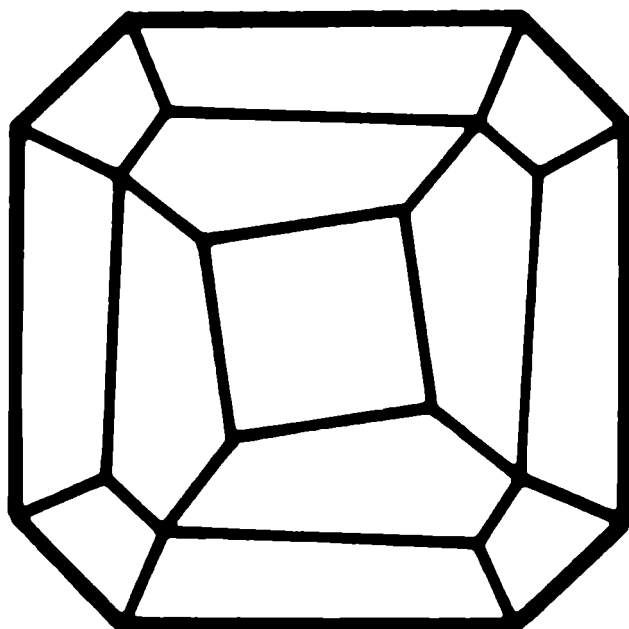


# **Mitteilungen der Österreichischen Mineralogischen Gesellschaft**



**Band 146**

**2001**

Herausgegeben von der Österreichischen Mineralogischen Gesellschaft  
für das Vereinsjahr 2000  
Eigenverlag

# Mitteilungen der Österreichischen Mineralogischen Gesellschaft

Band 146

2001



Vereinsjahr 2000

Gefördert aus Mitteln des Bundesministeriums für Wissenschaft und Verkehr in Wien.

#### Impressum:

Eigentümer, Herausgeber und Verleger: Österreichische Mineralogische Gesellschaft  
p.A. Mineralogisch-Petrographische Abteilung, Naturhistorisches Museum Wien

Burgring 7, A-1014 Wien

Homepage: <http://www.univie.ac.at/Mineralogie/Oemg.htm>

ISSN 1609-0144

#### Redaktion:

Friedrich Koller, Institut für Petrologie, Universität Wien  
Geozentrum, Althanstraße 14, A-1090 Wien

Anton Beran, Institut für Mineralogie & Kristallographie, Universität Wien  
Geozentrum, Althanstraße 14, A-1090 Wien

Richard Tessadri, Institut für Mineralogie & Petrographie, Universität Innsbruck  
Innrain 52, A-6020 Innsbruck

Gestaltung und Layout:  
R. Tessadri (Innsbruck)

Für den Inhalt sind die Autoren selbst verantwortlich.

Druck: Anton Riegelnik, Piaristengasse 19, A-1080 Wien

Printed in Austria

**INHALT**

MinPet 2001, 24.-26. September 2001, Vienna, Geocenter  
Anniversary Meeting Österreichische Mineralogische Gesellschaft (ÖMG) 1901-2001

Abart R., Badertscher N., Bernhard F., Burkhard M., Koller F. & Povoden E.: Syn-deformative fluid circulation at the Glarus Thrust, E-Switzerland	S. 13
Adamovič J., Melka K. & Ulrych J.: Fe-oxyhydroxide cementation in cretaceous sandstones, northern Bohemia: relation to young volcanic activity	S. 16
Akinin V. V., Ntaflos Th. & Richter W.: Augite megacrysts from Ennemelen volcanoes (Bering Sea basalt province)	S. 18
Andrut M. & Wildner M.: Lumineszenzspektroskopische Identifizierung spinverbotener Übergänge von Cr <sup>3+</sup> als Voraussetzung zur Anwendung des "Superposition Model" (SM) auf Uwarowite	S. 21
Andrut M., Hammer V. M. F., Lengauer C. L., Ntaflos T. & Redhammer G. J.: Untersuchungen zur Farbe des Lazoliths	S. 23
Andrut M., Hertweck B. & Wildner M.: Absorption- and Raman spectroscopic investigations of synthetic cobalt-boussingaultite (picromerite group), (NH <sub>4</sub> ) <sub>2</sub> Co(SO <sub>4</sub> ) <sub>2</sub> ·6H <sub>2</sub> O: refinement of Superposition Model (SM) parameters for Co <sup>2+</sup>	S. 26
Banerjee A. & Rager H.: Discrimination between sea water and fresh water tissue graft cultured pearls by EPR	S. 28
Barnert E. B., Müller W. F., Schmädicke E. & Franz G.: Transmission Electron Microscopy on eclogites from the lower schist cover and the eclogite zone (Tauern Window, Austria)	S. 31
Brandstätter F.: Kathodolumineszenz-Untersuchungen ausgewählter Mineralphasen mittels Rückstreuelektronendetektor: Eine REM-Studie	S. 34
Breiter K. & Koller F.: Mineralogy of extremely fractioned phosphorus-rich granite – Podlesí, Czech Republic	S. 37
Breiter K. & Scharbert S.: Geological mapping of the two-mica granites in the Weitra-Nové Hrady area	S. 40
Brereton N.R., Gallois R.W. & Whittaker A.: Improved lithological descriptions from downhole geophysical log data	S. 42
Brown J., Teetsra D. K. & Černý P.: Mineralogy and geochemical history of feldspars in the Tanco granitic pegmatite, southeastern Manitoba	S. 45
Brož M. & Losos Z.: Mineralogy and chemistry of the bi-metasomatic contact zone between gneiss and marble from Žulová, Czech Republic	S. 47
Buda G.: Lamprophyre-derived vaugneritic-durbachitic mafic enclaves in Variscan granitoids from Mecsek Mts. (South Hungary)	S. 50

Buriánek D. & Novák M.: Tourmaline-bearing leucogranites from the Moldanubicum	S. 51
Christensen A.-M. & Abart R.: A comparative study of contact metamorphism in the Oslo Graben, Norway	S. 54
Cina A. & Onuzi K.: Chromites related to the ultramafic south-eastern segment of Albania: a comparison with central and northern ones	S. 56
Copjáková R., Sulovský P. & Otava J.: Provenance of the lower carboniferous Culm sediments of the Drahany Upland (Czech Republic) derived from garnet chemistry	S. 58
Czuppon Gy., Harangi Sz., Ntaflos T., Lukács R., Szabó Cs. & Koller F.: Mixed andesite-rhyolite ignimbrite from the Miocene Bükkalja ignimbrite volcanic field, northern Hungary: evidence for magma mixing	S. 61
Dachs E. & Proyer A.: Time constraints on the metamorphic evolution of Tauern eclogites from diffusion modelling	S. 64
Dolníček Z.: Origin of the neoidic fluorite mineralization in the Brno Massif, Czech Republic: cathodoluminescence, REE, fluid inclusion and stable isotope study	S. 67
Effenberger H., Fleck M., Paar W., Topa D. & Criddle A. J.: Crystal-structure investigation of AgMS <sub>2</sub> minerals (M = As,Sb,Bi)	S. 69
Ertl A., Marler B. & Pertlik F.: Kristallchemische Überlegungen zur Besetzung "nichttetraedrischer" Kationenpositionen durch Silizium im Strukturtyp Turmalin	S. 72
Ertl A., Pertlik F. & Bernhardt H.-J.: Hellblaue Olenit-Schörl-Dravite von Ebersdorf, Niederösterreich: Chemismus und Kristallstruktur	S. 75
Falus Gy., van Roermund H. L. M., Drury M. R., Szabó Cs. & Gál Á.: The mechanism of development of a mantle shear zone: evidence from a xenolith (Szetbékálla, Bakony - Balaton Highland, Hungary)	S. 78
Faryad S. W. & Dianiška I.: Ti-bearing andradite with prehnite and epidote from the Malá Fatra granodiorite and tonalite (Western Carpathians)	S. 80
Faryad S. W., Hoinkes G. & Ivan P.: Pre-alpine eclogites and garnet-pyroxene-bearing metabasites in the Austroalpine units of the Eastern Alps and Western Carpathians	S. 82
Fojt B. & Kušnír I.: Sulphidische und oxidische Zn-Pb Vererzung der Lagerstätte Cho-Dien (Vietnam) – genetische Aspekte	S. 84
Franzen C. & Mirwald P. W.: Historical building materials in South Tyrol/Italy – a mineralogical study under the aspects of monument conservation	S. 87
Götzinger M. A. & Sauer R.: Die mineralogische Charakterisierung römischer Ziegel im Hinblick auf ihre Herkunft – erste Ergebnisse eines interdisziplinären Projektes	S. 89
Götzinger M. A. & Weisser S.: Das Pb-Zn-Fe-As-Vorkommen "Peitleralm" in der Stangalm-Trias, Nockberge, Kärnten – eine Detailstudie an Sediment und Mobilisat	S. 92
Götzinger M. A., Lein R. & Pak E.: Geologie, Mineralogie und Schwefelisotopie ostalpiner "Keuper"-Gipse: Vorbericht und Diskussion neuer Daten	S. 95
Gula A., Ferraris G., Ivaldi G. & Khomyakov A. P.: Crystal chemistry of some members of the eudialyte group	S. 97
Habler G., Linner M., Thiede R. & Thöni M.: Andalusitbildung im Schneeberger Zug (SE Ötzalkristallin, Italien/Österreich)	S. 100
Helmy H. M. & Kandl R.: Pyrite zonig and precipitation of gold in Atud and Sukkari gold deposits, Eastern Desert, Egypt	S. 103
Herbst G. & Kurzweil H.: Untersuchungen zur Ursache der Quellung technischer Asphalte	S. 105

Hertweck B., Fleck M., Wohlschläger A., Giester G. & Wildner M.: The isotopic crystal structures of $K_2Mn(SO_4)_2 \cdot 2H_2O$ and $K_2Cd(SeO_4)_2 \cdot 2H_2O$ : comparison with the kroehnikite-, collinsite- and fairfieldite-group	S. 107
Hertweck B., Libowitzky E. & Schultz A. J.: Neutron diffraction study of the low-temperature phase transition of Mn-leonite	S. 109
Hoinkes G., Faryad W. & Proyer A.: Pressure dominated Eo-Alpine metamorphism of the Austroalpine units of the Eastern Alps: new data from the Wölz complex	S. 111
Jelinek F., Leichmann J. & Nehyba S.: Contrasting evolution of the basal formation in the southern and central parts of the Boskovice Furrow	S. 113
Jeršek M., Mirtič B., Rečnik A., Zebec V., Bermanec V., Žorž M. & Dolenc T.: Wulfenite crystals from graben ore body of Mežica mines in Slovenia	S. 115
Johnson T. E., Ayalew T., Belete K. & Mogessie A.: Pan African metamorphism of the Western Ethiopian Shield	S. 117
Kaindl R., Abart R. & Hoinkes G.: Fluid inclusions in metamorphic garnet from selected Austroalpine basement areas	S. 119
Kaltenhauser G. & Tessadri R.: Die Kristallmodellsammlung aus dem 19. Jahrhundert des Instituts für Mineralogie und Petrographie der Universität Innsbruck	S. 122
Kempe U., René M. & Wolf, D.: Distribution of REE and REE-minerals in topaz-bearing granites of the Karlovy Vary pluton (Czech Republic)	S. 126
Kettrup B. & Deutsch A.: Chicxulub – Popigai: large impact craters and their distal ejecta. Isotopic characterisation of the melt products	S. 128
Klötzli-Chowanetz E. & Koller F.: Partial anatexis in the lower crust – where is the melt ? Examples from the Ötztal crystalline basement, Eastern Alps	S. 131
Klötzli-Chowanetz E., Klötzli U. & Sköld T.: Cambrian migmatisation and Ordovician tonalitic intrusion – Klopaijer area, Ötztal crystalline complex, Eastern Alps	S. 133
Kolitsch U.: Boron incorporation in rare-earth silicate apatites: a single-crystal X-ray study	S. 135
Kolitsch U.: The crystal structure of wycheproofite, a rare hydrated Na-Al-Zr-phosphate from Wycheproof, Victoria, Australia	S. 137
Kolitsch U.: Strong pseudosymmetry in the crystal structure of anthropogenic $Pb_2(OH)_3(NO_3)_2$ from a medieval mine dump	S. 139
Koller F., Hoeck V., Onuzi K., Knerringer E. & Meisel T.: From MORB to SSZ – the south albanian ophiolites and their Dinaric-Hellenic framework	S. 141
Konzett J. & Tropper P.: Domain formation in a staurolite-kyanite-amphibolite of the Schneeberg Complex, Southern Tyrol: applications of thermobarometry to local equilibrium domains	S. 143
Körner W., Weber L. & Weinke H. H.: Geochemische Untersuchungen von Grubenwässern mit Dithizon	S. 145
Koroneos A., Christofides G., Heaman L. & Krstic D.: Petrology, geochemistry and evolution of the peraluminous Monopigadon plutonite (Macedonia, Northern Greece)	S. 148
Kóthay K. & Szabó Cs.: Silicate melt inclusions in olivine phenocrysts in the Hegyestű Basalt, Bakony-Balaton Highland, Hungary	S. 151
Koubová M., Losos Z. & Malec J.: Ore-mineralogy of the Au-deposit near Voltyřov at Milevsko, Czech Republic	S. 153
Kovács I., Nédi Zs., Kóthay K., Bali E., Zajacz Z. & Szabó Cs.: Quartz and feldspar xenocrysts in mafic lavas from Nógrád-Gömör volcanic field, Bakony-Balaton Highland volcanic field and Villány Mountains (Hungary)	S. 155

Krause W., Bernhardt H.-J., McCammon C. & Effenberger H.: Neustädteleite and cobalt-neustädteleite, two new minerals of the medenbachite-group	S. 157
Kucha H., Schroll E. & Stumpf E. F.: Bacteriogenic ore formation in Bleiberg-type deposits	S. 160
Kudjelka A. P., Weber L., Punz W. & Weinke H. H.: Pflanzenverfügbarkeit und Mobilität von Schwermetallen von Bergwerkshalden der Pb-Zn Bergbaue des Grazer Berglandes (Steiermark)	S. 163
Kurat G., Dobosi G. & Maruoka T.: Diamondites and carbonatitic fluids: signals from trace elements in garnets and clinopyroxenes and from C isotope abundances	S. 166
Leichmann J. & Gaweda O.: Kłodsko-Złoty Stok and Niemcza zone granitoids – a shallow level intrusions of durbachites in the Rhenohercynian zone ?	S. 169
Leichmann J. & Zachovalová K.: Gabbros related to the durbachites (Jihlava Massif, Moldanubian Zone)	S. 171
Lenitz H., Seemann R. & Beran A.: Verteilung der Mineralien in den Klüften der Knappenwand; Hydroxid- und Fluor-Verteilung in Apatit und Sphen	S. 173
Leute M. A. & Götzinger M.A.: Einschluscharakterisierung von Zillertaler Schmuckgranaten, Tirol, Österreich	S. 175
Leute M. A., Wilhelm M. & Wruss W.: SiSiC-Keramiken – Eigenschaften und Anwendungsbereiche	S. 178
Lukács R., Harangi Sz. & Oláh I.: Correlation of Miocene pumice-bearing deposits in the Pannonian Basin	S. 180
Malitch K. N.: Unusual PGE-, REE-, Au- and U-rich mineral assemblage in mantle-derived chromitites from the Eastern Alps, Austria: a combined multi-disciplinary study	S. 183
Márton I., Gál J., Benoe É., Fall A., Gál Á., Török K. & Szabó Cs.: Fluid inclusions study in quartz, apatite and nepheline from Ditrău alkaline massif Transylvania (Romania)	S. 186
Masau M., Černý P., Cooper M. A., Chapman R. & Grice J. D.: Monazite-(Sm), a new member of the monazite group from the Annie Claim#3 granitic pegmatite, southeastern Manitoba	S. 189
Miletich R., Angel R. J., Rath S., Kunz M., Friedrich A., Schranz W. & Tröster A.: Elastische Anomalien bei Mineralen unter Druck	S. 191
Mirwald P. W.: Melting properties of Ice III, (V), VI and the isochoric gradient of water up to 20 kbar and 300°C – a review of literature data	S. 193
Mirwald P. W. & Tessadri R.: Thermal expansion behavior of disordered and ordered (Na)-Mg-cordierite between 25 and 700°C – a high resolution XRD study	S. 196
Mogessie A., Belete K., Hoinkes G. & Bowles J.: The Yubdo-Daleti and Tulu Dimtu ultramafic rocks: a potential source of economic deposits of platinum group minerals	S. 200
Morozov M., Brinckmann C., Kroll H., Lottermoser W., Tippelt G. & Amthauer G.: Mg <sup>2+</sup> , Fe <sup>2+</sup> - Verteilung in synthetischem Olivin (fa50fo50)	S. 202
Mrak M., Kolitsch U., Lengauer C., Kaučić V. & Tillmanns E.: Synthesis and crystal structure of a new layered hybrid gallophosphate containing oxalate groups	S. 204
Mukasa S. B. & Andronikov A. V.: Complex metasomatic enrichment of the upper mantle beneath Western Alaska: geochemical evidence from peridotite xenoliths in Cenozoic volcanics	S. 206
Mukasa S. B. & Andronikov A. V.: Upper mantle peridotites from Kigluaik Mountains: evidence of Cretaceous subduction zone existence beneath Western Alaska	S. 209
Niedermayr G.: Private Sammler und ihre Bedeutung für die Mineralogie in Österreich	S. 212

Niedermayr G., Brandstätter F., Ponahlo J. & Henhapl E.: Über ein Vorkommen von Vanadium-Beryllen aus dem östlichen Himalaya	S. 215
Novák M.: Are granitic pegmatites a toy for descriptive mineralogists or a useful tool for geologist ?	S. 217
Ntaflos Th., Bjerg E.A., Labudia C. H., Thöni M., Friscale C. & Günther M.: High temperature, low pressure garnet-bearing peridotites from Pragauniyu: evidence for plume activity in northern Patagonia	S. 220
Onuzi K. & Cina A.: Metallogenic features of Albanian ophiolitic complex	S. 223
Osman M. R. & Kurzweil H.: Provenance and palaeoenvironmental conditions of lacustrine sediments in the area east of Higaza, Nile Valley, Upper Egypt	S. 226
Parthé E.: Borate structures formed at ambient pressures: equally bonded O atoms as a key to understand the apportion of $\text{BO}_3$ triangles and $\text{BO}_4$ tetrahedra	S. 227
Piber A. & Tropper P.: Thermobarometry in low-grade metagranitoids: how reliable is stilpnomelane ?	S. 230
Potocan C., Vavtar F. & Tessadri R.: Preliminary results of steam processed slags produced by spray granulation (pilot-project DGM-Tribowent/Lorüns): mineralogical and physical parameters	S. 232
Poyer A.: Metamorphism of metapelites and metapsammites in NKFMASH – a new petrogenetic grid with comparison of natural assemblages and implications for the preservation of high-pressure rocks during exhumation	S. 233
Poyer A.: The preservation of high-pressure rocks during exhumation: eclogites, metapelites and metagranites	S. 236
Poyer A. & Hoinkes G.: The importance of paragonite-bearing micaschists in medium- to high-pressure metamorphism: a theoretical study and field evidence from the Austroalpine basement units of the Eastern Alps	S. 238
Poyer A., Schuster R., Hoinkes G. & Faupl P.: Permo-Triassic metamorphic evolution of the Kreuzeck-Goldeck mountains (Carinthia, Austria)	S. 240
Ramminger P.: Convolution based profile fitting in X-ray diffraction: instrumental effects and their description	S. 243
Recheis A. & Tropper P.: A compilation of thermobarometric data from the crystalline basement west of the Tauern Window (Ötztal-Schneeberg-Complex)	S. 244
Redhammer G. J., Amthauer G., Lottermoser W. & Roth G.: Strukturelle und mößbauerspektroskopische Untersuchungen an synthetischen trioktaedrischen $(\text{K})[\text{Me}_3]<\text{T}_4>\text{O}_{10}(\text{OH})_2$ : eine Zusammenfassung	S. 246
Redhammer G. J., Tippelt G., Roth G., Lottermoser W. & Amthauer G.: Strukturelle, mößbauerspektrometrische und magnetische Untersuchungen an der Brownmillerit-Mischkristallreihe $\text{Ca}_2\text{Fe}_{2-x}\text{Al}_x\text{O}_5$ bei 298 K und hohen Temperaturen	S. 249
Reif J.: Mercury polluted sites in Czech Republic and remediation technology	S. 251
Reif J. & Fojt B.: Mineralogy and geochemistry of iron ores from Horní Benešov deposit	S. 254
Reiter D. A., Weber L. & Kiesl W.: Geochemische Charakteristik primärer und sekundärer Blei- Zinkvererzung des Grazer Paläozoikums (Steiermark)	S. 256
René M.: Evolution of two-mica granites in the South Bohemian Batholith	S. 258
Rezek K., Reif J. & Parizek A.: Geochemical study of selected minor elements in polymetallic nodules and crust from eastern part of Clarion-Clipperton fracture zone, Pacific Ocean	S. 260

Sadiklar M. B., Hanedan A., Heide K. & Völksch G.: Breckzierung und entmischte Ti-Magnetite in Obsidianen der İkizdere Region (Rize/NE-Türkei): Hinweise auf Förderwege von Laven	S. 262
Schroffenegger V. & Kurzweil H.: Hydrogeology – water prospecting and management supported by GIS	S. 264
Schroll E.: Zur geochemischen Charakterisierung von Lagerstätten	S. 266
Schulz O., Vavtar F., Gu X. X., Liu J. M. & Zheng M. H.: Submarin-hydrothermale Metallanreicherung im Jung-Proterozoikum und metamorphogene Weiterentwicklung der stratiformen W-Sb-Au-Erzlagerstätten vom "Typ Woxi" in Hunan, Südost-China	S. 269
Schuster R. & Klötzli U.: Dating of andalusite by geochronological methods (Sm-Nd and U-Pb) – a failure	S. 272
Schuster R., Poyer A., Hoinkes G. & Schulz B.: Indications for a Permo-Triassic metamorphic imprint in the Austroalpine crystalline rocks of the Defreggen Alps (Eastern Tyrol)	S. 275
Sobolev N. V., Logvinova A. M. & Yefimova E. S.: Minerals in diamond aggregates and mineral inclusions in diamonds: a comparison	S. 278
Sulovský P. & Hlisnikovsky K.: Thorium mineralization in alkali feldspar syenite of the nordmarkite-type dyke in the Třebíč Pluton (Czech Republic)	S. 280
Thalheim K.: Die Sammlung Richard Baldauf (1848–1931) – eine bedeutende Mineraliensammlung aus der ersten Hälfte des 20. Jahrhunderts und ihr Bezug zu Österreich	S. 283
Thöny W., Tropper P. & Bernhard F.: The metamorphic evolution of stromatic migmatites from the western Ötztal-Stubai crystalline basement (Tyrol, Eastern Alps)	S. 286
Tóth E., Weiszburg T.G. & Pop D.: Celadonite: the colour-giving green clay mineral of the carbonate manganese ore, Úrkút, Transdanubian Central Range, Hungary	S. 288
Tropper P., Bernhard F. & Postl W.: Petrology of manganese silicate-carbonate rocks from the Veitsch Mn-deposit, Greywacke Zone, Eastern Alps	S. 290
Tufar W., Siewers U. & Weber Ch.: Die Spatmagnesit-Lagerstätte Breitenau (Steiermark), eine paläozoische Magnesit-Mineralisation aus dem Grazer Paläozoikum	S. 292
Tufar W., Siewers U. & Weber Ch.: Die Spatmagnesit-Lagerstätte Radenthein (Millstätter Alpe, Kärnten), eine voralpidische Magnesit-Mineralisation aus dem mittelostalpinen Altkristallin der Ostalpen	S. 295
Ulrych J., Svobodová J., Novák J. K. & Balogh K.: Synchronous contrasting late Miocene alkaline volcanic series related to the Cheb-Domažlice Graben, western Bohemia: geochemistry and mineralogy	S. 298
Vávra N.: Chemismus und Genese organischer Minerale in deutschen und österreichischen Braunkohlen	S. 301
Voll D., Beran A. & Schneider H.: Infrared band assignment of Al-Si mullite and SiO <sub>2</sub> -free compounds with mullite structure	S. 304
Wagner D. & Kurzweil H.: Einsatzmöglichkeiten von Tonen aus dem Bereich des Braunkohletagbaus Oberdorf, weststeirisches Tertiärbecken, als Rohstoff in der Industrie	S. 306
Walter F. & Ettinger K.: Andalusit, Sillimanit und Kyanit vom Schneestellkopf, Kreuzeckgruppe, Kärnten	S. 308
Walter F. & Ettinger K.: Die Kristallstrukturverfeinerung eines fast alkalifreien Minerals der Osumolithgruppe: K <sub>&lt;0,1</sub> (Fe,Mg) <sub>2</sub> (Mg,Fe) <sub>3</sub> [Si <sub>12</sub> O <sub>30</sub> ]	S. 311
Weinke H. H., Koller F. & Pernicka E.: Platinmetalle in mesozoischen Ophioliten der Ostalpen	S. 314

Wildner M. & Andrut M.: Synthetic cobaltomenite, CoSeO <sub>3</sub> .2H <sub>2</sub> O, and related Co-compounds as model phases for the application of the Superposition Model (SM) of crystal fields in geosciences	S. 316
Wilflingseder P., Abart R. & Bärnthaler K.: Ursachen für Restkarbonat im Gips aus einer Rauchgasentschwefelungsanlage	S. 318
Winkler W. & Kirchner E. Ch.: Petrographical data on the Lower Cretaceous fossil resin deposit, Golling/Salzburg, Austria	S. 320
Wohlschläger A., Kolitsch U. & Libowitzky E.: Large "gahnites" from near Okahua, Namibia: only Fe- and Zn-bearing spinels	S. 323
Zahiri R., Voll D., Beran A. & Schneider H.: Temperature-related dehydration and structural development of sol-gel prepared type I mullite precursors	S. 324
Zajacz Z., Szabó Cs. & Kovács I.: Petrogenetic significance of sulfide inclusions in ultramafic cumulate xenoliths from Nograd-Gömör volcanic field, Pannonian Basin	S. 326

## Exkursionen

Seeman R.: Gesteine - Lagerstätten und Karstlandschaften in Slowenien und im angrenzenden Italien ((Exkursion vom 18. bis 23. September 2001 anlässlich der Tagung MinPet2001 in Wien, 100 Jahre Österreichische Mineralogische Gesellschaft)	S. 331
---	--------

## Originalarbeiten

Faryad S. W. & Hoinkes G.: Alpine chloritoid and garnet from the Hochgrößen Massif (Speik Complex, Eastern Alps)	S. 387
Hammer V. M. F.: Sonderschau zum Thema "100 Jahre (Wiener) Österreichische Mineralogische Gesellschaft – ÖMG"	S. 397
Hammer V. M. F. & Pertlik F.: Ein Beitrag zur Geschichte des Vereines "Wiener Mineralogische Gesellschaft" (27. März 1901 – 24. November 1947)	S. 407
Hammer V. M. F. & Pertlik F.: Ehrentitel und Auszeichnungen, verliehen durch den Verein "Österreichische Mineralogische Gesellschaft"	S. 417
Niedermayr G.: Die Bedeutung privater Sammler in der Österreichischen Mineralogischen Gesellschaft (früher Wiener Mineralogische Gesellschaft)	S. 427
Schroll G. & Pertlik F.: Herbert Eduard Haberlandt: Ein Pionier der Geochemie in Österreich (*3.6.1904 Mödling †9.6.1970 Wien) – (Eine Biographie mit Schriftenverzeichnis)	S. 435

## Vorträge

Whittaker A.: Karl Ludwig Giesecke: his life, performance and achievements	S. 451
--	--------

## Diplomarbeiten und Dissertationen von österreichischen Universitäten (Auszüge)

Belete K. H.: The petrology of the mafic-ultramafic rocks and the surrounding basement, western Ethiopia and genesis of platinum-group minerals related to an alaskan-type ultramafic intrusions of Yubdo area	S. 483
Grasbon B.: Großmassenbewegungen im Grenzbereich Innsbrucker Quarzphyllit, Kellerjochgneis, Wildschönauer Schiefer	S. 486
Klötzli-Chowanetz E.: Migmatite des Ötztalkristallins – Petrologie und Geochronologie	S. 487
Lottner S.: Formation of minerals in hydrated high-calcium lignite fly ash influenced by elevated temperatures and their consequences for technological properties	S. 489
Nascimento F.: Distribution of trace metals in sediment profile of the Guajará estuary, North Brazil	S. 493
Nyakairu G. W. A.: Mineralogy, chemical composition and distribution of rare earth elements of clay-rich sediments, Central Uganda	S. 496
Sikazwe O. N.: The geology, geochemistry and genesis of the Lewis and Marie copper sulphide deposits, Mumbwa District, Central Zambia	S. 499
Tessema D. A.: Weathering and mobility of arsenic in soils	S. 501
Vianney T. J.: The petrology, geochemistry and petrogenesis of the Tororo Carbonatite Complex, eastern Uganda	S. 504

Vereinsnachrichten	S. 507
--------------------	--------

ÖMG-Nominierungen	S. 514
-------------------	--------

Autorenhinweise	S. 515
-----------------	--------

# **MINPET 2001**

**24.-26. SEPTEMBER 2001**

**VIENNA**

**ANNIVERSARY MEETING  
ÖSTERREICHISCHE MINERALOGISCHE  
GESELLSCHAFT (ÖMG)  
1901 - 2001**



SYN-DEFORMATIVE FLUID CIRCULATION AT THE GLARUS THRUST, E-SWITZERLAND

by

R. Abart<sup>1</sup>, N. Badertscher<sup>2</sup>, F. Bernhard<sup>3</sup>, M. Burkhard<sup>2</sup>, F. Koller<sup>4</sup> & E. Povoden<sup>1</sup>

<sup>1</sup>Institute of Mineralogy and Petrology  
Karl-Franzens-Universität, Graz, Austria

<sup>2</sup>Institute of Geology  
University of Neuchatel, Switzerland

<sup>3</sup>Institute of Applied Mineralogy  
Technical University Graz, Austria

<sup>4</sup>Institute of Petrology  
University of Vienna, Austria

The Glarus thrust in eastern Switzerland has been recognized as a major control on fluid flow associated with the Early Miocene emplacement of the Helvetic thrust mass on the Infrahelvetic realm.

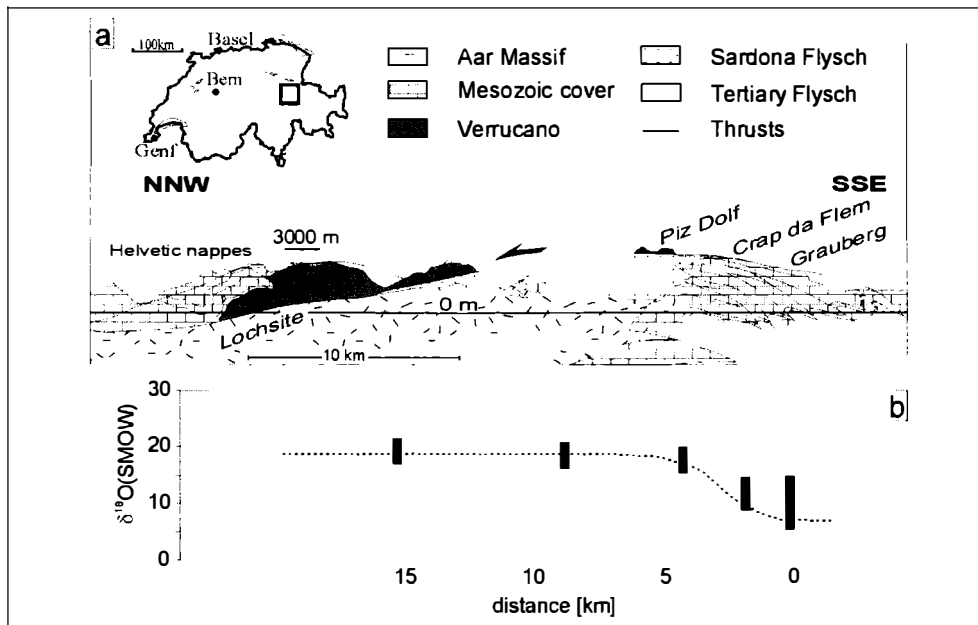
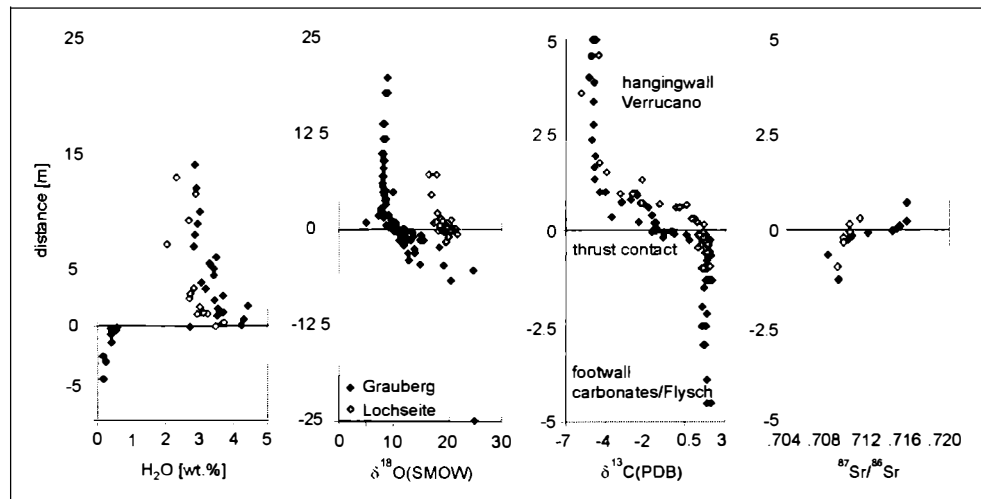


Figure 1

(a) Schematic cross section through the eastern Helvetic Alps, modified from Burkhard and Kerrich (1990) [1],  
(b) regional oxygen isotope trend in the Lochseiten Limestone, black bars are data form BURKHARD & KERRICH [1], dotted line represents the model interpretation as a large scale oxygen isotope front [2].

In the Lochseiten Limestone, a thin calc-mylonite at the thrust contact, a regional south to north  $^{18}\text{O}$  enrichment trend was documented by BURKHARD & KERRICH (1990) [1] (see Fig. 1) and interpreted in terms of one-dimensional flow with a thrust parallel time integrated volumetric flux on the order of  $10^3 \text{ m}^3/\text{m}^2$  [2]. In this communication we relax the assumption of purely one-dimensional transport and investigate the possible contributions of cross thrust transport components.

The sampling localities at Grauberg and at Lochseite represent two fundamentally different geological situations that occur in the southern (Grauberg) and northern (Lochseite) sections of the Glarus thrust. Whereas at Grauberg the footwall is represented by Cretaceous limestones, the footwall in the north is comprised of Tertiary Flysch. The hangingwall is represented by siltstones and metavolcanic rocks of the Verrucano formation over the entire length of presently exposed thrust. All along the thrust, there is a large difference in the background isotopic compositions between the footwall and hangingwall lithologies. The isotopic patterns as well as bulk rock water contents observed in sub-vertical sampling profiles at the Grauberg and Lochseite localities are shown in Fig. 2.



**Figure 2**

$\text{H}_2\text{O}$  contents, oxygen-, carbon- and strontium isotope variations across the Glarus thrust at the Grauberg (south) and Lochseite (north) localities.

In both profiles the isotopic compositions show a smooth transition across the thrust contact. At Grauberg only the lowermost one meter of the hangingwall Verrucano shows  $^{18}\text{O}$  and  $^{13}\text{C}$  enrichment and concomitant  $^{87}\text{Sr}$  depletion towards the thrust contact. The relatively  $^{18}\text{O}$  and  $^{13}\text{C}$  enriched and  $^{87}\text{Sr}$  depleted compositions of the footwall carbonates are gradually shifted towards the compositions of the Verrucano in the uppermost five meters below the thrust. This pattern may be explained by material exchange between the footwall and hangingwall lithologies. The fact that alteration is more pronounced in the footwall carbonates than in the hangingwall Verrucano suggests that net material transport was downwards directed. The geometry and the position of the isotopic fronts indicate a maximum time integrated flux on the order of  $6 \text{ m}^3/\text{m}^2$ .

At Lochseite isotopic alteration is only evident in the Verrucano, where the isotopic compositions are shifted towards typical Flysch values in the lowermost 10 to 20 meters of the hangingwall. The fact that the footwall Flysch does not show any sign of isotopic alteration indicates that at Lochseite fluid flow was upwards directed with a time integrated volumetric fluid flux on the order of  $3 \text{ m}^3/\text{m}^2$ . Although relatively small, cross thrust transport buffered the thin layer of Lochseiten Limestone towards the relatively  $^{18}\text{O}$ ,  $^{13}\text{C}$  depleted and  $^{87}\text{Sr}$  enriched composition of the hangingwall Verrucano in the south and towards the relatively  $^{18}\text{O}$  and  $^{13}\text{C}$  enriched and  $^{87}\text{Sr}$  depleted composition of the footwall Flysch in the north. The large scale  $^{18}\text{O}$  trend in the Lochseite limestone may at least in part be ascribed to the regional differences in cross thrust transport.

In both the Grauberg and Lochseite localities the  $\text{H}_2\text{O}$  content of bulk rock samples increases systematically in the hangingwall Verrucano towards the thrust contact (see Fig. 1). Whereas in the north, the dewatering footwall Flysch is a potential fluid source, the Cretaceous limestones in the south do not have any potential to release water during thrusting. At Grauberg, hydration of the lowermost Verrucano requires introduction of a water rich fluid along the thrust surface. Based on the assumption that hydration of the Verrucano is equally pronounced all along the thrust, time integrated volumetric fluxes on the order of  $200 \text{ m}^3/\text{m}^2$  are inferred for sub-horizontal thrust parallel flow.

## References

- [1] BURKHARD, M. & KERRICH, R. (1990): Fluid-rock interactions during thrusting of the Glarus nappe – evidence from geochemical and stable isotope data. - Schweiz. Min. Petrogr. Mitt., 70, 77-82.
- [2] BOWMAN, J. R., WILLET, S. D. & COOK, S. J. (1994): Oxygen isotope transport and exchange during fluid flow: One-dimensional models and applications. - Am. Journ. Sci., 294, 1-55.

**FE-OXYHYDROXIDE CEMENTATION IN CRETACEOUS SANDSTONES,  
NORTHERN BOHEMIA: RELATION TO YOUNG VOLCANIC ACTIVITY**

by

**J. Adamovič, K. Melka & J. Ulrych**

Institute of Geology, Academy of Sciences of the Czech Republic  
Rozvojová 135, 165 02 Praha 6, Czech Republic

Bodies of siliciclastic sediments hundreds of metres thick (Turonian to Coniacian) flank the northern margin of the Bohemian Cretaceous Basin and progressively thin out basinwards. They comprise quartzose and arkosic sandstones with variable amounts of clay and silt component [1]. Quartz pebbles are dispersed in the sandstone or form sharp-based conglomerate beds on tops of upwards-coarsening cycles. The distribution of Fe-oxyhydroxides in these sediments is controlled by high-permeability host lithologies, proximity of young bodies of basaltic rocks and high intensity of tectonic deformation.

Ferruginization is associated with age-contrasting volcanic series: 1) melilite-bearing rocks (olivine melilitites to olivine nephelinites and lamprophyres of polzenite type) of Late Cretaceous and Paleocene age and 2) alkali basaltic rocks (olivine nephelinites to basanites and camptonites) mostly of Eocene to Oligocene age. Both series represent typical near-primary mantle products [2]. The dissolved mineral content of iron-bearing fluids is of complex provenance, probably combining 1) primary magmatic source, 2) component leached from the adjacent upper crustal rocks (mostly granitic rocks in the area studied), and 3) component produced from decomposed volcanic rocks, the bodies of which may represent principal ascent paths for the iron-bearing fluids.

Twenty type localities with prominent ferruginization were studied using a combination of geophysical, geological and mineralogical methods in order to characterize sandstone lithology, distribution and mineralogy of Fe-oxyhydroxides and the presence of intrusive bodies and related tectonic structures. Macromorphological types of ironstones range from joint fillings and linings of basaltic dykes to complex undulating crusts in sandstone. Fe-oxyhydroxides bound to conglomerate beds may form extensive strata-bound bodies [3].

With the exception of two localities, close spatial relation was proved between the distribution of intrusive bodies of basaltic rocks and Fe-oxyhydroxides. Leaching of iron from young basaltic rocks after their emplacement, transport of ferrous iron in low-Eh hydrothermal fluids driven by the high thermal gradient, and precipitation of iron in zones of mixing with oxygenated meteoric waters seem to be the most probable ferruginization mechanisms. Two episodes of hydrothermal mineralization of different hydraulic parameters are suggested, which correspond to the two above mentioned age-contrasting volcanic series.

The study of macroscopic secondary structures as well as microscopic study allow to distinguish a continuous series with two end-members: laminated quartz-poor ironstones and massive quartz-rich ironstones. Quartz-poor ironstones contain 43.4 wt.% Fe<sub>tot</sub>, on average (20.98 - 67.01), quartz-rich ironstones contain 24.3 wt.% Fe<sub>tot</sub>, on average (11.75 - 32.68), with the oxidation ratio (0.9 Fe<sub>2</sub>O<sub>3</sub> + FeO/FeO wt.%) of 17.7 - 328.

The ironstones are enriched in incompatible elements relative to quartzose sandstones and, in the case of Fe<sub>tot</sub>, As and Zn, even relative to fresh volcanic rocks. With the exception of Ba and Sr, quartz-rich ironstones of different macromorphological types show similar major-element and trace-element composition.

According to mineralogical results based primarily on X-ray powder diffraction, quartz-poor ironstone was found to consist of goethite I, kaolinite, anatase, ± opal, ± detrital quartz, and a younger generation of goethite II ± lepidocrocite. Goethite I forms fine crystalline (crystal size < 500 nm) aggregates in the cement, fills of embayments, cracks and needle-like cavities in individual quartz grains. Goethite II and lepidocrocite form radially fibrous aggregates filling fractures in quartz grains and older goethite-SiO<sub>2</sub> groundmass. Quartz-rich ironstone is dominated by detrital quartz with accessory detrital minerals, cemented by goethite ± lepidocrocite ± hematite.

A higher than theoretically expected amount of water in goethite is observed on the thermogravimetric curve, corresponding to "hydrogoethite". A small endothermic reaction in the region of ~100°C on the DTA curve is indicative of the escape of adsorbed water from the surface of fine goethite particles.

## References

- [1] ADAMOVIC, J. (1994): Paleogeography of the Jizera Formation (Late Cretaceous sandstones), Kokorín area, central Bohemia. - Sbor. geol. Věd, Geol., 46, 103-123.
- [2] ULRYCH, J. & PIVEC, E. (1997): Age-related contrasting alkaline volcanic series in North Bohemia. - Chem. Erde, 57, 311-336.
- [3] ADAMOVIC, J., ULRYCH, J. & PEROUTKA, J. (2000): Geology of occurrences of ferruginous sandstones in N Bohemia: famous localities revisited. - Schr. Staatl. Mus. Miner. Geol. Dresden, 11: 49-50.

AUGITE MEGACRYSTS FROM ENMELEN VOLCANOES  
(BERING SEA BASALT PROVINCE)

by

V. V. Akinin<sup>1</sup>, Th. Ntaflos<sup>2</sup> & W. Richter<sup>2</sup>

<sup>1</sup>NEISRI FEB RAS

Magadan, Russian Federation

<sup>2</sup>Institute of Petrology

University of Vienna, Geozentrum, Althanstrasse 14, A-1090 Wien

The 10 to 4 million year old lavas at Enmelen volcanoes, Chukchi Peninsula, NE-Russia, consist of olivine melanephelinites and basanites, and include the most undersaturated lavas of the Bering Sea basalt province [1]. These intraplate lavas brought to the surface xenoliths of spinel lherzolites, pyroxenites, and gabbrorites along with megacrysts of clinopyroxene, orthopyroxene, olivine, ilmenite and biotite. Previous study showed that most of the spinel lherzolites xenoliths are Mg-rich and have relatively high CaO, Al<sub>2</sub>O<sub>3</sub> and Na<sub>2</sub>O contents compared to the depleted peridotites found in the ocean basins. Chondrite-normalized REE patterns for those Groups I lherzolites range from relatively flat patterns to patterns with negative slopes, they equilibrated within a temperature range of 850 - 1030°C; two xenoliths equilibrated at much higher temperatures of 1230 - 1240°C and have relatively Fe-rich composition [2].

Among the nodules found in Chuckhi peninsula, approximately 7 - 10 % are pyroxene megacrysts that vary in size between 1 and 12 cm. The relative high abundance of the augite megacrysts indicates that their origin must be associated with major magmatic processes that influenced and modified the lithosphere in this region. We investigated in detail these pyroxene megacrysts using microprobe, ion probe, INAA, LA-ICP-MS, XRF and ICP-MS.

The pyroxene megacrysts are black in color, characteristically lacking cleavage and exhibiting conchoidal fracture. They are typically subcalcic augites with high Al<sub>2</sub>O<sub>3</sub> (7.5 wt.%), significantly elevated TiO<sub>2</sub> (1.42 wt.%) and Na<sub>2</sub>O (2.45 wt.%) and very low Cr (ca. 30 ppm) contents. Their CaO content, however, vary with Fe/Mg ratios allowing to classify pyroxenes in two groups: group one (augite1) with CaO = 17.3 wt.% and Fe/Mg = 0.38 and group two (augite2) with CaO = 14.6 and Fe/Mg = 0.26. This increase of Fe/Mg ratio with increasing of CaO has been interpreted as indicative for crystallization during slow upward moving of the magma [3].

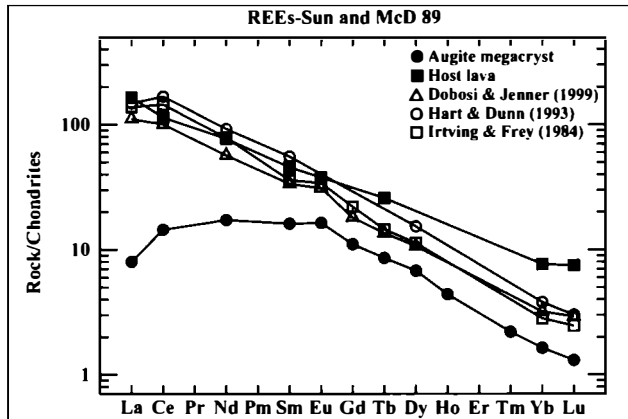


*Fig. 1*

*Host lavas and hypothetical compositions of liquids in equilibrium with augite megacrysts, calculated using partition coefficients of [4, 5, 6].*

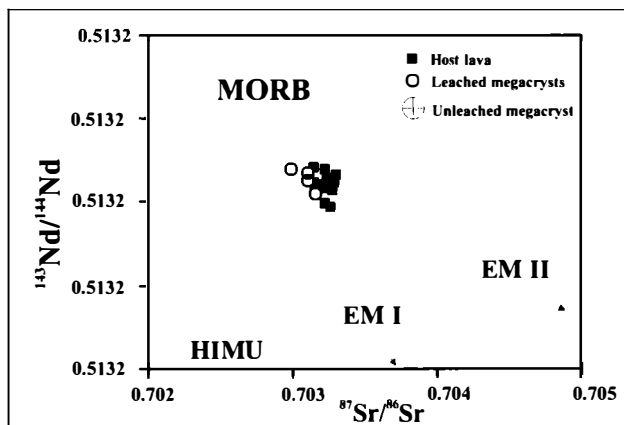


*Fig. 2*

*Correlation diagram of Sr-Nd isotopic ratios for augite megacrysts and host melanephelinitic lavas.*

The chondrite-normalized REE display LREE/MREE – enriched upward convex patterns with  $\text{La}_N/\text{Yb}_N = 6.4$  (Fig. 1). Using existing partition coefficients [4, 5, 6] we calculated the hypothetical melt in equilibrium with augite megacrysts. The calculated liquids, compared to the host olivine melanephelinite lavas have similar LREE but significantly lower middle and heavy REE. It implies that the parental source of the augite megacrysts was not the host lava, but rather a source which experienced, in an earlier stage of the evolution, garnet fractionation causing the strong HREE depletion.

Alternatively, partial melting of the source in the garnet peridotite field leaving residual garnet can also account for this HREE depletion (Fig. 1). In addition, megacrysts have isotopic compositions overlapping their host melanephelinites (Fig. 2). An initial alkali-picritic magma is proposed as possible source for their origin. However as inferred from the REE patterns, both, megacrysts and melanephelinites must have been formed under different conditions.

## Literature

- [1] AKININ, V. V & APT, J. E. (1995): Enmelen Volcanoes, Chukchi Peninsula: Petrology of Alkaline Lavas and Deep-Seated Inclusions. - ICAM-94 proceedings, 138-146.
- [2] AKININ, V. V. et al. (1997): Compositional and thermal state of the upper mantle beneath the Bering Sea Basalt Province: Evidence from the Chukchi Peninsula of Russia. - Can. J. Earth Sci. 1997. V. 34 (6), 789-800.
- [3] BINNS, R. A. et al. (1970): High Pressure megacrysts in alkaline lavas from north-eastern New South Wales. - Amer. J. Sci., 269, 132-168.
- [4] DOBOSI, G. & JENNER, G. A. (1999): Petrologic implications of trace element variation in clinopyroxene megacrysts from Nograd volcanic province, north Hungary: a study by laser ablation microprobe – inductively coupled plasma – mass spectrometry. - Lithos, 46, 731-749
- [5] HART, S. R. & DUNN, T. (1993): Experimental cpx/melt partitioning of 24 trace elements. - Contr. Mineral. Petrol. 113, 1-8.
- [6] IRVING, A. J. & FREY, F. A. (1984): Trace element abundances in megacrysts and other host basalts: constraints on partition coefficients and megacryst genesis. - Geochim. Cosmochim. Acta 48, 1201-1221.

**LUMINESZENZSPEKTROSKOPISCHE IDENTIFIZIERUNG SPINVERBOTENER  
ÜBERGÄNGE VON CR<sup>3+</sup> ALS VORAUSSETZUNG ZUR ANWENDUNG DES  
“SUPERPOSITION MODEL” (SM) AUF UWAROWITE**

von

**M. Andrut & M. Wildner**

Institut für Mineralogie und Kristallographie  
Universität Wien, Geozentrum, Althanstrasse 14, A-1090 Wien

Das Konzept des Kristallfeldes hat bei der Interpretation physikalischer und chemischer Eigenarten von Übergangs-metall-führenden Mineralen bisher eine breite und durchaus erfolgreiche Anwendung erfahren. Dazu zählen z.B. die Erklärung von Farbe und Pleochroismus, das inter- und intrakristallinere Verteilungsverhalten von Übergangsmetallionen oder der Einfluß der Kristallfeldstabilisierungsenergie CFSE auf thermodynamische Eigenschaften. Allerdings lag den bisherigen Kristallfeldberechnungen mit wenigen Ausnahmen die Annahme einer idealen oktaedrischen bzw. tetraedrischen Geometrie des lokalen Kristallfeldes als Näherung zugrunde. Diese ideale O<sub>h</sub>- bzw. T<sub>d</sub>-Symmetrie stellt im Vergleich mit den tatsächlichen Koordinationsverhältnissen zumeist eine grobe Vereinfachung dar.

Das ‘Superposition Model of Crystal Fields’ (SM) wurde von NEWMAN [1] entwickelt, um die geometrische und physikalische Information, welche durch verschiedene Kristallfeldparameter beschrieben wird, zu trennen. Seither wurde das SM erfolgreich für Verbindungen mit Lanthaniden eingesetzt, während es bisher nur einige wenige Anwendungen für die geowissenschaftlich relevanteren 3d<sup>N</sup> Ionen gibt [2, 3, 4].

Ziel der gegenwärtigen Untersuchungen ist die Bestimmung verlässlicher, sog. intrinsischer SM-Parameter verschiedener 3d<sup>N</sup> Übergangsmetallionen für zukünftige Anwendungen in den Geowissenschaften. Erste Untersuchungen wurden an Cr<sup>3+</sup>-führenden Phasen durchgeführt. Dazu wurden Einkristalle von Uwarowit bei 1000°C aus einer Mischung von 80 % Oxiden und 20 % Flux der Zusammensetzung Na<sub>2</sub>O K<sub>2</sub>O 1.3 B<sub>2</sub>O<sub>3</sub> synthetisiert [5]. Zur Kristallstrukturverfeinerung wurden Röntgenbeugungsintensitäten bis 100° 2θ an einem Nonius Kappa CCD Diffraktometer gemessen.

Lumineszenzspektren wurden mit einem Renishaw RM 1000 Ramanspektrometer mit gekoppltem Leica-Mikroskop DMLM aufgenommen. Die Spektren wurden mit der 6328-Å Linie eines He-Ne-Lasers angeregt. Aus den Lumineszenzspektren wurden die Lagen der durch Spin-Bahn Kopplung und trigonale Kristallfeldsymmetrie aufgespaltenen Folgeterme der spinverbotenen Übergänge <sup>4</sup>A<sub>2g</sub> → <sup>2</sup>E<sub>g</sub> und <sup>4</sup>A<sub>2g</sub> → <sup>2</sup>T<sub>1g</sub> bestimmt.

Die Kenntnis der Lage dieser Energieterme ist Voraussetzung für die richtige Zuordnung der entsprechenden Banden im Absorptionsspektrum und somit für die Bestimmung der Racah-Parameter  $B_{55}$  und C, sowie für die Abschätzung des Spin-Bahn Kopplungsparameters  $\zeta$ . Polarisierte Einkristall-spektren wurden im Bereich  $32000 \text{ cm}^{-1}$  bis  $10000 \text{ cm}^{-1}$  an einem Bruker IFS66v/S FT-Spektrometer mit IRScopeII Mikroskop gemessen. Die Absorptionsbanden [ $\text{cm}^{-1}$ ] wurden folgenden dd-Übergängen von  $\text{Cr}^{3+}$  zugeordnet:  $14272 ({}^4\text{A}_{2g} \rightarrow {}^2\text{E}_g, 'R_1')$ ,  $14375 ({}^4\text{A}_{2g} \rightarrow {}^2\text{E}_g, 'R_2')$ ,  $15905 ({}^4\text{A}_{2g} \rightarrow {}^4\text{T}_{2g})$ ,  $20905 ({}^4\text{A}_{2g} \rightarrow {}^2\text{T}_{2g}, 'B')$  und  $22775 ({}^4\text{A}_{2g} \rightarrow {}^4\text{T}_{1g})$ . Weiters zeigt sich im Spektralbereich zwischen  $14400$  und  $15000 \text{ cm}^{-1}$  eine Bandeneinstruktur, in der ‘phonon sidebands’ das sehr schwache und daher schwer beobachtbare  ${}^4\text{A}_{2g} \rightarrow {}^2\text{T}_{1g}$  Niveau überlagern. Mittels der Lumineszenzmessungen konnte schließlich ein Detail der Bandenstruktur bei  $14575 \text{ cm}^{-1}$  als  ${}^4\text{A}_{2g} \rightarrow {}^2\text{T}_{1g} 0'' - 0''$  Übergang identifiziert werden. In den nachfolgenden SM-Berechnungen wurde der Geometrie und Symmetrie des Ligandenfeldes durch die Polar-koordinaten der Liganden Rechnung getragen, welche aus der Strukturverfeinerung gewonnen wurden. Dadurch konnten die notwendigen 14 Kristalfeldparameter auf zwei intrinsische  $\bar{B}_k$  und zwei Exponentialparameter  $t_k$  reduziert werden, welche durch Anpassung an die optischen Absorptionsspektren gewonnen wurden. Die Berechnung der Energieniveaus aus den gewonnenen Parametern erfolgte mit dem HCFLDN2 Kristalfeld-Programmpaket von YEUNG [6]. Die beste Übereinstimmung fand sich für folgende Parameter:  $\bar{B}_4 = 9525 \text{ cm}^{-1}$ ,  $t_4 = 7$ ,  $\bar{B}_4 = 4650 \text{ cm}^{-1}$ ,  $t_2 = 3$ , Racah  $B_{35} = 714 \text{ cm}^{-1}$ ,  $B_{55} = 740 \text{ cm}^{-1}$  und  $C = 2980 \text{ cm}^{-1}$ . Diese Werte der SM-Parameter  $\bar{B}_k$  und  $t_k$ , welche an dem Uwarowit-Endglied bestimmt wurden, sollen nun in weiteren Unter- suchungen als Startwerte für  $\text{Cr}^{3+}$ -haltige Mischkristalle der Granatreihe eingesetzt werden.

## Literatur

- [1] NEWMAN, D. J. (1971): Theory of lanthanide crystal fields. - *Adv Phys*, 20, 197-256.
- [2] YEUNG, Y. Y., QIN, J., CHANG, Y. M. & RUDOWICZ, C. (1994): Correlation of spectroscopic properties and substitutional sites of  $\text{Cr}^{3+}$  in aluminosilicates: I. Kyanite. - *Phys Chem Min*, 21, 526-531.
- [3] QIN, J., RUDOWICZ, C., CHANG, Y. M. & YEUNG, Y. Y. (1994): Correlation of spectroscopic properties and substitutional sites of  $\text{Cr}^{3+}$  in aluminosilicates: II. Andalusite and sillimanite. - *Phys Chem Min*, 21, 532-538.
- [4] WILDNER, M. & ANDRUT, M. (1999): Crystal structure, electronic absorption spectra, and crystal field superposition model analysis of  $\text{Li}_2\text{Co}_3(\text{SeO}_3)_4$ . - *Z Kristallogr*, 214, 216-222.
- [5] LOWELL, J., NAVROTSKY, A., & HOLLOWAY, J. R. (1971): Synthesis of Uvarovite using a sodium-potassium borate flux. - *J Ceram Soc*, 54, 466.
- [6] CHANG, Y. M., RUDOWICZ, C. & YEUNG, Y. Y. (1994): Crystal field analysis of the  $3d^N$  ions at low symmetry sites including the “imaginary” terms. - *Computers in Physics*, 8, 583-588.

UNTERSUCHUNGEN ZUR FARBE DES LAZULITHS

von

**M. Andrut<sup>1</sup>, V. M. F. Hammer<sup>2</sup>, C. L. Lengauer<sup>1</sup>, T. Ntaflos<sup>3</sup> & G. J. Redhammer<sup>4</sup>**

<sup>1</sup>Institut für Mineralogie und Kristallographie  
Universität Wien, Geozentrum, Althanstrasse 14, A-1090 Wien

<sup>2</sup>Mineralogisch-Petrographische Abteilung  
Naturhistorisches Museum, Burgring 7, A-1010 Wien

<sup>3</sup>Institut für Petrologie  
Universität Wien, Geozentrum, Althanstrasse 14, A-1090 Wien

<sup>4</sup>Institut für Kristallographie  
RWTH Aachen, D-52056 Aachen

Unter verschiedenen Fundortangaben wurden in den letzten Jahren aus Pakistan tiefgrüne Lazulithe von ungewöhnlicher Größe bekannt, darunter ein etwa faustgroßes Kristallfragment (NHMW, N 160) mit zum Teil schleifwürdigen Partien. Gemmologische Charakterisierung: Spez.Gew.: 3.12 gcm<sup>-3</sup>, Härte: 5.5 - 6.0, Brechungsindex: 1.61 - 1.64, Pleochroismus: gelb- nach blaugrün, Chelsafilter: blaugrau, Fluoreszenz: matt orange (UV<sub>lang</sub>). An Einschlüssen konnten Scharen von Flüssigkeitsfahnen und oktaedrischen Kristallen, sowie Rutilnadeln beobachtet werden [1]. Im Gegensatz dazu kommt massig derber Lazolith relativ häufig vor, blaue klare Kristalle in schleifwürdiger Qualität hingegen werden vereinzelt von Vorkommen in Brasilien und Indien beschrieben.

Röntgenographische Voruntersuchungen identifizierten das Material eindeutig als Vertreter der Lazolith-Gruppe, genauere chemische Analysen ergaben jedoch einen sehr geringen Eisengehalt (FeO: 0.48(2) Gew.%) wonach in diesem Fall das fast reine Mg-Endglied der Mischkristallreihe Lazolith MgAl<sub>2</sub>[PO<sub>4</sub>]<sub>2</sub>(OH)<sub>2</sub> – Scorzalith Fe<sup>2+</sup>Al<sub>2</sub>[PO<sub>4</sub>]<sub>2</sub>(OH)<sub>2</sub> vorliegt und als natürliches Vorkommen noch nicht beschrieben wurde (LAZ-gr). Die gute Qualität des Fragments ermöglichte außerdem eine umfassende, kristallographisch-spektroskopische Bearbeitung mit weiteren Erkenntnissen zum Farbverhalten der Lazulithe. Als Vergleichsmaterial standen tiefblaue Lazolith-kristalle (LAZ-bl) vom Cross Cut Creek, Yukon, Kanada zur Verfügung (NHMW, M 998). Beide Varietäten wurden mit Hilfe von Röntgendiffraktometrie an Pulver und Einkristallen, Mikrosondenanalyse, Thermogravimetrie, Mössbauer Spektroskopie, sowie optischer und IR-Absorptionsspektroskopie charakterisiert.

Die Mikrosondenanalysen und thermoanalytischen Messungen ergaben für LAZ-gr eine einheitliche chemische Zusammensetzung, die der Formel Mg<sub>0.99</sub>Fe<sub>0.02</sub>Al<sub>1.99</sub>[P<sub>1.99</sub>O<sub>8</sub>](OH)<sub>1.93</sub> und einem Scorzalithanteil von 2 % entspricht. TiO<sub>2</sub> kann mit 0.09(2) Gew.% in Spuren nachgewiesen werden.

An den Proben von LAZ-bl hingegen lässt sich eine größere Varianz der Ergebnisse beobachten, wobei FeO (3.4 - 4.2 Gew.%) und TiO<sub>2</sub> (0.03 - 0.3 Gew.%) positiv miteinander korrelieren. Die gemittelte Formel kann mit Mg<sub>0.87</sub>Fe<sub>0.15</sub>Al<sub>1.98</sub>[P<sub>1.99</sub>O<sub>8</sub>]OH<sub>1.98</sub> angegeben werden. Weitere farbgebende Elementoxide wie MnO oder Cr<sub>2</sub>O<sub>3</sub> waren nicht nachweisbar. Die thermische Stabilität (Endset) unter N<sub>2</sub> Atmosphäre beträgt für LAZ-gr 1040 K und ist für LAZ-bl wegen des höheren Fe-Anteils erwartungsgemäß auf 1020 K reduziert. Beide Werte liegen jedoch deutlich über der von [2] bestimmten Stabilitätsgrenze von synthetischem Lazulith unter hydrothermalen Bedingungen. An Zerfallsprodukten konnten bei beiden Proben als Hauptphasen Mg<sub>3</sub>(PO<sub>4</sub>)<sub>2</sub> (Farringtonit) und AlPO<sub>4</sub> (Berlinit), in Spuren Al<sub>2</sub>O<sub>3</sub> und Fe<sub>2</sub>O<sub>3</sub> (LAZ-bl) röntgenographisch nachgewiesen werden.

Da der 'InterValence Charge Transfer' (IVCT) von Fe<sup>2+</sup>-Fe<sup>3+</sup> Paaren hauptsächlich für die intensive Farbgebung und das Polarisationsverhalten der blauen Lazulithe verantwortlich ist [3], wurden an beiden Proben <sup>57</sup>Fe Mössbauer Resonanzspektren gemessen. Unter Berücksichtigung der Fe<sup>3+</sup> Nachweisgrenze, die bei ca. 1 % des Gesamteisens liegt, konnte in LAZ-gr kein Fe<sup>3+</sup> Anteil festgestellt werden. Das Eisen liegt in diesem Fall lediglich als Fe<sup>2+</sup> vor, wobei die ermittelte große Quadrupolaufspaltung (QS) von 3.321(4) mm s<sup>-1</sup> mit den Werten von [4] für Fe<sup>2+</sup> als Substituent der oktaedrisch koordinierten Mg-Position übereinstimmt. In LAZ-bl dominiert mit 93.6(2) % ebenfalls Fe<sup>2+</sup> auf der Mg-Position, die QS ist allerdings auf 3.302(1) mm s<sup>-1</sup> reduziert, was mit dem häufig beobachteten inversen Trend für Fe<sup>2+</sup>, zunehmende Polyeder verzerrung = sinkende QS, korreliert. Mit einer QS und Isomerieverschiebung von 0.60(1) bzw. 0.385(8) mm s<sup>-1</sup> ist Fe<sup>3+</sup> mit 6.4(3) % nachweisbar. Da diese Resonanzwerte einer Platznahme von Fe<sup>3+</sup> auf der oktaedrisch koordinierten Al-Position entsprechen [5], ergibt sich für LAZ-bl die Strukturformel VI(Mg<sub>0.87</sub>Fe<sup>2+</sup><sub>0.14</sub>)VI(Al<sub>1.98</sub>Fe<sup>3+</sup><sub>0.01</sub>)[P<sub>1.99</sub>O<sub>8</sub>]OH<sub>1.98</sub>.

Die Zellparameter aus Rietveldverfeinerungen von Pulverdaten sind a = 7.1291(3), b = 7.2741(3), c = 7.1431(3) Å, β = 119.170 °, V = 323.44(2) Å<sup>3</sup> für LAZ-gr und a = 7.1331(5), b = 7.2790(5), c = 7.1467(5) Å, β = 119.160 °, V = 324.05(4) Å<sup>3</sup> für LAZ-bl. Die Verfeinerung der Ein-kristalldaten bestätigte die Ergebnisse von [6]. Die Struktur besteht aus Trimere flächenverknüpfter Al-Mg-Al Oktaeder, die über Wasserstoffbrückenbindungen zu Ketten entlang [110] angeordnet sind. Die Ketten wiederum sind über eckenverknüpfte P-Tetraeder verbunden. Wie zu erwarten, weisen in beiden Lazulithstrukturen die P-Tetraeder und Al-Oktaeder nahezu identische mittlere Bindungslängen auf (Δ = 0.001 Å). In Bestätigung der Ergebnisse der Mößbauer Spektroskopie lässt sich nur im zentralen Mg-Oktaeder eine Zunahme der anisotropen Verzerrung in Folge der Fe<sup>2+</sup> Substitution feststellen, z.B. Mg – OH in LAZ-gr 2.0767(7), in LAZ-bl 2.0820(6) Å. Der OH – H Abstand beträgt in beiden Varietäten 0.82(2) Å und die Wasserstoffbrückenbindung zum den benachbarten Trimer ist zweifach aufgespalten. Das entspricht den Beobachtungen der IR-Spektroskopie, die neben der OH-Bande bei 3404 cm<sup>-1</sup> eine Schulter bei 3464 cm<sup>-1</sup> erkennen lässt.

Das optische Absorptionsspektrum von LAZ-bl ist parallel Ny und Nz durch eine breite starke Bande bei 15000 cm<sup>-1</sup> dominiert, die durch Fe<sup>2+</sup>-Fe<sup>3+</sup> IVCT verursacht wird. Das Polarisationsverhalten lässt sich zwanglos erklären, indem ein Fe<sup>2+</sup>-Fe<sup>3+</sup> Paar benachbarte kantenverknüpfte Polyeder der Trimere besetzt. Weitere schwache Banden im Bereich zwischen 27300 und 22950 cm<sup>-1</sup> werden durch spin-verbotene Fe<sup>3+</sup> dd-Übergänge hervorgerufen, zwei Schultern bei 11665 und 9800 cm<sup>-1</sup> durch spin-erlaubte Fe<sup>2+</sup> dd-Übergänge.

Im Gegensatz dazu zeigt das Absorptionsspektrum von LAZ-gr wegen des kleineren Gesamt-eisengehaltes auch geringere Bandenintensitäten. Da außerdem der Fe<sup>3+</sup>-Anteil am Fe-Gehalt in dieser Probe wesentlich kleiner ist als in den blauen Lazulithen, wird nur eine sehr schwache Bande bei 15950 cm<sup>-1</sup> aufgrund des Fe<sup>2+</sup>/Fe<sup>3+</sup> IVCT beobachtet. Wegen der relativ geringen Intensität dieser Bande können in dieser Polarisationsrichtung nun aber die spin-erlaubten Fe<sup>2+</sup> dd- Banden bei 11450 und 9550 cm<sup>-1</sup> ebenfalls beobachtet werden. Eine breite Bande bei 25000 cm<sup>-1</sup> wird einem Fe<sup>2+</sup>/Ti<sup>4+</sup>-Ladungstransfer zugeordnet. Das Polarisationsverhalten parallel Ny und Nz unterstützt die Auffassung, daß Ti<sup>4+</sup> bevorzugt auf der Al-Position eingebaut wird.

## Literatur

- [1] ANDRUT, M., HAMMER, V. M. F., LENGAUER, C. L., NTAFLOS, T. & REDHAMMER, G. J. (2001): Schleifwürdiger grüner Lazulith aus Pakistan. - Z.Dt.Gemm.Ges. (im Druck).
- [2] CEMIĆ, L. & SCHMID-BEURMANN, P. (1995): Lazulite stability relations in the system Al<sub>2</sub>O<sub>3</sub>-AlPO<sub>4</sub>-Mg<sub>3</sub>(PO<sub>4</sub>)<sub>2</sub>-H<sub>2</sub>O. - Eur.J.Mineral., 7, 921-929.
- [3] AMTHAUER, G. & ROSSMANN, G. R. (1984): Mixed valence of iron in minerals with cation clusters. - Phys.Chem.Minerals, 11, 37-51.
- [4] SCHMID-BEURMANN, P., KNITTER, ST. & CEMIĆ, L. (1999): Crystal chemical properties of synthetic lazulite-scorzalite solid-solution series. - Phys.Chem.Minerals, 26, 496-505.
- [5] REDHAMMER, G. J., TIPPELT, G., ROTH, G., LOTTERMOSEN, W. & AMTHAUER, G. (2000): Structure and Mössbauer spectroscopy of barboselite Fe<sup>2+</sup>/Fe<sup>3+</sup><sub>2</sub>[PO<sub>4</sub>]<sub>2</sub>(OH)<sub>2</sub> between 80 and 300 K. - Phys.Chem.Minerals, 27, 419-429.
- [6] GIUSEPPETTI, G. & TADINI, C. (1983): Lazulithe, MgAl<sub>2</sub>[PO<sub>4</sub>]<sub>2</sub>(OH)<sub>2</sub>: structure refinement and hydrogen bonding. - N.Jb.Mineral.Mh., Jg.1983, 410-416.

**ABSORPTIONS- AND RAMAN SPECTROSCOPIC INVESTIGATIONS OF SYNTHETIC  
COBALT-BOUSSINGAULTITE (PICROMERITE GROUP),  $(\text{NH}_4)_2\text{Co}(\text{SO}_4)_2 \cdot 6\text{H}_2\text{O}$ :  
REFinement OF SUPERPOSITION MODEL (SM) PARAMETERS FOR  $\text{Co}^{2+}$**

by

**M. Andrut, B. Hertweck & M. Wildner**

Institut für Mineralogie und Kristallographie  
Universität Wien, Geozentrum, Althanstrasse 14, A-1090 Wien

Crystals of cobalt-boussingaultite  $(\text{NH}_4)_2\text{Co}(\text{SO}_4)_2 \cdot 6\text{H}_2\text{O}$  up to several mm in size were obtained by controlled evaporation of an aqueous solution of an equimolar mixture of  $(\text{NH}_4)_2\text{SO}_4$  and  $\text{CoSO}_4$  at 293K. The transparent crystals are orange-red in colour and exhibit weak pleochroism in polarized light.

Cobalt-boussingaultite belongs to the picromerite group,  $A^+ \text{Me}^{2+}(\text{SO}_4)_2 \cdot 6\text{H}_2\text{O}$ , with  $A^+ = \text{NH}_4^+$ , K, Cs, Tl and  $\text{Me}^{2+} = \text{Mg}, \text{Co}, \text{Ni}, \text{Fe}, \text{Cu}, \text{Zn}, \text{V}$  and Cd, crystallising in space group  $P2_1/a$ . The  $\text{Me}^{2+}$  cations are sixfold coordinated to oxygen atoms of the water molecules. A recent structure refinement of  $\text{K}_2\text{Co}(\text{SO}_4)_2 \cdot 6\text{H}_2\text{O}$  by KIRFEL et al. [1] reveals that the  $\text{Co}^{2+}$  cation is [2+4] coordinated, thus forming a pseudo-tetragonal compressed octahedron, whereas the  $\text{SO}_4$  tetrahedron is only slightly distorted.

Corresponding polyhedral distortions could also be detected in  $(\text{NH}_4)_2\text{Co}(\text{SO}_4)_2 \cdot 6\text{H}_2\text{O}$  by spectroscopic methods: single crystal Raman measurements in the range 100 to 4000  $\text{cm}^{-1}$  were conducted with a Renishaw RM 1000 spectrometer equipped with a Leica DMLM series microscope. The spectra were excited with the  $\text{Ar}^+$  488 nm line. Raman lines (in  $\text{cm}^{-1}$ ) caused by the  $\text{SO}_4$  group are observed at 455 ( $\nu_2$ ), 622 ( $\nu_4$ ), 982 ( $\nu_1$ ), and in the range 1068 - 1150 ( $\nu_3$ ). Bands at 1425 and 1675  $\text{cm}^{-1}$  are assigned to the normal modes  $\nu_4$  and  $\nu_2$ , respectively, of the ammonium ion. Its fundamentals  $\nu_1$  and  $\nu_3$  are superimposed by stretching frequencies of the water molecules in the spectral range 3100 to 3400  $\text{cm}^{-1}$ .

IR absorption powder spectra were measured in the spectral range 350 to 4000  $\text{cm}^{-1}$  under vacuum using a Bruker IFS 66v/S FTIR-spectrometer. Bands were assigned as follows: 613, 639  $\nu_4(\text{SO}_4)$ ; 1097, 1143  $\nu_3(\text{SO}_4)$ ; 1400, 1428, 1470  $\nu_4(\text{NH}_4^+)$ ; 2850 2 $\nu_4(\text{NH}_4^+)$ . The fundamental  $\nu_3(\text{NH}_4^+)$  which is expected at ~3200  $\text{cm}^{-1}$  is again superimposed by stretching frequencies of the water molecules (3000 - 3500  $\text{cm}^{-1}$ ). The  $\text{H}_2\text{O}$  combination modes are centred around 4800  $\text{cm}^{-1}$ .

In order to provide new Superposition Model (SM) parameters [cf. e.g. 2] for the  $\text{Co}^{2+}$  cation, polarized single crystal UV-VIS absorption spectra were measured at room temperature in the spectral range between 35000  $\text{cm}^{-1}$  and 4000  $\text{cm}^{-1}$  on the Bruker IFS 66v/S FTIR-spectrometer using the attached mirror optics microscope IRscopeII.

The optical spectra are characterised by two main regions of absorption around  $8200\text{ cm}^{-1}$  and  $18000\text{--}22000\text{ cm}^{-1}$  which are correlated predominantly with spin-allowed d-d transitions from the ground state  ${}^4T_{1g}(^4F)$  to the  $\rightarrow {}^4T_{2g}(^4F)$  and  $\rightarrow {}^4T_{1g}(^4P)$  states in ideal octahedral  $O_h$  symmetry, respectively. A weak and broad band at  $\sim 16500\text{ cm}^{-1}$  is attributed to the spin-allowed  ${}^4T_{1g}(^4F) \rightarrow {}^4A_{2g}(^4F)$  transition which in the strong field limit represents an electronically forbidden two-electron jump ( $t_{2g}{}^5e_g{}^2 \rightarrow t_{2g}{}^3e_g{}^4$ ) with low probability [e.g. 3]. The observed splitting and structure of the intense VIS band system indicates on one hand the tetragonal perturbation of the octahedral crystal field, on the other hand the significant contribution of intensity enhanced spin-forbidden quartet $\rightarrow$ doublet transitions and further splitting due to spin-orbit coupling. Preliminary SM calculations, based on the octahedral geometry of the potassium compound [1], indicate that both ‘intrinsic’ SM parameters  $\bar{B}_k$  for  $(\text{NH}_4)_2\text{Co}(\text{SO}_4)_2 \cdot 6\text{H}_2\text{O}$  will be comparable to those extracted previously for  $\text{Co}(\text{OH})_2$  ( $\bar{B}_4 = 5320$ ,  $\bar{B}_2 = 3900\text{ cm}^{-1}$ ) [4], i.e.  $\bar{B}_4$  is somewhat higher than refined for  $\text{Li}_2\text{Co}_3(\text{SeO}_3)_4$  ( $\bar{B}_4 = 4740\text{ cm}^{-1}$ ) [5]. This corresponds to the expectations in that  $\text{H}_2\text{O}$  as well as  $\text{OH}^-$  molecules occupy similar positions in the spectrochemical series of ligands, whereas it has been shown that oxygen atoms of  $\text{SeO}_3^{2-}$  groups consistently have a comparatively low position within the series of oxygen based ligands [6]. In order to obtain ‘correct’ global SM parameters for a particular  $3d^N$  cation in coordination to varying or mixed ligands, a slight modification of the Superposition Model formalism is currently proposed and tested [7].

## References

- [1] KIRFEL, A., KLAPPER, H., SCHÄFER, W. & SCHWABENLÄNDER, F. (1998): The crystal structure of Tutton’s salt type  $\text{K}_2[\text{Co}(\text{H}_2\text{O})_6](\text{SO}_4)_2$ . A combined X-ray and neutron study. - *Z Kristallogr.*, 213, 456-460.
- [2] NEWMAN, D. J. & NG, B. (1989): The superposition model of crystal fields. - *Rep Prog Phys.*, 52, 699-763.
- [3] LEVER, A. B. P. (1984): Inorganic electronic spectroscopy. - 2nd ed. Amsterdam, Oxford, New York, Tokyo, Elsevier.
- [4] ANDRUT, M. & WILDNER, M. (2001): Superposition Model analysis from polarised electronic absorption spectra of  $\text{Co}^{2+}$  in trigonally distorted octahedra in brucite-type  $\text{Co}(\text{OH})_2$ . - *J Phys Cond Matter* (submitted).
- [5] WILDNER, M. & ANDRUT, M. (1999): Crystal structure, electronic absorption spectra, and crystal field superposition model analysis of  $\text{Li}_2\text{Co}_3(\text{SeO}_3)_4$ . - *Z Kristallogr.*, 214, 216-222.
- [6] WILDNER, M. (1998): Beiträge zur Kristallchemie von Sauerstoffsalzen der Übergangsmetalle mit  $3d^3$  ( $\text{Cr}^{3+}$ ,  $\text{Mn}^{4+}$ ) und  $3d^7$  ( $\text{Co}^{2+}$ ) Elektronenkonfiguration unter besonderer Berücksichtigung der Korrelation von strukturellen Details mit UV-VIS-spektroskopischen Daten. - Habilitation thesis, Vienna university.
- [7] WILDNER, M. & ANDRUT, M. (2001): Synthetic cobaltomenite,  $\text{CoSeO}_3 \cdot 2\text{H}_2\text{O}$ , and related Co-compounds as model phases for the application of the Superposition Model (SM) of crystal fields in geosciences. - *Mitt Österr Min Ges*, 146 (this volume).

**DISCRIMINATION BETWEEN SEA WATER AND FRESH WATER  
TISSUE GRAFT CULTURED PEARLS BY EPR**

by

**A. Banerjee<sup>1</sup> & H. Rager<sup>2</sup>**

<sup>1</sup>Institute of Geosciences  
Mainz University, D-55099 Mainz, Germany  
<sup>2</sup>Institute of Crystallography  
Marburg University, D-35032 Marburg, Germany

As known pearls are produced in certain molluscs under some favourable circumstances by accumulation of nacre around a foreign matter, that has become lodged inside the shell. According to the habitat of the molluscs there are two kinds of pearls, e.g. fresh water and sea water pearls. While natural pearls are formed by accidental entry of a foreign matter inside the body of pearl-producing molluscs, cultured pearls are grown artificially in molluscs under controlled environmental conditions, after the insertion either of a mother-of-pearl bead or of a tissue graft as nucleus. Pearls grown by the first method are commercially known as bead nucleated cultured pearls and those grown by the second method are called tissue graft cultured pearls.

Besides natural pearls cultured pearls from sea water as well as from fresh water are offered in the market. In the last years the quality and size of cultured pearls have been improved to such an extent, that X-ray radiography, which is the mostly used diagnostic tool for testing of pearls, fail to distinguish between natural and cultured pearls. Moreover this method can not be successfully applied to make distinction between sea water tissue graft cultured pearls and fresh water tissue graft cultured pearls of larger sizes, as the growth structure inside the pearls can not be recognised properly in their radiographs due to the thickness of the pearl substance. These problems can be solved only by more sophisticated tools like EPR. The purpose of the present paper is to show that natural and cultured sea water pearls can be distinguished from natural and cultured fresh water pearls by EPR according to their Mn<sup>2+</sup> content.

The following whole pearls and fragments of pearls were investigated by EPR:

(1) a natural sea water pearl, (1a) a natural freshwater pearl, (2) a Chinese freshwater tissue graft cultured 'biwa' pearl, (3) a fragment of a nacreous layer taken from a Mabe South-sea cultured pearl, (4) a tissue graft South-sea cultured 'keshi' pearl and (5) a fragment of a nacreous layer taken from a bead nucleated South-sea pearl. In addition to the samples mentioned above, two crystals, e.g. an aragonite crystal from Aragon (Spain) and a calcite crystal from Island, both of which contained manganese as trace element, as proved by electron microprobe analyses, were also measured as standards in order to compare their EPR-spectra with those of biogenic aragonite and calcite originating from pearls.

The EPR measurements were performed both at room temperature and at low temperature using an Oxford EPR 900 A cryostat. The spectra were taken with a Varian X-band spectrometer and 100 kHz modulation. The external magnetic field could be varied between 0 and 1 T and was monitored by a gaussmeter (Bruker BH 15). At room temperature the resonance frequency was about 9.51 GHz and around 50 K about 9.24 GHz. The frequency was measured by a frequency counter (HP 5340).

The results of the EPR investigation of the samples (1 to 5) are shown in Table 1.

No.	Signal due to Mn <sup>2+</sup>	single line at g=1.999
1		++
1a	++	not observable
2	++	not observable
3		++
4		++
5		?

(++) = strong and (--) = absent

Table 1  
EPR signals of pearls.

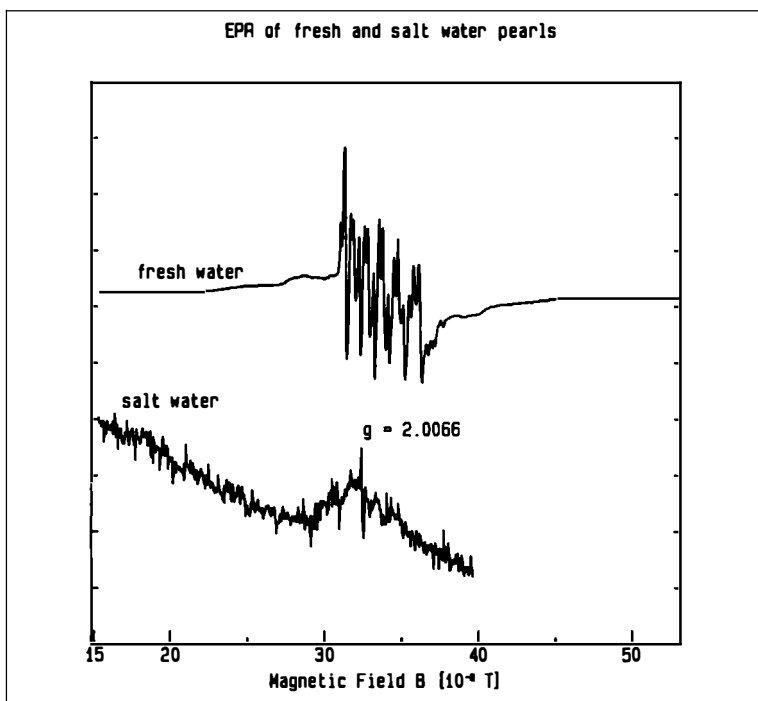


Fig. 1  
EPR-spectra of pearls: fresh water pearl (above) and salt water pearl (below).

EPR spectra of pearls are characterised either by a Mn<sup>2+</sup> EPR pattern or by a single EPR line at  $g_{\text{eff}} = 2.0066$ . The latter is of low intensity and could only be detected in samples without Mn<sup>2+</sup> EPR pattern. Its effective g-value indicates an electronic defect but a more exact cause of this effect can be given only after further studies. The Mn<sup>2+</sup> EPR powder pattern ranges from approximately 0.25 to approximately 0.4 T.

Decreasing the temperature down to 50 K no new ESR spectrum or no new line appears in the spectra and the Mn<sup>2+</sup>-EPR does not exhibit any change with respect to room temperature spectrum except the increase of intensity. The signal at  $g_{\text{eff}} = 2.0066$  could only be detected in distinct layers of pearls. Crushing the pearl, layers of different thickness and slightly different tinge can be distinguished from one another. It was found that the single EPR line is rather present in thin and transparent layers than thick and slightly coloured layers. All freshwater pearls exhibit a Mn<sup>2+</sup>-EPR spectrum, whereas the EPR spectra of sea water pearls do not (Fig. 1).

TRANSMISSION ELECTRON MICROSCOPY ON ECLOGITES FROM THE  
LOWER SCHIST COVER AND THE ECLOGITE ZONE (TAUERN WINDOW, AUSTRIA)

by

E. B. Barnert<sup>1</sup>, W. F. Müller<sup>1</sup>, E. Schmädicke<sup>1,2</sup> & G. Franz<sup>3</sup>

<sup>1</sup>Institut für Mineralogie  
Technische Universität Darmstadt, Schnittspahnstrasse 9, D-64287 Darmstadt  
<sup>2</sup>Institut für Geologie und Mineralogie  
Universität Erlangen, Schloßgarten 5a, D-91054 Erlangen  
<sup>3</sup>Institut für Angewandte Geowissenschaften  
Technische Universität Berlin, Strasse des 17. Juni, D-10623 Berlin

We are studying the microstructure of the mineral constituents of eclogites from the Tauern Window, Austria, by transmission electron microscopy (TEM). The eclogites occur in two different units: the Lower Schist Cover and the Eclogite Zone, where they experienced a different thermal and mechanical history.

**a) Lower Schist Cover:** Most of our studies have been made on TEM specimens of sample LT 26c-87, locality Frosnitztal, Keespöllach [1]. Mineral chemistry, phase relations and geothermometry point to low formation temperatures (400 - 500°C) at 8 - 12 kbar [1]. The eclogites formed from rocks of basaltic composition during the Silurian subduction about 420 Ma ago [2]. Omphacite (Omp), barroisite (Bst), glaucophane (Gln), albite, muscovite, paragonite, garnet, epidote, rutile, and titanite were seen in the TEM. The rock was heavily deformed as revealed by high densities of dislocations in Omp and amphibole; dislocations in the other minerals were rarely encountered.

Omphacite: Structurally, it is almost always characterized by a primitive Bravais lattice. Most grains contain rather small (around 50 nm in size) equiaxed roundish antiphase domains (APDs) with the displacement vector 1/2[110] (for literature on omphacite, see [3], [4]). Their small size is well in agreement with their formation at low temperatures. Occasionally, within the same grain, areas a few μm in width occur which are free or nearly free of antiphase domain boundaries (APBs). Faults parallel to (010) up to 1 μm in length are probably chain multiplicity faults (CMFs). The partial dislocations at their ends have the Burgers vector b parallel to [101] or [-101]. The CMFs may have been formed by the dissociation reaction  $[001] = 1/2[101] + 1/2[-101]$  (cf. [5]). Recovery processes are evident from frequent low angle grain boundaries (LAGB). Rather conspicuous are dynamically recrystallized Omp grains, ca. 5 μm in size, free of dislocations, which grow into the heavily deformed Omp matrix with a dislocation density up to  $10^{14} \text{ m}^{-2}$ . The size of the APDs in the recrystallized grains was also around 50 nm. Lamellar Bst precipitates near (010), 0.5 μm in width and a few μm long, were seen in a grain with frequent CMFs and LAGBs subparallel to (010); the lattices of Bst and Omp share (010) and (10<sup>-1</sup>).

Wavy exsolution lamellae on (100) occurred in Omp of more Fe-rich composition in a specimen of the same thin section, but in another layer of the banded eclogite (see [1]).

**Amphibole:** Bst is characterized by the occurrence of CMFs parallel to (010). Densities up to about  $45 \mu\text{m}^{-1}$  (measured along a line of about 1  $\mu\text{m}$  length perpendicular to (010)) have been noted. Gln does not show CMFs.

**Epidote:** The only one epidote studied so far contained a wedge-shaped twin lamella, from about 0.1  $\mu\text{m}$  to 0.2  $\mu\text{m}$ , according to the twin law m parallel to (100).

**Titanite:** Titanite was encountered as sub-idiomorphic inclusions of a few to several  $\mu\text{m}$  in size in Omp. Electron diffraction patterns showed the absence of reflections of the type  $k + l$  odd and streaks parallel to  $b^*$ . According to [6], the space group A2/a is attained when > 4 mole percent of Ti is substituted by Al and Fe, as is the case in our titanite.

**Mica:** In one case, a mica with about the same amount of Na and K was found, which is perhaps a paragonite/muscovite intergrowth in the unit cell range.

**b) Eclogite Zone:** Samples "Gatter" and "Knappenhaus" (Frosnitztal, [7]), geothermo-barometry: 550 - 630°C, ~ 20 kbar [8]. Omp-1, Omp-2, Grt, Gln, Tr, Ab, Tlc, Qtz, Ms, Pg, Ky, Ep, Czo, Dol, Mgs, Rt and Zr were identified by polarising microscopy, electron microprobe analysis and analytical TEM, in terms of selected area electron diffraction (SAED) and energy dispersive x-ray microanalysis (EDX). Omp shows APDs which are partially coarsened. The average diameter of the domains is 80 - 200 nm in both specimens which is in agreement with eclogites taken from the neighbouring Dorfer- and Timmeltal (50 - 200 nm, samples from T.J.B. Holland) described by CARPENTER [3]. Most APDs are equiaxed, their APBs smoothly curved. Occasionally, APBs parallel to (010) occur which are surrounded by a zone without APBs (Fig. 1).

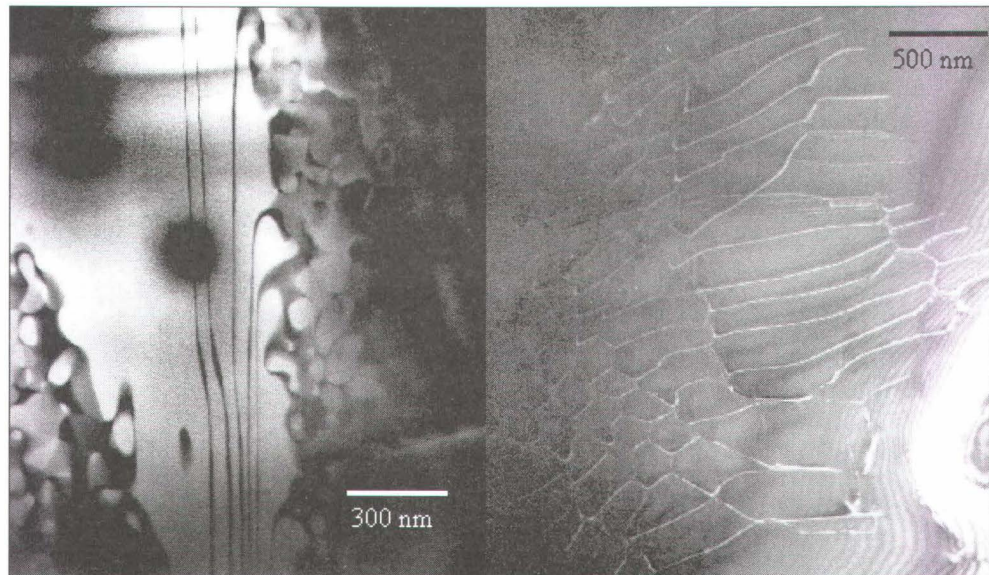


**Fig. 1**  
Dark field image of omphacite-2 with  
APB's parallel (010) (Eclogite Zone).

**Fig. 2**  
Weak beam dark field image of a dislocation  
network in omphacite-2 (Eclogite Zone).

We found the (010) APBs in contact with and as a continuation of the equiaxed APBs. The area with the oriented APBs does not exhibit chemical differences to the other APDs as verified by EDX. The (010) APBs in Fig. 1 seem to be induced by a sinistral shear deformation of the crystal. Perhaps these APBs can be used as an intracrystalline "micro-shear sense indicator"

The SAED patterns of lamellae parallel to (100), where maximum splitting of reflections in  $a^*$ -direction occurs, can be interpreted as twin or exsolution lamellae. The lamellae show pressure shadows due to deformation twinning. In case of exsolution,  $\text{omp}$  should decompose into jadeite and augite. We observed, however, APBs in and around the lamellae, crossing the lamellae without being influenced by them. Hence, these are twin lamellae which seem to have been formed by a deformation process before the APD-building phase transition C2/c to P2/n took place. The dislocation network (Fig. 2, note split dislocations!) is a result of dynamic recovery processes, probably during lasting deformation (dynamic recovery). We did not observe any interaction between the dislocations and the APBs. Epitaxial intergrowth parallel (001) between  $\text{omp}$  and tremolite is determined by SAED patterns. Epitaxial overgrowth of clinopyroxene with tremolite is a typical retrograde phenomenon. This is another argument for tremolite as a post eclogitic amphibole and not being part of the primary assemblage.

## References

- [1] ZIMMERMANN, R. & FRANZ, G. (1988): Die Eklogite der Unteren Schieferhülle; Frosnitztal/Südvenediger (Tauern, Österreich). - Mitt. österr. geol. Ges. 81: 167-188.
- [2] VON QUADT, A., GÜNTHER, D., FRISCHKNECHT, R., ZIMMERMANN, R. & FRANZ, G. (1997): The evolution of the pre-Variscan eclogites of the Tauern Window (Eastern Alps): A Sm/Nd-, conventional and Laser ICP-MS zircon U-Pb study. - Schweiz. Min. Petrogr. Mitt. 77: 265-279.
- [3] CARPENTER, M. A. (1981): Omphacite microstructures as time-temperature indicators of blueschist- and eclogite-facies metamorphism. - Contrib. Mineral. Petrol. 78: 441-451.
- [4] BRENKER, F. E. (1998): Mikrogefügethermochronometrie für Eklogite. - Diss., FB 17, Univ. Frankfurt/ M.
- [5] SKROTZKI (1995): Dislocation dissociation in chain silicates. - Plastic Deformation of Ceramics (R.C. BRADT et al., eds.): 75-86, Plenum Press, New York
- [6] HIGGINS, J. B. & RIBBE, P. H. (1976): The crystal chemistry and space groups of natural and synthetic titanites. Amer. Mineral. 61, 878-888.
- [7] THOMAS, S. & FRANZ, G. (1988): Kluftminerale und ihre Bildungsbedingungen in Gesteinen der Eklogitzone/Südvenediger-Gebiet (Hohe Tauern, Österreich). - Mitt. österr. geol. Ges. 81: 189-218.
- [8] KURZ, W., NEUBAUER, F. & DACHS, E. (1998): Eclogite meso- and microfabrics: implications for the burial and exhumation history of eclogites in the Tauern Window (Eastern Alps) from P-T-d paths. - Tectono-physics 285: 183-209.

**KATHODOLUMINESZENZ-UNTERSUCHUNGEN AUSGEWÄHLTER MINERALPHASEN  
MITTELS RÜCKSTREUELEKTRONENDETEKTOR: EINE REM-STUDIE**

von

**F. Brandstätter**

Mineralogisch-Petrographische Abteilung  
Naturhistorisches Museum, Burgring 7, A-1010 Wien

**Einleitung**

Die Untersuchung der Kathodolumineszenz (KL) von Mineralen ist eine Standardmethode, die in vielen Bereichen der Geowissenschaften eingesetzt wird [1]. Allen KL-Geräten gemeinsam ist eine Elektronen emittierende Kathode und ein für den Nachweis der Lumineszenzstrahlung geeigneter Detektor. In der konventionellen KL-Mikroskopie wird entweder eine "Kaltkathode" [2] oder eine "Heißkathode" [3] mit einer lichtmikroskopischen Einheit kombiniert. Eine weitere Gerätekonfiguration, die von diversen Herstellerfirmen standardmäßig angeboten wird, ist die Anbindung einer KL-Einheit an ein Rasterelektronenmikroskop (REM). Bei der letztgenannten Gerätekombination können die Vorteile des REM (insbesondere die hohe Ortsauflösung des Elektronenstrahls) mit den Möglichkeiten des jeweiligen Lumineszenzdetektors verknüpft werden. Zusätzlich können *in situ* im mm- bis  $\mu\text{m}$ -Bereich Rasteraufnahmen des KL-Signals mit anderen Probensignalen (z. B. Sekundärelektronen, RückstreuElektronen (BSE) oder charakteristischer Röntgenstrahlung) verglichen werden. Bei REM-Untersuchungen wird der Materialkontrast einer Probe meistens mittels BSE bestimmt. Der Nachweis der rückgestreuten Elektronen erfolgt dabei durch Halbleiterdetektoren oder Detektoren, die aus einer Szintillator-Photomultiplier-Kombination bestehen. Die letzgenannte Detektorvariante enthält den lichtempfindlichen Photomultiplier und sollte somit prinzipiell auch zum Nachweis von KL-Strahlung geeignet sein.

Im folgenden wird gezeigt, daß – unter bestimmten Voraussetzungen – mit einem konventionellen BSE-Detektor die in einer Mineralprobe angeregte KL-Strahlung nachgewiesen werden kann.

**Experimentelles**

Diese Studie wurde mit einem JEOL JSM-6400 Rasterelektronenmikroskop (Meßbedingungen: 15 kV Beschleunigungsspannung; 1.2 - 1.5 nA Strahlstrom) durchgeführt. Das REM ist mit zwei BSE-Detektoren ausgestattet: (i) einem zweigeteilten Halbleiterdetektor und (ii) einem Szintillator-Photomultipler ROBINSON Detektor (RB), der im Rahmen dieser Arbeit versuchsweise als KL-Detektor eingesetzt wurde. Ein mit dem REM kombiniertes KL-System (OXFORD MonoCL 2) wurde dazu verwendet, die mittels RB-Detektor erhaltenen und fotografisch dokumentierten KL-Aufnahmen *in situ* mit "echten" KL-Aufnahmen zu vergleichen. Zur Untersuchung wurden polierte und mit Kohlenstoff bedampfte Proben von Diamant, Fluorit, Benitoit und Zirkon verwendet.

## **Ergebnisse**

Bei allen untersuchten Proben konnten die mittels des KL-Systems erhaltenen KL-Aufnahmen in reproduzierbarer Weise auch mit dem RB-Detektor nachgewiesen werden.

Beim REM ist die Ausbeute an rückgestreuten Elektronen - und somit die Intensität des BSE-Signals- mit der mittleren Ordnungszahl ( $Z_m$ ) der Probe positiv korreliert. Der RB-Detektor sollte daher vor allem bei jenen Mineralen als KL-Detektor einsetzbar sein, die (i) ein niederes  $Z_m$  und eine kräftige Lumineszenz aufweisen oder (ii) bei höherem  $Z_m$  chemisch möglichst homogen sind. Für Möglichkeit (i) ist Diamant ein optimaler Kandidat. Von mehreren Diamantproben wurden Lumineszenzfotos von kristallographisch orientierten Wachstumszonen aufgenommen. Aus diesen Aufnahmen (Abb. 1, 2) ist ersichtlich, daß KL- und RB-BSE-Detektor durchaus vergleichbare Resultate ergeben.

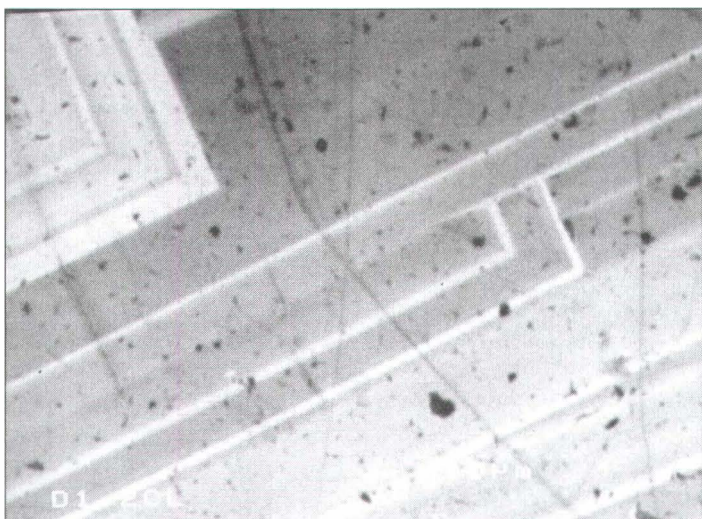


*Abb. 1  
Kristallographisch orientierte Wachstumsbereiche in natürlichem Diamant.  
REM-Aufnahme,  
KL-Detektor,  
Bildbreite 0.23 mm.*

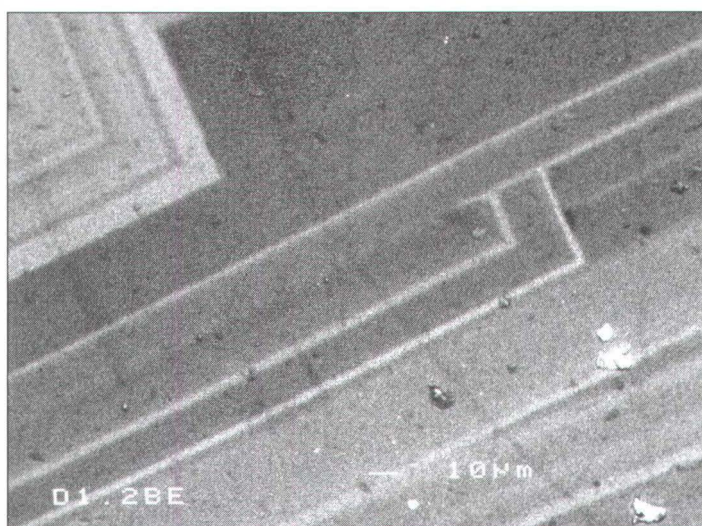


*Abb. 2  
Kristallographisch orientierte Wachstumsbereiche in natürlichem Diamant.  
REM-Aufnahme,  
RB-BSE -Detektor.,  
Bildausschnitt wie in Abb. 1.*

Ebenso zeigten Proben von Fluorit und Benitoit, die im BSE-Bild (Halbleiterdetektor) eine homogene Beschaffenheit aufwiesen, im RB-BSE-Bild Intensitätsverteilungen, die eindeutig den entsprechenden KL-Aufnahmen zuordenbar sind.

Ein Mineral mit kräftiger Lumineszenz und chemisch inhomogenem Aufbau ist der Zirkon, dessen Morphologie und Zonarbau – wegen seiner Bedeutung für die Geochronologie – in zahlreichen Publikationen beschrieben wurde. Bei kombinierten Untersuchungen von Zirkonen mittels KL- und BSE-Detektor ergab sich stets eine negative Korrelation von  $Z_m$  und KL-Intensität. Diese Antikorrelation zwischen Chemismus und Lumineszenzintensität zeigte sich in den RB-BSE-Aufnahmen dadurch, daß diese – im Vergleich zu den Halbleiter-BSE-Aufnahmen – eine merkliche Kontrastminderung aufwiesen. RB-BSE-Aufnahmen von Zirkon können somit als Resultat der Überlagerung von KL-Signal und antikorriertem BSE-Signal interpretiert werden.

## Literatur

- [1] PAGEL, M. et al. [Hrsg.] (2000): Cathodoluminescence in Geosciences. - Springer-Verlag: 514 S.
- [2] MARSHALL, D. J. (1988): Cathodoluminescence of Geological Materials. - Allen & Unwin: 146 S.
- [3] GÖTZE, J. (1998): Principle and advantages of cathodoluminescence microscopy. -European Microscopy and Analysis, September Vol.: 21-23.

MINERALOGY OF EXTREMELY FRACTIONATED PHOSPHORUS-RICH GRANITE –  
PODLESI, CZECH REPUBLIC

by

K. Breiter<sup>1</sup> & F. Koller<sup>2</sup>

<sup>1</sup>Czech Geological Survey  
Geologická 6, CZ-15200 Praha 5

<sup>2</sup>Institut für Petrologie  
Universität Wien, Geozentrum, Althanstrasse 14, A-1090 Wien

The Podlesí granite system represents one of the best known examples of a highly fractionated peraluminous fluorine- and phosphorus-rich Li, Rb, Sn, W, Nb, Ta-bearing granite. Well exposed outcrops and several drillings from this granite define an outstanding object for study of nature and structural evolution of P-rich granite.

### Geological setting

The Podlesí granite system ( $0.1 \text{ km}^2$ ) is situated in the western part of the Krušné Hory Mts., Czech Republic. It is the youngest intrusion of the multistage late-Variscan peraluminous tin-specialised Eibenstock-Nejdek pluton.

The main rock type is an albite-protolithionite-topaz granite (stock granite). Within a depth of 40 - 100 m the stock granite is intercalated by flat layers of albite-zinnwaldite-topaz granite (dyke granite).

Prominent manifestation of unidirectional solidification textures (UST) has been recently found in the upper part of a major flat dyke. Individual Q-Afs laminae are separated by comb quartz layers and/or by layers of oriented fan-like zinnwaldite aggregates. Two pegmatite-like layers with oriented megacrysts of Kfs up to 6 cm long have been found in the uppermost part of the dyke. The UST consist also of crenulated quartz layers, segregations of Mn-rich apatite and small pegmatite pods

Both types of granites were later transformed into greisen but only a in small scale: the dyke granite was transformed to massive mica-poor quartz-topaz greisen, the stock granite into joint-related mica-rich quartz-biotite-apatite-topaz greisen.

### Li-F-rich micas

Micas are the best mirror of evolution of crystallising melt and/or fluids interaction. Magmatic fractionation from the biotite granite of the Eibenstock-Nejdek pluton through the stock granite to the dyke granite is well documented by enrichment of fluorine and lithium (and also of Rb and Cs) in the micas: they range from Li-biotite through protolithionite to zinnwaldite (Fig. 1).

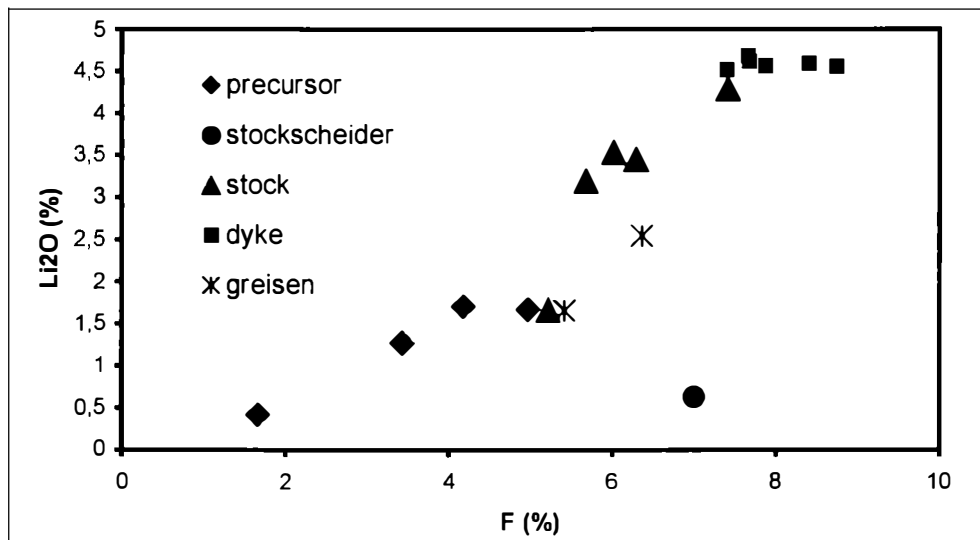


Fig. 1

The Li<sub>2</sub>O vers. F relations in micas from Podlesí (chemical analyses of mineral concentrates, laboratory of Czech Geological Survey, Praha). Precursor – biotite granite of the Nejdek massif foregoing the Podlesí intrusion, stockscheider – border pegmatite, stock – stock granite, dyke – dyke granite, greisen – dark mica-rich greisen.

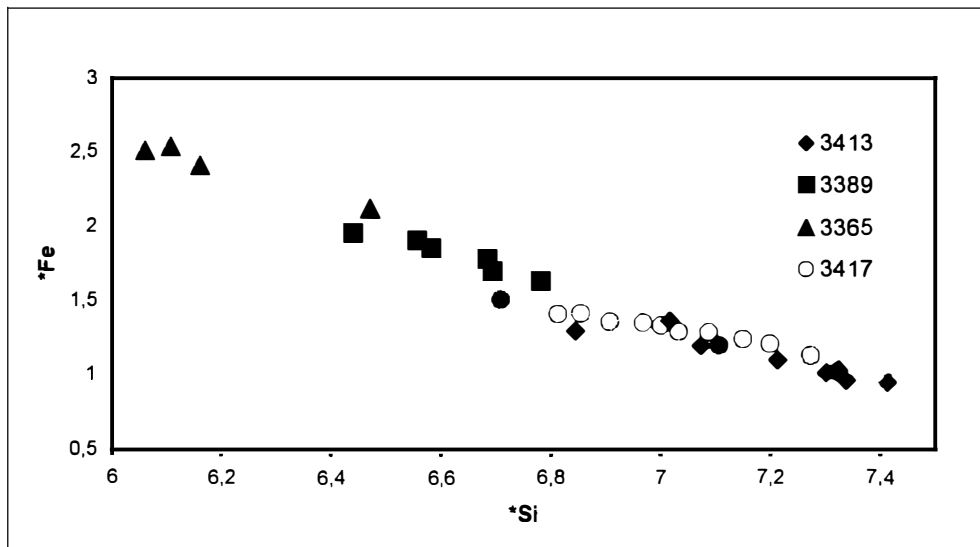


Fig. 2

Si vs. Fe plot for Li-rich micas from the Podlesí intrusion (expressed in atoms per formula unit). 3365 – dark mica-rich greisen, 3389 – light mica-poor greisen, 3413 – dyke granite, 3417 – dyke granite with the UST. (EMPA analyses in University Wien).

During greisenisation, again protolithionite and biotite appear in greisens. This documents that the F- and mainly Li-contents of micas decrease with decreasing temperature in fluids during greisenisation stage. This is well documented also by the decrease of Si and the increase of Fe in structural formulae of the micas (Fig. 2).

### **Feldspars**

Alkali feldspars are generally rich in phosphorus (1 - 2 wt.% of  $P_2O_5$ ) and rubidium (0.2 - 0.5 wt.% of Rb). They are often distinctly zoned. Rubidium is firmly bound in the Kfs-lattice and preserves well its magmatic signature during post-magmatic processes. In contrast, phosphorus can be easily released from the feldspar lattice and the P-content serves as a sensitive indicator of the late- and/or post-magmatic fluid-related reactions.

### **Apatite**

Apatite is full-saturated in fluorine. The Mn-content significantly increase during magmatic evolution (up to 3.5 wt.% of MnO) and decrease later during greisenisation.

### **Topaz**

Topaz is also close to the F-endmember. Often we found unexpected contents of phosphorus, locally reaching up to 0.3 - 0.4 wt.% of  $P_2O_5$ .

### **Conclusions**

The high grade of fluorine saturation in micas, topaz and apatite and the high content of phosphorus in alkali feldspars prove the unusually high concentration of F and P in the crystallising melt. High amount of phosphorus in the melt seems to favour also the incorporation of P into the crystal lattice of topaz. The contents of rubidium in the Kfs preserve well its magmatic signature during post-magmatic processes. In contrast, phosphorus can be easily released from the feldspar and is a sensitive indicator of the late- and/or post-magmatic fluid-related reactions forming greisens.

### **Acknowledgement**

The paper was supported by T. Ntaflos (University Wien) with his help during microprobe work.

GEOLOGICAL MAPPING OF THE TWO-MICA GRANITES  
IN THE WEITRA – NOVÉ HRADY AREA

by

**K. Breiter<sup>1</sup> & S. Scharbert<sup>2</sup>**

<sup>1</sup>Czech Geological Survey  
Geologická 6, CZ-15200 Praha 5  
<sup>2</sup>Geologische Bundesanstalt  
Rasumovskygasse 23, A-1031 Wien

Geological maps published by the Czech and Austrian Geological Services differ significantly in the interpretation of the internal structure of the South Bohemian Pluton in the Weitra–Nové Hrady area. "Eisgarn" type granite of the Austrian map comprises all varieties of two-mica granites while on the Czech maps the "Mrákotín" type granite and several types of coarse-grained granites are distinguished. Thus, apart from fieldwork we undertook petrological and geochemical revision of the two-mica granites in the border area.

The following granite types have been distinguished within the area:

1. "Aussengranit" - fine-grained granites build up the external part of the pluton, often along the contact with the biotite bearing Weinsberg granite to the E, S and SW of Weitra. In Bohemia, an identical granite appears between the "Jelení hrábet" hill and Besednice. This granite is generally equigranular, only locally porphyritic (between Schwarzau and Pohorská Ves, Kfs up to 1 cm). The content of biotite is much higher than that of muscovite. This granite petrographically resembles the granite from Mrákotín in the northern part of the SBP and is chemically similar to the Čímér granite. Typical content of  $\text{SiO}_2$  is 69 - 72 %,  $\text{K}_2\text{O}$  reaches 5.2 - 5.5 %,  $\text{Na}_2\text{O}$  2.6 - 2.7 %,  $\text{MgO}$  0.4 - 0.9 % and  $\text{CaO}$  0.7 - 1.0 %.
2. Eisgarn granite s.s., a generally coarse-grained two-mica granite builds the central part of the area between Weitra and Nové Hrady. This body, similar to the Eisgarn body N of Gmünd, is chemically concentrically zoned with a less fractionated rim and more fractionated core. The core is enriched in Na, Rb, Li, F, and U. In the central part of this body, an intrusion of strongly fractionated muscovite granite occurs near Pyhrabruk [1]. The typical content of  $\text{SiO}_2$  reaches 71 - 73 %,  $\text{K}_2\text{O}$  4.5 - 5.0 %,  $\text{Na}_2\text{O}$  3.0 - 3.3 %,  $\text{MgO}$  0.2 - 0.4 % and  $\text{CaO}$  0.5 - 0.8 %.
3. Fine- to medium grained biotite granite with high magnetic susceptibility crops out between the villages of Karlstift and Langschlag (Karlstift granite sensu KLOB [2] ). Typical content of  $\text{SiO}_2$  is only 67 - 69 %,  $\text{K}_2\text{O}$  reaches 4.2 - 4.5 %,  $\text{Na}_2\text{O}$  3.2 - 3.4 %,  $\text{MgO}$  0.8 - 1.3 % and  $\text{CaO}$  1.9 - 2.9 %.
4. Fine-grained biotite granite was found in several areas near St. Martin and Nebelstein. Characteristic features of this granite are the high contents of Sr and Th and often displays also high magnetic susceptibility. This rock most likely does not belong to the family of Eisgarn granite s.l. Typical contents are:  $\text{SiO}_2$  71%,  $\text{K}_2\text{O}$  up to 4.7 - 4.9 %,  $\text{Na}_2\text{O}$  2.9 - 3.1 %,  $\text{MgO}$  c.0.7 % and  $\text{CaO}$  1.3 - 1.5 %.

5. A small body of pegmatoidal muscovite granite was found near the center of the St. Martin magnetic anomaly. This type of muscovite granite is, in contrast to muscovite granites accompanying the Eisgarn intrusion, geochemically primitive, more enriched in silica, but without any enrichment of F, Rb, Li, Sn, U etc. Typical contents are: SiO<sub>2</sub> up to 75 %, K<sub>2</sub>O 4.1 - 4.4 %, Na<sub>2</sub>O 3.3 - 3.6 %, MgO max. 0.1 % and CaO max. 0.5 %.

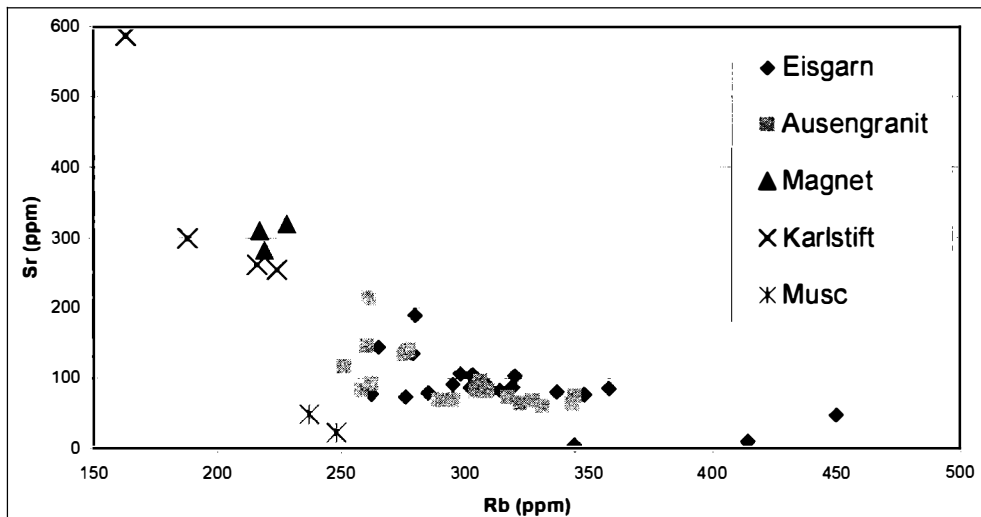


*Fig. 1*

The Rb-Sr plot of granites under investigation: Eisgarn – coarse-grained two-mica granites of Eisgarn type in central part of the pluton, Aussengranit – fine-grained granites in external part of the pluton, Magnet – biotite granites with elevated magnetic susceptibility from the area St.Martin-Nebelstein, Karlstift – biotite granite from the Karlstift area, Musc – muscovite granite from St. Martin magnetic anomaly.

#### Acknowledgement

This work was supported by Austrian-Czech agency ACTION.

#### References

- [1] BREITER, K. & SCHARBERT, S. (1998): Latest intrusions of the Eisgarn pluton (South Bohemia – Northern Waldviertel). - Jb.Geo.B.-A., 141: 25-37.
- [2] KLOB, H. (1970): Über das Vorkommen eines porphyrischen Granites im Raume Sandl – Karlstift – Liebenau bei Freistadt im oberösterreichischen Mühlviertel (Granit vom Typ "Karlstift"). - Tscherm. Min. Petr. Mitt., 3F, 14: 311-323.

**IMPROVED LITHOLOGICAL DESCRIPTIONS FROM  
DOWNHOLE GEOPHYSICAL LOG DATA**

by

**N. R. Brereton, R. W. Gallois & A. Whittaker**

British Geological Survey

Kingsley Dunham Centre, Keyworth. Nottingham NG12 5GG, United Kingdom

Rock material from deep boreholes in sedimentary sections is mainly available as cuttings, only occasionally as cores. Lithological descriptions are normally based upon visual assessment of the rocks, using primarily rock composition, colour and textural contrasts. However, within a particular sequence the descriptions may become more subjective, especially in relatively thick lithologically monotonous units such as the late Jurassic Kimmeridge Clay Formation, a principal source rock for North Sea oil.

Downhole geophysical wireline logs deliver a range of quantitative rock properties, usually including resistivity, sonic velocity, bulk density, neutron porosity and natural gamma radiation. For lithostratigraphic purposes marker beds are identified and then correlated between boreholes. However, the use of several logs simultaneously often presents visually complex data making it increasingly difficult to disentangle the patterns of multiple curves.

To overcome this, a 3D colour cube based on the additive properties of red, green and blue has been used. The three orthogonal axes of an x-y-z cross-plot are assigned these colours with maximum values coded 100, 010, and 001 respectively. Thus the cube origin has no colour (black; 000); the point in 3D space represented by the maximum of all three axes (red+green+blue) is white (111); and the other three end members are magenta (101), cyan (011) and yellow (110). Any point in the cube is thus represented by a specific mix of colour. If each of the red, green and blue axes is equated with a wireline log, then at any given depth in the borehole, the properties of the rock will be represented by the values of each of those three logs which will correspond to a particular colour. This, in turn, can be translated into a colour-coded pseudo-lithology log plotted against depth, which effectively comprises a four-dimensional cross-plot (that is, three logs and depth).

Instead of representing the logs as a continuum of colour, each axis can be subdivided into three so that the cube forms 27 discrete cells each with a specific colour. The planes between the layers of cells can be chosen to coincide with log properties that mark the boundaries between data clusters or different rock types.

The logs are arithmetically combined so as to include data from five or more logs. Of the five commonly run wireline logs, natural gamma is the only one which in many circumstances gives a general indication of lithology in terms of clay, mudstone or shale content ('shaliness') rather than its physical properties. It reflects the abundance of K, U and Th in sedimentary rocks, so that a high gamma is often characteristic of shales, clays or mudrocks. Resistivity is a measure of the electrical conductivity of the bulk rock and in sedimentary rocks there is often a negative correlation with natural gamma. The sonic velocity, bulk density, and neutron porosity logs all relate to physical properties and in particular are a function of porosity. In general, zones of low porosity coincide with zones of high sonic velocity and high density, and vice versa.

It is necessary to standardise all property variables by subtracting the mean of the distribution from each data value and dividing the result by the standard deviation of the distribution. The resultant values are measured in units of standard deviation and have a mean of zero and a standard deviation of one. Standardisation is applied to all the logs comprising the colour cube but, because resistivity is an exponential function, the logarithm of this log is taken prior to standardisation. The combination of standardised sonic velocity (VPS), bulk density (RHS) and neutron porosity (NPS) gives rise to the enhanced porosity log (EPL) by the relationship  $EPL = VPS + RHS - NPS$ . The standardised equivalents of natural gamma and the logarithm of shallow resistivity are given as GRS and LSS, respectively.

The x-y-z axes of the colour cube are represented by GRS, LSS, and EPL respectively. Because the effect of standardisation is to render each property dimensionless, with mean of zero and a standard deviation of one, the logs can be compared on equal terms. Thus the choice of colour cube boundary values can be made in terms of standard deviation rather than absolute log values; the choice depends upon the specific objectives of the study. If a broad lithological differentiation between a number of boreholes is required then a wide boundary range displays the principal lithological formations present. In the case of the British Jurassic and Triassic mudrocks used here, the colour cube representation of the wireline log characteristics was based upon boundary values of  $\pm 0.85$  standard deviation.

The Kimmeridge Clay Formation recently has been studied for its long term climatic cycles in a project sponsored by the UK Natural Environment Research Council. The formation was chosen because it consists of an apparently unbroken sequence of highly fossiliferous marine mudstones that represent about 3 million years of Earth history. The mudstones contain rhythmic variations in clay mineralogy, fauna and organic content that are believed to reflect climatic and sea level changes. The borehole sequences studied in detail comprise mudstones that vary in colour from dark grey to pale grey (with variable amounts of shell debris, silt and organic kerogen) and several thin dolomitic limestone beds. The organic-rich horizons give rise to distinctive thin beds of oil shale, and bituminous mudstone. Much of the remainder of the sequences examined in the drill holes consists of mudstones that show only minor colour and/or textural differences; they were grouped together as 'undifferentiated' mudstone.

Comparison of the lithologies from the core descriptions and those generated by the colour cube ('pseudo-lithology') method show clear recognition of the limestone beds which are given blue colour on graphic core logs but are shown as white stripes on the colour cube logs (end, or 'maximum' values) with low gamma and porosity, but high sonic velocities, high densities and relatively high resistivities. Likewise, oil shales and bituminous mudstones are easily recognised.

Thick 'undifferentiated' mudstones of the borehole sections are shown in a pale grey colour on the graphic core logs and make up the bulk of the section in terms of thickness and volume. However, they are represented in the colour cube column by numerous stripes of grey, blue, red and green hues, allowing considerable lithological refinement and subdivision of the 'undifferentiated' mudstone. Results suggest that the refined mudstone lithological units are grouped into metre-scale Milankovitch rhythms of the type which occur at many levels in the Kimmeridge Clay but which have not previously been recognised in the 'undifferentiated' mudstones.

This account is published with the approval of the Director, British Geological Survey (NERC).

MINERALOGY AND GEOCHEMICAL HISTORY OF FELDSPARS  
IN THE TANCO GRANITIC PEGMATITE, SOUTHEASTERN MANITOBA

by

J. Brown, D. K. Teertstra & P. Černý

Department of geological Sciences  
University of Manitoba, Winnipeg, MB, R3T2N2, Canada

The giant Tanco pegmatite at Bernic Lake, one of the globally significant producers of Ta, Cs, refractory spodumene and numerous industrial minerals, is located close to the southwestern margin of the Superior Province of the Canadian Shield in southeastern Manitoba. The pegmatite consists of nine concentric and layer-like internal zones with variable contents of alkali feldspars (albite, K-feldspar and Rb-dominant feldspar). Aplitic zones (10) and (30) contain virtually exclusively albite, whereas the near-central zones (50) and (60) are Kfs-dominant. Feldspar-rich zones (20) and (40) have substantial amounts of both albite and K-feldspar, as do the feldspar-poor innermost zones (80) and (90). The quartz zone (70) is feldspar-free. Selected batches out of a total of 461 samples were examined optically, by wet-chemical and/or EMP analysis, and by powder XRD to track down the phase and geochemical evolution of the feldspars.

Most of the "primary" blocky K-feldspar is tartan-twinned microcline-perthite, secondary after a primary magmatic homogeneous K>Na feldspar. Bulk compositions show, in wt.%, Rb<sub>2</sub>O (1.45 - 3.08), Cs<sub>2</sub>O (0.11 - 0.29), radiogenic Sr (0.014 - 0.026 oxide) increasing from the outer to the inner pegmatite zones, whereas Li<sub>2</sub>O (0.014 - 0.108) and P<sub>2</sub>O<sub>5</sub> (0.33 - 0.47) culminate in the amblygonite- and petalite-dominated zones (40) and (50) and drop off afterwards. In contrast, Na<sub>2</sub>O (2.46 - 1.10), K/Rb (9.0 - 4.1) and K/Cs (117 - 39) decrease, and CaO (0.13 - 0.08), BaO (0.004 - 0.17) and Ga<sub>2</sub>O<sub>3</sub> (0.006 - 0.010) show minor random variation. Rb-poor microcline is close to fully (Si,Al)-ordered, but the degree of order is somewhat reduced in Rb-enriched samples.

(Si,Al)-ordered albite is dominantly fine-grained aplitic, rarely saccharoidal. Subordinate platy cleavelandite is virtually never associated with the fine-grained varieties. The Ca content is negligible in all varieties (0.03 - 0.09 wt.%) but decreases slightly from the outer to the inner zones. Variations in SrO (b.d.l. to 0.04 wt.%) match those of Rb and Sr in associated K-feldspar, suggesting incorporation of radiogenic Sr lost from the latter.

Late feldspars precipitated under subsolidus conditions include (a) crystals of albite in miarolitic cavities, (b) veinlets of Rb-enriched untwinned microcline in pollucite (2 - 4 wt.%  $\text{Rb}_2\text{O}$ ), (c) Rb-dominant feldspar (up to 24.84 wt.%  $\text{Rb}_2\text{O}$ , 1.43 wt.%  $\text{Cs}_2\text{O}$ ;  $\leq 58$  mole % Rbf) associated with Rb-free end-member adularia, abundant on microscopic scale as replacements in microcline and pollucite, and (d) adularia with albite in leaching cavities or porous metasomatic pods (all of pure end-member compositions). Outer zones of cavity-grown adularia contain appreciable quantities of light elements (Li ?, H ?, B ?), which cannot be analyzed by EMP. Albite is fully ordered whereas the potassic adularia is totally disordered high sanidine; the structural state of the Rb-dominant feldspar is uncertain, but a high degree of disorder is suspected.

Gross textural features of primary feldspars are largely preserved, but details of the blocky, "primary" K-feldspar show widespread compositional, structural and textural adjustments under subsolidus conditions. Significant loss of  $\text{Na}_2\text{O}$  is suspected, increasing toward the inner zones of the pegmatite, which distorts the bulk composition of the feldspar relative to the features expected from experimental petrology: the sodium content of magmatic K-feldspar should at least slightly increase inwards. In the subsolidus assemblages, thermodynamic considerations seem to forbid the coexistence of K- and Rb-dominant feldspar phases, but experimental proof is not available.

MINERALOGY AND CHEMISTRY OF THE BI-METASOMATIC CONTACT ZONE  
BETWEEN GNEISS AND MARBLE FROM ŽULOVÁ, CZECH REPUBLIC

by

**M. Brož & Z. Losos**

Department of Mineralogy, Petrology and Geochemistry  
Faculty of Science, Masaryk University, Kotlářská 2, 611 37 Brno

The typical occurrences of contact zones – "tactites" between granitoid rocks and marbles in the area of Žulová massif (localities Žulová, Vápenná) in the Czech Republic were studied. The Žulová (Friedeberg) massif (age about 300 M.A.) is located at the NE margin of the Bohemian Massif.

This article presents results of the study of the bimetasomatic contact zone between calcite marble and biotite gneiss in the vicinity of the described direct contact bodies. The bi-metasomatic zone is located about 5 m from the direct contact of metasedimentary rocks with biotite granite on the locality Žulová – Boží hora (old quarry). Similar bimetasomatic contact zones were described by Losos [3] at Česká Ves near Jeseník, in the distance X0-X00 m from the plutonic rocks of the Žulová massif. The studied bimetasomatic contact zone has vertical orientation, parallel to the foliation of gneiss. The zone thickness is about 20 cm and it is composed of the following subzones (the middle part of this contact zone /subzones 2b, 2c/ are strongly silicified):

1. Dark biotite gneiss /Plg, Bi, K-fs, Qtz/ with enormous enrichment of biotite
2. Bimetasomatic contact zone
  - a) Transformed gneiss rich in Cpx /Plg, Bi, Cpx/
  - b) Plg-Cpx-zone /Plg, Cpx, Grs, Qtz/, Plg is transformed into zoisite and prehnite
  - c) Grs-Hd-zone /Grs, Hd, Qtz/
  - d) Wo-zone /Wo, Ves, accessory Di/
3. Coarse-grained calcite marble /Cal, accessory Di, Qtz/

Chemical analyses of the subzones give the following results: the Al-content decreases in the direction from biotite gneiss towards calcite marble. The highest content of Fe-total and Mn is in the Grs-Hd-zone (the source of Fe and Mn can be connected with magmatic fluids). Distribution curves of Fe<sup>3+</sup> and Fe<sup>2+</sup> have opposite trends, which were induced by a different oxygen fugacity over subzones of the contact. An excess of Fe<sup>2+</sup> in pyroxenes and Fe<sup>3+</sup> in garnets is a typical phenomenon for Grs-Hd-subzone. Garnets in this zone have a higher proportion of andradite and spessartite, the hedenbergite component is dominant in pyroxenes. The Si-content is high in the whole profile of the bi-metasomatic zone. Especially high Si-content in the middle subzones is connected with secondary silicification of these subzones. The low Si-content in marble is in correlation with accessory diopside and quartz grains.

A decrease of K signalizes disappearance of K-Fs in the Plg-Cpx-zone. The Ca content increases from marble toward gneiss. The opposite trend of Na and Ca curves is connected with albitization of Plg caused by Ca depletion during the crystallization of contact minerals.

The small Al content in the studied pyroxenes is typical for contacts with marble. The pyroxenes from the Grs-Hd-subzone have a dominant hedenbergite component, accessory pyroxenes from the W-zone and Cal-zone are diopsides. Most of pyroxenes from the direct large contacts on the locality Boží hora at Žulová have dominance of hedenbergite as well (Fig. 1). In contrast, pyroxenes of bimetasomatic contact zones between parametamorphites in the metasedimentary host rocks of Žulová massif from Česká Ves at Jeseník are practically pure diopsides [3].

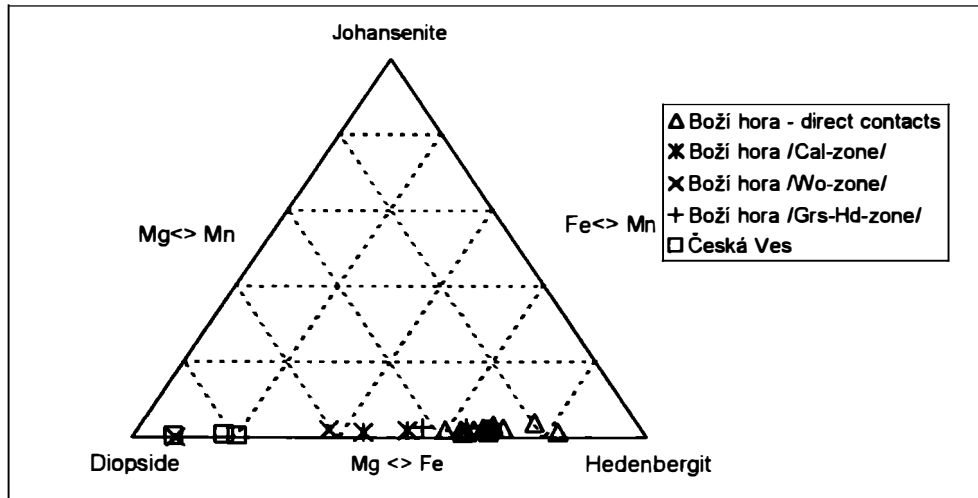


*Figure 1*  
*Chemistry of pyroxenes*

Grossulars from Grs-Hd-subzone in the studied bi-metasomatic contact have even higher contents of Anr (20 - 22 mol.%) and Spes (1 - 2 mol.%) than garnets in the one near Česká Ves (Anr 15 mol.%, Spes 0.2 mol.%). The Pyr and Ti-Grs component are low in both described garnets (at most 0.5 mol.%). In comparison, the known "floating garnets" in marble from Vycpálek quarry at Vápenná are rich in Pyr (6 - 7 mol.%) and Ti-Grs (7 - 9 mol.%) components.

The ratio between  $\text{Fe}^{2+}$  in pyroxens and  $\text{Fe}^{3+}$  in garnets of the bimetasomatic contact zone from Žulová indicates a reduction type of skarn with W-mineralization [1, 6]. Scheelite is known as the accessory mineral of contacts at Žulová. The influence of magmatic fluids on the origin of the bimetasomatic contact zone from Boží hora is documented by a high Fe content in the contact minerals, silicification, a low  $P_{\text{CO}_2}$ , and a high  $P_{\text{H}_2\text{O}}$  (the presence of vesuvianite). P-T conditions for the formation of the contact zones at Žulová were estimated:  $T = 600 - 620^\circ\text{C}$  – graphite-carbonate isotopic thermometry /Boží hora quarry/[5]. Host rocks of the Žulová massif:  $P = 200 \text{ MPa}$  – sphalerite geobarometry [4, 5],  $T = 650 - 680^\circ\text{C}$  – garnet-biotite thermometry [2] /both Česká Ves/.

## **References**

- [1] EUNAUDI, T. M. & BURT, M. D. (1982): Introduction – Terminology, classification and composition of skarn deposits. - Econ. Geol., 77, 4: 745-754, New Haven.
- [2] CHAB, J. & ŽAČEK, V. (1994): Geology of the Žulová pluton mantle (Bohemian Massif, Central Europe). - Věst. ZGÚ, 69, 4: 1-12, Praha.
- [3] LOSOS, Z. (1985): Studium minerálních paragenezí pláště Žulovského masívu v okolí České Vsi u Jeseníku. - MS, Dipl. práce přírod. fak. UJEP v Brně, 1-111.
- [4] LOSOS, Z. et al (1986): Mineralogická charakteristika sulfidického zrudnění u České Vsi u Jeseníku. - Scr. Univ. Purkyn. brun., Geol., 16, 3: 143-170, Brno.
- [5] LOSOS, Z. & HLADÍKOVÁ, J. (1988): Izotopické složení grafitů a karbonátů z pláště žulovského masívu a jeho využití pro výpočet teplot metamorfozy. - Scr. Univ. Purkyn. brun., Geol., 18, 7: 261-272, Brno.
- [6] SATO, K. (1980): Characteristics of Tungsten Skarns in Japan, Two Contrasting Types. - Proc. Symp. Tungsten Geology, 203-209, Jiangxi.

**LAMPROPHYRE-DERIVED VAUGNERITIC-DURBACHITIC MAFIC ENCLAVES  
IN VARISCAN GRANITOIDS FROM MECSEK MTS. (SOUTH HUNGARY)**

by

**Gy. Buda**

Department of Mineralogy  
Eötvös Loránd University, Múzeum krt. 4/a, H-1088 Budapest, Hungary

Variscan microcline megacryst-bearing granitoids contain several chromite-bearing mafic enclaves of various sizes from few cms to several hundreds of metres in Mórág Hills (South Hungary) occurring in the northwest part of the Tisza Megaunit.

The mineralogical, petrological and geochemical compositions of these enclaves correspond with lamprophyre-derived vaugnerites/durbachites, which are widespread in the Variscan collision belt e. g. French Massif Central, Vosges, Schwarzwald, South part of Central Bohemian Plutonic Complex. The host magnesio-potassic granitoid is consanguinous with mafic enclaves due to the mutual effect of acid and basic magmas. The basic melt originated from the upper mantle revealed by the presence of Cr- and Fe-rich chromites. The upper mantle was enriched in compatible and incompatible elements probable due to a previous older subduction. Acidic melt formed as a result of partial melting of the continental crust. The two rock types are mineralogically different but they show many geochemical similarities e.g. chondrite normalized REE patterns and  $^{87}\text{Sr}/^{86}\text{Sr}_{(350)}$  ratios,  $\epsilon\text{-Nd}_{(\text{CHUR } 350)}$  values. Both melts crystallized simultaneously and affected each-other. Mafic enclaves became more lamprophyric and the acidic one transformed to magnesio-potassic rich. The melts formed and crystallized in a postcollisional Variscan (350 Ma) uplifted tectonic regime due to extension which was followed by compression. The old acidic continental crust is presumed to be of Pan-African origin with Cadomian age [1].

**Reference**

- [1] KLÖTZLI, U. S., BUDA, G. & KOLLER, F. (1999): Geochronological evidence for the derivation of the Mecsek Mountains, South Hungary, from Variscan Central Europe. - Beih. Eur. J. Miner. 11, 1: 126.

TOURMALINE-BEARING LEUCOGRANITES FROM THE MOLDANUBIKUM

by

D. Buriánek & M. Novák

Department of Mineralogy, Petrology and Geochemistry  
Masaryk University, Kotlářská 2, 611 37 Brno, Czech Republic

Peraluminous leucogranites with accessory tourmaline derived from crustal sources are widespread in mountain belts formed by continental collision [1]. They are common in the Moldanubium as well, and two distinct types of leucocratic, medium- to fine-grained, dominantly muscovite-biotite granites with accessory tourmaline were distinguished [2].

(i) Granites with tourmaline concentrated in orbicules (OTG) compose small intrusive bodies and dykes, scarcely up to 200 m thick, cutting or spatially associated with durbachite plutons (Třebíč, Jihlava, Rastenberg, Čertovo břemeno, Písek area). Quartz + tourmaline  $\pm$  feldspars orbicules, up to 10 cm in diameter, or rare veins, up to 2 cm thick, are randomly distributed or concentrated in several m thick zones within bodies of leucocratic granites. Subhedral tourmaline is interstitial between euhedral grains of feldspars and quartz, and it replaces dominantly plagioclase. Leucocratic halo around orbicules is mica-free and enriched in feldspars. The accessory minerals include apatite, andalusite, cordierite, ilmenite, zircon, allanite and monazite in granite; apatite is fairly abundant in orbicules. The tourmaline-quartz orbicules and veins seem to be a product of crystallization of evolved, B-rich medium (melt and/or fluid) during late solidus to early subsolidus stage of the granite formation.

(ii) Granites with disseminated tourmaline (DTG) form relatively large intrusive bodies and dykes, up to several km<sup>2</sup>. They do not exhibit apparent spatial relationship to durbachite plutons as OTG; however, they also occur in the regions involving durbachitic rocks. Euhedral to subhedral tourmaline grains, up to several mm long, are rather regularly distributed in the rock. The accessory minerals include apatite, zircon and garnet. In contrast to OTG, disseminated tourmaline evidently crystallized from granitic melt.

Tourmaline from OTG and DTG exhibits similar chemical composition and individual grains are commonly rather homogeneous. Assuming the Z-site is fully occupied by Al, YAl = 0.96 - 0.24, Fe = 1.89 - 1.18, Mg = 1.10 - 0.36, Na = 0.70 - 0.54, Ca = 0.13 - 0.03, Ti, Mn, Zn and F contents are low. The tourmaline compositions correspond to those from granites and Li-poor granitic pegmatites [3]. Biotite is annite  $X_{Mg} = 0.49 - 0.25$  and  $YAl = 2.83 - 0.40$ ; plagioclase has  $An_{1.4-26.9}$ . The OTG and DTG have very similar geochemical characteristics corresponding to leucocratic and peraluminous, syn- to post-collisional S-type granites [4,5]:  $K_2O = 2.77 - 5.91$ ,  $Fe_2O_3\text{ tot} = 0.42 - 1.77$ ,  $CaO = 0.49 - 0.87$  (1.71 - Lavičky) in OTG and 0.36 - 0.66 in DTG;  $Rb = 194 - 234$  ppm,  $K/Rb = 134 - 368$ ,  $Rb/Sr = 1.00 - 5.56$  in OTG and 5.24 - 7.34 in DTG,  $Mg/Fe = 0.08 - 0.33$ .

The normalized REE patterns are very similar for both granite types; low REE concentrations  $\Sigma$ REE = 20.08 - 99.81 ppm and slight LREE enrichment ( $\text{La}_N/\text{Lu}_N = 1.9 - 6.8$ ). Similar mineral assemblages, whole rock major, minor and trace chemistry suggest that positive and negative europium anomalies found in both OTG and DTG rather reflect different  $f_{\text{O}_2}$  during crystallization than different degree of fractionation or different protoliths.

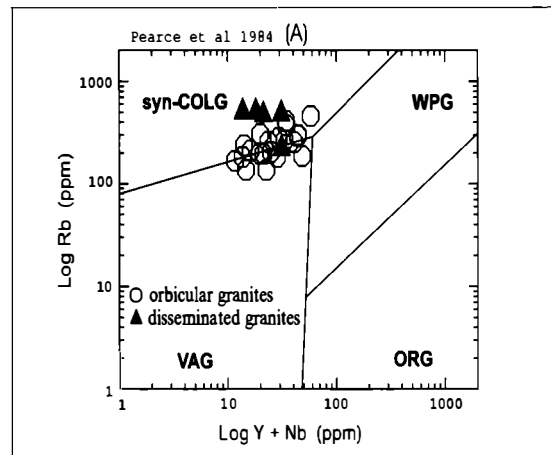


*Fig. A*  
Tectonic discrimination diagrams [4].

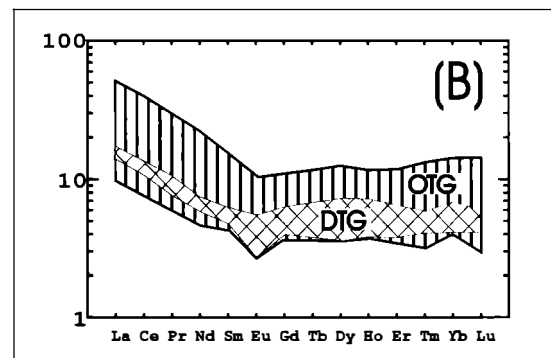


*Fig. B*  
Chondrite-normalised REE diagram for OTG and DTG. Normalising values from [5].

Most geochemical signatures exhibit rather primitive character of both OTG and DTG, despite slightly higher fractionation characteristics found in DTG. Disregarding distinct textures and origin of tourmaline, similar geochemical signatures and mineral chemistry of OTG and DTG suggest similar protoliths (metasediments) and conditions of melting. The observed differences in textures and development of OTG and DTG rather stem from different conditions of their emplacement. The DTG likely intruded into deeper level of the crust with no apparent relation to durbachitic rocks; the OTG are spatially related to durbachite emplacement and presence of andalusite indicate the conditions with lower pressure relative to those of DTG.

This work was supported by the grant GAČR No. 205/99/0434.

## **References**

- [1] LONDON, D., MORGAN, G. B. VI. & WOLF, M. B. (1996): Boron in granitic rocks and their contact aureoles. - In: Boron: Mineralogy, Petrology and Geochemistry (GREW, E. S. & ANOVITZ, L. M. eds). Rev. Mineral., 33, 299-330.
- [2] NOVAK, M. & BURIANEK, D. (2000): Chemistry of tourmaline from leucocratic orthogneisses and granites in the Moldanubian Zone, Czech Republic. - Symposium Magurka 2000.
- [3] HENRY, D. J. & GUIDOTTI, C.V. (1985): Tourmaline as a petrogenetic indicator mineral: an example from the staurolite-grade metapelites of NW Maine. - Amer. Mineral., 70, 1-15.
- [4] PEARCE, J. A., HARRIS, N. B. W & TINDLE, A. G. (1984): Trace element discrimination diagrams for the tectonic interpretation of granitic rocks. - J. Petrol. 25, 956-983.
- [5] BOYNTON, W. V. (1984): Cosmochemistry of the rare earth elements: meteoritic studies. In: Rare Earth Elements Geochemistry. (HENDERSON, P ed.). - Amsterdam: Elsevier, 63-114.

**A COMPARITIVE STUDY OF CONTACT METAMORPHISM IN THE  
OSLO GRABEN, NORWAY**

by

**A.-M. Christensen & R. Abart**

Institute for Mineralogy and Petrology  
Karl-Franzens-University Graz, Universitätsplatz 2, A-8010 Graz

The Oslo paleo rift is situated in the south-western part of the Baltic Shield and formed during an Permo-Carbonifereous rifting event. The presently exposed parts of the rift consist of Carboniferous and Lower Paleozoic sedimentary rocks along with alkaline extrusives and intrusives; the latter emplaced during intensive intrusive activity in the time-interval 300 - 250 Ma and the cause of widespread contact-metamorphism and hydrothermal activity in the surrounding sediments [e.g., 1].

This study deals with the attempt to compare the effect of contact metamorphism from 2 shallow intrusive complexes on Ordovician lithologically similar sediments. 1) The Drammen granitic intrusion is considered small ( $650 \text{ km}^2$ ) with a relative low solidus temperature ( $680^\circ\text{C}$ ) and considered a "wet" melt 2) The larvikite complex is large ( $2500 \text{ km}^2$ ) with a high solidus temperature ( $850^\circ\text{C}$ ) and considered a "dry" melt.

The phase-assemblage found in the Drammen aureole are wollastonite, andradite-grossular garnet and diopsidic-hedenbergitic diopside; whereas the phase-assemblage found in the Larvikite contact aureole also contain tremolite, biotite and chlorite. Scapolite is locally present. The phase assemblage is stable till 500 meter from the contact in the Drammen granitic aureole and 2500 meter in the Larvikite aureole. The difference in the aureole sizes is consistent with stable and radiogenic isotopic data for both aureoles.

In terms of stable isotopes the Drammen granitic aureole shows a steep front in oxygen ( $\delta^{18}\text{O}$ : 5 - 25 ‰) and no front in  $\delta^{13}\text{C}$ . The larvikite aureole shows a smooth front in both of the stable isotopes ( $\delta^{18}\text{O}$ : 10 - 25 ‰ and  $\delta^{13}\text{C}$ : -4; 2).  $^{87}\text{Sr}/^{86}\text{Sr}$  isotopic data shows initial  $^{87}\text{Sr}/^{86}\text{Sr}$  from 0.708 to 0.710 in the Drammen granitic aureole and initial  $^{87}\text{Sr}/^{86}\text{Sr}$  from 0.708 to 0.714 in the larvikite aureole.

The Drammen granitic aureole can be divided in two trends dependant on type of lithology. Pure carbonates and limestones which can be modelled in type of processes: decarbonation acting in the pure carbonates and an external infiltration of a water-rich ( $< 0.1 \text{ CO}_2$ ) fluid for the limestones. The highest degree of metamorphism is around  $590^\circ\text{C}$ .

The larvikite aureole can only be modelled with locally very CO<sub>2</sub>-rich fluids (< 0.6 CO<sub>2</sub>). The origin of these fluids are considered to be internally derived and not related to the magmatic source. The highest degree of metamorphism can have been as high as 800°C, which must be considered due to the size and prolonged heating of this area by this intrusive complex.

## References

- [1] JAMTVEIT, B. et al. (1996): Flow and transport during contact metamorphism and hydrothermal activity: Examples from the Oslo rift. - In: Fluid flow and transport in rocks (eds. JAMTVEIT & YARDLEY), Chapman & Hall, 57-82.

**CHROMITES RELATED TO THE ULTRAMAFIC SOUTH-EASTERN SEGMENT OF  
ALBANIA: A COMPARISON WITH CENTRAL AND NORTHERN ONES**

by

**A. Cina & K. Onuzi**

Institute of Geological research  
Blloku Vasil Shanto. Tirana, Albania

Jurassic ophiolite complex of Albania, located between Dinarides in north and the Helenides in south, is constituted of two belts, the Western Ophiolite belt (WOB) and the Eastern one (EOB). The two belts show distinctive petrologic, geochemical and metallogenetic features. The first of them belongs to the HOT-LOT type (harzburgite-lherzolite ophiolite-type) and displays MORB affinity, whereas the second one of HOT-type (harzburgite ophiolite-type) indicate a IAT-BSV nature. The segment of Albania EOB has its normal northward and northeastern continuation with Gjakova, Orahovac, Brezovica and Ljuboten-Radusa massifs, while in south its continuation follows with Vourinos massif. This segment shows more or less an homogeneity in comparison to other ophiolite segments. Relevant differences are traced also in the longitudinal direction with respect to northern continuation (Ozren, Zlatibor ect. ophiolite massifs) and to southern elongation (Othrys ect. ophilite massifs).

The Eastern ophiolite belt with a pyroxenite cumulate sequence consist of highly depleted mantle represented by harzburgite-dunite interbedding and transitional dunite in the upper part, a crustal plutonic sequence by a large variety of gabbro rocks and quartz-diorite-plagiogranite ones. Low-Ti basaltic to rhyodacitic volcanics and bonnites are characteristic.

EOB is wellknown for its high chromium-bearing potential and the metallurgic grade of chromitites. Nevertheless the general petrologic geochemical and metallurgic nature of EOB, along strike, through the different ophiolite massifs, especially those of northern group and southern one, significative differences are evident. The variations of lithologic thickness, the different sequence development, the diversity of the ore grade potential and the ore grade of chromitite, the heterogeneous distribution of the chromitite bodies through the ophiolite column and the PGE mineralization linked with some massifs only, are several of the most relevant different features.

The chromite chemistry of the northern group of ultramafic massifs (Tropoja, Kukesi, Lura, Bulqiza and Shebaniku) is more or less the same. The average of  $100 \times Y(Cr / (Cr + Al))$  ratio and the  $100 \times MF / (Mg + Fe^{2+})$  ratio for chromite of this group are respectively 80.4 and 64.4, that testify Cr-high and Mg-high nature of their chromitites.

The MOR (western)-type ophiolites are characterized by mantle harzburgite to Cpx-harzburgite (-lherzilite) with rare thin dunite intercalations, plagioclase-bearing lherzolite and dunites, Ol-hornblendite, troctolites, gabbros and Fe-gabbros and scarce trondhjemites. High-Ti basaltic pillow lavas form the top of MOR-type ophiolites. Nevertheless this type ophiolite of western Albania are characterized by intermediary features, between those of western Mediterannien and Eastern-type ophiolites as a consequence of a low grade of partial melting of upper mantle, the presence of harzburgite and dunite rocks of mantle suite, a relatively high-Mg and low-Ca and Al and the presence of Al-rich and Cr-rich chromitites in comparison with lherzolitic-type, as protolites of upper mantle (Western - type ophiolites of Apennines ect) .

A particular ophiolitic massifs are those of SE part of Albanian ophiolitic complex, that especially distinguished from other ones of Central and Northern Albanian ophiolites. The former care Shpati, Vallamara, Devolli, Voskopoja and Morava massifs and several sheets in the Korca-Kolonja regions which are associated with Tithonian ophiolitic melange. The magmatic chambres have a limited development and are represented by ultramafic cumulate rocks only, whereas the gabbroic are missed. The volcanic sequences are absent too. Another distinctive feature is a scarce chromitite mineralization related to Cpx-harzburgite with dunite interbedding and to plagioclase -bearing ultrabasic rocks, nearby to cumulate sequences, especially within Vallamara, Voskopoja and Morava massifs. The chromitite ore bodies have limited dimensions and are represented by middle ore grade. The chromite chemistry display a large variety, from those of Cr-rich type up to Al-rich: the chromite of Vallamara massif is of Cr-rich type (YCr ratio = 0.70 ); with Voskopoja massifs are related variable chromites with YCr ratio from 0.45 up to 0.79, i.e. Al-rich up to Cr-rich type. In the Morava massif the chromite is of very rich Al-type ( YCr ratio 0.34). In the contrary, the Bitincka massif, situated in the Eastern part, is distinguished by a Cr-rich chromite (YCr ratio up to 0.74). The chromite chemistry of SE ultramafic massifs is more or less the similar with NW one but is too much different from NE chromites. These difference supposed to be the consequence of low-grade partial melting of upper mantle peridotite and of limited development of melt-peridotite interaction in comparison with NE part of Albanian ophiolites.

PROVENANCE OF THE LOWER CARBONIFEROUS CULM SEDIMENTS OF THE  
DRAHANY UPLAND (CZECH REPUBLIC), DERIVED FROM GARNET CHEMISTRY

by

R. Čopjaková<sup>1</sup>, P. Sulovský<sup>1</sup> & J. Otava<sup>2</sup>

<sup>1</sup>Department of Mineralogy, Petrology and Geochemistry  
Masaryk University, Kotlářská 2, 611 37 Brno, Czech Republic  
<sup>2</sup>Czech Geological Survey  
Leitnerova 22, 600 00 Brno, Czech Republic

The Lower Carboniferous Moravian-Silesian Culm Basin in the eastern part of the Czech Republic is exposed in a NNE-SSW trending and northwards widening belt stretching from Brno surroundings in the south to the Odra Lineament in the north (southern Poland). Culm Basin sediments are exposed in two main areas, southern Drahany Upland and northern Nízký Jeseník Mts., now separated by the Elbe Lineament. The sequence belongs to the foreland flysh basin (conglomerates, greywackes, siltstones, mudstones, shales and related rhythmites and laminites) of Viséan to Lowermost Namurian age [1]. The presented study concerns only the southern, unmetamorphosed part of the basin.

The provenance of Culm sediments was earlier studied by a number of different methods – analysis based on petrography of lithic fragments, pebbles, of translucent heavy mineral assemblage [2]. The results did not show up to be sufficiently specific (lithic fragments, bulk chemistry, heavy mineral assemblages), or applicable in all lithostratigraphic levels (pebble analysis). We have therefore acceded to the varietal study of garnet, as it is a mineral with broad, source-specific elemental substitution, and owing to it known to be usable in provenance studies [3].

Garnet is very abundant heavy mineral at all stratigraphic levels in the psammitic and psefitic Culm sediments of the Drahany Upland. It often makes up to 80% of the total heavy mineral budget. The garnet chemistry was studied on a set of 37 heavy mineral concentrates sampled all over the area of the Drahany Upland. The concentrates were embedded in epoxy resin and polished. Within each polished section, usually 100 garnet grains were analysed by electron microprobe for all major garnet composing elements, including Cr and Ti. Such high number of analyses per sample provides information usually not acquired in provenance studies. Being statistically more representative, it reveals in the detrital garnet populations:

- garnet types derived either from rocks relatively poor in accessory garnet,
- garnets from garnet-rich rocks with limited occurrence in the provenance area,
- garnet zonation, not directly observed in individual fragments of larger, zoned grains.  
It manifests itself by continuous trails of garnet plots, with endpoints indicating the range of substitution.

The electron-microscopic study of detrital garnet from even the deepest levels (expected to have been buried to more than 2.500 metres) has shown that they did not suffer significant dissolution. Moreover, the etching patterns in grossular-rich garnets were not distinctly more developed than those in pyrope- or almandine-rich garnets, as it should be in sediments significantly influenced by intrastratal dissolution. The assumption that the garnet assemblage is probably unaltered is also supported by simultaneous presence of apatite and epidote, i.e. minerals which are typically less stable than garnet during diagenesis.

Garnet occurs in a wide variety of metamorphic and igneous rocks; compositions from the rock types is also varying, making provenance determination by a simple graphical comparison of garnet plots difficult. To make it more exact and justified, we have collected a number of data (directly or from literature) on the chemistry of garnets from a variety of potential source rocks – both in terms of rock types and geological position.

In the lower part of the Culm sequence, ranging from Protivanov- through Rozstání- and lower part of the Myslejovice Formation, the garnet assemblages are polymict, suggesting the basin was fed from a number of sources. These stratigraphically distinguished formations do not differ significantly in number and type of garnet supplying sources, the resulting garnet-type assemblage being rather monotonous over the whole mentioned stratigraphic span. The almandine-rich nature of the majority of garnets from the lower part of the sedimentary sequence suggests they were predominantly derived from metapelitic rocks – mica schists, biotite/amphibole gneisses, amphibolites. Such rocks are common within the Moldanubicum and also in adjacent crystalline units in the north.

A dramatical switch in garnet source occurred in the Upper Viséan - Goniatite zone Go- $\alpha$ , before the onset of Luleč conglomerate sedimentation, the polymict garnet assemblages turning into oligomict ones over only a very short transient zone in the middle of Myslejovice Formation. This change in the nature of garnet assemblages (see Fig. 1) suggests a relatively sudden occurrence of a new, strong source of garnets with distinctly different, pyrope-enriched almandine chemistry. Such garnets can be found in Moldanubian granulites, leptynites and associated ultramafic rocks, mostly garnet-rich. The chemistry of Moldanubian granulite garnets is not uniform, which enables to identify the most abundant garnet types as coming from granulites of the Moravian part of the Moldanubicum. Other, less abundant garnets in the upper part of the Myslejovice Formation can be assigned to metapelitic rocks of the Moldanubicum, of Polička and Svatka Crystalline Units (gneisses, mica-schists, amphibolites), and to Gföhl orthogneiss. The younger levels of the sequence contain less and less garnets from the northern and north-western territories (Svinov-Vranov and Orlice-Kladsko Crystalline Units and Silesicum) and acquired more material from W and SW directions (Moravicum, Moldanubicum), the general influx turning anti-clockwise.

Besides new insight on the stratigraphy of Culm sediments and their provenance, the results also extended the evidence of the high exhumation rate of the Lower Carboniferous granulites at the eastern margin of the Bohemian Massif [4].

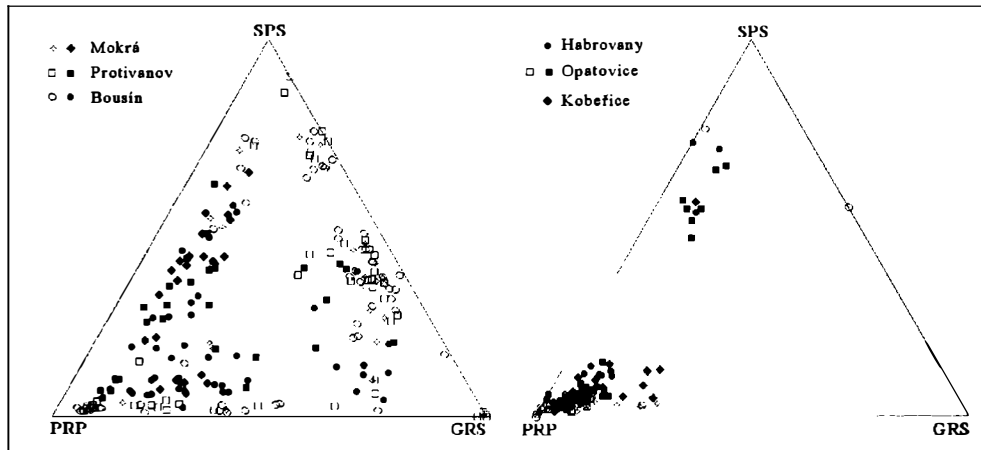


*Fig. 1*

*Comparison of garnets of polymict (left) and oligomict (right) assemblages from six localities in Drahany Upland. Empty symbols – almandine below 65 %; full symbols – almandine over 65 %.*

## References

- [1] HARTLEY, A. J. & OTAVA, J. (2001): Sediment provenance and dispersal in a deep marine foreland basin: the Lower Carboniferous Culm Basin, Czech Republic. - *Jour. of the Geological Society (London)*, 158(1), 137-150.
- [2] ŠTELCL, J., sen. (1962): Overview of the petrography of the Drahany Culm. - *Acta Musei Silesiae*, 11, 113-125.
- [3] MORTON, A. C. & HALLSWORTH, C. R. (1994): Identifying provenance-specific features of detrital heavy mineral assemblages in sandstones. - *Sedimentary Geology*. 90, 241-256.
- [4] KOTKOVA, J., GERDES, A. & PARRISH, R. R. (2000): Lower Carboniferous granulite metamorphism of clasts from the Upper Visean conglomerates – evidence for high exhumation rate at the E margin of the Bohemian Massif. Abstracts from the 6th PACE meeting, Zakopane, Poland, 17-19.9.2000, <http://www.esci.keele.ac.uk/pace/abs6/>.

**MIXED ANDESITE-RHYOLITE IGNIMBRITE FROM THE MIOCENE  
BÜKKALJA IGNIMBRITE VOLCANIC FIELD, NORTHERN HUNGARY:  
EVIDENCE FOR MAGMA MIXING**

by

**Gy. Czuppon<sup>1</sup>, Sz. Harangi<sup>1</sup>, T. Ntaflos<sup>2</sup>, R. Lukács<sup>1</sup>, Cs. Szabó<sup>1</sup> & F. Koller<sup>2</sup>**

<sup>1</sup>Department of Petrology and Geochemistry

Eötvös University, Múzeum krt 4/A, H-1088 Budapest, Hungary

<sup>2</sup>Institute of Petrology

University of Vienna, Geocenter, Althanstrasse 14, A-1090 Vienna, Austria

Many rhyolitic ignimbrite sequences are compositionally zoned, reflecting pre-eruptive gradients in magma chambers (e.g. [1]). Studies of these volcanic products can help to have a better understanding on the processes operating in the high-level magma chambers and the magmatic processes occurring in either intra-continental areas or destructive plate margins. Compositional zonation in rhyolitic magma chambers is often resulted by intrusion of mafic magmas. The subsequent processes depend on the time between the intrusion and the eruption. Convective mixing producing hybrid magma occurs within long-lived magma chambers. Over time, the magma chamber becomes compositionally stratified. If there is insufficient residence time in the magma chamber, syn-eruptive mixing can develop during simultaneous withdrawal of two or more magmas from the magma chamber (e.g. [2]). In this paper, we present examples for various mixing processes operating in silicic magma chamber under the Miocene Bükkalja Ignimbrite Volcanic Field.

The Bükkalja Ignimbrite Volcanic Field (BIVF) is located in the Northern Pannonian Basin, North Hungary. It exposes a silicic pyroclastic sequence originated roughly continuously between 20 Ma and 13.5 Ma [3], at the beginning of the Neogene volcanism of the Carpathian-Pannonian Region. The pyroclastic products are mainly unwelded and welded ignimbrites and subordinately phreatomagmatic fall deposits [4,5]. The pyroclastic sequence is divided into three horizons and named as Lower, Middle and Upper Ignimbrite Units (LIU, MIU, UIU; [3]).

The MIU is represented by dominantly welded ignimbrites and provides a key horizon in the BIVF. These pyroclastic flow deposits contain plagioclases, orthopyroxenes, biotite, amphibole and quartz. Composition of plagioclases and orthopyroxenes shows large variation: the An-content of plagioclases is in the range of 28 % and 90 %, whereas En-content of orthopyroxenes is in the range of 50 % and 92 %. This large geochemical variation cannot be explained by simple fractional crystallization, but suggests magma mixing process. This suggestion is supported by the occurrence of a mixed ignimbrite deposit in certain localities of the BIVF. The mixed deposit overlies a fiamme-bearing welded ignimbrite and shows reverse gradation.

It contains different kinds of juvenile fragments, such as dark and light scoriae, pumice and composite clasts. In addition to these juvenile components, hybrid clasts showing a transitional character between pumice and scoria also occur. Among these juvenile fragments, scoria clasts dominate and have the largest size (up to 10 cm), whereas pumices are rare (less than 10 vol.%) and are smaller (up to 3 cm). The composite clasts show a dark scoria-type core and a light rim. Composition of the glasses of these fragments is in the range of dacite (dark scoria and core of the composite clasts) to rhyolite (pumices and fiamme; Fig. 1).

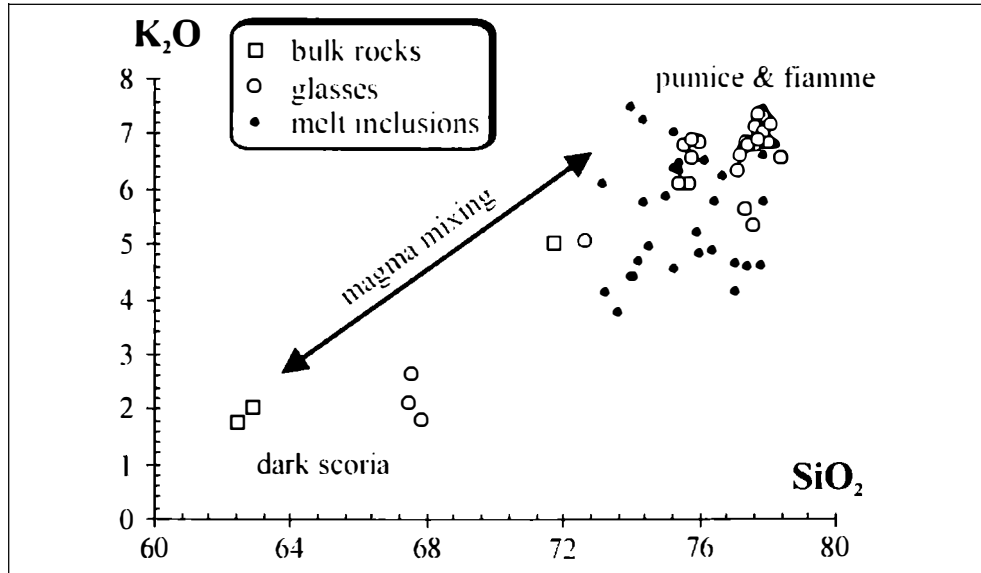


**Figure 1**

*Compositional variation in bulk rocks (dark and light scoriae), glasses of scoria, hybrid clasts, pumices and fiamme and silicate melt inclusions hosted by various phenocrysts. The nearly linear trend with strong increase of  $K_2O$  content can be best explained by magma mixing.*

Dacites are sodic ( $K_2O/Na_2O < 1$ ), whereas rhyolites are strongly potassic ( $K_2O/Na_2O > 2$ ). It is remarkable that composition of glasses shows linear trends in the Harker diagrams and the hybrid clasts are between the two end-members.

Silicate melt inclusions (smi) are common in each phenocryst (orthopyroxenes, plagioclases, ilmenite, quartz, biotite) of the MIU. They represent trapped magmas during different phases of magma evolution; therefore they provide important information on the processes operating in the high-level magma chamber. During the first stage of our study we analysed first the composition of glasses of the smi without apriori homogenisation [6]. Compositional variation of the smi glasses overlaps that of the bulk rocks and the glasses of the juvenile clasts (Fig. 1).

Based on the volcanological, petrologic and geochemical study, we propose various mixing process operated in the high-level magma chamber beneath the Miocene BIVF. Intrusion of andesitic magma into the rhyolitic magma chamber triggered explosive eruption of the most differentiated rhyolitic magma producing strongly welded ignimbrite.

Withdrawal of the rhyolitic magma was associating with suction of the deep-seated more mafic magma resulting in mixing and mingling between the two magmas. Local hybridisation could occur at the contact of the two magmas. The next explosive eruption removed both magmas from the chamber and syn-eruptive incomplete mixing took place producing a mixed ignimbrite deposit.

## References

- [1] HIDRETH, W. (1987): The Bishop Tuff: evidence for the origin of compositional zonation in silicic magma chambers. - *Geol. Soc. Am. Spec. Papers*, 180, 43-75.
- [2] HIDRETH, W. (1987): New perspectives on the eruption of 1912 in the Valley of Ten Thousand Smokes, Katmai National Park, Alaska. - *Bulletin of Volcanology*, 49: 680-693.
- [3] MARTON, E. & PÉCSKAY, Z. (1998): Complex evaluation of paleomagnetic and K/Ar isotope data of the Miocene ignimbritic volcanics in the Bükk Foreland, Hungary. - *Acta Geol. Hung.*, 41/: 467-476.
- [4] SZAKACS, A., ZELENKA, T., MARTON, E., PÉCSKAY, Z., POKA, T. & SEGHEDI, I. (1998): Miocene acidic explosive volcanism in the Bükk Foreland, Hungary: Identifying eruptive sequences and searching for source locations. - *Acta Geol. Hung.*, 41/4: 413-435.
- [5] HARANGI, SZ., LUKACS, R., SZABO, ZS. & KARATSON, D (2000): The Miocene Bükkalja ignimbrite volcanic field, northern Hungary: Volcanology, mineralogy, petrology and geochemistry. *Vijesti Hrvatskoga Geološkog Društva*, Vol.37, sv.3, Zagreb, p.51.
- [6] LUKACS, R., CZUPPON, GY., NTAFLOS, T., HARANGI, SZ., KOLLER, F. & SZABO, CS. (2001): Silicate Melt Inclusions in the mineral phases of the Bükkalja Ignimbrite Volcanic Field. Northern Hungary - ECROFI XVI, Abstracts, Porto 2001, Edited by F. NORONHA, A. DORIA & A. GUEDES, p. 275-277.

**TIME CONSTRAINTS ON THE METAMORPHIC EVOLUTION OF  
TAUERN ECLOGITES FROM DIFFUSION MODELLING**

by

**E. Dachs<sup>1</sup> & A. Poyer<sup>2</sup>**

<sup>1</sup>Institut für Mineralogie und Petrologie  
Universität Salzburg, Hellbrunnerstrasse 34, A-6020 Salzburg  
<sup>2</sup>Institut für Mineralogie und Petrologie  
Universität Graz, Universitätsplatz 2, A-8010 Graz

Discontinuous zoning profiles in garnet can be used as geo-speedometers, giving good constraints on the time span between the formation of a discontinuous growth zone in garnet and the time of closure to intracrystalline cation diffusion by modelling the time required for the observed compositional profile to form from an assumed original sharp compositional step, such as caused by a hiatus in growth, either during one metamorphic episode or during a polymetamorphic history.

An eclogite sample from the Glockner area of the Hohe Tauern, Austria [1] contains garnet with a very pronounced compositional discontinuity between a Mn-rich core with inclusions of amphibole, calcite and magnetite and an Fe-rich rim with inclusions of omphacite and dolomite. Epidote, paragonite and quartz occur as inclusions in both zones. The jump in composition (pronounced in  $X_{Fe}$  and  $X_{Mn}$ , Fig. 1) also marks a microtextural discontinuity (the core hosts a large number of generally small inclusions, the rim has very few inclusions of generally larger size) and is interpreted as the result of an omphacite-forming and garnet-consuming reaction.

A solution to the problem of the interdependent diffusion of the four cations Fe, Mg, Mn and Ca within a single phase can be obtained analytically by one-dimensional modelling of a half-infinite space with fixed (plateau-) compositions on either side of the discontinuity. In this case a number of simplifications and assumptions are necessary: An "effective binary diffusion coefficient (EBDC)" is calculated from the four single diffusion coefficients; single values for temperature and for the difference in composition have to be used in the calculation throughout.

A much higher flexibility can be obtained by (one-dimensional) numerical modelling: Each point along the compositional profile is used in the calculation, so any shape of the original (pre-diffusion) profile can be conceived and tested. No EBDC is needed and any PT-path, or segment of it, as obtained from petrologic reasoning, may be used for the geologic time span in question. This gives an additional flexibility of modelling the changes in composition as a function of position (in the profile), pressure, temperature and time. Diffusion coefficients (calculated according to [2]) are also reevaluated as functions of P, T and composition during each iteration.

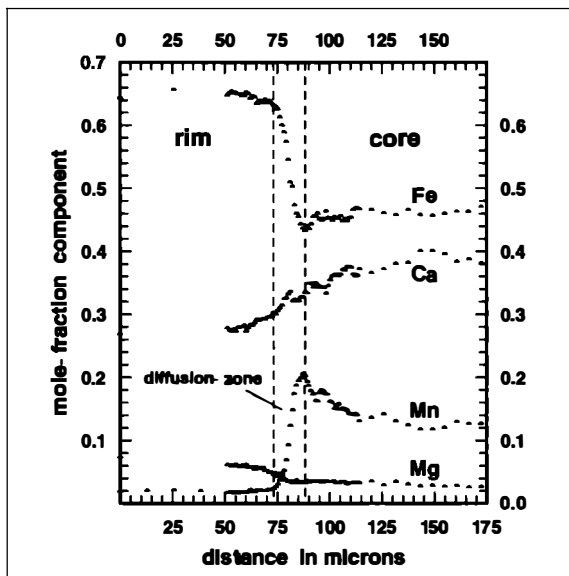


Figure 1

Discontinuous zoning profile preserved in a garnet from eclogite sample G5 (locality Gamsgrube, Grossglockner area), showing the development of a  $\sim 15 \mu\text{m}$  wide diffusion zone between the compositionally contrasting core- and rim regions.

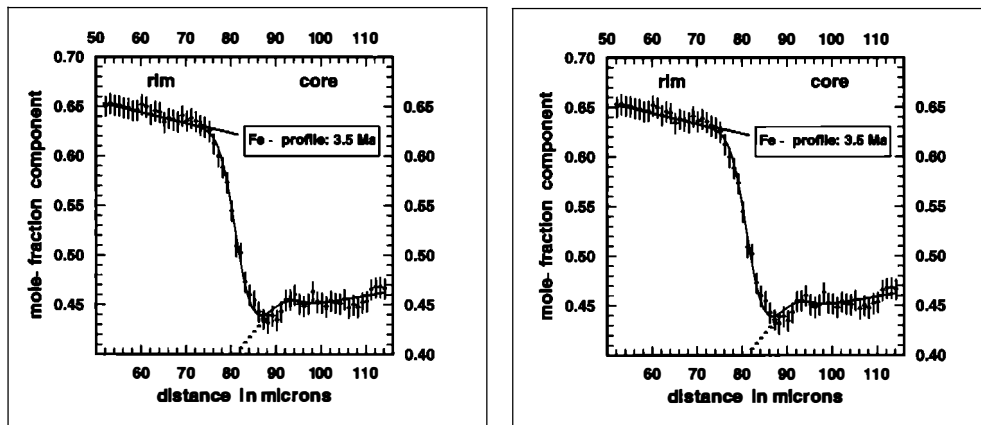


Figure 2

Numerical modelling of the diffusion-zone from the garnet-profile of Fig. 1. The pre-diffusional composition in the diffusion zone has been extrapolated from the compositional trends visible in the adjacent internal core- and external overgrowth zone (dots). Error bars mark  $\pm 0.01$  in the mole-fractions of the measured profile. Results of the numerical diffusion modelling are shown by the solid curve that fits the pronounced step in the Fe- and Mn-profile at 3.5 Ma. The imposed PT-path is that derived for the Grossglockner eclogites by [1].

The garnet investigated has a very complex zoning pattern which also varies in different directions. Despite of these complexities it was possible to obtain similar times not only for different elements from one profile but also for different profiles. Diffusion lasted from the time of rim growth along the prograde path through peak conditions (17 kbar/570°C) to about 450°C, 4 kbar on the retrograde path for maximal 3.5 Ma (Fig. 2) which points to rapid tectonic events related to exhumation of these Tauern eclogites.

## References

- [1] DACHS, E. & PROYER, A. (2001): Relics of high-pressure metamorphism from the Grossglockner region, Hohe Tauern, Austria: Paragenetic evolution and PT-paths of retrogressed eclogites. - Eur J Min 13 : 67-86.
- [2] CHAKRABORTY, S. & GANGULY, J. (1992): Cation diffusion in aluminosilicate garnets: experimental determination in spessartine-almandine couples. evaluation of effective binary diffusion coefficients, and application. - Contrib Mineral Petrol 111:74-86.

**ORIGIN OF THE NEOIDIC FLUORITE MINERALIZATION  
IN THE BRNO MASSIF, CZECH REPUBLIC:  
CATHODOLUMINESCENCE, REE, FLUID INCLUSION AND STABLE ISOTOPE STUDY**

by

**Z. Dolníček**

Department of Geology  
Palacky University, tř. Svobody 26, 771 46 Olomouc, Czech Republic

The Brno massif is the largest and oldest igneous massif at the eastern margin of the Bohemian Massif. From the mineralogical point of view, numerous small occurrences of fluorite are typical for this granitoid unit. Detailed mineralogical and formation conditions study allow to distinguish several types of fluorite mineralization in granitoid rocks. The youngest one is most likely a neoidic mineralization (Mesozoic?-Quaternary?). This type has been found at three sites (Tetčice near Rosice u Brna, Rakšice near Moravský Krumlov and Květnička Hill near Tišnov). Studied hydrothermal veins containing fluorite trend NW-SE, less NE-SW, with a steep dip. Drusy coating, inexpressive banding and breccias are typical structures of the mineralization. A mineral composition is very simple at all localities. The veins consist only of quartz, fluorite and calcite. Fine-grained quartz is present only in a little quantity. A light to dark violet, light green or colourless fluorite predominates. Considerable amount of calcite is present only in veins near Tetčice. Minerals precipitated in following succession: quartz-fluorite-calcite. Several methods were used to evaluate origin of the mineralization: cathodoluminescence microscopy, REE geochemistry of fluorite, fluid inclusion and stable isotope study.

**Cathodoluminescence study**

Fluorites often exhibit distinct growth zonation in CL microscope. Central parts of the crystals are green, margins show oscillatory zoning in blue hues. There are very interesting irregular, corroded boundaries between individual growth zones. Calcite has orange luminescence without growth zones. Younger population (light orange CL) crosscuts older one (dark orange CL) in a shape of tiny veinlets.

**REE in fluorite**

Total content of REE in analyzed fluorites vary between 46 and 273 ppm. REE chondrite-normalized patterns differ at different localities (flat curve without any anomaly and LREE enrichment at Tetčice, a well-balanced curve and a strong positive Eu anomaly at Rakšice), however, both total content and distribution of REE correspond well with those for surrounding rocks. The level of REE fractionation (in the Tb/Ca vs. Tb/La plot) indicate hydrothermal origin of all studied fluorites.

## **Fluid inclusions**

Primary and pseudosecondary fluid inclusions have been studied in fluorites. Inclusions are always two-phase (type L+V), with 2 - 5 vol.% of vapour phase. Homogenization temperatures range between 83 and 165°C. Inclusions completely freeze at temperatures from -29 to -47°C. Eutectic temperatures around -20 °C indicate presence of the NaCl-H<sub>2</sub>O fluid. Last ice crystal melts between 0.0 and -2.6°C, so the given range for T<sub>m</sub> values corresponds to the very low salinity of the trapped solution (between 0 and 4.3 wt.% NaCl<sub>eq</sub>). Distribution of the measured data in the Th/salinity plot indicate mixing of more saline and warmer fluid with less saline and cooler one. In fluid inclusion is further probably present small amount of CO<sub>2</sub>. Fluid inclusions in associated minerals exhibit, in fact, the same fluid characteristics as those in fluorites.

## **Stable isotopes**

Isotopic composition of C and O was determined for calcites from Tetčice. δ<sup>13</sup>C and δ<sup>18</sup>O values are between -6.7/-9.9 ‰ and -7.5/-15.0 ‰ PDB, respectively. Calculated carbon isotopic composition of the parent fluid is around -11 ‰ PDB. Source of carbon was probably in the host rocks, but some admixture of organic carbon cannot be excluded. Calculated δ<sup>18</sup>O values of the fluid between 0 and -7.5 ‰ SMOW are typical for meteoric water.

## **Conclusion**

The investigated mineral assemblages precipitated from low-saline fluids at temperatures of 80 - 150°C. These fluids were probably shallow-circulating meteoric waters. Components of mineralising fluids has been extracted from the host rocks as is documented by REE in fluorites or by carbon isotopes in calcites. The studied fluorite mineralization from the Brno massif could be compared to the Tertiary fluorite mineralization described from the North Bohemia region (Teplice, Jílové u Děčína [1]).

## **Reference**

- [1] ŽAK, K., ČADEK, J., DOBEŠ, P., ŠMEJKAL, V., REICHMANN, F., VOKURKA, K. & SANDSTAT, J. S. (1990): Vein barite mineralization of the Bohemian Massif: Sulfur, oxygen and strontium isotopes and fluid inclusion characteristics and their genetic implications. - In: POOLE, F. G. & DOBEŠ, P. (editors): Proceedings of the symposium on barite and barite deposits, Praha, pp. 35-49.

CRYSTAL STRUCTURE INVESTIGATIONS OF AgMS<sub>2</sub> MINERALS (M = As, Sb, Bi)

by

**H. Effenberger<sup>1</sup>, M. Fleck<sup>1</sup>, W. H. Paar<sup>2</sup>, D. Topa<sup>2</sup> & A. J. Criddle<sup>3</sup>**

<sup>1</sup>Institut für Mineralogie und Kristallographie

Universität Wien, Geozentrum, Althanstrasse 14, A-1090 Wien

<sup>2</sup>Institut für Mineralogie

Universität Salzburg, Hellbrunnerstrasse 34, A-5020 Salzburg

<sup>3</sup>Department of Mineralogy

The Natural History Museum, London SW75 BD, UK

Baumstarkite is a new mineral coating miargyrite from the San Genaro mine, Huancavelica Department, Peru. Baumstarkite is triclinic and is the third naturally occurring modification of AgSbS<sub>2</sub> besides monoclinic miargyrite [1,2] and cubic cuboargyrite [3]. The composition is usually close to the ideal formula. However, several grains of baumstarkite show sharply defined and chemically strongly zoned lamellae with As substituting for Sb according to Ag<sub>3</sub>(Sb,As)<sub>2</sub>SbS<sub>6</sub> to a maximum As content of 11.5 wt.% (10.6 at.%). Baumstarkite is isotypic with aramayoite [4], ideally Ag<sub>3</sub>Sb<sub>2</sub>BiS<sub>6</sub>, solid solutions are in accordance with Ag<sub>3</sub>Sb<sub>2</sub>(Bi,Sb)S<sub>6</sub>.

The crystal-structure investigation of baumstarkite is based on single-crystal X-ray data:  $a = 7.766(2)$ ,  $b = 8.322(2)$ ,  $c = 8.814(2)$  Å,  $\alpha = 100.62(2)$ ,  $\beta = 104.03(2)$ ,  $\gamma = 90.22(2)^\circ$ ,  $Z = 2\{\text{Ag}_3\text{Sb}_3\text{S}_6\}$ , space group P $\bar{1}$ ;  $R1(F) = 0.057$ ,  $\omega R2(F^2) = 0.128$ . To facilitate the chemical separation of baumstarkite from aramayoite, and to enable a structural comparison with miargyrite the crystal structures of these two minerals were refined [samples of aramayoite came from the Mina Armonia, El Quevar, Argentina:  $a = 7.813(2)$ ,  $b = 8.268(2)$ ,  $c = 8.880(2)$  Å,  $\alpha = 100.32(2)$ ,  $\beta = 104.07(2)$ ,  $\gamma = 90.18(2)^\circ$ ,  $Z = 2\{\text{Ag}_3\text{Sb}_2\text{BiS}_6\}$ , space group P $\bar{1}$ ,  $R1(F) = 0.034$ ,  $\omega R2(F^2) = 0.084$ ; and the samples of miargyrite were those associated with baumstarkite type material,  $a = 12.862(3)$ ,  $b = 4.409(1)$ ,  $c = 13.218(3)$  Å,  $\beta = 98.48(2)^\circ$ ,  $Z = 8\{\text{AgSbS}_2\}$ , space group C2/c,  $R1(F) = 0.031$ ,  $\omega R2(F^2) = 0.082$ ]. Their space-group symmetries had to be revised, the refinements unambiguously showed that the three investigated minerals are centrosymmetric.

In baumstarkite, aramayoite, and miargyrite the surrounding of the Ag atoms is roughly characterized by the coordination numbers [2], [2+2], [4] or [2+2+2]. The gaps between the first and second coordination spheres differ but correlate with the shortest of the Ag–S bonds. Ag–S bond lengths start for Ag<sup>[2]</sup> atoms at 2.38 Å, for Ag<sup>[2+2]</sup>/Ag<sup>[4]</sup>/Ag<sup>[2+2+2]</sup> atoms between 2.51 and 2.54 Å. Additional S ligands exhibit a wide spread distribution of bond distances up to the same range as further cations. The S–Ag–S bond angles between the two nearest neighbours are 146° to 163°; but for the Ag<sub>2</sub><sup>[2]</sup> atom in miargyrite the bond angle is 180° due to the site symmetry  $\bar{1}$  of the central atom.

An analysis of the displacement parameters of the Ag atoms shows that their anisotropies correlate with the bond length distribution rather than with the S–Ag<sup>[2]</sup>–S bond angles.

The M = As, Sb, Bi atoms exhibit two different coordination figures in minerals with formula AgMS<sub>2</sub>. Most M atoms are [3+3] coordinated. The individual bond lengths M–S for the first coordination sphere are 2.44 to 2.54 Å (average bond lengths 2.463 to 2.492 Å). Next ligands have M–S > 3.09 Å. In baumstarkite and aramayoite, the positions M3 = Sb and Bi feature [2+2+2] coordination and a huge difference in the short M3–S bond lengths due to the predominant occupation by Sb and Bi atoms, respectively. The shortest and medium M3–S bond lengths in baumstarkite (~ 2.51 Å and 2.76 Å) are smaller than in aramayoite (~ 2.64 Å and 2.81 Å) to allow for the different size of the Sb and Bi atoms, respectively. Two further ligands are at a distance of ~ 3.0 Å indicating only moderate chemical interactions. It is worth mentioning that these fifth and sixth M3–S bond lengths are larger for baumstarkite than for aramayoite. This causes a stronger distortion for the M3S<sub>6</sub> polyhedron in baumstarkite (SbS<sub>6</sub>) than in aramayoite (BiS<sub>6</sub>). Probably steric reasons caused by the structure type are responsible for the reverse of the Bi–S / Sb–S bond lengths. In addition, the steric activity of the lone-pair electrons of the Sb<sup>3+</sup> atoms seems to be more pronounced as compared to Bi<sup>3+</sup> atoms.

The different size of the coordination of the M atoms reflects the chemical variability of baumstarkite and aramayoite. Despite ideal compositions of Ag<sub>3</sub>Sb<sub>3</sub>S<sub>6</sub> and Ag<sub>3</sub>Sb<sub>2</sub>BiS<sub>6</sub>, extensive substitution between As/Sb and Sb/Bi was found by chemical analysis. Due to the different size and geometry of the M1<sup>[3]</sup>S<sub>3</sub> and M2<sup>[3]</sup>S<sub>3</sub> pyramids as compared to the M3<sup>[2+2]</sup>S<sub>4</sub> polyhedra any significant As content substitutes for Sb at the M1 and M2 position whereas the M3 position is occupied either by Sb or by Bi atoms. Only small portions of Bi substituting for Sb at the M1 and M2 position in aramayoite were observed. Consequently the crystal chemical formula for the structure type is roughly Ag<sub>3</sub>(As,Sb)<sub>2</sub>(Sb,Bi)S<sub>3</sub>. The compositions of baumstarkite and aramayoite are described as Ag<sub>3</sub>(Sb,As)<sub>2</sub>SbS<sub>3</sub> and Ag<sub>3</sub>Sb<sub>2</sub>(Bi,Sb)S<sub>3</sub>, respectively. However, samples of baumstarkite with small contents of both As and Bi according to Ag<sub>3</sub>(Sb<sub>0.95</sub>As<sub>0.05</sub>)<sub>2</sub>(Sb<sub>0.9</sub>Bi<sub>0.1</sub>)S<sub>3</sub> were also detected.

Authors of the earlier papers dealing with X-ray work of AgMS<sub>2</sub> minerals have considered structural relations within this group of compounds and they mentioned the PbS type as the parental structure. Additionally, this structural relation is deduced from the phase transitions observed by the previous authors. Cubic high-temperature modifications of AgMS<sub>2</sub> are described as crystallizing in the PbS type; Ag and M atoms are octahedrally coordinated and occupy statistically one atomic site. The low-temperature modifications of these compounds exhibit a full order between Ag and M atoms accompanied by distinct coordinations. According to more detailed investigations of sulfosalts by [5] the type structure of the AgMS<sub>2</sub> minerals should be considered as derivatives of the SnS archetype to account for their special coordinations and the bond-strength distributions. Despite the derivation from one structure type, the linkage among the short connected atoms in the AgMS<sub>2</sub> minerals is quite different.

Considering only the nearest-neighbour environment the type structure of baumstarkite and aramayoite features zig-zag chains parallel to [010] with formula [AgMS<sub>2</sub>]. The MS<sub>3</sub> pyramids are corner-connected to the MS<sub>4</sub> polyhedra. All Ag<sup>[2]</sup>–S bonds are within the chains.

The chains are interlocked among each other by additional Ag–S and M–S bonds to layers parallel to (001). The Ag–S bonds between the layers are > 2.93 Å and they are responsible for only weak chemical interactions. Miargyrite is formed by (MS<sub>2</sub>) chains running parallel to [010] of corner connected SbS<sub>3</sub> pyramids. The chains are linked by Ag atoms. Comparing the cell volumes recalculated for one AgSbS<sub>2</sub> unit indicates distinct packing densities. Miargyrite (92.9 Å<sup>3</sup>) is less densely packed as compared to baumstarkite (90.3 Å<sup>3</sup>) and cubargyrite (90.2 Å<sup>3</sup>). It is worth mentioning that aramayoite has only a volume of 91.2 Å<sup>3</sup> for one AgSb<sup>2/3</sup>Bi<sup>1/3</sup>S<sub>2</sub> unit, i.e., less than miargyrite. Structural data of the further minerals of the AgMS<sub>2</sub> group need a re-investigation: smithite, M = As [6], trechmannite, M = As [7], and matildite, M = Bi [8].

## References

- [1] KNOWLES, C. R. (1964): A redetermination of miargyrite, AgSbS<sub>2</sub>. - Acta Cryst. 17, 847-851.
- [2] SMITH, J. V., PLUTH, J. J., & SHAO-XU HAN (1997): Crystal structure refinement of miargyrite, AgSbS<sub>2</sub>. Min. Mag. 61, 671-675.
- [3] WALENTA, K. (1998): Cuboargyrite, ein neues Silbermineral aus dem Schwarzwald. - Lapis, 23/11, 21-23.
- [4] MULLEN, D. J. E. & NOWACKI, W. (1974): The crystal structure of aramayoite Ag(Sb,Bi)S<sub>2</sub>. - Z. Krist. 139, 54-69.
- [5] MAKOVICKY, E. (1993): Rod-based sulphosalt structures derived from the SnS and PbS archetypes. - Europ. J. Min. 5, 545-591.
- [6] HELLNER, E. & BURZLAFF, H. (1964): Die Struktur des Smithits AgAsS<sub>2</sub>. Die Naturwissenschaften, 51, 53-54.
- [7] MATSUMOTO, T. & NOWACKI, W. (1969): The crystal structure of trechmannite, AgAsS<sub>2</sub>. - Z. Krist. 129, 163-177.
- [8] HARRIS, D. C. & THORPE, R. I. (1969): New observations on matildite. - Can. Min. 9, 655-662.

**KRISTALLCHEMISCHE ÜBERLEGUNGEN ZUR BESETZUNG "NICHTTETRAEDRISCHER"  
KATIONENPOSITIONEN DURCH SILIZIUM IM STRUKTURTYP TURMALIN**

von

**A. Ertl<sup>1</sup>, B. Marler<sup>2</sup> & F. Pertlik<sup>1</sup>**

<sup>1</sup>Institut für Mineralogie und Kristallographie  
Universität Wien. Geozentrum, Althanstrasse 14, A-1090 Wien  
<sup>2</sup>Institut für Geologie, Mineralogie und Geophysik  
Ruhr-Universität Bochum, D-44780 Bochum

In den letzten Dezenien wurden eine Reihe von Turmalinanalysen mit Werten für SiO<sub>2</sub> veröffentlicht, die einer Anzahl > 6 an Si-Atomen pro Formeleinheit entsprechen. Die zur Diskussion stehenden Turmaline sind überwiegend einer Reihe Olenit - Schörl - Dravit zuzuordnen [1,2]. Während eine Substitution des Si durch B im Si<sub>6</sub>O<sub>18</sub> - Ring in einem Al-reichen Turmalin nach der ersten experimentellen Belegung [3, 4] anhand von Strukturuntersuchungen an weiteren Individuen bestätigt wurde [5, 6], kann die Besetzung nichttetraedrisch koordinierter Kationenpositionen durch Si aufgrund fehlender experimenteller Beweise nur vermutet werden. Da sich derartige Substitutionen auch nur in engen Grenzen von wenigen Atomprozent bewegen können, erscheinen daher vorerst kristallchemische Überlegungen angebracht, um Vertreter für weitere Untersuchungen (z. B. SIMS - secondary ion mass spectrometry) möglichst effizient auswählen zu können. Ganz allgemein ist zu bemerken, daß Korrelationen zwischen dem Si-Gehalt der Turmaline und deren genetischen P-T-Bedingungen sowie dem Chemismus der Ausgangslithologien in groben Zügen nachweisbar sind [7].

Welche Atomlagen im Strukturtyp Turmalin könnte Si zusätzlich zur tetraedrisch vierkoordinierten Kationposition, zumindest teilweise, besetzen und somit andere Elemente substituieren? In keiner der bis heute mit modernen Methoden an Turmalinen durchgeföhrten Strukturanalysen wurden neben den aus der Formel XY<sub>3</sub>Z<sub>6</sub>(BO<sub>3</sub>)<sub>3</sub>(Si<sub>6</sub>O<sub>18</sub>)(O,OH)<sub>3</sub>(OH,F) resultierenden Atompositionen weitere mögliche Positionen beschrieben. Da aufgrund des geringen Streuvermögens sämtlicher am Aufbau einer Turmalinstruktur beteiligter Elemente die Lagen der Wasserstoffatome neben den übrigen Atomlagen heute experimentell zweifelsfrei belegbar sind, scheint auch eine statistische Besetzung einer weiteren zusätzlichen Atompositon ausschließbar zu sein. "Überschüssiges Silizium" kann somit nur in eine der übrigen Kationpositionen als Gastelement eintreten.

Ein Ersatz des planar dreikoordinierten Bors erscheint aufgrund der unterschiedlichen Elektronenkonfiguration der beiden Elemente höchst unwahrscheinlich. Desgleichen kann ein Ersatz der Elemente der neunkoordinierten X-Position wegen der Größe der mittleren < X-O > Abstände im Bereich von 2.67 Å bis 2.74 Å [1] kristallchemisch ausgeschlossen werden. Die vorliegende Diskussion soll sich daher auf zwei Atompositionen, Y und Z, beschränken.

Diese zwei, je oktaedrisch sechsgekoordinierten Atompositionen, Y und Z, unterscheiden sich prinzipiell durch die mittleren  $\text{YO}_6$ - und  $\text{ZO}_6$ -Abstände sowie durch die zugehörigen Volumina der Voronoi-Dirichlet-Polyeder. Die mittleren Abstände  $\text{ZO}_6 < 1.933 > \text{\AA}$  sind deutlich kleiner als die  $\text{YO}_6$ -Abstände  $< 2.033 > \text{\AA}$ , gleiches gilt für die oben erwähnten Volumina [1].

Die Substitution eines Kations an den Positionen Y oder Z durch Si-Atome bedarf jedoch noch weiterer kristallchemischer Überlegungen. Beide Positionen werden auch von O-Atomen koordiniert, die aufgrund von Bindungsstärkenberechnungen mögliche Donoratome für H-Brücken darstellen bzw. durch F-Atome ersetzt werden können. Für die Y-Position sind dies zwei, für die Z-Position ein koordinierendes Atom. Da die Substitution eines O-Atoms durch F in einem  $\text{SiO}_x$ -Polyeder in natürlich vorkommenden Verbindungen unwahrscheinlich erscheint, ergibt sich als Konsequenz: Si kann nur in Polyeder ohne koordinierendes F eintreten. Dies wird durch fluorarme bis fluorfreie Paragenesen begünstigt.

Die Substitution von Al in der Z-Position durch Si von mehr als 5 Atom % würde den mittleren  $\text{ZO}_6$ -Abstand in Al-reichen Turmalinen (Elbait - Liddicoatit - Olenit-Reihe) um ungefähr 2 % verkleinern. Das bedeutet, daß mittlere  $\text{AlO}_6$ -Abstände von  $< 1.90 > \text{\AA}$  ein Hinweis auf eine Substitution des Al durch Si sein können.

In Tabelle 1 sind ausgewählte Parameter von fünf Turmalinstrukturen zusammengestellt, deren Volumina für die Voronoi-Dirichlet-Polyeder der Z-Position Werte  $< 7.1 \text{ \AA}^3$  ergeben und die somit Anwärter für weitere Untersuchungen darstellen. Es sind dies Al-reiche Turmaline, unter denen sich allerdings auch Vertreter finden, in denen aufgrund borreicher Ausgangslithologien das Si in der Tetraederposition in geringem Ausmaß durch B ersetzt sein kann.

	1.)	2.)	3.)	4.)	5.)
a [ $\text{\AA}$ ]	15.967(2)	15.916(3)	15.875(3)	15.846(3)	15.838(1)
c [ $\text{\AA}$ ]	7.126(1)	7.130(1)	7.126(2)	7.119(1)	7.103(1)
V [ $\text{\AA}^3$ ]	1573.3	1564.2	1555.3	1548.1	1543.1
Y	$\text{Fe}^{2+}_{1.5}\text{Al}_{1.0}\text{Mn}^{2+}_{0.2}\text{Li}_{0.2}$	$\text{Al}_{1.5}\text{Mn}^{2+}_{0.9}\text{Li}_{0.4}\square_{0.2}$	$\text{Al}_{1.6}\text{Li}_{1.4}$	$\text{Al}_{1.5}\text{Li}_{1.0}\text{Mn}^{2+}_{0.4}$	$\text{Al}_{1.6}\text{Li}_{1.2}\text{Mn}^{2+}_{0.2}$
V <sub>y</sub> [ $\text{\AA}^3$ ]	8.846	8.747	8.625	7.992	8.435
Z	$\text{Al}_{5.9}\text{Fe}^{2+}_{0.1}$	$\text{Al}_{6.0}$	$\text{Al}_{6.0}$	$\text{Al}_{6.0}$	$\text{Al}_{6.0}$
V <sub>z</sub> [ $\text{\AA}^3$ ]	7.066	7.067	7.062	7.031	7.021
T	$\text{Si}_{6.0}$	$\text{Si}_{6.0}$	$\text{Si}_{6.0}$	$\text{Si}_{6.0}$	$\text{Si}_{6.0}$
V <sub>T</sub> [ $\text{\AA}^3$ ]	7.177	7.217	7.236	7.172	7.168
1.) Schörl, [11]	4.) Olenit - Elbait, [8]				
2.) Olenit (mit Mangan), [10]	5.) Olenit - Elbait, [9]				
3.) Olenit - Elbait, [12]					

Tabelle 1

Gitterkonstanten (Standardabweichungen in Klammern), Volumina der Elementarzellen und individuelle Besetzungen der Kationpositionen Y, Z (=Oktaeder) und T (=Tetraeder) von Al-reichen Turmalinen aus der Literatur. Weiters sind die Volumina der Voronoi-Dirichlet Polyeder für diese Positionen angeführt.

## Literatur

- [1] ZANG, J.W. (1994): Zur Kristallchemie der Turmaline. - Dissertation, Universität Mainz.
- [2] DYAR, M. D., TAYLOR, M. E., LUTZ, T. M., FRANCIS, C. A., GUIDOTTI, C. V & WISE, M. (1998): Inclusive chemical characterization of tourmaline: Mössbauer study of Fe valence and site occupancy. - Amer. Mineral. 83, 848-864.
- [3] ERTL, A., PERTLIK, F. & BERNHARDT, H. J. (1997): Investigations on olenite with excess boron from the Koralpe, Styria, Austria. - Österr. Akad. Wiss. Math.-naturw. Kl., Anzeiger 134, 3-10.
- [4] ERTL, A. & PERTLIK, F. (1999): Replacement of silicon in tourmaline- and mica-type structures. - Bull. Soc. Franç. Min. Crist. 11, 115.
- [5] TAGG, S. L., CHO, H., DYAR, M. D. & GREW, E. S. (1999): Tetrahedral boron in naturally occurring tourmaline. - Amer. Mineral. 84, 1451-1455.
- [6] HUGHES, J. M., ERTL, A., DYAR, M. D., GREW, E. S., SHEARER, C. K., YATES, M. G. & GUIDOTTI, C. V (2000): Tetrahedrally coordinated boron in a tourmaline: boron-rich olenite from Stoffhütte, Koralpe, Austria. - Canad. Mineral. 38, 861-868.
- [7] SCHUSTER, R. (persönliche Mitteilung).
- [8] GRICE, J. D. & SCOTT ERCIT, T. (1993): Ordering of Fe and Mg in the tourmaline crystal structure: the correct formula. - N. Jb. Miner., Abh. 165, 245-266.
- [9] DONNAY, G. & BARTON, R. Jr. (1972): Refinement of the crystal structure of elbaite and the mechanism of tourmaline solid solution. - Tschermaks Min. Petr. Mitt. 18, 273-286.
- [10] NUBER, B. & SCHMETZER, K. (1984): Structural refinement of tsilaisite (manganese tourmaline). - N. Jb. Miner. Mh. 301-304.
- [11] MACDONALD, D.J., HAWTHORNE, F.C. & GRICE, J.D. (1993): Foitite,  $\square[Fe_2^{2+}(Al,Fe^{3+})]Al_6Si_6O_{18}(BO_3)_3(OH)_4$ , a new alkali-deficient tourmaline: description and crystal structure. - Amer. Mineral. 78, 1299-1303.
- [12] NUBER, B. & SCHMETZER, K. (1981): Strukturverfeinerung von Liddicoatit. - N. Jb. Miner. Mh. 215-219.

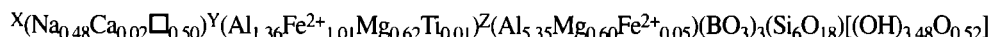
HELLBLAUE OLENIT-SCHÖRL-DRAVIT MISCHKRISTALLE VON EBERSDORF,  
NIEDERÖSTERREICH: CHEMISMUS UND KRISTALLSTRUKTUR

von

A. Ertl<sup>1</sup>, F. Pertlik<sup>1</sup> & H.-J. Bernhardt<sup>2</sup>

<sup>1</sup>Institut für Mineralogie und Kristallographie  
Universität Wien, Geozentrum, Althanstrasse 14, A-1090 Wien  
<sup>2</sup>Z. Elektronen-Mikrosonde der RUB  
Ruhr-Universität Bochum, D-44780 Bochum

Aus einem Pegmatit der Gföhler Einheit bei Ebersdorf, Niederösterreich, wurden stark zonierte Turmaline beschrieben, die einen dunkelbraunen Kern (Schörl-Dravit) und eine hellblaue Außenzone besitzen [1]. Chemische Analysen der Außenzone (Mikrosonden-Analysen) sind in Tabelle 1 wiedergegeben. Diese Analysen lassen sich unter Berücksichtigung des Strukturtyps zu folgender Formel verrechnen:



(mit X, Y und Z sind neun- (1x) und sechskoordinierte (2x) Kationpositionen ausgewiesen).

Die Analysenwerte für die Elemente K, Ba, Cr, Mn, Cu, Zn sowie F und Cl skalieren in Größenordnungen um die Nachweisgrenze. Da F- und Li-Gehalte in Al-reichen Turmalinen positiv korrelieren und Mg-reiche Turmaline generell einen unbedeutenden Li-Gehalt aufweisen, ist in vorliegendem Turmalin nur ein vernachlässigbarer Li-Gehalt zu erwarten. Für Eisen wurde die Wertigkeitsstufe 2+ angenommen, der Gehalt an B<sub>2</sub>O<sub>3</sub> und H<sub>2</sub>O nicht bestimmt. Der Mg Anteil an der Z Position wurde anhand der Abbildung 3 aus [2] in Korrelation mit dem Fe<sup>2+</sup> Anteil an der Y Position ermittelt, B<sub>2</sub>O<sub>3</sub> mit 3.0 in der Formelberechnung berücksichtigt und H<sub>2</sub>O als Differenz auf 100 ausgewiesen.

Eine Strukturanalyse des hellblauen Turmalins (Außenzone) mit  $a = 15.935(3)$  Å und  $c = 7.164(2)$  Å konvergierte für 3111 Intensitäten ( $h, k, l$  und  $-h, -k, -l$  nicht gemittelt) und  $2\theta_{\max} = 90^\circ$  bei R (konventionell): 0.033 für 97 variable Parameter. Ausgewählte interatomare Abstände sind in Tabelle 2 angeführt.

Generell wurden die Besetzungsfaktoren für die Atompositionen X, Y und Z zusammen mit den jeweiligen Ortsparametern verfeinert und so rechnerisch folgende Besetzungen ermittelt: Position X ist ~50 % mit Na besetzt (~50 %  $\square$ ), Y zu ~70 % mit (Al+Mg) und zu ~30 % mit Fe, Z zu 100 % mit (Al+Mg). Eine Differenzierung zwischen Al und Mg war aufgrund des praktisch gleichen Streuvermögens dieser Atome nicht möglich.

Eine Verfeinerung Si  $\leftrightarrow$  B an der Tetraeder-Position ergab keine signifikante Unterbesetzung, bezogen auf das Streuvermögen eines Si-Atoms. Des weiteren entspricht der mittlere  $\langle \text{Si}-\text{O} \rangle$  Abstand von 1.619 Å einer Vollbesetzung dieser Position mit Si. Die Mikrosondenanalysen (Si: 6.00 apfu) weisen ebenfalls darauf hin, daß die Tetraeder-Position vollständig mit Si besetzt sein muß. Somit sind in diesem Turmalin im Gegensatz zu Olenit-Elbait Mischkristallen, die immer einen gewissen Anteil von  $^{14}\text{B}$  aufweisen, sowohl signifikante Anteile von  $^{14}\text{B}$ , wie auch von  $^{14}\text{Al}$  auszuschließen. [3,4].

Die Alkalidefizienz des untersuchten Turmalins (Position X ~ 50 % □) und der mittlere  $\langle \text{X}-\text{O} \rangle$  Abstand mit 2.704 Å sind mit einem als Schörl bezeichneten Turmalin aus dem vulkanischen Tuff der Jack Creek Lagerstätte direkt vergleichbar [5], wobei an letzterem bei gleicher Besetzung der X-Position ein mittlerer  $\langle \text{X}-\text{O} \rangle$  Abstand von 2.713 Å bestimmt wurde. Die anhand letzterer Turmalinstruktur im Vergleich mit etwa einem Dutzend Literaturdaten ermittelte Korrelation zwischen dem  $\langle \text{X}-\text{O} \rangle$  Abstand (= Größe des  $\text{XO}_9$ -Polyeders) und der Verzerrung des  $\text{Si}_6\text{O}_{18}$ -Ringes stimmt innerhalb des einfachen Fehlers mit den vorliegenden Ergebnissen überein. Bei relativ großen  $\text{XO}_9$ -Polyedern weisen alkalidefizierte Turmaline mit geringem Ca-Gehalt den geringsten Verzerrungsgrad des Tetraederringes auf [5]. Der  $\langle \text{Z}-\text{O} \rangle$  Abstand von 1.922 Å ist deutlich größer als bei Turmalinen, die an der Z-Position nur mit Al besetzt sind (~1.90 Å). Diese Vergrößerung wird hauptsächlich durch Anteile von Mg an dieser Position hervorgerufen.

Anhand der an fünfzig Turmalinen unterschiedlicher Genese bestimmten Kristallstruktur und deren chemischer Zusammensetzung konnte PIECZKA [6] eine einfache Korrelation zwischen mittlerer Größe der oktaedrisch koordinierten Kationpolyeder und Chemismus ableiten. Die mittleren Abstände  $\langle \text{Y}-\text{O} \rangle$  mit 2.012 Å und  $\langle \text{Z}-\text{O} \rangle$  mit 1.922 Å, (Maß für die Größe der Kationpolyeder) sowie die für diese Kationpositionen berechneten Elektronendichten [Chemismus ausgedrückt als Verhältnis (Al+Mg)/Fe] bestimmt am Turmalin von Ebersdorf, stehen in guter Übereinstimmung zu dieser Korrelation.

Unter Berücksichtigung der Strukturanalyse und der Mikrosondenanalysen ergibt sich für den untersuchten Turmalin ein Olenit-Anteil von ~50 %, nebst ~30 % Schörl- und ~20 % Dravit-Anteilen.

	A	B
<b>Na<sub>2</sub>O</b>	1.49 (4)	1.50
<b>MgO</b>	5.14 (15)	5.00
<b>CaO</b>	0.1 (2)	0.11
<b>Al<sub>2</sub>O<sub>3</sub></b>	35.88 (12)	35.24
<b>SiO<sub>2</sub></b>	36.58 (14)	36.58
<b>TiO<sub>2</sub></b>	0.08 (4)	0.05
<b>FeO</b>	7.72 (16)	7.72
<b>B<sub>2</sub>O<sub>3</sub></b>	n. b.	10.62
<b>H<sub>2</sub>O</b>	n. b.	3.18
<b>Σ</b>		100.00

*Tabelle 1*

Analysenwerte für den hellblauen Turmalin (Außenzone) mit Standardabweichungen in runden Klammern.  
A: Gew. % (Analyse); B: Gew. % (der angegebenen Formel entsprechend). Analytiker: H.-J. Bernhardt.

X-	O(1) = 2.519(2); 3x	Z	O(5) = 1.883(1)	Si-	O(5) = 1.608(1)
	O(4) = 2.761(1); 3x		O(6) = 1.891(1)		O(6) = 1.609(1)
	O(2) = 2.832(2); 3x		O(7) = 1.891(1)		O(2) = 1.622(1)
Y-	O(1) = 1.975(1); 2x		O(7') = 1.923(1)		O(4) = 1.636(1)
	O(5) = 2.006(1); 2x		O(6') = 1.954(1)	B-	O(1) = 1.364(2)
	O(3) = 2.114(1)		O(3) = 1.990(1)		O(7) = 1.379(1); 2x
	O,F = 1.995(1)				

*Tabelle 2*

*Ausgewählte interatomare Abstände in Å. Standardabweichungen in runden Klammern.*

### Literatur

- [1] ERTL, A. (1995): Elbait, Olenit, Dravit-Buergerit-Mischkristalle, Dravit, Uvit und ein neuer Al-Turmalin(?) von österreichischen Fundstellen. - Mitt. Österr. Miner. Ges., 140, 55-72.
- [2] BLOODAXE, E. S., HUGHES, J. M., DYAR, M. D., GREW, E. S. & GUIDOTTI, C. V. (1999): Linking structure and chemistry in the schorl-dravite series. - Amer. Min. 84, 922-928.
- [3] ERTL, A., PERTLIK, F. & BERNHARDT, H.-J. (1997): Investigations on olenite with excess boron from the Koralpe, Styria, Austria. - Österr. Akad. Wiss., Math.-Naturw. Kl., Abt. I, Anzeiger, 134, 3-10.
- [4] TAGG, S. L., CHO, H., DYAR, M. D. & GREW, E. S. (1999): Tetrahedral boron in naturally occurring tourmaline. - Amer. Min., 84, 1451-1455.
- [5] FOIT, F. F. Jr. (1989): Crystal chemistry of alkali-deficient schorl and tourmaline structural relationships. Amer. Min. 74, 422-431.
- [6] PIECZKA, A. (1997): Statistical interpretation of structural parameters of tourmalines: iron ordering in octahedral sites. - "TOURMALINE 1977", Int. Symp. on Tourmaline, Abstracts 70-71.

THE MECHANISM OF DEVELOPMENT OF A MANTLE SHEAR ZONE:  
EVIDENCE FROM A XENOLITH  
(SZETBÉKKALLA, BAKONY-BALATON HIGHLAND, HUNGARY)

by

Gy. Falus<sup>1</sup>, H.L.M. van Roermund<sup>2</sup>, M.R. Drury<sup>2</sup>, Cs. Szabó<sup>1</sup> & Á. Gál<sup>3</sup>

<sup>1</sup>Department of Petrology and Geochemistry

Lithosphere Research Group, Eötvös University, Múzeum hrt. 4/a, 1088 Budapest, Hungary

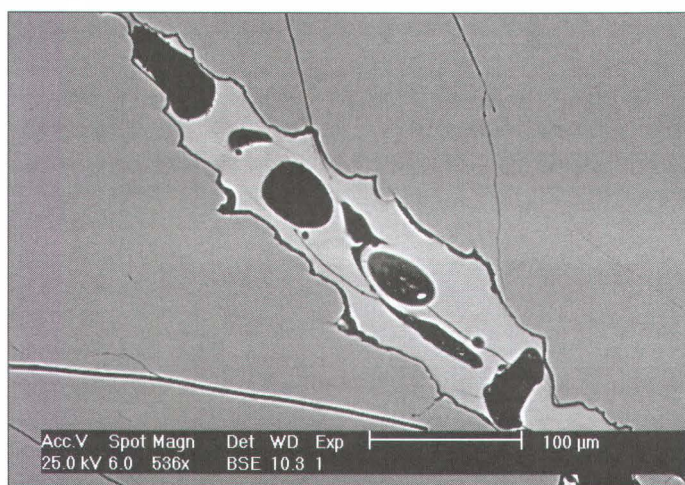
<sup>2</sup>Department of Structural Geology

Faculty of Earth Sciences, Utrecht University, Budapestlaan 4, 3584 CD Utrecht, Netherlands

<sup>3</sup>Department of Mineralogy and Petrology

Babeş-Bolyai University, Cluj-Napoca (UBB) str., Romania

A strongly deformed composite peridotite-pyroxenite mantle xenolith from the Pannonian Basin has been studied with optical microscope, SEM and electron microprobe to describe melt topology and pores pace partially filled with three immiscible fluids (silicate glass + CO<sub>2</sub> + sulfide). The two rock types (peridotite and pyroxenite) build up the xenolith approximately in the same volume ratio. Large amount of euheadral neoblasts related to the infiltrating fluid was also found. A narrow (300 - 600 mm) shear zone, running along the boundary of the two rock types and then continuing in the peridotite, can be observed even in the hand specimen. The peridotite part of the xenolith is a partially recrystallized porphyroclastic spinel lherzolite. Pods (d ~ 100 mm) of homogenous glass were detected, mostly in close relation with large porphyroblast (and porphyroblasts).



Large empty bubbles in dimensions of 30 - 50 mm possibly representing the exsolved vapor phase from the melt are observed in these pockets (Fig. 1).

Fig. 1

Some neoblasts are inbedded or next to the interstitial glass that has the same composition as those in the larger melt pockets. Neoblasts here are dominantly euhedral in shape (Fig. 2).

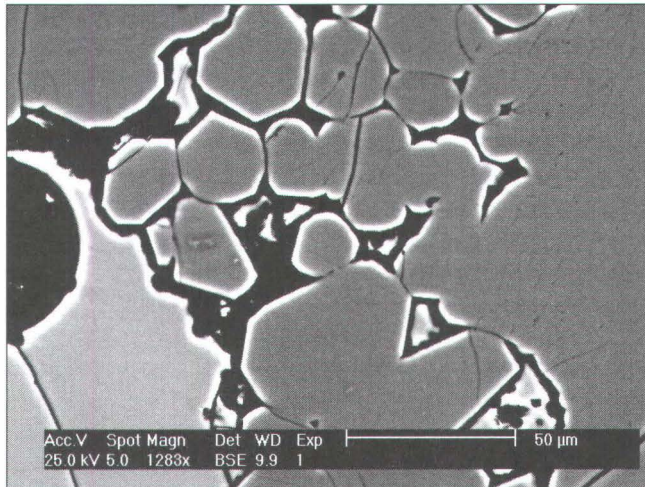


Fig. 2

Geothermometer of BREY & KÖHLER (1990) were used to estimate the changes in conditions during the deformation and recrystallization of porphyroclasts into neoblasts associated with the melt infiltration. The data suggest that an increase of temperature occurred in a range of 90 - 100°C during the recrystallization from 1090 to 1180°C. Thermometric calculations for co-existing liquid and clinopyroxene were performed to estimate the equilibrium temperature of infiltrating silicate melt using method of PUTIRKA et al. (1996). The results are in good agreement with the temperature estimates derived from the previous geothermometer showing an equilibrium temperature of  $1082 \pm 27^\circ\text{C}$ .

Dimensions of olivine tablet grains, grown in deformed porphyroclasts, were used to estimate the approximate period of annealing and tablet grain growth. Starting with temperatures of around 1100°C, cooling rates in the range of 1 - 100°C/Ma and an average tablet grain size of 300 mm, the annealing period lasted for 1 - 1000 years before the sampling by the host basalt. This suggests that the tectonic event (presumably one or more earthquakes) that developed the shear zone in the mantle is in close association with the alkali basaltic volcanism (WILSHIRE & KIRBY, 1989) which sampled the mantle rock.

Large volume of infiltrating fluids (vapor saturated silicate melt) was stable in the mantle and led to brittle/plastic deformation. As a consequence of its different softening effect in the two rock types, the fluids possibly led to strain localization and the formation of the shear zone observed in the sample. Furthermore, the exsolution of CO<sub>2</sub> from the evolving melt could have enhanced the localization even more drastically.

## References

- [1] BREY, G. P. & KÖHLER, T. (1990): Geothermobarometry in four-phase Iherzolites II. New thermobarometers and practical assessment of existing thermobarometers. - *J. Petrol.*, 31, 1353-1378.
- [2] PUTIRKA, K., JOHNSON, M., KINZLER, R., LONGHI, J. & WALKER, D. (1996): Thermobarometry of mafic igneous rocks on clinopyroxene-liquid equilibria, 0-30 kbar. - *Contrib. Mineral. Perol.*, 123, 92-108.
- [3] WILSHIRE, H. G. & KIRBY, S. H. (1989): Dikes, joints and faults in the upper mantle. - *Tectonophysics*, 161, 23-31.

**TI-BEARING ANDRADITE WITH PREHNITE AND EPIDOTE FROM THE  
MALÁ FATRA GRANODIORITE AND TONALITE (WESTERN CARPATHIANS)**

by

**S.W. Faryad<sup>1</sup> & I. Dianška<sup>2</sup>**

<sup>1</sup>Department of Geology and Mineralogy  
Technical University Košice, Letná 9, 04011 Košice, Slovakia  
<sup>2</sup>Mierová 16, Rožňava

Calc-silicate minerals with chlorite, muscovite occur in the Malá Fatra granodiorite and tonalite. The main constituents of the Malá Fatra rocks are plagioclase, quartz, biotite and K-feldspar. Accessory phases are epidote, garnet, prehnite, white mica, calcite, apatite and zircon. Some samples may additionally contain amphibole. Plagioclase is usually replaced by fine-grained white mica and epidote, especially in the more calcic cores. Biotite is altered to chlorite and partly contains epidote, titanite, garnet and prehnite. Garnet is present in most samples and, additional to chlorite and epidote, is often accompanied by titanite, prehnite and locally by K-feldspar (adularia), muscovite and calcite. In most cases garnet forms thin strips, lenses, pods (0.1 - 0.6 mm in length) or bulbous grains of near colorless or pale brown shade. The garnet is slightly anisotropic and its elongated crystals follow cleavage in biotite. Many of the chlorite and biotite contain lenses of prehnite, epidote and titanite. In one case epidote overgrowing and rimming garnet was found. Accessory hornblende is partly replaced by chlorite, epidote and titanite.

The garnet composition varies in the range of 32 - 42 mol % grossularite, 50 - 60 % andradite, 1 - 10 % schorlomite, 0 - 7 % morimotoite, 0.5 - 2.5 % spessartine, 0 - 1 % pyrope, 0 - 2 almandine. The low analysis total < 100 wt % and the Si deficient in mineral formulae suggest the presence of H<sub>2</sub>O in garnet. The garnet exhibits irregular zonation, but generally grossularite increase and andradite and schorlomite + morimotoite decrease toward rim. Some garnet may have three zones, where cores and rims are relatively poor in Ti. Some small domains in the second zone correspond to Fe-rich and Ti-poor garnet with up to 74 mol % andradite content. Correlation of major element contents in garnet indicates exchange of TiSi<sub>1.1</sub>, Fe<sup>3+</sup>Al<sub>1.1</sub> and TiFe<sup>2+</sup>Al<sub>2</sub>.

Epidote is rich in Fe<sup>3+</sup> with very small amounts of zoisite ( $100[(-2+Al_{tot})]/(-2+Al_{tot}+Fe_{tot})] = 3 - 17\%$ ). The high zoisite content come from epidote located in plagioclase. Accessory brown allanite is also present. X<sub>Fe<sup>3+</sup></sub> values of prehnite range between 0.3 - 1.0. The Si values of phengite are in the range of 3.15 - 3.29 a.p.f.u. based on 11 oxygens.

Textural relations from the Malá Fatra granodiorite and tonalite indicate that metamorphic minerals were probably formed by both hydrothermal alteration and metamorphism. Zeolite forming drusy veins in tectonic zone and the occurrence of white mica and epidote in shear cracks suggest their formation after cooling of intrusive body. Adularia and calcite forming veinlets that cross cut other matrix minerals in granodiorite and tonalite also belong to later formed phases in the rocks. Relation of prehnite and some epidotes and chlorites to hydrothermal alteration is probable, but rule of metamorphism on these minerals as well on grandite is not well clear. Mineral assemblages and thermodynamic calculation indicate temperature less than 350°C for the calc-silicates formation.

PRE-ALPINE ECLOGITES AND GARNET-PYROXENE-BEARING METABASITES IN THE  
AUSTROALPINE UNITS OF THE EASTERN ALPS AND WESTERN CARPATHIANS

by

S. W. Faryad<sup>1</sup>, G. Hoinkes<sup>2</sup> & P. Ivan<sup>3</sup>

<sup>1</sup>Department of Geology and Mineralogy  
Technical University Košice, Letná 9, 04011 Košice, Slovakia

<sup>2</sup>Institute of Mineralogy and Petrology  
Universität Graz, Universitätsplatz 2, A-8010 Graz

<sup>3</sup>Department of Geochemistry  
Comenius University, Mlynská dolina 842 15 Bratislava, Slovak Republic

The Austroalpine tectonic units in the Eastern Alps and the Western Carpathians basement rocks are indicative of similar metamorphic evolution during Pre-Alpine history. The classical Variscan metamorphism of medium-pressure conditions was followed by Upper Carboniferous granite intrusions. According to petrological and geochronological data, basement rocks from both area record early Variscan or Pre-Variscan high-grade, mostly high-pressure metamorphism. Because of multiply deformation and recrystallization during Variscan and Alpine metamorphic events, evidences of earlier metamorphic processes are only locally preserved. Some metabasites may contain lens-shaped enclaves (1 - xx m in length) of massive eclogites or high-pressure amphibolites that were spared from deformation and hydration.

In the Eastern Alps, amphibolized eclogites occur at Hochgrößen massif, east of the Tauern Window (RICHTER, 1973). Together with host serpentines, they are part of the Speik Complex in the Austroalpine basement nappes. Fresh eclogites are rare and contain omphacite with a maximum of 39 mol % jadeite content, garnet ( $Py_{15-19}$ ) and amphibole. An average temperature of 700°C was obtained for eclogite facies metamorphism using garnet-pyroxene thermometries. A minimum pressure of 1.5 GPa is indicated by the maximum jadeite content in omphacite. Thermobarometric calculations for amphibole with coexisting omphacite and garnet give pressures of 1.8 GPa at 700°C. Retrogression to ca 0.6 - 0.8 GPa at 590 - 640°C is documented by the equilibrium assemblage of Na-poor clinopyroxene, albite, amphibole and zoisite in the symplectites.  $^{40}Ar/^{39}Ar$  radiometric dating of edenitic amphibole in textural equilibrium with omphacite gave a plateau age of  $397.3 \pm 7.8$  Ma (FARYAD et al., 2001), and probably indicates retrograde cooling through the closure temperature for amphibole ( $\sim 500^\circ C$ ). The age of the HP metamorphism thus must be pre-Variscan and points to one of the earliest metamorphic events in the Austroalpine nappes known to date.

Several petrological works from the Western Carpathians (HOVORKA & MÉRES, 1990; JANAK et al., 1996) indicated evidences of granulite or eclogite facies metamorphism. Similar rocks were recently found in the eastern part of the western Carpathians from Branisko Mts. (MÉRES et al., 2000). Detail mineralogy of these rocks indicates high-grade metamorphism, appropriate to triple point of amphibolite - eclogite - granulite facies boundaries. The rocks are derived from MORB type basalts and contain Ca- and Mg- rich garnet ( $Grs_{20-32}$ ,  $Py_{18-20}$ ), diopsidic clinopyroxene and plagioclase ( $An_{10-40}$ ). Garnet encloses clinopyroxene, plagioclase, ilmenite and K-feldspar. P-T conditions of  $750^{\circ}\text{C}$  and 13 - 14 kbar were estimated using various exchange thermometries and equilibrium reactions. Such pressure conditions are assumed also by accessory phengite ( $Si = 3.38$ ) with K-feldspar in the matrix. Besides inclusions in garnet, pyroxene forms symplectites with plagioclase and amphibole in the matrix. The high-grade metamorphism was followed by amphibolite facies metamorphism at  $650^{\circ}\text{C}$  and 7 - 8 kbar. Textural relations in metabasites with combination of geochronological data from other basement rocks suggest long-termmed and polyphase evolution of the Western Carpathians basement during Pre-Alpine history.

The presented data from the Eastern Alps and Western Carpathians suggest subduction of continental and oceanic elements during Silurian-Devonian and continent-continent collision between Gondwana-derived continental elements and northern portion of Central European Variscan Belt and Fennosarmatia (VON RAUMER, 1998). Really eclogites, derived from ocean-floor basalts, occur in the Esatern Alps, while the high-pressure amphibolites transitioning to eclogites were formed in the Western Carpathians.

## References

- FARYAD, S. W., HOINKES, G., MELCHER, F., PUHL, J., MEISEL, T. & FRANK, W. (2001): Eclogites from the Speik Complex at Hochgrößen; middle Austroalpine unit, Eastern Alps. - Mineralogy and Petrology (in print).
- HOVORKA, D. & MÉRES, Š. (1990): Clinopyroxene-garnet metabasites from the Tribeč Mts. (Central Slovakia). - Mineralia Slovaca, 22, 533-538.
- JANAK, M., O'BRIEN, P. J., HURAI, V & REUTEL, CH. (1996): Metamorphic evolution and fluid composition of garnet-clinopyroxene amphibolites from the Western Tatra Mts., Western Carpathians. - Lithos, 39, 57-79.
- MÉRES, Š., IVAN, P. & HOVORKA, D. (2000): Garnet-pyroxene metabasite and antigorite serpentinites – evidence of leptino-amphibolite complex in the Branisko Mts. (Tatric unit, central estern Carpathians). - Mineralia Slovaca, 32, 479-486.
- RICHTER, R. (1973): Vergleichende Untersuchungen an ostalpinen Eklogiten. - Tschermaks Min Petr Mitt 19: 1-50.
- VON RAUMER, J. F. (1998): The Palaeozoic evolution of the Alps: from Gondwana to Pangea. - Geol. Rundschau 87: 407-435.

**SULFIDISCHE UND OXIDISCHE ZN-PB VERERZUNGEN DER LAGERSTÄTTE  
CHO-DIEN (VIETNAM) – GENETISCHE ASPEKTE**

von

**B. Fojt<sup>1</sup> & I. Kušnir<sup>2</sup>**

<sup>1</sup>Lehrstuhl für Mineralogie, Petrologie und Geochemie

Masaryk Universität Brno, Kotlářská 2, 611 37 Brno, Tschechische Republik

<sup>2</sup>22, Avenue de Guyenne, 92 160 Antony, Frankreich

Der nördliche Teil Vietnams ist durch die Anwesenheit von mehr als 300 Erzvorkommen gekennzeichnet. Das Lagerstätten-führende Gebiet Cho-Dien befindet sich ungefähr 300 km NO von Ha-noi und ist Bestandteil der gefalteten Viet-Bac Region. Diese Region liegt zwischen dem Yang-Tze im Norden und Indochina Kratons im Süden. In diesem Gebiet treten Metasedimente des Mitteldevons (überwiegend niedrig metamorphe Kalksteine und Phyllite) auf. Granitoid-Massiv (Pia-Biok) ist von Cho-Dien 11 km östlich entfernt. Die Metamorphose und Verfaltung gehören in die Untere Trias; weitere tektono-metamorphe Aktivitäten wurden im jüngeren Mezozoikum gefunden [1]. Das gesamte Gebiet (ungefähr 30 km<sup>2</sup>) wurde durch subparallele Bruchstrukturen in NNO-SSW Richtung mit Längen von 300 bis 1000 m zerlegt. Die darin auftretenden Vererzungen können in folgende Typen gegliedert werden:

**A. Primäre Erze:**

1. Stratiforme Sulfid-führende Lager
2. Sulfidische Gänge (mit der gleichen stofflichen Zusammensetzung wie A.I), die die stratiforme Lager durchdringen. Die Gänge sind ohne jede ökonomische Bedeutung.

**B. Sekundäre Erze:**

1. In-situ verwitterte Lager (bedeckt A.I)
2. Verwitterungsprodukte in karstigen Erdfällen (sog.Amas)
- 3.Umgelagerte Verwitterungsprodukte (= deluviale Anreicherungen)

Die Erze betragen: A: ~ 1.2 Mil. t Zn+Pb (10 - 30 % Zn, 0.5 - 6 % Pb)

B: ~ 4.5 Mil. t Zn+Pb (10 - 15 % Zn, < 0.5 % Pb)

Die reichsten Erze (mit 25 - 48 % Zn) wurden bereits in den Jahren vor dem II.Weltkrieg durch französische Aktivitäten abgebaut.

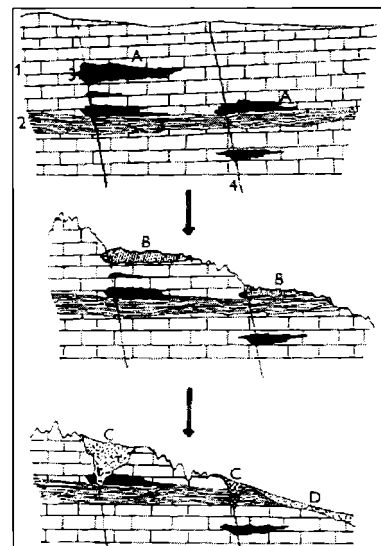
Die primäre, stratiforme Vererzung (A.I) bildet mehrere massive linsenförmige Lager mit Mächtigkeiten von 20 cm bis 3 m, die vorwiegend im Hangenden der Bruchstrukturen auftreten. Um die massiven Erze verteilt treten vereinzelt Sulfide auf, entweder fein verteilt oder in Form unregelmässig gebänderter Gefüge. Die Nebengesteine dieser Vererzungen sind silifiziert, chloritisiert und dolomitisiert. Als Erzmineralien treten am häufigsten Sphalerit und Galenit, in manchen Erzlinsen auch Pyrit und Arsenopyrit auf.

Daneben finden sich weitere Erzmineralien, die aber nur untergeordnet und daher akzessorische Bestandteile sind (Chalkopyrit, Pyrrhotin, Pyrargyrit, Canfieldit, Ag-Tetraedrit, Cassiterit, Magnetit). Als Nichterze wurden vorwiegend Quarz, Calcit, Karbonate der Dolomit-Reihe, manchmal auch Siderit, Chlorit und Muskovit beobachtet. Sphalerit enthält 0.8 - 12 % Fe, 0.25 - 0.62 % Cd, 0.1 - 1.1 % Mn und in Spuren auch Sn, In, Ag. Der Silbergehalt des Galenits schwankt zwischen 0.08 - 0.45 Gew.% - je nach der Menge der mikroskopisch erkennbaren Einschlüsse von Sulphosalzen. Bei unterschiedlichen Gehalten an Co+Ni im Pyrit (Variation von 3 bis 187 ppm) bleibt das Verhältnis von 1:1 zwischen diesen beiden Elementen stets gleich und weist somit einen linearen Trend aus. Die Arsenopyrit-Geothermometrie weist eine Kristallisationstemperatur zwischen 270 - 300°C aus, die Sphalerit-Geobarometrie einen Druck zwischen 0.236 - 0.252 GPa. Diese Daten entsprechen einer ursprünglichen Tiefe der Mineralisation von ungefähr 6 km. Der an Pyrrhotin bestimmte Wert  $N_{FeS} = 0.92 - 0.94$  zeugt von Verwachsungen von monoklinem mit hexagonalen Pyrrhotin. Die isotopische Zusammensetzung des Schwefels der Sulfide bewegt sich zwischen -5.9 bis +1.2 ‰  $\delta^{34}S$  (CDT), und entspricht demgemäß näherungsweise dem Wert für abysalen Schwefel. Aus den isotopischen Daten (der Paare Sphalerit-Galenit, Sphalerit-Pyrit und Galenit-Pyrit) errechnet sich für die stratiforme Lager eine Kristallisationstemperatur im Bereich zwischen 325 - 335°C und für die Gänge zwischen 216 - 290°C. Isotopische Pb-Werte ( $^{206}Pb/^{204}Pb : ^{207}Pb/^{204}Pb$ ) sind ± entlang der Kurve von Blei orogenen Ursprungs angehäuft.

Obwohl man die Genese der primären Erze von Cho-Dien rein phenomenologisch auch auf andere Genesemodelle zurückführen könnte (wie z.B. auf den "Mississippi Valley type" oder den "Sediment-hosted massive sulphide type"), korrelieren die oben angeführten Daten mit einer Vererzung, die mit der klassischen hydrothermalen Entstehung erklärt werden kann. Wie schon im Jahre 1965 bekannt wurde [2], sind die sulphidischen Erzvorkommen rund um die Granitoide der Massive Pia-Ouac, Pia-Bioc, Tam-Tao und Cho-Chu versammelt. Alterbestimmungen an Biotiten der Granite von Pia-Bioc führen zu Werten, die zwischen 210 und 271 Ma (K/Ar Methode) schwanken, während an Galenit von Cho-Dien (Pb/Pb Methode) ein Alter von ~ 230 Ma [3] ermittelt wurde.

**Fig. 1**  
*Idealisiertes Schema der Entstehung der Verwitterungslagerstätten der Zn-Pb Erze im Cho-Dien Revier.*

1. Kristalline Kalksteine
  2. Calcitische Phyllit
  3. Erzkörper
  4. Hauptbrüche.
- A. Primäres Erz  
 B. Oxidisches Erz der "in situ" verwitterten Sulphiden  
 C. Erz in den karstigen Erdfällen (sog. Armas)  
 D. Kataklastische Anhäufungen in den deluvialen Sedimenten.



In den sekundären Erzen (B) treten überwiegend folgende Mineralien auf: Hemimorphit, Hydrozinkit, Smithsonit, Pyrolusit, Goethit und andere Oxihydroxide des Eisens (sog.Limonit). Akzessorien sind: Saukonit, Beudantit, Halloysit, Anglesit, Cerusit, Pyromorfit, Vanadinit, Arseniosiderit, Farrnakosiderit, Skorodit. Cuprit, ged.Kupfer, Chalkosin und Greenockit. Erz-Typus B1 hat wegen seiner starken Anreicherung von Hydrozinkit und Smithsonit ökonomische Bedeutung. Das Alter der Verkarstung und die mit ihr zusammenhängende Verwitterung der Sulfidlagerstätten, konnte nicht eindeutig bestimmt werden. Die subtropischen Bedingungen geben die Möglichkeiten den weitgehenden Verwitterungsprozessen zu gleicher Zeit.

### Literatur

- [1] FEDIUK, F. & KUŚNIR, I (1967): Groupe de gites polymétalliques de Cho-Dien en République Démocratique du Vietnam. - Acta Univ.Carol., Geologica, I: 29-58. Praha.
- [2] FEDIUK, F., FOJT, B. & KUŚNIR, I. (1965): K probleme zonalnosti na primere rudnych mestorozdenij severovastocnoj casti Vietnamu. - Symp. Problems of Postmagmatic Ore Deposition, II: 171 - 174. Prague.
- [3] NHAN, V. N. (1988): Formacje endogenicznych zloz i prejawow okruszcowania w Wietnamie. - Zes.Nauk. AGH, 38, 1161: 1-134. Kraków.

**HISTORICAL BUILDING MATERIALS IN SOUTH TYROL/ITALY –  
A MINERALOGICAL STUDY UNDER THE ASPECTS OF MONUMENT CONSERVATION**

by

**C. Franzen & P. W. Mirwald**

Institute of Mineralogy and Petrography  
University of Innsbruck, Innrain 52, A-6020 Innsbruck

A combined study on the material inventory of churches in South Tyrol/Italy as well as on the properties and weathering behaviour of prominent building materials of that area was conducted. The first part of the study was concerned with mapping on a regional scale aiming at the documentation of historic building materials and a survey of its distribution. The project comprises the following South Tyrolian areas: Vinschgau, Etsch Valley, Eissack Valley, Pusteria Valley and Unterland.

In order to document all information in one map a spectrum of symbols has been developed which allows to distinguish the kind of constructions (church, chapel, house, castle, memorial, tombstone, wall etc.) architectural elements (base, wall, tower, roof, door, window, decoration elements etc.), and materials (stone, brick, mortar, masonry etc.). This scheme provides a comprehensive survey of relevant material data useable as primary information source for conservation and restoration concepts.

The results of this mapping survey suggest a very close correlation between stone materials employed for historic objects and the local geology. This applies particularly for more remote valley areas. Petrographic mapping reveals in addition in many cases a close correlation between the functional construction task and the choice of materials. This fact is additionally constrained by the local availability of materials. A simplified map is given in Fig. 1.

The data allow to distinguish five stone provinces:

- 1) Northern granitic province (Eissack - Pusteria Valley). - Main building material in that area is the permian Brixen Granite. The middle to fine grained Biotite Granite exhibits seldom dark inclusions. A weak foliation is often the only difference to the also used Granite-Gneiss.
- 2) Sandstone province – There the Gröden Sandstone as the important building and architectural stone in the Etsch valley area [1] (Bozen-Meran) exhibits an interesting mineral indicator for weathering: Dawsonite, a fibrous carbonate ( $\text{NaAl}_2[(\text{OH})_2/\text{CO}_3]$ ), to be found frequently in pristine Gröden sandstone decreases in terms of building stone weathering and disappear due to weathering impact [2].
- 3) Porphyry province – The Bozen Quartzporphyry, recently gained reputation as pavement material, was often used in walls, but examples for the use as architectural elements such as columns are also known.

4) Marble province – The Laas Marble as very decorative material a far exported material for architectural use. As general building material it can be found in the middle Vinschgau Area [3].  
 5) Gneiss province - In the upper Vinschgau Area most churches exhibit various Gneisses.  
 A yet unsolved problem is where the stone materials for the different objects have actually been quarried. Very little documentation about that is available.

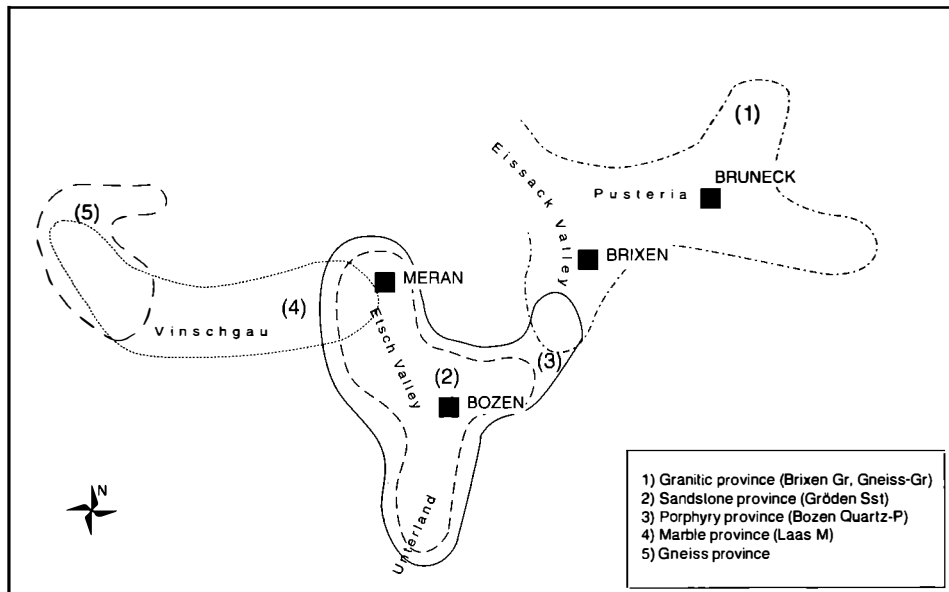


*Fig. 1  
Building stone provinces of historic material in South Tyrol.*

The second part of the study is concerned with the determination of basic petrographical, chemical and physical parameters, such as mineralogy, sedimentary fabrics, salt content, pore and hygric properties of the main materials. Weathering simulation experiments augment the data body about on weathering behaviour. The major problem in this study is the considerable material variation (especially within the sandstones) in combination with a broad spectrum of climatic/environmental factors. This requires long term monitoring of the climatic/environmental impact factors on building materials. However, the available data is still scarce.

## References

- [1] FRANZEN, C., LAIMER, M. & STAMPFER, H. (2000): St. Katharina in der Scharte in Hafling. - Messerschmitt Stiftung München, 36 p.
- [2] FRANZEN, C., HOFMANN, H. & MIRWALD, P. W. (2000): Mineralogical, petrophysical and weathering behaviour of Gröden Sandstone. - Annual Meeting 2000, Vol. 12, Beih. 1, p. 49. German Mineralogical Society, European Journal of Mineralogy.
- [3] FIMMEL, R. (1996): Verwitterungsverhalten der alpinen Marmore von Laas und Sterzing. - Diss. Univ. Innsbruck, p. 116.

**DIE MINERALOGISCHE CHARAKTERISIERUNG RÖMISCHER ZIEGEL  
IM HINBLICK AUF IHRE HERKUNFT – ERSTE ERGEBNISSE EINES  
INTERDISZIPLINÄREN PROJEKTES**

von

**M. A. Götzinger<sup>1</sup> & R. Sauer<sup>2</sup>**

<sup>1</sup>Institut für Mineralogie und Kristallographie

Universität Wien, Geozentrum, Althanstrasse 14, A-1090 Wien

<sup>2</sup>Institut für Konservierungswissenschaften und Restaurierungs-Technologie (ICORT)

Universität für Angewandte Kunst, Salzgries, A-1013 Wien

Am Südufer der Donau in Ober- und Niederösterreich verlief der Limes als Nordgrenze des römischen Reiches. Bis etwa 460 n. Chr. bestanden eine Reihe von Militärlagern und Zivilstädten [1]. Neben eindrucksvollen Gebäude- und Mauerresten (z.B. Traismauer) sind uns Grab- und Inschriftsteine sowie viele Ziegel- und Keramik(bruchstücke) erhalten geblieben. Auffällig sind bei fast allen "römischen" Ausgrabungen die häufig auffindbaren Dachziegelstücke mit ihren charakteristischen Wulsträndern. Manche Ziegel wurden mit Legions-Stempeln oder privaten Ziegelei-Stempeln versehen, wodurch die Hersteller oftmals bekannt sind. Nach heutigem Wissen ist jedoch nur eine römische Ziegelei (zwischen Enns/Lauriacum und Carnuntum) nachweislich bekannt (in Wien, 17. Bez.) und eine weitere im Bereich des 1. Bezirkes in Wien vermutet. So bleibt oftmals die Frage nach der Herkunft der Ziegel bzw. ihres Rohtones offen (Transport oder Gewinnung vor Ort ?).

Das Ziel dieser Untersuchungen ist die mineralogische Charakterisierung römischer Ziegel im Hinblick auf ihre Herkunft: Es ist bislang unklar, wie weit Ziegel von zentralen Ziegeleien transportiert wurden, oder vor Ort erzeugt wurden (wenn die Qualität des Tones dies zuließ). Römische Ziegel zeichnen sich üblicherweise durch sehr hohe Qualität aus (gut durchgebrannt, homogen, feinkörnig und druckfest). Es stellt sich daher die Frage: Welche Rohstoffe/Tone welchen Alters wurden wo abgebaut ?

**Voraussetzungen:** Durch unterschiedliche Ausgangsgesteine und Abtragungsbedingungen im ursprünglichen Liefergebiet und durch unterschiedliche Transport- und Ablagerungsbedingungen sowie durch spätere diagenetische Veränderungen ergeben sich Schwermineralzusammensetzungen, die häufig eine eindeutige Charakterisierung der Ablagerungen zulassen. Dies gilt auch für die Keramikrohstoffe und der daraus erzeugten Keramik (Ziegel), die ebenfalls reichlich Schwerminerale führen.

**Probenahme:** Von den aus der Literatur bekannten Siedlungsplätzen wurden eindeutig zuordenbaren (Dach)Ziegelproben (tegula, imbrex) von Feldern oder Aushubmaterial entnommen bzw. von autorisiertem Grabungspersonal erhalten: Traismauer, Zwentendorf, Tulln, Zeiselmauer, Mauerbach, Wien/Unterlaa und Biedermannsdorf, (Carnuntum). Boden- und Wandziegel blieben bisher eher unberücksichtigt.

**Untersuchungsmethoden:** Von den Ziegelstücken wurden sowohl Dünnschliffe, als auch Anschliffe (je mit etwa 5 – 6 cm<sup>2</sup> Beobachtungsfläche) hergestellt. Die Dünnschliffuntersuchungen erlauben die Charakterisierung bezüglich Homogenität, Textur, Gehalt an Karbonatmineral-Resten, (Mikro)Fossilien, Kristallinbruchstücken, Verhältnis Tonmatrix zu Magerungsmittel und deren Bestandteile (Punktzählmethode, Vergleichsschaubilder, Bildanalyse zu Farbe und Form) sowie die mineralogische Charakterisierung und Quantifizierung der Magerungsmittel bzw. Schwerminerale (Kornzählmethode bzw. Mengenabschätzung). Mit Rasterelektronenmikroskopie (REM) und energiedispersiver Analytik (EDX) werden die Einzelminerale (Magerungsmittel/Schwerminerale) auf ihre chemische Zusammensetzung und eventuellen Zonarbau untersucht (speziell bei Spinellen, Zirkon, Klinozoisit-Epidot-Allanit). Die Durchmesser der Mineralkörper in der Tonmatrix liegen zwischen 5 und etwa 100 µm, so daß REM-EDX eine ideale Methode darstellt. Die Kombination der Einzelergebnisse dieser Methoden ist für jeden Ziegeltyp kennzeichnend. Parallel dazu laufen mineralogisch-petrographische Untersuchungen der Ziegel-Rohstoffe, die in der Nähe der römischen Siedlungen vorliegen, bzw. es werden (die spärlichen) Literaturdaten darüber ausgewertet. Als Rohstoffquellen im besagten Raum S der Donau kommen vorrangig quartäre Lößlehme, marine Ablagerungen, wie Tone des Pannonien ("Inzersdorfer Tegel"), des Sarmatiens und des Badenien ("Badener Tegel"), aber auch lokale Schwemmmlehme in Frage.

**Vorläufige Ergebnisse:** Die quantitative Schwermineralanalyse für die Herkunftsanalyse von antiker Gefäßkeramik wurde im Wiener Raum und in Niederösterreich bereits mehrfach erfolgreich eingesetzt [2, 3, 4] und wird nun auf römische Ziegel ausgeweitet. Für die verschiedenen Ablagerungen des Wiener Beckens und der daraus erzeugten Keramik sind beispielsweise das Auftreten bzw. das Fehlen von Hornblende, der Reichtum an Epidot und Klinozoisit, das Überwiegen von Granat, höhere Beimengungen von Staurolith und Chloritoid wichtige Unterscheidungsmerkmale. Vereinzelt können sich auch noch sehr lokale Unterschiede im Liefergebiet, wie z.B. bei Umlagerungen aus dem Flysch oder von Gosau-Ablagerungen, durch typische Schwermineralspektren bemerkbar machen (erhöhte Beimengungen von Chromspinell, Chloritoid, Turmalin, Zirkon, Rutil, Glaukophan, etc.). Besonders gut lassen sich auch verschiedene Verwitterungslehme und Tonlagerstätten aus dem Bereich der Böhmisches Massiv (z.B. Dunkelsteiner Wald) durch ihre oft auffällige Schwermineralführung erkennen (z.B. die wichtigen Tone aus Oberfucha, Tiefenfucha): Granat, Rutil, Disthen, Sillimanit, Andalusit, Diopsid und Chromspinell [4].

Da für Ziegel wesentlich mehr lokale Rohstoffe in Frage kommen, als für die qualitativ höherwertige Gefäßkeramik, ist mit einer größeren Variabilität der Rohstoffe zu rechnen. Dies zeigte sich beispielsweise bereits deutlich bei Voruntersuchungen an römischen Ziegeln aus den Grabungen von Wien-Unterlaa (Stadtarchäologie, Frau K. Adler-Wölfel) und Biedermannsdorf, NÖ. (Frau D. Talaa). Gleichzeitig gilt unser Dank an die genannten und ungenannten ArchäologInnen, auch seitens des Bundesdenkmalamtes, für die bisherige gute Zusammenarbeit.

## **Literatur**

- [1] FRIESINGER, H. & KRINZINGER, F. (1997): Der römische Limes in Österreich. - Vlg. Österr. Akad. Wiss. 312 S.
- [2] SAUER, R. (1989/90/91): Die Anwendung der Schwermineralanalyse für die Herkunftsbestimmung von antiker Keramik anhand von Beispielen aus Carnuntum und St. Pölten. - Wiener Berichte über Naturwissenschaften in der Kunst, Bd. 6/7/8, S 121 ff.
- [3] SAUER, R. & GASSNER, V. (1995): Archäometrische Untersuchungen zur Gebrauchskeramik aus Carnuntum. - In: Naturwissenschaften in der Kunst, M. SCHREINER (Hrsg.) Böhlau Wien
- [4] SAUER, R. (2000): Archäometrische Untersuchungen zur Keramik von Mautern. - In: Das Kastell Mautern - FAVIANIS. Der römische Limes in Österreich V., GASSNER, V. et al., Heft 39; Verlag der Akademie der Wissenschaften.

**DAS PB-ZN-FE-AS-VORKOMMEN "PEITLERALM" IN DER STANGALM-TRIAS,  
NOCKBERGE, KÄRNTEN – EINE DETAILSTUDIE AN SEDIMENT UND MOBILISAT**

von

**M. A. Götzinger & S. Weisser**

Institut für Mineralogie und Kristallographie  
Universität Wien, Geozentrum, Althanstrasse 14, A-1090 Wien

Im Stangalm-Mesozoikum, Bereich Nationalpark Nockberge, Kärnten sind drei Vererzungstypen von Pb-Zn-F-(Cu-Fe-As)-Mineralisationen bekannt [1]:

- 1) lagenweise feinkörnig-disseminierte Pb-Zn-Fe-As-Erze mit teils massiven Imprägnationen in dolomitischen Sedimenten und Mobilisaten in Klüften (z.B. "Peitleralm"; diese Studie);
- 2) kluftgebundene Pb-Zn-Vererzungen (z.B. Predigerstuhl-Zunderwand);
- 3) kluftgebundene Zn-F-(Pb-Cu)-Vererzungen (z.B. Erlacher Bock, Kaning-Scharte).

Lage und Geologie der Vererzung "Peitleralm": Das kleine Vorkommen liegt ca. 500 m östlich der Ob. Kollerhütte (1869 m) im steilen Waldgelände SE des Peitlerocks (2244 m) auf etwa 1700 m SH. Zwei kleine Halden zeugen von der einstigen Schurf- oder Bergbauaktivität. Es sind Mundlöcher vorhanden, die Stollen sind verstürzt. Laut geologischer Karte [2; dort zu weit nördlich eingetragen!] liegt das Vorkommen in dunklen Dolomiten des Anis (Mitteltrias).

Die Zusammensetzung der Dolomite schwankt in Abhängigkeit von ihrem Erzmineralgehalt und ihrem Auftreten (vgl. Abb. 1): Der Pyrit und Arsenkies führende Dolomit enthält zwischen 2.5 und 3.1 Mol.% FeCO<sub>3</sub> und zwischen 0.6 und 1.1 Mol.% MnCO<sub>3</sub>. Die fast erzfreien Dolomite, die Dolomite mit fein verteilem Sphalerit und in den Pb-Zn-Erzklüften enthalten zwischen 0.5 und 1.8 Mol.% FeCO<sub>3</sub> und zwischen 0.3 und 0.7 Mol.% MnCO<sub>3</sub>. Die Fe-As-Mineralisation bedingt höhere Fe- und Mn-Gehalte des Dolomites.

Die Vererzungen sind lagenweise, teils feinkörnig-dissemiert im Dolomit, teils in Klüften und teils massiv ausgebildet. Die Ausdehnung ist gering, obertags sind aufgrund der schlechten Aufschlüsse (Waldgelände mit Unterholz und einzelnen Felsrissen) kaum Erze anzutreffen. Die Erze führen einerseits Galenit, Sphalerit und Pyrit (+ Limonit) sowie Pyrit und Arsenkies, wobei eine gewisse räumliche Trennung Pb+Zn(+Fe) - Fe+As gegeben ist (auch zwei getrennte Einbauten mit je einer kleinen Halde).

Aus dem unteren Stollen stammen die Fe-As-Erze: Pyrit (Korngröße ≤ 0.5 mm) zeigt Ansätze zu Idiomorphie und ist regellos im grauen Dolomit verteilt, wobei einzelne Sedimentlagen durch detritäre Glimmer (Phlogopit und Muskovit) getrennt sind. Arsenkies bildet idiomorphe Kristalle (charakteristische, rautenförmige Querschnitte bis 0.2 mm). Hier treten praktisch keine Kluftvererzungen auf.

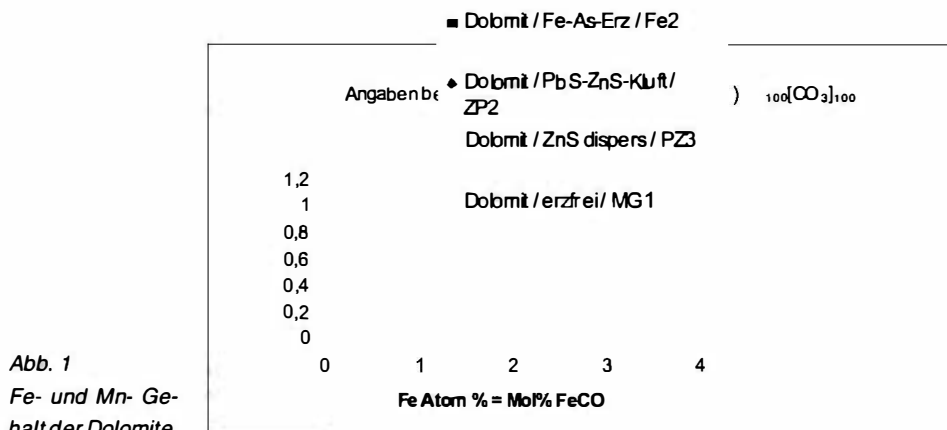


Abb. 1  
Fe- und Mn- Gehalt der Dolomite.

Aus dem oberen Stollen wurden vor allem die Pb-Zn-Erze gefördert; es gibt drei Erztypen, ineinander übergehende:

- a) ZnS feinkörnig-dispers (10 - 100  $\mu\text{m}$ ) im Dolomit;
- b) ZnS, PbS und Dolomit (Korngröße um 1 mm) in Klüften des Dolomits (Abb. 2);
- c) ZnS-PbS-Massiverz im Dolomit (Korngröße um 1 mm).

Von allen dreien gibt es Übergänge zur Fe-As-Vererzung, wobei aber hier nur Pyrit in unterschiedlichen Mengen auftritt. Der Fe-Gehalt des Sphalerites ist in allen drei genannten Pb-Erztypen jeweils gleich, steigt aber in Abhängigkeit vom zunehmenden Pyritgehalt von knapp unter 4 Gew.% bis knapp über 6 Gew.% (energiedispersive Analyse/EDX, Link ZAF-4 Anistik). Ein geringer Cd-Gehalt bis etwa 0.6 Gew.% ist charakteristisch.

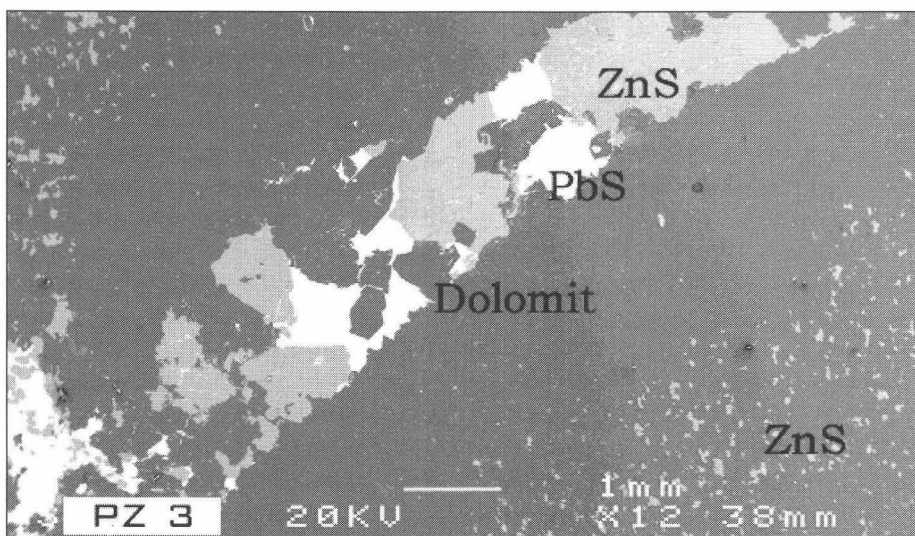


Abb. 2  
REM-Bild; Kluftgebundene Pb-Zn-Vererzung in nahezu erzfreiem Dolomit, etwas entfernt disseminierte Sphaleritvererzung im Dolomit.

Die fein-disperse ZnS-Vererzung kann als erhaltene, primäre, sedimentäre Anlage gesehen werden, wenn auch schwach metamorph überprägt und rekristallisiert. Daraus bildete sich (während der abklingenden Metamorphose ?) eine kleinräumige intraformationale Mobilisationsvererzung. Die Mobilisation in Klüfte (im cm-Bereich) und die Bildung der Massiv-Erze hatte offenbar keine nachweisbare chemische Veränderung der Minerale zur Folge (Dolomit und ZnS), wobei sich jedoch um die Klüfte eine erzarme Zone bildete (Abb. 2).

## Literatur

- [1] GÖTZINGER, M. A. & LEUTE, M. A. (1998): Die Pb-Zn-F-(Cu-Fe)-Mineralisationen der Stangalm-Trias, Nationalpark Nockberge, Kärnten.- Mitt. Min. Ges. 143, 281-283.
- [2] PISTOTNIK, J. (1996): Geologische Karte der Republik Österreich, Geol. B.-A. Wien, Bl. 183 Radenthein.

GEOLOGIE, MINERALOGIE UND SCHWEFELISOTOPIE  
OSTALPINER "KEUPER"-GIPSE: VORBERICHT UND DISKUSSION NEUER DATEN

von

M. A. Götzinger<sup>1</sup>, R. Lein<sup>2</sup> & E. Pak<sup>3</sup>

<sup>1</sup>Institut für Mineralogie und Kristallographie  
Universität Wien, Geozentrum, Althanstrasse 14, A-1090 Wien

<sup>2</sup>Institut für Geologie  
Universität Wien, Geozentrum, Althanstrasse 14, A-1090 Wien

<sup>3</sup>Institut für Isotopenforschung und Kernphysik  
Universität Wien, Boltzmanngasse 3, A-1090 Wien

Frühe Bemühungen [1, 2, 3] um eine Erfassung der aus Evaporiten abgeleiteten Schwefel-Isotopenverteilung der Weltmeere in Raum und Zeit haben zur Erstellung der bekannten Schwefelisotopen-Alterskurve geführt, die inzwischen, von wenigen strittigen Punkten abgesehen, als gut abgesichert gelten kann [4, 5, 6]. Allerdings ist die Datenlage dieser Kurve, was Probenanzahl und stratigraphische Auflösung betrifft, nicht homogen.

Verglichen mit den reichen Befunden aus dem Oberperm stellt die Obertrias diesbezüglich – vor allem jene des alpinen Raumes – einen eher ungenügend erfaßten Zeitabschnitt dar.

Probenahme: Um diese Lücke zu schließen, wurde in den Nördlichen Kalkalpen (Oberostalpin) mit einer systematischen Beprobung oberkarnischer Evaporitvorkommen begonnen. Weitere obertriadische Evaporitproben von nicht näher geklärter detailstratigraphischer Position ("Keuper") stammen aus dem Unterostalpin (Semmering-System) und aus dem Pennin (Unterengadiner Fenster), vgl. auch [7].

In den bisher untersuchten Gipsvorkommen und Lagerstätten im W-Abschnitt der Nördlichen Kalkalpen bildet Gips tektonisch stark verfaltete Körper, die im Zentimeter-Bereich eine charakteristische, vermutlich primäre Bänderung aufweisen. Diese wird sowohl durch bräunlich gefärbten Gips (organisches Material ?), als auch durch Dolomit, Quarz und Tonminerale verursacht. Der farbliche Gesamtcharakter des Gipes schwankt zwischen hellgrau und graubraun. Auffallend sind in vielen Vorkommen zur Bänderung diskordant verlaufende Klüfte und Gängchen, die von schneeweißem Gips ausgefüllt sind. Nach den Ortsbildern sind kleinräumige Mobilisationen zu vermuten. Anhydrit ist in oberflächennahen Bereichen bisher noch nicht nachgewiesen worden.

An Schwefelisotopenwerten obertriadischer Gipse liegen von einzelnen österreichischen Vorkommen (bisher oft unpublizierte) Daten vor (siehe Tab. 26 in [8]). Diese etwa ein Dutzend Werte schwanken zwischen +14.8 ‰ und +16.7 ‰ (CDT).

Aus dem Bereich Reutte, Weißenbach und Oberlech (Tirol), sowie aus dem Rellstal und dem Montafon (Vorarlberg) liegen nunmehr neue S-Isotopenwerte vor, die in ihrer Gesamtheit sehr einheitlich sind: Der Mittelwert über vorläufig 18 gemessene Einzelproben aus diesen Bereichen liegt bei +15.85 ‰ (CDT;  $s = \pm 0.40$ ). Damit stellt die Standardabweichung der 18 Einzelmessungen nur den doppelten Wert der methodischen Standardabweichung von  $\pm 0.2$  dar. Kein isotopischer Unterschied konnte zwischen den gebänderten und den weißen (mobilisierten) Gipsen festgestellt werden. Dies zeigt, daß diese schneeweissen Gipse durch die lokale, räumlich beschränkte Mobilisation keine isotopische Veränderung erfahren haben.

Diskussion: Aus der zur Zeit zwar noch nicht abgeschlossenen Auswertung ergibt sich folgendes Bild: Die zahlreichen kalkalpinen Proben, die aus dem Niveau der Raibler Schichten bzw. der Opponitzer Rauhwacke stammen, ergaben ein erstaunlich einheitliches isotopisches Bild von +15.85 ‰ (CDT;  $s = \pm 0.40$ ). Auffallend ist, daß kleinräumige Mobilisationen, kenntlich an diskordant verlaufenden Klüften und Gängen, in keinem Fall das bestehende Isotopenverhältnis verändert haben. Nach wie vor ungeklärt ist die genaue stratigraphische Korrelation der obertriadischen "Keuper"-Gipse des Pennins und des Unterostalpins (Semmering) in Bezug zu den verschiedenen Evaporitniveaus der germanischen Keuperentwicklung und zu den ostalpinen Gipsen der Raibler Schichten. Allerdings zeigen die wenigen bisher isotopisch ausgewerteten Proben [%o, CDT] aus dem Pennin (Tauernfenster: +15.8; Engadiner Fenster: +15.7) und aus dem Unterostalpin (Semmeringsystem: +15.9) auffallend ähnliche Werte zu jenen aus den Kalkalpen. Vor dem Hintergrund der beträchtlichen Schwankungsbreite der Schwefelisotopen-Verteilung, die in randmarinen Bereichen und in abgeschlossenen Becken auftreten kann, bedeuten die obigen sehr einheitlichen Ergebnisse aus den obertriadischen Evaporiten aus dem Ostalpin und aus dem Pennin, daß in beiden Fällen ein gut durchmischter Meeresbereich vorgelegen haben muß und sich daher die Isotopenwerte dieser Region ausgezeichnet für eine weitere Verdichtung der Schwefelisotopen-Alterskurve eignen.

**Dank:** Dieses Projekt wurde in dankenswerter Weise von der Hochschuljubiläumsstiftung der Stadt Wien gefördert.  
Herrn Mag. Rufus Bertle danken wir für die wertvolle Hilfe bei der Geländearbeit in Tirol und Vorarlberg.

## Literatur

- [1] NIELSEN, N. & RICKE, W. (1964): Geochim. Cosmochim. Acta, 28, 577-591.
- [2] NIELSEN, N. (1965): Geol. Rundschau 55/1, 160-172.
- [3] HOLSER, W. T. & KAPLAN, I. R. (1966): Chem. Geol. I, 93-135.
- [4] CLAYPOOL, G. E. et al. (1980): Chem. Geol. 28, 199-260.
- [5] HOLSER, W. T. (1984): in HOLLAND, H. D. & TRENALL, A. F. (eds.): Patterns of Change in Earth Evolution, 123-143.
- [6] HOLSER, W. T., MAGARITZ, M. & RIPPERDAN, R. L. (1995): in WALLISER, O. H. (ed.): Global events and event stratigraphy in the Phanerozoic results of the international interdisciplinary Cooperation in the IGCP Project 216 "Global Biological Events in Earth History", Springer Berlin, 63-84.
- [7] GÖTZINGER, M. A., LEIN, R. & PAK, E. (2001): Mitt. Ges. Geol. u. Bergbaustud. in Österr. 44/2001 (im Druck).
- [8] WEBER, L. et al. (1997): Archiv f. Lagerstättenforschung 19, 607 S, Geol. B.-A. Wien.

CRYSTAL CHEMISTRY OF SOME MEMBERS OF THE EUDIALYTE GROUP

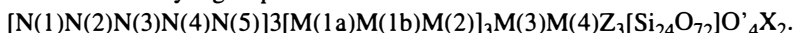
by

A. Gula<sup>1</sup>, G. Ferraris<sup>1</sup>, G. Ivaldi<sup>1</sup> & A. P. Khomyakov<sup>2</sup>

<sup>1</sup>Dipartimento di Scienze Mineralogiche e Petrologiche  
Via Valperga Caluso 35, 10100 Torino, Italy

<sup>2</sup>IMGRE, RAS  
Moscow, Russia

The eudialyte minerals belong to a complex group of cyclosilicates which occur in peralkaline rocks. So far 6 members (alluaivite [1], eudialyte [2], kentbrooksite [3], khomyakovite [4], manganokhomyakovite [4], oneillite [5]) are known in literature, but several new eudialytes are being studied and the number of species in the eudialyte group is expected to rapidly increase. This is due to the presence of a large number of independent sites in the structure and to the wide possibility of isomorphous substitutions. Under these aspects, the eudialyte group can be compared to the labuntsovite group in which continuously new species are described (see, e.g., [6, 7]). The following general formula describes in the most general way the schematic composition of the eudialyte group:



In this formula:

- N(1), N(2), N(3), N(4), N(5) are normally occupied by Na and in literature [2] they are usually labeled Na(1), Na(2), Na(3), Na(4) and Na(5) (however, the sites N can contain also other cations like REE, Sr, Ca, K);
- M(1a) and M(1b) = Ca, Mn, REE, Y, Zr;
- M(2) = Fe, Mn;
- M(3) = Nb, Ti, W;
- M(4) = Si, □;
- Z = Zr, Ti;
- O' = O, OH, H<sub>2</sub>O;
- X = Cl, F, O, OH, CO<sub>3</sub>.

The crystal structure of eudialytes is characterised by a (001) layered sequence of cations. The following (001) building modules can be individuated:

- (1) a tetrahedral sheet (*Th*) consisting of three-member rings, [Si<sub>3</sub>O<sub>9</sub>]<sup>6-</sup>, and nine-member rings, [Si<sub>9</sub>O<sub>27</sub>]<sup>18-</sup>;
- (2) a polyhedral (001) sheet (*Ph*) where rings of six [M(1)O<sub>6</sub>] octahedra are linked by [M(2)O<sub>n</sub>] (n = 4 or 5) polyhedra to form a nine-member ring;
- (3) a sheet formed by isolated (Z)-octahedra (*Oh*).

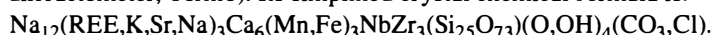
Each sheet *Ph* is sandwiched between two sheets *Th* thus forming a 2:1 composite layer. In their turn two 2:1 layers are connected by a *Oh* sheet of (Z)-octahedra. Within the main layer-framework described above, other sites shown in the general formula are located as follows:

- (i) the sites N(1), N(2) and N(5) show coordination numbers between 6 and 10 and are within cavities of the sheet *Oh* surrounded by the (Z)-octahedra;
- (ii) the sites N(3) and N(4) are close to the *Th/Ph* interfaces within the 2:1 layer;
- (iii) the sites M(4) and M(3) can coexist only in the non-centrosymmetric structures [in this case they occupy the center of two nine-member silicate rings occurring on the opposite polar sides of the 2:1 layer];
- (iv) O' represents extra silicate framework oxygens: one forms a tetrahedron around M(4) and the other three are coordinated by cations occupying M(3), M(2) and N(4) sites;
- (v) the sites X are within the *Th* sheet and connect three  $[\text{Si}_9\text{O}_{27}]_{18^-}$  rings; these sites are disordered and occupy positions both on and closely around the three-fold axis.

All known eudialyte minerals are rhombohedral and belong to one of the following space group types:  $\bar{R}\bar{3}m$ ,  $R\bar{3}m$  and  $R\bar{3}$ . Their cell parameters are  $a \sim 14.2$  and  $c \sim 30.0$  Å, but some members have double *c* axis, due to ion ordering. With respect to the  $\bar{R}\bar{3}m$  type, lack of the symmetry centre augments the number of the independent sites (the number of tetrahedral sites increases from 3 to 6). The lack of the mirror plane in  $R\bar{3}$  results in a doubling of several sites [the independent tetrahedral sites become 8 and M(1) site degenerates into M(1a) and M(1b)]. Due to the presence of several chemical elements which can occupy at the same time different sites in the structure, eudialytes can be fully characterised only by structural methods.

We are characterising several samples of eudialytes by microprobe chemical analyses and X-ray single-crystal diffractometry. A satisfactory crystal chemical formula can thus be obtained by matching the amount of analysed chemical elements with the refined electron density contents of the independent crystallographic sites. However the chemical and structural information would not be sufficient if some step procedure in assigning the cations to the different sites is not taken into account. Since the total number of anions is not easily determined because of complex and fractional occupancies of O' and X sites, it is suggested [2] to calculate the crystal chemical formula by setting  $\text{Si}+\text{Al}+\text{Zr}+\text{Ti}+\text{Hf}+\text{Nb}+\text{W}+\text{Ta} = 29$  apfu = to the content of the Si sites plus M(3) and M(4). However, even this procedure is not completely satisfactory since some, e.g., some Zr can occur in other sites and does take into account possible vacancies in the considered sites.

The sample we have best characterised is from peralkaline pegmatites of the Dara-i-Pioz alkaline massif (Tajikistan). This eudialyte group mineral shows  $a = 14.239(3)$  Å,  $c = 30.039(8)$  Å, space group  $R\bar{3}$ . The crystal structure has been refined to  $R = 0.026$  for 3454 observed reflections (P4 Siemens diffractometer, Torino). Its simplified crystal chemical formula is:



The Dara-i-Pioz mineral represents a new member of the eudialyte group. It corresponds to a Ca-rich oneillite [5] with Ca dominating both in M(1a) and M(1b) sites; in oneillite, instead, M(1b) is dominated by Mn. As already reported for oneillite, the infrared spectrum clearly shows the presence of  $(\text{CO}_3)^{2-}$ . The positions of  $(\text{CO}_3)^{2-}$  has been identified in the structural refinement on the three-fold axis and is alternative to a small quantity of Cl.

For other three samples of eudialytes, from Russian localities, X-ray single-crystal diffraction data (Nonius Kappa diffractometr with CCD area detector, Vienna) are being processed:

1. Si-rich sample from Khibina [ $a = 14.278(3)$  Å,  $c = 30.08(1)$  Å];
2. second sample from Dara-i-Pioz [ $a = 14.248(2)$  Å,  $c = 30.076(6)$  Å];
3. sample from Kirovsk [ $a = 14.291(2)$  Å,  $c = 30.041(6)$  Å].

Structural data and crystal chemical formulae will be presented at the meeting.

## References

- [1] RASTSVETAeva, R. K. et al. (1990): Crystal structure of alluaivite. - Dokl. Akad. Nauk SSSR 312: 1379-1384 (in Russian).
- [2] JOHNSEN, O. & GRICE, J. D. (1999): The crystal chemistry of the eudialyte group. - Canad. Mineral. 37: 865-891.
- [3] JOHNSEN, O. et al. (1998): Kentbrooksite from the Kangerdlugssuaq intrusion, East Greenland, a new Mn-REE-Nb-F end-member in a series within the eudialyte group: Description and crystal structure. - Eur. J. Mineral. 10: 207-219.
- [4] JOHNSEN, O. et al. (1999a): Khomyakovite and manganokhomyakovite, two new members of the eudialyte group from Mont Saint-Hilaire, Quebec. - Canad. Mineral. 37: 893-899.
- [5] JOHNSEN, O. et al. (1999b): Oneillite: a new Ca-deficient and REE-rich member of the eudialyte group from Mont Saint-Hilaire, Quebec, Canada. - Canad. Mineral. 37: 1295-1301.
- [6] FERRARIS, G. et al. (2000): Crystal structures of three new members of the labuntsovite group. - 80° Convegno SIMP, Pavia, 11-13 settembre 2000, Plinius, n° 24: 107.
- [7] CHUKANOV, N. V. et al.: Recommended nomenclature for labuntsovite group. - Eur. J. Mineral. in press.

ANDALUSITBILDUNG IM SCHNEEBERGER ZUG  
(SE ÖTZTALKRISTALLIN, ITALIEN/ÖSTERREICH)

von

G. Habler<sup>1</sup>, M. Linner<sup>2</sup>, R. Thiede<sup>3</sup> & M. Thöni<sup>1</sup>

<sup>1</sup>Institut für Geologie

Universität Wien, Althanstrasse 14, A-1090 Wien

<sup>2</sup>Geologische Bundesanstalt

Rasumofskygasse 23, A-1031 Wien

<sup>3</sup>Institut für Geowissenschaften

Universität Potsdam, Karl-Liebknecht-Strasse 24, D-14476 Golm

Die Metamorphoseprägung des Ostalpinen Schneeberger Zuges (SC) im südlichen Ötzalkristallin (ÖSC) umfasst ein druckbetontes Ereignis mit anschliessender statischer Mineralbildung und Rekristallisation [1]. Dieses Ereignis wird mit der eklogitfaziellen Metamorphose des ÖSC südlich des SC korreliert. Neue Andalusitfunde in Metapeliten der "Monotonen Serie" (Grt-Glimmerschiefer aus dem Kern der SC-Synformen), ermöglichen die Eingrenzung des PT-Pfades während der Dekompression. Eine interdisziplinäre (petrologische, strukturgeologische und geochronologische) Bearbeitung der Metapelite im zentralen SC lieferte neue Ergebnisse zur Klärung der tektonometamorphen Entwicklung.

Metapelite der "Monotonen Serie" besitzen durchschnittliche Gesamtgesteinschemismen (WR) mit geringen Ca- und Mn-Gehalten. Diese Gesteine können im KNFMASH (+ ms + qtz + H<sub>2</sub>O) System, mit Pa und Ab als einzigen Na-Phasen, beschrieben werden. Die Al<sub>tot</sub> Gehalte variieren, sodaß "Al-reiche" (Als-führende) und "Al-arme" (Als-freie) Metapelite unterschieden werden können. Eine kontinuierliche Abfolge von 4 (Re)Kristallisationsphasen (K1-K4) ist an Mineralzonierungen, Mikrostrukturen und Paragenesen zu beobachten.

### Al-reiche Metapelite

**K1:** Euhedraler Grt1 bildet die einzige Ca-führende Phase ( $X_{\text{grs}} = 0.12$ ) und weist leicht steigendes  $X_{\text{Mg}}$  (= Mg/(Mg+Fe<sup>2+</sup>)), sowie fallendes  $X_{\text{sps}}$  vom Kern zum Rand auf. Als Einschlüsse treten Qtz, Iilm, Mt und selten Ab und St auf. Die Matrix bilden phengitische Hellglimmer (Si<sup>IV</sup> 3.20 - 3.2/11O), Pg, Qtz, Bt, Chl, Ky, Ab und Iilm. K1 erfolgte syn-, inter- und postkinematisch bezüglich der intensiven Mylonitisierung und Isoklinalfaltung D1, die NW-WSW orientierte Streckungslineare und Isoklinalfaltenachsen ausbildet.

**K2:** Grt2 bildet euhedrale Anwachssäume um Grtl und zeigt fallende  $X_{\text{grs}}$  und  $X_{\text{Mg}}$ -Werte. Ein zweites Mn-Maximum in Grt weist auf eine Chl-Abbaureaktion hin. Grobkörniger Ky2 und St2 kristallisieren durch Pg-Abbau. Die Matrix besteht aus phengitischem Hellglimmer ( $\text{Si}^{\text{IV}} 3.15 - 3.18/11\text{O}$ ), Qtz, Bt, Pg, Ab und Ilm. K2 erfolgt synkinematisch zu einer engen S-vergenten Faltung um E-W-Achsen (D2), die den Grossfaltenbau des SE ÖSC bildet.

**K3:** Postkinematisch bezüglich der duktilen Deformation zeigen euhedrale Grt3 Ränder neuerlich ansteigendes  $X_{\text{Mg}}$  bei weiterhin fallendem  $X_{\text{grs}}$ . Grobkörniger Bt, Ab und Ky sowie mittelkörniger St (re)kristallisieren in der Matrix.

**K4:** dm-grosse Andalusit-Blasten und Oligoalbit sprossen in der Matrix durch Pg-Abbau. Bt und St bilden die stabilen FM-Phasen während der Andalusitbildung.

### Al-arme Metapelite

Diese Metapelite weisen nur die erste Grt-Generation (Grt 1) auf, während K2 und K3 erfolgte Grt-Resorption. St ist nur selten zu beobachten und Alumosilikat fehlt völlig.

### PT-Pfad

Thermodynamische Berechnungen unter Anwendung des Programmes THERMOCALC [2, 3] zeigen, daß die Grt-Stabilität in der Andalusit-führenden Lithologie auf PT-Bedingungen nahe  $P_{\text{max}}$  beschränkt ist ( $P > 0.7 \text{ GPa}$ ). Neue Daten bestätigen Bedingungen von  $580 - 600^\circ\text{C}/0.8 - 1 \text{ GPa}$  [1] für den Druckhöhepunkt. Die Paragenese K1 liegt im KFMASH-divarianten Feld Grt-St-Chl. Aufgrund lokaler Variationen in der Gesamtzusammensetzung von Gleichgewichtsdomänen kann die Paragenese Ky-Chl-St (v.a. in unmittelbarer Umgebung von Grt), sowie eine Bt1-Generation in der Matrix auftreten. Die erste Ky-Bildung ist auf kontinuierliche Reaktionen im KFMASH-System zurückzuführen, während Ky in der Folge vor allem durch eine (im SC weit verbreitete) Pg-Abbaureaktion gebildet wurde [4].

Mit dem Einsetzen der Dekompression (K2-D2) wurde die KFMASH-univariante Reaktion  $\text{Grt} + \text{Chl} + \text{Ms} = \text{St} + \text{Bt} + \text{Qtz} + \text{H}_2\text{O}$  überschritten, und die divariante Paragenese Grt-St-Bt stabil. Diese Reaktion führte zu Chl-Abbau (an dem Mn-Maximum in Grt2 zu beobachten), sowie signifikantem Anstieg im St-Modalbestand. Unter Annahme von  $a_{\text{H}_2\text{O}} = 1$  wird diese Mineralreaktion bei etwa  $600^\circ\text{C}/0.75\text{GPa}$  überschritten. Allerdings könnte das Einsetzen dieser Reaktion mit einer Reduktion der  $\text{H}_2\text{O}$ -Aktivität im Zuge der Dekompression in Zusammenhang stehen. Unter Annahme von  $a_{\text{H}_2\text{O}} = 0.7$  würde die univariante Chl-Abbaureaktion bei etwa  $565^\circ\text{C}/0.75\text{GPa}$  einsetzen.

Die postkinematische Mineralbildung beginnt noch im divarianten Grt-St-Bt Feld (= K3). Grt3 zeigt einen kontinuierlichen, signifikanten  $X_{\text{Mg}}$  Anstieg zum Rand. Während der Dekompression, kann diese Zonierung durch eine kontinuierliche Reduktion der  $\text{H}_2\text{O}$ -Aktivität erklärt werden. Ein T-Anstieg ist unwahrscheinlich, da die  $X_{\text{Mg}}$  Grt-Isoplethen im Grt-St-Bt Feld eine sehr geringe Steigung haben, d.h. T-insensitiv sind. Grobkörniger Ky und Ab wurden durch die Reaktion  $\text{Pg} + \text{Qtz} = \text{Ab} + \text{Ky} + \text{H}_2\text{O}$  gebildet und übersprossen D2-Strukturen statisch. Im Zuge isothermaler Dekompression führte die kontinuierliche, im KNFMASH-System divariante Reaktion  $\text{Bt} + \text{Pg} + \text{Qtz} = \text{Ab} + \text{St} + \text{Ms} + \text{H}_2\text{O}$  zu Reequilibration von Bt und St, mit höherem  $X_{\text{Mg}}$  als Bt und St der K3-Paragenese. Grt3 zeigt jedoch während des gesamten retrograden Pfades nach K3 keine diffusive Reequilibration, retrograde Zonierung oder Resorption.

Die zweite Phase statischen Mineralwachstums erfolgte im Andalusit-Stabilitätsfeld. Die Pg-Abbaureaktion zu Ab und Als wurde fortgesetzt, allerdings führte sie nun zu Andalusitbildung.

Da Bt und St die stabilen FM-Phasen während der Andalusitbildung anstelle von Chl darstellen, sind T-Bedingungen von über 500°C (bei  $a_{\text{H}_2\text{O}} = 0.5$ ) bis über 540°C (bei  $a_{\text{H}_2\text{O}} = 1$ ) unter Niederdruckbedingungen (0.2 - 0.4GPa) erforderlich. Die absoluten T-Bedingungen sind in dieser Lithologie stark von der H<sub>2</sub>O-Aktivität abhängig, die aufgrund der Stabilität von St im Andalusitfeld für K4 als reduziert angenommen werden muß.

Zur zeitlichen Eingrenzung dieses Metamorphoseereignisses wurden 0.5 - 1 cm grosse Grt-Körner mit der Sm-Nd-Methode analysiert. Die Fe-ärmere Grt Fraktion (Grt1) ergab ein Alter von 94.1 ± 2.2 Ma, die Fe-reichere Fraktion (Grt 2/3) 92.7 ± 1.2 Ma. Der gesamte Grt-Wachstumszeitraum, und somit die Hauptmetamorphose- und Strukturprägung sind damit auf das eo-Alpine Ereignis beschränkt. Eo-Alpine Abkühlung unter 300°C ist durch das Bt-WR Alter von 79.5 ± 0.8 Ma der selben Probe sowie zahlreichen Daten aus der Literatur belegt.

## Literatur

- [1] KONZETT, J. & HOINKES, G. (1996): Paragonite-hornblende assemblages and their petrological significance: an example from the Austroalpine Schneeberg Complex, Southern Tyrol, Italy. - *J. metamorphic Geol.* 14: 85-101.
- [2] POWELL, L. L. & HOLLAND, T. J. B. (1988): An internally consistent thermodynamic dataset with uncertainties and correlations. 3. Application to geobarometry, worked examples and a computer program. - *J. metamorphic Geol.* 6: 173-204.
- [3] HOLLAND, T. J. B. & POWELL, L. L. (1998): An internally consistent thermodynamic data set for phases of petrological interest. - *J. metamorphic Geol.* 16: 309-343.
- [4] HOINKES, G. (1981): Mineralreaktionen und Metamorphosebedingungen in Metapeliten des westlichen Schnebergerzuges und des angrenzenden Altkristallins (Ötztaler Alpen). - *TMPM* 28: 31-54.

PYRITE ZONING AND PRECIPITATION OF GOLD IN  
ATUD AND SUKKARI GOLD DEPOSITS, EASTERN DESERT, EGYPT

by

H. M. Helmy<sup>1</sup> & R. Kaindl<sup>2</sup>

<sup>1</sup>Geology Department

Faculty of Science, Minia University, Minia, Egypt

<sup>2</sup>Institute of Mineralogy and Petrology

Karl-Franzens University Graz, Austria

The Sukkari and Atud gold mines are located in the Eastern Desert of Egypt (Fig. 1). These deposits are of the vein-type hosted in late Precambrian granite. Different generations of quartz are observed within the same vein. The large and small veins are usually surrounded with extensive alteration (Fig. 2).

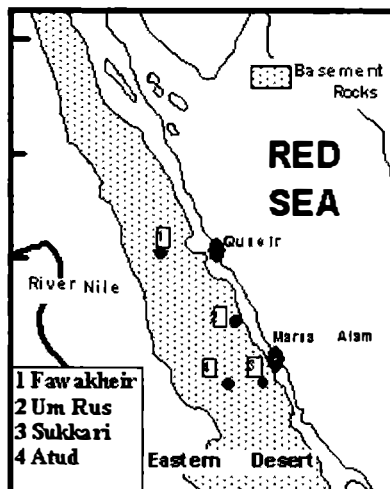


Fig. 1  
Location map of the studied gold deposits.

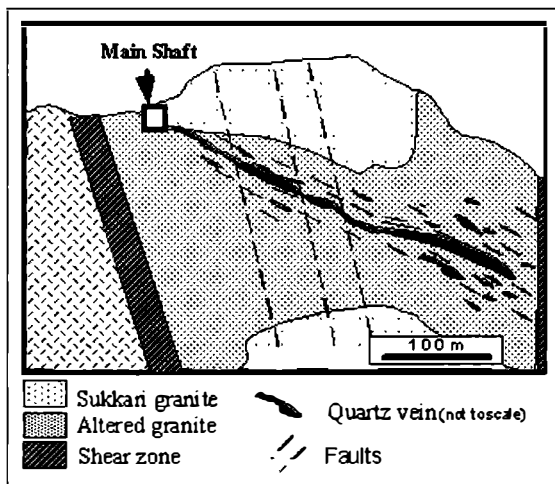


Fig. 2  
Cross section in the Sukkari gold mine.

In these deposits, gold is associated with sulphides in quartz veins and in alteration zones. The sulphide ore comprises pyrite and arsenopyrite, as major constituents, and minor sphalerite, chalcopyrite and galena. More than one pyrite generation is recognized in each deposit; large subhedral As-poor pyrite (PI), large euhedral arsenian pyrite (PII) and fine-grained angular and deformed euhedral As-poor pyrite (PIII).

Two types of pyrite zoning are recognized in the Sukkari and the Atud mine (Fig. 3, 4):  
 a) Simple zoning, with a core of As-poor pyrite (PI) surrounded by a thick zone of As-rich pyrite (PII), and b) Oscillatory zoning of coarse-grained, euhedral pyrite. In this type, As-rich zones alternate with As-poor ones. High arsenic contents (up to 2.6 and 3.4 wt.% in the Sukkari and Atud deposits, respectively) were detected in zoned pyrite while gold contents in As-rich and As-poor pyrite are below the microprobe detection limit.

Gold occurs in three distinct positions; 1) anhedral grains (GI) at the contact between As-rich zones within the arsenian pyrite; 2) randomly distributed anhedral grains and along cracks in arsenian pyrite and arsenopyrite (GII) and 3) large gold grains (GIII) interstitial to fine-grained PIII pyrite and arsenopyrite. Gold from different textures is always alloyed with 12 - 14 wt.% silver (electrum).

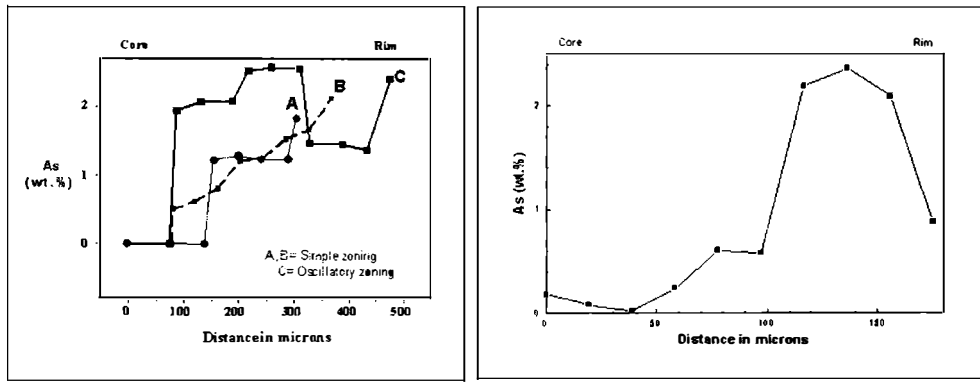


Fig. 3  
*Microprobe stepscans across zoned pyrite grains from Sukkari mine.*

Fig. 4  
*Microprobe stepscans across zoned pyrite grains from Atud mine.*

The textural positions of gold indicate strong relationship with arsenic concentration in the ore forming fluids. At early stage, before fluids attained saturation with gold and arsenic, gold deposition was controlled by the fluctuation in the arsenic content where both were incorporated in the pyrite structure. When the ore fluids attained As and Au saturation, gold was contemporaneously deposited with arsenopyrite. It is suggested that the concentration of arsenic in the ore forming fluids plays an important role in gold siting in the studied deposits.

**UNTERSUCHUNGEN ZUR URSACHE DER QUELLUNG TECHNISCHER ASPHALTE**

von

**G. Herbst<sup>1,2</sup> & H. Kurzweil<sup>2</sup>**

<sup>1</sup>Boden- und Bauprüfstoffstelle  
NÖ Strassendienst, A-3100 St. Pölten

<sup>2</sup>Institut für Petrologie  
Universität Wien, Geozentrum, Althanstrasse 14, A-1090 Wien

Technische Asphalte für Straßendecken und darunterliegende Schichten sind ein Gemisch von Gesteinskörnungen und Bitumen. Ihre Haltbarkeit gegen Wassereinfluß hängt von der Art und Qualität der Gesteine ab. Letztere bestimmt Schäden durch Quellung, die in der Literatur Mineralneubildungen im Feinkornanteil < 90 µm (Füller) der Sande zugeschrieben wurden [1].

Frühere Forschungen aus Anlaß von Schadensfällen [2] ergaben die Volumsvergrößerung von Asphaltprobekörnern nach Wasserlagerung (Quellversuch n. ÖNORM B3681 [3] als für die Bau-praxis ausreichendes Kriterium zur Feststellung ungeeigneter Gesteinskörnungen mit Erfassung gegenseitiger Mineraleinflüsse.

Die mineralogischen Ursachen wurden jedoch nicht ausreichend erfaßt. Offene Probleme blieben die Rolle der Sandfraktion 0.09/2 mm, die notwendige Verbesserung des bestehenden Kriteriums für die Füller [4] und eine Quantifizierung des Effekts der Quellung auf die Verkehrsbelastung.

Zur Klärung dieser Fragen wurden 6 Steinbrüche und 4 Kiesgruben beprobt und RD-Analysen [5] für Tonminerale in der < 20 µm Fraktion der Füller, die innere Oberfläche der Füller und Sande und statistisch gesicherte quantitative Erfassungen des Mineralbestandes der Sandfraktion an Dünnschliffen dem Wasseraufnahmevermögen [6] der Füller und der Quellung [3] von Sand-asphaltprobekörpern mit Erfassung der Änderung des dyn. Verformungsmoduls [7] gegenübergestellt.

Zwei Beispiele zeigen den Zusammenhang der Quellung mit der inneren Oberfläche, dem Ton-mineralbestand der Füller und dem Anteil stark veränderter Feldspäte in der Sandfraktion > 90 µm.

## Literatur

- [1] SCHELLENBERG, K. (1977): Hervorragende Eigenschaften d. Kalksteinmehls. Aktueller Kongreßbericht - Füllertagung Düsseldorf; Straße und Tiefbau, Heft 31: 31-32
- [2] HERBST, G. (1983): The Assessment of Water Susceptibility of Aggregates. - Beitrag im öst. Nationalbericht zum XVII Weltstraßenkongreß der AIPCR i. d. Publikation zu Question II, Construction and Maintenance of Pavements. Sydney - Paris: 361 - 379.
- [3] ÖNORM B3681: Prüfung bituminöser Massen für den Straßenbau, Quellversuch, 1982.
- [4] RICHTLINIEN UND VORSCHRIFTEN F. D. STRASSENWESEN RVS 8.01.11 (1993): Baustoffe, Steinmaterial, Gesteinskörnungen f. d. Straßenbau.
- [5] GRUBER, S. (1998): Mineralogische und petrologische Untersuchungen zur Klärung d. Quellverhaltens v. bitumengebundenen Schichten im Straßenoberbau. - Dissertation am Institut für Angewandte Geologie, Universität f. Bodenkultur, Wien.
- [6] RICHTLINIEN UND VORSCHRIFTEN F. D. STRASSENWESEN RVS 11.062 (1987): Grundlagen, Prüfverfahren, Steinmaterial, Teil VI, Wasseraufnahme der Kornklassen kleiner 0.125 mm (Enslinversuch).
- [7] HERBST, G. & PIBER, H. (1997): The Deformation Modulus, a Possibility to Define the Behaviour of Asphalt. - Proceedings d. 5. Internationalen RILEM Symposiums über "Mechanical Tests for Bituminous Materials; Recent Improvements and Future Prospects" von DI BENEDETTO, H. & FRANKEN, L., Verlag A. A. Balkema, Rotterdam/Brookfield.

THE ISOTYPIC CRYSTAL STRUCTURES OF  $K_2Mn(SO_4)_2 \cdot 2H_2O$  AND  $K_2Cd(SeO_4)_2 \cdot 2H_2O$ :  
COMPARISON WITH THE KROEHNKITE-, COLLINSITE-, AND FAIRFIELDITE-GROUP

by

B. Hertweck, M. Fleck, A. Wohlschläger, G. Giester & M. Wildner

Institut für Mineralogie und Kristallographie  
Universität Wien, Geozentrum, Althanstrasse 14, A-1090 Wien

The crystal structures of the isotopic compounds  $K_2Mn(SO_4)_2 \cdot 2H_2O$  and  $K_2Cd(SeO_4)_2 \cdot 2H_2O$  (space group  $P\bar{1}$ ,  $Z = 2$ ) have been investigated by single-crystal X-ray diffraction using a CCD area detector. The crystal structure of  $K_2Mn(SO_4)_2 \cdot 2H_2O$  was determined by Patterson methods and refined to  $R = 0.023$  with cell parameters  $a = 6.574(1) \text{ \AA}$ ,  $b = 7.332(1) \text{ \AA}$ ,  $c = 10.700(1) \text{ \AA}$ ,  $\alpha = 72.89(1)^\circ$ ,  $\beta = 73.91(1)^\circ$ ,  $\gamma = 69.77(1)^\circ$ ,  $V = 453.6(1) \text{ \AA}^3$ . The crystal structure of  $K_2Cd(SeO_4)_2 \cdot 2H_2O$ , previously described by Peytavin et al. [1], was refined to  $R = 0.025$  with cell parameters  $a = 6.625(1) \text{ \AA}$ ,  $b = 7.542(1) \text{ \AA}$ ,  $c = 11.349(1) \text{ \AA}$ ,  $\alpha = 72.17(1)^\circ$ ,  $\beta = 74.55(1)^\circ$ .

A large number of sulphate, phosphate, and arsenate minerals with the general formula  $A_2M^{II}(XO_4)_2 \cdot 2H_2O$ , with  $A = Na$  or  $Ca$ , and  $M^{II} = Cu$ ,  $Mg$ ,  $Co$ ,  $Mn$ ,  $Fe$ ,  $Ni$ , or  $Zn$ , and  $X = S$ ,  $P$ , or  $As$  have been found up to date. These natural compounds have triclinic or monoclinic symmetry. The triclinic minerals (space group  $P\bar{1}$ ) are the Ca-arsenates talmessite ( $M = Mg$ ) [2],  $\beta$ -roselite ( $M = Co$ ) [3], gaitite ( $M = Zn$ ) [4], and the Ca-phosphates collinsite ( $M = Mg$ ,  $Fe$ ,  $Zn$ ) [5], fairfieldite ( $M = Mn$ ) [6], messelite ( $M = Fe$ ,  $Mn$ ) [3] and cassidyite ( $M = Ni$ ) [7]. The monoclinic minerals (space group  $P2_1/c$ ) are the Ca-arsenates brandtite ( $M = Mn$ ) [8], roselite ( $M = Co$ ,  $Mg$ ) [9], Zn-roselite ( $M = Zn$ ) [10], and wendwilsonite ( $M = Mg$ ) [11], as well as kroehnkite,  $Na_2Cu(SO_4)_2 \cdot 2H_2O$  [12, 13].

The crystal structures of the synthetic compounds  $K_2Mn(SO_4)_2 \cdot 2H_2O$  and  $K_2Cd(SeO_4)_2 \cdot 2H_2O$  are closely related with the minerals of the  $A_2M^{II}(XO_4)_2 \cdot 2H_2O$  type. In all these compounds chains built up by  $MO_6$  and  $XO_4$  polyhedra are interconnected via  $A-O$  bonds and hydrogen bonds, forming layers parallel to  $(010)$ . While the topology of the chains is similar in all these structures, there are differences concerning their linkage to layers as well as the stacking of the layers. Based on these features, four structure types can be distinguished.

Compared with the crystal structures of  $K_2Mn(SO_4)_2 \cdot 2H_2O$  and  $K_2Cd(SeO_4)_2 \cdot 2H_2O$  (type I,  $P\bar{1}$ ), adjacent layers are shifted by  $c/2$  in the monoclinic structures of the isotopic minerals kroehnkite, brandtite, roselite, and wendwilsonite (type II,  $P2_1/c$ ). Consequently, the translation period along  $[010]$  is doubled referring to  $K_2Mn(SO_4)_2 \cdot 2H_2O$  and  $K_2Cd(SeO_4)_2 \cdot 2H_2O$ .

The crystal structures of collinsite, talmessite and cassidyite are isotopic with the synthetic compounds  $\text{Na}_2\text{Cu}(\text{SeO}_4)_2 \cdot 2\text{H}_2\text{O}$  [14],  $\text{K}_2\text{Co}(\text{SeO}_4)_2 \cdot 2\text{H}_2\text{O}$ , and  $\text{Na}_2\text{Ni}(\text{SeO}_4)_2 \cdot 2\text{H}_2\text{O}$  (both WILDNER, pers. comm.) (type III,  $\text{P}\bar{1}$ ). There, all A- and X-atoms, respectively, are crystallographically equal, resulting in a unit cell halved along [001] in comparison to the  $\text{K}_2\text{Mn}(\text{SO}_4)_2 \cdot 2\text{H}_2\text{O}$  and  $\text{K}_2\text{Cd}(\text{SeO}_4)_2 \cdot 2\text{H}_2\text{O}$  structures.

Finally, the formation of the chains and layers of the isotopic structures of fairfieldite and messelite (type IV,  $\text{P}\bar{1}$ ) is analogue to that of  $\text{K}_2\text{Mn}(\text{SO}_4)_2 \cdot 2\text{H}_2\text{O}$  and  $\text{K}_2\text{Cd}(\text{SeO}_4)_2 \cdot 2\text{H}_2\text{O}$ . However, the stacking of the layers is modified: two adjacent layers are shifted along [100], which results in  $\gamma$  being nearly  $90^\circ$  in the fairfieldite-type structure.

## References

- [1] PEYTAVIN, S., PHILIPPOT, E. & LINDQVIST, O. (1974): Étude structurale du sel double dihydraté  $\text{K}_2\text{Cd}(\text{SeO}_4)_2 \cdot 2\text{H}_2\text{O}$ . - Rev. Chim. Min. 11, 37-47.
- [2] CATTI, M., FERRARIS, G. & IVALDI, G. (1977): Hydrogen bonding in the crystalline state. Structure of talmesite,  $\text{Ca}_2(\text{Mg},\text{Co})(\text{AsO}_4)_2 \cdot 2\text{H}_2\text{O}$ , and structure chemistry of related minerals. - Bull. Soc. Fr. Minéral. Cristallogr. 100, 230-236.
- [3] FRONDEL, C. (1955): Neomesselite and beta-roselite: two new members of the fairfieldite group. - Am. Min. 30, 828-833.
- [4] STURMAN, B. D. & DUNN, P. J. (1980): Gaitite,  $\text{H}_2\text{Ca}_2\text{Zn}(\text{AsO}_4)_2(\text{OH})_2$ , a new mineral from Tsumeb, Namibia (South West Africa). - Can. Min. 18, 197-200.
- [5] BROTHERTON, P. D., MASLEN, E. N., PRYCE, M. W. & WHITE, A. H. (1974): Crystal structure of collinsite. Austr. J. Chem. 27, 653-656.
- [6] FANFANI, L., NUNZI, A. & ZANAZZI, P. F. (1970): The crystal structure of fairfieldite. - Acta Cryst. B26, 640-645.
- [7] WHITE, J. S., HENDERSON, E. P. & MASON, M. (1967): Secondary minerals produced by weathering of the Wolf Creek meteorite. - Am. Min. 52, 1190-1197.
- [8] HEJNY, C., GIESTER, G., WILDNER, M. & GÖTZINGER, M. (1997): Die Kristallstruktur von Brandtit,  $\text{Ca}_2\text{Mn}(\text{AsO}_4)_2 \cdot 2\text{H}_2\text{O}$ . - Beihefte Eur. J. Min 9, 150.
- [9] HAWTHORNE, F. C. & FERGUSON, R. B. (1975): Refinement of the crystal structure of kroehnkite. - Acta Cryst. B31, 1753-1755.
- [10] KELLER, P., INNES, J. & DUNN P. J. (1986): Zincroselite,  $\text{Ca}_2\text{Zn}(\text{AsO}_4)_2 \cdot 2\text{H}_2\text{O}$ , a new mineral from Tsumeb, Namibia. - N. Jb. Miner. Mh. 11, 523-527.
- [11] DUNN, P. J., STURMAN, B. D. & NELEN, J. A. (1987): Wendwilsonite, the Mg analogue of roselite, from Morocco, New Jersey, and Mexico, and new data on roselite. - Am. Min. 72, 217-221.
- [12] DAHLMAN, B. (1952): The crystal structures of kröhnkite,  $\text{CuNa}_2(\text{SO}_4)_2 \cdot 2\text{H}_2\text{O}$  and brandtite,  $\text{MnCa}_2(\text{AsO}_4)_2 \cdot 2\text{H}_2\text{O}$ . - Arkiv Min. Geol. 1, 339-366.
- [13] LEONE, M. (1953): La struttura della kronkite. - Rend. Soc. Min. Ital. 9, 251.
- [14] PEYTAVIN, S., PHILIPPOT, E. & LINDQVIST, O. (1974): Étude structurale du sel double dihydraté  $\text{Na}_2\text{Cu}(\text{SeO}_4)_2 \cdot 2\text{H}_2\text{O}$ . - J. Solid State Chem. 9, 63-68.

NEUTRON DIFFRACTION STUDY OF  
THE LOW-TEMPERATURE PHASE TRANSITION OF MN-LEONITE

by

B. Hertweck<sup>1</sup>, E. Libowitzky<sup>1</sup> & A. J. Schultz<sup>2</sup>

<sup>1</sup>Institut für Mineralogie und Kristallographie  
Universität Wien, Geozentrum, Althanstrasse 14, A-1090 Wien  
<sup>2</sup>Argonne National Laboratory  
IPNS Division, Argonne, Illinois 60439, USA

Single-crystal Time-Of-Flight (TOF) neutron diffraction data of Mn-leonite,  $K_2Mn(SO_4)_2 \cdot 4H_2O$ , were obtained at the Intense Pulsed Neutron Source (IPNS) at Argonne National Laboratory, Illinois, using a four-circle single-crystal diffractometer and a position-sensitive detector. Two reversible phase transitions at low temperatures have been previously confirmed by optical, calorimetric [1], and X-ray data [2]. The cause for the phase transitions of Mn-leonite is a dynamic disorder of sulphate groups  $S_dO_4$  at room temperature ( $C2/m$ ), that freeze to an ordered structure ( $I2/a$ ) at 205(1) K. At 169(1) K the crystal structure switches to another ordered phase ( $P2_1/a$ ).

At room temperature the structure of Mn-leonite consists of two crystallographically different  $MnO_6$  octahedra, assembled in the form of  $Mn[(H_2O)_4(SO_4)_2]_2^-$  units, with the sulphate groups in trans conformation and the S–Mn–S axes oriented nearly parallel to [100]. They form layers parallel to (001), with each layer consisting solely of  $S_o$ – $Mn_1$ – $S_o$  (ordered layer) or  $S_d$ – $Mn_2$ – $S_d$  (disordered layer) units, respectively. The units are interconnected by potassium cations in [9]- or [10]- coordination and by hydrogen bonds of the  $H_2O$  molecules.

Because X-ray methods locate electron densities rather than nuclei of atoms, the obtained H coordinates represent the delocalized H electrons. In the case of Mn-leonite with a dynamic disorder in the room temperature crystal structure an additional influence of proton dynamics is probable. Hence, neutron diffraction is an excellent method to investigate the hydrogen bonds, which influence the cooperative arrangement of tetrahedra across the layers.

The crystal for the data collection was a clear, synthetic specimen, that was ground to an ellipsoid with a size of 2.5 x 2 x 2 mm, elongated parallel to a. The neutron diffraction data were collected at room temperature, in the interval between the two indicated transition temperatures at 185 K, and below the second transition at 110 K. Least-squares refinements of the neutron diffraction data were carried out using the program system PC-GSAS [3]. Lattice parameters and starting values for the atomic positional parameters were obtained from the X-ray refinements [2] at the corresponding temperatures.

The results at room temperature are in good agreement with the neutron diffraction refinement of SRIKANTA et al. [4] with a deviation of the atom coordinates of less than 1 %. The refined atomic positional parameters confirm the X-ray diffraction data, obtained at identical temperatures. With the neutron diffraction data the coordinates of the hydrogen nuclei are determined, by which the evolution of the hydrogen bonds during the transformation process is elucidated.

Comparison of the O–H···O angles confirms the rule, that stronger hydrogen bonds are straighter than weaker ones. Within the ordered layer the distortion of the structure with decreasing temperature is accompanied by continuous decreasing and increasing, respectively, of the two O–H···O bond lengths surrounding the So tetrahedra. In general, the H···O distances surrounding the S<sub>d</sub> tetrahedra (disordered at room temperature) are longer <1.78 Å> than the H···O distances surrounding the So tetrahedra <1.72 Å>.

The interatomic distances and angles of the H<sub>2</sub>O molecules are close to those of free water molecules [5], i.e. O–H = 0.98 Å and H–O–H = 104.5°. At room temperature the O–H distances show the most significant deviations from the ideal value with the two shortest distances of 0.945(5) Å and 0.955(5) Å, belonging to the Ow3 molecule, connecting the disordered sulphate tetrahedra with the ordered layers via hydrogen bonds. Hence, the dynamics of the Ow3 molecule leads to the apparently shortened O–H distances, and, in addition, to enlarged U<sub>ij</sub> values. The Ow2 molecule, connecting the ordered tetrahedra within the ordered layer, is straightened to H–O–H = 110° in all three crystal structures.

## References

- [1] HERTWECK, B., ARMBRUSTER, T. & LIBOWITZKY, E. (2001): Multiple phase transitions of leonite-type compounds: optical, calorimetric, and X-ray data. - Mineral. Petrol. 72, in press.
- [2] HERTWECK, B., GIESTER, G. & LIBOWITZKY, E. (2001): The crystal structures of the low-temperature phases of leonite-type compounds, K<sub>2</sub>Me(SO<sub>4</sub>)<sub>2</sub>·4H<sub>2</sub>O (Me = Mg, Mn, Fe). - Am Mineral 86, in press.
- [3] LARSON, A. C. & VON DREELE, R. B. (1994): General structure analysis system – GSAS. - Los Alamos National Laboratory, Report LA-UR, 86-748.
- [4] SRIKANTA, S., SEQUEIRA, A. & CHIDAMBARAM, R. (1968): Neutron diffraction study of the space group and structure of manganese-leonite, K<sub>2</sub>Mn(SO<sub>4</sub>)<sub>2</sub>·4H<sub>2</sub>O. - Acta Crystallogr. B24, 1176-1182.
- [5] FRANKS, F. (ed) (1973): Water – A comprehensive Treatise, Volume 2. - Plenum Press, New York.

PRESSURE DOMINATED EO-ALPINE METAMORPHISM OF THE AUSTROALPINE UNITS  
OF THE EASTERN ALPS: NEW DATA FROM THE WÖLZ COMPLEX

by

G. Hoinkes<sup>1</sup>, W. Faryad<sup>2</sup> & A. Poyer<sup>1</sup>

<sup>1</sup>Institut für Mineralogie und Petrologie  
Karl-Franzens Universität, Universitätsplatz 2, A-8010 Graz  
<sup>2</sup>Katedra Geologie a Mineralogie  
BF, TU Letná 9, 04011 Kosice, Slovakija

Eclogites are the classical rocks indicating pressure dominated metamorphism. Eclogite occurrences of the Eastern Alps are known from the very beginning of the introduction of the term eclogite by [1] for "diallag (omphacite) - garnet - kyanite - quartz - zoisite - assemblages" from Kupplerbrunn (Saualpe) which generally is accepted as type locality of eclogites [2]. Most eclogites are spread from east to west in the Eastern Alps within a narrow zone of eo-Alpine exhumation ages of eclogite- to amphibolite facies assemblages which are of eo-Alpine age [3]. Only a few eclogite bodies occur in eo-Alpine low-temperature areas and therefore must be of pre-Alpine age. These pre-Alpine eclogites are dated as Variscan in the Ötztal basement [4] and preliminary age-data for the Hochgrößen eclogites point to a pre-Variscan age (FRANK pers. com.). Hence, modern geochronological and petrological investigations in the Austroalpine basement changed the geodynamic picture of the Eastern Alps significantly and the post-Variscan rock forming processes are now known to be dominant in many parts of the Austroalpine basement.

The post-Variscan metamorphic overprint starts with a temperature increase at low pressures and the emplacement of acid to basic magmatic bodies (Permian LP/HT-event). It is succeeded by a high pressure metamorphism at low to medium temperature (eo-Alpine HP/LT event). The metamorphic overprint of the LP/HT-assemblages and the magmatic bodies of Permian age by HP/LT-assemblages clearly dates this last pressure dominated metamorphism as Alpine metamorphic overprint of the Austroalpine units.

The regional distribution of this last metamorphic overprint is characterized by a continuous increase from N to S within the Austroalpine basement from low greenschist- to epidote-amphibolite and eclogite-facies conditions with a sudden end of regional PT increase at a tectonic line (SAM = southern limit of Alpine Metamorphism) still within the Austroalpine basement. The geothermal gradient of this regional metamorphism must be rather small (15 - 20° C/km) in order to cross the stability field of paragonite and hornblende before entering the omphacite stability field. The key rocks of such geothermal gradients are paragonite-amphibolites which occur N to the SAM and the eclogite facies assemblages as indicators of the epidote-amphibolite facies due to decreasing metamorphic conditions.

The Wölz complex east of the Pennine Tauern window and north of the type locality of eclogites (Saualpe) is, similar to the Ötztal complex west of the Tauern window, a good example for this P-dominated metamorphic gradient.

The Wölz complex turns out to consist of two tectonic units which differ in terms of pre-Alpine metamorphism. Only one suffered from Variscan amphibolite facies overprint (Rappold unit) whereas the other (Wölz unit) suffered from post-Variscan metamorphism only. Both units were overprinted together during eo-Alpine pressure dominated metamorphism: P- and T-increase from 8 kbar (500°C) in the N (Ennstal), 10 kbar (< 600°C) in the center and 17 kbar (> 600°C) in the S (Murtal) at the transition to the Saualpe complex where the first omphacite relics are present as inclusions in garnet, is derived by geothermobarometry.

These rock units continuously grade into the Saualpe complex where they may represent polymetamorphic and monometamorphic units which suffered from even higher PT-conditions of ~ 700°C/20 kbar approaching the SAM.

### Acknowledgements

This work was supported by the Austrian Science Fund (FWF-project P13058-GEO and LM 00417-GEO).

### Literature

- [1] HAÜY, R. J. (1822): *Traité de minéralogie*. 2nd ed., (Bachelier).
- [2] MOTTANA, A., CHURCH, W. R. & EDGAR, A. D. (1968): Chemistry, mineralogy and petrology of an eclogite from the type locality/Saualpe, Austria. - *Contrib. Mineral. Petrol.*, 18: 338-346.
- [3] THÖNI, M. (1999): A review of geochronological data from the Eastern Alps. - *Schweiz. Mineral. Petrogr. Mitt.*, 79, 209-230.
- [4] MILLER, CH. & THÖNI, M. (1995): Origin of eclogites from the Austroalpine Ötztal basement (Tirol, Austria): geochemistry and Sm-Nd vs Rb-Sr isotope systematics. - *Chem. Geol. (Isotope Geoscience Section)*, 122, 199-225.

**CONTRASTING EVOLUTION OF THE BASAL FORMATION IN  
THE SOUTHERN AND CENTRAL PARTS OF THE BOSKOVICE FURROW**

by

**F. Jelinek, J. Leichmann & S. Nehyba**

Department of Geology and Paleontology  
Masaryk University, Kotlářská 2, 611 37 Brno

Two profiles in the basal formation were studied in the southern half of the Boskovice Furrow. The first profile is situated in the Svatka valley, west from Veverská Bíťůška. The second is located more southerly, in the Oslava valley by Oslavany village. Sandstones from transgressive contact with the basement (by both examples from the West to the East) to the roof is the objective of the study. The metamorphic rocks of the Moravian window form the basement in both cases. The sedimentation started in both profiles with coarse basal conglomerates, breccias and sandstones [1]. The first sediments fill dominantly depressions in the paleorelief. The clastic material was derived from the close vicinity. Very similar character of the sedimentation – alluvial depositional environments, and accumulation of coarse-grained local material indicate poor communication within the basin during the first stage of its evolution.

Serpentinesed ultramafic, Sillimanite, and big K-feldspars derived from durbachites indicate that the Moldanubian material plays an important role in the roof sediments in the southern, Oslavany profile. These sediments represent river and lacustrine systems already. Some sandstones contain up to 30 % of volcanic material, ranging from rhyolite to dacite. The traces of erosion of the basin fill itself (cannibalism) were discovered in the uppermost part of the profile. The calcite to Fe-calcite, rarely corrosive, cement is locally abundant.

The lithological character of the deposits was examined using gammaspektrometric measurement. The sandstones, which were derived from Třebíč Massif are characterised by high K (3.5 wt.%), U (7 ppm), and Th (20 ppm), whereas other sandstones are depleted in all three elements (K – 2.7, U – 5.9, Th – 10). The shales are generally enriched in Th comparing with sandstones. The highest U concentration (73 ppm) was measured in the coal layer.

The northern profile is much more monotonous. Moldanubian material was not identified in this part of Boskovice Furrow. The whole material seems to be derived from the Moravian unit, especially from the Bites gneiss.

The differences between both profiles indicate, that even during its oldest evolution the furrow was separate into the individual subbasins [2]. The basal alluvial sedimentation is rapidly changed by river and lacustrine sedimentation on the south. Provenance study indicates broad source area. Whereas the local provenance, and the alluvial system sedimentation dominates the whole profile in the central part of the basin.

### Literature

- [1] HOUZAR, S. (1981): Petrografie permokarbonických slepenců boskovické brázdy mezi Veverskou Bítyškou a Moravským Krumlovem. - MS, dipl. práce Přf MU Brno
- [2] JAROŠ, J. (1963): Litostratigrafie permokarbonu bosk. brázdy. - Věst. Ústř. Ústř. Geol., 38, 2, 115-118. Praha.

WULFENITE CRYSTALS FROM GRABEN ORE BODY OF MEŽICA MINES IN SLOVENIA

by

**M. Jeršek<sup>1</sup>, B. Mirtič<sup>2</sup>, A. Rečnik<sup>3</sup>, V. Zebeč<sup>4</sup>, V. Bermanec<sup>5</sup>, M. Žorž<sup>6</sup> & T. Dolenec<sup>2</sup>**

<sup>1</sup>Slovenian Museum of Natural History  
Prešnerova 20, 1000 Ljubljana, Slovenia

<sup>2</sup>Faculty of Natural Sciences and Engineering  
University of Ljubljana, 1000 Ljubljana, Slovenia

<sup>3</sup>Ceramics Department  
Jožef Stefan Institute, Jamova 39, 1000 Ljubljana, Slovenia

<sup>4</sup>Croatian Natural History Museum  
Demetrova 1, 10000 Zagreb, Croatia

<sup>5</sup>Department of Geology  
Faculty of Science, Horvatovac b.b., 10000 Zagreb, Croatia

<sup>6</sup>Prešernova 53, 1290 Grosuplje, Slovenia

An isolated part of the Mežica Mines is the ore deposit Graben. It is situated on the right bank of the Meža river, south from the village of Žerjav. Mineralization of the ore minerals, mostly galena and sphalerite, is syngenetic. Due to the late diagenesis, epigenesis and retrograde epigenesis ore minerals have been oxidised into the secondary minerals. Discordant and metasomatic ores and minerals of the oxidation zone, e.g. wulfenite, have been formed[1, 2, 3].

Wulfenite crystals from the Graben ore body are unique from the morphologic point of view. They are of brown colour with dull, terraced and twisted faces. Unusually developed acicular crystals of wulfenite from Graben were first reported in 1972 by GRAFENAUER & MIRTIČ [4] who determined steep pyramids {441}, while ŠTRUCL [5] reported that the crystals from the Graben ore body were combination of pyramid **o**{111} and prism **m**{110} and stressed the roughness of pyramidal faces. Crystals were modified by prisms **a**{010}, **g**{120}, **f**{150} and **v**{1.11.0} that alternate with pyramids ( $a : c = 1 : 1.55767$ ).

In the recent study ŽORŽ et al.[6] determined by single-crystal X-ray diffractometry that the crystals were rotated by 45° about the c-axis and determined the corresponding **n**{011} and **m**{010} and several other previously not determined crystallographic forms on wulfenite crystals from Mežica Mines ( $a : c = 1 : 2.2308$ ).

The crystals studied in our investigation were collected at the 511 m level of the Graben ore deposit. Because of their unusual colour and crystal habit we performed powder X-ray diffractometry and energy dispersive X-ray spectroscopy in order to prove that the mineral is in fact wulfenite. In the first stage of growth crystals develop the bipyramidal morphology with the prevailing forms **n**{011} and **d**{021}, as reported by ŽORŽ et al. [4] in 1998. In the later growth stage the acicular brown wulfenite crystals overgrew the bipyramidal crystals of wulfenite.

They measure up to 3 mm in length and may reach elongated form where length to thickness (c/a) ratio can reach the value of 10 or more. Wulfenite crystals have been frequently found on galena. In this case they always grow on cerusite which is the first product of galena oxidation. According to the scanning electron microscopy investigation the wulfenite crystals from the 511 m level at Graben deposit initially developed an extremely elongated prismatic morphology. Crystals look as if they were composed out of infinite number of tiny crystals that together form the sheave-shaped aggregates that are only occasionally terminated by pedions. We determined them with energy dispersive X-ray spectroscopy. In addition to wulfenite we have determined cerusite and dolomite crystals from Graben locality by energy dispersive X-ray spectroscopy and scanning electron microscopy. The fact that there were at least two wulfenite growth generations may help us in better understanding of the local re-crystallisation processes and the transport of the ore metals within the Graben ore body as well as their leaching out of it.

### Literature

- [1] ZORC, A. (1955): Rudarsko geološka karakteristika rudnika Mežica. - Geologija (Ljubljana) 3: 24-80.
- [2] ŠTRUCL, I. (1970): Poseben tip mežiškega svinčeve cinkovega orudjenja v rudišču Graben. - Geologija (Ljubljana) 13: 21-43.
- [3] DOLENEC, T., PEZDIC, J. & KUŠEJ, J. (1993): Izotopska sestava kisika in ogljika v karbonatih iz Mežiškega rudišča Graben. - Rudarsko-metalurški zbornik (Ljubljana) 1-2: 133-144.
- [4] GRAFENAUER, S. & MIRTIČ, B. (1972): O nenavadnih kristalih wulfenita iz Mežice. - Rudarsko-metalurški zbornik (Ljubljana) 4: 329-330.
- [5] ŠTRUCL, I. (1984): Geološke, geokemične in mineraloške značilnosti rude in prikamnine svinčeve - cinkovih orudjenj mežiškega rudišča. - Geologija (Ljubljana) 27: 215-327.
- [6] ŽORŽ, M., ALEKSANDER, R., MIRTIČ, B. & KRIVOGRAD, F. (1998): Morphology of wulfenite crystals from Mežica Mines. - Materials and Geoenvironment (Ljubljana) Vol. 45, 3-4: 315-344.

**PAN AFRICAN METAMORPHISM OF THE WESTERN ETHIOPIAN SHIELD**

by

**T. E. Johnson<sup>1</sup>, T. Ayalew<sup>2</sup>, K. Belete<sup>1</sup> & A. Mogessie<sup>1</sup>**

<sup>1</sup>Institut für Mineralogie und Petrologie

Karl-Franzens Universität, Universitätsplatz 2, A-8010 Graz

<sup>2</sup>Department of Geology and Geophysics

Faculty of Science, Addis Ababa University, PO Box 1176, Addis, Ethiopia

The Precambrian basement of Ethiopia occupies a position of particular geological importance where juvenile metavolcano-sedimentary rocks of the Arabian-Nubian Shield (ANS) are in contact with higher-grade, gneissic rocks of probable Mozambique Belt (MB) affinity. In the Western Ethiopian Shield, the ANS Birbir domain largely comprises chlorite-rich meta-tuffs with subordinate pelites and psammites and contains a broadly N-S oriented linear belt of highly altered mafic and ultramafic intrusions – the Yubdo-Daleti-Tulu Dimtu belt. The margins of the Birbir domain are marked by mylonitic shear-belts where the Birbir is in tectonic contact, to the east and west respectively, with the gneissic (MB) Geba and Baro domains. The Geba and Baro domains are dominated by banded quartzofeldspathic biotite- and/or hornblende-bearing orthogneisses and contain rare slivers of quartzite, calc-silicate and pelitic paragneiss. The pronounced (subsequently folded) gneissose layering and the preservation of both subsolidus and anatetic migmatites suggest an early, high-temperature (Archean?) event not recorded in the Birbir rocks, implying that the Baro and Geba domains form an older crystalline basement to the Birbir. All domains were strongly deformed by the subsequent Pan African (c. 900 - 550 Ma) tectonothermal event, resulting in N-S trending Dp1-folds and ductile Dp2-shear-zones, polyphase intrusion and metamorphism.

The Pan African metamorphic event (Mp1) affected the entire area. Porphyroblast-matrix relationships suggest Mp1 occurred at an early stage within the Pan African structural framework, either pre- or syn-Dp1. Thermobarometric calculations on gneisses from the Geba and Baro domains yield mid- to upper-amphibolite facies conditions for this event, with peak temperatures of around 650 - 700°C and pressures in the range 7 - 10 kbar. The abundant metabasite parageneses within the Birbir domain generally indicate greenschist to lower-amphibolite facies conditions, both within and away from Dp2 shear-zones. Calculations on a low-variance garnet-chloritoid-staurolite-bearing pelitic schist from a metamorphosed clastic shelf sequence within the Birbir domain gives results of 560 - 580°C at c.7 - 10 kbar. Such high pressures have not previously been recorded in the ANS of Western Ethiopia and, when combined with lithological considerations, may imply the existence here of a discrete lithostratigraphical group, possibly equivalent to the “Middle Complex” of Kazmin [1].

The Pan African metamorphic peak within the region was evidently attained prior to, or during the earliest stages of, continent-continent collision (i.e. of east and west Gondwana [2]) and maintained throughout much of the period of deformation. An overall anti-clockwise P-T-t evolution is implied. A significant contribution to the heat required for this widespread metamorphic event was probably provided by intraplated mafic and/or ultramafic intrusions emplaced within an extensional back-arc setting [3], examples of which are preserved as the Yubdo-Daleti-Tulu Dimtu belt.

This work was financed by FWF project P13643-GEO.

## References

- [1] KAZMIN, V. (1971): Precambrian of Ethiopia. - *Nature* 230: 176-177.
- [2] STERN, R. J. (1994): Arc assembly and continental collision in the Neoproterozoic East African orogen: implications for the consolidation of Gondwanaland. - *Annu. Rev. Earth Pl. Sci.* 22: 319-351.
- [3] BRAATHEN, A., GREENE, T., GEBRESELLASSIE, M. & WÖRKU, T. (2001): Transpressional juxtaposition of Meso-Neoproterozoic units; the Wombara-Kilaj transect within the Pan-African belt of Western Ethiopia. - *Precambrian Res.* (in press).

**FLUID INCLUSIONS IN METAMORPHIC GARNET  
FROM SELECTED AUSTROALPINE BASEMENT AREAS**

by

**R. Kaindl, R. Abart & G. Hoinkes**

Institut für Mineralogie und Petrologie  
Karl-Franzens University Graz, Universitätsplatz 2, A-8010 Graz

The investigation of the fluid phase, which is involved in most metamorphic reactions and plays a major role for a number of rock-forming processes, has become one of the most active fields in metamorphic petrology. The direct approach is the study of fluid remnants preserved as inclusions in minerals. Interpretation of fluid inclusion data can only be done by comparison with independent P-T estimates [1].

Within the Austroalpine basement sequences of the Radenthein Complex (RC) and the Schneeburg complex (SC) east and west of the Tauern window the index minerals garnet and kyanite occur commonly together with quartz and contain frequently fluid inclusions. By combining various methods such as petrography, microthermometry, Raman spectroscopy, mineral chemistry, oxygen isotope measurements, geochronology and phase petrology with fluid inclusion data an improved pressure-temperature-time-path of the Eoalpine and pre-Alpine metamorphic event can be derived.

Amphibolite facies metapelites of the Radenthein Complex contain fluid inclusions in garnet, kyanite and quartz. Geothermobarometry, stable isotope data and fluid inclusion studies revealed inconsistencies between peak metamorphic pressure-temperature conditions on one hand and the observed fluid composition and density of fluid inclusions trapped within the peak metamorphic minerals garnet and kyanite on the other hand. Oxygen isotope thermometry on several mineral pairs yielded concordant peak metamorphic temperatures in the range of 560 to 590°C. Combining these temperature estimates with the analysis of phase relations suggests that the pressure was between 5.5 and 7.5 kbars and that  $X_{\text{H}_2\text{O}}$  was between 0.4 and 0.5 during peak metamorphism. The fluid inclusion assemblages within garnet and kyanite are dominantly -  $\text{CO}_2\text{-N}_2$ , and  $\text{CO}_2\text{-H}_2\text{O}$  respectively. The generally low  $X_{\text{H}_2\text{O}}$  ( $< 0.26$ ) of the fluid and the high fluid molar volumes of 42 to 70  $\text{cm}^3/\text{mole}$  are inconsistent with the estimated peak metamorphic conditions.

Scanning electron images, as well as Raman and infrared spectra of solid phases in fluid inclusions indicate retrograde closed system reactions producing chlorite within garnet-hosted and aluminum sheet silicates within kyanite-hosted inclusions. Fluid modeling corroborates this mechanism.

A virtual fluid inclusion that trapped the presumed peak metamorphic fluid ( $X_{H_2O} = 0.46$ , molar volume =  $33 \text{ cm}^3/\text{mole}$ ) changes its composition and density by producing chlorite and quartz at the expense of garnet and the water fraction of the fluid. The final density of such an inclusion is consistent with the observed density range of the fluid inclusion assemblage entrapped in garnet. Alternative reequilibration phenomena such as leakage or diffusive water loss cannot be excluded but are not necessary to explain the present day composition and density of the fluid inclusion assemblages in garnet and kyanite.

The mostly monometamorphic Schneeberg complex (SC) was intensely folded into the polymetamorphic Ötztal-Stubai complex (OSC) during the Eoalpine orogeny. The metapelites and metacarbonates of the SC differ significantly from the dominantly quartzo-feldspathic rocks of the OSC. It is considered to represent the remnants of a Palaeozoic sedimentary cover unit overlying the OSC and missing in other parts of the OSC due to erosion.

P-T data from the literature [2] and this study yielded peak metamorphic temperatures between  $550 - 600^\circ\text{C}$  and pressures from  $8 - 10 \text{ kbar}$  for the SC. Rims of mica schist garnet from the transition zone between the SC and the OSC grew during the Eoalpine orogeny which is confirmed by monazite inclusions yielding an average age of  $93 \pm 11 \text{ Ma}$ . A clearly pre-Alpine origin of the garnet cores is indicated by garnet zoning profiles and aqueous fluid inclusions with low salinity and density ( $0.57 - 0.72 \text{ g/cm}^3$ ). These inclusions may have been trapped after the Variscan high-pressure event during pressure release and contemporaneous heating. Their low densities can be explained by reequilibration of these inclusions during a low-P/high-T extensional event affecting large areas of the Austroalpine basement [3], [4]. Few monazite ages above  $200 \text{ Ma}$  in the matrix of the garnet-mica schist and K-Ar hornblende ages within various parts of the SC [5] as well as numerous post-Variscan – pre-Alpine diabase dikes distributed all over the OSC [6] confirm increased heat-flow and extension in the late Permian – early Triassic. Alternatively, the garnet cores and the inclusions may be of Permo-Triassic age. Their low density and high resistance of garnet against plastic deformation prevented these inclusions from resetting to Eoalpine metamorphic conditions.

In conclusion, fluid inclusions in monometamorphic metapelitic garnet from the Eoalpine metamorphic RC were changed due to metamorphic reaction involving the host mineral and the trapped metamorphic fluid. In contrast garnet from the transitions zones between the polymetamorphic OSC and the monometamorphic SC records pre-Alpine trapped fluid inclusions which remained unchanged during Eoalpine high-pressure overprint. The most common preferential water diffusion or leakage of quartz during the Eoalpine metamorphic event cannot be excluded for inclusion assemblages in garnet but is not necessary to explain their observed composition and density.

## References

- [1] TOURET, J. L. R. (2001): Fluids in metamorphic rocks. - *Lithos* 55:1-25.
- [2] KONZETT, J. & HOINKES, G. (1996): Paragonite-hornblende assemblages and their petrological significance: an example from the Austroalpine Schneeberg Complex, Southern Tyrol, Italy. - *J. Metam. Geol.* 14: 85-101.
- [3] SCHUSTER, R. & FRANK, W. (1999): Metamorphic evolution of the Austroalpine units east of the Tauern Window: indications for Jurassic strike slip tectonics. - *Mitt. Ges. Geol. Bergbaustud. Österr.* 42: 37-58.
- [4] THÖNI, M. & MILLER, C. (2000): Permo-Triassic pegmatites in the eo-Alpine eclogite-facies Koralpe complex, Austria: age and magma source constraints from mineral chemical, Rb-Sr and Sm-Nd isotope data. *Schweiz. Mineral. Petrograph. Mitt.* 80:169-187.
- [5] MAURACHER, J. (1980): Alpidische und voralpidische Metamorphose und Strukturprägung am Westende des Schneeberger Zuges (Ötztaler Alpen). - Dissertation, Universität Wien.
- [6] PURTSCHELLER, F. & RAMMLMAIR, D. (1982): Alpine metamorphism of the diabase dikes in the Ötztal-Stubai metamorphic complex. - *Tscherm. Mineral. Petrograph. Mitt.* 29: 205-221.

**DIE KRISTALLMODELLSAMMLUNG AUS DEM 19. JAHRHUNDERT  
DES INSTITUTS FÜR MINERALOGIE UND PETROGRAPHIE  
DER UNIVERSITÄT INNSBRUCK**

von

**G. Kaltenhauser & R. Tessadri**

Institut für Mineralogie und Petrographie  
Universität Innsbruck, Innrain 52, A-6020 Innsbruck

Die Kristallmorphologie war für die Bestimmung von Mineralen schon immer ein wichtiges Kriterium, ist sie doch das Abbild jener regelmäßigen inneren Raumgitterstruktur, die den jeweiligen Mineralen zu eigen ist. Da in der Natur aber unregelmäßig gewachsene Formen weit- aus überwiegen und ideal gewachsene Kristalle sich nur unter den allerbesten Bedingungen entwickeln können, hat man seit den Anfängen der Kristallographie als Wissenschaft Modelle von ideal geformten Kristallen hergestellt, um diese Gesetzmäßigkeiten der inneren Raumstruktur an Habitus und Tracht makroskopisch sichtbar zu machen.

Am Institut für Mineralogie und Petrographie der Leopold-Franzens-Universität Innsbruck wird eine historisch und kristallographisch interessante Sammlung von Kristallmodellen verwahrt, die wohl wert ist hier kurz vorgestellt zu werden.

Diese Sammlung besteht aus mehreren Serien, die zu verschiedenen Zeiten und unter verschiedenen Institutsvorständen erworben wurden. Somit spiegelt diese Sammlung auch einen Teil der Institutsgeschichte wider. Sie ist seit der Übersiedlung des Institutes von der "alten" Universität in das Bruno-Sander-Haus in 22 Laden eines, für Universitätsverhältnisse durch sein Dekor aufwendigen, Schrankes untergebracht. Der Schrank besteht aus Eichenholz, weist unterhalb der Abdeckung ein Zahnfries auf und hat in den vier Füllungen der Flügeltüren ornamentale Schnitzereien. An der Stirnseite der Laden ist eine Vertiefung ausgearbeitet, in welche ursprünglich kleine Schildchen für eine Beschriftung gesteckt werden konnten.

In den alten Inventarbüchern des Institutes findet sich kein Hinweis über den Erwerb dieses wertvollen Möbelstückes; es scheint erst in einer modernen Kartei auf. Wohl aber ist durch den Schriftverkehr, den Institutsvorstand Bruno Sander mit dem Bevollmächtigten bezüglich des Erwerbes von Mineralien und Büchern nach Alois Cathrein – seinem Amtsvorgänger – führte, die Herkunft dieses Kastens gesichert. Im Schreiben vom 17. September 1942 heißt es "*Ihre Schätzung der beiden eichenen Mineralienkästen (zu 22 Schubladen) à 300.- RM halte ich für angemessen, angesichts der erstklassigen Ausführung (was z.B. Staubdichte anlangt)*"

Demnach waren es zwei Einrichtungsgegenstände, die ehemals in privatem Eigentum des im Jahre 1890 ernannten Extraordinarius des mineralogisch-petrographischen Institutes waren. Wir können so mit Bestimmtheit annehmen, daß Alois Cathrein sich diese zwei Kästen wohl anlässlich seiner Bestellung im Jahre 1890 oder kurz nachher hat anfertigen lassen. Das vorhin erwähnte zweite Stück befindet sich ebenfalls im Institut.

In den ersten fünf Laden sind auf schwarz gestrichenen gefachten Einsätzen die Modelle der Serie A eingeordnet. Über diese Einsätze ist im Inventar-Buch I zu lesen “*G 60 gefächerter Einsatz für Mineralien und Krystallmodelle, 9 Stück 1877 von M. Jeggle hergestellt*”. Mit Bleistift ist noch der Zusatz vermerkt, daß Josef Blaas, der zwischen 1883 bis 1890 interimistisch das Institut leitete, vier Stück davon in das inzwischen errichtete Geologisch-Paläontologische Institut mitgenommen hat. Interessant ist aber dabei, daß die Einsätze genau in die Läden des Kastens passen, obwohl sie älter sein müßten als die Schubladen.

Die Serie A, die heute in diesen Einsätzen eingeordnet ist, beinhaltet 224 Formen aus Birnholz. Die Oberfläche der Modelle erscheint leicht gebeizt und weist leichten Seidenglanz auf. Die darauf angebrachten Nummern beziehen sich wahrscheinlich auf die von der Herstellerfirma festgelegten Fabrikationsnummern. Die Serienbezeichnung A wurde wahrscheinlich erst später im Institut aufgestempelt. Auf nicht ganz einheitlichen Begleitzetteln (ca. 45 x 65 mm) ist handschriftlich die Bezeichnung des Modells, sowie die kristallographische Kennzeichnung, sowohl in der Nomenklatur nach Samuel Weiss, wie auch in jener nach Miller festgehalten. Die ersten 13 Modelle sind die Grundformen des kubischen Kristallsystems. Im Anschluß daran folgen zwei- und dreigliederige Kombinationen aller Systeme – einige sogar mit drehbaren Hälften. Aus dem alten Inventarbuch ist zu entnehmen, daß diese Serie am 13.XII.77 von Dr. C. Hintze, Straßburg um 116.60 fl (= Gulden) angekauft wurde.

Die Serie B besteht aus 62 Formen, die aus Lindenholz gefertigt sind. Die Modelle sind ungebeizt – weisen also eine unbehandelte Oberfläche auf. Bei dieser Serie handelt es sich um durchwegs mehrgliedrige Formen, die in schwarz kaschierten Kartons (63 x 70 mm) untergebracht sind. Die Begleitzettel sind denen der Serie A ähnlich und von gleicher Hand beschriftet. Dabei wurde große Sorgfalt aufgewendet, denn der Inventator mußte scheinbar an jedem Modell jeden Winkel genau nachgemessen haben, um jeden kleinsten Verschnitt am Begleitzettel kritisch zu vermerken. Allem Anschein nach wurden diese beiden Serien durch den neuen Vorstand des im Jahre 1876 neu gegründeten Extraordinariates, Edmund Neminar, angekauft. Diese aufwendige Inventararbeit wird man aber nicht ihm sondern eher Josef Blaas zuschreiben können, der seit 1879 in diesem Institut als Demonstrator arbeitete und nach dem Weggang von Neminar interimistisch das Institut leitete und in dieser Zeit für die Ordnung und Inventarisierung der Sammlungen verantwortlich war.

Serie C umfaßt 158 Modelle aus rohem (unbehandeltem) Birnenholz, die in schwarz kaschierte Kartons (80 x 85 mm) eingeordnet sind. Als Begleitzettel werden nun einheitliche Vordrucke mit dem Format 64 x 58 mm verwendet. Darauf ist erstmals auch die Institutsbezeichnung festgehalten. Die Namen und kristallographischen Bezeichnungen sind auch hier handschriftlich eingetragen. Die Schrift weist wesentlich andere Züge auf, als auf den Begleitzetteln der Serien A und B. Zum weiteren Unterschied sind hier die kristallographischen Bezeichnungen nur mehr in den Miller'schen Indizes angegeben. Aus dem bereits erwähnten Inventarbuch ist zu entnehmen, daß diese Serie in 5 Etappen in den Jahren 1892/93 “aus der Krantz'schen Sammlung nach Groth” angekauft wurde. Aus diesen Eintragungen scheint auch hervorzugehen, daß es damals zwei Sätze nach Groth gegeben habe – einen zu 412 und einen zweiten zu 743 Formen. Die in Innsbruck verwahrte Serie stellt demnach nur einen Bruchteil der von Groth vorgestellten Formen dar. Die eingetieften Zahlen sind als Produktionsnummern daher nicht lückenlos durchgehend. Der Ankauf dieser Serie erfolgte zu einem Zeitpunkt, als Alois Cathrein, der Schüler von Groth war, die Lehrkanzel bereits zwei Jahre innehatte. Man kann daher erwarten, daß die Eintragungen auf den Begleitzetteln seiner Hand entstammen.

Serie D mit der Inventarbezeichnung B 204 besteht aus 56 Modellen, die ebenfalls aus Birnenholz gefertigt sind. Das Inventarbuch gibt darüber Auskunft, daß diese Serie im Jahre 1913 durch Ankauf an das Institut kam. Wie weiters vermerkt ist, handelt es sich dabei um Verzerrungen nach Hirschwald. Eine kurze Notiz besagt weiters, daß diese Serie anscheinend nicht bei den anderen Modellen verwahrt wurde, sondern sich „*im Glaskasten im Hörsaal*“ befand. Die Begleitzettel gleichen jenen der Serie C.

Mit der Bezeichnung E ist eine Serie von 172 Modellen zusammengefaßt, die nach ihren unterschiedlichen Größen, ihren verschiedenen Holzarten und der zum Teil eigenwilligen Behandlung der Formoberflächen wohl verschiedenen Produktionsstätten entstammen müssen.

Die ersten 50 Modelle stellen Grundformen der sieben Kristallsysteme dar. Darauf folgen Modelle, die laut Beschreibung verschiedenen Mineralgruppen zugeordnet werden. Eine Ordnung in kristallographischer Hinsicht ist nicht erkennbar. Insoferne weist aber diese Serie eine Besonderheit auf, weil die Flächen der Modelle zum Teil bunt bemalt sind. Einige sind mit Papier überklebt und transparent bemalt. An einigen Formen sind Weiss'sche Indizes angebracht. Die Begleitzettel weisen keine kristallographischen Angaben auf. Weiters lassen die knappen handschriftlichen Vermerke für die Begleitzettel eine jüngere Entstehung vermuten. Somit wird der Eindruck erweckt, als hätte man Restbestände verschiedener Gruppen in späterer Zeit zu einer Serie zusammengefaßt. Die Handschrift der Begleitzettel kann derzeit noch keiner bestimmten Person zugeschrieben werden.

In den beiden untersten Laden (Nr. 11 und 22) sind insgesamt 230 Kristallmodelle aus Gips verwahrt. Auf den ersten Blick ist in dieser Serie, die keine eigene Bezeichnung trägt, kein festes System erkennbar. Hier sind die Modelle zum Teil in schwarzen Kartons unterschiedlicher Größe verwahrt, zum anderen Teil in einheitlichen Schächtelchen (100 x 65 mm) aus grauem Karton, der außenseits mit grünem Papier kaschiert ist, untergebracht.

Die Modelle in den schwarzen Kartons sind durch eingravierte und aufgemalte Inventarnummern gekennzeichnet, wobei einige Stücke mehrere Zahlen in schwarzer oder roter Farbe aufweisen, also mehr als einmal inventarisiert wurden. Bei diesen Modellen handelt es sich um zwei- und mehrgliedrige Kombinationen verschiedener Kristallsysteme, weiters um Zwillingssbildungen und um „*durch ungleichmäßige und unvollständige Flächenentwicklung*“ entstandene Verzerrungen. Ihnen sind Begleitzettel beigelegt, die in Form und Handschrift jenen der Serie A und B gleichen. Man erkennt in diesen Eintragungen wieder die Handschrift von Josef Blaas. Als späterer Zusatz durch fremde Hand findet sich auch ein Hinweis auf das alte Inventarbuch. Unter der Bezeichnung B 207 ist dort über die Herkunft zu lesen „*Kristallmodelle aus Gips (aus dem Pichler Inventar) 48 Stück*“ Diese Eintragung ist nicht mit dem Eingangsdatum versehen, doch muß die Erwerbung nach 1913, also viele Jahre nach Pichlers Tod erfolgt sein. Wo diese Modelle sich bis dahin befunden haben und warum die Begleitzettel nicht Pichlers Handschrift zeigen, sondern jene von Josef Blaas, kann vorerst nicht geklärt werden.

Wenn man nach Ausgliederung der vorhin beschriebenen Formen jene Modelle der grünen Kartons näher betrachtet, kann man sehr wohl ein System erkennen, nach dem diese Serie aufgebaut war. Die Nummern der Modelle sind am Boden der Schächtelchen mit Mineralnamen und der kristallographischen Bezeichnung – hier aber lediglich in der heute nicht mehr gebräuchlichen Nomenklatur nach Samuel Weiss – versehen. Auch die Schrift – „*deutsche Schreibschrift*“ – mutet altertümlich an und ist heutzutage für viele nicht mehr lesbar.

Vielleicht mag das auch der Grund gewesen sein, warum diese Serie nach der letzten Übersiedlung des Institutes nicht mehr richtig eingeordnet wurde. Sie ist erst ab der Nummer 36 einigermaßen vollständig erhalten. Es gibt aber Hinweise, daß die vorausgehenden Nummern, die heute leider fehlen, einfache Formen, Zwillinge und Verzerrungen des kubischen Kristallsystems enthalten haben.

Die vorhandenen Modelle liegen meist zu zweit oder zu dritt in einer Schachtel. Dabei handelt es sich durchwegs um binäre Formen, die nach Kristallsystemen eingeordnet sind. Formen des triklinen Systems fehlen vollständig. Durch die Einordnung der Modelle zu zweit und zu dritt sollte offenbar die abwechselnde Dominanz der auftretenden Glieder und die dadurch bedingte Veränderung der Kristallflächen veranschaulicht werden.

Über die Herkunft dieser Serie ist weiter nichts überliefert. Im bereits erwähnten Inventarbuch Bd. I findet man jedoch unter der Bezeichnung B 209 die Eintragung "*Kristallmodelle aus Holz und Gips 359 Stück um 600.- (Schilling) am 6.2.29 aus dem geol. Institut übernommen*". Leider hat sich aber dort die Spur dieser Sammlung nicht weiter verfolgen lassen, weil ältere Aufzeichnungen, die über die Herkunft des Inventars Auskunft geben könnten, nicht aufscheinen. Es darf aber wohl mit Sicherheit angenommen werden, daß man in dieser Serie den ältesten Teil der Innsbrucker Kristallmodellsammlung erblicken kann. Man wird weiters auch nicht fehlgehen, den Erwerb dieser Serie mit der Institutsgründung bzw. der Ernennung Adolf Pichlers zu dessen erstem Ordinarius im Jahre 1867 anzusetzen. Offen bleibt dabei aber die Frage, ob diese Gipsformen, die heute in einer Serie zusammengefaßt sind, auch ursprünglich zusammengehört haben, oder aus zwei verschiedenen Sammlungen stammen. Unbeantwortet bleibt weiterhin auch, warum die einfachen Formen des kubischen Systems fehlen.

Schließlich sind noch 8 Modelle aus Glas zu erwähnen, die einfache Formen der verschiedenen Kristallklassen darstellen. Sie tragen weder Inventarnummer, noch eine Serienbezeichnung. Ihre Herkunft ist ungewiß. Sicherlich kann es sich nicht um jene, im alten Inventarbuch verzeichneten Stücke handeln, die dort mit Inv.Nr. B 9 angeführt sind, denn diese hatten angeblich sichtbare Achsen. Sie wurden 1884 von Löwensohn in Fürth gekauft, waren aber bereits vier Jahre später als "Abfall" gemeldet.

Wenn es auch noch nicht gelungen ist, alle Fragen, die diese Sammlung aufwirft, bis ins Letzte zu klären, so kann doch mit diesem Überblick etwas Licht in den Ablauf ihres Zustandekommens geworfen werden. Es ist somit auch ein Beitrag zur Aufhellung der Institutsgeschichte. Man kann froh sein, daß sich diese Sammlung mit ihren insgesamt 909 Modellen, abgesehen von einigen Abgängen, bis zum heutigen Tag erhalten hat und sich nun im Institut als Einheit präsentieren kann.

DISTRIBUTION OF REE AND REE-MINERALS IN TOPAZ-BEARING GRANITES  
OF THE KARLOVY VARY PLUTON (CZECH REPUBLIC)

by

**U. Kempe<sup>1</sup>, M. René<sup>2</sup> & D. Wolf<sup>1</sup>**

<sup>1</sup>Institut für Mineralogie

Technische Universität, Bergakademie Freiberg, Brennhausgasse 14, D-09596

<sup>2</sup>Institute of Rock Structure and Mechanics

Academy of Sciences of the Czech Republic, V Holešovičkách 41, 182 09 Prague 8

Topaz-bearing granites are significant variety of high-evolved granite plutons. In the Erzgebirge/Krušné Hory batholith topaz-bearing granites form the youngest phases of younger magmatic complex. High-peraluminous and high-P topaz-bearing granites occur in some granite bodies in the western part of the Erzgebirge/Krušné Hory batholith. Very typical occurrences of more varieties of topaz-bearing granite were found in the Krudum massif. Krudum massif in the SW part of the Karlovy Vary pluton forms relatively independent magmatic body that is composed entirely of intermediate to high-differentiated Variscan granites with various content of topaz. The youngest topaz-albite granites on the southeastern margin of this oval body are associated with Sn-W mineralization of greisen type. This mineralization is bounded on various topaz-albite granite stocks, mainly on Hub and Schnöd stocks, in which were Sn-W ores mined from 13<sup>th</sup> century to 1991. Exploitation in last fifty years was focused mostly on low-grade impregnation ores containing on average 0.2 - 0.3 % Sn. Krudum massif has a markedly zoned internal structure with the oldest porphyritic biotite granites of the Trídomí type in its central part and younger two-mica granites and topaz-albite granites on its periphery. The youngest granite phase of aplitic albite granite form small stock on the southeast margin of the Krudum massif by Vysoký Kámen hill. In this granite stock occur also irregular, mostly subhorizontal lenses and layers of feldspathites. From hidden stock granite structures of Sn-W ore deposit Krásno-Horní Slavkov with elevations Hub and Schnöd made by topaz-albite granites is stock of aplitic aplite granite separated by thick shear zone of Vysoký Kámen.

Two-mica, finely porphyritic granites of the Milicie type are medium grained, sometimes contain minute phenocrysts of perthitic K-feldspar an their groundmass consists of K-feldspar, plagioclase ( $An_{5-20}$ ), quartz, biotite, muscovite, topaz and accessory minerals (zircon, monazite, rare apatite and magnetite). Medium-grained equigranular topaz-albite granites of the Čistá type are generally grey, greyish white and whitish in colour. They contain quartz, albite ( $An_{0-10}$ ), K-feldspar, Li-mica and topaz. Accessory minerals are represented by apatite, fluorite, zircon, Nb-Ta-rutile, columbite, tantalite, monazite, xenotime, uraninite, thorianite, pyrite, scheelite and cassiterite and by rare REE-minerals of As-crandallite-As-florencite-As-goyazite group. Cathodoluminescence and microprobe analyses allowed distinguishing several generations of apatites.

The equigranular topaz-albite granites are locally accompanied by fine-grained porphyritic topaz-albite granites with characteristic oval phenocrysts of quartz. Three generations of quartz were distinguished by cathodoluminescence microscopy. The K-feldspar phenocrysts are generally markedly perthitic. Groundmass is composed of quartz, albite ( $An_{03-05}$ ), K-feldspar, Li-mica, topaz and muscovite. Accessory minerals are formed by apatite, zircon, monazite, magnetite, hematite and cassiterite. The emplacement of granite stocks of topaz-albite granites was associated with intensive protrusion of lithologically favourable metamorphic rocks (migmatized biotite paragneisses) and evolution of intrusive breccias. Intrusive breccias are cemented by topaz-albite microgranites. These microgranites are fine grained to very fine grained, rarely porphyritic rocks. Groundmass of microgranites is composed of quartz, albite, Li-mica, K-feldspar and topaz. Accessory minerals of the topaz-albite microgranites are formed by apatite, Nb-Ta-rutile, monazite, zircon, brabantite, xenotime, gahnite and Sn-Zn-spinel. For zircon is characteristic very variable content of U and Th. The higher content of  $UO_2$  (1.2 - 7.2 wt.%) is characteristic for all analysed monazites from topaz-albite granites of the Krudum massif. Content of  $UO_2$  in analysed xenotimes is 2.0 - 5.2 wt.%.

Aplitic albite granites are fine grained to middle grained, white or pale pink rocks that contain albite ( $An_{0-8}$ ), K-feldspar and smaller quantity of quartz and accessory amount of Li-mica or muscovite. Other accessory minerals in aplitic albite granites are formed by apatite, Nb-Ta-rutile, columbite, tantalite, monazite, zircon, wolframite and uraninite. For apatite is characteristic very variable content of Mn, which also strongly influences its cathodoluminescence. The feldspathites are composed mostly of albite and K-feldspar, with subordinate content of quartz. In granite stock were also found irregular lenses and dykes of pegmatites. Schliers of the older pegmatites are probably comagmatic with aplitic albite granite and represent parts of original granite melts with enrichment of some volatile and incompatible elements (F, Be, Sc). Younger, but also Variscan pegmatite dykes are oriented in NE-SW, NW-SE and NNW-SSE directions and are formed by K-feldspar, quartz and Li-mica with some rare minerals (beryl, bertrandite, kolbeckite). The small time interval between emplacement of aplitic albite granite and evolution of pegmatite dykes is confirmed by hydrothermal alteration (albitization, muscovitization, greisenization) of both rock types. After mineral composition of pegmatites should be distinguished three subtypes of these pegmatites - quartz - feldspars, quartz-Li-mica and quartz-Li-mica-beryl pegmatites.

Topaz-bearing granites of the Krudum massif are strongly peraluminous. The prominent excess of aluminium is also expressed by the content of normative corundum, mean value of which is 3.8 for two-mica granites of the Milíře type and 4.5 for topaz-albite granites of the Čistá type. In comparison with common Ca-poor granites the topaz-bearing granites of the Krudum massif are poor in Ca, Fe, Mg, Sr, Ba, Zr, Sc and strongly enriched in incompatible elements such as Li, Rb, Cs, Sn, Nb, and W. The Milíře type two-mica granites are characterised by higher ratios  $Th/U = 1.1$  and  $La_N/Yb_N = 5.47 - 8.13$ . These two-mica granites show negative europium anomaly, which is, however, less distinct than that of younger topaz-albite granites of the Čistá type ( $Eu/Eu^* = 0.29 - 0.40$ ). Topaz-albite granites of the Čistá type display lower ratio  $Th/U = 0.4$ , reflecting presence of accessory uraninite and lower monazite content in these granites. Values of  $La_N/Yb_N$  ratio in the Čistá types granites are 3.82 - 4.81 and a prominent negative europium anomaly is very characteristic for these granites ( $Eu/Eu^* = 0.28 - 0.32$ ). The topaz-albite granites of the Čistá type are also characterised by a higher  $P_2O_5$ -content (0.24 - 0.54 wt.%).

**CHICXULUB – POPIGAI: LARGE IMPACT CRATERS AND THEIR DISTAL EJECTA.  
ISOTOPIC CHARACTERISATION OF THE MELT PRODUCTS**

by

**B. Kettrup & A. Deutsch**

Institut für Planetologie  
Universität Münster, Wilhelm-Klemm-Strasse 10, D-48149 Münster

In this study, we characterize impact melt products and target lithologies at impact sites, and compare them with ejected impact melt products, such as tektites, micro-tektites, impact melt glass, micro-krystites. We utilize isotopic "fingerprinting" techniques which have a much higher sensitivity than conventional geochemical analyses [1, 2].

With this investigation, we search answers to the following questions:

What is the depth of the melt zone? How intense is the mixing of impact melt that stays inside the crater? Can we characterize the target from the study of clast populations and/or from geochemical data for impact melt lithologies? In which depth originate ejected impact melt products? Which methods allow an unambiguous correlation of ejected melt products with their respective source crater?

The below listed material has been studied:

- Impact melt breccias, suevites and their clast content from Chicxulub PEMES drill cores. The 65 m. yrs. old Chicxulub structure, the "smoking gun" of the K/T mass extinction has a diameter of  $\approx 180$  km. The crater is buried beneath about 1 km of post-impact sediments.
- Ejected impact melt products separated from K/T boundary sediments.
- For comparison, we investigate melt lithologies, and target rocks from the excellently exposed 35.7 m. yrs. old, about 100 km large Popigai impact structure.

**Chicxulub.** In the  $\epsilon_{\text{Nd}}$  vs.  $\epsilon_{\text{Sr}}$  plot of Figure 1, the Chicxulub melt lithologies display a surprisingly large variation in Nd isotopic compositions [3]. We have explained this observation with a major contribution of a mafic target component to the impact melt lithologies. Such mafic rocks have not yet been described to occur as clasts in impact breccias of the Chicxulub crater. Despite the restricted data set (due to the non-availability of samples!), our isotopic investigation yielded one fundamental result [3]: The Chicxulub impact melt lithologies are not the product of simple mixing of two components, i.e., Cretaceous platform sediments and a homogeneous crystalline basement (cf. Fig. 1).

**Popigai.** Impactites from this crater display a wide range in  $\epsilon_{\text{Sr}}$  values (Fig. 2) [4]. It is not constrained yet whether this observation reflects variable contributions of specific target components to individual melt volumes or post-impact alteration. Variations in  $\epsilon_{\text{Nd}}$  of the Late Eocene ejecta material [5] are relatively high compared to impactites. The data for micro-krystites and micro-spherules, plot with one exception in a field defined by target lithologies (Fig. 2).

This data alignment and the Nd model ages support the view that Popigai is the source crater for this kind of ejecta material. Impactites and ejecta material, however, form two, only partially overlapping clusters. The ejecta materials have a higher affinity to the younger sedimentary cover than impactites whose data alignment can be explained by melting of basement gneisses and granites only (Fig. 2). A contribution of sedimentary rocks to the impactites is not obvious, though the sediments occur as clasts in the tagamites.

**Ejecta.** The geochemistry of tektites, formed early in the cratering process, match the composition of the uppermost target lithologies (sediments), which not necessarily resemble the composition of deeper seated target material. Generally, tektites from one strewn field show only restricted variations in  $\epsilon_{\text{Sr}}$  and  $\epsilon_{\text{Nd}}$ . Impact melt glass, derived from deeper target levels, have a more variable compositions (e.g., Late Eocene ejecta in Fig. 3). A correlation with the parent crater was so far only possible in a few cases [1, 2]. We would like to emphasize in this context that only parts of the terrestrial crater population are known, and that systematic isotope studies on impact craters are still very scarce.

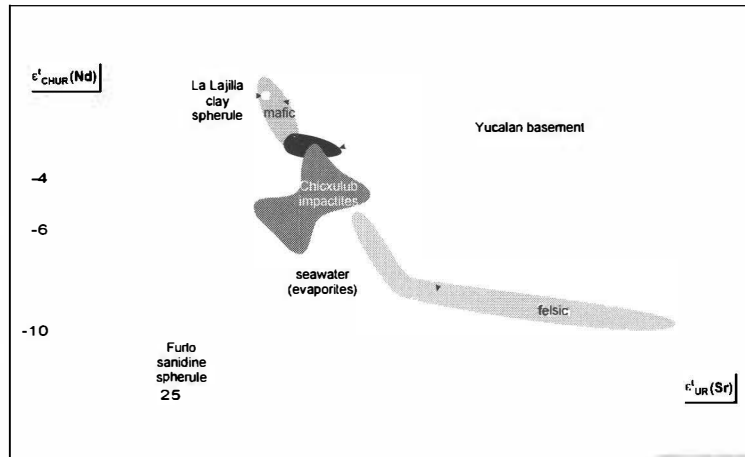


**Figure 1**  
Time-corrected  $\epsilon_{\text{Sr}}\text{-}\epsilon_{\text{Nd}}$  diagram ( $t=65$  Ma) for impactites and target rocks from the Chicxulub crater and related ejecta material for K/T boundary sediments [3, with refs.].

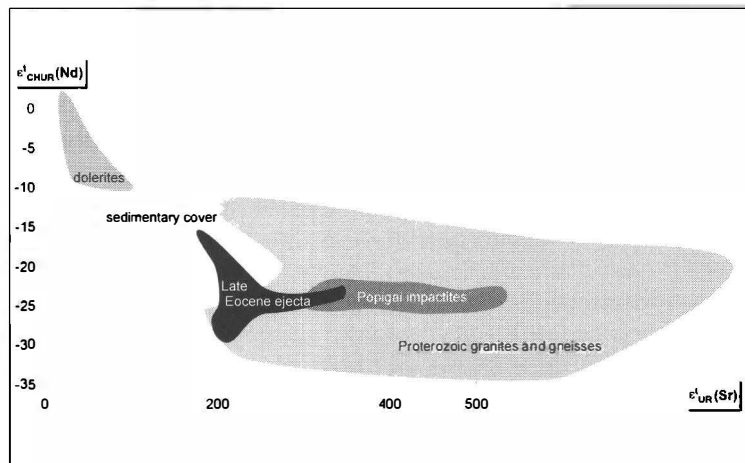


**Figure 2**  
Time-corrected  $\epsilon_{\text{Sr}}\text{-}\epsilon_{\text{Nd}}$  diagram ( $t=35.7$  Ma) for impactites and target rocks from the Popigai crater [4, with refs.] and Late Eocene ejecta material (microkrystites, micro-spherules [5]).

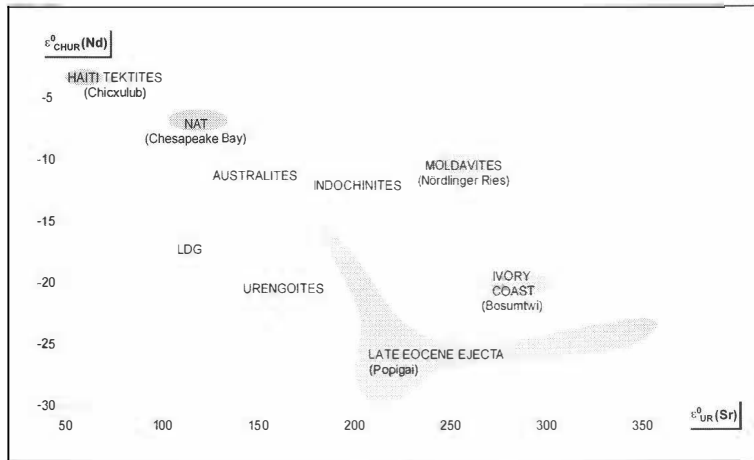


**Figure 3**

$\epsilon_{\text{Sr}}-\epsilon_{\text{Nd}}$  diagram for tektites, tektite-like objects, and ejected impact glass. Note large variations for the Late Eocene Ejecta. Data sources: [2, with refs.; 5]. LDG: Libyan Desert Glass; NAT: North American tektites.

We appreciate support by the DFG (grants De 401/12, and GRK 189/3. This work is part of B.K. Ph.D. thesis.

## References

- [1] SHAW, H. F. & WASSERBURG, G. J. (1982): Age and provenance of the target material for tektites and possible impactites as inferred from Sm-Nd and Rb-Sr systematics. - Earth Planet. Sci. Lett. 60: 155-177.
- [2] DEUTSCH, A. et al.. (1997): Geochemistry and neodymium-strontium isotope signature of tektite-like objects from Siberia (urengoites, South-Ural glass). - Meteoritics Planet. Sci. 32: 679-686.
- [3] KETTRUP, B. et al. (2000): Chicxulub impactites: geochemical clues to the precursor rocks. - Meteoritics Planet. Sci. 35: 1229-1238.
- [4] KETTRUP, B. et al. (2001): Sr, Nd isotope composition of impact melt coated gneiss bombs and tagamites, Popigai crater, Russia. - Lunar Planet. Sci. 32, 1290 (CD-ROM).
- [5] WHITEHEAD, J. et al. (2000): Late Eocene impact ejecta: geochemical and isotopic connections with the Popigai impact structure. - EPSL 181: 473-487.

**PARTIAL ANATEXIS IN THE LOWER CRUST – WHERE IS THE MELT ?  
EXAMPLES FROM THE ÖTZTAL CRYSTALLINE BASEMENT, EASTERN ALPS**

by

**E. Klötzli-Chowanetz & F. Koller**

Institut für Petrologie  
Geozentrum, Universität Wien, Althanstrasse 14, A-1090 Wien

Partial anatexis of biotite-plagioclase-paragneisses is known to have taken place in several sites within the Ötztal crystalline complex, a polymetamorphic basement unit of the Eastern Alps in Austria. Petrological investigations were made in the Ordovician Winnebach migmatite [1] and the Cambrian Klopaijer migmatite [2]. Both are schollen-migmatites build up by a granodioritic matrix surrounding Bt-Pl-gneiss-schollen.

The genesis of the Winnebach migmatite is currently explained by an in situ melting of paragneisses leading to granodioritic neosome with a nonoriented texture enclosing schollen that have withstood melting and preserved their layering [3]. In another model the schollen have been interpreted as migmatite s. str. and the matrix as tonalitic intrusion [4].

This matrix or "neosome" shows fine-grained aggregates of plagioclase, resorbed K-feldspar and minor amounts of quartz [2]. We interpret these patches as having been the actual melt. Most of the quartz originally present in this melt has precipitated on neighbouring quartz grains, thus forming large quartz-islands surrounding the melt pockets [5]. Biotite in contact with the melt pockets shows beginning of melting. The "neosome" has therefore to be regarded as only partially molten (about 20%). This low degree of melting and the dispersed distribution of the melt pockets within the "neosome" imply the remaining of the melt in situ.

A first generation of coarse grained kyanite occurring only within the "neosome" in the vicinity of melt pockets and not within the schollen favors a crossing of the muscovite breakdown reaction curve within the stability field of kyanite. This requires pressures above 0.8 GP for the onset of the anatexis. Fe/(Fe+Mg) ratios in garnet below 0.7 suggest temperatures exceeding 750°C [6]. These conditions are achieved for instance in a continent-continent collision regime.

A postanatectic metamorphic overprint, attributed to the Variscan cycle, is marked by a second kyanite generation growing within migmatite and surrounding paragneisses and is thought to have exceeded 500°C (reequilibrated garnets, appearance of staurolite). However, the preservation of Ordovician white mica Rb-Sr ages within the Winnebach migmatite does not permit the temperature to have risen significantly above 550°C.

The anatetic P-T conditions within the Klopaijer migmatite have reached a similar state of melting as in the Winnebach migmatite. The melt phase is represented by fine-grained aggregates of plagioclase, K-feldspar and quartz. Biotite is involved in the melting reaction. However the kyanite present can be the result of an anatetic muscovite breakdown as well as of a postanatetic metamorphic overprint, which has lead sillimanite (or even andalusite) to recrystallise. Since the formation of kyanite in the Klopaijer migmatite cannot be attributed without doubt to the anatetic event, the pressure estimates for this older anatexis remain uncertain.

## Literature

- [1] KLÖTZLI-CHOWANETZ, E., KLÖTZLI, U. & KOLLER, F. (1997): Lower Ordovician migmatisation in the Ötztal crystalline basement (Eastern Alps, Austria): linking U-Pb and Pb-Pb dating with zircon morphology. - *SMPM*, 77, 315-324.
- [2] KLÖTZLI-CHOWANETZ, E. (2001): Migmatite des Ötzalkristallins – Petrologie und Geochronologie. - Diss. Univ. Wien, 165 p.
- [3] HOINKES, G. (1973): Die Anatexis des Winnebachgranites (Ötzaler Alpen, Österreich) am Beispiele eines Aufschlusses. - *TMPM*, 20, 225-239.
- [4] SCHINDLMAYR, A. (1999): Granitoids and Plutonic Evolution of the Ötztal-Stubai Massif – A Key for Understanding the Early Palaeozoic History of the Austroalpine Crystalline Basement in the Western Eastern Alps - Diss. Univ. Salzburg, 288 p.
- [5] CLEMENS, J. D. & HOLNESS, M. B. (2000): Textural evolution and partial melting of arkose in a contact aureole: a case study and implications. - *Electronic Geosciences* (2000) 5:4 Springer.
- [6] SPEAR, F. S., KOHN, M. J. & CHENEY, J. T. (1999): P-T paths from anatetic pelites. - *Contr. Mineral. Petrol.*, 134, 17-32.

CAMBRIAN MIGMATISATION AND ORDOVICIAN TONALITIC INTRUSION –  
KLOPAIER AREA, ÖTZTAL CRYSTALLINE COMPLEX, EASTERN ALPS

by

E. Klötzli-Chowanetz<sup>1</sup>, U. Klötzli<sup>2</sup> & T. Skiöld<sup>3</sup>

<sup>1</sup>Institut für Petrologie

Geozentrum, Universität Wien, Althanstrasse 14, A-1090 Wien

<sup>2</sup>Institut für Geologie

Geozentrum, Universität Wien, Althanstrasse 14, A-1090 Wien

<sup>3</sup>Swedish Museum of Natural History

Box 50007, SE-104 05 Stockholm

Elongated enclaves of anatetic paragneisses can be seen in a tonalite near the Klopaiер Spizе in the SW part of the polymetamorphic Öztal crystalline complex (Eastern Alps, Austria). In an attempt to decide whether or not anatexis and tonalite intrusion are contemporaneous, single zircon Pb-Pb evaporation and ion microprobe (Cameca 1270) U-Th-Pb dating have been carried out on both the Klopaier tonalite and the Klopaier migmatite.

Evaporation data of magmatic type zircons (typological subgroups S 23 – S 25) from the tonalite yield a mean plateau-age of  $487 \pm 16$  Ma. In contrast, different types of zircon populations extracted from the Klopaier migmatite suggest three or four zircon growth events, the first around 640 - 630 Ma, the second and possibly third within the Cambrian. In this case evaporation data alone did not resolve the number of events. An Ordovician event at around 490 Ma is commonly encountered with in the region, but surprisingly enough this age figure is not depicted among the migmatite zircons. The youngest record in the evaporation results hint to a Late Ordovician – Early Silurian overprint.

The ion microprobe analyses from the migmatite document three events of zircon growth, namely at  $585 \pm 8$  Ma,  $531 \pm 11$  Ma, and  $430 \pm 6$  Ma. These sets of data were obtained from long prismatic zircons. Spheroidal zircons which are thought to have grown exclusively during the anatexis [1, 2] fall in the 531 Ma age group.

The comparison of zircon populations from the migmatite and the tonalite demonstrates a wall-rock assimilation of the anatetic metasediments by the tonalite, field relations give also evidence for stoping. This implies an anatetic event preceding the tonalitic intrusion which is in agreement with the older age result of  $531 \pm 11$  Ma for the spheroidal zircons from the migmatite, whereas the magmatic zircons of the tonalite give a younger, namely Ordovician intrusion ages of  $487 \pm 16$  Ma.

On a regional scale, i.e. throughout the Ötztal and the Silvretta crystalline complexes the high temperature event at  $531 \pm 11$  Ma encountered in the Klopaiers migmatite appears to correspond to the Late Cambrian formation of granitoids such as the Mönchhalpgneiss [3 and references therein]. The age of 487 Ma of the tonalite intrusion fits well into the model of an extended acidic magmatic activity in the Ordovician. Similarly, the age of  $430 \pm 6$  Ma can be compared with orthogneisses in the southernmost Kaunertal dated at  $435 \pm 8$  Ma [4] and crosscutting granites in the Winnebach area (central Ötztal) dated at  $444 \pm 4$  Ma [5]. These combined evidences of detailed age dating support the presence of another widespread acidic magmatic event in Early Silurian time.

#### Literature

- [1] KLÖTZLI-CHOWANETZ, E. (2001): Migmatite des Ötztalkristallins – Petrologie und Geochronologie. - Diss. Univ. Wien, 165 p.
- [2] SKIÖLD, T., BOGDANOVA, S., GORBATSCHEV, R. & BIBIKOVA, E. (in press): Timing of Palaeoproterozoic metamorphism in the northern Belomorian Belt, White Sea region: conclusions from U-Pb isotopic data and P-T evidence. - Bull. Geol. Soc. Finland.
- [3] POLLER, U. (1997): U-Pb single zircon study of gabbroic and granitic rocks of Val Barlas-ch (Silvretta nappe, Switzerland). - SMPM, 77, 351-359.
- [4] LICHÉM, C. (1993): Petrologische und geochemische Untersuchungen an Orthogneisen des westlichen Ötztal-Stubai Kristallins (Kaunertal). - Diplomarbeit, Univ. Graz, 139 p.
- [5] SÖLLNER, F. & HANSEN, B. T. (1987): "Pan-afrikanisches" und "kaledonisches" Ereignis im Ötztal-Kristallin der Ostalpen: Rb-Sr- und U-Pb-Altersbestimmungen an Migmatiten und Metamorphiten. - Jb. Geol. B.-A., 130, Heft 4, 529-569.

BORON INCORPORATION IN RARE-EARTH SILICATE APATITES:  
A SINGLE-CRYSTAL X-RAY STUDY

by

**U. Kolitsch**

Institut für Mineralogie und Kristallographie  
Geozentrum, Universität Wien, Althanstrasse 14, A-1090 Wien

As part of studies of the system  $\text{Y}_2\text{O}_3\text{-TiO}_2\text{-SiO}_2$ , a B-rich Y silicate apatite has been grown as whitish hexagonal prisms with the help of a  $\text{PbO}_2\text{-PbF}_2\text{-MoO}_3\text{-B(OH)}_3$  flux (for details see Refs. [1],[2]). The crystal structure has been refined in space group  $\text{P}6_3/\text{m}$  typical of rare-earth (RE) silicate apatites  $(\text{RE}_{3.33}\square_{0.67})^{\text{IX}}\text{RE}_6^{\text{VII}}(\text{Si}^{\text{IV}}\text{O}^{\text{IV}}_4)_6\text{O}^{\text{III}}_2$  ( $\square$  = cation vacancy; roman numbers = coordination numbers). For the refinement single-crystal X-ray diffraction data were used (Mo-K $\alpha$  radiation, CCD area detector, room temperature).

Crystal data and R factors are:  $a = 9.260(1)$ ,  $c = 6.748(1)$  Å,  $V = 501.10(11)$  Å $^3$ ,  $R_1 = 2.88\%$  for 743 'observed' reflections [ $F_o > 4\sigma(F_o)$ ]. SEM-EDS analyses showed only the presence of Y and Si. The refinement provided convincing evidence that ~20 % of the Si has been replaced by B, with a concomitant filling-up of the cation-deficient Y 4f site. The charge-balanced formula,  $(\text{Y}_{3.73}\square_{0.27})_{\Sigma 4.00}\text{Y}_6[(\text{SiO}_4)_{4.80}(\text{BO}_4)_{1.20}]_{\Sigma 6.00}\text{O}_2$ , is also in accordance with a refinement of the occupancies of the two Y sites (4f, 6h). As expected, the B incorporation results in a considerably decreased average (Si,B)-O bond length of 1.592 Å, and in decreased unit-cell parameters by comparison to B-free Y silicate apatites. A strong decrease is especially observed for the  $a$  parameter.

The present results confirm the work of ITO (1968)[3] who prepared polycrystalline B-bearing Y silicate oxyapatites at 1150°C and inferred the existence of two complete solid solution series  $\text{Y}_{10}\text{Si}_4\text{B}_2\text{O}_{26} \leftrightarrow \text{Mg}_2\text{Y}_8\text{Si}_6\text{O}_{26}$  and  $\text{Y}_{10}\text{Si}_4\text{B}_2\text{O}_{26} \leftrightarrow \text{Ca}_2\text{Y}_8\text{Si}_6\text{O}_{26}$ , based on the observation of linear changes of unit-cell parameters along the respective series. The given formula,  $\text{Y}_{10}\text{Si}_4\text{B}_2\text{O}_{26}$ , can be rewritten as  $\text{Y}_4\text{Y}_6[(\text{SiO}_4)_4(\text{BO}_4)_2]_{\Sigma 6}\text{O}_2$ , thus demonstrating that this apatite is characterised by completely filled Y sites and a replacement of every third  $\text{SiO}_4$  tetrahedron by a  $\text{BO}_4$  tetrahedron. A comparison of the unit-cell parameters of  $\text{Y}_{10}\text{Si}_4\text{B}_2\text{O}_{26}$ ,  $a = 9.15$ ,  $c = 6.75$  Å[3], with those of  $(\text{Y}_{3.73}\square_{0.27})_{\Sigma 4.00}\text{Y}_6[(\text{SiO}_4)_{4.80}(\text{BO}_4)_{1.20}]_{\Sigma 6.00}\text{O}_2$ ,  $a = 9.260(1)$ ,  $c = 6.748(1)$  Å, shows that the further increase of the incorporated amount of B leads to a distinct decrease of the  $a$  parameter, but apparently does not affect the  $c$  parameter to any significant degree.

Very recently, a B-rich La silicate apatite was prepared and characterised by Rietveld refinement of neutron powder diffraction data.[4] The given formula,  $\text{La}_5\text{Si}_2\text{BO}_{13}$ , can be reformulated as  $\text{La}_4\text{La}_6[(\text{SiO}_4)_4(\text{BO}_4)_2]\Sigma_6\text{O}_2$ , again demonstrating that in rare-earth silicate apatites every third  $\text{SiO}_4$  tetrahedron can be replaced by a  $\text{BO}_4$  tetrahedron. Similar B incorporation could also occur in natural (RE,Ca)-silicate-phosphate apatites (britholites).

Further comparisons are drawn with the solid solutions series  $\text{RE}_{9.33+2x}(\text{Si}_{1-x}\text{Al}_x\text{O}_4)_6\text{O}_2$  [5].

The financial support of the Deutsche Forschungsgemeinschaft (DFG) via a Research Fellowship to the author is gratefully acknowledged.

## References

- [1] KOLITSCH, U. (2001): Flux growth, crystal data and crystal chemistry of silicates, titanates, titanate-molybdates and molybdates of Nd, Gd, Y and Sc. - To be submitted.
- [2] KOLITSCH, U. (2001): Crystal chemistry of four flux-grown neodymium, gadolinium and yttrium silicate apatites: incorporation of Pb, Li and B, and implications for ionic conductivity. - To be submitted.
- [3] ITO, J. (1968): Silicate apatites and oxyapatites. - Am. Mineral., 53, 890-907.
- [4] MAZZA, D., TRIBAUDINO, M., DELMASTRO, A. & LEBECH, B. (2000): Synthesis and neutron diffraction study of  $\text{La}_5\text{Si}_2\text{BO}_{13}$ , an analog of the apatite mineral. - J. Solid State Chem., 155, 389-393.
- [5] KOLITSCH, U., SEIFERT, H. J. & ALDINGER, F. (1998): Phase relationships in the systems  $\text{RE}_2\text{O}_3\text{-Al}_2\text{O}_3\text{-SiO}_2$  (RE = rare earth element, Y, and Sc). - J. Phase Equilibria 19, 426-33.

THE CRYSTAL STRUCTURE OF WYCHEPROOFITE, A RARE HYDRATED  
NA-AL-ZR-PHOSPHATE FROM WYCHEPROOF, VICTORIA, AUSTRALIA

by

**U. Kolitsch**

Institut für Mineralogie und Kristallographie  
Geozentrum, Universität Wien, Althanstrasse 14, A-1090 Wien

Wycheproofite is a rare phosphate mineral species known only from pegmatite veins in a granite quarry at Wycheproof, Victoria, Australia. The original description[1] reports the formula  $\text{NaAlZr}(\text{PO}_4)_2(\text{OH})_2 \cdot \text{H}_2\text{O}$ , triclinic symmetry and the preliminary unit-cell parameters  $a = 10.926(5)$ ,  $b = 10.986(5)$ ,  $c = 12.479(9)$  Å,  $\alpha = 71.37(4)$ ,  $\beta = 77.39(4)$ ,  $\gamma = 87.54(3)$ °,  $V = 1375.9$  Å<sup>3</sup>, determined with the help of electron diffraction. The mineral occurs as compact, finely fibrous masses in small cavities in the pegmatite. The fibrous crystals of the type material are only 5 - 10 µm wide but up to several mm long.[1]

To determine the previously unknown crystal structure of wycheproofite, a single-crystal X-ray study (CCD detector, MoKα radiation) was undertaken, using a tiny, elongate crystal fragment with the dimensions 0.02 x 0.03 x 0.08 mm. It gave a completely revised unit cell,  $a = 5.263(1)$ ,  $b = 9.251(2)$ ,  $c = 9.480(2)$  Å,  $\alpha = 109.49(3)$ ,  $\beta = 98.57(3)$ ,  $\gamma = 90.09(3)$ °,  $V = 429.60(15)$  Å<sup>3</sup>,  $Z = 2$ . The crystal structure was solved in space group  $\bar{P}\bar{1}$  (no. 2) to  $R1 = 4.18$  % for 1731 'observed' reflections. It contains zigzag chains of edge-sharing  $\text{AlO}_2(\text{OH})_4$  octahedra along [100] which are linked via corners to  $\text{PO}_4$  tetrahedra. Each corner of the  $\text{ZrO}_6$  octahedron is shared with these  $\text{PO}_4$  tetrahedra. All mentioned polyhedra are fairly regular and average Al-O, Zr-O and P-O bond lengths are 1.898, 2.063 and 1.529 Å, respectively. A Na site, partially occupied (~ 88 %) and slightly disordered, is located in a void of the resulting three-dimensional framework, and forms a  $\text{NaO}_3(\text{OH})_{2-x}(\text{H}_2\text{O})_{2-x}$  ( $x \sim 0.7$ ) polyhedron. Three of its O ligands (Ow12 and 2x Ow11) are also only partially occupied and somewhat disordered, in agreement with bond-valence calculations. The originally given formula is therefore an idealised formula. Only very weak hydrogen bonding is present.

Comparisons are drawn to the structures of the few other known natural and synthetic zirconium phosphates (e.g., kosnarite -  $\text{KZr}_2(\text{PO}_4)_3$ ; selwynite -  $\text{NaK}(\text{Be}, \text{Al})\text{Zr}_2(\text{PO}_4)_4 \cdot 2\text{H}_2\text{O}$ ; mahlmoodite -  $\text{FeZr}(\text{PO}_4)_2 \cdot 4\text{H}_2\text{O}$ ; synthetic  $\text{ZrKH}(\text{PO}_4)_2$  and  $\text{Zr}_2(\text{NaPO}_4)_4 \cdot 6\text{H}_2\text{O}$ ) and related metal phosphates. Common structure features are pointed out.

Dr. Bill Birch, Museum Victoria, Melbourne, is thanked for kindly furnishing the studied sample. The financial support of the Deutsche Forschungsgemeinschaft (DFG) via a Research Fellowship to the author is gratefully acknowledged.

## References

- [1] BIRCH, W. D., PRING, A., KHARISUN & BEVAN, D. J. M. (1994): Wycheoproofite: a new hydrated sodium aluminium zirconium phosphate from Wycheoproof, Victoria, Australia and a new occurrence of kosnarite. - *Mineral. Mag.* 58, 635-39.

STRONG PSEUDOSYMMETRY IN THE CRYSTAL STRUCTURE OF  
ANTHROPOGENIC  $\text{Pb}_2(\text{OH})_3(\text{NO}_3)$  FROM A MEDIEVAL MINE DUMP

by

**U. Kolitsch**

Institut für Mineralogie und Kristallographie  
Geozentrum, Universität Wien, Althanstrasse 14, A-1090 Wien

Recently, an anthropogenic occurrence of the well-known synthetic basic lead nitrate  $\text{Pb}_2(\text{OH})_3(\text{NO}_3)$  was briefly described from the Altemannfels dump of the medieval Pb-Zn-Ag mining district Badenweiler, Black Forest, Germany [1]. The ruler-shaped colourless crystals have formed by anthropogenic processes, probably involving black gunpowder used in the blasting of ore.  $\text{Pb}_2(\text{OH})_3(\text{NO}_3)$  is associated with elyite,  $\text{Pb}_4\text{Cu}(\text{SO}_4)\text{O}_2\cdot(\text{OH})_4\cdot\text{H}_2\text{O}$ , hydrocerussite,  $\text{Pb}_3(\text{CO}_3)_2(\text{OH})_2$ , and, rarely, another anthropogenic lead nitrate with formula  $\text{Pb}_{13}\text{O}_8(\text{OH})_6(\text{NO}_3)_4$  (rhombohedral, space group  $R\bar{3}$ ,  $a = 10.263(1)$ ,  $c = 25.454(5)$  Å); its recently solved crystal structure contains a unique  $[\text{Pb}_{13}\text{O}_8(\text{OH})_6]^{4+}$  cluster characterised by a near-icosahedral arrangement of two Pb atoms around a third Pb atom at the centre of the cluster [2, 3].

The previously unknown crystal structure of  $\text{Pb}_2(\text{OH})_3(\text{NO}_3)$  was determined from single-crystal X-ray intensity data (CCD detector, MoK $\alpha$  radiation). The compound is metrically orthorhombic, with  $a = 8.31$ ,  $b = 8.55$ ,  $c = 17.19$  Å, but is strongly pseudosymmetric (pseudo-space group  $I\overline{m}mm$ ). The true space group is  $P1$ , with  $a = 8.314(2)$ ,  $b = 8.545(2)$ ,  $c = 10.467(2)$  Å,  $\alpha = 114.08(3)$ ,  $\beta = 113.40(3)$ ,  $\gamma = 90.00(3)^\circ$ ,  $V = 611.3(2)$  Å $^3$  and  $Z = 4$  ( $R1 = 3.95\%$  for 4759 'observed' reflections).

The dominant structure element is a cuboid  $[\text{Pb}_8(\text{OH})_{12}]^{4+}$  cluster previously unknown from inorganic lead compounds. The cluster can be described as eight Pb atoms at the corners of a 'cube', with kinked Pb–OH–Pb bonds representing the cube edges. Strong to weak hydrogen bonds within the cluster provide an internal stabilisation. The clusters are arranged in a plane parallel to (001) to form Pb–OH 'layers', which are separated by layers composed of fairly distorted  $\text{NO}_3^-$  groups. Connection between the  $[\text{Pb}_8(\text{OH})_{12}]^{4+}$  clusters is achieved by weak hydrogen bonds within the Pb–OH 'layer'. Linkage to the  $\text{NO}_3^-$  groups is achieved by very weak Pb–O<sub>nitrato</sub> bonds. All Pb atoms exhibit stereochemical activity of their  $6s^2$  lone electron pairs. The distinct pseudosymmetry results from the orthorhombic arrangement of the Pb atoms. Reported data on  $[\text{Pb}_x^{2+}(\text{O},\text{OH})_y]^{n+}$  clusters and basic lead nitrates are summarised and critically discussed. The probable conditions of formation of  $\text{Pb}_2(\text{OH})_3(\text{NO}_3)$  and  $\text{Pb}_{13}\text{O}_8(\text{OH})_6(\text{NO}_3)_4$  are evaluated, and Raman spectroscopic data for both compounds are reported.

Hans-Werner Graf of Niederzier-Ellen, Germany, is thanked for kindly furnishing the studied samples. The financial support of the Deutsche Forschungsgemeinschaft (DFG) via a Research Fellowship to the author is gratefully acknowledged.

## References

- [1] WALENTA, K. (1998): Neue Mineralfunde aus dem Schwarzwald. - 7. Folge, 2. Teil. Lapis, 23 (12), 43-8. (in German)
- [2] LI, Y., KRIVOVICHEV, S. V. & BURNS, P. C. (2001): Crystal chemistry of lead oxide hydroxide nitrates. II. The crystal structure of  $Pb_{13}O_8(OH)_6(NO_3)_4$ . - J. Solid State Chem. (in press).
- [3] KOLITSCH, U. (2001): The crystal structures of two anthropogenic basic lead nitrates: two new  $Pb-(O,OH)$  clusters. - Mineral. Mag. (submitted).

**FROM MORB TO SSZ – THE SOUTH ALBANIAN OPHIOLITES  
AND THEIR DINARIC-HELLENIC FRAMEWORK**

by

**F. Koller<sup>1</sup>, V. Hoeck<sup>2</sup>, K. Onuzi<sup>3</sup>, E. Knernerger<sup>1</sup> & T. Meisel<sup>4</sup>**

<sup>1</sup>Institut of Petrology

University of Vienna, Geozentrum, Althanstrasse 14, A-1090 Wien

<sup>2</sup>Institute of Geology

University of Salzburg, Hellbrunnerstrasse 34, A-5020 Salzburg

<sup>3</sup>Geological Institute of Tirana

Blloku Vasil Shanto, Tirana, Albania

<sup>4</sup>Institute of General and Analytical Chemistry

Montanistic University of Leoben, Franz-Josefstrasse 18, A-8700 Leoben

Within the eastern Mediterranean ophiolites the Albanian portion forms very well developed sections. They are part of the western ophiolitic belt, ranging from Croatia in the north over Bosnia, Montenegro, Albania to Greece in the south. Generally, the Albanian ophiolites, locally named Mirdita ophiolites, are divided in a western and an eastern zone, where the former shows MORB and the latter SSZ signatures according to SHALLO, 1992; BORTOLOTTI et al., 1996, ROBERTSON & SHALLO, 2000. They continue towards the south into the Pindos ophiolites and the Central Greek ophiolites. Towards the north they are connected with the Bosnian and Croatian ophiolites.

The ophiolite complex of Voskopoja, one of the major ophiolite bodies of the South Albanian ophiolites is located in the southernmost part of the Albanian (Mirdita) ophiolites and forms, together with the complexes of Shpati, Devolli, Vallamare, Morava, Shebeniku, and Bitincka, the southern Mirdita ophiolites. Except for the latter two complexes they are interpreted to be a continuation of the western zone, the Shebeniku and Bitincka are compared to the ophiolites of the eastern zone (SHALLO, 1992). The contrast between the western and the eastern ophiolites, well developed in northern Albania, is not so clearly recognizable in southern Albania.

According to our own investigations most of the ophiolitic mantle sections in the Voskopoja and neighbouring ophiolites such as Rehove or Morava, contain lherzolite together with a subordinate amount of harzburgite and dunite. Individual ultramafic thrustsheets in Voskopoja and Morava are separated by metamorphic soles. Wehrellites are common and form the majority of the ultramafic cumulates, which indicates that pyroxenites and wherlites are not only restricted to the Shebeniku and Spati Massif as believed earlier.

Troctolites, metagabbros and olivinegabbros represent the mafic cumulates, clinopyroxene gabbros, occur in Devolli, Voskopoja and Rehove, but are not so common. Gabbronorites occur only in Morava, plagiogranites seem to be mainly absent.

Fragments of a sheeted dike complex were found recently in the Rehove section. Only four ophiolites (Shpati, Devolli, Vallamare, and Voskopoja) contain a volcanic section directly overlying the ultramafic and/or mafic cumulate sequence. Ultramafic cumulates, gabbros and basalts underwent an oceanic metamorphism of variable degree. For example, amphibole, hydrogrossular and serpentinite result from a metamorphic overprint.

Geochemical data of lavas of the Voskopoja and Rehove (an extrusive section is missing in Morava) indicate a relatively wide range of geochemistry intermediate between typical MORB and island arc tholeiites erupted in a SSZ environment. They can be grouped into four groups: a high Ni-group; a low Ni-group; a high Ti-Zr Group and a low Ti-Zr group. The first two groups are apart from the Ni concentration relatively similar, the high Ni group contains additional olivine and spinell xenocrysts from the mantle causing the high Ni concentration. In the spider diagrams both groups are similar to MORBs, but often slightly depleted as observed in back arc basins. The High Ti-Zr basalts are significantly enriched, the low Ti-Zr group is markedly depleted. This variation in element concentrations and element ratios can not be explained by crystal fractionation or partial melting processes alone but requires most probably a tapping of geochemical heterogeneous mantle portions.

Compared with other ophiolites in the Dinaric-Hellenic realm (e.g.: the Pindos ophiolite in Greece, a continuation of the western zone of the south Albanian ophiolites) there is obviously a wide variety in lithology and geochemistry of the ophiolite. This indicates a geochemical variation from MORB to SSZ tholeiites, not only between the eastern and the western zone, but also in a north-south direction along the main axis of the ophiolites on a regional scale. The same mid- to upper Jurassic formation age, the occurrence of metamorphic soles and comparable sediments on top indicate a common formation and emplacement history.

## References

- BORTOLOTTI, V., KODRA, A., MARRONI, M., MUSTAFA, F., PANDOLFI, L., PRINCIPI, G. & SACCANI, E. (1996): Ophioliti, 21, 3-20.  
ROBERTSON, A. & SHALLO, M. (2000): Tectonophysics 316, 197-254.  
SHALLO, M. (1992): Geol. Rdsch, 81, 681-692.

**DOMAIN FORMATION IN A STAUROLITE-KYANITE AMPHIBOLITE  
OF THE SCHNEEBERG COMPLEX, SOUTHERN TYROL:  
APPLICATIONS OF THERMOBAROMETRY TO LOCAL EQUILIBRIUM DOMAINS**

by

**J. Konzett & P. Tropper**

Institute of Mineralogy and Petrography  
University of Innsbruck, Innrain 52, A-6020 Innsbruck

Within the Paleozoic Austroalpine Schneeberg Complex, unusual Al-rich staurolite-bearing assemblages occur. These assemblages form within the contact between calcite marble, interlayered calc-micaschists and amphibole-bearing metamarls.

In one of these localities, the assemblage staurolite + Ca-amphibole was found within a garnet amphibolite sample containing the assemblage staurolite + Ca-amphibole + margarite + kyanite + clinozoisite. Careful textural examination revealed that Ca-amphibole and staurolite are part of entirely different kinds of domains: staurolite occurs within Al-rich domains in the assemblage staurolite + margarite + kyanite + clinozoisite/epidote + plagioclase + biotite + muscovite without quartz, while Ca-amphibole is confined to Al-poor domains containing the assemblage Ca-amphibole + calcite + clinozoisite/epidote + biotite + plagioclase + quartz. Although both assemblages occur within a thin section, they show different reaction histories. The Al-poor domains are characterized by the breakdown of the assemblage Ca-amphibole + muscovite according to the model reaction in the system KCMASH:  $5\text{muscovite} + 3\text{tremolite} \leftrightarrow 2\text{clinozoisite} + 5\text{phlogopite} + 2\text{anorthite} + 14\text{quartz} + 2\text{H}_2\text{O}$ . The Al-rich domains show an equilibrium assemblage containing margarite + kyanite + plagioclase + clinozoisite/epidote, which probably developed by a complete consumption of quartz.

P-T-a(H<sub>2</sub>O) estimates of sample K34 were calculated with the program THERMOCALC v 2.7. with the thermodynamic data base of HOLLAND & POWELL (1998). Within the assemblage zoisite + clinozoisite + margarite + kyanite in the Al-rich domain, several reactions can be calculated. Since no quartz is present in this domain anymore, a quartz-absent invariant point can be calculated involving the reaction kyanite + zoisite/clinozoisite  $\leftrightarrow$  anorthite + margarite and the transition reaction zoisite  $\leftrightarrow$  clinozoisite. These calculations yields  $9.3 \pm 0.5$  kbar and  $569 \pm 24^\circ\text{C}$  for the Al-rich domain of sample K 34. The a(H<sub>2</sub>O) from this sample has also been estimated by calculating a P-a(H<sub>2</sub>O) diagram, after estimating the P-T conditions with the H<sub>2</sub>O-independent reactions as discussed above. For these claculations, muscovite and biotite were also added to the calculations. The resulting a(H<sub>2</sub>O) is low and ranges from 0.39 to 0.47 at pressures between 9.3 and 9.5 kbar.

Application of WEBINVEQ thermobarometry (GORDON, 1992) to the adjacent rocks yields pressures of 8 - 10 kbar at temperatures of 540 - 590°C. These high pressures may be interpreted in favour of an overall pressure increase of the Eo-Alpine metamorphism from NW towards SE within the Ötztal-Stubai Crystalline Complex, culminating in the formation of Eo-Alpine eclogites in the southwest of the Schneeberg Complex (HOINKES et al., 1991).

### References

- GORDON, T. (1992): *Geochim. Cosmochim. Acta* 56, 1793-1800.  
HOINKES, G., KOSTNER, A. & THÖNI, M. (1991): *Mineral. Petrol.* 43, 237-254.  
HOLLAND, T. J. B. & POWELL, R. (1998): *J. Metam. Geol.* 8, 89-124.

**GEOCHEMISCHE UNTERSUCHUNGEN VON GRUBENWÄSSERN MIT DITHIZON**

von

**W. Körner<sup>1</sup>, L. Weber<sup>2</sup> & H. H. Weinke<sup>1</sup>**

<sup>1</sup>Institut für Geochemie

Geozentrum, Universität Wien, Althanstrasse 14, A-1090 Wien

<sup>2</sup>Montanbehörde

Bundesministerium für Wirtschaft und Arbeit, Wien

## **Einführung**

Die Belastung von Grubenwässern mit den Schwermetallen Blei und Zink in ehemaligen Bergbauern des Grazer Paläozoikums wird mittels der Dithizonmethode [1, 2] analysiert. Im Mittelpunkt der Untersuchungen stehen zahlreiche kleine Gruben sowie Halden des Grazer Paläozoikums [3], wo seit dem Mittelalter bis zum Beginn dieses Jahrhunderts Erz abgebaut wurde.

## **Untersuchungen**

Das als Nachweisreagens für Schwermetalle verwendete Dithizon (Diphenyl-thiocarbazone,  $H_2Dz$ ) ist in Wasser und verdünnten Säuren kaum, in verdünntem Ammoniak und organischen Lösungsmitteln wie Chloroform und Tetrachlorkohlenstoff gut löslich. Über die Verwendung in der Mikro- und Spurenanalyse gibt es die ausgezeichnete Übersicht von G. IWANTSCHEFF [4]. Blei und Zink gehören zu den Elementen, die stabile Metalldithizonate  $MeHDz$  bilden. Das in den organischen Lösungsmitteln smaragdgrün vorliegende Dithizon bildet mit den Schwermetallen größtenteils rote Chelatkomplexe.

Die Entfärbung von noch im Überschuß vorliegendem grünen Dithizon erfolgt durch Zugabe von Ammoniak. Die resultierende rote Färbung der Schwermetall-komplexe wird bei 520 nm nach dem Einfärbenverfahren quantitativ photo-metriert werden.

Für die gleichzeitige Bestimmung der Elemente Blei und Zink in einer Wasserprobe müssen zur Maskierung geeignete Komplexierungsmittel verwendet werden. Mit jeder Probe werden vier Bestimmungen ausgeführt:

1. die Summe von Blei und Zink,
2. Blei unter Maskierung von Zink mit Cyanid,
3. Zink unter Maskierung von Blei mit Thiosulfat,
4. weitere störende chelatbildende Elemente durch Maskierung beider Elemente.

Für die Einstellung der Reagenzien ist wesentlich, daß die photometrischen Eichkurven bis zu 100 ppb im linearen Bereich liegen.

Die gemessenen Extinktionen der Schwermetalle sowie die berechneten Regressionsgeraden sind in Abb.1 dargestellt. Die Blei- und Zinkgehalte von Bergbauwässern aus dem ehemaligen Blei-Zinkbergbau Arzberg, Steiermark, werden in Tabelle 1 angegeben.

Vergleichsmessungen mit der Atomabsorption in der Konfiguration, Zink mit Flamme und Blei mit Graphitrohr, zeigen sehr gute Übereinstimmung.

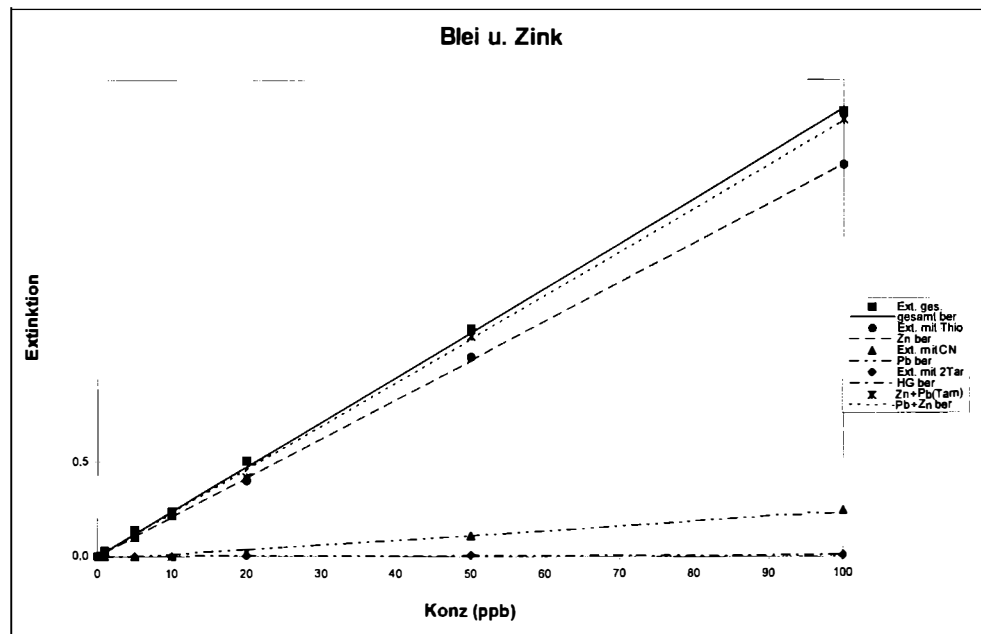


*Abb. 1  
Photometrische Eichgerade nach Dithizon-Einfarbenmethode.*

### Schlußfolgerungen

Für die geochemische Prospektion von Wässern, die mit Blei- und Zinkerzen in Berührung gekommen sind, ist die vorliegende Methode bis zu einer Nachweisgrenze von 1 ppb für Zink und etwa 5 ppb für Blei, infolge der wesentlich geringeren Farbintensität, hervorragend geeignet. Als obere Grenze in Laboruntersuchungen unter Verwendung eines Filterphotometers ist der Meßbereich bis etwa 100 ppb für beide Elemente ausreichend linear. Für Geländearbeiten ist eine 0.001%-ige H<sub>2</sub>Dz-lösung besser geeignet. Vor allem, wenn als obere Erfassungsgrenze 25 ppb Blei bzw. Zink festgelegt werden kann. Durch den geringeren H<sub>2</sub>Dz-Gehalt kann eine semi-quantitativen Abstufung der Metallgehalte direkt vorgenommen werden.

Überraschend sind die geringen Konzentrationen an Schwermetallen in stehenden Grubenwässern. Dies ist auf den hohen pH-Wert zurückzuführen. Demgegenüber sind die Schwermetalle im (karbonathältigen) Schlamm angereichert. Fließ- oder Tropfwässer zeigen in Abhängigkeit einer Erznähe deutliche Schwermetallführung, weswegen sich dieser Schnellnachweis als ausgezeichnete Prospektionsmethode empfiehlt.

Probe:	Verd.	Ext.ges.	Ext. Zn	Zn	Ext. Pb	Pb	Ext.sum.
AS		0,230	0,212	10	0,008	9	0,220
AS1		0,150	0,080	4	0,073	35	0,153
AS2		0,222	0,120	6	0,076	36	0,196
ERS		0,030	0,026	1	0,008	9	0,034
ES4	1:5	1,400	1,340	65			1,342
	1:1			325	0,010	9	
ES5	1:5	0,850	0,840	41			0,850
	1:1			204	0,050	26	
ES7		0,730	0,710	34	0,007	8	0,717
LKS		0,670	0,635	31	0,043	23	0,678
MH		1,634	1,590	77	0,026	16	1,616
RS		1,058	0,960	47	0,074	36	1,034
URS/W		1,090	0,083	4	0,011	10	0,094
ZL		0,126	0,096	5	0,010	9	0,106

AS	Arbergschacht	MH	Mariahilfstollen
ERS	Eingang Raabstollen	RS ...	Raabstollen
ES	Erbstollen	URS/W ...	Unt. Raabstollen West
LKS	Nordschlag	ZL	Zwischenlauf

Tabelle 1

Blei- und Zinkkonzentrationen in ppb.

## Literatur

- [1] KOCH, O. G. & KOCH-DEDIC, G. A. (1974): Handbuch der Spurenanalyse. - Springer Berlin-Heidelberg-New York, 1597 S.
- [2] HÜTTER, L. A. (1992): Wasser und Wasseruntersuchung. - Salle + Sauerländer Frankfurt, 515 S.
- [3] WEBER, L. (1992): Die Blei-Zinkvererzung des Grazer Paläozoikums. - Archiv für Lagerstättenforschung der Geol. B.-A., H 12, Wien.
- [4] IWANTSCHEFF, G. (1972): Das Dithizon und seine Anwendung in der Mikro- und Spurenanalyse. - Verlag Chemie Weinheim, 330 S.

PETROLOGY, GEOCHEMISTRY AND EVOLUTION OF THE PERALUMINOUS  
MONOPIGADON PLUTONITE (MACEDONIA, NORTHERN GREECE)

by

A. Koroneos<sup>1</sup>, G. Christofides<sup>2</sup>, L. Heaman<sup>2</sup> & D. Krstic<sup>3</sup>

<sup>1</sup>Department of Mineralogy, Petrology and Economic Geology

School of Geology, Aristotle University of Thessaloniki, GR-540 06 Thessaloniki, Greece

<sup>2</sup>Department of Earth and Atmospheric Sciences

University of Alberta, Edmonton, Alberta, Canada T6G 2E3

<sup>3</sup>Geospec Consultants Limited

4632 151 Street, Edmonton, Alberta, Canada

The Upper Jurassic Monopigadon plutonite intrudes both the Chalkidiki ophiolites, which are part of the Late Triassic to Middle Jurassic Vardar ophiolitic belt and a supra-ophiolitic formation [1]. The granite occupies an area of about 10 km<sup>2</sup> in the NW part of Chalkidiki. The plutonite is covered by Tertiary and Neogene sediments and is unconformably overlain by the Kimmeridian-Tithonian Petralona limestones. An arkosic layer occurs locally at the base of Petralona limestones, and a conglomerate a few meters above it [1]. Drillings made for the investigation of the Epanomi gas field (15 km SW of Monopigadon), found a granodiorite at ca 3400 m depth below the Peonia limestones considered as the continuation of the Monopigadon plutonite [2]. The age of the Monopigadon plutonite is constrained both by stratigraphic evidence and radiometric measurements. It is unconformably overlain by the Kimmeridgian – Tithonian Petralona limestones [3] while an age of  $141 \pm 3$  Ma was obtained by K/Ar method on biotite separates [1]. Since a weak greenschist facies metamorphism affects the plutonite and its cover, it is concluded [1] that this K/Ar age is likely younger than the magmatic emplacement age, which is close to 150 Ma as at Fanos. Recently a single zircon evaporation Pb/Pb age of  $192.5 \pm 3.8$  Ma has been reported [4]. Preliminary zircon U/Pb datings gave a minimum emplacement age of 161 Ma, although an intercept age of 184 Ma was obtained using line fitted through slightly different data points (our unpubl. data).

The Monopigadon plutonite consists of biotite granodiorite (BGrd) and biotite to two-mica (BGr to TMG) granite cut by aplitic dykes (Apl). The BGrd contains xenoliths and enclaves. The BGrd is fine to medium-grained consisting of quartz, not perthitic K-feldspar ( $Or_{84}Ab_{16}$  -  $Or_{95}Ab_5$ ) and slightly zoned plagioclase with core ranging from  $An_{29}$  to  $An_{34}$  and rim ranging from  $An_{27}$  to  $An_{29}$ . Biotite exists in higher amounts relative to the rest rock-types (20 vol. %). Zircon, apatite and sphene are present as accessories. The BGr is coarse to medium-grained intruding BGrd. The main mineral constituents are quartz, perthitic K-feldspar ( $Or_{94}Ab_6$ ), zoned plagioclase ( $An_{21-14}$ ). Biotite is present in lesser amount (7 vol. %) relative to BGrd. Zircon, apatite and sphene are present.

The TMG is a fine to medium-grained leucocratic rock. Their perthitic K-feldspars ( $\text{Or}_{95}\text{Ab}_5$ ) are kaolinized and the plagioclases are zoned (core  $\text{An}_{20}$ , rim  $\text{An}_{16}$ ) and often altered to sericite. Biotite does not exceed 5 vol.%. The Apl are rich in quartz and K-feldspar with minor amounts of biotite. Xenoliths, 3 to 20 cm in length, are fine- to medium-grained, spheroidal, and dark-green to black in colour. They are surrounded by a biotite-rich rim. Some times only biotite-concentrates, 0.3 to 2 cm in dimension, are found. The enclaves are fine-grained rocks, with small amount of quartz, K-feldspar, plagioclase altered to sericite, biotite and magnetite. They have the same mineralogy with the host rock differing in the amount and size of apatite and zircon. The latter form more abundant, bigger and euhedral crystals. Biotite is reddish-brown to brown, Mg-rich ( $\text{Mg}/(\text{Mg}+\text{Fe}) = 0.46$  to 0.49) in BGrd and BGr while it is yellow-brown to brown, Mg-poor ( $\text{Mg}/(\text{Mg}+\text{Fe}) = 0.31$ ) in TMG. The ASI number of biotites, ranges from 1.5 to 2.0 reflecting increased alumina activity in the magma. Muscovite is present only in the more acid rock-type (TMG), in amount less than 4 vol.%). Although textural and chemical criteria ( $\text{TiO}_2 < 0.6$  wt.%) cannot distinguish between a primary and a post-solidus origin of muscovite the latter seems more plausible.

The Monopigadon plutonite is slightly peraluminous (ASI = 1.0 - 1.2). With increasing  $\text{SiO}_2$  content,  $\text{TiO}_2$ ,  $\text{MnO}$ ,  $\text{CaO}$ ,  $\text{FeO}$ ,  $\text{MgO}$  decrease in BGrd and from BGr to TMGr and Apl. A compositional gap between BGrd and BGr+TMGr exists except for  $\text{CaO}$  and  $\text{MnO}$ .  $\text{K}_2\text{O}$  and  $\text{Na}_2\text{O}$  are almost constant in BGrd while the former increases from BGr to TMGr and Apl and the latter decreases from BGr to TMGr and Apl. Total alkalies are constant both in BGrd and in BGr+TMGr with a significant compositional gap c.a. 2 %.  $\text{Fe}_2\text{O}_3$  increases in BGrd and then decreases from BGr to TMGr and Apl.  $\text{P}_2\text{O}_5$  generally decreases in BGrd and increases from BGr to TMGr.  $\text{Al}_2\text{O}_3$  forms two subparallel decreasing trends one for BGrd and another for BGr and TMGr.

From the less evolved towards the more evolved BGrd rocks V, Cr, Cu, Ga, Co, Ni, Zn, Rb and Sr decrease and Zr, Pb, Y, Nb, Ce, Th increase while La and Ba are almost stable. From BGr to TMG, V, Ga, Co, Sr, Ba, Zr, Nb, La, Ce, Th decrease and Cr, Zn, Rb, Pb increase, while Cu, Ni, Y are almost constant. A significant compositional gap, with or without change in the compatible/incompatible behaviour, exists between BGrd and (BGr+TMG) for V, Cr, Cu, Ni, Zn, Rb, Sr, Y, Ce. The REE patterns are very similar implying a common origin for all the rocks. The  $\Sigma\text{REE}$  increases indicating that the REE behaviour is not essentially controlled by the accessories. The  $(\text{La}/\text{Yb})_{\text{CN}}$  ratio decreases with increasing  $\text{SiO}_2$ . All the samples show negative Eu anomalies varying from 0.8 in BGrd to 0.3 in BGr and TMGr. The high negative correlation between  $\text{Eu}/\text{Eu}^*$  and Sr suggests plagioclase fractionation.

Field and petrographic relations along with mineralogical and geochemical features suggest that the plutonite consists of two main different groups of rocks (except enclaves and aplites), possibly with common origin, not related by a fractionation process. At least in the half of the presented Harker diagrams the BGrd are separated from the group of BGr+TMG. In each one of the two groups the differentiation is due to a fractional crystallization process (or AFC) since no mixing or mingling phenomena are obvious. This is supported also by the presence of normal zoning in plagioclases, the decrease of anorthite content in them and the decrease of Mg-number of biotites with  $\text{SiO}_2$  content of the rocks. Major element fractional crystallization models, tested by trace elements, support an AFC process for the evolution of the rocks. 50 % fractionation of  $\text{Pl}_{41}\text{Kf}_{4}\text{Bi}_{32}\text{Ap}_1\text{Mt}_1\text{Qz}_{21}$  is required for the evolution of BGrd while TMG is formed from BGr through 40 % fractionation of  $\text{Pl}_{52}\text{Kf}_{16}\text{Bi}_{13}\text{Ap}_1\text{Mt}_2\text{Sph}_1\text{Qz}_{15}$ .

## **References**

- [1] MICHARD, A. et al. (1988): The Chalkidiki supra-ophiolitic formations, and their bearing on the Vardarian obduction process. - Bull. Geol. Soc. Greece, XXXII/1: 59-64.
- [2] SOUSOUNIS, G. (1993): Estimation of the hot dry rocks (HDR) with data from boreholes and seismic data. - Proc., 2nd Congress of GGA, Florina, Greece, 2: 276-287.
- [3] KOCKEL, F. & MOLLAT, H. (1977): Erlauterungen zur geologischen Karte der Kalkidiki und angrenzender Gebiete 1/100.000 (Nord-Griechenland). - Bund. Geowiss. Rohst., Hannover, 119 p.
- [4] KOSTOPOULOS, D. et al. (2001): Palaeozoic and Early Mesozoic Magmatism and Metamorphism in the Serbo-Macedonian Massif, Central Macedonia, Northern Greece. - EUG Abstr., LS03:Tham01:F2, 318.

SILICATE MELT INCLUSIONS IN OLIVINE PHENOCRYSTS  
IN THE HEGYESTŰ BASALT, BAKONY-BALATON HIGHLAND, HUNGARY

by

K. Kóthay & Cs. Szabó

Department of Petrology and Geochemistry  
Lithosphere research Group, Eötvös University, Múzeum krt. 4/A, H-1088 Budapest

In the Carpathian-Pannonian Region post-extensional alkaline basalt volcanism (EMBEY-ISZTIN et al., 1993) followed the Miocene-Pliocene (BALOGH et al., 1983) subduction-related calc-alkaline magmatism (SZABÓ et al., 1992). The principal goal of this work is to use primary silicate melt inclusions in olivine phenocrysts occurring in Hegyestű basalt, a monovolcano in the Bakony-Balaton Highland Volcanic Field, to better understand the evolution of alkaline basaltic magma.

The Hegyestű alkaline basalt shows porphyritic texture and contains forsteritic olivine phenocrysts and minor Ti-rich augite microphenocrysts. The groundmass consists of Ti-rich clinopyroxene, labradoritic plagioclase, magnetite, leucite and minor glass. The olivine phenocrysts and clinopyroxene microphenocrysts contain primary multiphase silicate melt, CO<sub>2</sub> fluid, Cr-spinel inclusions and some secondary silicate melt and CO<sub>2</sub> fluid inclusions.

The silicate melt inclusions in olivine phenocrysts consist of TiO<sub>2</sub> and Al<sub>2</sub>O<sub>3</sub> rich augite, TiO<sub>2</sub> and FeO-rich rhönite, pure CO<sub>2</sub>, sulfide blebs (pyrrhotite + chalcopyrite ± pentlandite), ± Al-spinel, ± apatite, ± ilmenite, ± rutile, ± carbonate and ± trapped Cr-spinel can be recognized in glassy groundmass. The glass is extremely rich in alkalis and some inclusions contains two immiscible glass phases with nepheline- and leucite-like composition.

The homogenization temperature of the silicate melt inclusions in olivines are between 1270 - 1300°C. However, most of the silicate melt inclusions were partially leaked prior to complete homogenization. During the heating of inclusions the glass melting occurred at 900 - 950°C, the major daughter phases disappeared consequently at 1000 - 1060°C (apatite?), 1190 - 1210°C (augite) and 1220 - 1245°C (rhönite). The homogenization temperatures of silicate melt inclusions in core and in rim of clinopyroxenes are between 1230 - 1255 °C and 1180 - 1220°C, respectively.

The bulk composition of olivine hosted silicate melt inclusions, based on mass balance calculations and furnace technique, show more mafic character and richer in alkalis: SiO<sub>2</sub> (40 - 46 wt.%), Al<sub>2</sub>O<sub>3</sub> (15 - 20 wt.%), FeO (5 - 12 wt.%), MgO (3 - 11 wt.%), TiO<sub>2</sub> (2 - 3.5 wt.%), CaO (10 - 15 wt.%), Na<sub>2</sub>O (3 - 6 wt.%), K<sub>2</sub>O (2 - 5 wt.%) compared to that of host Hegyestű basaltic magma.

## **References**

- BALOGH, K., ÁRVA-SÓS, E., PÉCSKAY, Z. (1986): *Acta Miner.-Petrogr.*, v. 27, p. 75-93.
- EMBEY-ISZTIN, A., DOWNES, H., JAMES, D. E., UPTON, B. G. J., DOBOSI, G., INGRAM, G. A., HARMON, R. S., SCHARBERT, H. G. (1993): *J. Petrol.*, v. 34, p. 317-343.
- KUNZMANN, T. (1999): *Eur. J. Mineral.*, v.11, p. 743-756.
- SZABÓ, CS., HARANGI, SZ., CSONTOS, L. (1992): *Tectonophysics*, v. 208, p. 243-256.

**ORE-MINERALOGY OF THE AU-DEPOSIT  
NEAR VOLTÝŘOV AT MILEVSKO, CZECH REPUBLIC**

by

**M. Koubová<sup>1</sup>, Z. Losos<sup>1</sup> & J. Malec<sup>2</sup>**

<sup>1</sup>Department of Mineralogy, Petrology and Geochemistry

Faculty of Science, Masaryk University, Kotlářská 2, 611 37 Brno, Czech Republic

<sup>2</sup>Institute of Raw Materials

Vitězná 425, 284 03 Kutná Hora, Czech Republic

Small Au-deposit near Voltýřov at Milevsko is located at the contact between rocks of granitic Middle-Bohemian pluton and rocks of Sedlčany-Krásná Hora "island" composed of metamorphosed host rocks. Ore-mineralization is presented in both of rock sequences: in Sázava granodiorite, Těchnice granodiorite and their rock veins – aplite and porphyric granodiorite, resp. in host rocks – orthogneisses with hornfelses. The variegated rocks (granodiorites and hornfelses) with sulphide-ores represent the contact zone of the pluton.

The ore-mineralization in surface parts of the deposit is connected with irregular vein systems and impregnations. Ore-assemblages are identical in granodiorites and orthogneisses. Ore-assemblage is composed of dominant arsenopyrite with minor pyrite. Accessory sulphides are represented by chalcopyrite, pyrrhotite, sphalerite. They have allotriomorphic form of grains and are probably younger than arsenopyrite and pyrite. All the mentioned ore-minerals are without inclusions. Gold grows together with arsenopyrite and quartz only exceptional. Quartz is typical mine waste of the veins.

Ore-assemblage of veins is characterized by accessory galenite, pure Bi, Au, Bi-tellurides and sulphosalts of Bi, Te and Pb). Maldonite and hedleyite were determined by JANATKA et al. [3]. Size of all described rare minerals (as well as gold) averages between X - X0 µm. Accessory ore-minerals often grow together. Au forms small izometric grains and very small plates, short Au-microveinlets among quartz grains are found in orthogneiss. Single Au-grains are disseminated in ores or gold grains form areas with X0 - X00 gold individuals together. Ore assemblage of veins is accompanied by scheelite.

The orthogneiss contains more pyrite than granodiorite. Pyrite, often secondary altered in markasite, is in the same position as arsenopyrite. Both of minerals in orthogneiss form euhedral grains or aggregates. These aggregates are arranged in small veins in quartz too. Quartz often has saccharoidal structure. Rare Bi, Te-minerals and Au form orbiculate inclusions in quartz among its grains. These minerals often grow together, and are located particularly at the boundary of arsenopyrite-pyrite bands in saccharoidal quartz.

In the granitoids the ores are represented by small veins of arsenopyrite, which are cataclased. Ores mainly form allotriomorphic aggregates and sometimes are dragged into the middle of veins. The veins are filled with the massive quartz or with the slips of rocks. Pyrite is probably younger than arsenopyrite and it is formed idiomorphic to allotriomorphic aggregates on the contact of arsenopyrite and quartz or of arsenopyrite and rocks. Pyrite is mostly changed into marcasite, and is far less present than arsenopyrite. Minerals of Bi, Te, and Au are above all related to the slips of rocks in the middle of the veins, or to the spurs of arsenopyrite. The impregnated ores are typical for granitoids, when the ore-minerals are broadly regularly placed in rock.

In the area of the Voltýřov Au-deposit younger Mn-mineralization occurs too, which is connected with overthrust fault zones with NE direction in orthogneisses. These zones are filled with chalcedonic quartz with lenses of pyroluzite, hematite and nontronite. These zones content remobilised gold too [3].

Except primary ores, the gold occurs far much in disintegrate rocks in this area (weathered outcrop of primary Au-ores) [2]. The cementation zone was denuded and mined in past centuries. JANATKA et al. [3] found anomalies of gold, which follow contact of the granitoid rocks with the rocks of metamorphosed "island". This Au-anomaly is extend in NE orientation and is about 2.5 km long.

Proterozoic volcanic rocks, which are equivalent of the rocks of the Jílové zone are obviously presumptive resources of gold in the deposit near Voltýřov. "Starosedelské" orthogneisses may be second source of gold. The consequential metamorphism related to the origin of granitoids caused to mobilization and redistribution of gold. The genesis of the ore-bearing is metamorphic [1]

## References

- [1] BERNARD, J. H. & POUBA, Z. et al. (1986): Rudní ložiska a metalogeneze československé části Českého masívu. - ÚÚG, Academia, Praha.
- [2] BŘEZINA, S. et al. (1992): Dílčí závěrečná zpráva úkolu rozsypová ložiska Voltýřov. - GMS, a. s. Praha, Jihlava.
- [3] JANATKA, J. et al. (1986): Dílčí závěrečná zpráva úkolu VoltDílčí závěrečná zpráva úkolyrov. - Geofond, Praha.

QUARTZ AND FELDSPAR XENOCRYSTS IN MAFIC LAVAS FROM NOGRAD-GÖMÖR  
VOLCANIC FIELD, BAKONY-BALATON HIGHLAND VOLCANIC FIELD AND  
VILLÁNY MOUNTAINS (HUNGARY)

by

I. Kovács<sup>1</sup>, Zs. Nédli<sup>2</sup>, K. Kóthay<sup>1</sup>, E. Bali<sup>1</sup>, Z. Zajacz<sup>1</sup> & Cs. Szabó<sup>1</sup>

<sup>1</sup>Department of Petrology and Geochemistry

Lithosphere Research Group, Eötvös University, Múzeum krt. 4/a, 1088 Budapest

<sup>2</sup>Department of Mineralogy, Geochemistry and Petrology

University of Szeged, Egyetem utca 2-6, 6722 Szeged

Quartz and plagioclase xenocrysts occur in mafic lavas all over the world. These are significant arguments to crustal contamination and magma – wallrock interaction (LHUR et al., 1995). Most of these xenocrysts show an interaction rim composed mostly of glass and clinopyroxene (Fig. 1). Where the glass is replaced by sanidine it refers to longer cooling period (SATO, 1974). Using experimental data, ascent velocities of the uprising magma, assessing its temperature, and the depth where the xenocrysts might have been incorporated into the magma can be estimated (WATSON, 1982).



Fig. 1

*Interaction products, coexisting glass and clinopyroxene, between quartz xenocryst and mafic lavas from the Bakony-Balaton Highland Volcanic Field (BSE image).*

Quartz and plagioclase xenocrysts were found in mafic dyke rocks in the Villány Mts. and alkali basalts in the Nógrád-Gömör and the Bakony-Balaton Highland Volcanic Field (Hungary). We present here the results of our petrographic and geochemical studies.

Quartz xenocrysts in size of 1 - 20 mm in diameters from the Villány Mountains, where the host rock is Mesozoic lamprophyre like basaltic dyke in Triassic-Jurassic limestone, have a 10 - 30 mm thick glass rim and 50 - 150 mm thick clinopyroxene corona. Composition of the clinopyroxenes in the reaction rims is augite similarly to those of the groundmass. The grain size of clinopyroxenes gradually increases from the quartz towards the host rock.

All the quartz crystals are strongly resorbed. The border of the clinopyroxene corona with the glass rim is rounded and sharp. The border towards the groundmass is also sharp: the clinopyroxenes irregularly grow into the groundmass.

In samples from Nógrád-Gömör Volcanic Field quartz and feldspar xenocrysts show size of 1.25 - 0.5 mm diameters and the glass is absent around them. However, the xenocrysts are also surrounded by clinopyroxene corona. Grain size of the clinopyroxenes (15 - 100 mm) decreases continuously from the quartz and feldspar xenocrysts towards the groundmass. Reaction rims of these xenocrysts show sharp and irregular border with the xenocrysts. The clinopyroxenes grow gradually into the groundmass forming a rounded shape border. The composition of clinopyroxenes in the rim is aegirine which is different from those in the groundmass.

Alkali basalts from the Bakony-Balaton Highland Volcanic Field also contain quartz xenocrysts which are surrounded by 0.2 - 1 mm wide glass and 0.3 - 0.8 mm wide clinopyroxene rims. Reaction rims, where carbonate minerals (siderite) often occur in the glass, show border similar to those of Nógrád-Gömör Volcanic Field.

Glasses in the interaction rims between quartz and the basaltic host rocks, based on microprobe analysis, are inhomogeneous and show very high silica content. The petrographic characteristics and geochemical data of the xenocrysts and the surrounded interaction rims confirm that the glass and clinopyroxene corona is formed via interaction of the melt and the xenocrysts. Different sizes and chemical composition of the clinopyroxene corona from the three distinct volcanic areas refer to either different composition and/or temperature of the melt interacting with the quartz/feldspar xenocrysts. The xenocrysts in compositions likewise diffused quartz xenocrysts all over the word in mafic lavas (LHUR et al., 1995) were incorporated into the melt from the crust. Xenocrysts found in mafic lavas from the Villány Mts. following their trapping into the mafic magma melted and resorbed, and may act as nucleation core for the clinopyroxene crystallization. The lack of volcanic glass in interaction rims of quartz xenocrysts from the Nógrád-Gömör Volcanic Field may be the result of the low temperature of the incorporation. The fine-grained crystals and gradually change in grain size of clinopyroxenes, as well as sharp contact with the xenocrysts probably refer to solid state diffusion in agreement with the relatively low temperature of the incorporation. Relatively thick glass rims around xenocrysts from the Bakony-Balaton Highland Volcanic Field could be explained by the high temperature of the mafic melt or the great depth of the xenocryst entrapment. The clinopyroxene bearing interaction rims are generally similar to those described from Nógrád-Gömör Volcanic Field. The presence of carbonate bearing volcanic glass in the rims of the basalts in the Villány Mts. and the Bakony-Balaton Highland may refer to high CO<sub>2</sub> content of the mafic melt.

## References

- [1] LHUR, F. J., PIER, G. J., ARANDA-GOMEZ, J. J. & PODOSEK, A. F. (1995): Crustal contamination in early Basin-and-Range hawaiites of the Los Encinos Volcanic Field, central Mexico. - Contrib. Mineral. Petrol. 118, 321-339.
- [2] SATO, H. (1975): Diffusion coronas around quartz xenocrysts in andesite and basalt from Tertiary volcanic region in Northeastern Shikoku, Japan. - Contrib. Mineral. Petrol. 50, 46-64.
- [3] WATSON, B. E. (1982): Basalt contamination by continental crust: some experiments and models. - Contrib. Mineral. Petrol. 80, 73-87.

NEUSTÄDTELITE AND COBALTNEUSTÄDTELITE,  
TWO NEW MINERALS OF THE MEDENBACHITE-GROUP

by

W. Krause<sup>1</sup>, H.-J. Bernhardt<sup>2</sup>, C. McCammon<sup>3</sup> & H. Effenberger<sup>4</sup>

<sup>1</sup>Henriette-Lott-Weg 8, 50354 Hürth, Germany

<sup>2</sup>Institut für Mineralogie

Ruhr-Universität Bochum, Universitätsstrasse 150, 44780 Bochum, Germany

<sup>3</sup>Bayerisches Geoinstitut

Universität Bayreuth, 95440, Bayreuth, Germany

<sup>4</sup>Institut für Mineralogie und Kristallographie

Universität Wien, Geocenter, Althanstrasse 14, A-1090 Wien, Austria

The minerals of the medenbachite group have space-group symmetry  $P\bar{1}$  and have the chemical formula  $\text{Bi}_2\text{M}_1\text{M}_2(\text{O},\text{OH})_2(\text{OH})_2(\text{AsO}_4)_2$ ; end-member composition of medenbachite [1] / cobalt-neustädtelite / neustädtelite is  $\text{M}_1 = \text{Fe}^{3+}$ ,  $\text{M}_2 = \text{Cu}^{2+}/\text{Co}^{2+}/\text{Fe}^{3+}$ . On the average, the three minerals have the same crystal structure. Medenbachite is isotypic with cobaltneustädtelite; neustädtelite is isostructural. The medenbachite-group minerals with  $\text{M}_2^{3+}$ , two OH groups, and two oxo-oxygen groups p.f.u. have a "small" unit cell with  $Z = 1$  (neustädtelite); in cases with  $\text{M}_2^{2+}$ , three OH groups, and one oxo-oxygen atom p.f.u. the unit cell is "large",  $Z = 2$  (medenbachite and cobaltneustädtelite). The intensities of the superstructure reflections responsible for the change of the unit cell originate from order phenomena of the split Bi site.

Neustädtelite and cobaltneustädtelite were found on samples from the dumps of the Güldener Falk Mine (Schneeberg-Neustädtel, Saxony, Germany). The appearance of the two new minerals is very similar: small tabular crystals up to 0.2 mm in diameter, transparent to translucent, with a brown color and a light brown streak; the lustre is adamantine. Both minerals are biaxial negative,  $2V = 65(5)^\circ$ ,  $n_x = 2.02(2)$ ,  $n_y = 2.09$  (calc.),  $n_z = 2.12(2)$ ; pleochroism is strong with X = brown to opaque, Y = yellow, Z = pale yellow. Mohs' hardness is  $4\frac{1}{2}$ . The cleavage parallel to {001} is good. The chemical composition was derived by means of electron-microprobe analyses. Average contents for neustädtelite / cobaltneustädtelite are (in wt.%):  $\text{Bi}_2\text{O}_3$  52.58/51.54,  $\text{PbO}$  0.08/0.08,  $\text{CaO}$  0.15/0.32,  $\text{Fe}_2\text{O}_3$  13.92/10.90,  $\text{Al}_2\text{O}_3$  0.29/0.07,  $\text{CoO}$  3.35/5.47,  $\text{NiO}$  0.34/1.61,  $\text{ZnO}$  0.09/0.39,  $\text{CuO}$  0.07/0.00,  $\text{As}_2\text{O}_5$  26.82/25.91,  $\text{P}_2\text{O}_5$  0.23/0.43,  $\text{H}_2\text{O}$  (calc.) 2.56/3.01, total 100.48/99.73.

Based on 12 oxygen atoms the empirical formulas for the neustädtelite and cobaltneustädtelite type material are

$\text{Bi}_{1.94}\text{Ca}_{0.02}\Sigma_{1.96}\text{Fe}_{0.99}(\text{Fe}_{0.51}\text{Co}_{0.38}\text{Ni}_{0.04}\text{Al}_{0.05}\text{Zn}_{0.01}\text{Cu}_{0.01})\Sigma_{1.00}[(\text{OH})_{2.44}\text{O}_{1.54}\Sigma_{3.98}[(\text{AsO}_4)_{2.01}(\text{PO}_4)_{0.03}\Sigma_{2.04}$   
and

$(\text{Bi}_{1.91}\text{Ca}_{0.05})_{\Sigma 1.96}\text{Fe}_{1.02}(\text{Co}_{0.63}\text{Fe}_{0.16}\text{Ni}_{0.19}\text{Zn}_{0.04}\text{Al}_{0.01})_{\Sigma 1.03}[(\text{OH})_{2.88}\text{O}_{1.14}]_{\Sigma 4.02}[(\text{AsO}_4)_{1.95}(\text{PO}_4)_{0.05}]_{\Sigma 2.00}$ , respectively. Extensive solid solution is observed between these two minerals.

The valence state of iron in cobaltneustädteleite and medenbachite was investigated by Mössbauer spectroscopy. Both spectra were fitted to two Lorentzian doublets. The doublets in the medenbachite spectrum are sufficiently resolved to conclude that there are at least two distinct environments for  $\text{Fe}^{3+}$ , which are octahedral based on the centre shifts. These could tentatively be assigned to M1 and M2 in the structure, where  $\text{Fe}^{3+}(\text{I})$  corresponds to M1 and  $\text{Fe}^{3+}(\text{II})$  corresponds to M2 based on the values of quadrupole splitting and the relative site distortion.  $\text{Fe}^{3+}$  is therefore preferentially partitioned into the M1 site, although some  $\text{Fe}^{3+}$  appears to occupy also the M2 site, which is mainly occupied by Cu. Determining accurate site occupancies is not possible, however, due to the line overlap. For the cobaltneustädteleite spectrum the linewidths of both doublets were constrained to be equal since the doublets were not sufficiently resolved; the fitting to two Lorentzian doublets is consistent with the observations of medenbachite.

Neustädteleite / cobaltneustädteleite have space group  $\text{P}\bar{1}$ :  $a = 4.556(1)$  /  $9.156(1)$ ,  $b = 6.153(2)$  /  $6.148(1)$ ,  $c = 8.984(2)$  /  $9.338(1)$  Å,  $\alpha = 95.43(2)$  /  $83.24(1)$ ,  $\beta = 99.22(2)$  /  $70.56(1)$ ,  $\gamma = 92.95(3)$  /  $86.91(1)$ °,  $V = 246.9$  /  $492.2$  Å<sup>3</sup>,  $Z = 1$  / 2. Structure investigations were performed on single-crystal X-ray data. A structural reinvestigation of medenbachite proved isotypy with cobaltneustädteleite:  $a = 9.162(2)$ ,  $b = 6.178(1)$ ,  $c = 9.341(2)$  Å,  $\alpha = 83.50(1)$ ,  $\beta = 71.04(1)$ ,  $\gamma = 85.15(1)$ °,  $V = 496$  Å<sup>3</sup>,  $Z = 2$ . The crystal structure investigations of neustädteleite / cobaltneustädteleite / medenbachite was based on 873 / 1729 / 1749 unique data; 796 / 1579 / 927 had  $\text{Fo} > 4\sigma(\text{F}_o)$ . R1 was 0.047 / 0.090 / 0.083 and  $\omega\text{R}2$  was 0.107 / 0.192 / 0.233 after refinement of the 95 / 108 / 108 free variables.

In neustädteleite the Bi atoms feature a site disorder; they are split onto two half occupied positions separated by 0.486(3) Å. No indications for ordering of the Bi atoms were detected. A trial to obtain order by reducing the symmetry to P1 failed. Superstructure reflections were not seen even after long exposed X-ray investigations. Cobaltneustädteleite and medenbachite display topologically the same building principles as found in neustädteleite, but the unit-cell volume is twice as large. Their average cells correspond with the neustädteleite cell. The most striking difference concerns the actual position of the Bi atoms and the environment of one of the oxygen atoms with respect to its coordination by Bi and H atoms. In cobaltneustädteleite and medenbachite all atoms except Bi exhibit an exact translation vector [1/2 0 0]. 50 % of the Bi atoms show a site disorder; their separation is larger as compared to neustädteleite and amounts to 0.587(3) and 0.762(4) Å, respectively. The other half of the Bi atoms are on a fully occupied atomic site (Bi12). This fully occupied Bi site corresponds approximately to the average position between Bi1 and Bi2 after application of the pseudotranslation vector (the deviations are 0.017(4) and 0.019(7) Å in the two minerals).

The coordination of the  $\text{Bi}^{[3+4]}$  and  $\text{Bi}^{[4+3]}$  atoms is irregular. The nearest ligands are in the range of 2.02 to 2.34 Å, additional ligands are up to 2.91 Å. The gaps between nearest and next-nearest neighbour environments as well as the spreading of the outer coordination sphere are unequally developed. Half of the O atoms not belonging to an arsenate tetrahedron are linked to a M1Ø<sub>6</sub> and a M2Ø<sub>6</sub> octahedron; bonds to Bi atoms are ≥ 2.70 Å. Despite the actual position of the Bi atom, the cations yield a too small contribution to the bond strength reaching this O atom to compensate for its valence (1.05 to 1.19 v.u.) and it has to be considered as a hydroxyl group.

The other oxygen atoms not belonging to  $[AsO_4]$  are oxo-oxygen atoms in neustädtelite but they are half oxo-oxygen atoms and half hydroxyl groups in cobaltneustädtelite and medenbachite. They balance the charge according to the formula  $M^{3+} + O^{2-} \leftrightarrow M^{2+} + (OH)$ . These O atoms are exclusively coordinated by two or three Bi atoms, featuring a varying distribution of the O–Bi bond lengths; two O–Bi bonds are  $\leq 2.21$  Å. For compensation of the bond valences the Bi–O bond lengths are adopted by shifting the Bi atoms. The actual bond length to the coordinating cations depends on the respective position of the Bi atom due to site disorder.  $Fe^{3+}$ ,  $Co^{2+}$ , and  $Cu^{2+}$  atoms occupy two six-coordinated M positions. The average bond lengths indicate that M1 is  $Fe^{3+}$  and M2 is  $(Fe^{3+}, Co^{2+}, Cu^{2+})$ .

The medenbachite-type structures are characterized by chains of edge-connected  $M\ddot{O}_6$  octahedra (neustädtelite and cobaltneustädtelite) and of alternating octahedra and tetragonal bipyramids (medenbachite) running parallel to [010]. Layers in (001) are formed by corner connection of the chains with the arsenate tetrahedra. The layers may be described as formed by densely packed oxygen atoms in (001). Half of the octahedral sites are occupied by M atoms. The other sites are vacant; however an arsenate tetrahedron is alternately at the top and bottom face of the vacant tetrahedra, which results in  $M^{[6]}(OH)(XO_4)$  layers. They are linked by Bi atoms. The structure may also be regarded as columns of edge-sharing octahedral columns  $\text{ }_{\infty}^1[MO_4]$  running parallel to [010] and by  $\text{ }_{\infty}^1[Bi(O,OH)]$  chains running parallel to [100], i.e., the two chemically different chains are approximately perpendicular to each other.

## References

- [1] KRAUSE, W., BERNHARDT, H.-J., GEBERT, W., GRAETSCH, H., BELENDORFF, K. & PETITJEAN, K. (1996): Amer. Miner. 81, 505-512.

**BACTERIOGENIC ORE FORMATION IN BLEIBERG-TYPE DEPOSITS**

by

**H. Kucha<sup>1</sup>, E. Schroll<sup>2</sup> & E. F. Stumpf<sup>3</sup>**

<sup>1</sup>Institute of Geology and Mineral Deposits  
Av. Mickiewicza 30, PL-30-059 Krakow

<sup>2</sup>Institut für Mineralogie und Kristallographie  
Universität Wien, Geocenter, Althanstrasse 14, A-1090 Wien  
<sup>3</sup>Institut für Geowissenschaften, Mineralogie und Petrologie  
Montanuniversität, A-8700 Leoben

We present new microscopic and analytical evidence in favour of bacteriogenic ore formation at Bleiberg. This should be viewed against the background of previous work, which is summarised below.

Negative sulphur isotope values of sulphide ores of Bleiberg and other Alpine Pb-Zn deposits have been interpreted by SCHROLL et.al. [1] as products of bacteriogenic reduction of sulphate in Triassic seawater. The finegrained texture of zinc sulphides and the presence of framboids, especially in stratiform mineralisations have been used as indicators for bacteriogenic metal deposition. This has, however, not been generally accepted and negative sulphur isotope values have traditionally been attributed to abiogenic processes [2].

Microthermometry of some sphalerite and fluorite samples from Bleiberg and Mezica, Slovenia, gave formation temperatures in excess of 100°C, which exclude bacteriogenic processes [3]. The Mississippi Valley type (MVT) model was then postulated for the genesis of ore deposits in the Alpine Trias. This involved epigenetic metal supply during subsidence at the time of the Alpine orogeny. However, thermal reduction of sulphate sulphur can only result in heavier sulphur, i.e. positive isotopic values - a feature observed in MVT deposits.

Bacteriogenic sulphate reduction (BRS) in mineralisations with sedimentary textures can be reconciled only with a model involving ore deposition which is coeval with the stratigraphic age of the host sediments [4].

To clarify this problem, we selected ore samples of finegrained sulphide associations from Bleiberg and from other occurrences within the Camian and Anisian sediments, such as Topla, Slovenia. These have been investigated microscopically, by scanning electron microscopy (SEM), by electron microprobe and by RAMAN spectroscopy. Measurements of sulphur valence by microprobe have also been performed. In reflected light samples of the stratiform Cardita mineralisation reveal microtextures of peloids. These represent relicts of bacteria which have also been identified in carbonate hosted mineralisations in Ireland, Belgium and Poland [5].

These sphalerite peloids show a ZnS core with 30–50 mm diameter. The rim is made up by pyrite, oxisulphide and an outer layer (10–20 mm) of ZnS. Sphalerite recrystallisation is widespread. Sulphur valences of the oxisulphides vary considerably from sulphide to thiosulphate; this is considered indicative for bacterial sulphur reduction. In addition, Zn-calcite peloids have been observed which are mantled by ZnS. Their core reveals large elongate or circular textures which can be interpreted as individual fossil bacteria.

Syndiagenetic textures have been described from the Cardita mineralisation at Bleiberg [6]; our data and observations now provide definite proof for syndiagenetic Pb-Zn mineralisation in the Alpine Trias. The giant carbonate hosted deposit of Navan, Ireland, occurs in Lower Carboniferous rocks and carries 9 mt Zn+Pb. It has recently been ascribed to the activity of sulphate reducing bacteria: "No bacteria, no ore deposit" [7]. This discovery is considered an extraordinary coincidence and provides additional support for our concept.

Bacteriogenic sulphate reduction (BSR) takes place below ~80°C and plays a significant role in Pb-Zn mineralisation in the alpine Trias and in the economically important deposits of the Lower Carboniferous in Ireland. The latter do, however, occur in tectonically undisturbed platform sediments while deposits of the Bleiberg type have been affected by deep subsidence during Alpine orogeny. Thus, bacteriogenic mineralisations co-exist with products of epigenesis and redeposition. The combined application of gas chromatography and isotopic methods will provide better understanding of the links between carbohydrates, ores and the thermal evolution of mineralised sequences. Examples for the distinction between bacteriogenic and thermally overprinted organogenic sediments components have been presented by MACHEL [8].

The response of carbohydrates in ores and rocks to different thermal regimes has also been elucidated [9]. Carbohydrate and isotope data from Topla, Slovenia, support synsedimentary, bacteriogenic origin for sphalerite ores [10].

This contribution reports first results of a working group which owes its existence to the support of the Raw Materials Commission of the Austrian Academy of Science.

## Literature

- [1] SCHROLL, E., et.al. (1983): Sulphur isotope distribution in the Pb-Zn deposit Bleiberg, Carinthia, Austria. - Mineralium Deposita 18: 17-25.
- [2] HOEFS, J. (1987): Stable isotope geochemistry. - Berlin, Springer-Verlag, 241 pp.
- [3] ZEEH, S. & BECHSTÄDT, T. (1994): Carbonate-hosted Pb-Zn mineralisation at Bleiberg-Kreuth (Austria): Compilation of data and new aspects. - In: FONTBOTÉ, L. & BONI, M. (eds.): Sediment-hosted Zn-Pb-ores. Spec. Publ. 10 SGA, pp 271-298, Springer-Verlag, Berlin etc.
- [4] BRIGO, L. et.al. (1977): Comparative reflections on four alpine Pb-Zn deposits. In: KLEMM, D. D. & SCHNEIDER, J. (eds.): Time and strata bound ore deposits, pp. 273-293, Springer-Verlag, Berlin etc.

- [5] KUCHA, H. et.al. (2001): Direct evidence for bacterial sulphur reduction in Bleiberg-type deposits. - (SGA 2001; in press)
- [6] SCHULZ, O. (1960): Studien an Zinkblenden im Bereich der erzführenden Raibler Schichten der Grube Max, Kreuth, Kärnten. - Berg- und Hüttenmänn. Monatshefte 105: 1-11, Springer-Verlag, Wien.
- [7] FALLICK, A. E. et.al. (2001): Bacteria were responsible for the magnitude of the world-class hydrothermal base-metal orebody at Navan, Ireland. - Nature (in press).
- [8] MACHEL, H. G. (2001): Bacterial and thermochemical sulphate reduction in diagenetic settings - old and new insights. - Sedimentary Geology 140: 143-175
- [9] RANTITSCH, G. et.al. (1999): Hydrocarbon-bearing fluid inclusions in the Drau range (Eastern Alps, Austria): implications for the genesis of Bleiberg Pb-Zn deposit. - Mineralogy & Petrology 65: 141-159.
- [10] SPANGENBERG, J. E. et.al. (2001): Carbonate-hosted Zn-Pb mineralisation at Topla (Slovenia): Inorganic and organic geochemical constraints. - Abstracts Volume EUG XI, p. 546, Cambridge Publications.

**PLANZENVERFÜGBARKEIT UND MOBILITÄT VON SCHWERMETALLEN VON  
BERGWERKSHALDEN DER PB-ZN BERGBAUE DES GRAZER BERGLANDES  
(STEIERMARK)**

von

**A.P. Kudjelka<sup>1</sup>, L. Weber<sup>2</sup>, W. Punz<sup>3</sup> & H. H. Weinke<sup>1</sup>**

<sup>1</sup>Institut für Geochemie

Geozentrum, Universität Wien, Althanstrasse 14, A-1090 Wien

<sup>2</sup>Bergbau-Montanbehörde

Bundesministerium für Wirtschaft und Arbeit, Dennisgasse 31, A-1200 Wien

<sup>3</sup>Institut für Ökologie und Naturschutz

Universität Wien, Althanstrasse 14, A-1090 Wien

## **Einleitung**

Im Bereich des Arzwaldgrabens und der näheren Umgebung von Frohnleiten im Grazer Paläo-  
zoikum (Steiermark) wurden bis in die 20-iger Jahre des 20. Jahrhunderts Pb-Zn Erze berg-  
männisch gefördert. Durch diese Bergwerkstätigkeit entstanden zahlreiche Abraum- und  
Schlackenhalden. In dieser Arbeit soll nun der umweltrelevante Einfluss durch jene Erzhalden  
untersucht werden.

Spurenelementen wie Pb, Zn, Cu, Cd, As, Hg etc. kommen aus ökotoxikologischer Sicht eine  
wichtige Rolle zu. Diese stellen pflanzenphysiologische Gifte dar, die zum Teil bereits in  
Konzentrationen von einigen ppm hochtoxisch wirken können. In Ökosystemen können Unter-  
suchungen an speziellen Spurenelementen, Aussagen zu deren Transport und Akkumulation  
innerhalb des Systems Boden/Pflanze geben. Darüber hinaus sind auch Rückschlüsse auf die  
Spurenelement-situation der Fauna möglich.

Alle Pflanzen decken ihren Bedarf an Hauptnährelementen (H, C, N, O, P, S, K, Ca, Mg, Fe) aus  
der Luft und vor allem aus dem Boden. Einerseits werden auch essentielle Spurenelemente (Mn,  
Zn, Cu, Mo etc.) aus der Bodenlösung aufgenommen, andererseits kann es, durch ein zu großes  
Angebot dieser, zu physiologischen Schädigungen – bis zum Absterben – kommen. Aus diesem  
Grund sollten Flächen, auf denen durch anthropogen/geogene Einträge (Erzausbisse, Berg-  
werkshalden, ...) mit einer möglicherweise toxischen Fracht zu rechnen ist, entsprechend  
beobachtet werden; dabei ist auch der Eintrag über die Atmosphäre zu berücksichtigen.

## Geländearbeit

Die integrierte Betrachtung des komplexen Systems Gestein-Boden-Pflanze findet in folgenden Untersuchungen Ausdruck:

- Geologische Begehungen
  - Regionale Geologie des Gebietes (Arzwaldgraben und Umgebung)
  - Geologie/Petrologie der Probenahmestandorte
  - Pedologische Untersuchungen
  - Bodenart, Bodentyp, Bodenfarbe etc.
  - Floristische Aufnahmen
  - Vorkommen von Mettallophyten
  - Forstökologische Untersuchungen
  - Standortskundliche Aufnahmen mit Betrachtung von forstökologischen Aspekten
  - Probenahme
    - Probenahme von Pflanzen (krautige Pflanzen und Fichtennadeln)
    - Probenahme von Bodenmaterial (horizontweise)
    - Probenahme von Gesteinen in der Umgebung der Probenahmepunkte (vererzte, unvererzte Gesteine)

## Chemische Analyse der Proben

- Gesamtgehalte (Totalaufschlüsse) der Pflanzenproben und Messung der Spurenelemente und dadurch Quantifizierung der Aufnahme von Schadelementen in den Pflanzenkörper

erste Ergebnisse (in ppm):	Pb	Cd
Fichtennadeln von 2-jährigen Sämlingen (Bergwerkshalde)	12.6	0.62
Fichtennadeln von 2-jährigen Sämlingen (Vergleichsstandort)	< 0.01	0.01
Farnblätter (Bergwerkshalde)	68.7	0.10
Farnblätter (Vergleichsstandort)	< 0.01	0.03

- Extraktionen der Bodenproben mit BaCl<sub>2</sub>, NH<sub>4</sub>NH<sub>3</sub> und EDTA und daraus Ermittlung von Pflanzenverfügbarkeit und Mobilität, sowie chemischer Bindungsarten von Elementen
- Gesamtgehalte (Totalaufschlüsse) in Böden und Gesteinen von Hauptnährelementen und Spurenelementen und dadurch chemische Charakterisierung der Böden

Die chemische Charakterisierung der Untersuchungsproben, sowohl der ausgewählten Pflanzenproben als auch des zugehörigen Bodens, setzt eine instrumentelle Analytik mit hoher Richtigkeit und hoher Reproduzierbarkeit voraus. Diese Forderung wird in der vorliegenden Arbeit mittels Flammen-AAS, Graphitrohr-AAS, DCP-OES und ICP-MS erfüllt.

Weitere wichtige Parameter zur Feststellung von Pflanzenverfügbarkeit von Schwermetallen werden ermittelt, um das Verhältnis von Nährstoffangebot im Substrat (Boden) zur Aktivität der Pflanze festzustellen. Hierzu zählen:

- pH-Wert
- Redoxpotential (Eh-Wert)
- Nährstoffverfügbarkeit (C-, N-, P-, S-Gehalt)
- Karbonat-Gehalt
- Anwesenheit chelatbildender Ionen
- (Mikroorganismen)

### **Interpretation der Analysenergebnisse**

Es wird versucht die Analysenergebnisse in Verbindung mit der Fragestellung nach einer Interpretation dieser umweltanalytischen Daten zu diskutieren:

- Quantität irgendeines Elements
- Beziehung zu irgendeiner Pflanze
- zu einem bestimmten Zeitpunkt
- an einem bestimmten Ort

DIAMONDITES AND CARBONATITIC FLUIDS: SIGNALS FROM TRACE ELEMENTS IN  
GARNETS AND CLINOPYROXENES AND FROM C ISOTOPE ABUNDANCES

by

G. Kurat<sup>1</sup>, G. Dubosi<sup>2</sup> & T. Maruoka<sup>3</sup>

<sup>1</sup>Naturhistorisches Museum  
Vienna, Austria

<sup>2</sup>Hungarian Academy of Sciences, Laboratory for Geochemical Research  
Budapest, Hungary

<sup>3</sup>Department of Geochemistry  
University of Vienna, Austria

Diamondites are fine- (< 100 µm) to coarse-grained (> 1 mm) rocks consisting of diamonds and occasionally some silicates and oxides [1]. They are usually porous rocks with abundant open and mostly interconnected cavities. The walls of the open cavities are covered by euhedral diamond crystals (druses). Silicates (mostly garnets) are present preferentially interstitially or fill the space in cavities and often contain inclusions of euhedral diamonds.

Silicates from 10 diamondites have been analyzed for trace element contents by laser ablation ICP-MS [2]. Four diamondites contain lilac "peridotitic" garnets with low CaO contents (3.6 - 5.7 wt.%), high Mg-numbers (0.83 - 0.84) and high Cr<sub>2</sub>O<sub>3</sub> contents (3.9 - 6.4 wt.%). Occasionally, they are accompanied by Cr-diopside. "Peridotitic" garnets have heavy rare earth element (HREE)-enriched and light rare earth element (LREE)-depleted chondrite-normalized patterns, commonly with a small hump at Eu and Sm (Fig. 1). The remaining 6 diamondites contain orange "eclogitic" garnets with low Cr<sub>2</sub>O<sub>3</sub> contents (< 1 wt%). These "eclogitic" garnets can be divided into two subgroups: E-I garnets have high Mg-numbers (0.84 - 0.85, as high as those of the "peridotitic" garnets) and higher Cr<sub>2</sub>O<sub>3</sub> and TiO<sub>2</sub> and lower HREE contents than the E-II garnets (Fig. 1).

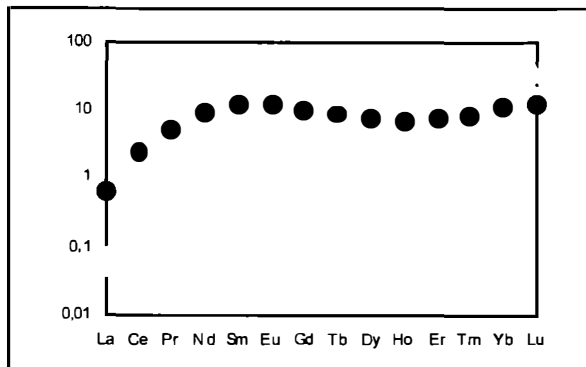


Fig. 1  
Chondrite-normalized REE abundances in garnets from diamondites. Solid circles: "peridotitic"; open squares: "eclogitic" I; open triangle: "eclogitic" II.

The chondrite-normalized trace element patterns of the two subgroups of "eclogitic" garnets are all depleted in LREE with respect to the HREE and have significant positive anomalies of Zr and Hf. "Eclogitic" garnets are more depleted in highly incompatible elements (LREE, Nb and Ta) than the "peridotitic" garnets.

Diamondites and their silicates very likely are the product of a fluid phase. The hypothetical fluids in equilibrium with the "peridotitic" garnets have trace element abundances which are similar to those in kimberlitic and carbonatitic liquids. Therefore, diamondites very likely formed from a highly alkaline fluid/liquid in the presence of carbonates. A predominantly alkali carbonatitic fluid/melt could provide the proper environment for mobilization of incompatible elements and precipitation of diamond [e.g., 3]. Hypothetical melts in equilibrium with "eclogitic" garnets are highly magnesian but depleted in LREE and other highly incompatible elements relative to the typical kimberlitic, lamproitic or carbonatitic liquids. This is surprising as eclogites should be richer in trace elements than peridotites, as should be the fluids in equilibrium with these rocks. The differences in trace element contents of fluids which precipitated, beside diamonds, "peridotitic" and "eclogitic" garnets, respectively, therefore, must be the result of different properties of these fluids rather than of different source rocks [1].

Diamonds (117 samples) from 35 diamondites have been analyzed for C isotope abundances (Fig. 2). Delta  $^{13}\text{C}$  values vary between and within diamondites with a total range from -3.24 to -24.36 ‰ for 13 "peridotitic" diamondites, from -18.30 to -23.59 ‰ for 4 which in addition to garnet also contain clinopyroxene and from -5.27 to -22.22 ‰ for 19 "eclogitic" diamondites. Three diamondites without silicates have a range in  $\delta^{13}\text{C}$  from -5.44 to -27.87 ‰.

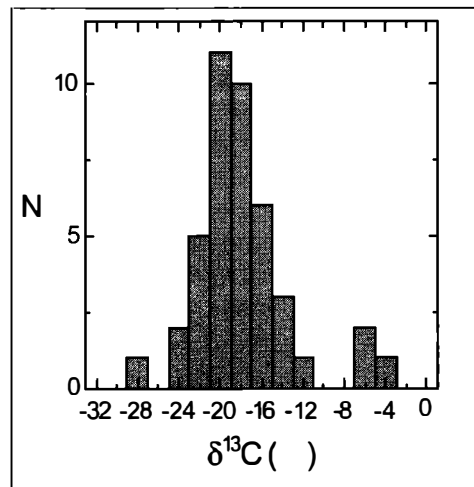


Fig. 2

*Carbon isotope composition of diamondite diamonds.*

Carbon in our diamondites is clearly lighter than that previously reported from diamond crystals [e.g., 4] and polycrystalline diamonds from Yakutia ( $\delta^{13}\text{C}$ : -6.1 to -2.6 ‰, [5]) but similar to that reported for polycrystalline diamonds from South Africa [6, 7]. Surprisingly, only 3 out of 35 diamondites have C isotope abundances that are compatible with unfractionated upper mantle C [see 5] and they represent all three types of silicate-bearing diamondites. The C isotope abundances are apparently not correlated with the type of garnet ("eclogitic" or "peridotitic") present, nor with the absence of silicates. The dominantly light C is probably the product of mass fractionation between oxidized ( $\text{CO}_2$ ) and reduced ( $\text{CH}_4$ ) carbon [e.g., 8] indicating diamond precipitation via  $\text{CH}_4$ , probably at fairly low temperatures. The degree to which mass fractionation occurred could simply reflect the mass ratio of reduced to oxidized C in the local environment. Variable isotopic compositions of C within diamondites (up to almost 4 ‰  $\delta^{13}\text{C}!$ ) likely reflect changing conditions during diamond growth. The few diamondites with upper mantle C isotope composition could indicate precipitation of diamond directly from carbonates [e.g., 3].

In conclusion, diamondites seem to be the product of large scale mass transfers taking place in the Earth's mantle. Carbonatitic fluids/melts appear to be the main vehicle for major, minor and trace element transfers, transfers of heat and of C, presumably from the deeper to the shallower mantle. Depending on local conditions in the mantle, some of the mobilized elements react with mantle rocks they invade (e.g., carbonatitic metasomatism) or are precipitated into the space created by the moving fluids/melts (e.g., diamondites). As the main mass of the mobilisates continues to migrate, highly fractionated products are left behind, the most common of which seem to be pyroxenites, olivinites, garnetites and diamondites.

#### Acknowledgements

Support by the Austrian FWF, the Austrian Academy of Sciences, the Ermann-Fonds, G. Jenner and M. Tubbrett, St. John's, and C. Koeberl, Vienna, is gratefully acknowledged.

#### References

- [1] KURAT, G. & DOBOSI, G. (2000): Garnet and diopside-bearing diamondites (framesites). - *Mineral. Petrol.* 69, 143-159.
- [2] DOBOSI, G. & KURAT, G. (2001): Trace element abundances in garnets and clinopyroxenes from diamondites - a signature of carbonatitic fluids. *Mineral. Petrol.*, in press.
- [3] LITVIN, U. A. & ZHARIKOV, V. A. (2000): Experimental modeling of diamond genesis: Diamond crystallization in multicomponent carbonate-silicate melts at 5-7 GPa and 1200-1570 °C. - *Doklady Earth Sci.*, 373, 867-870.
- [4] DEINES, P. (1980): The carbon isotopic composition of diamonds - relationship to diamond shape, color, occurrence and vapor composition. - *Geochim. Cosmochim. Acta* 44, 943-962.
- [5] REUTSKII, V. N. et al. (1999): Carbon isotopic composition of polycrystalline diamond aggregates with chromite inclusions from the Mir kimberlite pipe, Yakutia. - *Geochem. Internat.* 37, 1073-1078.
- [6] JACOB, D. E. et al. (2000): Remobilization in the cratonic lithosphere recorded in polycrystalline diamond. - *Science* 289, 1182-1185.
- [7] BURGESS et al. (1998): He, Ar and C isotopes in coated and polycrystalline diamonds. - *Chem. Geol.* 146, 205-217.
- [8] BOTTINGA, Y. (1969): Calculated fractionation factors for carbon and hydrogen isotope exchange in the system calcite-carbon dioxide-graphite, methane-hydrogen-water vapor. - *Geochim. Cosmochim. Acta* 33, 49-64.

**KLODSKO-ZLOTY STOK AND NIEMCZA ZONE GRANITOIDS - A SHALLOW LEVEL  
INTRUSION OF DURBACHITES IN THE RHENOHERCYNIAN ZONE ?**

by

**J. Leichmann<sup>1</sup> & O. Gaweda<sup>2</sup>**

<sup>1</sup>Department of Geology and Palaeontology  
Masaryk University, Kotlářská 2, 611 37 Brno

<sup>2</sup>Department of Mineralogy, Geochemistry and Petrography  
University of Silesia, Bedzinska 60, Sosnowiec

Klodosko-Zloty Stok (KZSM) and Niemcza Zone granitoids are located at the north-eastern margin of the Bohemian Massif, on the southern termination of the western Sudets. Rocks of mainly granodioritic composition dominate both massifs. But some melanocratic granites or syenites resemble strongly the durbachites from the moldanubian part of the Bohemian massif. The common features are mainly: K-Feldspar phenocryst with inclusions of biotite and plagioclase, presence of actinolite with relicts of Cpx together with biotite, high content of MgO (4.69 wt.%), K<sub>2</sub>O (4.54 wt.%), Rb (184 ppm), Sr (442 ppm), REE (174 ppm) and Zr (178 ppm). The SiO<sub>2</sub> (58.81 wt.%) and Al<sub>2</sub>O<sub>3</sub> (14.46) are low on the other hand [1].

The U-Pb dating of the Niemcza Zone syenites define a discordia with a lower intercept age of  $338 \pm 3$  Ma and an upper intercept age of about 1800 Ma [2]. Ar-Ar ages on amphiboles from the Niemcza Zone reveal values 340 Ma [1] or  $335 \pm 5$  Ma [3]. The ages around 340 Ma were reported from durbachites in Austria as well [4]. Rb-Sr study [5] didn't allow unequivocal geochronological interpretation, indicating rather an important role of magma mixing in the origin of these granitoids. Just the very complex U-Pb [4] and Rb-Sr [6] systematic are typical for durbachites from the eastern moldanubian zone. The rocks of the KZSM are penetrating, similar to the durbachites, by veins of spessartites, vingesites, microsyenites etc.

Apart from similarities, some differences between durbachites and studied granitoids could be traced in the geology mainly. Typical durbachites from the eastern moldanubian zone intrude high-grade gneiss's, migmatites, granulites and other high-grade rocks, and are surrounded by migmatitic contacts. The Klodosko-Zloty stok massif intrudes partly to the unmetamorphosed visean, Culm-facies sediments and it is surrounded by hornfels contacts indicating much shallower conditions of intrusion. The shallow level intrusion and crystallisation is probably responsible for the strong inhomogeneity of the KZSM caused by incomplete magma mixing, with an only low contribution of the melt derived from country rocks. The intrusion of the durbachites into the Culmian = Rhenohercynian sediments indicates, that the durbachite magmatic activity is not restricted to the moldanubian zone only.

## Literature

- [1] PUZIEWICZ, J., (1992): Geneza Granodioritu z Kozmic. - Arch. Mineralogiczne, XLVII, 2, 95-141.
- [2] OLIVER, G. J. H. et al. (1993): U-Pb Ages from SW Poland: Evidence for a Caledonian Suture Zone between Baltica and Gondwana. - J. Geol.Soc.London., 150, 355-369.
- [3] DUDEK, K. et al. (2000): Ar-Ar Dating of Hornblende from Pegmatite in Quartz Monzodiorite from Przedborowa (lower Silesia, Poland). - Preliminary Results. Miner. Pol. 31, 2, 75-83.
- [4] KLOETZLI, U. S. & PARRISH, R. R. (1996): Zircon U/Pb and Pb/Pb Geochronology of the Rastenberg Granodiorite, South Bohemian Massif. - Austria. Miner. Petrol., 58, 197-214.
- [5] LORENC, M. W. (1998): Badania Izotopowe Metoda Rb/Sr Skal Intruzyjnych Strefy Niemczy. - Arch. Mineralogiczne, LI, 1/2, 153-161.
- [6] SCHARBERT, S. & VESELA, M. (1990): Rb-Sr Systematic of Intrusive Rocks from the Moldanubicum around Jihlava. Thirty Years of Geological co-operation between Austria and Czechoslovakia. - CGU and GBA Prague, 262-272.

GABBROS RELATED TO THE DURBACHITES (JIHLAVA MASSIF, MOLDANUBIAN ZONE)

by

J. Leichmann & K. Zachovalová

Department of Geology and Palaeontology  
Masaryk University, Kotlárská 2, 611 37 Brno

Approximately 2 km long body of mafic rocks ranging from gabbros to monzodiorites was found in the northern part of the Jihlava durbachite batholith. The nature of the body – intrusion or inclusion in durbachites – could not be determinated directly in the field because of poor outcrop evidence. The interpretation of gravimetry and the occurrence of hT kinzigites in association with gabbros indicate rather intrusive nature of the body. Another similar body of mainly biotite bearing gabbros intrudes the Moldanubian gneises approximately 6 km NE from the northern termination of the Jihlava batholith.

The concentrations of MgO (7 - 16 wt.%), SiO<sub>2</sub> (49 - 52 wt.%), CaO (7.8 - 10.3 wt.%), Na<sub>2</sub>O (0.9 - 3.4 wt.%) and FeO (8.3 - 9.6 wt.%) are typical for basaltic chemistry. However, the elevated concentration of mainly LIL elements like K<sub>2</sub>O (1.9 - 3.6 wt.%), Rb (95 - 222 ppm), Ba (1100 - 1400 ppm), but also P<sub>2</sub>O<sub>5</sub> (0.4 - 0.8 wt.%), and REE (209 ppm) with week negative Eu anomaly and preponderance of LREE over HREE indicate more complex origin of the rocks.

Two mineralogical associations were found in the rock. The primary paragenesis is characterised by unzoned labradorite (An<sub>52</sub>), Ti-rich biotite ( $X_{mg}$  0.5 - 0.6), Opx, Cpx1 ( $X_{mg}$  0.75), and apatite. The secondary paragenesis originated via decomposition of biotite into perthitic K-feldspar with common rutile inclusion and Cpx2 ( $X_{mg}$  0.5). Corrode relics of plagioclase, An-rich perthites in K-feldspar and high Ca content in Cpx indicate, that the plagioclase was involved in the reaction too. Myrmekites appear at the reaction contacts between primary biotite and secondary K-feldspar or Cpx, indicating that the equilibrium was not reached during the reaction. The temperature of K-feldspar crystallisation was estimated from recalculated composition of primary, ternary feldspar of around 1100°C. The biotite breakdown reaction can indicate the infiltration of CO<sub>2</sub>-rich fluids at hT conditions [1]. The input of CO<sub>2</sub>-rich fluids could explain the reaction history, but cannot explain the enrichment on LIL and other elements. For instance, biotite contains 0.5 wt.% BaO in average only. But the secondary K-feldspar contains usually six times higher concentration of BaO. This could be clarified by a reaction between the primary biotite bearing gabbro and K-rich melt. The melt could be derived from the surrounding Moldanubian paragneises as a consequence of the intrusion of hot gabbro into the lower crust, leaving garnet-sillimanite kinzigites as a restite [2].

Both associations were affected by low temperature overprinting in addition. The primary Opx is mostly totally replaced by cummingtonite and Cpx partly by actinolite. Biotite is rarely chloritised., plagioclase replaced by prehnite. The decomposition of Px, Plg and Bt indicate the infiltration of aqueous fluids in the medium to low temperture environment.

#### **Literature**

- [1] IONOV, I. (1999): Mantle Metasomatism by Fluids with Low Water Activity: Feldspar – Ti oxide bearing peridotite Xenoliths in basalts from SE Siberia.- J Conf. Abstr. EUG 10, 4, 1, 364-365.
- [2] LEICHMANN, J., NOVAK, M., ZACHOVALOVA, K. & TOPA, D. (2000): Ultrahigh Temperature event in their Moldanubian Zone: its Significance for the Origin of Durbachites. - Geolines, 10, 47-48.

**VERTEILUNG DER MINERALIEN IN DEN KLÜFTEN DER KNAPPENWAND;  
HYDROXID- UND FLUOR-VERTEILUNG IN APATIT UND SPHEN**

von

**H. Lenitz<sup>1</sup>, R. Seemann<sup>2</sup> & A. Beran<sup>1</sup>**

<sup>1</sup>Institut für Mineralogie und Kristallographie  
Universität Wien, Geocenter, Althanstrasse 14, A-1090 Wien

<sup>2</sup>Mineralogisch-Petrographische Abteilung  
Naturhistorisches Museum, Burgring 7, A-1010 Wien

Im Zuge von Gebirgsbildung und Metamorphose kam es auch im Bereich der Ostalpen zur Ausbildung von alpinen Klüften, den sogenannten Zerrklüften [1]. In diese Klüfte drangen heiße Lösungen aus den umgebenden Gesteinsverbänden ein, die Stoffe aus dem Nebengestein gelöst hatten. Aus diesen Lösungen schieden sich dann in einer charakteristischen Abfolge entsprechend der Abkühlung im Zuge der Hebung der Alpen die typischen Kluftmineralien ab [2].

Es wurden die Kluftmineralien aus der Knappenwand (Untersulzbachtal) untersucht, die im Rahmen eines Forschungsprojektes in den Jahren 1977 bis 1992 von den Mitarbeitern des Naturhistorischen Museums Wien geborgen wurden und im Museum für weitere Bearbeitung zur Verfügung stehen. Im Zuge dieser Arbeiten wurden insgesamt 70 Klüfte erschlossen. Die historische Fundstelle Knappenwand wurde wegen der beachtlichen Epidotvorkommen weltberühmt.

Die Mineralien wurden nach den Kluftvorkommen sortiert, nach Mineralparagenesen bei abnehmender Temperatur (Byssolith, Epidot, Apatit, Albit, Calcit, Adular, Quarz/Bergkristall, Sphen, Chlorit) gereiht und ihre relative Häufigkeit bestimmt [3].

Aus dem Spektrum der angeführten Kluftmineralien wurden gezielt Apatit- und Sphenproben aus unterschiedlichen Klüften verwendet, um den F- und OH-Gehalt festzustellen. Das gemeinsame Auftreten von Apatit und Sphen in einer Kluft ist auf wenige Vorkommen beschränkt. Die Bestimmung des Fluorgehaltes wurde mittels F-sensitiver Elektrode durchgeführt. Die Fluorwerte für Apatite aus Sphen-freien Klüften betrugen 2.00 bzw. 1.91 Gew.%. Dies ist geringfügig höher als der theoretisch errechnete Wert für Fluorapatite, der bei 1.89 % liegt. Die Fluorwerte für Apatite aus den Klüften in denen Sphen und Apatit gemeinsam vorkamen, waren deutlich niedriger und zwar lagen sie bei 1.25 bis 1.50 Gew.% Fluor. Für die Sphenproben aus diesen Klüften lagen die Werte bei 0.17 bis 0.24 Gew.% Fluor [3].

Die OH-Bestimmung erfolgte mittels IR-Spektroskopie und ergab für alle Apatitproben ähnliche Werte bei 0.06 Gew.% H<sub>2</sub>O. Bei den Sphenproben, ergaben sich Werte zwischen 0.17 und 0.22 Gew.% H<sub>2</sub>O [3].

Unter dem Mikroskop waren in einigen Apatitproben Einschlüsse zu erkennen, die in drei unterschiedlichen Formen ausgebildet waren. In den Einschlüssen zeigten sich Gasblasen, Tochterkristalle und Flüssigkeit. Bei Untersuchungen mittels Heiz- und Kühlisch wurde die Salinität auf Grund der Schmelztemperatur mit ~ 11% ermittelt [4]. Durch Kombination der Homogenisierungstemperatur, die zwischen 220 und 260°C lag, und der Salinität konnte die Bildungsdichte der salinaren Lösung mit 0.85 - 0.91 g/cm<sup>3</sup> bestimmt werden [5].

Sowohl um eventuell vorhandenes Chlor im Apatit festzustellen, als auch um die Beschaffenheit von Kristallisaten in und um geöffnete Cavitäten zu klären, wurden Untersuchungen von Apatitproben mit dem Rasterelektronenmikroskop durchgeführt [6]. Ergebnis dieser Untersuchungen war, dass innerhalb der Nachweisgrenze dieses Systems kein Chlor angezeigt wurde, und dass es sich bei den Kristallisaten um NaCl und KCl handelte.

## Literatur

- [1] NIEDERMAYR, G. (1990): Mineralabfolgen in alpinen Klüften der Ostalpen und ihre Bedeutung für den Bau der Alpen. - Mitt. Österr. Min. Ges. 135, 59-60.
- [2] SEEMANN, R. (1990): Die Mineralfundstelle Knappenwand – Geschichte und Mineralogie. Mitt. Österr. Min. Ges. - 135. 80- 81.
- [3] LENIT, Z. H. (2001): Mineralogische Untersuchungen an Kluftmineralien der Epidotfundstelle Knappenwand, Untersulzbachtal. - Unveröff. Diplomarbeit, Univ. Wien, 73S.
- [4] POTTER, R. W., CLYNNE, M. A. & BROWN, D. L. (1978): Freezing point depression of aqueous sodium chlo-ride solutions. - Econ. Geol. 73, 284-285.
- [5] SHEPHERD, T. J., RANKIN, A. H. & ALDERTON, D. H. M. (1985): A Practical Guide to Fluid Inclusion Studies.
- [6] GÖTZINGER, M. A. (1994): Einschluss-Untersuchungen mittels Rasterelektronenmikroskopie und EDX-Analytik. - Mitt. Österr. Min. Gesellschaft, 139, 159-168.

**EINSCHLUSSCHARAKTERISIERUNG VON  
ZILLERTALER SCHMUCKGRANATEN, TIROL, ÖSTERREICH**

von

**M. A. Leute<sup>1</sup> & M. A. Götzinger<sup>2</sup>**

<sup>1</sup>Institut für Chemische Technologie anorganischer Stoffe

TU Wien, Getreidemarkt 9/161, A-1060 Wien

<sup>2</sup>Institut für Mineralogie und Kristallographie

Universität Wien, Geocenter, Althanstrasse 14, A-1090 Wien

Im Zillertal (Tirol), wurden in den Jahren von 1782 bis 1913 Almandine für Schmucksteinzwecke abgebaut. Für die Unterscheidung von Schmuckgranaten aus verschiedenen Bereichen des Zillertales, aber auch aus dem Raum Radenthein (Kärnten) haben sich neben der chemischen Charakterisierung die Form, Anzahl und Größe {in mm} von Mineraleinschlüssen bewährt, die mittels Auflichtmikroskopie und Rasterelektronenmikroskopie (REM) mit energiedispersiver Analyse (EDX) unterschieden werden konnten [1].

#### **ROSSRÜCKEN (ROSSRUGG)/ZEMMGRUND**

Am Rossrücken wurde auf 2 Fundstellen abgebaut (West- und Ostseite), was das Einschlusbild der Granate geringfügig unterscheidet. Im Almandin-Granat der Westseite treten häufig idiomorphe Ilmenitleisten und Quarzkörnchen als Einschlüsse auf, die regelmäßig verteilt sind. Überdurchschnittlich oft wird Apatit, Epidot und Allanit-(Ce) beobachtet. Zirkone mit geringen Hf-Gehalten sind mäßig oft vertreten und erreichen eine Kantenlänge bis zu 70 µm. Die Granate auf der Ostseite des Rossrückens haben verhältnismäßig viele Ilmenitleisten (50 - 400) eingeschlossen. Relativ oft kann man im Rasterelektronenmikroskop Apatite (40 - 100), Epidote (40 - 100), xenomorphe Quarzkörper {500} und Allanite-(Ce) {60} finden. Neben Cer und Neodym konnten geringe Gehalte an Thorium und Uran im Allanit-(Ce) detektiert werden. An einigen Stellen wurden kleine, aber meßbare Kristalle als Cerianit identifiziert.

Charakteristisch und unverwechselbar sind Apatitkristalle im Almandin von der Ostseite des Rossrückens. Schon mit geringer Vergrößerung können im Mikroskop hauchdünne und durchsichtige Nadeln beobachtet werden, die sich durch den ganzen Granat ziehen. Diese ungewöhnliche morphologische Ausbildung ist bislang nur von diesem Vorkommen bekannt.

#### **HORNKEES/ZEMMGRUND**

Selten sind Mineraleinschlüsse wie Biotite {bis 800}, die mit Quarz verwachsen sind und Rutile {100 - 200}, die in der Granatklamm nur in einem Granat gefunden wurden. Ankerit-Dolomit-Mischkristalle {100 - 500}, sind randlich mit Ilmenit, Rutil und Apatit vergesellschaftet.

Reine Calcite sind sehr selten, Ankerite treten aber häufiger auf und wurden ausschließlich im Kernbereich beobachtet.

Ilmenit ist entweder solitär {50 - 600} im Granat in Form von idiomorphen Leisten verteilt, oder liegt in Form von Nestern mit anderen Ilmenitleisten im Granat vor.

#### GRANATKLAMM/ZEMMGRUND

Die Granate von der Granatklamm im Zemmgrund haben nur wenige gut zu unterscheidende Mineraleinschlüsse, die sie von den anderen Granaten aus dem Zillertal unterscheiden. Die Einschlüsse können in zwei Gruppen unterteilt werden, wobei eine Gruppe sich durch dominierende Ilmenitleisten {200 - 300} und durch mäßig viel Apatit auszeichnet, die andere hingegen mäßig (Fe, Mg)-Chlorit enthält.

Auffällig sind kleinste Einschlüsse von Paragonit im Ilmenit, die nicht größer als 10 µm sind.

#### SCHÖNBICHLER HORN/ZEMMGRUND

Das Einschlusssbild vom Schönbichler Horn ist am vielfältigsten. Ilmenit {30 - 60} als dominierende Ti-Phase, Epidot {10 - 30}, Quarz {20 - 100}, Allanit-(Ce) und Apatit {20 - 50} bilden die Hauptmenge der Einschlüsse im Granat. Idiomorphe Zirkone und verschiedene Erzminerale, wie oktaedrisch ausgebildeter Magnetit, Pyrit, Zinkblende und Chalkopyrit werden nur selten als "Gäste" im Granat beobachtet. Weiters trifft man Calcit, Ankerit sowie Plagioklas im Granat an. Ferner kommen Ankerit-Aggregate und Apatite mit Magnetit im Granat nebeneinander vor.

#### GREINERGRÜNDL/ZEMMGRUND

Typisch für die Granate vom Greinergründl ist das Auftreten von Ankerit-Dolomit- Mischkristallen.

Das Einschlusssbild ist außerdem durch einen großen Anteil an Quarz im Granat charakterisiert, der auch die dominierende Rolle unter den Einschlüssen spielt. Mäßig viele, aber kleine Epidote {10 - 50} ergänzen das Erscheinungsbild im Granat. Große, aber selten auftretende Ilmenitleisten liegen im Bereich Rand/Mitte der einzelnen Granatkristalle.

#### LAPENKAR/STILLUPGRUND

Häufig auftretendes Einschlusmineral ist hier Rutil {70 - 200}, der nur selten von großen Ilmenitleisten {100 µm - 3.5 mm} am Kristallrand begleitet wird. Quarz, Allanit-(Ce) und Klinochlor treten ebenfalls öfters auf. Epidot bildet einen dünnen Saum um idiomorphe Allanit-(Ce) Kristalle. Große Biotit-Plättchen, die vermutlich aus protogenetischen Mineralbeständen übernommen wurden, konzentrieren sich auf verschiedene Stellen im Granat.

#### LÖFFLERKEES/STILLUPGRUND

Apatit {70} und Zirkon {30} sind als "Einschluss-Gäste" ebenso vertreten wie Ankerit-Dolomit-Mischkristalle {100} und Ilmenit {80 - 600}. Margarit {40 - 110} als seltenes Einschlusmineral tritt nur in den Granatkristallen vom Löfflerkees auf und konnte in keinem anderen Granat aus dem Zillertal gefunden werden.

### **STAPFENALM/STILLUPGRUND**

Das Einschlusbild wird hauptsächlich von Ilmenit geprägt. Selten treten Zirkon, Apatit und Biotit auf. Interessant ist der Randbereich der Granate, der syngenetisch auskristallisierte Rutilkristalle an den Kristallrändern von Granat erkennen lässt.

### **EISKAR/STILLUPGRUND**

Im Kernbereich dominiert Ilmenit, der zum Rand hin an Eisen verarmt und in Rutil übergeht. Quarze und SEE-reiche Allanite (Ce, La, Nd) sind auch Hauptbestandteile der Mineraleinschlüsse. Solitäre Epidotkristalle liegen regellos im Granat verteilt, sind aber nicht mit Allanit-(Ce, La, Nd) zoniert.

### **GRANATKLAMM/GUNGGL**

Wichtigste Einschlusminerale sind Epidot {100 - 300}, Allanit {50 - 200} und xenomorphe Quarzkörper. Selten tritt Ilmenit {30}, Apatit, Plagioklas {100 - 400}, Calcit {50} und Chlorit {70 - 300} im Granat auf.

### **VORDERE STANGENSPITZE/ZILLERGRUND**

Auffallend viele Ankerit-Dolomit Mischkristalle {100 - 500} wurden in diesen Granaten gezählt. Verschiedene morphologische Erscheinungsformen zeigt Epidot, der entweder als unzonierte Spindeln ausgebildet ist, oder als Saum um Allanit-(Ce) zoniert ist.

### **Literatur**

- [1] LEUTE, M. A. (2000): Mineralogische Charakterisierung der Radentheiner und Zillertaler Schmuckgranate, Österreich. - Diplomarbeit Univ. Wien, 129S.

SiSiC-KERAMIKEN – EIGENSCHAFTEN UND ANWENDUNGSBEREICHE

von

**M. A. Leute, M. Wilhelm & W. Wruss**

Institut für Chemische Technologie anorganischer Stoffe  
TU Wien, Getreidemarkt 9/161, A-1060 Wien

Siliziumfiltriertes Siliziumcarbid ist ein keramischer Verbundwerkstoff, der neben Siliziumcarbid als Bindephase freies Silizium in den Poren enthält. Die Herstellung erfolgt durch eine Nass-Mischung von SiC mit Kohlenstoff (Ruß oder Graft). Das Suspensionsmedium kann ein organisches, bzw. anorganisches Lösungsmittel sein. Zu diesem Schlicker werden Plastifizierer und Bindemittel beigemengt und zu einem Formkörper trocken verpresst. Nach einem Trocknungsvorgang wird das Bindemittel polymerisiert und anschließend unter Schutzgasatmosphäre zu Kohlenstoff verkrackt.

Mittels einer Auflageinfiltration, die über dem Schmelzpunkt des Siliziums ( $> 1420^{\circ}\text{C}$ ) stattfindet, wird der sg. Grünkörper mit elementarem Silizium infiltriert. Die Umsetzung des Kohlenstoffes zu SiC erfolgt nach folgendem Reaktionsschema:



Durch die Kapillarwirkung des porösen Grünkörpers wird das flüssige Silizium aufgesaugt und reagiert mit dem vorhandenem Kohlenstoff zu sekundärem SiC. Durch das Aufwachsen auf den vorhandenen primären SiC-Körnern, bzw. durch das Hineinwachsen des sekundären SiC<sub>s</sub> in die vorhandene Porosität, werden beide SiC-Phasen miteinander verbunden und es entsteht ein zusammenhängendes Gerüst, was letztendlich zu hohen mechanischen Festigkeiten führt. Der verbleibende offene Porenraum wird mit flüssigem Silizium aufgefüllt, wodurch ein gasdichter Verbundwerkstoff entsteht.

**Chemische Eigenschaften:**

Zu den wichtigsten chemischen Eigenschaften zählen neben der guten Oxidationsbeständigkeit, die durch eine passivierende SiO<sub>2</sub>-Schutzschicht hervorgerufen wird, die sehr gute Korrosionsbeständigkeit im sauren Milieu (mit Ausnahme HF!). Im alkalischen Bereich sind SiSiC-Keramiken vor korrosiven Angriffen nicht geschützt, da die SiO<sub>2</sub>-Phase bereits in verdünnten Laugen zerstört und die Si-Bindefase unter Bildung von Silikaten gelöst wird.

**Physikalische Eigenschaften:**

Durch die geringe Dichte ( $\sim 3.1\text{g/cm}^3$ ), sowie durch den geringen thermischen Ausdehnungskoeffizient, als auch die gute Temperaturwechselbeständigkeit und hohe thermische Leitfähigkeit ist SiSiC in der industriellen Anwendung vielseitig einsetzbar. Die elektrische Leitfähigkeit, die sich aus den Halbleitereigenschaften des Siliziums ergibt, ermöglichen eine funken-erosive Bearbeitung von SiSiC-Konstruktionsteilen.

### **Mechanische Eigenschaften:**

Neben einer hohen Härte, sind bei Keramiken im allgemeinen die mechanischen Eigenschaften, wie Biegebruchfestigkeit und -zähigkeit von großer Bedeutung, da verschiedene Einsatzbereiche bestimmte mechanische Eigenschaften voraussetzen.

Im wesentlichen werden die Festigkeit und die Zähigkeit durch die Dichte, durch die SiC-Korngröße, durch den freien Silizium Gehalt, sowie durch das Verhältnis SiC:Si beeinflusst [1]. Im Gegensatz zu metallischen Werkstoffen kann bei SiSiC-Keramiken ein Ansteigen der Biegebruchfestigkeit bis 1200°C beobachtet werden [2]. Erst bei einer Anwendungstemperatur von über 1300°C beginnen die Festigkeitswerte von SiSiC zu sinken, da die Siliziumbindephase über 1410°C komplett aufschmilzt.

### **Anwendungsbereiche:**

Aus allen genannten Eigenschaften resultiert eine Vielzahl von Vorteilen dieser Keramik, die diesen Werkstoff zu einem kostengünstigen Hochtemperatur- und verschleißarmen Konstruktionswerkstoff machen.

Schon seit Jahren finden SiSiC-Keramiken Einsatz als Wärmetauscher, Gleitringdichtungen, Schweiß- und Brennerdüsen, wo insbesondere Eigenschaften, wie hohe thermische Leitfähigkeit, gute Warmfestigkeit und der geringe Verschleiß vorausgesetzt werden.

Weitere Anwendungsbereiche für SiSiC-Keramiken sind die Solarenergietechnik, Müllverbrennungs- und Kraftwerksanlagen, sowie in der Umwelttechnik und im Verschleißschutz.

Im Bereich der Verschleißtechnik stehen vor allem die hohe Härte, das gute Reibverhalten und die chemische Passivität im Vordergrund. Verschleißbeanspruchte Bauteile wie Gleitlager, Gleitringdichtungen werden in Zukunft pulvermetallurgische Werkstoffe vom Markt drängen.

Die schwindungsfreie Herstellung kombiniert mit guten Hochtemperatureigenschaften und sehr guten Temperaturwechselbeständigkeit lassen den Einsatz im Ofen- und Anlagenbau zu.

Erfolgreich eingesetzt werden heute erosiv und korrosiv beanspruchte Anlagenteile wie Röhren, Rohrbögen und Ventile.

Zukunftsträchtig sind die Entwicklungen von keramischen Substratschichten für Solarzellen auf Basis von SiSiC-Keramiken [3], Leichtbau-Laserspiegel mit integrierten Kühlkanälen, sowie Komponenten für Diffusionsöfen in der Mikroelektronik.

### **Literatur**

- [1] COHRT, H. (1985): Herstellung, Eigenschaften und Anwendung von reaktionsgebundenem, siliziumfiltrierten Siliziumcarbid. - Z. f. Werkstofftechn. 16: 277-285.
- [2] KENNEDY, P. & SHENNAN, J. V. (1973): An Assessment of the Performance of Refel Silicon Carbide under Conditions of Thermal Stress. - Proc. Brit. Ceram. Soc. 22: 67-87.
- [3] RÄUBER, A., EYER, A. & POHLMANN, H.-J. (1998): Ceramic substrate for solar cells with a thin crystalline silicon layer. - PCT Int. Appl., 1-28.

**CORRELATION OF MIOCENE PUMICE-BEARING PYROCLASTIC DEPOSITS  
IN THE PANNONIAN BASIN**

by

**R. Lukács, Sz. Harangi & I. Oláh**

Department of Petrology and Geochemistry  
Eötvös University, Múzeum krt, 4/A, H-1088 Budapest, Hungary

Discrimination and correlation of pyroclastic flow deposits is important in structurally complex regions, where long-lived volcanic activity took place and therefore these volcanic products provide keys to the regional stratigraphic framework. The Neogene evolution of the Carpathian-Pannonian Region (CPR) was accompanied by various volcanic activities [1]. Among them, repetitive explosive eruptions of silicic magmas resulted in large volume pyroclastic deposits covering a large area (more than 200 000 km<sup>2</sup>) during the Miocene (from 20 to 13 Ma). These volcanic products are traditionally divided into three horizons, called as 'Lower Rhyolite Tuff' (LRT), 'Middle Rhyolite Tuff' (MRT) and 'Upper Rhyolite Tuff' (URT), respectively (e.g. [2]). However, recent studies (e.g. [3]), questioned this rigid classification and suggested nearly continuous multiple eruptions of silicic magmas from different volcanic centres during the Miocene. These volcaniclastic horizons are separated by fossiliferous sediments in the basement of the basins, but it is very difficult to distinguish them in other areas. Thus, one of the major challenges in the study of the silicic volcanic rocks of the CPR is to find tools to correlate the scattered deposits extending over the Pannonian Basin. The K/Ar radiometric age data appear to have not enough resolution to distinguish clearly the main volcaniclastic horizons (e.g. [4]). In this paper, we present the results of a combined physical volcanology, zircon morphology, petrographic, mineral and bulk rock geochemical study on the Miocene silicic pyroclastic rocks of the Pannonian Basin. We emphasize that the simultaneous use of these criteria provides a powerful tool in discrimination and correlation of scattered pyroclastic deposits.

In comparative studies of volcaniclastic deposits it is important to define first the volcanic activity units. An eruption unit is a deposit defined as a thickness of volcanic material deposited from an eruptive pulse (lasting for a few minutes to a few hours), an eruptive phase (lasting for days) or an eruption (lasting for years; [5]). These eruption units could be single pyroclastic flow or fall units among others. Furthermore, we can define larger volcanic units, such as volcanic complexes produced by an eruptive epoch (lasting for thousands of years) and volcanic fields built up by eruptive periods (lasting for millions of years; [5]). The resolution of the comparative studies (i.e. what kinds of volcanic activity units are compared) depends on the amount and quality of the exposed deposits.

In the southern slope of the Bükk Mts. (Bükkalja Ignimbrite Volcanic Field), a large number of outcrops of fresh silicic volcanic products can be found that cover a formation age between 21 Ma and 13.5 Ma [4]. Therefore, this region provides an excellent opportunity to test various tools to correlate the scattered localities. Paleomagnetic data are powerful tools in correlating the volcaniclastic horizons (volcanic complexes) of the Bükkalja region ([4]; Lower Ignimbrite Unit, LIU; Middle Ignimbrite Unit, MIU, Upper Ignimbrite Unit, UIU west and east), because two major rotations occurred during the period of the volcanic activity [6]. Thus, paleomagnetic rotation data serve as a strong framework in the comparative study of volcanic complexes. Furthermore, based on detailed physical volcanological studies, even smaller units have been distinguished such as pyroclastic flow and fall units. This allowed us to test various criteria how eruption units can be correlated in terms of their petrologic, geochemical etc. features.

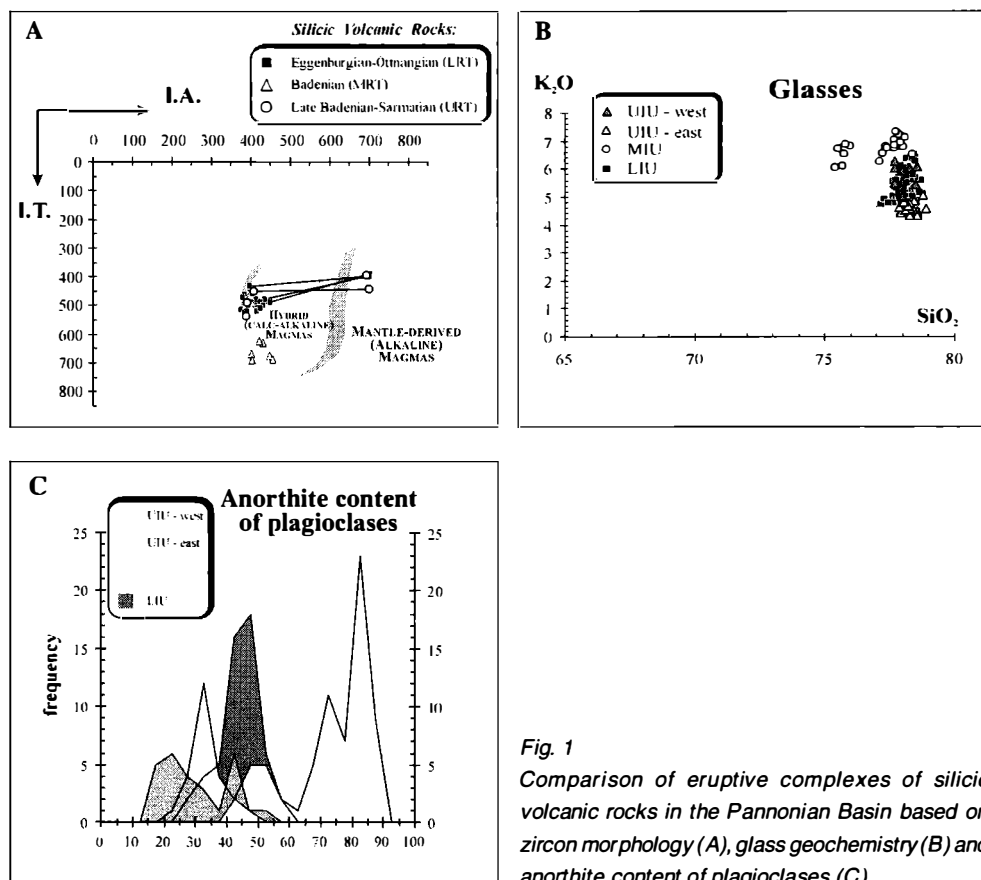


**Fig. 1**  
Comparison of eruptive complexes of silicic volcanic rocks in the Pannonian Basin based on zircon morphology (A), glass geochemistry (B) and anorthite content of plagioclases (C).

We demonstrate that the combined use of zircon morphology (Fig. 1A), petrography, glass geochemistry (Fig. 1B), mineral chemistry (e.g. anorthite content of plagioclases; Fig. 1C; FeO content of biotites) and composition of silicate melt inclusions hosted by quartz provides a powerful tool to discriminate and correlate the Miocene silicic volcanic complexes and even eruptive units in the Pannonian Basin.

## **References**

- [1] HARANGI, SZ. (2001): Neogene to Quaternary Volcanism of the Carpathian-Pannonian Region - a review. - *Acta Geol. Hung.* in press.
- [2] HAMOR, G., RAVASZ-BARANYAI, L., HALMAI, J., BALOGH, K. & ÁRVA-SOS, E. (1987): Dating of Miocene acid and intermediate volcanic activity in Hungary. - *Ann. Inst. Geol. Publ. Hung.*, 70: 149-154.
- [3] OLAH, I. & HARANGI, SZ. (2000): Does a unique "Lower Rhyolite Tuff Horizon" exist in the Pannonian Basin? - *Vijesti Hrvatskoga geoloskog drustva*, 37/3: 93.
- [4] MARTON, E. & PÉCSKAY, Z. (1998): Complex evaluation of paleomagnetic and K/Ar isotope data of the Miocene ignimbritic volcanics in the Bükk Foreland, Hungary. - *Acta Geol. Hung.*, 41/: 467-476.
- [5] FISHER, R. V. & SCHMINCKE, H.-U. (1984): Pyroclastic rocks - Springer Berlin Heidelberg New York, p. 472.
- [6] MARTON, E. & FODOR, L. (1995): Combination of paleomagnetic and stress data - a case study from North Hungary. - *Tectonophysics*, 242: 99-114.

**UNUSUAL PGE-, REE-, AU- AND U-RICH MINERAL ASSEMBLAGE  
IN MANTLE-DERIVED CHROMITITES FROM THE EASTERN ALPS, AUSTRIA:  
A COMBINED MULTI-DISCIPLINARY STUDY**

by

**K. N. Malitch**

Institute of Geological Sciences  
University of Leoben, Peter-Tunner Strasse 5, A-8700 Leoben, Austria

Highly unusual assemblages of platinum-group minerals (PGM), rare earth-, gold- and uranium-rich accessory minerals from geologically and compositionally distinct chromitites (podiform and banded types) at Kraubath and podiform chromitite at Hochgrössen have been evaluated during FWF-Projects M505 and M601-CHE "Platinum-group element geochemistry and mineralogy in Eastern Alpine ultramafic massifs". Parts of these results have been summarized recently [1, 2].

The Kraubath and Hochgrössen dunite-harzburgite massifs, two large mantle relicts in the Eastern Alps, have been interpreted as part of a dismembered Precambrian to Early Paleozoic, strongly deformed and metamorphosed ophiolite complex, which originated in a supra-subduction setting [3-6, etc.]. However, the age of ultramafic protoliths is unknown. Preliminary data on Os-isotope composition of laurite, presented for the first time, help constrain the age of protolith(s) formation.

The predominant chromitite type at Kraubath and Hochgrössen is schlieren, deformed stringers and streaks of massive chromite not more than a few centimeters thick. These are considered to be typical of podiform chromitite. However, at Kraubath another, less abundant type of chromitite (i.e. sheet-like orebodies, banded type) is present as layers in a stratigraphically higher level of the massif (the Sommergraben area). Various accessory minerals from 3 different bedrock chromitites have been investigated by several techniques, including highly effective hydroseparation method and electron-microprobe analysis (EMPA). However, negative thermal ionization mass-spectrometry (NTIMS), to date, has only been applied to monophase Ru-Os sulfides in the size range of 45 - 100  $\mu\text{m}$  from the podiform chromitite of the Kraubath massif.

**Mineralogy and PGE-geochemistry**

Chemical composition of chromite varies from Cr# [100\*Cr/(Cr+Al)] = 73 - 77 in the banded-type to Cr# = 81 - 86 in the podiform chromitite at Kraubath and Hochgrössen.

About 15 different PGM, one gold-rich mineral (tetrauricupride AuCu) and uraninite are firstly observed in the banded chromitite with pronounced enrichment of Pt and Pd relative to more refractory platinum-group elements (PGE) of IPGE-group (Os, Ir, Ru) like in those characteristic of crustal section of ophiolites. On the contrary, the podiform chromitites at Kraubath and Hochgrössen display a negatively sloping chondrite-normalized PGE pattern. This pattern is similar to typical ophiolitic-podiform chromitite. Twenty-one different PGM are recorded in the podiform chromitite from Kraubath, compared to 3 PGM and 2 unnamed rare earth minerals in the podiform chromitite at Hochgrössen. Distinct PGE distribution patterns of different chromitites correspond well to variable PGM assemblages.

Banded chromitite is dominated by sperrylite (53 % of all PGM), which occurs in polyphase assemblages with an unnamed Pt-base metal (BM) alloy and Pd-rich minerals such as stibiopalladinite, mayakite, mertieite II, palladoarsenide, unnamed Pd-Rh-As and Pd(Pt)-(As,Sb) minerals. Banded type also contains PGE-sulfides (about 7 %), which are represented by a wide compositional range of the laurite-erlichmanite series and irarsite (8 %). Iridian osmium, geversite, unnamed Pt-Pd-Bi-Cu, tetrauricupride and Pb-Th-rich uraninite are present in minor amounts. Uraninite is characterised by high contents of PbO (13.63 - 17.04 wt.%) and ThO<sub>2</sub> (9.54 - 11.44 wt.%), yielding model ages between 1520 and 1780 Ma.

In contrast, podiform chromitite is dominated by laurite, which occurs in complex polyphase assemblages with PGE-alloys (Ir-Os, Os-Ir, Pt-Fe), PGE-sulfides (kashinite, bowieite, cupro-iridsite, cuprorhodsite, unnamed Ir-rich variety of ferrorhodsite, braggite, unnamed Ni-Fe-Cu-Rh- and Ni-Fe-Cu-Ir sulfides) and Pd telluride (keithconnite). A variety of PGE-sulfarsenides (33 %) including irarsite, hollingworthite, platarsite, ruarsite and a number of intermediate species have been identified, while sperrylite and stibiopalladinite are subordinate (2 %). Unnamed rare earth minerals are present as mono- and polyphase grains. Their composition is dominated by Ce<sub>2</sub>O<sub>3</sub> (51.15 - 52.85 wt.%), La<sub>2</sub>O<sub>3</sub> (25.32 - 26.32 wt.%), Nd<sub>2</sub>O<sub>3</sub> (14.89 - 15.83 wt.%) and Gd<sub>2</sub>O<sub>3</sub> (6.19 - 7.6 wt.%).

### **Os-isotope constraints**

The <sup>187</sup>Os/<sup>188</sup>Os ratio was used to identify the substantial source and model (mantle-derived) osmium-isotope age of PGM. The <sup>187</sup>Os/<sup>188</sup>Os value, measured by NTIMS, in single Os-rich laurite grains from podiform chromitite at Kraubath was found to range from 0.1158 to 0.1162. Therefore, first age estimates on the formation of the ultramafic protoliths, based on osmium isotopic composition of Ru-Os sulfides, yield model ages in the range of 1630 - 1685 Ma, assuming chondritic mantle reservoir. The model ages obtained indicate that the matter source for PGE-mineralization had been the Proterozoic mantle. The Rb-Sr isotope-geochemical system identifies several younger metamorphic events that occurred in the vicinity of the Kraubath and Hochgrössen massifs at c. 400 and 100 Ma [6, FARYAD et al. unpublished data]. In this context, the model Os-isotope ages obtained (1630 - 1685 Ma) indicate the high stability of the Os-isotope system within PGM, despite the occurrence of later thermal events. Os-isotope stability has also been demonstrated for detrital 3.1 Ga Os-rich alloys from the Evander goldfield, Eastern Witwatersrand, South Africa [7]. This feature is considered a promising sign in the evaluation of Os-isotope composition of various PGM (e.g., Os-rich alloys, sulfides and sulfarsenides) from geologically and compositionally distinct chromitites at Kraubath as well as from podiform chromitite at Hochgrössen.

## **Conclusions**

The occurrence of about 30 PGM, two rare earth minerals, tauriccupride and Pb-Th-rich uraninite from only three bedrock chromitite samples is highly unusual for an ophiolitic environment. Such unusual diversity, firstly observed in or close to the mantle section of an ophiolite, is due to the novel investigation approach undertaken in this study. Consequently, geologically, geochemically and mineralogically distinct banded chromitite from Kraubath might be considered as indicative for the transition zone of an ophiolite, closely above the mantle section with podiform chromitite, rather than representative of the crustal cumulate pile. Model ages of Ru-Os sulfides vary from 1630 to 1685 Ma. Therefore, they indicate the existence of Precambrian parent ultramafic protolith originated at the PR2-PR3 boundary.

## **Acknowledgements**

Financial support by the Austrian Science Fund and productive atmosphere in the Institute of Geological Sciences is gratefully acknowledged.

## **References**

- [1] MALITCH, K. N., MELCHER, F. & MÜHLHANS, H. (2001): Palladium and gold mineralization in podiform chromitite at Kraubath, Austria. - *Mineral. Petrol.* 73 (In press).
- [2] MALITCH, K. N., THALHAMMER, O. A. R., KNAUF, V. V. & MELCHER, F. (in press): Diversity of platinum-group mineral assemblages in banded and podiform chromitites from the Kraubath ultramafic massif, Austria: evidence for an ophiolitic transition zone? - *Mineral. Deposita*.
- [3] STUMPFL, E. F. & EL AGEED, A. (1981): Hochgrößen und Kraubath - Teile eines paläozoischen Ophiolit-Komplexes. - *Mitt. Abt. Geol. Paläont. Bergr. Landesmuseum Joanneum* 42: 161-169.
- [4] NEUBAUER, F. (1988): Bau und Entwicklungsgeschichte des Rennfeld-Mugel- und des Gleinalm-Kristallins (Ostalpen). - *Abh Geol B-A.* 42: 1-137.
- [5] MELCHER, F. (2000): Chromite and platinum-group elements as indicators of mantle petrogenesis. - Unpubl. Habil. thesis. Mining University Leoben, 202 pp.
- [6] PUHI, J. (2000): Vergleichende Petrologie und Geochemie von ultramafischen Massiven der Ostalpen. - Unpubl. PhD thesis, Mining University Leoben, 332 pp.
- [7] MALITCH, K. N., KOSTOYANOV, A. I. & MERKLE, R. K. W. (2000): Mineral composition and osmium isotopes of PGE-mineralization of Eastern Witwatersrand, South Africa. - *Geology of Ore Deposits* 42: 253-266.

**FLUID INCLUSIONS STUDY IN QUARTZ, APATITE AND NEPHELINE FROM THE  
DITRAU ALKALINE MASSIF, TRANSYLVANIA (ROMANIA)**

by

**I. Márton<sup>1,2</sup>, J. Gál<sup>1,2</sup>, E. Benö<sup>1,2</sup>, A. Fall<sup>1,2</sup>, Á. Gál<sup>1</sup>, K. Török<sup>3</sup> & Cs. Szabó<sup>2</sup>**

<sup>1</sup>Department of Mineralogy and Petrology

Babeş-Bolyai University, Cluj-Napoca (UBB), str. M. Kogalniceanu, nr.1., Romania

<sup>2</sup>Department of Petrology and Geochemistry

Lithosphere Research Group, Eötvös University, Múzeum krt. 4/A, 1088 Budapest, Hungary

<sup>3</sup>Department of Geophysics

Eötvös University (ELTE), Ludovika tér 2, 1083 Budapest, Hungary

Formation of the Ditrău Alkaline Massif (East-Transylvania, Romania) could have been related to the opening of the Tethys Ocean between 230 Ma and 115 Ma (KRÄUTNER & BINDEA, 1998). The rifting process was accompanied by a complex igneous activity. According to MOROGAN et al. (2000), the whole massif is inferred to have originated from basanitic magmas of OIB-like character, generated by small degrees of melting of asthenospheric garnet lherzolite. However, the relatively hydrous nature of the Ditrău magmas leads to speculation that the primitive melts may have been modified by passage through hydrated (possibly amphibole-bearing) lithospheric rocks.

The main aim of our fluid inclusion study is to provide more information to better understand the evolution of the Ditrău Alkaline Massif. We have examined all the major rock types (alkali granites, syenites, monzonites, nepheline syenites, diorites/gabbros, hornblendites) collected from the best-known and studied locations (STRECKEISEN, 1960; PÁL-MOLNÁR, 2000).

Based on a careful petrographic study, primary fluid inclusions have been found in apatites (Figure 1) from diorites/gabbros and hornblendites, in nephelines (Figure 2) from nepheline syenites, and in quartzes from alkali granites. Fluid inclusions in apatite are rounded or negative crystal shaped. Their sizes are between 5 - 30 µm in diameters. They contain two phases: liquid and vapor (Figure 1). Fluid inclusions in quartz show rounded and irregular shapes. Their sizes range from 5 to 17 µm in diameters. They also contain liquid and vapor phases. Fluid inclusions in nepheline are elongated negative crystal shaped. Their emplacement is always parallel to the cleavage direction of the host mineral. Size of the fluid inclusions is between 2 - 40 µm in diameters. Two types of fluid inclusions can be distinguished in nephelines: 1) two-phase fluid inclusions containing liquid and vapor; and 2) multiphase fluid inclusions consisting of liquid, vapor and solid phase(s) (Figure 2). Among the solid phases only halite has been identified. However, unknown salt crystal(s) and/or trapped silicates are also visible.

Secondary two-phase fluid inclusions, occurring along intragranular healed fractures, can be seen in grains of apatite, quartz, calcite and titanite. However, these inclusions were ignored in this study.

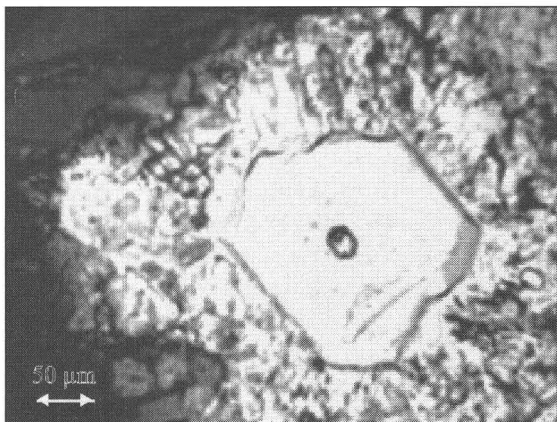


*Fig. 1*  
*Two-phase negative crystal shaped fluid inclusion in apatite in diorite/gabbro.*

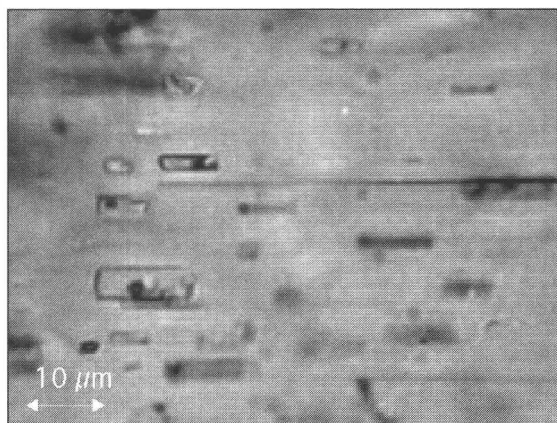


*Fig. 2*  
*Two-phase and multiphase negative crystal shaped fluid inclusions in nepheline in nepheline syenite. Emplacement of the fluid inclusions is the same as cleavage direction of the host mineral.*

Based on the microthermometric data and properties of the two-phase fluid inclusions, the fluid represent a simple NaCl-H<sub>2</sub>O system with different NaCl content. Fluid inclusions in apatite ( $T_h = 119 - 223^\circ\text{C}$ ) show high salinity (average 23 NaCl equ. wt.%), whereas those in quartz ( $T_h = 170 - 212^\circ\text{C}$ ) have low salinity (average 6.5 NaCl equ. wt.%). Two-phase fluid inclusions in nepheline ( $T_h = 196 - 288^\circ\text{C}$ ) have moderate salinity (NaCl ranging from 10.73 equ. wt.% to 17.43 equ. wt.%). However, the microthermometric properties of the multiphase fluid inclusions in nepheline have not been constrained properly, yet. These fluid inclusions represent complex salty water containing probably ions of Na<sup>+</sup>, K<sup>+</sup>, Mg<sup>2+</sup>, Ca<sup>2+</sup>, SO<sub>4</sub><sup>2-</sup>, Cl<sup>-</sup>, CO<sub>3</sub><sup>2-</sup>.

Based on the microthermometric data obtained for NaCl-H<sub>2</sub>O fluids (BODNAR & VITYK, 1994), experimental data for water saturated alkali granite (KONNERUP-MADSEN & ROSE-HANSEN, 1984), and the PT conditions of crystallization for nepheline in intrusive environment (KOGARKO & ROMANCHEV, 1977), the trapping conditions for the two-phase NaCl-H<sub>2</sub>O fluid inclusions in quartz and nepheline can be estimated by use of isochore intercept techniques.

Accordingly, trapping of fluid inclusions in quartz could have occurred at ranges of  $P = 4.5 - 6$  kbar and  $T = 510 - 530^\circ\text{C}$ . Whereas, trapping of fluid inclusion in nepheline could have occurred at range of  $P = 2.5 - 5$  kbar and  $T = 420 - 710^\circ\text{C}$

## References

- [1] KRÄUTNER, H. G. & BINDEA, G. (1998): Timing of the Ditrău intrusive complex (Eastern Carpathians, Romania). - Slovak Geol. Mag., 4, pp. 213-223.
- [2] MOROGAN, V., UPTO, B. G. & FITTON, J. G. (2000): The petrology of the Ditrău alcalinecomplex, Eastern Carpathians. - Min. and Petr. 69, pp. 227-265.
- [3] STRECKEISEN, A. (1960): On the structure and the origin of the Nephelinsyenite Complex of Ditró (Transsilvania). - 21th IGC. 13, pp. 228-238.
- [4] PÁL MOLNÁR, E. (2000): Hornblendites and diorites of the Ditró syenite massif. - University of Szeged, Szeged, pp. 172.
- [5] BODNAR, R. J. & VITYK, M. (1994): Interpretation of microthermometric data for  $\text{H}_2\text{O}-\text{NaCl}$  fluid inclusions. - in: Fluid inclusions in minerals: methods and applications, Short Course of Working Group (IMA) in "Inclusions in Minerals" (Pontignano-Siena, 1-4 September 1994).
- [6] KONNERUP-MADSEN, J. & ROSE-HANSEN, J. (1984): Composition and significance of fluid inclusions in the Illicmussaq peralkaline granite, South Greenland. - Bull. Mineral., 107, pp. 317-326.
- [7] KOGARKO, L. N. & ROMANCHEV, B.P. (1977): Temperature, pressure, redox conditions and mineral equilibria in agpaitic nepheline syenites and apatite-nepheline rocks. - Geokhimiza, No. 2, pp. 19-216.

MONAZITE-(SM), A NEW MEMBER OF THE MONAZITE GROUP  
FROM THE ANNIE CLAIM #3 GRANITIC PEGMATITE, SOUTHEASTERN MANITOBA

by

M. Masau, P. Černý<sup>1</sup>, M. A. Cooper<sup>1</sup>, R. Chapman<sup>1</sup> & J. D. Grice<sup>2</sup>

<sup>1</sup>Department of Geological Sciences  
University of Manitoba, Winnipeg, MB R3T 2N2, Canada  
<sup>2</sup>Canadian Museum of Nature  
Research Division, Ottawa, ON K1P 6P4, Canada

Monazite-(Sm) was found in the Annie Claim #3 pod of lepidolite-subtype granitic pegmatite, within the Greer Lake intrusion of pegmatitic leucogranite, in the Archean Bird River Subprovince of the Superior Province, in southeastern Manitoba. The subellipsoidal, subhorizontal body of the pegmatite is approximately 10 x 7 metres in size, with distinct concentric zoning. The zones show an inward progression of changing texture and mineral assemblage, exemplified by a border-to-core succession of five main types of mica (from muscovite to lithian muscovite and lepidolite), associated mainly with albite and quartz. Microcline-perthite is sporadic in the outermost zones and absent from the intermediate and inner zones. Accessory minerals include spessartine, cesian beryl, cassiterite with exsolved zirconian-hafnian wodginite, manganocolumbite, manganotantalite and rare primary wodginite, microlite, uranpyrochlore, ferrotapiolite, probable formanite-(Y), apatite, zircon with exsolved coffinite, uraninite, dysprosian xenotime-(Y) and monazite-(Sm). The pegmatite and the parent pegmatitic granite do not contain any minerals of B or phosphates of Li, Al, Fe or Mn, and sulphides are extremely rare.

Monazite-(Sm) forms tabular crystals  $\leq 0.4$  mm in size, associated with manganocolumbite, quartz, albite and lithian muscovite. Monazite-(Sm) is yellowish, translucent, with a white streak, vitreous to greasy luster and no observed fluorescence. One good cleavage is present, tenacity is brittle, and the fracture is uneven. Monazite-(Sm) has no observable pleochroism;  $\alpha = 1.768(5)$ ,  $\beta = 1.771(3)$ ,  $\gamma > 1.808(3)$ ;  $2V$  meas. =  $28(8)^\circ$ ,  $X = b$ ,  $Z \wedge c = 9^\circ$  ( $\beta$  obtuse). It is monoclinic, space group  $P2_1/n$ ; refinement from single-crystal and powder X-ray-diffraction data gave  $a = 6.725(1)$ ,  $6.739(3)$ ,  $b = 6.936(1)$ ,  $6.951(3)$ ,  $c = 6.448(1)$ ,  $6.462(3)$  Å,  $\beta = 104.02(1)^\circ$ ,  $104.03(4)^\circ$ ,  $V = 291.8(1)$ ,  $293.6(2)$  Å<sup>3</sup>,  $Z = 4$ ;  $D_{\text{calc.}}$  from average chemical composition 5.512 and 5.548 g/cm<sup>3</sup>. The strongest lines of the (Gandolfi) X-ray diffraction pattern [d in Å(I)(hkl)] are: 4.647(5)(011), 4.164(8)(-111), 3.492(4)(111), 3.264(7)(200), 3.065(10)(120), 2.857(9)(-112).

The monazite-(Sm) contains, in wt.%, up to 14.29 Sm<sub>2</sub>O<sub>3</sub>, 13.48 Gd<sub>2</sub>O<sub>3</sub> and 6.28 Nd<sub>2</sub>O<sub>3</sub>, and moderate percentages of huttonite and brabantite components.

The most Sm-rich composition gives:



The middle-REE-dominant signature of the Annie Claim #3 monazite-(Sm) is shared with the broadly associated Y(Ta,Nb)O<sub>4</sub> mineral (probably formanite-(Y)) and dysprosian xenotime-(Y). This exotic pattern of REE abundances is possibly generated by selective and differential complexing of REE in the granite-to-pegmatite solidification sequence.

**ELASTISCHE ANOMALIEN BEI MINERALEN UNTER DRUCK**

von

**R. Miletich<sup>1</sup>, R. J. Angel<sup>2</sup>, S. Rath<sup>1</sup>, M. Kunz<sup>1,3</sup>, A. Friedrich<sup>1</sup>, W. Schranz<sup>4</sup> & A. Tröster<sup>4</sup>**

<sup>1</sup>Labor für Kristallographie  
ETHZ, Ch-8092 Zürich, Schweiz

<sup>2</sup>Department of Geological Sciences  
Virginia Polytechnic Institute, VA 24060 Blacksburg, USA

<sup>3</sup>Naturhistorisches Museum  
Augustinergasse 2, CH-4001 Basel, Schweiz

<sup>4</sup>Institut für Experimentalphysik  
Universität Wien, A-1090 Wien

Die elastischen Konstanten eines Materials, die den Zusammenhang zwischen externen mechanischen Kräften und der Deformation eines kristallinen Festkörpers beschreiben, zeigen normalerweise eine gleichmässige und annähernd lineare Entwicklung über einen weiten Bereich von Druck und Temperatur. Variationen in P und T können mitunter aber auch spontane, relativ drastische Änderungen der strukturellen Konfiguration auf atomarer Ebene bedingen. Materialien, die einer solchen Phasentransformation unterliegen, zeigen oft – bei Approximation ihrer Stabilitätsgrenzen – anormale Verhaltensweisen, die mitunter starke Variationen einzelner die Elastizität beschreibender Tensorkomponenten mit sich bringen [1]. Derartige Anomalien manifestieren sich durch betont nichtlineare Abhängigkeiten der Druckentwicklung der elastischen "Konstanten" über einen gewissen P,T-Bereich in unmittelbarer Nähe der kritischen Übergangspunkte. Hinsichtlich temperaturinduzierter Phasenübergänge existiert eine Vielzahl an Beispielen experimentell belegter Anomalien [2], aber nur wenige sind für druckinduzierte Effekte bekannt [3], was primär auf die experimentellen Meßschwierigkeiten bei Hochdruckuntersuchungen zurückzuführen ist.

Mit den erzielten Fortschritten in der Hochdruck-Röntgendiffraktometrie [4] ist es nun möglich auf Basis hochauflösender Beugungsexperimente an Einkristallen in der Diamant-Stempelzelle extrem gute Datensätze statischer isothermaler Kompressibilität zu erzielen. In dieser Studie wurden von Mineralphasen, die bekannterweise einem druckinduzierten Phasenübergang unter hydrostatischen Bedingungen  $\leq 100$  kbar unterliegen, die statischen Kompressibilitäten untersucht, vor allem ihr Verhalten in unmittelbarer Nähe der Phasen-Übergänge. Die Untersuchungen erfolgten an Pyroxenen, Akermannit, Titanit-Malayait, Cordierit, und Effenbergerit-Gillespit.

Das Versagen von konventionellen Modellen [5] zur Beschreibung der thermodynamischen Zustandsgleichung verlangt im Fall stark elastischem Verhaltens einen neuen theoretischen Ansatz zur Beschreibung der Kompressibilität im kritischen Bereich des Übergangsdruckes  $P_c$ . Basierend auf einem erweiterten Modell der Landautheorie, in der die Beschreibung der freien Energie mit einem nichtlinearen Term für die Elastizität erstmals verwendet wird, konnten die experimentell bestimmte Datensätze erstmals physikalisch sinnvoll dem geringen Messfehler entsprechend präzis nachvollzogen werden [6]. Hinsichtlich der überraschenden Größenordnung, sowohl des Ausmaßes die Kompressibilität betreffend (bis zu 300 % der "normalen" Entwicklung) als auch den vom abnormalen Verhalten betroffenen Druckbereich soll auf die potentielle Bedeutung im Rahmen geophysikalischer Modellierungen verwiesen werden.

## References

- [1] CARPENTER, M. A. & SALJE, E. K. H. (1998): Eur. J. Mineral. 10, 693.
- [2] CARPENTER, M. A., SALJE, E. K. H., GRAEME-BARBER, A., WRUCK, B., DOVE, M. T. & KNIGHT, K. S. (1996): Am. Mineral. 83, 2 und KITYK, A., SOPRUNYUK, V. P., FUITH, A., SCHRANZ, W. & WARHANEK, H. (1996): Phys. Rev. B 53, 6337.
- [3] HAUSSÜHL, S. (1983): Solid St. Comm., 46, 423.
- [4] MILETICH, R., ALLAN, D. R. & KUHS, W. F. (2001): MSA Rev. in Min. and Geochem. 41, 445 und ANGEL, R. J., DOWNS, R. T. & FINGER, L. W. (2001): MSA Rev. in Min. and Geochem. 41, 559.
- [5] ANGEL, R. J. (2001): MSA Rev. in Min. and Geochem. 41, 35 (2001) und ANDERSON, O. L. (1995): Equations of State of Solids for Geophysics and Ceramic Sciences, Oxford University Press, Oxford.
- [6] TRÖSTER, A., SCHRANZ, W. & MILETICH, R.: Phys. Rev. Lett. (submitted) und MILETICH, R., SCHRANZ, W. TRÖSTER, A., ANGEL, R. J. & FRIEDRICH, A.: Science (submitted)

MELTING PROPERTIES OF ICE III, (V), VI AND THEIR ISOCHORIC GRADIENT  
OF WATER UP TO 20 KBAR AND 300°C – A REVIEW OF LITERATURE DATA

by

P. W. Mirwald

Institute of Mineralogy and Petrography  
University of Innsbruck, Innrain 52, A-6020 Innsbruck

A reexamination of literature data on the melting of ice I-VII and the PVT-behavior of water the range of -20 to 300°C and 1 to 20 Kbar has been conducted.

The basic data for the melting of different ice-modifications has been produced by TAMMANN (1900) and BRIDGMAN (1912 a,b; 1935; 1937) which only have been modified in slight details by later workers (PETRENKO & WHITNORTH, 1999). As to the reevaluation of the PVT-behavior of water the NBA Steam tables served for this study being augmented by some low temperature data by BRIDGMANN (1912a,b).

Starting point of this study was the reexamination of the melting of ice of which the P-T phase diagram is displayed in Fig. 3. While ice I, V and VII show a fairly regular melting behaviour the melting curves of ice II and VI exhibit an abnormally curved course with a "kink" at 2.3 and at 8.3 kbar. From a phase theoretical point of view this insinuated a more complex situation between solid, melting and liquid than previously assumed.

The inspection of the PVT-data of water revealed some irregularities when plotted in isothermal and isobaric sections respectively. The compression and thermal expansion of materials, expressed by its coefficients  $dV/dP_T$  and  $dV/dT_P$ , are related to the isochoric gradient by the expression  $dV/dT_P / dV/dP_T = -dP/dT_V$ . The isochoric gradients were calculated for the above outlined P-T-frame. Some examples of the gradient curves plotted versus pressure and temperature respectively are displayed in Fig. 1 and 2.

The data reveal systematic changes in slope what may be interpreted as irregular and/or discontinuous volume behaviour of water. In addition, for a more precise determination of the P-T-position of slope changes the derivative have been used in some cases.

The results derived from the isochoric gradient curves have been incorporated in Fig. 3. They reveal a systematic volume/density variation of over the P-T-range reviewed what enables to construct a tentative pattern of P-T regions of different volume behaviour of water.

Generally, three major regimes (I, II, III) may be distinguished within the P-T-range studied. They are separated by two "boundaries" starting off at the "kink" in the melting curve of ice II and VI. These boundaries are in principle little pressure dependent exhibiting an average slope in the range of 25 to 35 bars/K. A further boundary of rather isothermal character is likely in the temperature range between 60 - 100°C which seems to subdivide the two lower pressure regions I and II. Generally, the available data do not allow a precise allocation of the boundaries so far.

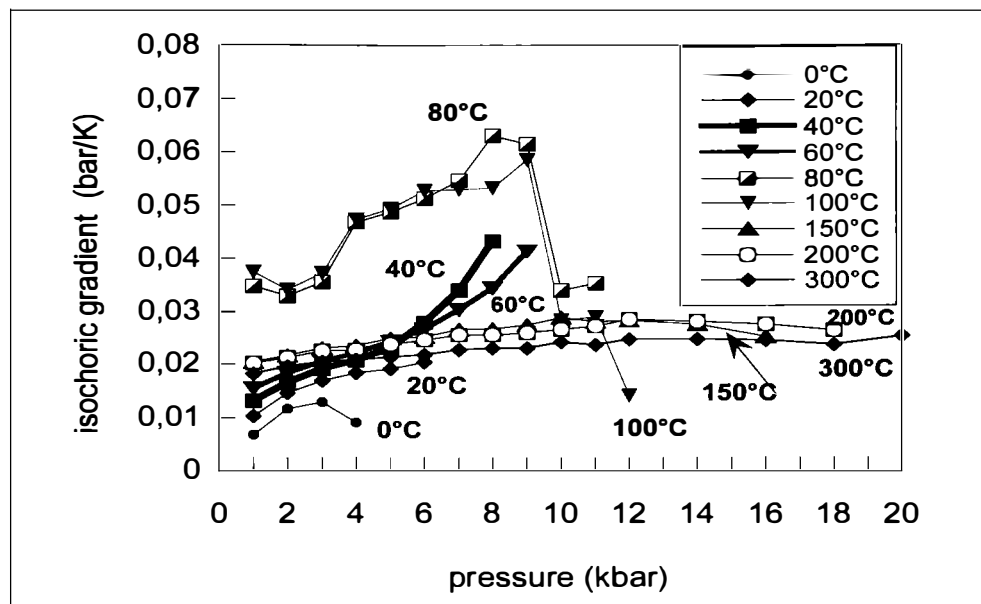


Fig. 1

Isobares of the isochoric gradient of water plotted versus pressure between 1 and 18 kb (cf. fig. 3:  $T_{isoch/p}$ ).

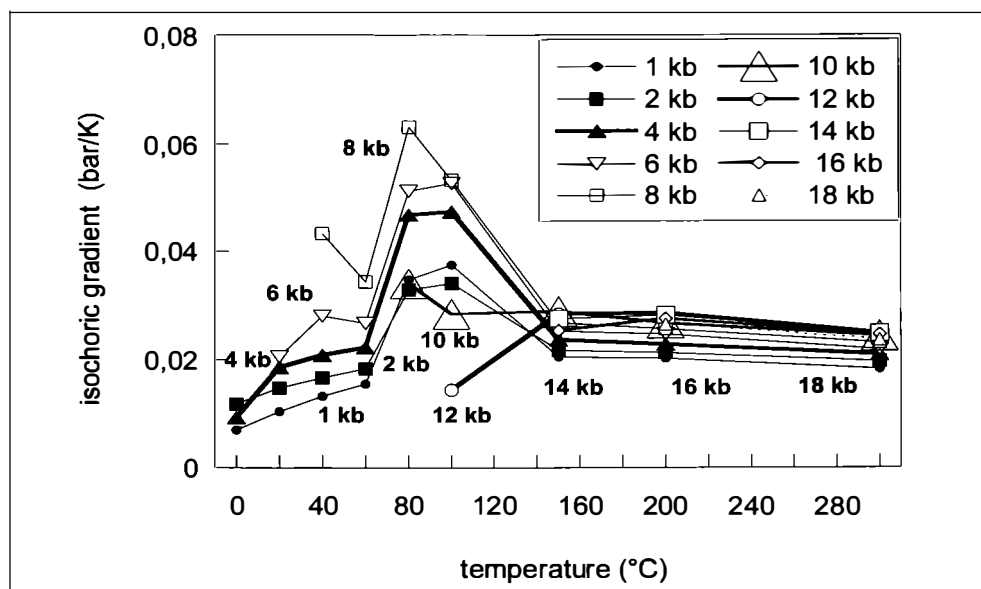


Fig. 2

Isotherms of the isochoric gradient of water plotted versus temperature between 0 and 300°C (cf. fig. 3:  $T_{isoc/t}$ ).

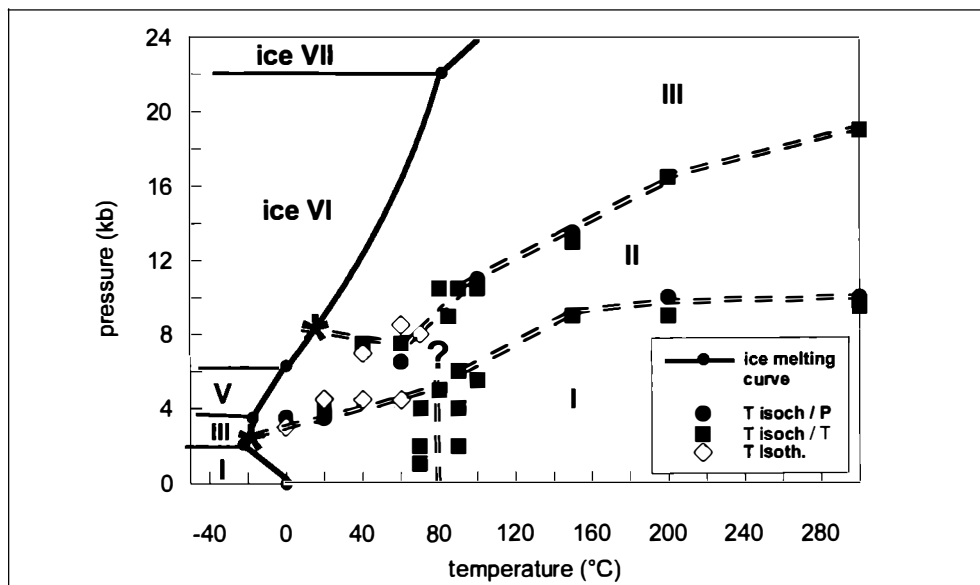


Fig. 3

Phase diagram of  $\text{H}_2\text{O}$ ; the melting curve of ice I, III, V, VI, VII and a tentative outline of P-T-regimes of different behaviour of the specific volume of water (dashed double lines). Symbols:  $T_{\text{isoch}}/t$  and  $T_{\text{isoch}}/p$  taken from isochoric gradient curves, see fig. 1 and 2;  $T_{\text{isoch}}$ : data taken from isothermal compression curves; stars: "kinks" in the melting curve of ice III and VI.

The finding of different P-T regimes for the specific volume behaviour of water insinuates different structural states. Possibly, this might also explain the often observed discontinuous solution rate behaviour of minerals in the temperature range 50 to 100°C, e.g. ANDERSON et al., (1991). A similar assumption might be valid for high P-T solution data e.g. by BECKER et al. (1985) and MANNING (1994), which indicate, at 700°C a first discontinuous rate change at 10 kbar and a second one at 19 kbar. If this proves true the slope of boundary I/II and II/III would significantly decrease.

For verification of these assumptions and for a more precise determination of the "boundaries" which separate the different P-T-regimes specific experiments are in progress.

#### Literature

- ANDERSON, CASTET, SCHOTT & MESNER (1991): Geochim. Cosmochim. Acta 55, 1769-1779.
- BECHER, CEMIC & LANGER (1983): Geochim. Cosmochim. Acta, 47, 1573-1578.
- BRIDGMAN (1912a): Proc. Am. Acad. Arts Sciences, 47, 441-558.
- BRIDGMAN (1912b): Proc. Am. Acad. Arts Sciences, 48, 310-362.
- BRIDGMAN (1935): J. Phys. Chem. 3, 597-605.
- BRIDGMAN (1937): J. Phys. Chem. 5, 964-966.
- HAAR, GALLAGHER & KELL (1984): NBS/NRC Steam Tables, Mc-Graw-Hill Book Comp., 1984.
- MANNING (1994): Geochim. Cosmochim. Acta 58, 4831-4839.
- PETRENKO & WHITNORTH (1999): Physics of Ice, Oxford Univ. Press, 1999.
- TAMMANN (1900): Ann. Phys., Ser. 4, 2, 1-31.

**THERMAL EXPANSION BEHAVIOR OF DISORDERED AND ORDERED  
(NA)-MG-CORDIERITE BETWEEN 25 AND 700°C – A HIGH RESOLUTION XRD STUDY**

by

**P. W. Mirwald & R. Tessadri**

Institut of Mineralogy and Petrography  
University of Innsbruck, Innrain 52, A-6020 Innsbruck

Cordierite ( $[Mg, Fe]_2Al_4Si_5O_{18} \cdot n[Na, H_2O, CO_2, \text{etc.}]_{\text{channel}}$ ), a framework silicate with characteristic channel elements, is an interesting mineral phase in granulitic metapelites and applied ceramics as well. Besides variable Mg/Fe ratios, sodium which is accommodated in the centre of the channel forming six membered ring elements, may be incorporated up to 0.6 mol% (WOLFSDOFF & SCHREYER, 1992; MIRWALD, 1999).

Cordierite occurs in two structural modifications, high and low temperature cordierite. In nature the orthorhombic low temperature form prevails which is with respect to its Si-Al distribution ordered. In ceramics where cordierite is produced as polycrystalline material for numerous applications, it is of hexagonal symmetry being characterised by Si-Al disorder.

With respect to its physical properties the low thermal expansion behaviour of cordierite is very striking. Most studies have been performed on synthetic material (e.g. IKAWA et al., 1986). Measurements on natural material are rare (HOCELLA et al., 1979; ARMBRUSTER, 1986; SCHNEIDER & MIRWALD, 1999) due to the fact that fluid compounds in the structural channels as well as complex chemical compositions (MIRWALD, 1998) impair to reproducible conditions.

A reinvestigation of the thermal expansion on Mg-cordierite by X-ray powder diffractometry has been conducted between 25 - 700°C at 1 atm. The major goal was to study the influence of variable sodium content on its thermal behaviour, in particular with respect to the recently established thermal discontinuities (SCHNEIDER et al., 2001; MIRWALD, 1999) at some 250 - 300 and 500 - 600°C.

The material has been prepared from oxide mixes (cf. WOLFSDOFF & SCHREYER, 1992). Pure cordierite (indialite) was used from BAM (PEPLINSKI et al., 2000). For the thermal expansion measurements a Siemens D-5005 diffractometer (parallel beam optics, scintillation counter, Cu-target, 40kV, 40mA, 0.02 steps, 4 sec measuring time per step, 8 - 100 degrees  $\theta/2\theta$ ) equipped with a Paar HTK 1200 high temperature device (heating ramp 0.2%/sec in 10°C intervals from 20°C to 700°C) was used. Data evaluation have been done by using the Rietveld-algorithm implemented in TOPAS 2.0 (Bruker AXS).

In Fig. 1 a data compilation of the system synthetic Mg-cord. – NaMg-cord. is given – including our samples – relating the sodium content of Mg-cordierite by the elementary cell volume at some 25°C. Our samples cover the whole range of miscibility. Five compositions have been prepared (9, 15, 33, 53 and 55 mol%). After crystallisation from the glass all samples crystallised in the hexagonal high temperature form. Only the sodium free sample could be transformed into the rhombic low temperature form by heating at 1400°C for 20 days; the sample of 9 mol% Na-content turned out to be structurally and chemically inhomogeneous. In a first measurement campaign detailed thermal expansion measurements have been done on the chemical endmembers, hexagonal and rhombic 0.00 NaMg-cordierite as well as on hexagonal 0.60 NaMg-cordierite.

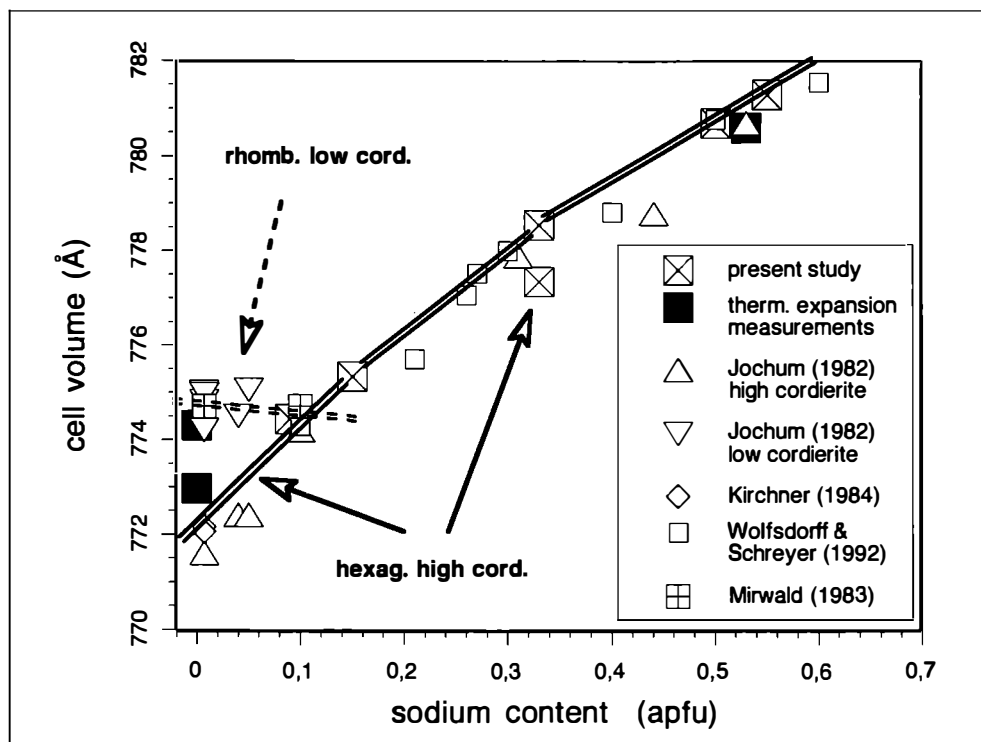


*Fig. 1*  
Plot of sodium content vs. cell volume compiled from different sources.

In a general way the data confirm the previous studies: small positive thermal expansion for the basis parameters and a negative expansivity for the c-parameter. However, detailed analysis of the three data sets reveals that the expansion behaviour is specifically different with respect to structural state as well as to the sodium content in the low temperature region up to 300°C (Fig. 2). In addition, the course of expanding volume curves show an irregular slope behaviour in the temperature region at 250 - 300°C and 550 - 600°C which is in relation to the sodium content of the samples. For comparison with the present data the volume expansion of White Well cordierite is also given in Fig. 2.

SCHNEIDER et al. (2001) recently have found a structural discontinuity in the temperature range 250 - 300°C. This discontinuity appears as a subtle kink in the lattice parameters, specially in the c-parameter, and is accompanied with a intensity jump of reflection peaks. A further discontinuity seems to be at 500 - 600°C. Both discontinuities are indicated in Fig. 2.

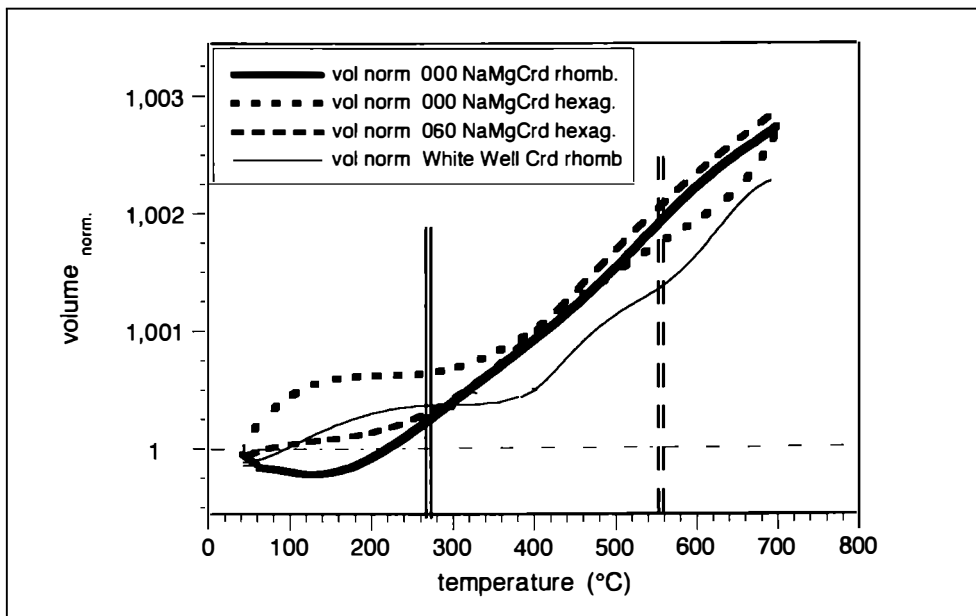


*Fig. 2*  
Temperature vs. cell volume (normalization: 25°C).

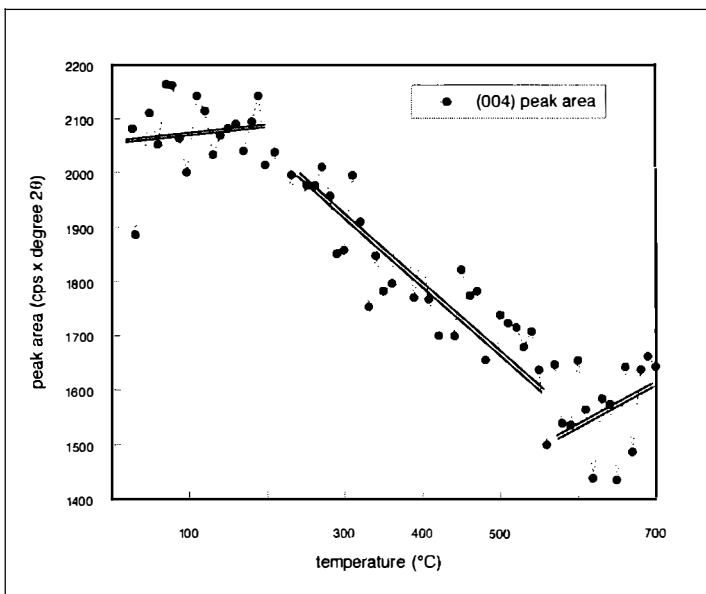


*Fig. 3*  
Temperature vs. peak area of the (004)-reflection of low cordierite ordered from high 000 NaMg-cordierite (indialite).

A comparable situation is encountered in the present data. While the cell parameters show only an indication of a kink, the change in intensity of the reflections is quite obvious as demonstrated by the peak area of the (004) reflection of the orthorhombic 000 NaMg-cordierite in dependence of temperature in Fig. 3.

These findings confirm previous work (MIRWALD, 1981, SCHNEIDER, TESSADRI & MIRWALD, 2001). They are supported by results obtained in electrical conductivity measurements (SCHMIDBAUER & MIRWALD, 1988a,b)) as well as by the H<sub>2</sub>O incorporation behaviour as reflected by changing slopes of the isohydrons (MIRWALD et al., 1979).

## References

- ARMBRUSTER, TH. (1986): Crystal structure refinement and thermal expansion of a Li, Na, Be-cordierite between 100 and 500 K. - Z. Krist. 174, 205-217.
- HOCELLA, M.F., ROSS, F.K. & GIBBS, G.V. (1979): High-temperature crystal chemistry of hydrous Mg-Fe-cordierites. - Am. Mineral., 64, 337-351.
- IKAWA, H., OZAGIRI, T. & IMAI, O. (1986) Thermal expansion of high cordierite and its solid solutions. - Yogyo Kyokai-Shi, 94, 3, 42-48.
- JOCHUM, C. (1982): Kinetik des H<sub>2</sub>O-Austausches und des Abbaus von synthetischem Mg-Cordierit. - Unpubl. diploma thesis, Ruhr-Universität Bochum, 74p.
- KIRCHNER, D. (1984): Experimenteller Lithium-Einbau in Mg-Cordierit. - Unpubl.diploma thesis, Ruhr-Universität Bochum, 142 p.
- MIRWALD, P. W. (1983): Crystal chemical effects of sodium on the incorporation of H<sub>2</sub>O and CO<sub>2</sub> in Mg-cordierite. - Terra cognita, 3:163.
- MIRWALD, P. W. (1981): Evidence of phase transition in cordierite at elevated pressure and temperature. - Terra cognita, EUG, 1: 90.
- MIRWALD, P. W. (1999): Sodium incorporation into cordierite. - Ber. Dtsch. Mineralog. Ges., Beih 1, p. 157.
- MIRWALD, P. W., MARESCH, W. V. & SCHREYER, W. (1979): Der Wassergehalt von Mg-Cordierit zwischen 500 und 800°C sowie 0.5 und 11 Kbar. - Fortschr. Mineral., 57, 1: 101.
- PEPLINSKI, B., MÜLLER, R., WENZEL, J., SOJRET, R. & SCHULTZE, D. (2000): An X-ray powder diffraction investigation of a fine-grained synthetic  $\alpha$ -cordierite powder. - Materials Science Forum, Vols. 321-324, 150-155.
- SCHMIDBAUER, E. & MIRWALD, P. W. (1998): Elektrische Eigenschaften von Cordierit - Frequenzabhängigkeit der elektrischen Leitfähigkeit und Kapazität zwischen 20 und 800°C. - Ber. Deutsche Mineralog. Ges. No.1, 1998, p.253.
- SCHMIDBAUER, E. & MIRWALD, P.W (1998): Elektrische Eigenschaften und strukturelle Variationen in Cordierit zwischen 200 und 800°C. - Mitt. Österr. Mineralog. Ges., 143, 345-348.
- SCHNEIDER, J. & MIRWALD, P.W. (1999)
- SCHNEIDER, J., TESSADRI, R. & MIRWALD, P. W. (1999): Re-examination of the thermal expansion of natural and synthetic cordierite between 25 and 800°C. - EUG XI, J. Conf Abstr. 6, (to be published).
- WOLFSDORFF, P. & SCHREYER, W. (1992): Synthesis of sodian cordierites in the system Na<sub>2</sub>O-MgO-Al<sub>2</sub>O<sub>3</sub>-SiO<sub>2</sub>. - N. Jb. Miner. Mh. 1992, 2: 80-96.

**THE YUBDO-DALETI AND TULU DIMTU ULTRAMAFIC ROCKS:  
A POTENTIAL SOURCE OF ECONOMIC DEPOSITS OF PLATINUM GROUP MINERALS**

by

**A. Mogessie<sup>1</sup>, K. Belete<sup>1</sup>, G. Hoinkes<sup>1</sup> & J. Bowles<sup>2</sup>**

<sup>1</sup>Institut für Mineralogie und Petrologie

Universität Graz, Universitätsplatz 2, A-8010 Graz

<sup>2</sup>John F. W. Bowles Mineral Science Ltd.

109 Asheridge Road, Chesham, Buckinghamshire, England HP5 2PZ

The 9 km long and 45 km wide ultramafic intrusion of Yubdo lies on the southern tip of a NNE–SSW striking lineament which includes the Daleti and Tulu Dimtu ultramafic intrusions covering a distance of 100 kms in western Ethiopia. Although the presence of platinum group minerals in both the Daleti and Tulu Dimtu ultramafic intrusions has yet to be proved, the platinum group element (PGE)/chondrite normalized plots show that all three intrusions display an Alaskan type layered intrusion trend as opposed to the ophiolitic origin that has been proposed by previous researchers in the region.

These ultramafic rocks are underlain by precambrian basement consisting mainly of gneisses, mica schists, quartzites and chlorite schists. Acidic intrusive rocks include syn-tectonic granodiorites, hybrid granites, quartz diorite and diorite porphyries which intrude the ultramafics.

There is an estimated 12.060 kg of platinum reserves in the weathered lateritic deposit of Yubdo with an average platinum content of 0.336 g/t of ore. Placer platinum and gold workings are common in the Yubdo area along the Alfe and Birbir rivers in addition to the known elluvial-alluvial lateritic placer deposits on the top of the birbirite and dunitic rocks belonging to the ultramafic intrusion.

The platinum group minerals are found in the form of Pt-Fe nuggets. They contain a wide variety of inclusions ranging from hollingworthite, irarsite, erlichmanite, laurite, genkinite, stibio-palladinite, and osmium laths with iron oxide coatings (MOGESSIE et al., 1999; BOWLES, 1986) suggested that a chemical agent must have been responsible for their sculpting and the extreme polishing observed on some alluvial platinum nuggets from Yubdo. The embayed and sculpted surfaces of the platinum-iron nuggets and their intimate association with fine grained iron oxides in the cavities of the nuggets documented from Yubdo are also features of gold grains considered to have grown in a lateritic environment. The similarities between gold and the platinum-group elements (PGM) indicate that the processes of formation of gold in laterites are likely to be paralleled by comparable development of PGM.

Based on the investigation made one can conclude that 1) the occurrence of droplets of PGM in chromites from bore hole ultramafic samples at depth suggests a magmatic origin; and 2) a remobilization and transport of the Pt-Fe alloys have taken place from a possible dunitic source and concentrated them in the laterites. Since the remobilization of the PGE is related to a hydrothermal fluid and structurally controlled, there is a possibility of finding an enriched platinum deposit as an offshoot mineralization in the basement intruded by the ultramafic rocks.

This work was financed by FWF project PI3643-GEO.

### References

- [1] BOWLES, J. F. W. (1986): The development of Platinum-Group Minerals in Laterites. - *Econ. Geol.* 81: 1278-1285.
- [2] MOGESSIE, A., BELETE, K., HOINKES, G., & ETTINGER, K. (1999): Platinum mineralisation in the Yubdo ultramafic rocks, western Ethiopia. - In *Mineral Deposits: Processes to Processing*, STANLEY et al. (eds), Balkema, Rotterdam. 751-754.

**Mg<sup>2+</sup>, Fe<sup>2+</sup> - VERTEILUNG IN SYNTHEtISCHEm OLIVIN (FA50FO50)**

by

**M. Morozov<sup>1</sup>, C. Brinckmann<sup>2</sup>, H. Kroll<sup>2</sup>, W. Lottermoser<sup>1</sup>, G. Tippelt<sup>1</sup> & G. Amthauer<sup>1</sup>**

<sup>1</sup>Institut für Mineralogie  
Universität Salzburg, Hellbrunnerstrasse 34, A-5020 Salzburg

<sup>2</sup>Institut für Mineralogie  
Universität Münster, Corrensstrasse 24, D-48149 Münster

In der Olivin Mischkristallreihe Mg<sub>2</sub>SiO<sub>4</sub> Forsterit (fo) - Fe<sub>2</sub>SiO<sub>4</sub> Fayalite (fa) mit der Raumgruppe Pnma besetzen Mg<sup>2+</sup> und Fe<sup>2+</sup> zwei kristallographisch unterschiedliche Gitterplätze: 4c mit der Punktsymmetrie m (M2) und 4a mit der Punktsymmetrie (M1). Wie mehrere Untersuchungen gezeigt haben ist die Mg<sup>2+</sup>, Fe<sup>2+</sup>-Verteilung auf M2 und M1 temperaturabhängig [e.g. 1, 2, 3].

In der vorliegenden Untersuchung wurden Olivine mit der Zusammensetzung 50 mol% fo und 50 mol% fa aus stöchiometrischen Mischungen der Oxide MgO, Fe<sub>2</sub>O<sub>3</sub>, and SiO<sub>2</sub> bei hohen Temperaturen und kontrollierten Sauerstoff-Fugazitäten (CO/CO<sub>2</sub>) synthetisiert. Diese Proben wurden dann bei Temperaturen zwischen 500°C und 800°C in Abständen von 25°C getempert und dann abgeschreckt. Von diesen Proben wurden <sup>57</sup>Fe Mössbauer Spektren mit einem üblichen Mössbauer Spektrometer mit Heizvorrichtung für den Absorber aufgenommen.

Die bei Zimmertemperatur des Absorbers aufgenommenen Spektren zeigen nur 2 Resonanzabsorptionslinien, die sich für quantitative Zwecke nicht genügend genau durch 2 Dubletten auswerten lassen. Bei höheren Absorbertemperaturen ist das Spektrum besser aufgelöst und ermöglicht eine quantitative Auswertung durch 2 Dubletten, die sich dem M1- bzw. dem M2-Platz zuordnen lassen. Deshalb wurden alle Spektren bei einer Absorbertemperatur von 300°C aufgenommen. Bei dieser Temperatur ist auch kein Kationenaustausch zwischen den M1- und M2-Positionen innerhalb der Messzeit eines Spektrums (5 Tage) zu erwarten.

Die Ergebnisse unserer Messungen zeigen, dass Fe<sup>2+</sup> die M1-Plätze bevorzugt, und dass der Anteil an Fe<sup>2+</sup> auf M1 mit steigender Temperatur von 52.4 % bei 500°C auf 55.7 % bei 750°C zunimmt. Dies übersteigt deutlich den Messfehler von ± 1 %. Diese Resultate werden mit denen von Röntgen- und Neutronenbeugungsuntersuchungen verglichen [1, 2, 3] und thermodynamisch ausgewertet.

## References

- [1] HEINEMANN, R., STAAK, V., FISCHER, A., KROLL, H., VAD, T. & KIRFEL, A. (1999): Temperature dependence of Fe, Mg partitioning in Acapulco olivine. - Amer. Mineral. 84: 1400-1405.
- [2] RINALDI, R., ARTIOLI, G., WILSON, C. C. & MCINTIRE, G. (2000): Octahedral cation ordering in olivine at high temperature. I: in situ neutron single-crystal diffraction studies on natural mantle olivines (Fa12 and Fa10). - Phys. Chem. Minerals 27: 623-629.
- [3] REDFERN, S. A. T., ARTIOLI, G., RINALDI, R., HENDERSON, C. M. B., KNIGHT, K. S. & WOOD, B. J. (2000): Octahedral cation ordering in olivine at high temperature. II: an in situ neutron powder diffraction study on synthetic MgFeSiO<sub>4</sub> (Fa50). - Phys. Chem. Minerals 27: 630-637.

SYNTHESIS AND CRYSTAL STRUCTURE OF  
A NEW LAYERED HYBRID GALLOPHOSPHATE CONTAINING OXALATE GROUPS

by

**M. Mrak<sup>1</sup>, U. Kolitsch<sup>2</sup>, C. Lengauer<sup>2</sup>, V. Kaučič<sup>1</sup> & E. Tillmanns<sup>2</sup>**

<sup>1</sup>National Institute of Chemistry

Hajdrihova 19, 1000 Ljubljana, Slovenia

<sup>2</sup>Institut für Mineralogie und Kristallographie

Universität Wien, Geozentrum, Althanstrasse 14, A-1090 Wien

The field of open framework materials has expanded dramatically during the last few years by introducing suitable organic ligands as part of the crystal structures, thus allowing a more flexible tailoring of the atomic architecture. The resulting materials can be described as hybrid inorganic-organic frameworks [1].

We have investigated the use of oxalic acid as an organic ligand having four potential donor sites for cation coordination. The compound  $(C_2N_2H_{10})_3[Ga_4(C_2O_4)_4(HPO_4)_4(H_2PO_4)_2]$  was prepared by hydrothermal synthesis under autogenous pressure using ethylenediamine (en) and oxalic acid as organic structuring agents. The title compound was accompanied by a second new oxalate-bearing gallophosphate,  $(C_2N_2H_{10})_2[Ga_2(C_2O_4)_2(HPO_4)_3] \cdot H_2O$ , described elsewhere [2]. The starting mixture, corresponding to the molar composition 0.5 Ga<sub>2</sub>O<sub>3</sub>, 2 H<sub>3</sub>PO<sub>4</sub>, 2 H<sub>2</sub>C<sub>2</sub>O<sub>4</sub> · 2 H<sub>2</sub>O, 4 H<sub>3</sub>BO<sub>3</sub>, 2 en and 202 H<sub>2</sub>O, was placed in a Teflon-lined stainless-steel autoclave and heated at 165°C for five days. The structure was determined by single-crystal X-ray diffraction (CCD detector, MoKa radiation, room temperature).

It crystallises in triclinic space group P1 with  $a = 8.730(1)$ ,  $b = 11.575(1)$ ,  $c = 11.696(1)$  Å,  $\alpha = 115.12(1)$ ,  $\beta = 90.07(1)$ ,  $\gamma = 111.23(1)$ °,  $V = 950.52(16)$  Å<sup>3</sup>,  $Z = 2$ ,  $R(F) = 5.63\%$  for 2452 observed data with  $F_0^2 > 2\sigma(F_0^2)$ . The compound consists of anionic chains built of corner-linked alternating GaO<sub>6</sub> octahedra and PO<sub>4</sub> tetrahedra. Parallel chains are corner-linked to form corrugated sheets parallel to (011). Each GaO<sub>6</sub> octahedron is coordinated to four mono- or di-protonated PO<sub>4</sub> tetrahedra and one bidentate oxalate group. Charge neutrality is achieved by the incorporation of en in its diprotonated form. The en molecules, situated between and within the polyhedral sheets, interact with the inorganic framework via multipoint hydrogen bonding. Slight orientational disorder is observed for one of the three PO<sub>4</sub> groups, and two of the three en molecules. These disorder features are interrelated. Thermogravimetric analyses indicate that the structure remains stable until ~ 250°C, when the loss of en leads to a collapse of the structure. The total mass loss of 39.2 % corresponds to the weight of oxalate and en. A further characterisation using IR absorption and Raman spectroscopy is in progress.

This research has been supported by a Marie Curie Fellowship of the European Community programme 1.4.1 IHP under contract number HPMT-CT-2000-00138.

## References

- [1] RAO, C. N. R., NATARAJAN, S., CHOUDHURY, A., NEERAJ, S. & VAIDHYANATHAN, R. (2001): Synthons and design in metal phosphates and oxalates with open architectures. - *Acta Cryst.*, B57: 1-12.
- [2] MRAK, M., LENGAUER, C., KOLITSCH, U., KAUČIČ, V. & TILLMANNS, E. (2001): Synthesis and crystal structure of a novel layered microporous phosphate-oxalate  $(C_2N_2H_{10})_2[Ga_2(C_2O_4)_2(HPO_4)_3]\cdot H_2O$ . - *Eur. J. Mineral.*, 13, Beih. 1 (in press).

**COMPLEX METASOMATIC ENRICHMENT OF THE UPPER MANTLE  
BENEATH WESTERN ALASKA: GEOCHEMICAL EVIDENCE FROM  
PERIDOTITE XENOLITHS IN CENOZOIC VOLCANICS**

by

**S.B. Mukasa & A.V. Andronikov**

Department of Geological Sciences  
University of Michigan, Ann Arbor, MI 48109-1063, USA

Upper mantle peridotite xenoliths from Cenozoic volcanics of Seward Peninsula, St. George Island (Pribilof Islands) and Nunivak Island were studied in terms of major oxide and trace element compositions. Xenoliths were found in volcanics displaying a time sequence of emplacements from 6 Ma (Seward Peninsula) through 2.5 Ma (St. George Island) to 0.5 Ma (Nunivak Island). Most peridotite xenoliths display evidences of complex metasomatic enrichment pronounced in terms of both major oxide and trace element abundances. Xenoliths show various types of major oxide and trace element distributions due to the existence of different tectonic environments in the region over time.

By the time of the Seward Peninsula volcanics eruption (6 Ma), rift-related metasomatism influenced the upper mantle beneath the region. The peridotite xenoliths display only signs of metasomatic enrichment by silicate melts through fractures: deviation of major oxide compositions from the depletion trend (Fig. 1), and steady enrichment of peridotites from more compatible to strongly incompatible trace elements (Fig. 2). No influence of subduction-related processes (such as metasomatism by fluids or recrystallisation front [1]) can be suggested for the region on the basis of chemical composition of the xenoliths. This observation is consistent with the suggestion about continental rift volcanism developed on Seward Peninsula [2].

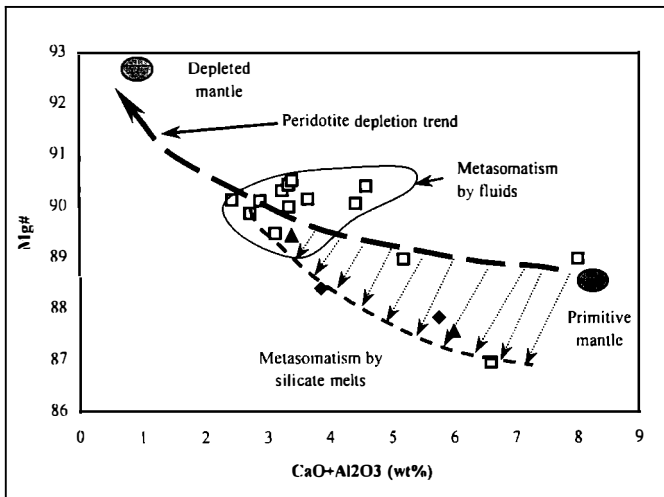
St. George xenoliths also do not display any signs of metasomatism by fluids or any traces of recrystallisation front influence. Metasomatism, as well as in the case of Seward Peninsula xenoliths is pronounced in the deviation of major oxide compositions from the depletion trend (Fig. 1), and in steady enrichment of peridotites from more compatible to strongly incompatible trace elements (Fig. 2). Since this closest to the Aleutian arc xenolith location does not display any signs of the subduction influence onto the upper mantle rocks, one can suggest that the rest of the studied region (located farther northward from the Aleutian arc) did not experience compression tensions by that time either. However, the subduction front from the Aleutian arc might have reached Pribilof Islands soon after 2.5 Ma.

On the other hand, Nunivak xenoliths (0.5 Ma) display fingerprints of the influence of both silicate melt- and fluid-induced metasomatism. In particular, the presence of abundant amphibole was noted in some xenoliths. Major oxide and trace element abundances of the Nunivak xenoliths are very variable (Figs. 1 & 2).

Fig. 1

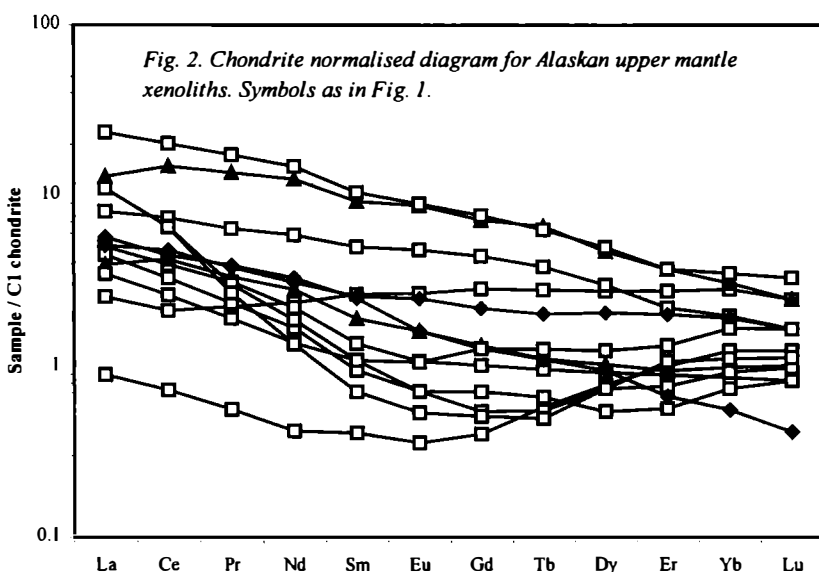
Plot Mg# vs. weight percent ( $\text{CaO}+\text{Al}_2\text{O}_3$ ) for Alaskan upper mantle xenoliths.

Squares: Nunivak peridotites; diamonds, Seward Peninsula peridotites; Triangles: St. George peridotites.



All the variability of the Nunivak xenolith compositions can be due to the depletion in basalt components (with increase of the rocks Mg#) and in strongly incompatible trace elements (resulted from melting and melt extraction) followed by metasomatism by silicate melts, and by metasomatism by ascending recrystallisation front (resulted in selective depletion of the rocks in MREE and enrichment in LREE [3]). Although by 0.5 Ma fluid flux from the subduing ocean lithosphere slab reached the Nunivak Island region, this flux did not have sufficient time yet to erase all signatures of the previously existed continental rift tectonic regime, and some isolated mantle fragments even have kept nearly primitive mantle characteristics (Figs. 1 & 2).

Fig. 2. Chondrite normalised diagram for Alaskan upper mantle xenoliths. Symbols as in Fig. 1.



If subduction-related processes started to influence the lithosphere beneath St. George Island shortly after the xenolith-bearing volcanics eruption (2.5 Ma), it would take ~2 m.y. for the subduction front to travel 150 - 170 km (the distance from St. George Island to Nunivak Island with respect to the Aleutian arc). Thus, the rate of the northward horizontal movement of the subduction front in the Late Cenozoic should be about 7 - 8 cm/year, which is consistent with the present-day North Pacific Plate movement at 5 - 10 cm/year [4].

## References

- [1] KELEMEN, P. B. et al. (1992): Formation of harzburgite by pervasive melt/rock reaction in the upper mantle. - Nature 358: 635-641.
- [2] TURNER, D. L. et al. (1981): Continental rifting – a new model for geothermal exploration of the central Seward Peninsula, Alaska. - Geoth. Res. Council Trans. 5: 213-216.
- [3] BODINIER, J.-L. et al. (1990): Mechanism of mantle metasomatism: geochemical evidence from the Lherz orogenic peridotite. - J. Petrol. 31: 597-628.
- [4] MAHLBURG KAY, S. & KAY, R. (1994): Aleutian magmas in space and time. - In: The Geology of North America, G-1, Geol. Soc. Amer.: 687-722.

**UPPER MANTLE PERIDOTITES FROM KIGLUAIK MOUNTAINS:  
EVIDENCE OF CRETACEOUS SUBDUCTION ZONE EXISTENCE  
BENEATH WESTERN ALASKA**

by

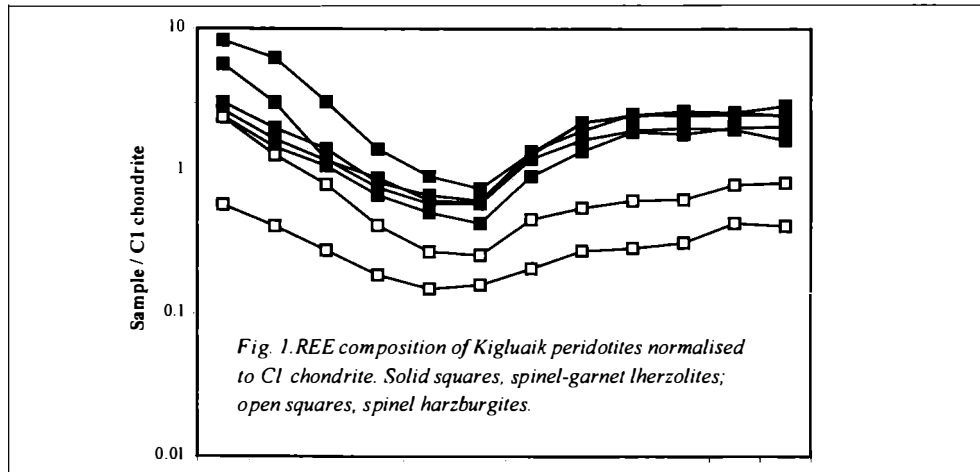
**S.B. Mukasa & A.V. Andronikov**

Department of Geological Sciences  
University of Michigan, Ann Arbor, MI 48109-1063, USA

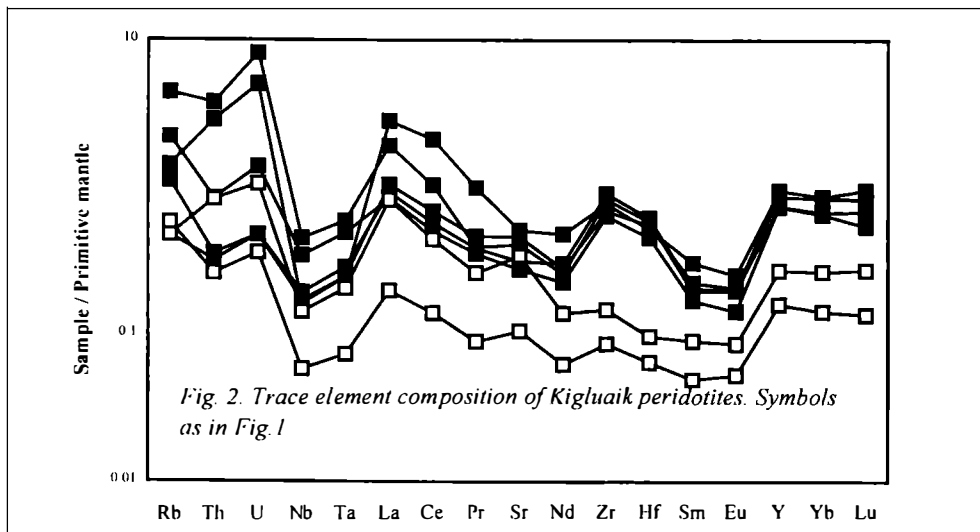
Amphibole- and phlogopite-bearing spinel-garnet lherzolite, spinel harzburgite, and composite rocks consisting of the host harzburgite and veinlets of amphibole clinopyroxenite were collected in the Kigluaik Mountains region on Seward Peninsula. Kigluaik Mountains is a part of a broad Cretaceous magmatic belt that extends from northern Alaska to eastern Russia [1].

Kigluaik peridotites display major oxide features consistent with various degrees of the rocks melting and melt extraction. These events lead to the progressive depletion of the rocks in basalt components and to increase of Mg#. Since all high-Mg# Kigluaik peridotites are garnet-free varieties, the shallowest upper mantle horizons should have experienced intensive melting and melt extraction, whereas garnet-bearing peridotites do not display signs of intensive melting. In terms of mantle thermal regime, it is unusual that the shallower horizons experienced intensive heating resulted in partial melting, whereas the deeper horizons did not. The uppermost mantle horizons were probably separated from a mantle convection cell, whereas deeper mantle horizons might be involved into the mantle convection. Garnet-free peridotites can be considered then as fragments of mantle preserved in part ancient characteristics.

Kigluaik peridotites display pretty steady HREE chondrite-normalised patterns, which are changing by sharp MREE depletion, and then by strong enrichment in LREE (Fig. 1). Primitive mantle normalised diagram for spinel-garnet lherzolites shows that such trace elements as Zr and Hf display marked peaks, whereas Nb and Ta display a deep trough (Fig. 2). The rest of the trace elements displays steady enrichment from Nd to La. Harzburgites do not display peaks at Zr-Hf, but also display pronounced troughs at Nb-Ta (Fig. 2). It is known that if melt segregated from the Earth's mantle into the crust flows pervasively through porous peridotite, the reaction surface (recrystallisation front) is nearly unlimited, and large volumes of melt and host peridotite are likely to interact [2, 3]. Combined chromatographic effect and solidification of the small melt fractions at distance from the recrystallisation front are to create moderate to very strong U-shaped REE patterns in peridotites ahead of the front [3]. Variation in melt fraction across the front explains the spatial variation in the degree of recrystallization, REE fractionation, and HFSE abundances. The depletion in incompatible elements toward the recrystallisation front in particular affects the MREE.



The favorable conditions for porous melt flow could exist in the upper mantle hanging wall of subduction zones, due to the presence of volatiles in the melt migration system [4]. The presence of volatiles also accounts for the generation of hydrous phases in peridotite that can be one of the distinctive features of convergent tectonic settings in contrast to the extensional settings where volatiles are not so abundant. The presence of Nb-Ta troughs for Kigluaik peridotite trace element patterns along with high U- and Th-concentrations, and marked peaks at Zr-Hf (only for garnet-bearing peridotites) can suggest influence of crustal component-bearing arc melts on the upper mantle rocks [5]. Since the U-shaped REE patterns are observed for peridotites from different upper mantle horizons, the recrystallisation front influenced the whole "sampled" upper mantle section with the strongest influence onto the deepest horizons. Since both Nb-Ta troughs and Zr-Hf peaks are imposed onto the U-shaped peridotite patterns, one can suggest that the crustal component was introduced into peridotites at the latest stages of peridotite evolution when the deeper mantle levels became close to the ascending recrystallisation front.



The influence of subduction-related processes onto the upper mantle beneath Western Alaska was mainly due to the ascending recrystallisation front, which left its fingerprints in the trace element composition of Kigluaik peridotites. Before the setting up of the subduction-related environment in the Cretaceous, the upper mantle sections beneath the region experienced melting and melt extraction. However, mantle convection separated the deeper levels from the uppermost mantle horizons, and the signs of melting and melt extraction were preserved only in the shallowest mantle rocks of the spinel-stability field.

## References

- [1] AMATO, J. M. & WRIGHT, J. E. (1997): Potassic mafic magmatism in the Kigluaik gneiss dome, northern Alaska: A geochemical study of arc magmatism in an extensional tectonic setting. - *J. Geophys. Res.* 102: 8065-8084.
- [2] NAVON, O. & STOLPER, E. (1987): Geochemical consequences of melt percolation – the upper mantle as a chromatographic column. - *J. Geol.* 95: 285-307.
- [3] BODINIER, J.-L. ET AL. (1990): Mechanism of mantle metasomatism: geochemical evidence from the Lherz orogenic peridotite. - *J. Petrol.* 31: 597-628.
- [4] KELEMEN, P. B. (1990): Reaction between ultramafic rock and fractionating basaltic magma. I. Phase relations, the origin of calc-alkaline magma series, and the formation of discordant dunite. - *J. Petrol.* 31: 51-98.
- [5] MOLL-STALCUP, E. J. (1994): Latest Cretaceous and Cenozoic magmatism in mainland Alaska. - In: *The Geology of North America*, G-1, *Geol. Soc. Amer.*: 589-619.

**PRIVATE SAMMLER  
UND IHRE BEDEUTUNG FÜR DIE MINERALOGIE IN ÖSTERREICH**

von

**G. Niedermayr**

Mineralogisch-Petrographische Abteilung  
Naturhistorisches Museum, Burgring 7, A-1010 Wien

Wie viele andere Wissenschaftsdisziplinen hat auch die erdwissenschaftliche Forschung ihre Wurzeln u.a. in der Beobachtungsgabe und im Eifer privater Sammler. Sie waren es in erster Linie, die in den vergangenen Jahrhunderten oft bedeutende Kollektionen von Naturobjekten zusammengetragen haben und aufgrund der Fülle dieses Materials auch Anstoß für eine systematische Ordnung dieser Objekte gaben (vgl. [1], [2], [3], [4] ). Der Wechsel vom bloß kuriosen Naturobjekt zum wissenschaftlich wertvollen Baustein in einer systematischen Ordnung vollzog sich demnach in der mineralogischen Wissenschaft in der zweiten Hälfte des 18. Jahrhunderts. Auch das für eine wissenschaftliche Untersuchung notwendige Instrumentarium entwickelte sich erst nach und nach. Die Mineralogie ist dementsprechend eine verhältnismäßig junge Wissenschaft (vgl. [5] ).

Die Basis jeder Wissenschaft war und ist auch heute das Sammeln von Objekten und Beobachtungen, wobei hier insbesondere in der mineraltopographischen Bestandsaufnahme dem privaten Engagement auch heute noch eine sehr bedeutende Rolle zukommt. Das belegten bzw. belegen die vorbildlich gepflegten systematischen Sammlungen von Dir. Viktor Vavrovsky (jetzt im Landesmuseum für Kärnten), Reg.Rat. Friedrich Hermann (jetzt im Stadtmuseum Villach) und Helmut Prasnik in Kärnten, von Simone und Mag. Peter Huber in Niederösterreich, von Otmar Wallenta in Oberösterreich (jetzt Stiftssammlung Kremsmünster) und Dr. Wolfgang Gabriel in Vorarlberg, um hier nur einige Beispiele zu nennen. So ergänzen sich Wissenschaft und privater Sammeleifer in positiver Weise. Das war den Proponenten der Gründungsversammlung der Wiener Mineralogischen Gesellschaft vor 100 Jahren bereits klar. Nicht von ungefähr weist August Ritter von Loehr, der gemeinsam mit dem Direktor der Mineralogisch-Petrographischen Abteilung am k.k Naturhistorischen Hofmuseum, Friedrich Berwerth, den eigentlichen Anstoß zur Bildung der Gesellschaft gegeben hat, auf den großen wissenschaftlichen Wert privater Sammlungen hin und gibt die Anregung, dass die Besitzer solcher Sammlungen ihre Bestände den Mitgliedern der neu gegründeten Gesellschaft zugänglich machen. An den viele Jahre üblichen, einen Vortrag begleitenden Ausstellungen beteiligten sich so bekannte österreichische Sammler, wie u.a. Buschmann, Distler, Kürschner, Lechner, Loehr, Perlep, Schwarz, Veidl und Weinberger. Nach dem 2. Weltkrieg waren es insbesondere Kontrus, Metzger und Siegmund, die immer wieder Anschauungsmaterial für Vorträge zur Verfügung stellten.

Private Initiative zeigt aber nicht nur ihr Material, sie stellt auch bereitwilligst Untersuchungsmaterial für wissenschaftliche Zwecke zur Verfügung. Insbesondere die mineraltopographische Forschung wäre ohne die Unterstützung der privaten Sammler nie in dem Umfang möglich gewesen, wie das tatsächlich der Fall war und auch heute noch ist. Ein gutes Beispiel dafür sind die in mehrere hundert Einzelbeiträge gehenden Arbeiten von Heinz Meixner. Dazu kommt aber noch eine große Zahl jener Sammler, die – heute oft eingebunden in wissenschaftliche Projekte – in ihrer Freizeit unentgeltlich ihren wichtigen Beitrag zur Mineraldokumentation des Bundesgebietes leisten (z.B. Nationalparke "Hohe Tauern" und "Nockberge").

Naturgemäß ist nicht jeder Sammler gewillt und auch nicht in der Lage, fachlich fundierte Artikel, die auch einem gewissen wissenschaftlichen Anspruch gerecht werden, zu verfassen, aber auch in dieser Hinsicht haben eine Reihe von Personen sehr viel für die Mineralogie Österreichs getan. Namen wie August von Loehr, auf dem Sektor der Edelsteinkunde, Otto Fitz, auf sammlungsgeschichtlichem Gebiet, oder insbesondere auf dem Sektor der Mineraltotopographie Simone und Peter A. Huber, Dietmar Jakely, Ludwig Kiesewetter, Karl Kontrus, Helmut Offenbacher, Manfred Puttnar, Albert Strasser, Josef Taucher und andere sind im Schrifttum immer wieder anzutreffen. Albert Strasser hat darüber hinaus die vorläufig letzte Landesmineralogie von Salzburg vorbildlich zusammengestellt, und die Zeitschriften "Mineralobserver" bzw. "Mineralogisches Archiv Salzburg" wurden bzw. werden von ihm im Eigenverlag herausgebracht. Und auch die Zeitschriften "Die Eisenblüte", "MatriXX", "Mefos" und "Der steirische Mineralog" waren bzw. sind der Eigeninitiative privater Sammler zu verdanken. Darüber hinaus sind gerade in den letzten Jahren einige weltweit neue Mineralspezies beschrieben worden, deren Auffindung, Erkennung und teils auch wissenschaftlich korrekte Untersuchung auf private Initiative zurückzuführen ist. Dazu gehören etwa Galgenbergit, Leogangit, Mallestigit und Weinebeneit.

Natürlich erstreckt sich die Tätigkeit privater Sammler nicht nur auf das österreichische Bundesgebiet. Der steirische Sammler Franz Lammer etwa galt nicht nur als hervorragender Systematiker und Spezialist für das Mineral Lazolith sowie für die Mineralisationen der Magnesit-Talk-Lagerstätte Oberdorf an der Laming sondern er war auch ein besonderer Kenner der Lagerstätte von Tsumeb. Aufgrund seiner großen Verdienste um die Mineralogie wurde das von ihm als neues Mineral vermutete Cu-Arsenat von Laurani, Bolivien, ihm zu Ehren benannt (Lammerit).

Die wenigen hier genannten Beispiele zeigen, dass privaten Sammlern insbesondere bei der Mineraldokumentation des Bundesgebietes und darüber hinaus auch heute noch eine sehr wichtige Rolle zukommt und sie daher mit vollem Recht gewissermaßen als Helfer der Wissenschaft bezeichnet werden müssen. Ohne ihre Unterstützung wäre die mineralogische Erforschung Österreichs nicht so weit gediehen, wie wir das heute feststellen dürfen. Wir können aber auch davon ausgehen, dass auch außerhalb Österreichs private Sammlerinitiative einen sehr wesentlichen Beitrag bei der Erforschung der Mineralvorkommen der Welt leistet und auch in Zukunft weiterhin leisten wird (müssen).

## Literatur

- [1] GÜSSMANN, F. (1785): *Lithophylacium Mitisianum*. - Viennae: J. Kurzbeck, 692 S.
- [2] KARSTEN, D. L. G. (1789): *Museum Leskeanum Regnum Minerale. Des Herrn Nathanael Gottfried Leske hinterlassenes Mineralienkabinet systematisch geordnet und beschrieben*. - Leipzig: J. G. Müllersche Buchhandlung, 2 Bde., 578 und 280 S.
- [3] BORN, I. v. (1796): *Catalogue methodique et raisonne de la collection des fossils de Mlle. Eleonore de Raab*, 2 Bde. - Wien: J. V. Degen (I. Alberti), 500 und 499 S.
- [4] MOHS, F. (1804): *Des Herrn J. F. von der Null Mineralien-Kabinet, nach einem, durchaus auf äussere Kennzeichen gegründeten System geordnet* 2 Bde. - Wien: Camesinische Buchhandlung, 594 und 730 S.
- (5) FABIAN, E. (1986): *Die Entdeckung der Kristalle. Der historische Weg der Kristallforschung zur Wissenschaft*. - Leipzig: VEB Deutscher Verlag für Grundstoffindustrie, 196 S.

**ÜBER EIN VORKOMMEN VON VANADIUM-BERYLLEN  
AUS DEM ÖSTLICHEN HIMALAYA**

von

**G. Niedermayr<sup>1</sup>, F. Brandstätter<sup>1</sup>, J. Ponahlo<sup>2</sup> & E. Henhapl<sup>3</sup>**

<sup>1</sup>Mineralogisch-Petrographische Abteilung  
Naturhistorisches Museum, Burgring 7, A-1010 Wien

<sup>2</sup>Slattngasse 6/Top a 5, A-1130 Wien

<sup>3</sup>Fa. Swietyl Peony Perlen  
Westbahnstrasse 21/1/1, A-1070 Wien

Schon seit mehr als 20 Jahren sind die Vorkommen von Smaragden aus dem Hindukush-Gebirgszug in Pakistan und Afghanistan bekannt (Swat, Bucha, Sassi und Panjshir); sie sind zum größten Teil an Serpentinit-Randgesteinassoziationen geknüpft [1]. Der Fa. Swietyl Peony Perlen, Wien, wurden schon vor vielen Jahren im Zuge einer Einkaufstour in Jaipur (Indien) von einem Schleifer einige Steine eines angeblich neuen, nur zeitweise beschürften, Smaragd-Vorkommens aus der östlichen Himalaya-Region (mit einiger Wahrscheinlichkeit aus Sikkim oder Bhutan stammend) angeboten. Es handelt sich dabei um insgesamt 8 Steine im Gewicht von 0.22 - 0.48 ct. Nähere Angaben zur Fundortsituation waren nicht zu erhalten, doch zeigen die Steine trotz teils typischer Dreiphaseneinschlüsse keine Übereinstimmung mit den überlicherweise auf dem Markt gehandelten Smaragden aus Rußland, Afrika, Indien, Brasilien oder Kolumbien.

Das Material unterscheidet sich hinsichtlich Chemismus und Einschlüssen auch grundsätzlich von den Smaragden aus dem Hindukush. Die Steine sind deutlich gelblichgrün gefärbt, mit einem Pleochroismus von gelblich zu bläulichgrün, reich an Einschlussphänomenen (Fluideinschlüsse und Festkörperphasen) und zeigen unter dem Chelseafilter eine deutliche Rotfärbung, was auf einen gewissen Anteil an Cr<sup>3+</sup> bzw. V<sup>3+</sup> schließen ließ. Nach Erscheinungsbild und Einschlusssphänomenen sind zwei Typen zu unterscheiden. Ein etwas hellerer, an Festkörperphasen reicher Typus (Typ 1) steht einem dunkleren, einschlusärmeren und damit deutlich transparenterem Typus (Typ 2) gegenüber. Die Steine letzteren Typs zeigen kaum Festkörperphasen aber Fluid-einschlüsse in Formtypischer Dreiphaseneinschlüsse sowie parallel orientierter Hohlkanälchen. Die zum Teil clusterartig aggregierten Festkörperphasen im Typ 1 konnten mittels EDS-Analyse als in der Hauptsache aus Karbonat (Calcit) und Quarz bestehend identifiziert werden, zusätzlich ist noch Titanit anzugeben. Die Lichtbrechungswerte betragen unabhängig vom Typ für  $n_o = 1.590 - 1.600$  und für  $n_e = 1.582 - 1.592$ ; die Doppelbrechung schwankt zwischen -0.006 und -0.008.

Auch chemisch zeigen die beiden genannten Typen keine gravierenden Unterschiede. Die entsprechenden Werte wurden mittels EMS-Analyse bestimmt und sind anzugeben mit (Angabe in Gew.%): Na<sub>2</sub>O 0.80 - 2.13, Al<sub>2</sub>O<sub>3</sub> 13.1 - 18.4 und SiO<sub>2</sub> 63.9 - 68.3; die Werte für K<sub>2</sub>O, CaO, TiO<sub>2</sub>, MnO und NiO liegen fast immer unter 0.02 Gew.% (Nachweisgrenze). Der BeO-Gehalt ist mittels EMS nicht bestimmbar. FeO schwankt zwischen 0.27 - 0.95 Gew.%, der V<sub>2</sub>O<sub>3</sub>-Gehalt liegt zwischen 0.24 - 0.81 Gew.% und ist deutlich höher als der Gehalt an Cr<sub>2</sub>O<sub>3</sub>. So weist Typ 1 einen Cr<sub>2</sub>O<sub>3</sub>-Gehalt von < 0.02 - 0.06 Gew.% auf; die Werte für Typ 2 liegen dagegen mit < 0.02 - 0.09 Gew.% geringfügig höher.

Dies steht in guter Übereinstimmung mit den Kathodenlumineszenzspektren der untersuchten Steine, die nur eingeschränkt auswertbar sind; ein Teil der Proben zeigt keinerlei Lumineszenz. Aufgrund des vorliegenden Datenmaterials handelt es sich bei dem Vorkommen von "Smaragden" aus dem östlichen Himalaya nicht um Smaragde im eigentlichen Sinn sondern gemäß dem Vorschlag von [2] um Vanadium-Berylle.

## Literatur

- [1] SCHWARZ, D. (1987): Esmeraldas. Inclusões em Gemas. - Ouro Preto: Imprensa Universitária Universidade Federal de Ouro Preto, 439 S.
- [2] HENN, U. (1992- ): Über die Farbe und Farbursachen grüner Berylle und ihre nomenklatorische Abgrenzung.  
- Z. Dt. Gemmol. Ges. 41, 4: 156-158.

**ARE GRANITIC PEGMATITES A TOY FOR DESCRIPTIVE MINERALOGISTS  
OR A USEFUL TOOL FOR GEOLOGIST ?**

by

**M. Novák**

Department of Mineralogy, Petrology and Geochemistry  
Masaryk University, Kotlářská 2, 611 37 Brno, Czech Republic

Most geologists consider granitic pegmatites solely an object for descriptive mineralogical studies or a source of gemstones and attractive mineral specimens, despite economic importance of Li, Be, Ta and other elements at some pegmatite deposits. Granitic pegmatites are only sporadically used in discussions of regional geological evolution. However, are they really only a toy for descriptive mineralogists or can we use granitic pegmatites as a potentially useful tool for geological interpretations? In order to answer this question, we have to introduce granitic pegmatites not only as a source of attractive minerals but also as a rock with a well-defined and experimentally verified genesis [1] and with specific geological positions in the evolution of the crust [1,2].

The current classification of granitic pegmatites includes several distinct classes, types and sub-types, and families, [3]; in this paper, only more evolved (highly fractionated) rare-element granitic pegmatites of the LCT family will be considered. The other granitic pegmatites (e.g., NYF family, abyssal class) are outside the scope of this presentation and primitive barren pegmatites with simple mineral assemblages related to more evolve rare-element (LCT) pegmatites are commonly less useful.

Specific features of the rare-element (LCT) granitic pegmatites, which can be utilized in geological interpretations, are given as follows:

- Granitic pegmatites are the most evolved members of intrusive granitic systems commonly derived from or along with leucocratic peraluminous granites.
- Characteristic mineral assemblages and chemistry of minerals allow classification of pegmatites and their regional and comparative studies.
- Mineral assemblages in pegmatites (and in exocontact zones) are useful for derivation of PT conditions of the pegmatite emplacement.
- Low viscosity and low solidus of pegmatitic melts facilitate long-range propagation from their sources (5 to 10 km or even more) and emplacement of melt into relatively cold rocks.
- Very rapid crystallization of crystal-free melts (with no inherited crystals) due to strong over-cooling and presence of minerals such as monazite, columbite, garnet, micas, zircon, apatite allow to use pegmatites for radiometric dating.

The following examples from the Bohemian Massif are presented to document how granitic pegmatites may contribute to discussions concerning geological interpretations in individual regions.

1. The distributions of specific types (subtypes) of granitic pegmatites in the Bohemian Massif open several questions concerning relationships between the individual geological regions. Beryl-phosphate-columbite pegmatites occur exclusively in the Bavarian Moldanubicum and in the Domažlice-Poběžovice area; complex (Li) pegmatites are typical for the Moldanubicum (exclusive Bavarian Moldanubicum and Central Moldanubian Pluton area) and the Saxonian Granulite Complex; beryl-columbite pegmatites were found in the Hrubý Jeseník Mts., Silesicum and in the Western Carpathians (Považský Inovec, Malé Karpaty, Žiar, Nízké Tatry). The same pegmatite types or subtypes present in these particular regions and evident similarities in mineral assemblages and chemistry of minerals suggest at least similar protoliths, PT conditions of melting and magmatic differentiation.

2. Several well-defined belts characterized by the same subtype of complex (Li) pegmatites were observed in the Moldanubicum (western Moravia, southern Bohemia). These belts occur in distinct Moldanubian subunits (nappes) and cut their borders. The distribution of the belts demonstrates that the nappe stacking and regional metamorphism predate the emplacement of the rare-element granitic pegmatites.

3. Radiometric dating of monazite from rare-element granitic pegmatites (beryl-columbite subtype with abundant tourmaline) in the Moldanubicum yielded the age  $337 \pm 2$  Ma, which dates the PT conditions of pegmatitic melt emplacement at  $P \sim 2$  kbar and  $T \sim 500 - 550$  °C [4]. As these pegmatites cut various rocks including granulites dated at 340 Ma [5, 6], average exhumation rates inferred from these data, indicate extremely rapid exhumation during the Variscan orogeny, see Fig. 1.

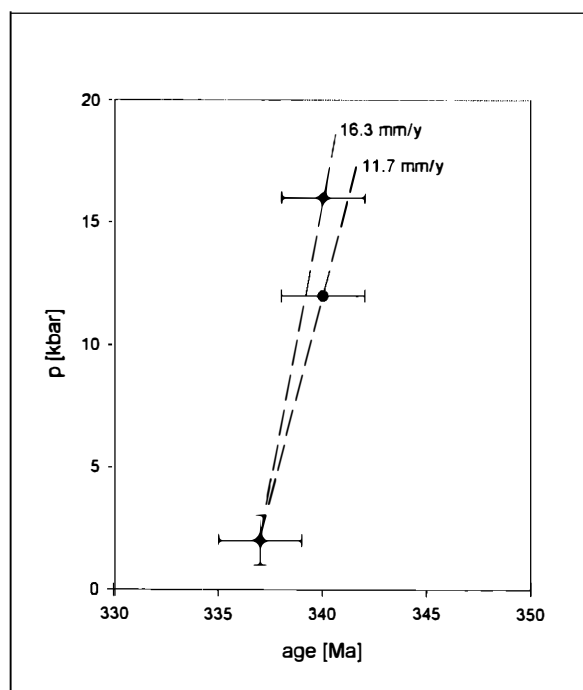


*Fig. 1*

Diagram showing radiometric data of monazite from rare-element granitic pegmatites [4] and of zircon from granulites [6] in the Moldanubicum; the calculated average exhumation rates are indicated by dashed lines; 1 kbar ~ 3.5 km.

In general, the study of rare-element granitic pegmatites may significantly contribute to our understanding of magmatic evolution of granitic complexes, and to metamorphism and late-tectonic to post-tectonic development during relatively low-pressure conditions. Radiometric data from rare-element granitic pegmatites can be used for calculation of exhumation rates in orogenic belts or other geological and geophysical interpretations.

This work was supported by the grant GAČR No. 205/99/0567.

### References

- [1] LONDON, D. (1996): Granitic pegmatites. - *Trans. Royal Soc. Edinburgh Earth Sci.*, 87, 305-319.
- [2] ČERNÝ, P. (1991): Rare-element granitic pegmatites. II Regional to global environments and paragenesis. - *Geosci. Canada*, 18, 68-81.
- [3] ČERNÝ, P. (1991): Rare-element granitic pegmatites. I. Anatomy and internal evolution of pegmatite deposits. - *Geosci. Canada*, 18, 49-67.
- [4] NOVAK, M., ČERNÝ, P., KIMBROUGH, D. L., TAYLOR, M. C. & ERCIT, T. S. (1998): U-Pb Ages of monazite from granitic pegmatites in the Moldanubium and their geological implications. - POCEEL International Symposium, Praha, September 30-October 2, *Acta Univ. Carol., Geol.*, 42, 2, 309-310.
- [5] KRÖNER, A., O'BRIAN, P. J., NEMCHIN, A. A. & PIDGEON, R. T. (2000): Zircon ages for high pressure granulites from South Bohemia, Czech Republic, and their connection to Carboniferous high temperature processes. - *Contrib. Mineral. Petrol.*, 138, 127-142.

HIGH TEMPERATURE, LOW PRESSURE GARNET-BEARING PERIDOTITES  
FROM PRAGAUNIYEU: EVIDENCE FOR PLUME ACTIVITY IN NORTHERN PARAGONIA

by

**Th. Ntaflos<sup>1</sup>, E. A. Bjerg<sup>2</sup>, C. H. Labudia<sup>2</sup>, M. Thöni<sup>3</sup>, C. Frisicale<sup>2</sup> & M. Günther<sup>4</sup>**

<sup>1</sup>Institute of Petrology

University of Vienna, Vienna, Austria

<sup>2</sup>Departamento de Geología

CONICET, Universidad Nacional del Sur, Bahía Blanca, Argentina

<sup>3</sup>Institute of Geology

University of Vienna, Vienna, Austria

<sup>4</sup>Forschungsinstitut und Naturmuseum Senckenberg

Frankfurt, Germany

**Introduction:** Garnet-bearing mantle xenoliths in Pali Aike, southernmost Patagonia have been repeatedly reported in the past. We present, chemical and isotopic data and PT estimates for garnet-bearing mantle xenoliths from Praguaniyu, a new locality close to the Meseta de Somuncura, in northern Patagonia.

**Results:** Xenoliths occur in tuffs, alkali basalts and basanites and comprise garnet-peridotites, garnet-spinel-peridotites and spinel-peridotites, and garnet-bearing spinel-clinopyroxenites. The majority of the xenoliths have equigranular texture. There is, however, a second suite of xenoliths with foliated textures. Minerals are homogeneous in composition and only the very outer opx and cpx rims have insignificantly lower  $\text{Al}_2\text{O}_3$  contents than the cores. Also very narrow kelyphite rims around garnet are present. In general, the equigranular garnet-bearing peridotites have higher  $\text{Al}_2\text{O}_3$  (~ 7 wt.%) and  $\text{Na}_2\text{O}$  (~1.8 wt.%) contents than the foliated (~ 4.5 and 1.0 wt.% respectively) ones. Garnets from both suites have similar mg# around 0.84, but different  $\text{Cr}_2\text{O}_3$  contents (1.2 and 2.5 wt.% respectively). Similar trends were also obtained for spinel peridotites: equigranular spinel-peridotites have higher  $\text{Al}_2\text{O}_3$  and  $\text{Na}_2\text{O}$  contents (4.8 and 1.5 wt.% respectively) than the foliated (4.0 and 1.0 wt.% respectively) ones.

The major elements  $\text{CaO}$  and  $\text{Al}_2\text{O}_3$  range from 4.5 to 0.80 wt.% and from 4.31 to 1.01 wt.%, respectively. In the  $\text{CaO}$  vs  $\text{Al}_2\text{O}_3$  diagram the most depleted samples define a linear trend which is different from the linear trend that define the most fertile samples (Fig. 2). It is therefore evident that Praguaniyu xenoliths are not residues after different degrees of partial meltings of an initial fertile source. Apparently the most depleted samples represent an older depleted lithosphere and the most fertile a recrystallized one. The REE patterns in a chondrite-normalized diagram are flat ( $\text{La}_N/\text{Yb}_N$  ratios vary from 0.7 to 3.1) suggesting a moderate cryptic metasomatism (no hydrous phases are present).

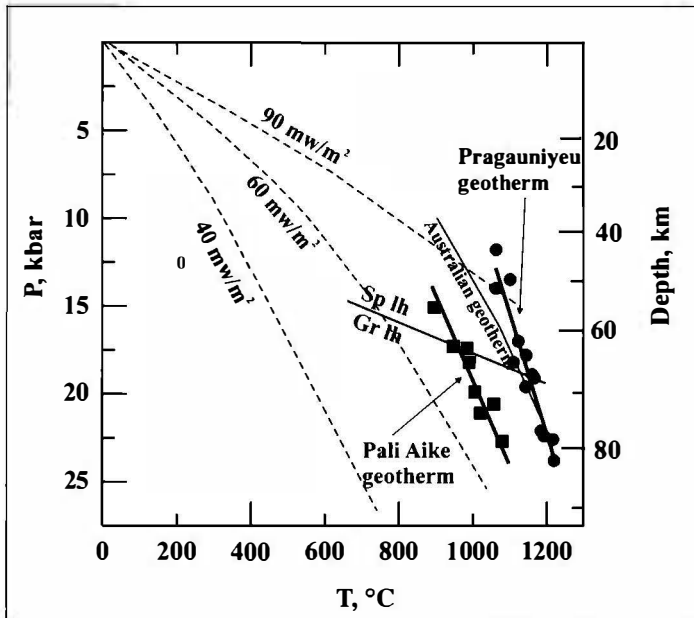


**Fig. 1**  
PT estimates for xenoliths from Pragauniyu, northern Patagonia. The xenolith geotherm implies very high temperatures at relative shallow depth. Steady state geotherms are from [4], Australian geotherm from [5] and Pali Aike geotherm from [6].

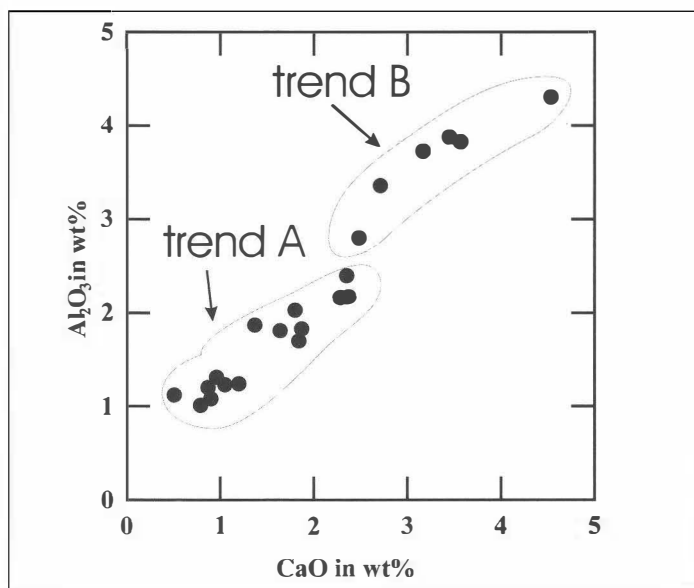


**Fig. 2**  
Plot of CaO vs. MgO for major elements from Pragauniyu xenoliths. Depleted and fertile xenoliths form different trends (trend A and trend B respectively).

Ion-probe analyses have shown that gt and cpx in the foliated garnet-peridotites are not in equilibrium in respect of REE, since LREE in cpx are strongly depleted, resembling patterns similar to those of garnets. There is a correlation between texture and degree of LREE depletion. The equigranular garnet-bearing peridotites have cpx that are in equilibrium with gt (La ~ 6x chondritic). Conversely, cpx in the moderate foliated samples have La around 2 times chondritic and in the strongly foliated samples the LREE depletion is very high (La ~ 0.2 times chondritic).

Equilibrium P-T estimates are calculated for garnet-bearing samples based on compositions of coexisting gt-cpx-opx and for spinel-bearing samples based on compositions of coexisting ol-cpx-opx. Temperature estimates were made with the two-pyroxene geothermometer of [1]. Pressure estimates were made with Al in opx coexisting with garnet [1] and Ca exchange between coexisting ol-cpx [2]. Tequil are unusual high and range from 1060°C to 1230°C, whereas Pequil are low, ranging from 12 to 24 kbars (Fig. 1).

The age of the equilibrated garnet-lherzolites as inferred from Sm-Nd mineral dating is  $29.4 \pm 5.7$  Ma (garnet-clinopyroxene;  $\epsilon_t = +9.9$ ).

**Conclusions:** The preliminary results demonstrate that xenoliths from Pragauniyeu in northern Patagonia lie on elevated geotherms and represent an extreme high temperature, probably related to extensional tectonics due to the uplift of the same source that generated the Meseta de Somoncura tholeiitic basalts. The young age of the subcontinental mantle in this area ( $29.4 \pm 5.7$ ), represents the closing of the Sm-Nd isotopic system between garnet-clinopyroxene after the Somoncura extensive magmatic event (about 40 Ma ago). These features of the subcontinental mantle and the OIB signature of the Somoncura basalts may suggest a rising plume in this area[3].

#### References

- [1] BREY, G. P & KÖHLER, T. P. (1990): J. Petrol. 3530-3550.
- [2] KÖHLER, T. P. & BREY, G. P (1990): GCA. 2375-2388.
- [3] KAY, S. M., et al. (1993): XII Congress Geologico Argentino. 236-248.
- [4] POLLACK, H. N. & CHAPMAN, D. S. (1977): Tectonophysics, 38, 279-296.
- [5] O'REILLY, S. Y & GRIFFIN, W. L. (1985): Tectonophysics, 111, 41-63.
- [6] KEMPTON, P. D., et al. (1998): in Proceedings of the VII<sup>th</sup> International Kimberlite Conference, (editors GURNEY et al.) volume I, 403-414.

#### Acknowledgements

The work was supported in part by the Hochschuljubiläumsstiftung der Stadt Wien Pr. Nr. H-168/2000

METALLOGENETIC FEATURES OF ALBANIAN OPHIOLITIC COMPLEX

by

**K. Onuzi & A. Cina**

Institute of Geological Research  
Blloku V, Shanto, Tirana

In Albania, the ophiolite belt, named Mirdita Ophiolitic Belt, is part of the Mesozoic Tethyan ophiolite belt. It is set on between the Dinarides in the north and the Hellenides in the south. The metallogenic picture of the Albanian ophiolites is of high economic importance. Its complex character is related to the complex lithotypes, the large spatial development and the big thickness of lithologic column. Due to favourable conditions of development of ore-forming processes, the Albanian ophiolitic complex is distinguished by a high metallogenic potential. This complex shows distinctive features from those of the Dinarides and Hellenides ophiolites because abundant and diverse ore assemblages are present. The ultrabasic and basic rocks predominance is determined by the metallogenic climax of the chromium and copper mineralizations. Different PGE, Ti-magnetite, Ni-sulfide and arsenide, Ni+Co+Cu, Cu+Fe, Cu+Zn+Pb+Au etc. mineralizations and asbestos, talc, magnesite, lateritic Ni-silicate and Fe-Ni are found as well. Starting from the deepest mantle section of the Iherzolite and cpx-bearing harzburgite composition to cumulate and volcanic sequences, a spectacular metallogenic evolution is recognized. This is expressed by the geochemical element fractionation and the mineral assemblages replacement.

The Albanian ophiolite complex exhibit features of mid oceanic ridge (MOR) and supra-subduction zone (SSZ) - type ophiolites. The first one is a HOT-LOT (harzburgite ophiolite type-Iherzolite ophiolite type) and characterized by Pl-rich cumulate sequences, high-Ti basaltic pillow lavas and less depleted mantle sequences. The second one is a HOT (harzburgite) and characterized by Px-rich cumulate sequences, low-Ti tholeites and boninitic lavas and extremely depleted mantle sequences.

The development of the two ophiolite belts, produced in the different geodynamic settings, led to the diverse metallogenic scenarios. The mantle sequence of the MOR-type ophiolites consist of homogenous cpx-bearing harzburgites- (Iherzolites) with very rare thin dunite bands. The high-Mg and low-Ca contents and small differences in trace element content related to mantle ultramafic rocks of the SSZ-type ophiolites differ from typical Iherzolite-type ophiolites of western Mediterranean ones. The ultramafic suite is completed by Pl-bearing Iherzolites and dunites and olivine-hornblendites. The gabbroic rocks of MOR-type ophiolite have a limited extension and are represented by several small massifs of troctolite, olivine gabbro, leucocratic gabbro, apatite-bearing gabbro and ferrogabbro. Ultramafic intrusions (Iherzolite-wehrlite and their plagioclase-bearing varieties) cut the upper parts of the ultramafic suite and the gabbros.

The uppermost part of the MOR-type ophiolite suite consists of volcanic rocks, represented by basaltic pillow lavas and massive flows. The lowermost part of this volcanic suite is represented by gabbro-diabase rocks, whereas the upper part contains andesite-basalts and pyroclastics.

The SSZ-type ophiolites make up the eastern part of the Albanian ophiolite belt and have larger ophiolite lithotypes. Its mantle sequence consists of harzburgites interbedded with dunite in the upper parts and has a consistent mineral and chemical composition. Abundant dunite bodies within the harzburgites represent the residues of extensive partial melting of upper mantle peridotite and/or the product of melt-peridotite interaction. Crustal sequences are extremely thick and show a marked lithological variety. A lower plutonic unit with ultramafic cumulates and layered gabbros and an upper unit of isotropic gabbros, quartz-diorites and plagiogranites are the constituent parts of these crustal sequences. Diabase and boninitic dykes are found within the gabbros.

Intrusive ultramafic rocks are recognized in the crustal sequence of Albanian ophiolites too. They occur as sills or irregular and relatively small intrusive bodies within the layered gabbros, isotropic gabbros and plagiogranites. The main lithotypes are wehrlite, pl-wehrlite and herzolite. The sheeted dyke complex is widely distributed in the Central Mirdita region and represents an important member of the SSZ-type ophiolitic suite. Its chemical composition indicates a range close to chemical composition of the associated volcanic rocks, i. e. Si-oversaturated, low-Ti tholeites with IAT and boninitic affinity. The upper part of the SSZ ophiolite suite compresses volcanoes, which constitute a complete, differentiated sequence. The lower, thicker part, consists of vesicular basaltic to basalt-andesitic pillow-lavas, and the upper part consists of finegrained to glassy vesicular pillowed and massive andesite-basaltic and boninitic lavas. Spherulitic, microlitic dacite and rhyodacite-rhyolite extrusives, pyroclastics and andesite-dacite and boninitic glasses overlie the andesite-basaltic lava sequence. Scarce podiform massive chromitite bodies, mainly of Al-rich, refractory type (although a limited Cr-rich metallurgic-type chromitite mineralization also exists) occur in the upper parts of the mantle sequence of MOR-type ophiolite (western Albanian ophiolite belt). Some occurrences of BMS disseminations and asbestos and talc deposits are related to plagioclase-bearing Iherzolites and dunites of this ultramafic suite of MOR-type.

A stratiform vanadium-bearing Ti-magnetite mineralization is related with ferrogabbros in the lower part of the gabbro rocks succession and in the gabbro-diabasic massifs. Several vein quartz-sulfide copper ores occur in the gabbroic sequences. Volcanogenic massive Cu-Fe sulfide (chalco-pyrite and pyrite) ores associated with sulfide disseminations are localized in different parts of the volcanic suite. Intermediate petrologic features of the MOR-type ophiolites determine the relatively high metallogenetic potential in comparison with typical Iherzolitic type western Mediterranean ophiolites.

The important deposits of mantle, mainly metallurgic-type, Cr-rich chromite, occur within the harzburgite-dunite interbending sequence of the mantle SSZ-type ophiolite. The morphology of these ore bodies are tabular subconcordant, concordant, folded concordant, discordant, pencil-like and podiform. A scarce Al-rich or Fe+Ti-rich chromite mineralization is related to the transition ultramafic cumulate rocks. The textural features of the chromitites (massive, disseminated, nodular, autinodular, layered, brecciated etc.) indicate a magmatic origin and plastic deformation. The formation of mantle chromitites in a suprasubduction zone setting is presumed to result from high grade partial melting of the peridotite upper mantle and from melt/peridotite interaction in the upper mantle .

Four types of PGE mineralization are distinguished: related to mantle chromitites, to upper mantle chromitites, to disseminated BMS within transition dunite sequence, and related to chromitite dykes. So, a clear element fractionation of PGE across ultramafic column is evident. Several lens-shape ore bodies of massive Cu-Ni sulfide occur within contact zones between ultramafic-mafic rocks. More important than the copper-sulfide mineralization is the quartz-sulfide vein and stockwork mineralization related to lower-middle part of gabbroic suite, plagiogranite and quartz-diorite sequence. The stockwork-type Cu-Fe sulfide mineralization is related to sheeted dyke complex. It is presumed to have formed below the seafloor where upwelling hot hydrothermal fluids mixed with cooler seawater circulated in the overlying volcanics. A widespread sulfide massive and stockwork mineralization related to volcanic series is represented by a large mineral assemblage of Cu+Zn+Pb+As+Au.

**PROVENANCE AND PALAEOENVIRONMENTAL CONDITIONS OF LACUSTRINE  
SEDIMENTS IN THE AREA EAST OF HIGAZA, NILE VALLEY, UPPER EGYPT**

by

**M. R. Osman<sup>1</sup> & H. Kurzweil<sup>2</sup>**

<sup>1</sup>Geology Department

Faculty of Science at Qena, South Valley University, Egypt

<sup>2</sup>Institute of Petrology

University of Vienna, Geozentrum, Althanstrasse 14, A-1090 Vienna

The present study is dealing with sediments that are known in literature as "Pliocene gulf deposits and conglomerates". These sediments were classified according to the distribution of facies into four lithostratigraphic units of formation rank [1], [2]. These units from older to younger are Khuzam Shale, Durri Limestone, Higaza Formation and Issawia Formation. Due to the lack of marine fauna in these sediments, the age of their deposition still is questionable. However, the previous workers assigned these sediments to Pliocene age. The origin of the studied succession also is controversial. Earlier authors believed that these rocks were accumulated either in fresh water lake [3], fluvial, estuarine [4], lake or gulf of sea [5] environments. Later, they were considered as brackish water lake sediments [2]. Nevertheless the question of the palaeoenvironmental conditions of the studied sediments still open.

Lithologically, the investigated sequence is composed of carbonates and clastic sediments. Grain size analysis data of the clastic type indicate that they were deposited in uniform suspension. The mineralogy of carbonates exhibits the presence of calcite, dolomite, quartz and clays together with minor amounts of k-feldspar and plagioclase. Analysis of the clay fraction of loose sediments shows the dominance of smectite as well as small contents of kaolinite, chlorite and mica. The final petrographical and geochemical investigations of the present study are still in progress.

**References**

- [1] ABDEL RAHMAN, M. (1980): Geology of the area southeast of Qena with special reference to the phosphate deposits. - M.Sc. Assiut Univ.: 177 p.
- [2] PHILOBBOS, E. R. & ABDEL RAHMAN, M. A. (1990): Remarks on lithostratigraphy and sedimentological history of the Pliocene (?) sediments of the Qena area. - Bull. Fac. Assiut Univ. 19(2F): 15-33.
- [3] BEADNELL, H. J. L. (1900): Recent geological discoveries in the Nile Valley and Libyan Desert. - Int. Geol. Cong., Paris: 839-866.
- [4] BALL (1939): Contributions to the geography of Egypt. - Survey Dept., Cairo: 300 p.
- [5] SANDFORD, (1929): The Pliocene and Pleistocene deposits of Wadi Qena and the Nile Valley between Luxor and Assiut. - J. Geol. Soc. London. 85: 493-548.

BORATE STRUCTURES FORMED AT AMBIANT PRESSURES:  
EQUALLY BONDED O ATOMS AS A KEY TO UNDERSTAND THE APPORTION OF  
 $\text{BO}_3$  TRIANGLES AND  $\text{BO}_4$  TETRAHEDRA

by

E. Parthé

Institut für Mineralogie und Kristallographie  
Geozentrum, Universität Wien

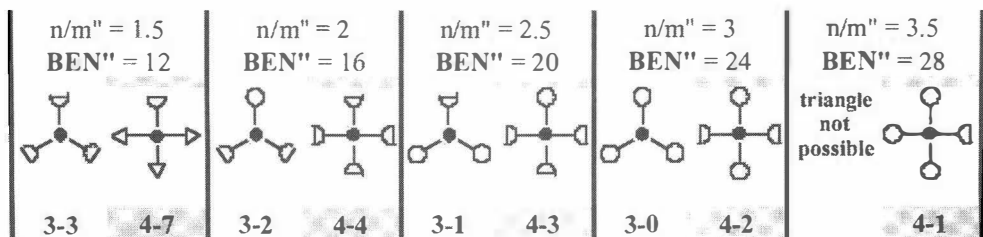
The anion complexes of borates, formed at ambiant pressures, are characterized by  $\text{BO}_3$  triangles and/or  $\text{BO}_4$  tetrahedra. which may be isolated or linked in different ways by means of shared O atoms. Borates formed at high pressure are, however, built up of only  $\text{BO}_4$  tetrahedra (or one gets there in steps with increasing pressure, e.g.  $\text{CaB}_2\text{O}_4$ ).

Comparing alkali borates formed at ambiant pressures previous investigators had noted that the more alkali in the compound the more  $\text{BO}_4$  tetrahedra occur. For other borates the partition of triangles and tetrahedra seemed arbitrary. Here will be given explanations.

The anion complex in a borate can be constructed with base triangles and/or base tetrahedra. Base polyhedra are the smallest building units consisting each of one central atom surrounded by anions, i.e. here 3 or 4 O atoms, respectively, the anion count being different depending if it is endstanding (1) or shared with other base polyhedra (1/2, 1/3). The base triangles and tetrahedra, for which the graphs are shown below, can be characterized by their anion to central atom ratio ( $\equiv n/m'$ , here it is the O/B ratio) and the Base polyhedron Electron Number ( $\equiv \text{BEN}''$ ), i.e. sum of the number of electrons for all central atom - anion bonds (2c2e) and lone-electron pairs (1c2e) on the anions which have completed octets. In the last line of the figure are given two-numeral codes of the base polyhedra with the coordination number of the central atom, on the left, and, on the right, the total number of bonds the anions extend to central atoms of other base polyhedra. One should take note that isoelectronic base triangles and base tetrahedra, i.e. those with some  $n/m'$  and  $\text{BEN}''$ , have different numbers of anion bonds to other base polyhedra.

The partition of base triangles and base tetrahedra in the anion complexes of borates, formed at ambiant pressures, can be explained based on the following hypothesis:

**The anion complex is preferably built with base triangles (if the O/B ratio permits), but precedence takes that all O atoms have the same number of O-(B,H) bonds, whenever possible.** This condition, attributable to entropy requirements, can be satisfied, if needed, by changing an appropriate number of base triangles into isoelectronic base tetrahedra, where, as seen in the figure, the anions extend a larger number of bonds to other base polyhedra.



**$1.5 \leq O/B_{a.c.} < 2$  ( $12 \leq BEN'' a.c. < 16$ ):** An anion complex (a.c.) constructed with base triangles alone would contain a mixture of 3-3 and 3-2 base triangles in the ratio  $(2 - O/B_{a.c.}) : (O/B_{a.c.} - 1.5)$ . But this combination of base triangles has both endstanding and shared O atoms. By changing all 3-2 base triangles into isoelectronic 4-4 base tetrahedra all O atoms in the structure are now shared, i.e. equally bonded to two B atoms.

Application: Predicted (and observed) ratios of 3-3 base triangles to 4-4 base tetrahedra in alkali borates without hydroxyl groups: -  $B_2O_3$  (1:0),  $CsB_9O_{14}$  (8:1),  $KB_5O_8$  (4:1),  $Na_2B_8O_{13}$  (3:1),  $K_5B_{19}O_{31}$  (14:5),  $CsB_3O_5$  (2:1),  $Li_3B_7O_{12}$  (4:3),  $K_2B_4O_7$  (1:1).

If the anion complex has hydroxyl groups the base polyhedra must have as many endstanding O atoms as there are hydroxyl groups for forming O-H bonds. Thus for a given B/O ratio the partition of base triangles and tetrahedra will vary depending on the number of OH groups.

Example:  $(NH_4)_3B_{15}O_{20}(OH)_8 \cdot 4H_2O$ : A complex with  $O/B = 28/15$ , constructed alone with base triangles, would consist of four 3-3 and eleven 3-2 base triangles, the latter with one endstanding anion. Eight endstanding O atoms are needed for the eight OH groups. If the remaining three 3-2 base triangles are changed to isoelectronic 4-4 base tetrahedra, then all O atoms have two bonds, i.e. five O to 2B and eight O to 1B and 1H. In this way one can explain why the complex is constructed of four 3-3, eight 3-2 and three 4-4 base polyhedra.

**$O/B = 2$  ( $BEN'' = 16$ ):** For borates without hydroxyl groups are available 3-2 base triangles (with one endstanding and two shared O atoms) and 4-4 base tetrahedra (where all anions are shared). Based on the preferred equi-bonding of O atoms one might expect to find only 4-4 base tetrahedra. However, the expected quartz-like structure of the anion complex would – given the small radius of B ( $r_B = 0.25\text{\AA}$ ) – not leave enough space for the cations. Thus in the borates without hydroxyl group occur only 3-2 triangles.

Mixtures of 3-2 triangles and 4-4 tetrahedra occur, however, in borates with hydroxyl groups. The triangle to tetrahedron ratio is as above determined by the number of hydroxyl groups in the formula. All O atoms have two bonds either to two B atoms or one B and one H.

Examples       $Ag_2B_4O_6(OH)_2 \cdot H_2O$       Two 3-2 triangles and two 4-4 tetrahedra  
                    $KB_5O_6(OH)_4 \cdot 2H_2O$       Four 3-2 triangles and one 4-4 tetrahedron

**$O/B = 2.5$  ( $BEN'' = 20$ ):** Pyroborates without hydroxyl groups, such as suanite  $Mg_2B_2O_5$ , are constructed with 3-1 base triangles. An incentive to change to the isoelectronic 4-3 base tetrahedra is lacking as also there the O atoms have unequal bonding.

**O/B = 3 (BEN'' = 24):** In borates without hydroxyl groups, such as kotoite  $Mg_3B_2O_6$ , occur 3-0 base triangles where all O atoms are endstanding, participating on one O-B bond.

In borates with hydroxyl groups, such as vimsite  $CaB_2O_2(OH)_4$ , two of the endstanding O per base polyhedron are used for the two OH groups. These O atoms have two bonds (1 to B and 1 to H). To allow two bonds also for the remaining O atom the 3-0 base triangle changes into the isoelectronic 4-2 base tetrahedron.

**O/B = 3.5 (BEN'' = 28):** Base triangles with  $O/B > 3$  do not exist, thus only 4-1 base tetrahedra will occur. The anion complex is similar to that found in sorosilicates. The six endstanding O are bonded to H atoms and the seventh bridging O atom to two B atoms. Thus all O atoms extend two bonds. A mineral example is pentahydroborite  $CaB_2O(OH)_6 \cdot 2H_2O$ .

**O/B = 4 (BEN'' = 32):** These borates are fully hydroxylated, as for example frovolite  $CaB_2(OH)_8$ . As anion complex can exist only an isolated tetrahedron (4-0 base tetrahedron) where all four endstanding O atoms extend a bond to an H atom.

**THERMOBAROMETRY IN LOW-GRADE METAGRANITOIDS:  
HOW RELIABLE IS STILPNOMELANE ?**

by

**A. Piber & P. Tropper**

Institut für Mineralogie und Petrographie  
Universität Innsbruck, Innrain 52, A-6020 Innsbruck

This investigation is part of the ongoing project on the tectonometamorphic evolution of the Austroalpine nappes in the northern Zillertal area, Eastern Alps. The two units studied are the Kellerjochgneiss and the underlying Innsbruck Quartzphyllite. Both lithological units show a polymetamorphic evolution under low- to high greenschist facies conditions. The Kellerjochgneiss contains the mineral assemblage muscovite + biotite + albite + chlorite + quartz ± stilpnomelane. Additionally a sample from a pegmatite in the Kellerjochgneiss contains the assemblage garnet1 ( $\text{Alm}_{68}\text{Spess}_{27}\text{Pyr}_3\text{Gro}_2$ ) + garnet2 ( $\text{Gros}_{52}\text{Alm}_{33}\text{Spess}_{15}$ ) + biotite + stilpnomelane + muscovite + chlorite + albite + quartz. Within the Innsbruck Quartzphyllite, small greenschist layers containing the mineral assemblage albite + chlorite + muscovite + clinozoisite + sphene + calcite + stilpnomelane ± ilmenite ± biotite also occur.

Stilpnomelane ( $\text{K}_{0.625}\text{Fe}_6\text{Si}_8\text{Al}(\text{O},\text{OH})_{27.2-4}\text{H}_2\text{O}$ ) occurs commonly at low temperatures (<450°C) and moderate to high pressures. In rocks containing the assemblage biotite + muscovite + chlorite + stilpnomelane + quartz, the assemblage biotite + chlorite + muscovite + quartz is used as a geothermobarometer (POWELL & EVANS, 1983; BUCHER-NURMINEN, 1987), in addition the assemblage stilpnomelane + chlorite + muscovite + quartz (CURRIE & VAN STAAL, 1999) may also yield useful information. The thermodynamic data of Fe-stilpnomelane and phengite were also included into the data base of MASSONNE (1998) and therefore can be used in multi-equilibrium calculations. These calculations were performed by calculating invariant points with the program TWQ v. 1.02 (BERMAN, 1988) and the data base of MASSONNE (1998). In addition, the empirically calibrated muscovite + chlorite + stilpnomelane + quartz thermobarometer by CURRIE & VAN STAAL (1999) was applied. These calculations yield pressures ranging from 8.3 to 9.5 kbar and temperatures ranging from 380 to 430°C for the biotite-muscovite-chlorite-quartz thermobarometer. The results achieved with the empirical thermobarometer of CURRIE & VAN STAAL (1999) are in good agreement and yield slightly lower pressures and temperatures ranging from 5.8 to 7.3 kbar and 310 to 400°C. Multi-equilibrium calculations involving Fe-stilpnomelan yield pressures of 7 - 9.5 kbar at temperatures of 310 - 350°C, which are also in good agreement with the results from the biotite-muscovite-chlorite-quartz thermobarometer. Overall, these data show that stilpnomelan can be used for thermobarometric purposes, if other P-T estimates are also available for comparison.

## **References**

- BERMAN, R. G (1988): *J. Petrol.* 29, 445-522.  
BUCHER-NURMINNEN, K. (1987): *Contr. Mineralogy and Petrol.* 96, 519-522.  
CURRIE, K.L. & VAN STAAL, C. R. (1999): *J. Metamorphic Geol.* 17, 613-620.  
MASSONNE, H. J. (1998): written communication.  
POWELL, R. & EVANS, J. A. (1983): *J. Metamorphic Geol.* 1, 331-336.

**PRELIMINARY RESULTS OF STEAM PROCESSED SLAGS PRODUCED BY  
SPRAY GRANULATION (PILOT-PROJECT DGM-TRIBOVENT/LORÜNS):  
MINERALOGICAL AND PHYSICAL PARAMETERS**

by

**C. Potocan, F. Vavtar & R. Tessadri**

Institute of Mineralogy and Petrography  
University of Innsbruck, Innrain 52, A-6020 Innsbruck

**Introduction**

In order to produce suitable precursor material for the production of cement a pilot plant (situated in Lorüns near Bludenz/Vorarlberg/Austria) based on spray granulation of melts has been built. Mineralogical characterisation and investigation of various physical parameters and the influence on processing parameters on the processed products will be the major work during this project. The project is carried out by the "TRIBOVENT process engineering company". Other members of this interdisciplinary project deal with the technical processing (Universities of Stuttgart and Bremen) and the aerodynamic behavior of hot melt (University of Erlangen and the German Aero Space Center).

**The material concept**

The main idea of the project is to substitute calc-clay as precursor cement material, which is not available everywhere and a relatively expensive raw material compared to the large amounts of slags, which are produced during various metallurgical processes. On the other hand this new production method should replace most of the grinding processes in cement industry, since these belong to the most cost-intensively procedures. The DGM ("Dampf Granulier Mühle")/STM ("Steam Granulation Mill") should produce a microgranulate, with a mean grain size of about 20 microns and a crystalline phase content below 1%.

**The technical concept**

Melt of about 1500 to 1600°C produced in rotating furnaces is poured into a nozzle-system consisting of SiC ceramics/high-T alloys. The actual granulation process is carried out with the aid of supersonic hot water steam.

**The first products**

The first run at the pilot plant already exhibited encouraging results concerning amorphous phase content and specific surface. However, the product itself did not show grains with more or less isomorphic shape – it showed fine needles. Varying the process parameters more isomorphic grains have been produced with grain sizes about 200 micrometers and crystalline phase content of about 10% (mainly quartz and gehlenite).

Further investigations and adjustments of the processing parameters (melt chemistry, melt viscosity, nozzle diameter variation, supersonic velocity variations etc.) are under way.

**METAMORPHISM OF METAPELITES AND METAPSAMMITES IN NKFMAH –  
A NEW PETROGENETIC GRID WITH COMPARISON OF  
NATURAL ASSEMBLAGES AND IMPLICATIONS FOR THE PRESERVATION OF  
HIGH-PRESSURE ROCKS DURING EXHUMATION**

by

**A. Poyer**

Institut für Mineralogie und Petrologie  
Universität Graz, Universitätsplatz 2, A-8010 Graz

There is a missing link in the description of metapelites between high and ultrahigh-pressure parageneses and their respective grids in NFMASH [1, 2] and medium- to low-pressure parageneses described by KFMASH-grids [e.g. 3, 4]. The missing link is important because most high-pressure metapelites undergo reactions during exhumation, which tend to wipe out their memory of the high-pressure past and make them appear medium-grade only. As these are the very reactions occurring at the transition between N- and K-FMASH, the new NKFMAH-grid clarifies the paragenetic evolution of metapelites over a broad PT-range and will be useful in the geotectonic interpretation of metapelite-bearing terranes.

The NKFMAH-grid has been calculated using the software THERMOCALC (v. 2.75) [5, 6] by superposition of the grids in ASH, NASH, FMASH and KFMASH. All reactions emanating from stable FMASH- or KFMASH invariant points were checked if they would pass through an invariant point from the corresponding sodic system (NFMASH or NKFMAH). Intersection of reactions emanating from these sodic invariant points would yield the rest of the stable invariant points in these systems.

The complexity was reduced a priori by assuming muscovite, quartz and a pure H<sub>2</sub>O-fluid to be present in excess. Consequently, the grid is only applicable to rocks falling under these constraints. The following phases were considered in the stability calculations: quartz (a+b), coesite, H<sub>2</sub>O, kaolinite, pyrophyllite, kyanite, andalusite, sillimanite, OH-topaz, albite, paragonite, jadeite, chlorite, chloritoid, carpholite, talc, staurolite, Fe-Mg-garnet, muscovite, biotite and Fe-Mg-glaucomophane. K-feldspar, cordierite and orthopyroxene were included but their stability fields plot mainly outside the PT-region shown.

Melting has been disregarded as well as very low-temperature and ultrahigh-pressure minerals (like sodoite, Mg-pumpellyite etc.), so some reactions will be metastable at the extreme ends of the grid.

The interpretation of the grid is facilitated by dividing the entire PT-range in three sections:

1) The high- and ultrahigh-pressure range can be discussed in the system NFMASH because phengite is the only stable potassic phase. This system has been discussed earlier [1, 2] and differs mainly because additional phases were included and a more recent dataset version was used.

2) A transitional region at moderately high pressures is characterised by four NKFMAH-invariant points which "shield" high-pressure glaucophane-bearing metapelites from lower-pressure biotite-bearing ones. The transition between NFMASH and KFMASH model systems is rather sharp because the change in Mg-buffer erases either a sodic or a potassic phase. The reactions connecting the four invariant points are flat-lying in PT-space and generally predict dehydration during decompression. Thus metapelites passing this region during exhumation usually dehydrate, which decreases the chance of preservation of glaucophane-bearing high-pressure parageneses above temperatures of around 550°C. This prediction is corroborated by estimated peak temperatures from a number of high-pressure metapelite occurrences, which are generally below 550°C [e.g. 7, 8].

3) The low- to medium pressure range contains a fifth NKFMAH-invariant point. This invariant point has been documented for the first time from field evidence [9]. Reactions emanating from this point terminate the large stability field of garnet-paragonite-biotite schists, which is a typical, but unsuspecting rock type that may be easily underestimated in its relevance as a high-pressure indicator. This paragenesis breaks down to staurolite, kyanite and plagioclase, and develops characteristic plagioclase porphyroblast textures during exhumation. Other examples of moderately high pressure paragonite-bearing micaschists are known from Newfoundland [10], the Bohemian Massif [11] and several units of the Austroalpine basement of the Eastern Alps.

Despite of its apparent chemical complexity the new grid is relatively simple to read. It finally integrates and completes the medium- and high-pressure range by incorporating all major components of non-carbonaceous metapelites and provides the basis for further analysis by pseudosections.

## References

- [1] GUIRAUD, M., HOLLAND, T. & POWELL, R. (1990): Calculated mineral equilibria in the greenschist-blue-schist-eclogite facies in  $\text{Na}_2\text{O}-\text{FeO}-\text{MgO}-\text{Al}_2\text{O}_3-\text{SiO}_2-\text{H}_2\text{O}$ . - Contrib. Mineral. Petrol., 104:85-98.
- [2] MASSONNE, H. J. (1995): Experimental and petrogenetic study of UHMP. - In: COLEMAN & WANG: Ultrahigh pressure metamorphism. Cambridge University Press, Cambridge, USA.
- [3] POWELL, R. & HOLLAND, T. (1990): Calculated mineral equilibria in the pelite system, KFMASH ( $\text{K}_2\text{O}-\text{FeO}-\text{MgO}-\text{Al}_2\text{O}_3-\text{SiO}_2-\text{H}_2\text{O}$ ). - Am. Min. 75:367-380.
- [4] SPEAR, F. S. & CHENEY, J. T. (1989): A petrogenetic grid for pelitic schists in the system  $\text{SiO}_2-\text{Al}_2\text{O}_3-\text{FeO}-\text{MgO}-\text{K}_2\text{O}-\text{H}_2\text{O}$ . - Contrib. Mineral. Petrol., 101:149-164.
- [5] POWELL, R. & HOLLAND, T. J. B. (1988): An internally consistent dataset with uncertainties and correlations: 3. Applications to geobarometry, worked examples and a computer program. - J. Metam. Geol., 6:173-204.

- [6] HOLLAND, T. J. B. & POWELL, R. (1998): An internally consistent thermodynamic data set for phases of petrological interest. - *J. Metam. Geol.*, 16:309-343.
- [7] GUILLOT, S., SIGOYER, J., DE LARDEAUX, J. M. & MASCLE, G. (1997): Eclogitic metasediments from the Tso Morari area (Ladakh, Himalaya): evidence for continental subduction during India-Asia convergence. - *Contrib. Mineral. Petrol.*, 128:197-212.
- [8] SISSON, V. B., ERTAN, I. E. & AVÉ LALLEMANT, H. G. (1997): High-pressure (~2000 MPa) kyanite- and glaucophane-bearing pelitic schists and eclogite from Cordillera de la Costa Belt, Venezuela. - *J. Petrol.* 38:65-83.
- [9] PROYER, A. (1989): Petrologie der Rahmengesteine der Pb-Zn-Lagerstätte Schneeberg, Südtirol. - Unpubl. Dipl. Arb. Universität Innsbruck, 1989.
- [10] KONOPASEK, J. (1998): Formation and destabilization of the high-pressure assemblage garnet-phengite-paragonite (Krusne hory Mountains, Bohemian Massif): The significance of the Tschermak substitution in the metamorphism of pelitic rocks. - *Lithos*, 42:269-284.
- [11] JAMIESON, R. A. & O'BEIRNE-RYAN, A. M. (1991): Decompression-induced growth of albite-porphyroblasts, Fleur de Lys Supergroup, western Newfoundland. - *J. Metam. Geol.*, 9:433-439.

Research on this topic was financed by a guest-professorship at the University of Graz and by the Austrian Science Fund (Project P13058-GEO).

**THE PRESERVATION OF HIGH-PRESSURE ROCKS DURING EXHUMATION:  
ECLOGITES, METAPELITES AND METAGRANITES**

by

**A. Poyer**

Institut für Mineralogie und Petrologie  
Universität Graz, Universitätsplatz 2, A-8010 Graz

The country rocks of eclogites rarely record the same or even comparable high- or ultrahigh-pressure conditions. This situation has caused prolonged discussions on the subject of in-situ HP-metamorphism versus tectonic emplacement of HP-rocks along the exhumation path for a number of high-pressure localities around the world.

Internal dehydration of a lithology, in combination with deformation, is the major factor governing the degree of reequilibration of a rock along the exhumation path. This study gives an overview and a quantitative outline of the most important reactions controlling dehydration in two important country rock lithologies (K-feldspar gneisses and high-pressure metapelites) and discusses the fluid interaction between eclogites and country rocks during subduction and exhumation.

Acidic orthogneisses with a typical paragenesis of K-feldspar + plagioclase + quartz + muscovite + biotite (+fluid) are 4-variant in the system NKCFMASH. Other minerals are usually accessory, even garnet and epidote are stable only as buffers of Mn and Fe<sup>3+</sup>. They require external hydration during prograde high-pressure metamorphism in order to equilibrate to ambient HP-conditions by producing more siliceous micas. Any lack of external fluid or the disappearance of biotite stops reequilibration and thus prevents recording of HP-conditions. The same reactions cause dehydration during exhumation. Orthogneiss from shear zones or adjacent to metapelites and metabasites will take up external fluid on the prograde path and record the highest PT-conditions, but will also be the first to dehydrate upon exhumation, now hydrating other lithologies and probably refuelling shearzones.

Metapelites generally have a more complex mineralogy. The fluid bound in the structures of hydrous mineral like chlorite and chloritoid is only partly released, but partly transferred to other minerals like paragonite or phengite during a prograde oceanic or continental subduction event and is given off in large quantities upon exhumation. High-pressure metapelites can be preserved only if the PT-path remains within the stability fields of chlorite and paragonite or passes through them again on the retrograde limb. Rapid exhumation (isothermal decompression) very likely destroys almost any indication of former HP-conditions, giving rise to typical Barrow-type garnet-biotite-staurolite or -kyanite schists.

Metapelites of different bulk composition – Al-rich, Al-poor and sodic varieties – differ significantly in their ability to record various sections or points along the PT-path and should be used together with eclogites and gneisses to deduce a well-constrained PT-evolution for a certain area.

A thorough understanding of the dehydration behavior of orthogneisses and metapelites explains how different lithologies may interact during their metamorphic evolution and thus advances the tectonic interpretation of high- and ultrahigh-pressure terrains.

Research on this topic was financed by a guest-professorship at the University of Graz and by the Austrian Science Fund (Project P13058-GEO).

THE IMPORTANCE OF PARAGONITE-BEARING MICA-SCHISTS  
IN MEDIUM- TO HIGH-PRESSURE METAMORPHISM:  
A THEORETICAL STUDY AND FIELD EVIDENCE FROM  
THE AUSTROALPINE BASEMENT UNITS OF THE EASTERN ALPS

by

A. Poyer & G. Hoinkes

Institut für Mineralogie und Petrologie  
Universität Graz, Universitätsplatz 2, A-8010 Graz

The existence of an NKFMAH-invariant point has been documented in a medium- to high-pressure metamorphic terrain in the southeastern part of the Ötztal-Stubai-Complex, which belongs to the Austroalpine basement west of the Tauern Window).

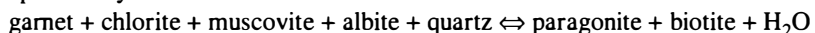
The unusual staurolite-forming reaction

$\text{garnet} + \text{biotite} + \text{paragonite} + \text{quartz} \leftrightarrow \text{staurolite} + \text{muscovite} + \text{plagioclase} + \text{H}_2\text{O}$

emanates from this invariant point (which has additional kyanite) and occurs at considerably higher temperatures than the well known staurolite-forming reactions resulting from the breakdown of chlorite.

In order to explain the evolution of paragonite-bearing micaschists, a petrogenetic grid for metapelites in the model system NKFMAH has been constructed for the PT-range in which two sodic phases (paragonite, albite) and two potassic phases (muscovite, biotite) are part of the mineral assemblages. The general relevance of two important invariant points for the interpretation of medium- to high-pressure metapelites in general is discussed and illustrated with field examples from the Austroalpine basement units. The presence of plagioclase destabilizes typical aluminous phases like chloritoid or staurolite at intermediate to high pressure conditions for a large range of bulk compositions. Thus unsuspecting, apparently low-grade assemblages like garnet + white-mica + chlorite or biotite occur over a wide range of PT-conditions up to around 600°C. The presence of a second white mica (paragonite) together with muscovite generally remains unnoticed in the field. Such rocks may be erroneously classified as low-grade chlorite- or biotite-zone rocks, as retrograde or just as too Al-poor to be a valuable sensor of metamorphic conditions.

The grid shows two large stability fields for garnet-white micas-chlorite and garnet-white micas-biotite, separated by the univariant reaction



The actual PT-conditions of a sample can be narrowed down within each of the two parageneses by modern geothermobarometry or isopleth contours within pseudosections. With an increase of pressure paragonite becomes stable in a larger range of bulk compositions, thus making the appearance of paragonite and the often coinciding reduction of the amount of biotite indicative of moderate- to high-pressure metamorphism.

This case study demonstrates that a "standard" KFMASH-view is insufficient and sodium is potentially important for a full appreciation of the metamorphic evolution of metapelites, especially in pressure-dominated metamorphism.

Research on this topic was financed by a guest-professorship at the University of Graz and by the Austrian Science Fund (Project P13058-GEO).

PERMO-TRIASSIC METAMORPHIC EVOLUTION OF  
THE KREUZECK-GOLDECK MOUNTAINS (CARINTHIA, AUSTRIA)

by

A. Poyer<sup>1</sup>, R. Schuster<sup>2</sup>, G. Hoinkes<sup>1</sup> & P. Faupl<sup>2</sup>

<sup>1</sup>Institute of Mineralogy and Petrology

University of Graz, Universitätsplatz 2, A-8010 Graz

<sup>2</sup>Institute of Geology

University of Vienna, Althanstrasse 14, A-1090 Vienna

**Introduction:** The Austroalpine basement units had long been regarded as a product of the Variscan and probably Caledonian orogeny only, until an increasing number of geochronologic and petrologic studies documented that an Eo-Alpine eclogite to amphibolite facies metamorphism was actually dominant in most of the units. Only the southernmost basement blocks remained almost unaffected by this geotectonic event, thus defining a boundary, the "Southern limit of Alpine Metamorphism (SAM)" within the Austroalpine [1]. Even more, a widespread Permo-Triassic high temperature/low pressure (HT/LP) metamorphic imprint of various grade has recently been recognised within the Austroalpine [2, 3]. A continuous section through Permo-Triassic middle and upper crust, up to the Permian sedimentary cover, has been preserved south of the SAM, in the Kreuzeck-Goldeck-Drauzug area. In this abstract we present geochronological and petrological data on the pre-Alpine evolution of the Strieden Complex which represents the lower part of this section.

**Petrography:** The Strieden Complex shows a zonation expressed in mineral assemblages, the occurrence of pegmatites and typical cooling ages for different structural levels. The deepest structural levels and rocks of highest metamorphic grade are exposed in the north, immediately south of the SAM. The whole sequence is tentatively divided from north to south in a lower and upper sillimanite zone, andalusite zone, staurolite zone and garnet zone.

**Garnet zone:** The uppermost part of the Strieden Complex consists of garnet-chlorite-muscovite-schists and subordinate amphibolites which exhibit a polyphase deformation ( $D_m$ ,  $D_n$ ). The metapelites are characterised by the syndeformational assemblages  $Grt + Chl + Ms + Pl + Qtz + Ilm \pm Bt \pm Pg$ . Garnet porphyroblasts are up to 1 cm in diameter and sometimes contain inclusions of chloritoid.

**Staurolite zone:** Going north, and downward in the section, gneisses occur, intercalated with layers of garnet-two-mica-schists. The mica schists exhibit an assemblage of  $Grt + St + Bt + Ms + Pl + Qtz + Ilm$ .

**Andalusite zone:** Further below centimeter-sized andalusite porphyroblasts occur, obviously restricted to staurolite- and garnet-rich layers. Andalusite, as well as large biotite flakes are overgrowing the pre-existing microfabrics and the garnet porphyroblasts.

Staurolite is resorbed and forms dismembered inclusions with identical optical orientation, indicating their formation during prograde breakdown of staurolite by the reaction  $\text{St} + \text{Ms} \rightleftharpoons \text{And} + \text{Bt} + \text{Qtz} + \text{H}_2\text{O}$ . In the lowermost part of the andalusite zone fibrolitic sillimanite appears.

**Sillimanite zones:** The upper sillimanite zone is characterised by the occurrence of sillimanite and the disappearance of staurolite [4]. An overprinting ductile deformation ( $D_6$ ) becomes more prominent with structural depth. Staurolite and garnet act as porphyroclasts during  $D_6$ ; sillimanite growth is syndeformational. The lower sillimanite zone is characterised by the absence of garnet. In the metapelites sillimanite is intergrown with biotite and aligned to the dominant schistosity of the rocks. Sillimanite also forms millimeter-sized patchy pseudomorphs after garnet, indicating prograde breakdown of garnet by the reaction  $\text{Grt} + \text{Ms} + \text{Qtz} \rightleftharpoons \text{Sil} + \text{Bt} + \text{Pl} + \text{H}_2\text{O}$ . The amount of muscovite is decreasing with depth. Anatetic melting is indicated locally by concordant neosome layers of  $\text{Pl} + \text{Or} + \text{Qtz} \pm \text{Bt} \pm \text{Sil}$  whereas plagioclase porphyroblasts are overgrowing the residual sillimanite-biotite schists. Pegmatites are frequent in the sillimanite zone.

**Petrology and Geothermobarometry:** Based on microfabrics and the deformation history two metamorphic events can be identified in the Strieden Complex: The older exhibits moderately high-pressure metamorphic conditions and is characterised by garnet-chlorite-muscovite-schists ( $\pm$  biotite, paragonite), grading northwards into staurolite- and rarely kyanite-bearing schists. Thermobarometric calculations yielded  $590 \pm 20^\circ\text{C}$ ,  $8.5 \pm 1.5$  kbar for the garnet-chlorite-muscovite-schists and  $570^\circ\text{C} \pm 50$  and  $8 \pm 1.5$  kbar for the staurolite zone. The overprinting HT/LP event produced andalusite-bearing mica-schists and andalusite-quartz-veins and transformed the northernmost rocks into biotite-rich sillimanite-mica-schists with local anatexis. Andalusite-bearing rocks apparently are only partly reset: Average-PT-data for the full assemblage (grt-sta-and-bt-mus-plag-qtz) yields around  $6.5 \pm 1.4$  kbar and  $600 \pm 50^\circ\text{C}$ , which is way outside the stability limit of andalusite. Based on the breakdown of staurolite in the andalusite stability field conditions of c.  $550 \pm 50^\circ\text{C}$  at  $3.5 \pm 1.0$  kbar would be expected. The sillimanite-schists and -gneisses are relatively well equilibrated, however the determined PT-conditions of  $580 \pm 40^\circ\text{C}$  and  $4.5 \pm 1.4$  kbar are low with respect to the occurrence of anatetic mobilisates and the prograde breakdown of garnet.

**Geochronologic data:** A Variscan age of the first event is indicated by a Sm-Nd garnet isochron age of  $342 \pm 3$  Ma from the staurolite-garnet micaschists and from Ar-Ar ages on muscovite of around 310 Ma (see below). The timing of the HT/LP event, which dominates the northern part of the section, was determined by Sm-Nd garnet isochron ages on magmatic garnets from a weakly deformed (RS35/00) and a deformed (RS43/99) pegmatite. Calculated with orthoclase and the whole rock they yielded well defined Permo-Triassic isochron ages of  $261 \pm 3$  Ma and  $229 \pm 2$  Ma. The cooling history of the rock pile was investigated by Ar-Ar and Rb-Sr ages on muscovite respectively biotite from several zones of the section. The Ar-Ar plateau ages on muscovite, which are interpreted as cooling ages below c.  $400^\circ\text{C}$  exhibit Variscan ages (RS7/00:  $316 \pm 4$  Ma; RS8/00:  $311 \pm 3$  Ma; RS24/00:  $312 \pm 3$  Ma) below the transgressive Permo-Mesozoic sediments and decrease with structural depth. From the garnet muscovite schists  $287 \pm 2$  Ma (RS55/99) and  $286 \pm 2$  Ma (RS58/00) were determined.

A staurolite-garnet-mica-schist yielded  $225 \pm 3$  Ma (RS4/00) and  $210 \pm 2$  Ma (RS14/97), whereas  $212 \pm 2$  Ma (RS69/00) and  $205 \pm 2$  Ma (RS13/97) have been measured for the andalusite zone. The lowest age of  $193 \pm 2$  Ma (RS43/00) has been found in the sillimanite zone.

**Conclusions:** The Strieden Complex represents a Variscan metamorphic basement that was situated at upper to middle crustal level in Permo-Mesozoic times. Extension caused a Permo-Triassic HT/LP overprint at an elevated geothermal gradient. Peak metamorphic conditions were reached at about 260 Ma. After that relaxation of the isotherms caused slow cooling. Middle crustal rocks cooled down below 400°C at about 200 Ma. A more detailed PT-profile and an interpretation of disequilibrium features in the transition zone between dominantly Variscan and Permo-Triassic metamorphism will be given at the conference.

## References

- [1] HOINKES, G., KOLLER, F., RANITSCH, G., DACHS, E., HÖCK, V., NEUBAUER, F. & SCHUSTER, R. (1999): Alpine metamorphism of the Eastern Alps. - Schweiz. Mineral. Petrogr. Mitt., 79:155-181.
- [2] SCHUSTER, R., SCHARBERT, S. & ABART, R. (1999): Permo-Triassic crustal extension during opening of the Neotethyan ocean in the Austroalpine-South Alpine realm. - Tübinger Geowissensch. Arb., Serie A, 52: 5-6.
- [3] THÖNI, M. (1999): A review of geochronological data from the Eastern Alps. – Schweiz. Mineral. Petrogr. Mitt., 79/1: 209-230.
- [4] HOKE, L. (1990): The Altkristallin of the Kreuzeck Mountains, SE-Tauern Window, Eastern Alps - Basement Crust in a Convergent plate Boundary Zone. - Jb. Geol. B.-A., 133: 5-87.

**CONVOLUTION BASED PROFILE FITTING IN X-RAY DIFFRACTION:  
INSTRUMENTAL EFFECTS AND THEIR DESCRIPTION**

by

**P. Ramminger**

Institute of Mineralogy and Petrography  
University of Innsbruck, Innrain 52, A-6020 Innsbruck

Due to the use of new X-ray geometries and large scale powder diffractometers such as synchrotron beam lines for the development of industrial materials and quality control, evaluation of XRD data needs to be adopted to these recent developments.

It is the aim not only to obtain structural informations such as the lattice parameters or the crystal structure of a crystalline substance but also to obtain informations about the physical properties of the crystalline materials by measuring the size of the crystallites and the microstrain within the sample. In order to determine the size of the crystallites and the microstrain (real structure) of a crystalline sample a close description of the obtained peak shapes and the instrumental contribution of the observed pattern is necessary.

This work introduces the experimentally-based convolution fitting method, which can be modeled by software modules, based on the Fundamental Parameter Approach (FPA). This FPA is performed with software modules such as TOPAS, developed by Bruker-AXS, which allow to describe the contribution of the instrumental function of physically complicated X-ray paths, such as modern parallel beam optics used in X-ray diffractometers.

The basis of this experimentally-based convolution fitting method is the strict separation of the instrumental contribution, the contribution due to the X-ray source and the sample contribution. This procedure is performed in three steps: (1) The basis of this procedure is a set of well defined aberrational functions which are used to model the instrumental contributions. (.) These aberrational functions are then convoluted over the profile of a well known sample specimen, such as CeO<sub>2</sub>, LaB<sub>6</sub> and Y<sub>2</sub>O<sub>3</sub>, to derive the unique instrumental function. In addition to the sample characteristics, the obtained function also strongly depends on the x-ray optics and wavelength characteristics used. (3.) In order to verify the quality of the data set presented here, the last step involves the comparison of the results to the ongoing round robin test by D. BALZAR [1].

The major advantage of this convolution based approach is (.) the capability of describing a wide range and variety of powder diffraction peak shapes with very high accuracy and (2) its applicability to XRD data which have been derived from both, conventional and synchrotron x-ray sources.

**Reference**

- [1] BALZAR, D. (2000): "Size/Strain Round Robin"; CPD-Project, [http://www.boulder.nist.gov/div853/balzar/s-s\\_rr.htm](http://www.boulder.nist.gov/div853/balzar/s-s_rr.htm).

**A COMPILATION OF THERMOBAROMETRIC DATA FROM  
THE CRYSTALLINE BASEMENT WEST OF THE TAUERN WINDOW  
(ÖTZTAL-SCHNEEBERG-COMPLEX)**

by

**A. Recheis & P. Tropper**

Institute of Mineralogy and Petrography  
University of Innsbruck, Innrain 52, A-6020 Innsbruck

The Ötztal Stubai basement complex (ÖSCB) and the Schneeberger Zug (SC) are large crystalline complexes, west of the Tauern Window. The Paleozoic SC consists of at least three narrow and structurally complicated synclines folded into the southern part of the polymetamorphic ÖSCB. Petrological as well as geochronological data indicate at least three periods of metamorphism in the ÖSCB: First, a Caledonian event (490 - 420 Ma) resulting in the local formation of migmatites, second a dominant Variscan amphibolite facies event (390 - 270 Ma) and the Eo-Alpine event from 90 to 65 Ma. The degree of the Eo-Alpine metamorphic overprint increases from greenschist facies conditions in the NW to eclogite facies conditions in the SE of the ÖSCB (HOINKES et al., 1991). Thermobarometric data of the Variscan- and Eo-Alpine metamorphic overprint in the ÖSCB and SC were obtained by investigating a wide range of samples from areas where Alpine metamorphism is almost lacking in the NW, to the SE where the dominant Eo-Alpine metamorphic overprint occurs.

The investigated metapelites contain the assemblage garnet + staurolite + biotite + muscovite + plagioclase  $\pm$  kyanite  $\pm$  sillimanite  $\pm$  andalusite and were used to reconstruct pressure and temperature conditions with multi-equilibrium methods. Phase equilibria in the system Na<sub>2</sub>O-CaO-MgO-Al<sub>2</sub>O<sub>3</sub>-SiO<sub>2</sub>-H<sub>2</sub>O (NCMASH) were calculated using the internally consistent data set of HOLLAND & POWELL (1998) and the program THERMOCALC v. 2.7. To avoid uncertainties due to poor knowledge of H<sub>2</sub>O activity, in a first attempt only H<sub>2</sub>O-absent reactions are taken into account to calculate an H<sub>2</sub>O-absent invariant point. These conditions are used subsequently to estimate  $a(\text{H}_2\text{O})$  by calculating P- $a(\text{H}_2\text{O})$  diagrams.

In addition to the multi-equilibrium approach, the inverse approach of GORDON (1992) was also applied to all samples. Instead of using a set of independent equilibria, P and T estimates are found by finding the best-fit hyperplane to the partial molar free energies of all phase components (GORDON, 1992). The program WEBINVEQ uses the data base of BERMAN (1988) with subsequent modifications (BERMAN, 1992, written com.).

The obtained P-T conditions of 470 - 710°C and 4 - 8 kbar were derived for the Variscan event in the ÖSCB and 500 - 600°C and 8 - 11 kbar were obtained for the Eo-Alpine event in the southern part of the ÖSCB and the SC. Textural and chemical data clearly indicate a continuous pre-Alpine metamorphic evolution.

## **References**

- BERMAN, R. G. (1988): J. Petrol. 29, 445-522.  
GORDON, T. (1992:) Geochim. Cosmochim. Acta 56 1793-1800.  
HOINKES, G., KOSTNER, A. & THÖNI, M. (1991:) Mineral. Petrol. 43, 237-254.  
HOLLAND, T. J. B. & POWELL, R. (1998:) J. Metam. Geol. 8, 89-124.

STRUKTURELLE UND MÖSSBAUERSPEKTROMETRISCHE UNTERSUCHUNGEN AN  
SYNTHETISCHEN TRIOKTAEDRISCHEN GLIMMERN  $\{K\}[ME_3] < T_4 > O_{10}(OH)_2$ :  
EINE ZUSAMMENFASSUNG

von

G. J. Redhammer<sup>1,2</sup>, G. Amthauer<sup>2</sup>, W. Lottermoser<sup>2</sup> & G. Roth<sup>1</sup>

<sup>1</sup>Institut für Kristallographie, LFG Angewandte Kristallographie und Mineralogie  
RWTH Aachen, Jägerstrasse 17/19, D-52056 Aachen

<sup>2</sup>Institut für Mineralogie  
Universität Salzburg, Hellbrunnerstrasse 34, A-5020 Salzburg

Die Mineralgruppe der Glimmer ist bekannt für ihre Eigenschaft, eine Vielzahl von Kationen und Anionen in ihre Kristallstruktur einbauen zu können. Dies gilt sowohl für die Zwischenschicht {K, Na, Ca}, die Oktaeder- [Mg, Zn, Fe, Mn, Al, Ti] und die Tetraederplätze <Al, Si, Fe>, als auch für den Hydroxylplatz (OH-, F-, Cl-). Dementsprechend schwierig ist eine kristallchemische Charakterisierung dieser relevanten Mineralgruppe, vor allem dann, wenn man auf natürliche Glimmer zurückgreift. So sind bislang mehr als 100 Einkristall – Strukturanalysen von natürlichen "echten" Glimmern bekannt [1 und Zitate darin]. Diese wurden im Rahmen dieser vorliegenden Untersuchung im Hinblick auf systematische Änderungen struktureller Parameter (Bindungslängen, Verzerrungsparameter) mit der chemischen Zusammensetzung untersucht. Es zeigten sich allerdings nur diffuse Trends. Deshalb sollte man – will man systematische kristallchemische Untersuchungen an den Glimmern durchführen – auf synthetisches Probenmaterial zurückgreifen [cf. 2 – 6].

Für eine systematische strukturelle und mößbauerspektroskopische Untersuchung wurde deshalb – ausgehend vom Mineral Annit  $\{K\}[Fe_3]<AlSi_3>O_{10}(OH)_2$  – oktaedrisch koordiniertes Fe systematisch und kontinuierlich durch  $Ni^{2+}$ ,  $Mg^{2+}$  und  $Co^{2+}$  substituiert, sowie nach einer Tschermak's Substitution teilweise durch  $Al^{3+}$  ersetzt [cf. 2], auch Mischkristalle zwischen dem  $Ni^{2+}$  und dem  $Co^{2+}$  Endglied wurden hergestellt. Tetraedrisch koordiniertes  $Al^{3+}$  im Annit wurde kontinuierlich durch  $Fe^{3+}$  ersetzt und in diesem sogenannten Tetraferriannit  $\{K\}[Fe_3]<Fe^{3+}Si_3>O_{10}(OH)_2$  wurde wiederum [Fe] durch  $Mg^{2+}$  und  $Ni^{2+}$  substituiert. Alle diese Proben wurden auf hydrothermalem Wege zwischen 600°C und 700°C, 0.2 - 0.4 GPa Druck und kontrollierten Sauerstoff – Fugazitäten hergestellt. Die Synthesen lieferten fast immer einphasige Glimmer Mischkristalle, die Korngrößen lagen bei maximal 5 mm. Eine nähere Charakterisierung dieser Proben erfolgte mittels Mößbauerspektroskopie und Röntgenbeugung am Pulver (Rietveld – Verfeinerung). Da die Aussagekraft der strukturellen Untersuchungen an den pulverförmigen synthetischen Glimmer gering ist, wurde in weiterer Folge versucht, bei Temperaturen zwischen 1300°C und 1350°C und Drucken von 3 GPa Einkristalle herzustellen.

Nach über einem Jahr Arbeit liegen bislang 14 qualitativ hochwertige Proben unterschiedlicher Zusammensetzung  $\{K\}[Me^{2+}]<AlSi_3>O_{10}(OH)_2$  mit Me = Ni, Mg, Co und Fe vor. Zusätzlich zu diesen synthetischen Proben wurden auch noch ein natürlicher Annit und ein natürlicher Siderophyllit, beide nahe der idealen Zusammensetzung, mit Einkristall – Röntgenbeugung untersucht.

Annit zeigt von den 16 unterschiedlichen Glimmern, die bisher mit Röntgenbeugung am Einkristall untersucht wurden, die am wenigsten verzerrte mittlere Kristallstruktur. Wird  $Fe^{2+}$  durch kleinere zweiseitige Kationen ersetzt, so nimmt die Verzerrung der mittleren Struktur, vor allem die der Oktaederschicht, deutlich zu. Im synthetischen Nickelannit  $\{K\}[Ni_3]<AlSi_3>O_{10}(OH)_2$  zeigen die Oktaeder die größte Verzerrung (Abweichung von der idealen Geometrie eines Oktaeders). In allen untersuchten Glimmern mit Ausnahme des natürlichen Siderophyllits, idealerweise  $\{K\}[Fe_2Al]<Al_2Si_2>O_{10}(OH)_2$  - sind sich der M1- und der M2-Oktaeder in ihrer Größe und Verzerrung sehr ähnlich und unterscheiden sich nur in der Anordnung der (OH) Gruppen. Dies ist für die Mößbauerspektroskopie besonders wichtig. Annit weist von allen untersuchten Glimmern die geringste Abflachung j der Oktaederschicht auf, Nickelannit die größte. Auch die trigonale Verzerrung der Tetraederschicht a ist im Annit wesentlich geringer als im Nickelannit. In Siderophyllit ist der M1-Platz deutlich kleiner als der M2-Platz. Die Ursache dafür liegt im bevorzugten Einbau des kleinen  $Al^{3+}$  auf der M2- Position. Die teilweise deutlichen Größenunterschiede der M1- und M2-Oktaeder, die für natürliche Glimmer in der Literatur gefunden wurden, haben ihre Ursache in dieser Platzbevorzugung von oktaedrisch koordiniertem  $Al^{3+}$ . Für die Mischkristalle der Reihen [Ni-Co] und [Mg-Fe] zeigten sich keinerlei Anzeichen für Platzbevorzugungen.

Die mößbauerspektroskopischen Untersuchungen an den Glimmern ergaben drei wichtige Ergebnisse. (i) Synthetischer Annit zeigt, selbst wenn er bei sehr reduzierenden Bedingungen hergestellt wird, immer einen geringen Gehalt an oktaedrisch koordiniertem  $Fe^{3+}$ . Dieser ist notwendig, um einen lateralen Größenunterschied der Oktaeder- und der Tetraederschicht in der - a-b Ebene auszugleichen. (ii) In den Mößbauerspektren von Annit kann zwischen  $Fe^{2+}$  auf den beiden M-Plätzen (M1 und M2) nicht unterschieden werden, deshalb ist es nicht möglich, M2/M1-Verhältnisse zu bestimmen, wie sie in der Literatur häufig angegeben wurden/werden. Zwar kann die Resonanzabsorption, die von oktaedrisch koordiniertem  $Fe^{2+}$  herrührt, nur zufriedenstellend ausgewertet werden, wenn zumindest zwei  $Fe^{2+}$  Komponenten verwendet werden, diese beiden Komponenten korrelieren allerdings nicht unmittelbar mit den beiden kristallographischen M-Plätzen sondern vielmehr mit lokalen geometrischen und/oder elektronischen Verzerrungszuständen. Dies gilt auch für alle weiteren mößbauerspektroskopisch untersuchten Glimmer. Die Auswertung der Mößbauerspektren der Glimmer erfolgt am besten mit einem Ansatz, bei dem die Verteilung der Quadrupolaufspaltung von  $Fe^{2+}$  auf den beiden M Plätzen bestimmt wird (QSD-Kurve). (iii) Die  $Fe^{2+}$  Quadrupolaufspaltungen der einzelnen Komponenten einer QSD-Kurve nehmen mit steigendem Ersatz von  $Fe^{2+}$  durch kleinere zweiseitige Kationen sukzessive zu. Dieses Verhalten zeigt, daß – lokal gesehen – die Verzerrung der (verbleibenden)  $Fe^{2+}$ -Oktaeder mit zunehmendem Gehalt an kleineren zweiseitigen Kationen in der Oktaederschicht abnimmt. Die lokale Baueinheit der  $Fe^{2+}$ -Oktaeder spiegelt also ein anderes Verhalten wider als die gemittelte Struktur, die aus Einkristall-Röntgenbeugungsdaten bestimmt wurde. Eine ausführliche Darstellung der Kristallchemie der Glimmer findet sich in [6].

## References

- [1] BRIGATTI, M. F. et al. (2000): Crystal chemistry of Al-rich biotites coexisting with muscovite in peraluminous granites. - American Mineralogist, 85, 436-448.
- [2] REDHAMMER, G. J. et al. (2000): Spectroscopic and structural properties of synthetic micas on the annite - siderophyllite binary  $\{K\}[Fe^{2+}_3] < AlSi_3 > O_{10}(OH)_2 - \{K\}[Fe^{2+}_2Al] < Al_2Si_2 > O_{10}(OH)_2$ . - American Mineralogist, 85(3-4), 449-465.
- [3] REDHAMMER, G. J. (1998): Characterization of synthetic trioctahedral micas by Mössbauer spectroscopy. - Hyperfine Interactions, 117: 85-115.
- [4] REDHAMMER, G. J. et al. (1995): Mössbauer spectroscopic and X-ray powder diffraction studies of synthetic micas on the join annite  $KFe_3AlSi_3O_{10}(OH)_2$  - phlogopite  $KMg_3AlSi_3O_{10}(OH)_2$ . - Physics and Chemistry of Minerals, 22, 282-294.
- [5] REDHAMMER, G. J. et al. (1993): A Mössbauer and X-ray diffraction study of annites synthesized at different oxygen fugacities and crystal chemical implications. - Physics and Chemistry of Minerals, 20, 382-394.
- [6] REDHAMMER, G. J. (2001): Kontrollierte chemische Substitutionen in ausgewählten Ketten und Schichtsilikaten: Beiträge von Mößbauerspektroskopie, und Einkristall – Röntgenbeugung zur Kristallstruktur, Kristallchemie und Magnetismus von Glimmern und Klinopyroxenen. - Habilitationsschrift, RWTH – Aachen, 333 Seiten.

STRUKTURELLE, MÖSSBAUERSPEKTROMETRISCHE UND MAGNETISCHE  
UNTERSUCHUNGEN AN DER BROWN MILLERIT-MISCHKRISTALLREIHE  
 $\text{Ca}_2\text{Fe}_{2-x}\text{Al}_x\text{O}_5$  BEI 298 K UND HOHEN TEMPERATUREN

von

G. J. Redhammer<sup>1,2</sup>, G. Tippelt<sup>2</sup>, G. Roth<sup>1</sup>, W. Lottermoser<sup>2</sup> & G. Amthauer<sup>2</sup>

<sup>1</sup>Institut für Kristallographie, LFG Angewandte Kristallographie und Mineralogie  
RWTH Aachen, Jägerstrasse 17/19, D-52056 Aachen

<sup>2</sup>Institut für Mineralogie  
Universität Salzburg, Hellbrunnerstrasse 34, A-5020 Salzburg

Brownmillerit  $\text{Ca}_2\text{FeAlO}_5$ , in der Zementnomenklatur auch als C4AF bezeichnet, ist eine der vier Hauptkomponenten des Portland-Zementklinkers. Bei Normaldruck existiert im ternären System  $\text{CaO}-\text{Fe}_2\text{O}_3-\text{Al}_2\text{O}_3$  für die Ferrite der Zusammensetzung  $\text{Ca}_2\text{Fe}_{2-x}\text{Al}_x\text{O}_5$  eine lückenlose Mischbarkeit bis zu  $x \approx 1.4$  [1]. Reines  $\text{Ca}_2\text{Fe}_2\text{O}_5$  (auch bekannt unter dem Mineralnamen Srebrodoskit) kristallisiert bei Raumtemperatur ( $RT = 25^\circ\text{C}$ ) in der Raumgruppe Pnma [2], bei Gehalten von  $x > 0.6$  kommt es zu einer Änderung der Raumgruppe. Die aluminiumreicherer Mischkristalle kristallisieren in der Raumgruppe Ibm2 [3, 4]. Darüber hinaus geht auch reines  $\text{Ca}_2\text{Fe}_2\text{O}_5$  bei etwa  $680^\circ\text{C}$  von Pnma in die Raumgruppe Ibm2 über [5, 6]. Reines  $\text{Ca}_2\text{Fe}_2\text{O}_5$  ist bei Raumtemperatur magnetisch geordnet, die Neél – Temperatur wird von [5] mit  $\approx 455^\circ\text{C}$  angegeben. Ziel unserer vorliegenden Untersuchungen im System  $\text{Ca}_2\text{Fe}_{2-x}\text{Al}_x\text{O}_5$  ist es, zum einen das Ausmaß der möglichen Substitution von  $\text{Fe}^{3+}$  durch  $\text{Al}^{3+}$ , die dabei einher gehende Änderung der Raumgruppe bei  $25^\circ\text{C}$  und die Verteilung von  $\text{Fe}^{3+}$  über die Oktaeder- und Tetraederposition der Struktur genau zu bestimmen, zum anderen auch das Hochtemperaturverhalten der einzelnen Mischkristalle (thermische Ausdehnung, Auftreten eines Pnma  $\rightarrow$  Ibm2 Phasenübergangs, Neél-Temperatur) eingehend zu untersuchen.

Zu diesem Zweck wurden insgesamt 20 pulverförmige Proben mit  $0 \leq x \leq 1.4$  bei Temperaturen von  $1200^\circ\text{C}$ , sowie zu Vergleichszwecken drei Proben bei  $1300^\circ\text{C}$  durch keramische Sinterung hergestellt (Versuchsdauer = 3 Wochen). Einkristalle bis zu 1 mm Größe konnten über eine Hochtemperatur-Lösungsmittelzüchtung unter Verwendung von  $\text{CaCl}_2$  als Mineralisator (Probe Flux = 1 : 3) durch langsames Abkühlen von  $1050^\circ\text{C}$  auf  $900^\circ\text{C}$  gezüchtet werden. An den als Einkristalle vorliegenden Proben wurden die Strukturen mit Röntgenbeugung am Einkristall verfeinert und daraus die Bindungslängen, -winkel sowie Verzerrungsparameter bestimmt. Die Kationenverteilung von  $\text{Fe}^{3+}$  und  $\text{Al}^{3+}$  über den Oktaeder- und den Tetraederplatz wurde sowohl aus den Einkristall-Datensätzen als auch über die Mößbauerspektroskopie bestimmt.

Wie in der Literatur beschrieben, kristallisiert reines  $\text{Ca}_2\text{Fe}_2\text{O}_5$  bei  $25^\circ\text{C}$  in der Raumgruppe Pnma,  $a = 5.4259(1)$  Å,  $b = 14.7632(2)$  Å,  $c = 5.5969(1)$  Å,  $V = 448.34(1)$  Å<sup>3</sup>. Der Phasenübergang von Pnma nach Ibm2 zeigt sich in unseren Messungen für  $\text{Ca}_2\text{Fe}_2\text{O}_5$  bei  $735^\circ\text{C}$ .

Der Einbau von  $\text{Al}^{3+}$  bewirkt ein Absinken der Gitterparameter. Besonders deutlich ist dies für den b- Gitterparameter zu beobachten, während in c-Richtung nur minimale Änderungen in der Gittermetrik auftreten. Die Änderung der Raumgruppe vom Pnma nach Ibm2 erfolgt bei 25°C bei  $\text{Al}^{3+}$  Gehalten zwischen  $x = 0.55$  und  $x = 0.60$ . Dies kann aus der Abnahme der integralen Intensität des Reflexes (131) sehr gut bestimmt werden. Mit den Phasenübergang sind keine nennenswerte Diskontinuitäten im Verlauf der Gitterparameter als Funktion des  $\text{Al}^{3+}$  Gehaltes verbunden. Der Einbau von  $\text{Al}^{3+}$  bewirkt auch ein Absinken der Temperatur des Pnma → Ibm2 Phasenüberganges. Für Zusammensetzungen mit  $x = 0.40$  liegt dieser bei 630°C, für  $x = 0.50$  bei  $\approx 450^\circ\text{C}$ . Ein genaues T-x Phasendiagramm für diese Änderung der Raumgruppe als Funktion von Temperatur und Zusammensetzung ist in Arbeit und wird vorgestellt. Ebenso erfolgt eine detaillierte Diskussion der Änderungen von strukturellen Parametern (Bindungslängen, -winkel, Polyederverzerrungen) als Funktion des  $\text{Al}^{3+}$  Gehaltes.

Das Mößbauerspektrum von  $\text{Ca}_2\text{Fe}_2\text{O}_5$  besteht aus zwei magnetisch aufgespaltenen Unterspektren, die auf Grund der  $^{57}\text{Fe}$  Mößbauerparametern eindeutig dem  $\text{Fe}^{3+}$  auf der Oktaeder-(O) und auf Tetraederposition (T) zugeordnet werden können. Das Verhältnis von  $\text{Fe}^{3+}$  auf O/T entspricht innerhalb des experimentellen Fehlers dem idealen Wert von 1:1. Sowohl Tetraeder als auch Oktaederposition zeigen eine für  $\text{Fe}^{3+}$  unüblich hohe Quadrupolaufspaltung (QS), die auf deutlich verzerrte Koordinationspolyeder hinweist. Die QS ist positiv für den Oktaederplatz und negativ für den Tetraederplatz, der polare Winkel  $\theta$  beträgt in beiden Fällen 85°. Mit zunehmendem Einbau von  $\text{Al}^{3+}$  werden die Spektren komplexer. Neben einem Unterspektrum für  $\text{Fe}^{3+}$  (O) können zwei Unterspektren für  $\text{Fe}^{3+}$  (T) beobachtet werden, die sich allerdings nur in der Größe des internen magnetischen Feldes  $H(o)$  am Kernort unterscheiden. Neutronenbeugungsuntersuchungen sind zur Klärung der magnetischen Spinstruktur in Planung. Bis zu einem  $\text{Al}^{3+}$  Gehalt von  $x = 1.1$  zeigen die Mößbauerspektren magnetisch aufgespaltene Unterspektren. Erst für Zusammensetzungen  $\geq 1.2$  liegt die Neél-Temperatur unterhalb von Raumtemperatur. Der Einbau von  $\text{Al}^{3+}$  erfolgt bei kleinen  $x$  vornehmlich auf der Tetraederposition. Auch bei  $\text{Al}^{3+}$  Gehalten über  $x = 1$  sind beide kristallographischen Plätze mit  $\text{Fe}^{3+}$  und  $\text{Al}^{3+}$  besetzt, wobei  $\text{Al}^{3+}$  den Tetraeder bevorzugt. Innerhalb der Mischkristallreihe zeigen sich keine Änderungen in der Größe der Quadrupolaufspaltung. Dies kann als ein Indiz gesehen werden für ein annäherndes Gleichbleiben der lokalen geometrischen/elektronischen Verzerrungszustände um die Eisenkerne.

## References

- [1] HANSEN, W. C. et al. (1928): Studies on the system calcium oxide-alumina-ferric-oxide. - J. Am. Ceramic Soc., 50, 396-408.
- [2] COVILLE, A. C. (1970): The crystal structure of  $\text{Ca}_2\text{Fe}_2\text{O}_5$  and its relation to the nuclear electric field gradient at the iron site. - Acta Cryst., B26, 1469-1473.
- [3] COVILLE, A. C. & GELLER, S. (1971) The crystal structure of brownmillerite,  $\text{Ca}_2\text{Fe}_2\text{O}_5$ . - Acta Cryst., B27, 2311-2315.
- [4] SMITH, D. (1962): Crystallographic changes with the substitution of aluminium for iron in Dicalcium ferrite. - Acta Cryst., 15, 1146-1152.
- [5] GELLER, S. et al. (1971): Crystal chemistry and magnetic structure of substituted  $\text{Ca}_2[\text{Fe}](\text{Fe})\text{O}_5$ . - Progress in Solid State Chemistry, Vol 5, 1-26.
- [6] KAHLENBERG, V., et al. (1998): Strukturelle Untersuchungen an  $\text{Ca}_2\text{Fe}_2\text{O}_5$  mittels Röntgen und Neutronenbeugung. - Europ. J. Mineral, 10, Beiheft 1, 147.

**MERCURY POLLUTED SITES IN CZECH REPUBLIC AND REMEDIATION TECHNOLOGY**

by

**J. Reif**

GEOtest Brno a.s.  
Šmahova 112, 65901 Brno

The soil and water contaminations with mercury in the Czech Republic are of technogenous character; these are mostly bounded to chemical factories in the towns of Neratovice and Ústí nad Labem, where obsolete electrolysis operations were located. Here, the production of NaOH and Cl<sub>2</sub> was kept going for tens of years, via the amalgam electrolysis of NaCl solution. This technology provides almost pure NaOH, containing very low levels of chlorides. Metal mercury used as the cathode, placed at the bottom of electrolyzers, does not enter the reaction and passes into products only in minimum quantities. The mercury is necessary to keep replenished; and all mercury migration pathways, except for the technological process, have not been explained in full.

Natural contamination with mercury comes into consideration only in locations where mercury ores (native mercury HgO, cinnabar HgS or calomel Hg<sub>2</sub>Cl<sub>2</sub>, oxyhydrochloride e.g. Hg<sub>2</sub>ClO, Hg<sub>4</sub>Cl<sub>2</sub>O was not observed) were exploited in the past [2]. There was a relatively small pocket Dědova Hora u Hořovic, that by far did not approach such metal contents as some European-important mercury mines, for example Idrija in Slovenia which represent strongly polluted area by mercury [4].

Environmental impact of mercury is done by possible methylation. This process was described by professional papers [6,9]. Products of methylation are monomethylmercury (CH<sub>3</sub>Hg<sup>+</sup>) and dimethylmercury (CH<sub>3</sub>-Hg-CH<sub>3</sub>). Consecutive changes of methylmercury was described as follows [3]: 2CH<sub>3</sub>Hg<sup>+</sup> + S<sup>2-</sup> ⇌ (CH<sub>3</sub>Hg)<sub>2</sub>S ⇌ (CH<sub>3</sub>)<sub>2</sub>Hg + HgS. The danger of organic substances that can evolve by mercury methylation is exemplified by the tragedy caused by organic mercury in Minamata, Kumamoto Prefecture in Kyushu [8]. Mercury poisoning has also occurred in countries including USA, China, Indonesia, Canada, Brazil and other [5, 6].

Mercury contamination in area of Neratovice town occurs within the foundation and vicinity of the building in which an old electrolysis technology was seated. For evaluation of the old ecological load, there were available results obtained from interpretation of 50 shallow boreholes [1]. Due to the irregular distribution of the observed contaminant, confirmed by investigation, the submitted scope of works is a compromise between the real demand of determination of the current status and the capability to finance the investigation within the given time period. The results of drilling work indicate that the rock environment below the building of the old electrolysis is very inhomogeneous; permeable layers (cinder, sand, gravel) diversify layers of low to very low permeability (various types of clay).

The man-made layer sickness ranges from 60 to 160 cm. The groundwater table level occurs between 1.15 and 2.80 m, mostly in an interval of 1.6 - 1.8 m. The borehole EL VIII confirmed an approximately 10 cm layer of grey-green compact clay at a depth of 5.2 m, and grey-green clayey shale underneath. The depth level corresponds to the occurrence of the aquitart represented by Turonian clays. The groundwater contamination is excessive namely in the area of the northern part of the building (max. 1000 mg/litre). The soil contamination maximum occurs below the central part of the building (max. 29187 ppm in dry soil). The way of selection of the remediation technology depends on the remediation target, which means on the establishment of the maximum acceptable residual contamination content in soil and on the remediation completion time period (which is given by the contamination migration potential regarding the surrounding environment). These criteria represent vector product responding to financial costs on the considered case of old ecological load. Another problem of the same importance as the establishment of the maximum acceptable residual contamination in the environment is the evaluation of the following possible processes which would take place (1) conservation of the existing state, (2) transfer of the environmental load to another environmental constituent, (3) decontamination.

In the event of disposal of Hg and Hg-compounds from the environment, we can proceed by combination of the selected remediation technologies depending on the established post-remediation limits, completion time horizon, and current real financial capabilities. The selected technologies and their evaluation are listed in the following Table 1.

Type of remediation technology	Environmental Contribution
Excavation of contaminated soil, landfill deposition	(1) Conservation
Contamination encapsulation	(1) Conservation
Underground cut-off walls with horizontal drainage, preventing lateral migration of Hg and Hg-compounds contamination	(1) Conservation
Sealing of subsoil by grouting, preventing further Hg penetration into subsoil but allowing capillary lift of methylated Hg	(1) Conservation (2) Transfer
In-situ vitrification using electrodes, subsequently providing reaction passivation of pollutant – most metastable chemically indefinable vitrified materials undergo devitrification with time	(1) Conservation (2) Transfer
Reaction underground barriers, bounding contaminants on active sorbents, providing reaction passivation of pollutant	(1) Conservation
Ex-situ chemical and physical separation of excavated soil, aimed at passivation of contaminant which remains in the environment as cinnabar, meta-cinnabar or other technogenous modification of HgS	(1) Conservation
Groundwater extraction preventing contamination migration, contaminated groundwater is pumped and treated to acceptable residual contaminant contents, (contaminant separation from water)	(3) Decontamination
In-situ electrochemical remediation using electrodes	(3) Decontamination
In-situ remediation by magnetic carriers with active surface ion exchanger (sorbent)	(3) Decontamination
Ex-situ thermal desorption of excavated soil, limited by contents of acids, caustics and organic substances which enter combustion processes	(3) Decontamination
Ex-situ chemical and physical separation of excavated soil, aimed at contaminant separation	(3) Decontamination
Microbial reduction of mercury, providing reduction of methylated Hg and complex-bound Hg to metallic Hg, separable in gravitational separators	(3) Decontamination

Table 1

*Summary of remediation technologies.*

## **References**

- [1] BARCHANEK, M. (1994): Závěrečná zpráva o výsledcích průzkumu znečistění horninového prostředí včetně podzemních vod pod budovou staré elektrolýzy a v blízkém okolí rtutí. - Archív GEOTest, str. 1-13. Nepublikováno.
- [2] BERNARD, J. H. et al (1981): Mineralogie Československa. - Academia. 645 stran. Praha.
- [3] CRAIG, P. J.(1986): Organometallic compounds in the environment, principles and reactions. - Longman Essex, 368p.
- [4] GOSAR, M., PIRC, S. & BIDOVEC, M. (1997): Mercury in the Idrijica River sediments as a reflection of mining and smelting activities of the Idrija mercury mine. - Journal of geochemical Exploration, 1496, 1-7. Elsevier.
- [5] GRAY, E. J.(2001): An overview mercury transport, cycling and environmental effects of mercury mining RMZ - Materials and Geoenvirónment, Vol. 48, No.1.pp.2-7, Ljubljana.
- [6] JAMES, A. I., WARWICK, J. J. & CARROLL, R. W. H. (2001): Advancements in modelling mercury transport and fate in dynamic fluvial system. RMZ – Materials and Geoenvironment, Vol. 48, No.1.pp.205-211, Ljubljana.
- [7] JENSEN, S. & JERNELÖV, A. (1969): Biological methylation of mercury in aquatic organisms. - Nature, 223, 753-754. London.
- [8] MASHIMOTO, T. (1996): Industrialization and Environment. The Association for Overseas technical Scholarship. - AOTS, 30-1, Senju-azumal-chome, Adachi-ku, Tokyo 120, Japan, 1-47.
- [9] POELSTRA, M., FRISSEL, N., VAN DER KLUGT, N. & BANNINK, D. W. (1973): Accumulation and distribution of mercury in Dutch soils. - Neth.J.agric.Sci. 21, 77-84.

MINERALOGY AND GEOCHEMISTRY OF IRON ORES FROM HORNÍ BENEŠOV DEPOSIT

by

J. Reif<sup>1</sup> & B. Fojt<sup>2</sup>

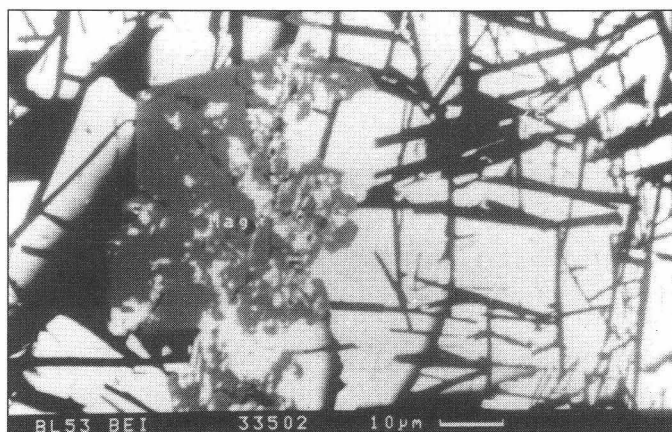
<sup>1</sup>GEOtest Brno a.s.

Šmahova 112, 65901 Brno

<sup>2</sup>Department of Mineralogy, Petrology and Geochemistry  
Masaryk University, Kotlářská 2, 611 37 Brno

The main stratabound ore deposit in the Jeseníky Mts. region (Zlaté Hory, Horní město and Horní Benešov – size according to decreasing intensity of regional metamorphism in the green schist facia) was interpreted as genetically equivalent – jointed by co-magmatic source of Devonian volcanites accompanied by small bodies of Lahn-Dill ores, commonly observed in the mentioned area [1]. The optimum object for the genesis study of polymetallic ores in Jeseníky Mts. seems to be the lower metamorphosed Horní Benešov deposit, being metamorphosed into metamorphic facies of prehnite-pumpellyite metagraywacke [2]. It contains some sedimentary relicts ores bearing many similarities to the accumulation of the polymetallic sulphides from the middle ocean ridges [5].

Detailed investigation on the lower metamorphosed Horní Benešov deposit proved that in the area there are two types of iron ores, which demonstrate mineralogical and geochemical significance [6]. The iron ores bear Pb, Zn, Ag sulphide ores in "Wester Devonian Scale" (type A) are accompanied by pyrite and represented by musketovite, magnetite with relicts of collo-morphous structure and with sporadic sphalerite, Fe-stilpnomelane, scarce siderite, rhodochrosite, Fe-rhodochrosite and mainly with occurrence of fine grained sheelite (see Picture 1).



Picture 1

Detail of scheelite – ferrostilpnomelane aggregate with automorphic magnetite crystal. Scheelite (white), ferrostilpnomelane (black needle), magnetite (black intergrows with white sheelite).

Other iron ores (Type B) are spatially bound to the "Central Devonian Scale", they are mineralogically identical with other occurrences of Lahn-Dill iron ores in Šternberk – Horní Benešov Belt. The mentioned differences in mineralogical compounds have direct consequences for microchemical composition of magnetite and pyrite, which is demonstrated by Table 1.

<b>Magnetite, Type A (Western Devonian Scales)</b>	<b>Magnetite, Type B (Central Devonian Scales)</b>
Zn (ppm) 123 – 1655 Ø 987 (13)*	Zn (ppm) 92 – 375 Ø 188 (5)*
V (ppm) 88 - 553 Ø 194 (13)	V (ppm) 190 - 887 Ø 612 (5)
Ti (ppm) 16 - 726 Ø 225 (13)	Ti (ppm) 19 - 265 Ø 115 (5)
V / Ti 0,3 – 18,3 Ø 3,7 (13)	V / Ti 1,8 – 10,8 Ø 7,4 (5)
$\delta^{18}\text{O}$ (‰ SMOW) from 2,5 to 6,7 Ø 4,7 (4)	$\delta^{18}\text{O}$ (‰ SMOW) from 8,4 to 8,5 Ø 8,5 (3)
<b>Pyrite, Type A (Western Devonian Scales)</b>	<b>Pyrite, Type B (Central Devonian Scales)</b>
Ni / Co 4,3 – 18,3 Ø 8,5 (9)	Ni / Co 1,0 – 2,9 Ø 1,7 (5)
$\delta^{34}\text{S}$ (‰ CDT) from -2,9 to + 20,4 Ø 10,3 (17)	$\delta^{34}\text{S}$ (‰ CDT) 17,0 až + 19,7 Ø 18,1(2)

*Table 1*

*Geochemical significance of magnetite and pyrite from two different type of iron ores, Horní Benešov, deposit.*

The presented observation and data illustrate not only the previously published theory of the origin of the Horní Benešov ore deposit by the type process of "hydrothermal cell" of Devonian sea basin in volcano-sedimentary conditions [3, 4] lead to the idea of the reinterpretation of the co-magmatic origin of the strataboud polymetallic sulphide deposits and Lahn-Dill type iron ores in Jeseníky region.

## References

- [1] HAVELKA, J., PALAS, M. & SCHARM, B. (1963): Nové pojetí metalogenese rud neželezných kovů jesenické provincie a jeho důsledky v geologickém průzkumu. - Geol. průzk. Roč. 5, 8, 225-227. Praha.
- [2] CHAB, J. & SUK, M. (1977): Regionální metamorfóza na území Čech a Moravy. - Knihovna Ústředního ústavu geologického, sv. 50, 5-156. Praha.
- [3] LARGE, D. E. (1983): Sediment-hosted massive sulphide lead-zinc deposits: an experimental model. - In: Short Course in Sediment-hosted stratiform lead-zinc deposits (SANGSTER, D. F.,ed.): 1-25. Victoria.
- [4] PLIMER, I. R. (1979): Sulphide rock zonation and hydrothermal alteration at Broken Hill, Australia. - Trans. Inst. Min. Metall. (Sec.B: Appl.Earth Sci.) 88, B 161.176.
- [5] REIF, J. (2000): Mineralogy of iron ores on Pb-Zn-Ag and barite Horní Benešov deposit. - Ph.D. theses, pp 1-49. Masaryk University, Brno.
- [6] REIF, J. & FOJT, B. (2000): Dva typy železných rud na lokalitě Horní Benešov v Nízkém Jeseníku. - Mineralogicko-petrologické Sympózium Magurka'2000, Editor: UHER, P., BROSKA, I., JELEN S., JANAK, M., p.35. Bratislava.

**GEOCHEMISCHE CHARAKTERISTIK PRIMÄRER UND SEKUNDÄRER  
BLEI-ZINKVERERZUNGEN DES GRAZER PALÄOZOIKUMS (STEIERMARK)**

von

**D.I. Reiter<sup>1</sup>, L. Weber<sup>2</sup> & W. Kiesl<sup>1</sup>**

<sup>1</sup>Institut für Geochemie

Universität Wien, Geozentrum, Althanstrasse 14, A-1090 Wien

<sup>2</sup>Montanbehörde

Denisgasse 31, A-1200 Wien

### **Einleitung**

Die Bergbaue auf silberhältige Blei- Zinkvererzungen des Grazer Paläozoikums erlebten ihre Blütezeit im 19. Jahrhundert. Die Bergbaue kamen jedoch um 1930 zum Erliegen.

Diese Blei- Zinkvererzungen, so auch jene von Arzberg, liegen in einer altpaläozoischen ober-ostalpinen Deckeneinheit, die diskordant und fernüberschoben auf dem kristallinen Untergrund auflagert: dem Gleinalm-Kristallin im Westen, dem Rennfeldkristallin im Norden und Nordosten, dem Angerkristallin im Osten bzw. Kristallin von St. Radegund im Süden. Im Süden taucht das Grazer Paläozoikum unter das Steirische Tertiär ab.

Die Vererzungen befinden sich ausschließlich in einer Beckenfazies in den basalen Anteilen des Deckenkomplexes und sind in die Arzbergschichten eingebunden.

Bei den Lagerstätten handelt es sich um stratiforme Blei-, Zink-, Barytvererzungen, die als SEDEX-Vererzungen anzusehen sind, (WEBER, L. 1990, 1997).

Dieser postuliert in seiner Arbeit eine synsedimentäre-exhalative Entstehung dieser Blei- Zink- vererzung, die im engen Zusammenhang mit einem Riftingereignis im Bereich ausgedünnter Kruste und der damit verbundenen Beckenentwicklung zwischen den Ablagerungsräumen der Rhannachfazies und Hochlantschfazies zu sehen ist.

Bestimmt wird die Bildung einer SEDEX-Lagerstätte durch folgende lagerstättenkonstruktive Parameter:

- Ein submarines Becken mit synsedimentären Bruchstrukturen, welche das Aufdringen hydrothermaler-metallhaltiger Lösungen begünstigen,
- Ein akzentuiertes Meeresbecken mit Schwellenzonen, da es beim Fehlen selbiger zur lateralen Verteilung der metallhaltigen Lösungen kommen würde,
- Ein synsedimentärer Vulkanismus, der einerseits als Antrieb und andererseits als Wärmequelle für die zirkulierenden Lösungen fungiert.

Diese lagerstättenkonstruktiven Voraussetzungen ermöglichen eine räumliche Differenzierung der verschiedenen Erze. Die unterschiedlichen Milieu-Bedingungen und die unterschiedlichen physikochemischen Gegebenheiten führten zu einer horizontalen und vertikalen Element-zonierung innerhalb des Beckens.

In der Blei-Zinklagerstätte Arzberg, in der insbesondere schichtkonkordante Vererzungen aufgeschlossen sind, wurden im Jahre 1996 im Zuge von Erweiterungsarbeiten im sogenannten "Nordschlag" diskordante (sekundäre) Vererzungen nachgewiesen, die wohl als jüngere Mobilisate interpretiert werden dürfen. Durch verschiedene Untersuchungsmethoden sollen die Charakteristika sowohl der primären als auch der sekundären Vererzung näher bestimmt werden.

### **Untersuchungsmethoden**

Die bisher durchgeführten Analysen mittels Massenspektrometer zur Ermittlung der Pb- und S-Isotope erbrachten die nachstehenden (vorläufigen) Ergebnisse:

Bei den S-Isotopen liegt eine merkliche Variation zwischen der primären und der sekundären Vererzung vor. Die  $\delta^{34}\text{S}$ -Werte der unter dem Binokular aussortierten Bleiglanze ergaben für die primäre Vererzung einen Mittelwert von +2.2 ‰ und für die sekundäre, mobilisierte Vererzung einen Mittelwert von +8.2 ‰. Die Erzproben weisen alle positive  $\delta^{34}\text{S}$ -Werte auf. Diese Werte lassen erstmals eine Differenzierung innerhalb der Lagerstätte, in eine primäre und eine sekundäre, mobilisierte Vererzung zu.

Die Blei-Isotopenanalysen lassen demgegenüber keine merkliche Drift zwischen der primären und der sekundären Vererzung erkennen, die Werte differieren lediglich um +/- 0.001 %. Die Berechnung des Bleimodellalters ergab jedoch Unterschiede hinsichtlich der primären und der sekundären Vererzung, die ebenso wie bei den S-Isotopen, eine Klassifizierung der Vererzung erlaubt.

Makroskopisch unterscheiden sich die primären von den sekundären Vererzungen durch feinste Verwachsungen im m-Bereich. Die typischen Minerale der Lagerstätte Arzberg sind Bleiglanz, Baryt, Pyrit, Magnetkies, Ilmenit, Magnetit, Siderit und untergeordnet Zinkblende. Die Gangart bilden Calcit, Dolomit und Quarz.

Äußerst schwierig gestalten sich die Untersuchungen an den Fluid Inclusions (FI), zumal die geringe Größe der Bläschen und der Einschlüsse deutliche Grenzen setzen. Die Fluid Inclusions der primären und der sekundären Vererzung sind offensichtlich miteinander verwandt, in sich jedoch völlig verschieden. Die bislang durchgeführten Analysen innerhalb der sekundären Vererzung ergaben Unterschiede bezüglich der Homogenisierungstemperatur (zwischen +36.4°C und +230°C). Hinsichtlich des Gefrierpunktes ergaben sich Werte zwischen -51°C und -67°C. Bei der Schmelztemperatur wurden Werte zwischen -6,9°C und +36°C festgestellt.

Die Analyse der Spurenelementgehalte in den Bleiglanzen mittels ICP-MS soll die Frage nach der Entstehung der Mobilisate abrunden.

### **Schlußfolgerung**

Das Ziel dieser Arbeit, durch verschiedene geochemische Analysenmethoden eine Differenzierung der primären und sekundären Vererzungen zu erzielen, konnte bereits durch die vorliegenden Untersuchungsergebnisse erreicht werden.

Die Projektarbeiten wurden aus Mitteln der Kommission für Grundlagen der Mineralrohstoffforschung der Österreichischen Akademie der Wissenschaften gefördert.

### **Literatur**

- [1] WEBER, L. (1997): Handbuch der Lagerstätten der Erze, Industriemineralien und Energierohstoffe Österreichs - Arch. f. Lagerstättenforschung Geol. B.-A., 19, p.343 ff.
- [2] WEBER, L. (1990): Die Blei-Zinklagerstätten des Grazer Paläozoikums und ihr geologischer Rahmen - Arch. f. Lagerstättenforschung Geol. B.-A., 12, p.39-41 ff.

**EVOLUTION OF TWO-MICA GRANITES IN THE SOUTH BOHEMIAN BATHOLITH**

by

**M. René**

Institute of Rock Structure and Mechanics  
Academy of Sciences of the Czech Republic, V Holešovičkách 41, 182 09 Prague 8

The South Bohemian batholith (SBB) is the largest granitoid complex ( $6\,000\text{ km}^2$ ) within the Bohemian Massif. It intruded high-grade metamorphic rocks (mainly various types of paragneisses and migmatites) of the Moldanubian zone. The SSB crops out in the area between Jihlava in the north and the Donau river in the south. Some parts of a batholith are partly covered by Cretaceous and Tertiary sediments of the České Budějovice and Třeboň basins. The SBB is a complicated intrusive complex built by many intrusions of granitoids of different types. Two mica granites are part of the younger Upper Carboniferous group. Their contacts with surrounding metamorphic complex are mostly sharp and discordant. Many of these magmatic bodies are totally undeformed except for the proximity of some major shear zones, where foliation is sometimes developed (Altenberg and Lásenice/Deštná subtypes). The most common Eisgarn type, described originally in southern part of the SBB is coarse-, medium- to fine-grained porphyritic or equigranular two-mica granite, which belongs to the S-type granitoids. Several varieties of two-mica granites built more than 90 % of the exposed surface of the SBB.

Two-mica granites on the Austrian side are designed as Eisgarn and Altenberg types, in the Czech part the structural and mineralogical variability of these granites is greater and here more various subtypes of two-mica granites can be delimited. On the base of gravimetric and gammaspectrometry measurements two-mica monzogranites and alkali-feldspar granites, which form younger stocks (Zvůle, Čerínek and Melechov stocks) can be divided as separate magmatic phase. For these stock granites are characteristic lower LREE/HREE and Th/U ratios.

For southern part of the SBB are typical medium-grained, more rarely coarse-grained muscovite-biotite porphyric granites of the Číměř subtype. In middle part of the SBB prevail medium-grained equigranular, sometimes drab porphyric two-mica granites of the Mrákotín subtype. Both subtypes are peraluminous granite with a value of A/CNK of 1.07 – 1.42. Their peraluminous character is expressed by the presence of magmatic andalusite, sillimanite and rare cordierite. In equigranular granites of the Mrákotín subtype is peraluminosity expressed also by often presented superiority muscovite above biotite. The same mineral compositions have granites in the northern part of the SBB (Kouty or Světlá subtype). For all these subtypes is characteristic higher ratio REE/LREE ( $\text{La}_N/\text{Yb}_N = 32 - 40$ ) and particularly remarkable negative Eu anomaly. There is a general decrease in compatible elements, LREE, Th, Zr with increasing Rb and Cs contents. The highest content of Th (40 - 46 ppm) was determined in muscovite-biotite granites of the Lipnice subtype that occur in northern part of the SBB.

These granites have also the highest value of LREE/HREE ratio ( $\text{La}_N/\text{Yb}_N = 32 - 42$ ). Variable, but very similar chemical composition of porphyric and equigranular subtypes of two-mica granites in the whole SBB support opinions about variable degree of partial melting of original pelite-dominated greywackes, which were the most probable source of granite melt of two-mica granites. Relatively smaller extend have fine-grained varieties of two-mica granites, which are sometimes delimited as independent subtypes (Sulzberg, Weitra, Trhové Sviny in southern part of the SBB, Bílý Kámen, Boršov, Pavlov and Jiřín in northern part of the SBB). Some of these subtypes are relatively enriched in Ba and Sr contents (Weitra, Boršov, Pavlov). Higher contents of Ba and Sr are also characteristic for fine-grained granites from the area between Besednice and Dobrkovská Lhotka in southern part of SBB, which contain older K-feldspars xenocrysts from older Weinsberg granite.

Relatively independent positions have two-mica granites of the Lásenice/Deštná subtype on western margin of SBB, which also form Klenov massif, NE-SW trending body northern of Jindřichův Hradec. Special positions have as well two-mica granites from small magmatic body between Linz and Altenberg in southern part of the SBB. For both varieties of two-mica granites is characteristic partly very strong deformation (ductile deformation, occurrence of mylonites) that is connected with NNO-SSW trending shear zones of the Rodl-Kaplice-Blanice system, which are evolved in the Early Permian extensional regime of central part of the Bohemian massif. In the Altenberg massif also occur numerous dykes of aplites. For part of these two subtypes of two-mica granites is typical plentiful occurrence of restites (inclusions of restitic biotite and sillimanite or xenoliths of biotite gneisses). Occurrence of variable in size xenoliths of biotite and sillimanite-biotite gneisses is also characteristic for other subtypes of two-mica granites in the whole SBB. The two-mica granites of the Lásenice/Deštná and Altenberg subtypes are also typical peraluminous granites with an elevated value of A/CNK (1.10 - 1.30). For both subtypes of granites are typical low contents of Zr and Th. Distribution of REE is particularly remarkable by decreasing of the all REE and by the absence of a negative europium anomaly. Origin of these both subtype of two-mica granites (Lásenice/Deštná and Altenberg) is connected with emplacement of early-evolved granite melt, that originated in conditions of the crustal melting during the thermal peak of the regional metamorphism.

The evolution of individual granite subtypes of the two-mica granites in the Moldanubian batholith is marked by variability in their mineral and chemical composition, which has been caused either by different composition of the protoliths or by different degree of partial melting. The lower proportion of REE and Zr in the Lásenice/Deštná and Altenberg subtypes is attributable to lower solubility by monazite, xenotime and zircon in granitic melt by lower temperature. The degree of partial melting of the source rocks, which influenced mineral and chemical composition of the individual granite subtypes to be the dominant process. Some variability of chemical composition of two-mica granites as expressed in variation of the Ba, Rb, Sr and REE contents can also be attributable to variability in composition of the source metasedimentary rocks that comprised both greywacke type rocks and rocks with a higher proportion of pelitic component.

Investigation of evolution two-mica granites of the Moldanubian batholith was supported by Ministry of Education of CR (Projects No. ME-458, ME-459).

**GEOCHEMICAL STUDY OF SELECTED MINOR ELEMENTS  
IN POLYMETALLIC NODULES AND CRUST FROM EASTERN PART OF  
CLARION-CLIPPERTON FRACTURE ZONE, PACIFIC OCEAN**

by

**K. Rezek<sup>1</sup>, J. Reif<sup>2</sup> & A. Pařízek<sup>3</sup>**

<sup>1</sup>Mineral Research Institute  
Vítězna 425, 28401 Kutná Hora, Czech Republic

<sup>2</sup>GEOtest Brno a.s.  
Šmahova 112, 65901 Brno, Czech Republic

<sup>3</sup>Interoceanmetal Joint Organization  
Szczecin, Poland

It becomes obvious that the deep sea mineral resources may be an important source of many valuable metals. They are the subject of commercial interests of industrialized countries. Superiority has been given to polymetallic nodules, cobalt crusts and massive polymetallic sulphides for their unique metal composition (e.g. copper, cobalt, nickel, manganese, iron, zinc, molybdenum, silver, gold), and the significant value of the selected rare earth elements (REE) and the platinum group elements (PGE) [1, 2, 3]. The latest investigation of the Clarion-Cliperton Fracture Zone (CCZ) within the Interoceanmetal (IOM) pioneer investor claim has been conducted to determine the major and minor metal elements, and namely the REE (La, Ce, Nd, Sm, Eu, Yb, Lu, Y) and the selected platinum group elements (Pt, Pd, Rh) in polymetallic nodules. The REE contents in powdered-nodule samples have been determined in the Mineral Resources Institute, Kutná Hora by the DCP-OES (Direct Content Plasma Optical Emission Spectrometry) method with a Beckmann Spectro Span IV on the Russian standard polymetallic nodules GSPN-3. The PGE analytical determination of PGE included ICP-MS method using the Canadian standards Astasol WGM and WPR in the laboratory of the Department of Geochemistry, Mineralogy and Natural Resources, Charles University, Praha.

The samples showed considerable differences in structure and texture. On the other hand, the analyses did not prove occurrence of any substantial mineralogical differences. The samples were represented by fine-grained mixtures of Mn-Fe hydrated oxides (todorokite > birnessite + goethite) and silicate phase (mica > plagioclase > potassium feldspar > smectite and amorphous silicate phase).

The contents of the major elements in the polymetallic nodules from the IOM area are given in Table 1; and the rare earth elements contents in Table 2.

Contents (mass%)	Depth (m)	Mn	Fe	Ni	Cu	Co	Mn/Fe	(Ni+Co+Cu).10
Min.	3415	15.79	0.21	0.73	0.59	0.07	1.63	14.1
Max.	4600	34.42	15.2	1.52	1.6	2.00	7.68	44.6
Mean	4352	30.37	5.96	1.25	1.23	0.18	5.3	26.6
Standard dev.	105	3.02	1.36	0.13	0.17	0.11	1.2	2.8

**Table 1**  
*Major elements.*

Contents (ppm)	La	Ce	Nd	Sm	Eu	Gd	Tb	Ho	Tm	Yb	Lu
Min.	100	80	80	17	1.0	16	0.8	3.7	1.5	1.9	0.4
Max.	460	940	340	67	22	113	10.3	31.5	5.7	17.4	3.2
Mean	227.3	392.7	217.3	35.3	10.6	48.9	3.6	7.5	3.0	6.9	1.4
Standard dev.	56.5	120.3	38.8	8.2	3.3	21.3	1.9	5.0	1.1	2.6	0.5

**Table 2**  
*Minor elements (REE).*

The PGE average contents in the polymetallic nodules were as follows: Pt - 55 ppb, Pd - 5.5 ppb, Rh - 6.3 ppb. The PGE average concentrations the nodular crust samples: Pt - 53.2 ppb, Pd - 7.2 ppb and Rh - 5.8 ppb. Three polymetallic nodules showed anomalous contents of Pt, in the range of 510 - 8100 ppb. Prominent positive correlation between Pt and the total content of REE, and also between Pd and Rh, were found. On the contrary, no relationship were proven in the case of Pt and Pd + Rh. The Pt distribution corresponds to the Weibull's partition law.

## References

- [1] GROMOLL, L. (1996): Geochemical Types of Polymetallic Nodules: An Application of Multivariate Analysis. Mar. - Geores. Geotech., No.14, pp 361-379.
- [1] KOTLINSKI, R. (1996): Morphogenetic Types of Polymetallic Nodules in the Clarion-Clipperton Ore Field. - International Seminar on Deep Sea-Bed Mining Technology, part II, pp. 1-12, Beijing.
- [1] KOTLINSKI, R., PARIZEK, A. & REZEK, K. (1997): Polymetallic Nodules – A Possible Source of Rare Earth Elements. - Proceedings of the Second Ocean Mining Symposium, Seoul, pp. 50-56, Korea.

**BRECKZIERUNG UND ENTMISCHTE TI-MAGNETITE IN OBSIDIANEN DER  
IKIZDERE REGION (RIZE/NE-TÜRKEI): HINWEISE AUF FÖRDERWEGE VON LAVEN ?**

von

**M.B. Sadiklar<sup>1</sup>, A. Hanedam<sup>1</sup>, K. Heide<sup>2</sup> & G. Völksch<sup>3</sup>**

<sup>1</sup>Jeoloji Bölümü

Karadeniz Teknik Üniversitesi, TR-61080 Trabzon

<sup>2</sup>Institut für Geowissenschaften

Abteilung für Mineralogie, FSU Jena, Burgweg 11, D-07749 Jena

<sup>3</sup>Otto-Schott-Institut

FSU Jena, D-07749 Jena

Auf dem Hochalm Büyük Yayla südlich der Küstenstadt Rize im NE der Türkei sind sehr mächtige (> 500 m) saure Naturgläser aufgeschlossen [1, 2]. Man kann sie in graue felsitische Rhyolith und schwarze bis rötliche Obsidiane unterteilen. In lithostratigraphischer Hinsicht liegen die Rhyolith tiefer als die Obsidiane und bilden somit die relativ älteren Partien des Glaskomplexes [3]. Der Übergang von Rhyolithen zu den Obsidianen erfolgt über eine Wechsel-lagerung, welche zuerst aus mm- bis cm- und später cm- bis dm-mächtigen Lagen von Rhyolith und Obsidian besteht. Nach oben hin werden die Obsidiane immer mächtiger und massiger.

Die kristallinen Phasen in den Obsidianen [4] erlangen mengenmässig keine grosse Bedeutung, aber sie sind dagegen relativ artenreich. Feldspäte (vor allem Orthoklas und Sanidin), Biotit, Apatit, Zirkon z.T. Hf-reich, Pyroxen, Anhydrit, Titanomagnetit, Magnetit, Hematit, Kupferkies, Pyrit u.a. sind die mikroskopisch beobachteten und mikrochemisch bewiesenen Mineralen.

Obwohl das Obsidianvorkommen eine Fläche von c.a. 7 - 8 km<sup>2</sup> bedeckt und eine grosse Mächtigkeit besitzt, konnten bis heute im Gelände keine garantiierte Förderwege der Laven gefunden werden. Dagegen tauchen an einigen Stellen der Obsidiane breckzierte Bereiche auf. An frischen Ausbrüchen solcher Bereiche sehen die Obsidiane "säulig" aus. Im Querschnitt zeigen diese "Säulen" einen Durchmesser von mm bis dm. Die aus Glas bestehenden Breckzien selbst sind mm- bis cm- gross und schwarz aussehend. Die Matrix zwischen den Breckzien besteht aus bräunlichem Glas.

In den Breckzien und der Matrix kommen Fe-Ti-Oxide vor, meist in Form von Titanomagnetiten. Fast alle Titanomagnetite in den Breckzien sind entmischt [5], während die in der Matrix kaum solche Erscheinungen aufweisen. Unentmischte Titanomagnetite treten auch in den schwarzen massigen Obsidianen in den oberen Bereichen des Gebietes auf, d.h. in jüngsten Partien.

Um die Zusammenhänge zwischen der Breckzierung der Obsidiane und der Entmischung der Titanomagnetite bestimmter Bereiche zu studieren, wurden im Labor an den Titanomagnetiten Temperversuche unter atmosphärischer Bedingungen durchgeführt. Zuerst wurden im Auflicht-Mikroskop unentmischt aussehende Titanomagnetite lokalisiert, phototechnisch aufgenommen und dann in einem elektrischen Ofen auf bis 1100°C temperiert. Nach der Abkühlung zeigten alle die vorher unentmischten Titanomagnetite hervorragende Entmischungen, die identisch waren mit denen in der Natur (Geschwindigkeit der Aufheizung bzw. der Abkühlung betrug 2°C/min). Daraus kann gefolgert werden, dass die Breckzierung der Obsidiane im Arbeitsgebiet nicht während des Abwärtsfliessens der Laven an der Erdoberfläche durch "Krustenbildung und Brechung" entstand, sondern eine Art von Schlottbreckzienbildung darstellt und die Entmischung der Titanomagnetite auf eine Temperung durch diese später hochdringenden sauren Laven basiert. Somit könnte besonders die Breckzierung der Obsidiane auf Förderwege der Laven hin-deuten.

## Literatur

- [1] HEIDE, K., SADIKLAR, M. B., GERT, K., VÖLKSCH, G. & HARTMANN, E. (1996): Obsidian from Büyükkale and Sirikli Tepe, EastPontides, Turkey: A Glass-Chemical Study. - Chemie der Erde. 56/4:313-322.
- [2] HANEDAN, A., SADIKLAR, M. B., HEIDE, K. & KLETTI, H. (2000): Mineralogische und chemische Zusammensetzung der felsitischen Rhyolithe von İkizdere (FIR) NE-Türkei. - Beih. Zum EJM, 12/1: 73.
- [3] SADIKLAR, M. B., HANEDAN, A., HEIDE, K. & KLETTI, H. (1999): Genetische Beziehung zwischen den Rhyolithen und den Obsidianen der İkizdere Region, NE-Türkei. - Beih. z. EJM, 11/1: 196.
- [4] SADIKLAR, M. B., HEIDE, K., KLETTI, H. & VÖLKSCH, G. (1997): Mikroparagenesen in Obsidianen des Rize-Massivs/Türkei. - Beih. z. EJM. 9/1: 302.
- [5] SADIKLAR, M. B. & HANEDAN, A. (1997): Entmischte Magnetite in Obsidian (İkizdere/NE-Türkei) und deren genetische Bedeutung. - Beih. z. EJM. 9/1: 301.

**HYDROGEOLOGY – WATER PROSPECTING AND MANAGEMENT SUPPORTED BY GIS**

by

**V. Schöffenegger & H. Kurzweil**

Institute of Petrology  
University of Vienna, Geozentrum, Althanstrasse 14, A-1090 Wien

The main tasks of this project carried out in an area of about 720 km<sup>2</sup>, Eastern Austria, were

- o Hydrogeological investigations, placing strong emphasis on the availability of subsurface water, with special consideration for renewal, dynamics and quality of waters

in connection with

- o Employment of a Geographic Information System (ArcView) for data management and to ensure uninterrupted collection of data to maintain up-to-date water conservation.

Brief background information concerning basic data, research methods, computer-drafted maps and graphics is shown on posters.

The project area is located about 120 km SSE of Vienna, Austria, east of the Central Alpine ridge, close to the Austrian/Hungarian border. Bounded by hills to the west, the area becomes rather flat open country to the east with a general discharge of water in this direction.

The regional geology is characterized by crystalline rocks mainly consisting of gneisses, quartzites etc., cropping out in the western part of the area, and a Tertiary sediments complex within the basin consisting of fine-grained sediments with intercalated sands and gravels acting as major ground-water reservoirs for this part of the country.

Changing sedimentary conditions as well as locally divergent tectonic evolutions limit availability of subsurface water. The large-scale groundwater renewal is restricted due to a very complicated hydrogeological situation, and also human activity becomes a criterion for restriction of ground-water resources development.

Based upon these data this research program has been created and carried out by the use of the following methods:

- o Hydrogeological reconnaissance of the area by mapping and data collection
- o Hydrogeochemical investigations of subsurface and surface water
- o Isotopic geophysical examinations of selected waters
- o Hydrological background information
- o Geophysical surveying by geoelectrics and seismic methods
- o Drilling activities, borehole geophysics and pumping tests
- o Sedimentary descriptive petrology

The great number of data obtained from these investigations were used afterwards to develop hydrodynamic pilot projections for drawing up an approximate groundwater balance model.

Furthermore, and this is the aim of this presentation, all data banks were transferred into a Geographic Information System (ArcView), and a group of people responsible for future use was entrusted with the entire project in digital form, in order to ensure an uninterrupted continuation of data collection and thus to maintain up-to-date water conservation data for the sustained and guaranteed drinking water supply of this area.

In order to make our system applicable in the most effective way, specific data banks, focusing on hydrological, hydrogeological or hydrogeochemical background information, should be available to access the Geographic Information System (ArcView) for successful and highly economic data management.

Data on hydrogeological research and water prospection data prepared and processed in this way have always attracted our customers who profit from this user-friendly method on account of its efficiency in linking even comprehensive databases in order to produce, compile, correlate, and print, without any delay, maps on varying subjects. A further advantage of this system is the possibility to insert and incorporate new data so as to update databases in a most efficient way – for instance, in the field of water supply, an uninterrupted collection of data on water quality, discharge and distribution requires an immediate digital data management to guarantee sustained water conservation and an uninterrupted supply of drinking water.

Development of strategic planning methodologies and scientific tools for the integrated management of water at catchment or river basin scale, taking into consideration the complex interaction between the natural and man made environments, the quality and quantity of water and the various uses of water.

The objectives are to support the development of integrated water management approaches at catchment or river basin scale.

The relation between the function and structure of aquatic ecosystems should be evaluated in order to distinguish between natural variability and anthropogenic impacts.

Development and demonstration of tools to determine socio-economic requirements for urban and suburban water management systems, and to evaluate the location and functioning of water supply. Assessment and auditing methods for water exchange between cities and their water supplying region.

**ZUR GEOCHEMISCHEN CHARAKTERISIERUNG VON LAGERSTÄTTEN**

von

**E. Schroll**

Institut für Mineralogie und Kristallographie  
Universität Wien, Geozentrum, Althanstrasse 14, A-1090 Wien

Die geochemische Charakterisierung geologischer Körper ermöglicht Gruppenbildungen, Klassifikation und genetische Abgrenzung. Bei Lagerstätten kommt es bisweilen zu Anwendungen dieser Methodik ohne vorliegende geologische Fakten und geochemische zu berücksichtigen.

Lagerstätten sind Sonderfälle der Petrogenese. Sie unterscheiden sich von den Massengesteinen durch eine überdurchschnittliche Anreicherung an Mineralen oder chemischen Elementen, die nutzbare Eigenschaften aufweisen. Sie werden daher nach wirtschaftliche Grundsätzen bewertet, die vom Bedarf und technologischem Fortschritt abhängig sind. Die geochemische Charakterisierung von Lagerstätten eher rückständig, obwohl gerade in der Lagerstättenexploration erhebliche Fortschritte in der Anwendung der Methoden der Geochemie erzielt worden sind. Dagegen ist heute die Anwendung petrochemischer und geochemischer Prinzipien zur Klassifikation und geochemischen Charakterisierung der Gesteine praktisch Routine geworden.

Die Rückständigkeit der Lagerstättengeochemie auf die Vielfältigkeit der Mineralparagenese und Elementassoziationen sowie auf Schwierigkeiten bei der Abgrenzung des Lagerstättenkörpers vom Nebengestein und bei der Entnahme representativer Proben zurückzuführen. Mehr ins Gewicht fällt jedoch die Abhängigkeit der wissenschaftlichen Aussagen vom Aufschlussgrad der Lagerstätte, der durch die Bergbauaktivitäten vorgegeben ist. Suche und Abbau von Rohstoffen richtet sich nach dem Bedarf sowie technischen und wirtschaftlichen Gesichtspunkten. Während in der Vergangenheit der Vorrat von einer Lagerstätte oft über ein Jahrtausends genutzt werden konnte, verkürzt sich heute durch maschinellen Einsatz die Lebenszeit eines Bergbaus je nach der Vorratslage bis auf Dezennien. Mit der Schließung eines Bergbaus ist in der Regel Besichtigung und Beprobung vor Ort nicht mehr möglich. Statt bergfrischen Proben stehen nur beschränkt lokalisierbares Probenmaterial aus Halden- und Sammlungsmaterial zur Verfügung.

Für das Aufsuchen und die Beurteilung von Rohstoffvorräten ist die Kenntnis der Genese der Lagerstätten von fundamentaler Bedeutung. Die Bodenschätze der Erde sind die einmalige Hinterlassenschaft der Evolution der Erdkruste und der Biosphäre. Dies unterstreicht die Notwendigkeit der geochemischen Charakterisierung von Lagerstätten. Die Möglichkeiten, Daten zu schaffen und zu verarbeiten, haben bereits einen hohen Standard erreicht. Die Analyse erfasst Atome, stabile und instabile Isotope und Moleküle.

Maßgebliche Objekte der Analytik sind technische Bergbauprodukte, wie Haufwerk oder Konzentrate, und für wissenschaftliche Zwecke Mineralphasen und Flüssigkeitseinschlüssen. Die In-situ-Analytik erschließt den submikroskopischen Bereich und verbessert die Einsicht in die Wachstumsgeschichte von Mineralen. Statistische Methoden und elektronische Datenverarbeitungstechniken ermöglichen die Bewältigung großer Datemengen. Für eine Methodik, bei der die multivariate Geostatistik benutzt wird, wurde der Terminus Geochemometrie vorgeschlagen (SCHROLL et al., 1996)1. Zur Zeit wird leider chemischen Daten zu wenig Bedeutung zugemessen, am ehesten noch in Hinsicht auf die Haupt- und Wertmetalle der Erzlagerstätten (SCHROLL, 2002).

Multivariate Messdaten eines geologischen Körpers stellen ein komplexes System korrelativer Beziehungen dar. Die Aussagen beschreibender Arbeitsmethodik, die sich vornehmlich bildlicher Darstellung bedient, gewinnen erst durch die Kontrolle mittels Messdaten allgemeine gültige Bestätigung. Extreme werden auch in der Wissenschaft zur Glaubensache. Allein aus der Bildhaftigkeit auf der Richtigkeit von Aussagen zu beharren, ist ebensowenig zielführend, Aussagen allein auf geochemischer Messdaten und deren Interpretation auzubauen. Man kann nicht darüber hinwegsehen, dass die klassischen Methoden der Lagerstättenkunde die Voraussetzung für die representative Beprobung und damit für die Anwendung der Methoden der analytischen Geochemie schaffen. So hat sich die Missachtung gefügkundlicher Befunde als Fehler erwiesen.

Geochemische Daten sind - unter Einschluss der geologischen und mineralogischen Fakten - das geeignete Hilfsmittel, um Lagerstätten objektiv zu vergleichen. Noch mangelt es an einheitlichen Datensätzen, wie ein Versuch am Beispiel von Stibnitlagerstätten in den Westkarpaten und Ostalpen zeigt (ANDRAS et al., 2000). Ergebnisse weiterer Untersuchungen sind trotzdem ermutigend, weil so ein Basis für eine einheitliche Interpretation der zeitlichen und genetischen Zuordnung geschaffen werden kann.

Dasselbe gilt für Gruppierung und Klassifikation anscheinend gleichartiger Erzmineralisationen, wie dies am Beispiel karbonatgebundener Pb-Zn-Lagerstätten der Fall gezeigt wurde (SCHROLL et al., 1996). Dabei ist die Schwefelisotopenverteilung eine charakteristische Eigenschaft. Schwefelisotope sind u.a. ein Indikator für bakteriogene Prozesse bei der Sulfatreduktion und ein wesentliches Kriterium für die Gliederung der karbonatgebundenen Pb-Zn-Vererzungen (SCHROLL, 2001). Die bakteriogene Mitwirkung wird durch zusätzliche Beobachtungen und Messdaten bestätigt (KUCHA et al., dieser Band). Siderit- und Magnesitlagerstätten sind in ihrer Genese umstritten. Als Ansatz für die genetische Gruppierung dieser karbonatischen Mineralisationen bieten sich die Sauerstoff- und Kohlenstoffisotope an. Versuche mit einer einzigen geochemischen Meßmethode, wie beispielsweise mit Hilfe der Analyse der Seltenen Erden, die genetischen Probleme zu lösen, halten der Konfrontation mit realen Fakten und anderen Daten nicht Stand. Generell ist in Betracht zu ziehen, daß die Interpretation von Daten vom jeweiligen Wissensstand abhängig ist..

Komplexe Naturprozesse, wie die Bildung von Lagerstätten, können nur mehr durch koordinierte Detailarbeit im lokalen und regionalen Rahmen sowie durch globale Zusammenschau unter Einbezug relevanter wissenschaftlichen Disziplinen entschlüsselt werden. Noch sind wesentliche Fragen der Lagerstättengenese unzureichend beantwortet, wie der Einfluss der Evolution der Erdkruste und der Lebensprozesse auf die Bildung von Lagerstätten, Herkunft und Transport der

Metalle, die hiefür erforderlichen Fluidumsätze sowie der Zusammenhang mit geotektonischen Ereignissen. In wissenschaftshistorischer Sicht bewegt sich der Stand der Erkenntnis in einer zeitabhängigen S-Kurve, die sich in ihrem oberen Abschnitt asymptotisch der Sättigung des Wissensstand nähert. Obwohl heute ein exponentieller Wissenszuwachs zu verzeichnen ist, sind wir in der Depositologie noch nicht allzu weit über den Wendepunkt der Erkenntniskurve hinausgekommen. Im Falle der geochemischen Charakterisierung von Lagerstätten wäre eine verstärkte Kooperation auf internationaler Ebene nötig.

## Literatur

- [1] SCHROLL, E., KÜRZL, H. & WEINZIRL, O. (1996): Geochemomerische Charakterisierung sedimentgebundener Blei-Zink-Vererzungen mittels Multivariate Techniken. - Berg- u. huttenm., Monatshefte 141, 156-164.
- [2] SCHROLL, E. (2002): Special metals in carbonate-hosted zinc-lead deposits. - Mineralium Deposita (im Druck).
- [3] ANDRAS, P. CHOVAN, M. & SCHROLL, E.: Comparison of antimony ore deposits of the Eastern Alpy and the Western Carpathians using geochemical data. - Abstracts, Carpathian- Balkan Geological Assoc. XVI Congress , Vienna 1998.,41, Geol. Surv. Austria.

**SUBMARIN-HYDROTHERMALE METALLANREICHERUNG IM JUNG-PROTEROZOIKUM  
UND METAMORPHogene WEITERENTWICKLUNG DER STRATIFORMEN  
W-SB-AU-ERZLAGERSTÄTTEN VOM “TYP WOXI” IN HUNAN, SÜDOST-CHINA**

von

**O. Schulz<sup>1</sup>, F. Vavtar<sup>1</sup>, X. X. Gu<sup>2</sup>, J. M. Liu<sup>3</sup> & M. H. Zheng<sup>2</sup>**

<sup>1</sup>Institut für Mineralogie und Petrographie

Universität Innsbruck, Innrain 52, A-6020 Innsbruck

<sup>2</sup>Department of Mineral Resources and Economics

Chengdu University of Technology, Sichuan, P.R.China

<sup>3</sup>Research Center of Mineral Resources and Exploration

Chinese Academy of Science, Beijing, P.R.China

Die polymetallische W-Sb-Au-Erzlagerstätte Woxi (Xiangxi) ist Typuslokalität für eine Serie von schichtgebundenen Anreicherungen in einem metallogenetischen Gürtel, der den Nordwesten der Provinz Hunan quert. Insbesondere das Xuefeng-Gebirge als Teil des NW-konvexen Bogens der Jiangnan-Orogenzone ist durch einen auffallenden Erzreichtum ausgezeichnet.

Schwach metamorphe Sedimentgesteine des mittleren und jüngeren Proterozoikums beherrschen mit einer monotonen Abfolge von pelitischen, siltigen bis psammitischen und kieseligen Schiefern und Phylliten die Region. Die über 10.000 m mächtigen Sedimente sind allerdings durch tuffitische Zwischenschaltungen auffallend bereichert.

Im Großbergbau Woxi sind in der Madiyi-Sedimentformation des Jung-Proterozoikums bis in die derzeitige Teufe von 650 m 12 stratiforme Erzlager auf geschlossen worden. Sie sind stratigraphisch gesehen auf ein 720 m mächtiges Sedimentpaket verteilt. Im Detail gesehen sind innerhalb von 200 m Sediment 6 Erzlager und in 130 m Sediment schon seit langer Zeit 4 Erzlager bekannt und in Abbau. Die Mächtigkeiten liegen statistisch gesehen um 0.30–1.50 m. Dabei handelt es sich in Einzelfällen auch um 1.50 m mächtiges Antimonitderberz, und um über 3 m mächtiges, laminiertes Scheeliterz. Die streichenden und im Schichtfallen bekannt gewordenen Längen reichen vorläufig an die 2300 bis 3500 m, dürften aber noch größer sein.

Das Erz der Schichterzkörper beinhaltet die Nutzminerale Antimonit, Scheelit und Gold, weiters Pyrit, Arsenkies, Wolframit, Bleiglanz, Zinkblende, Tetraedrit, Bournonit, Boulangerit, Gersdorffit, Kupferkies und Aurostibit. Begleitminerale sind: überwiegend Quarz, daneben Ankerit, Dolomit, Calcit, zurücktretend Baryt, Siderit und Apatit. Durch die feinschichtige Teilnahme von Nebengestein sowie durch die Einstreuung von sandigem und schlammigem Detritus im Erz sind noch zu ergänzen: Hämatit, Rutil, Anatase, Titanit, Leukoxen, Turmalin, Zirkon, Sericit, Kaolinit, Chlorit, Pyrophyllit und Semigrafit.

Die Bindung der teils stark, teils diskret angereicherten Erzminerale an den progressiven Sedimentaufbau in Form feinschichtiger Parallelgefüge, Schräg- und Kreuzschichten stellt einen genetisch signifikanten Hinweis auf einen primären sedimentären Ursprung dar. Außer dem Sedimentaufbau aus Erz und Begleitsediment bestätigen auch syndiagenetische Fältelungen, rupturelle Deformationen und lokale Erosionen mit geopetaler Relieffüllung eine polare sedimentäre Anreicherung des Erzes. Auch Sammelkristallisationen, Entröpfelungen, Mobilisationen und Neukristallisationen veränderten die Erzgefüge. Im Kontakt mit den Erzlagern entstanden bereichsweise schichtgebundene Netzwerkvererzungen und vererzte Deformationsbreccien.

Unmittelbares Erzträgergestein ist ein grünlichgrauer Pyrit-Ankerit-Chlorit-Quarz-Sericitschiefer. Er ist liegend und hangend von einer dunkelgrau-purpurroten Hämatit-Kieselschiefer-Bank (Hämatit-Sericit-Quarzit, Fe-Chert) umrahmt. Tuffitische Chloritlagen begleiten stellenweise die Schichterzkörper. Diese Leitgesteine und die Erzlager sind teils durch Wechsellagerung, teils durch scharfe Grenzen und teils durch allmähliche Übergänge, auch mit metasomatischem Stofftausch gekennzeichnet. Der Lagenbau im großen und im kleinen entstand durch einen lückenlosen Sedimentaufbau von feindetritischem allothigenem Sediment und authigener chemischer Anlagerung von "Fremdmineralen" in Form von Erz.

Mindestens drei Orogenesen und vermutlich Metamorphosen überprägten den Felsverband samt den Erzkörpern. Vor allem Zerrkluftvererzungen transversal zur Schichtung, in räumlichem Zusammenhang mit den Schichterzkörpern, bereichern die Vererzungstypen in der Lagerstätte. Groß- und Kleinfalten verformten, bzw. Gleitungsklüfte zerscherten die Gesteins- und Erzabfolge, führen selbst aber nur tektonisch verschlepptes Erz.

Trotz der metamorphogenen Überprägungen sind im kristallinen Erz noch ursprüngliche Gefüge aus der synsedimentären Entstehungsphase als Relikte durch Abbildungskristallisation erhalten. Das Gefüge der prämetamorph entstandenen Metallanreicherungen zeigt typische Erztektonite mit teilweiser Rekristallisation. Der metamorphosierende Einfluß läßt auf Grund von Mineralneubildungen und dem Carbonifizierungsgrad von Phytodetritus auf eine Subgrünschieferfazies schließen.

Geochemische Untersuchungen von Haupt- und Spurenelement- sowie Isotopen-Zusammensetzungen ( $\delta^{34}\text{S}$ ,  $\delta\text{D}/\delta^{18}\text{O}$ ,  $\delta^{13}\text{C}/\delta^{18}\text{O}$ , Gesteins- und Erzblei, Flüssigkeitseinschlüsse) bestätigen und erweitern die lithologischen, tektonischen, mineralogischen und petrologischen Befunde. So finden wir bestätigt, daß es sich bei den Ausgangsgesteinen des enormen proterozoischen Sedimentstapels um vorwiegend granitoide und intermediäre Magmatite und deren metamorphe Äquivalente handelt. Der chemische Index der Alteration (CIA) spricht für Verwitterung in einem gemäßigten Klimabereich. Die nur gering gestreuten  $\delta^{34}\text{S}$ -Werte um -2 ‰, gemessen an Antimoniten, lassen den Schluß auf eine homogene, abioogene S-Herkunft zu. Die  $\delta^{13}\text{C}$ - und  $\delta^{18}\text{O}$ -Daten der Karbonatgesteine und Erzcalcite unterscheiden sich nur gering durch leichteren C im Erzcalcit. Das Verhältnis  $\delta\text{D}/\delta^{18}\text{O}$  fällt mit weiter Streuung in einen Bereich, in dem sich magmatische und metamorphogene Wässer überschneiden. Die Modellalter der Erzbleie liegen mit 800–900 Mio. Jahren im Rahmen der Gesteinsalter. Allgemein besteht, mit Einbeziehung einer Reihe von Lagerstätten gleichen Vererzungstyps, eine enge Beziehung zwischen Begleitgestein und Erz. Flüssigkeitseinschlüsse, gemessen an Quarz, Scheelit und Calcit, ergeben Homogenisierungstemperaturen von 95°–185°C. Die geochemischen Daten beziehen sich selbstverständlich auf die relativ jungen Kristallisationen des metamorphen Erzes.

Der erzreiche metallogenetische Gürtel im Norden der Provinz Hunan dürfte in einem tiefen Randmeerbecken über einer, zwischen zwei alten Kontinentblöcken gelegenen ozeanischen Subduktionszone entstanden sein. Aufschmelzungsprozesse und Magmatismus könnten einen Hydrothermalkreislauf in Gang gebracht haben, der zu einer extrusiven Belieferung und Ausfällung von Metallen am Meeresboden geführt hat.

## Literatur

- GU, X. X., LIU, J. M., ZHENG, M. G., SCHULZ, O. & VAVTAR, F. (2000): Fabric and Geochemical Evidence for the Submarine Exhalative Sedimentary Origin of the Woxi W-Sb-Au Deposit, Hunan. - Bulletin of Mineralogy Petrology and Geochemistry, vol.19, 4, 235-238. Guiyang, China.
- GU, X. X., SCHULZ, O., VAVTAR, F., LIU, J. M. & ZHENG, M. H. (2000): Jung-proterozoische submarine Primärerichierung und metamorphogene Weiterentwicklung der stratiformen W-Sb- Au-Lagerstätten vom "Typ Woxi" in Hunan (Süd-China). - (Im Druck).

DATING OF ANDALUSITE BY GECHRONOLOGICAL METHODS  
(SM-Nd AND U-Pb) – A FAILURE

by

R. Schuster & U. Klötzli

Institute of Geology  
University of Vienna, Geozentrum, Althanstrasse 14, A-1090 Vienna

**Introduction:** Andalusite, sillimanite and cordierite are index minerals for high-temperature/low-pressure (HT/LP) metamorphic rocks. These rocks occur in different tectonic settings related to contact metamorphism, exhumation of thickened crust or lithospheric extension. Their formation age respectively the formation age of their peak metamorphic assemblages is of interest for some geodynamic questions. If they formed during contact metamorphism this age can be determined by dating the intrusion age of the related magmatic body. For the other cases dating is much more difficult because of the following reasons: The HT/LP assemblages contain andalusite, sillimanite, biotite, plagioclase, muscovite and quartz, whereas garnet suitable for dating by the Sm-Nd method is not in equilibrium with the HT/LP assemblage, respectively it is consumed by the aluminumsilicat-forming reactions. On the other hand dating of zircon or monazite by the U-Pb method is problematic, because it is difficult to prove their formation during the peak of the HT/LP event. The most convenient age determination would be dating of the index minerals andalusite, sillimanite or cordierite itself. Being aware of the bad chance, but facing that it has not been reported before, we launched dating of metamorphic and magmatic andalusite.

**Analytical techniques:** Minerals used for isotope determinations were hand-picked under a binocular microscope, except biotite which was separated on a vibrating table and by grinding in alcohol. Chemical sample digestion and element separation for the Sm-Nd method follows standard procedures [1]. To remove surface contaminations minerals were leached in 2.5 N HCl before decomposition for 5 minutes. Overall blank contributions are  $\leq 0.2$  ng for Nd and Sm. Errors quoted in table 1 correspond to  $2\sigma$  of the block mean (1 block = 10 isotope ratios). The  $^{143}\text{Nd}/^{144}\text{Nd}$  ratio for the La Jolla international standard during the course of this investigation was  $0.511846 \pm 8$  (35 runs). Errors for the  $^{147}\text{Sm}/^{144}\text{Nd}$  ratio are  $\pm 1\%$ , or smaller, based on iterative sample analysis and spike recalibration. The U/Pb leaching experiment was performed on 50.7 mg of andalusite with grain size 0.20 to 0.25 mm. It includes one cleaning step (A), three leaching steps (B: 1N HBr + 6N HCl, 2h, 70°C; C: 1N HBr, 16h, 70°C; D: 15N HNO<sub>3</sub>, 16h, 70°C) and complete dissolution (E: HF+ HNO<sub>3</sub>, 48h, 170°C). Element separation follows the normal U/Pb method of titanite [2].

**Sample material:** Three samples from Austroalpine basement units have been investigated: Samples RS13/97 [3] and NM93/128 [4] represent Al-rich metapelites with a polyphase metamorphic history. Andalusite formed by the breakdown of Variscan staurolite during a Permo-Triassic HT/LP event. It developed by the reaction  $\text{St} + \text{Ms} \leftrightarrow \text{And} + \text{Bt} + \text{Qtz} + \text{H}_2\text{O}$ . In both cases andalusite exhibits up to 1 cm large porphyroblasts which form a significant part of the rock. The third sample (92T32) is an andalusite-muscovite-quartz vein. Andalusite was separated from a several centimeter large, pinkish colored, euhedral crystal. A Variscan formation age of the vein is suggested by geochronological age data from the sample area [5].

**Results:** Andalusite from sample RS13/97 contains 0.25 ppm Nd and 0.035 ppm Sm. It is characterised by lower  $^{147}\text{Sm}/^{143}\text{Nd}$  and  $^{144}\text{Nd}/^{143}\text{Nd}$  ratios than the whole rock and two biotites. The spread of all four data points is too low to calculate an isochron age. Concentrations of 8.2 ppm Nd and 1.4 ppm Sm have been found in andalusite of sample NM93/128. Within the error bars andalusite shows the same isotopic ratios than the whole rock and the biotite but lower ratios than plagioclase. The much higher concentrations of Sm and Nd and the similar isotopic ratios might indicate a contamination of the andalusite by inclusions of REE-rich minerals such as zircon or monazite. Magmatic andalusite of sample 92T32 exhibits very low concentrations of 0.019 ppm Nd and 0.012 ppm Sm and a higher  $^{147}\text{Sm}/^{143}\text{Nd}$  and  $^{144}\text{Nd}/^{143}\text{Nd}$  ratio than the metapelites. The higher ratios might be due to partial melting during the mobilisation of the vein material.

Sample	unit / locality	Nd [ppm]	Sm [ppm]	$^{147}\text{Sm}/^{144}\text{Nd}$	$^{143}\text{Nd}/^{144}\text{Nd}$	+/-2s <sub>m</sub>
RS13/97 WR	Strieden Complex,	79,610	12,982	0,09856	0,511859	5,7E-06
RS13/97 And	Carinthia (Austria)	0,245	0,035	0,08545	0,511834	1,3E-05
RS13/97 Bt1		1,726	0,359	0,12590	0,511923	1,8E-05
RS13/97 Bt2		1,199	0,252	0,12697	0,511952	1,0E-05
NM93/128 WR	Öbrennberg-Kaltes	47,626	8,286	0,10516	0,511882	6,2E-06
NM93/128 Pl	Bründl Serie,	1,109	0,214	0,11682	0,511903	7,1E-06
NM93/128 And	Burgenland (Austria)	8,186	1,407	0,10389	0,511873	6,2E-06
NM93/128 Bt		2,399	3,296	0,83049	0,511871	1,1E-05
92T32 And	Ötztal C., Tyrol (Austria)	0,019	0,012	0,37968	0,512135	9,3E-06
sample	step	U [ppm]	Pb [ppm]	% Pb rad	Th/U	$^{207}\text{Pb}/^{206}\text{Pb}$
RS13/97 And	B	0.242	4.526	7.6	1.472	0.4432
	C	1.571	17.365	16.4	3.075	0.1732
	D	1.155	10.325	16.9	3.146	0.1841
	E	0.016	4.091	21.5	3.447	0.1632
						$^{207}\text{Pb}/^{235}\text{U}$
						$^{208}\text{Pb}/^{238}\text{U}$

Table 1

Sm-Nd and U-Pb analytical data from mineral concentrates and whole rocks.

Assuming that the andalusite preparate of sample RS13/97 was not contaminated by other mineral phases, it was used for investigations by the U/Pb leaching method. Observed concentrations are 0.016 to 1.57 for U and 4.09 to 17.4 for Pb. U/Th ranges from 1.5 to 3.4 and is comparably low. The content of radiogenic Pb is low and varies (7.6 - 21.5 %) during the leaching experiment. Obviously it is not possible to separate the common Pb component from the radiogenic lead with the applied leaching procedures.

It is therefore concluded, that the common Pb is included in the crystal lattice and not in the form of inclusions. Calculated  $^{207}\text{Pb}/^{206}\text{Pb}$ ,  $^{207}\text{Pb}/^{235}\text{U}$  and  $^{206}\text{Pb}/^{238}\text{U}$  ages are scattering and give no geological information. This might be due to primary unequilibrium or problems of the leaching technique. A Pb-Pb errorchron yields c. 2.0 Ga, a typical average "age" value for the Alpine basement units.

Conclusions: Pure andalusite is poor in Sm, Nd, U and Pb. Andalusite is fractionating the LREE and therefore it exhibits lower  $^{147}\text{Sm}/^{143}\text{Nd}$  and  $^{144}\text{Nd}/^{143}\text{Nd}$  ratios than the whole rock. The U-Pb leaching experiment yielded complex mixtures of common and radiogenic lead, leading to disequilibrium and meaningless age informations. Andalusite is not suitable for geochronological dating by the Sm-Nd method or the applied U-Pb leaching technique.

## References

- [1] THÖNI, M. & JAGOUTZ, E. (1992): Some new aspects of dating eclogites in orogenic belts: Sm-Nd, Rb-Sr and Pb-Pb isotopic results from the Austroalpine Saualpe and Koralpe type-locality (Carinthia/Styria, SE Austria). - *Geochim. Cosmochim. Acta*, 56: 347-368.
- [2] PERRISH, P. P., RODDICK, J. C., LOVERIDGE, W. D. & SULLIVAN, R. W. (1987): Uranium-lead analytical techniques at the geochronology laboratory, Geological Survey of Canada. - *Geol. Surv. of Canada Paper*, 87/2: 3-7.
- [3] SCHUSTER, R., SCHARBERT, S. & ABART, R. (1999): Permo-Triassic crustal extension during opening of the Neotethyan ocean in the Austroalpine-South Alpine realm. - *Tübinger Geowissenschaftl. Arb., Serie A*, 52: 5-6.
- [4] DRAGANITS, E. (1998): Seriengliederung im Kristallin des südlichen Ödenburger Gebirges (Burgenland) und deren Stellung zum Unterostalpin am Alpenostrand. - *Jb. Geol. B.-A.*, 141: 113-146.
- [5] THÖNI, M. (1981): Degree and evolution of the Alpine Metamorphism in the light of K/Ar and Rb/Sr age determinations on micas. - *Jb. Geol. B.-A.*, 124/1: 111-174.

**INDICATIONS FOR A PERMO-TRIASSIC METAMORPHIC IMPRINT IN THE  
AUSTROALPINE CRYSTALLINE ROCKS OF THE DEFREGGEN ALPS (EASTERN TYROL)**

by

**R. Schuster<sup>1</sup>, A. Proyer<sup>2</sup>, G. Hoinkes<sup>2</sup> & B. Schulz<sup>3</sup>**

<sup>1</sup>Institute of Geology

University of Vienna, Geozentrum, Althanstrasse 14, A-1090 Vienna

<sup>2</sup>Institute of Mineralog and Petrology

University of Graz, Universitätsplatz 2, A-8010 Graz

<sup>3</sup>Institute of Mineralogy

TU Bergakademie, Brennhausgasse 14, D-09596 Freiberg

In the past years a widespread Permo-Triassic high temperature/low pressure metamorphic (HT/LP) imprint of various grade has been recognised within the Austroalpine units [1][2]. We discuss the effects of this imprint for the Austroalpine unit in the Defereggener Alps. From the Uttenheim area, that forms the continuation to the west, "late Variscan" pegmatites and a HT/LP metamorphic imprint have been reported [3]. New geochronological data from the southern part of the Defereggener Alps demonstrates striking analogies to the Austroalpine unit in the Kreuzeck-Goldeck-Drauzug section c. 50 km in the east:

In the Kreuzeck-Goldeck-Drauzug, a section through a Permo-Triassic middle and upper crust and overlying sediments has been preserved [4]. The HT/LP imprint shows a characteristic zonation expressed in mineral assemblages, the occurrence of pegmatites and typical cooling ages for different structural levels. From the petrological point of view, a deeper sillimanite-zone with local anatexis, an upper sillimanite-zone with relicts of staurolite, an andalusite-zone and a zone of preserved pre-existing assemblages can be distinguished from bottom to the top [5]. Synmetamorphic pegmatites are frequent in the sillimanite-zone and die out in the andalusite-zone, where andalusite-quartz veins occur within staurolite and garnet-rich layers. Magmatic feldspars in the pegmatites exhibit syn- to post-intrusive ductile deformation at temperatures above 500°C. Formation ages of garnets from the pegmatites, determined by the Sm-Nd method are  $260 \pm 30$  Ma. Ar-Ar data from muscovite in the pegmatites and surrounding schists, yield plateau ages of  $190 \pm 10$  Ma which are interpreted as cooling ages below c. 400°C. Those from the andalusite zone are  $210 \pm 10$  Ma. Going upward in the section plateau-type Ar-Ar cooling ages increase up to c. 270 Ma until saddle-shaped age spectra with total gas ages of 270 to 310 Ma occur. Rocks below the transgressive Permo-Mesozoic sequences of the Drauzug experienced less than c. 400°C during the Permo-Triassic thermal event and exhibit Variscan Ar-Ar plateau ages of c. 310 Ma. The sequence is interpreted as the result of Permo-Triassic lithospheric extension, subsequent thermal relaxation and sedimentation of the cover series [4].

The Austroalpine basement of the Deferegger Alps is situated between the Penninic Tauern Window to the north and the Periadriatic Lineament to the south. It is subdivided by the Oligocene Defereggen–Antholz–Vals-Line (DAV) which is marked by slices of anchizinal lower Triassic sediments [6]. Both subunits show lithological similarities, but the northern one experienced a more intense Alpine overprint. The structurally deepest parts of the southern unit are cropping out immediate to the south of the DAV and in the core of an anticline in the Michelbach valley. The rock series consists of sillimanite-bearing biotite schists and biotite-plagioclase gneisses with intercalations of pegmatites, amphibolites and marbles [7]. In the metapelites sillimanite is intergrown with biotite and aligned to the dominant schistosity of the rocks. Sillimanite also forms millimeter-sized patchy pseudomorphs after garnet, indicative of prograde breakdown of garnet by  $\text{Grt} + \text{Ms} \leftrightarrow \text{Sil} + \text{Bt} + \text{Qtz} + \text{H}_2\text{O}$ . The pegmatites are mostly concordant and exhibit a magmatic mineral assemblage of  $\text{Grt} + \text{Tur} + \text{Kfsp} + \text{Pl} + \text{Qtz} + \text{Ms}$ . Garnet occur as up to 4 mm large ikositetraeders, the tourmalines are optically zoned. A ductile deformation which started at more than 500°C and continued to lower temperatures is expressed by dynamic recrystallisation and wavy extinction of feldspar and quartz. Above the sillimanite-bearing zone, fine grained biotite-plagioclase gneisses with intercalations of staurolite and/or garnet-rich micaschists occur [8]. Andalusite-quartz veins have been observed within the micaschists. The upper part of the unit is formed by garnet-micaschists, orthogneisses and phyllitic micaschists which continue into the Thurntal quartzphyllites [8].

Pegmatites also occur within biotite-rich schists and gneisses of the northern unit. Those from the Uttenheim area are interpreted as partial anatetic melts from the residual sillimanite-biotite schists. They formed during a HT/LP event at  $650 \pm 30^\circ\text{C}$  and  $0.6 \pm 0.1 \text{ GPa}$  [3]. To the east near Radlach a spodumene-bearing pegmatite has been found. A Permian age for the pegmatites from the Uttenheim area is confirmed by a Rb-Sr whole rock isochron of  $262 \pm 7 \text{ Ma}$  [9]. From the Michelbach valley, a Sm-Nd garnet isochron yields a Permian age of  $253 \pm 7 \text{ Ma}$  from the pegmatite. An Ar-Ar age on muscovite from the surrounding sillimanite-biotite-schist yielded  $193 \pm 2 \text{ Ma}$  and is interpreted to date cooling below c.  $400^\circ\text{C}$ . It is identical to those of the sillimanite-zone from the Kreuzeck area. The Rb-Sr isochron age of biotite from the same sample is  $204 \pm 2 \text{ Ma}$ . As closure temperatures for the Rb-Sr isotopic system in biotite are expected to be around  $300^\circ\text{C}$  and since the age was not reset during a later event, Alpine temperatures did not exceed  $300^\circ\text{C}$ . These observations signalize a Permian age of the high-temperature ductile deformation of the pegmatites, and implies a similar minimum age of the HT/LP imprint of the surrounding rocks.

Summarising the data the following conclusions can be deduced: The Austroalpine crystalline rocks from the Deferegger Alps experienced a Variscan metamorphic imprint [3] [8]. During Permo-Triassic times, extension of the lithosphere caused an elevated geothermal gradient and a HT-LP imprint. At middle crustal levels, sillimanite-bearing assemblages developed and pegmatites were emplaced. Subsequent cooling to the steady state geotherm produced Ar-Ar cooling ages of c.  $190 \text{ Ma}$  in the sillimanite-zone. In the southern block the Alpine temperatures were just below  $300^\circ\text{C}$ , in the northern unit upper greenschist facies conditions were reached [3].

## References

- [1] SCHUSTER, R., SCHARBERT, S. & ABART, R. (1999): Permo-Triassic crustal extension during opening of the Neotethyan ocean in the Austroalpine-South Alpine realm. - Tübinger Geowissensch. Arb., Serie A, 52: 5-6.
- [2] THÖNI, M. (1999): A review of geochronological data from the Eastern Alps. – Schweiz. Mineral. Petrogr. Mitt., 79/1: 209-230.
- [3] STÖCKHERT, B. (1987): Das Uttenheimer Pegmatitfeld (Ostalpines Altkristallin, Südtirol) Genese und alpine Überprägung. - Erlanger geol. Abh., 114: 83-106.
- [4] SCHUSTER, R. & FAUPL, P.: Permo-Triassic sedimentary record and contemporaneous basement evolution in the Drauzug-Goldeck-Kreuzeck transsect (Eastern Alps/Austria). - Mitt. Österr. Mineral. Ges., 146.
- [5] HOKE, L. (1990): The Altkristallin of the Kreuzeck Mountains, SE-Tauern Window, Eastern Alps - Basement Crust in a Convergent plate Boundary Zone. - Jb. Geol. B.-A., 133: 5-87.
- [6] STÖCKHERT, B. (1982): Deformation und retrograde Metamorphose im Altkristallin S' des westlichen Tauernfensters (Südtirol). - Thesis, Univ. Erlangen: 214pp, Erlangen.
- [7] SENARCLENS-GRANCY, W. (1972): Geologische Karte der westlichen Deferegger Alpen 1:25 000. - Geol. B.-A. Österreich, Wien.
- [8] SCHULZ, B., SIEGESMUND, S., STEENKEN, A., SCHÖNHOFER, R. & HEINRICH, T. (2001): Geologie des ostalpinen Kristallins südlich des Tauernfensters zwischen Virgental und Pustertal. - Z. dt. geol. Ges., 152 (in print).
- [9] BORSI, S., DEL MORO, A., SASSI, F. P., VISONA, D. & ZIRPOLI, G. (1980): On the existence of Hercynian aplites and pegmatites in the lower Aurina valley (Ahrntal, Austrides, Eastern Alps). - N. Jb. Miner. Mh., 1980/11: 501-514.

**MINERALS IN DIAMOND AGGREGATES AND MINERAL INCLUSIONS IN DIAMONDS:  
A COMPARISON**

by

**N. V. Sobolev, A. M. Logvinova & E. S. Yefimova**

Institute of Mineralogy and Petrography  
Russian Academy of Sciences, Siberian Branch, 3 Koptyug Ave, 630090 Novosibirsk, Russia

Minerals associated with diamonds from kimberlites and lamproites are represented by inclusions isolated within diamonds and intergrowths with polycrystalline diamond aggregates which are composed of microdiamond crystals of varied size and are described as boart, framesites [1, 5] or diamondites [3]. Series of Mg- and Cr-enriched minerals represent the ultramafic or peridotitic suite (U-type) and minerals (mostly garnets and pyroxenes) with varied Mg, Fe, Ca and Na represent eclogitic (E-type) suite with transitional type referred to as websterite-pyroxyenitic suite [1, 4, 8]. Diamond aggregates containing variable minerals are described from Yakutian diamond mines, in particular from the Mir pipe [7-10] with rare occurrences from Udachnaya, Yubileynaya, Sytykanskaya pipes. South African diamond mines also contain such aggregates, which are described for Orapa, Venetia and Premier [1-3, 6].

About 80 % of approximately 200 studied worldwide samples of diamond aggregates, containing U-type and E-type minerals are collected from the Mir pipe, Yakutia [7-11 and unpublished data by the authors]. Both harzburgitic (about 40 %) and lherzolitic (about 60 %) pyropes occur in diamond aggregates from this pipe, which confirm earlier observations [8]. More than 100 chromite samples known only from Yakutian diamond aggregates contain on average lower MgO and Al<sub>2</sub>O<sub>3</sub> compared with chromites included in diamonds, which is in agreement with earlier data [9].

We conclude that garnets, chromites and pyroxenes occurred in diamond aggregates are, in general, similar in their assemblages and compositions to the same minerals included in diamonds. However, some clinopyroxenes, especially, rich in Cr and Na represent a notable exception. They contain up to 15.6 wt.% Cr<sub>2</sub>O<sub>3</sub> and 10.1 wt.% Na<sub>2</sub>O [8]. E-type garnet compositions from Mir diamond aggregates cover all range for similar garnets included in diamonds worldwide [4, 11]. Temperature of equilibration of chromite bearing aggregates varies mainly from 900 up to 1050°C [10] which is relatively lower than that of similar diamond inclusions. The detailed geochemical study of minerals from diamond aggregates [2, 3] especially, for the same kimberlite pipes, where mineral inclusions from diamonds are systematically studied, may open new way in better understanding of a diamond formation in deep lithosphere.

## References

- [1] GURNEY, J. J. (1989): Diamonds. - In: ROSS, J. ed. Geol. Soc. Australia Spec. Publ. 14. Proc. Fourth International Kimberlite Conf. 2: 935-965.
- [2] JACOB, D. E., VILJOEN, K. S., GRASSINEAU, N. & JAGOUTZ, E. (2000): Remobilization in the cratonic lithosphere recorded in polycrystalline diamond. - Science. 289: 1182-1185.
- [3] KURAT, G. & DOBOSI, D. (2000): Garnet and diopside-bearing diamondites (framesites). - Mineralogy and Petrology. 69: 143-159.
- [4] MEYER, H. O. A. (1987): Inclusions in diamonds. - In: NIXON, P. H., ed. Mantle xenoliths, Chichester: 501-522.
- [5] ORLOV, YU. L. (1977): The mineralogy of the diamond. - (English translation of Russian edition. 1973. Izdatelstvo Nauka). Wiley: 235 pp.
- [6] ORLOV, YU. L. & SOBOLEV, N. V. (1980): Inclusions of pyrope and sub-calcic omphacite in a polycrystalline aggregate of diamond. - Dokl. Akad. Nauk SSSR. 250: 938-941.
- [7] REUTSKY, V. N., LOGVINOVA, A. M. & SOBOLEV, N. V. (1999): Carbon isotopic composition of diamond polycrystalline aggregates containing chromite from the Mir kimberlite pipe, Yakutia. - Geokhimiya: 1191-1196.
- [8] SOBOLEV, N. V. (1977): Deep-seated inclusions in kimberlites and the problem of the composition of the upper mantle. - (English translation of Russian edition. 1974. Izdatelstvo Nauka) American Geophysical Union, Washington DC: 279 pp.
- [9] SOBOLEV, N. V., POKHILENKO, N. P., LAVRENT'EV, Y. G. & USOVA, L. V. (1975): Characteristics of the compositions of chrome-spinels in diamonds from Yakutian kimberlites. - Soviet Geology and Geophysics. 16, II: 4-14.
- [10] SOBOLEV, N. V., SOBOLEV, A. V., POKHILENKO, N. P. & YEFIMOVA, E. S. (1989): Chrome spinels coexisting with Yakutian diamonds. - In: F. R. BOYD, H. O. A. MEYER & N. V. SOBOLEV, eds. Workshop on diamonds, Washington D.C.: 105-108.
- [11] SOBOLEV, N. V., YEFIMOVA, E. S. & USOVA, L. V. (1983): Eclogitic paragenesis of diamonds from the Mir kimberlite pipe. - In: Mantle xenoliths and problems of ultramafic magmas, Novosibirsk: 4-16.

**THORIUM MINERALIZATION IN ALKALI FELDSPAR SYENITE OF  
THE NORDMARKITE-TYPE DYKE IN THE TŘEBÍČ PLUTON (CZECH REPUBLIC)**

by

**P. Sulovský<sup>1</sup> & K. Hlisníkovský<sup>2</sup>**

<sup>1</sup>Department of Mineralogy, Petrology and Geochemistry  
Masaryk University, Kotlářská 2, 611 37 Brno, Czech Republic

<sup>2</sup>DIAMO State Enterprise  
Dolní Rožinka, Czech Republic

The Třebíč pluton, a large lakkolith occurring to the East of the Bohemian Massif, is formed mostly by melanosyenites or quartz syenites. These ultrapotassic rocks belong to the oldest members within the Variscan plutonic sequences, being documented along the whole Variscan chain under various local names - vaugnerites in the Massif Central and Vosges, redwitzites in the southwestern part of the Bohemian Massif and finally durbachites in the Czech and Austrian part of the Bohemian Massif. Common feature for the whole group is high content of light REE, LILE (K, Rb, Ba) and radioactive elements (U, Th), accompanied by elevated Mg, Cr, Ni at the same time. The origin of this geochemically unusual suite is still a matter of discussion. Anyhow, the origin by mixing of the mantle derived, ultrapotassic mafic magma with leukogranitic crustal melt prevails in the recent literature.

In spite of their relatively high basicity, durbachites of the Třebíč pluton are very rich in radioactive elements. On the average they contain around 10 ppm U and 45 ppm Th. The major part of these contents occurs in accessory minerals – both as major components in proper uranous and thorous minerals (buttonite, brabantite, thorianite, uraninite, brockite), and as minor components of common accessory minerals – allanite, zircon, monazite, xenotime, apatite. The minerals containing Th and/or U occur usually as very small (X - X0 mm) grains.

The high radioactivity of the Třebíč pluton has led in the past to an intensive radiometric survey of the area, which eventually led to finds of a number of anomalies, some of potential mining interest. The studied locality Vaneč belongs to the broader environs of the deposit Jasenice, surveyed in detail by the Uranium Survey Nové Město na Moravě in years 1954–1989.

Besides the prevailing syenitic rocks, the Třebíč pluton is penetrated by numerous dykes of aplitic or pegmatitic nature. These have usually much lower Th and U content than the durbachites: mean Th content in durbachites is  $36.2 \pm 3.0$  ppm, in aplites -  $12.8 \pm 4.6$  ppm; similarly U in durbachites =  $10.7 \pm 2.2$ , in aplitic rocks  $5.2 \pm 1.3$ . This, however, does not apply to all leucocratic rocks. One of the highly radioactive leucocratic rocks is long known from Naloučany, only a few hundred meters off the margin of the Třebíč pluton.

This extremely Zr-rich rock, containing locally up to 1000 ppm of Th in the form of thorite inclusions in zircon, was named by LEICHMANN (1997) as nordmarkite. The same name can be given also to a rock, which undoubtedly outcrops inside the Třebíč pluton in Vaneč, a place just about 3 km distant from Naloučany. The alkaline feldspar syenite (nordmarkite) dyke was discovered by trench J540, localised south of the Vaneč village, about 3 km NW of the Bíteš dislocation. The country rock is amphibole-biotite durbachite with K-spar phenocrysts up to 1.5 cm long. The dyke, at present intensively ferruginised, is composed practically only of alkaline feldspars, with minor amounts of biotite, chlorite, actinolite, and haematite, the latter three being probably not of primary origin. The bulk rock chemistry perfectly agrees with the chemistry of nordmarkite from the type locality Nordmark (Norway); it is much closer to it than the alkaline syenite from Naloučany. A striking feature, making the rock interesting from a genetic point of view, is its trace element pattern, which is very close to that of most durbachites (melanocratic syenites) and practically identical with leucocratic syenites from the Třebíč pluton. The shapes of all their patterns are practically identical, and only little displaced in the vertical direction. This seems to indicate that they were derived from the same magma. The same cannot be said about aplite dykes, penetrating the pluton – they are relatively more enriched in HREE and U (but not Zr), and show a weak positive Eu anomaly instead of a negative one as durbachites do.

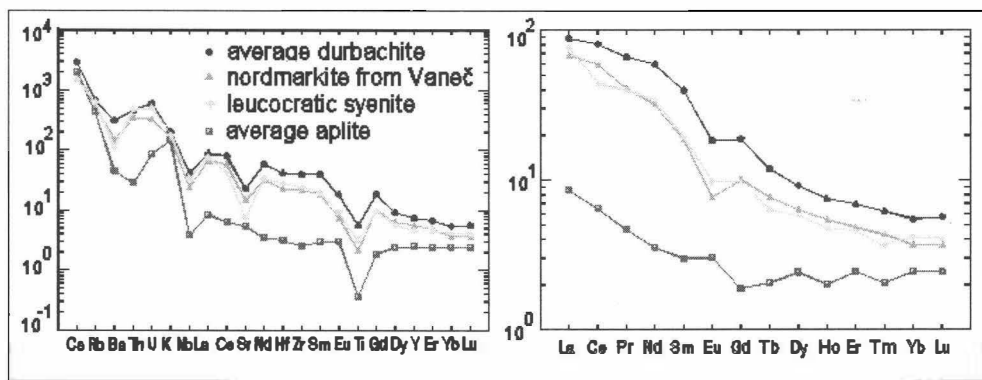


Fig 1

Normalised trace elements and REE patterns of nordmarkite from Vaneč, compared with average durbachite (melanocratic syenite), leucocratic syenite, and aplite from the Třebíč pluton.

Although the nordmarkite from Vaneč has been strongly ferruginised, its trace element chemistry remained generally unchanged. The ferruginization, manifested ultimately by development of haematite rims around many phases, has caused only local changes to the minerals of U and Th, originally represented by thorite and minerals of the monazite group, and to a lesser extent by thorianite and uraninite. The late magmatic to postmagmatic solutions locally dissolved the primary accessory minerals, especially monazite group minerals. As they also contained quite high amounts of Th and also some U, the resulting solutions were enriched in REE, Th and in places also in U or As, V and other trace elements, released by partial dissolution of accessory minerals. The solutions must have also been rich in fluorine and carbon dioxide, as the above elements precipitated often in the form of REE fluorocarbonates, along with neogenic silico-phosphates and phosphates, mainly brockite  $(\text{Ca}, \text{Th}, \text{Ce})(\text{PO}_4)_2 \cdot \text{H}_2\text{O}$ .

The precipitates did not form very far from the source, usually only several to tens microns, often making a kind of reaction rims directly engulfing the primary accessories. As a rule, all original grains of monazite or thorite or thorianite encrusted with neoformed phosphates or silicophosphates are rimmed by haematite. The neoformation of (silico)phosphates and fluorocarbonates of REE was in places connected with fractionation within the LREE group: while all primary monazite was Ce-dominant, the secondary REE minerals are in places La-dominant. The fact that the bulk REE pattern does not differ from the REE patterns of durbachites seems to imply that the ferruginization, visibly affecting the the rock very strongly, did not led to extensive migration of REE or Th.

### **References**

- [1] LEICHMANN, J., ŠTELCL, J., ZACHOVALOVA. K. (1997): A Highly Radioactive Syenite from the Moldanubian Zone (Western Moravia). - Journal of the Czech Geological Society, 42 (3), 63.

**DIE SAMMLUNG RICHARD BALDAUF (1848 - 1931) –  
EINE BEDEUTENDE MINERALIENSAMMLUNG AUS DER ERSTEN HÄLFTE  
DES 20. JAHRHUNDERTS UND IHR BEZUG ZU ÖSTERREICH**

von

**K. Thalheim**

Staatliche Naturhistorische Sammlung Dresden, Museum für Mineralogie und Geologie  
Königsbrücker Landstrasse 159, D-01109 Dresden

Mit dem Ankauf der Sammlung des "Mineralogischen Museums Baldauf" im Jahre 1940 durch das Museum für Mineralogie und Geologie in Dresden wurde eine der größten, wertvollsten und schönsten mineralogischen Privatsammlungen vom Anfang des 20. Jahrhunderts in sächsischen Landesbesitz überführt. Die Sammlung umfasst ca. 10 000 Mineralstufen und gliedert sich in eine systematische Sammlung (5113), eine Kollektion großer Schaustufen (1524), eine Kristallsammlung (2651) und eine Sammlung geschliffener Edel- und Halbedelsteine (894). Alle bis 1929 bekannten Mineralarten sind in der Sammlung Baldauf vertreten. Bis auf wenige Verluste durch die Wirrnisse der Zeit kurz nach 1945 ist die Sammlung vollständig erhalten geblieben.

Richard Baldauf wurde am 7.3.1848 in Chemnitz geboren. Er studierte an der Bergakademie Freiberg Bergbaukunde und war im Anschluss an sein Studium als Bergingenieur im Ausland sowie im sächsischen Steinkohlen- und böhmischen Braunkohlenbergbau tätig. 1891 gründete er im nordböhmischen Braunkohlenrevier ein eigenes Bergbauunternehmen, welches bis 1920 bestand. Nachdem Richard Baldauf im Jahre 1904 seinen Wohnsitz in Dresden genommen hatte und sein Sohn in die Geschäfte der Baldauf-Rudolphschen Braunkohlenwerke eingetreten war, wendete er sich verstärkt seinem geliebten Hobby, der Mineralogie und dem Mineraliensammeln zu. Die Anregung zu diesem Hobby verdankte Baldauf seinem interessanten Studium in Freiberg und seiner Tätigkeit im Bergbau. Die Reisen von Richard Baldauf ab 1905 dienten ausschließlich dem Mineraliensammeln und dem Besuch berühmter Lagerstätten sowie mineralogischer Museen. Mineralogische Reiseziele waren Island, Grönland, Spanien, Portugal, Schweden und Norwegen. Seine weiteste Reise unternahm er 1912 im Alter von 64 Jahren nach Südamerika (Brasilien, Uruguay, Argentinien). In den Jahren 1924 bis 1926 bereiste Richard Baldauf die europäischen Länder und studierte dort eingehend die mineralogischen Museen. In Österreich besuchte er das Naturhistorische Museum, die Universität und die Geologische Landesanstalt in Wien sowie die Museen und Sammlungen in Graz, Leoben und Klagenfurt. Sein geplantes Buch über die bedeutendsten mineralogischen Museen und Sammlungen in Europa konnte Baldauf leider nicht vollenden.

Richard Baldauf sammelte mit wissenschaftlicher Methode. Er stand in regem Kontakt mit vielen Mineralogen und Geologen seiner Zeit, denen er auch sein gastliches Haus öffnete. Enge Beziehungen pflegte er zu den Direktoren des Museums für Mineralogie und Geologie in Dresden Ernst Kalkowsky (1851–1938) und Eberhard Rimann (1882–1944) sowie zu den Mineralogen der Bergakademie Freiberg Friedrich Kolbeck (1860–1943), Richard Beck (1858–1919) und Friedrich Schumacher (1884–1975). Aus Österreich stand er mit Josef Emanuel Hirsch (1852–1940), der an der Hochschule für Bodenkultur in Wien lehrte und vor allem mit Rudolph Koechlin (1862–1939), dem Kustos am k.k. Naturhistorischen Hofmuseum in Wien in Verbindung. Koechlin war es auch, der im Jahre 1929 die Sammlung Baldauf bis ins Detail katalogisierte und nach dem damaligen Handelswert auf rund eine Million Reichsmark schätzte. Richard Baldauf war in der glücklichen Lage, durch seine Vermögenssituation bedeutende Geldmittel für seine Liebhäberei aufwenden zu können. So pflegte er zahlreiche Verbindungen zu Mineralienhändlern in aller Welt. Aus Österreich sind hier zu nennen: Anton Berger in Mödling, das Mineralien-Comptoir Julius Böhm in Wien sowie das Mineralogische Comptoir Anton Otto in Wien. Über die Mineralienhandlung Böhm erwarb Baldauf einige Stücke aus der berühmten Sammlung Johann Isidor Weinberger (1838–1915) für seine systematische Sammlung. Mit dem bedeutenden Mineraliensammler Hans v. Karabacek (1878–1963) aus Wien stand Baldauf beim Erwerb von besonders schönen Mineralstufen, vor allem aus Tsumeb, in Konkurrenz.

Im Jahre 1916 erklärte Baldauf die Sammlung in seiner Villa auf der Geinitzstraße in Dresden zum öffentlichen "Mineralogischen Museum". Dieses mineralogische Privatmuseum erlangte sehr schnell über Dresdens und Deutschlands Grenzen hinaus internationale Bekanntheit und Berühmtheit.

An Mineralen aus Österreich sind über 370 Stufen in der Baldauf-Sammlung vertreten, darunter mehr als 70 große Schaustufen.

Richard Baldauf trat in seiner sächsischen Heimat als Förderer der geologischen Wissenschaften und Mäzen von geowissenschaftlichen Sammlungen in Erscheinung. Die Bergakademie Freiberg, das Mineralogische Institut der TH Dresden und das Mineralogische Museum im Dresdner Zwinger kamen in den Genuss seiner großzügigen Donationen an Geldmitteln und an Mineralstufen.

Sein großzügiges Wirken auf sozialem und wissenschaftlichem Gebiet sowie seine freizügige Unterstützung wissenschaftlicher Institutionen und Sammlungen erfuhren mehrfach öffentliche Anerkennung und Ehrung. Im Jahre 1917 verlieh ihm die TH Dresden den Ehrendoktor der Technischen Wissenschaften. Baldauf zu Ehren wurde ein neues Phosphatmineral aus dem Pegmatit von Hagendorf in Bayern von Franz Müllbauer 1925 als Baldaufit benannt. Seit Hugo Strunz 1954 die Identität mit dem schon seit 1825 bekannten Mineral Huréaulith feststellte, gibt es leider kein anerkanntes Mineral Baldaufit mehr.

Am 28.4.1931 starb Richard Baldauf nach einem erfüllten Leben in Dresden.

Über den verdienstvollen Unternehmer und Mineraliensammler schrieb der damalige Direktor des Museums für Mineralogie und Geologie in Dresden, Eberhard Rimann 1932 im Nekrolog: "Der Name Richard Baldauf wird für alle Zeiten in der Mineralogie und im Bergbau ehrenvoll genannt werden: in der Mineralogie als der Name eines der wenigen Männer in Deutschland, der dieser Wissenschaft seine Förderung in reichem Maße zuteil werden ließ und der in viel-jähriger zielbewußter Arbeit ein einzigartiges Mineralogisches Museum geschaffen hat, im Bergbau als der Name einer führenden und neue Wege weisenden Persönlichkeit von überragender Bedeutung."

Die Sammlung Baldauf ist seit ihrer Übernahme einer der wertvollsten Bestände des Museums für Mineralogie und Geologie Dresden. Sie ist ein wichtiger Fundus für Forschungs- und Ausstellungszwecke. Schon oft wurde bei der Untersuchung seltener Minerale und bei der Präsentation von Ausstellungen auf diesen Fundus zurückgegriffen. Im Jahre 1983 wurde die Baldauf-Sammlung auf der Großen Wiener Mineralienschau vorgestellt und 1990 bereicherten drei besonders schöne Epidotstufen aus dieser Sammlung die Jubiläumsschau zum Symposium "125 Jahre Knappenwand" im Rahmen der MinPet 90 in Neukirchen am Großvenediger.

## Literatur

- [1] BALDAUF, M. (1957): Dr. Richard Baldauf (1848-1931). Seine Bedeutung für die Mineralogie. - Jb. Staatl. Mus. Mineral. Geol. 1956/57:116-237.
- [2] FITZ, O. (1993): Eine Sammlung erzählt. - Mitt. Inst. Bodenforschung etc. Wien Sh. I: 1-80.
- [3] NIEDERMAYR, G. & FRANCIS, C. (2000): Die Karabacek-Sammlung im Harvard Mineralogical Museum bei Boston, USA. - Mineralien-Welt 5: 32-43
- [4] NIEDERMAYR, G. & PERTLIK, F. (2000): Hans J. (Ritter von) Karabacek (\*5.3.1878 †9.6.1963) Ein später Nachruf. - Mitt. Österr. Miner. Ges. 145: 15-20
- [5] Archivmaterial zur Sammlung Richard Baldauf am MMG Dresden

THE METAMORPHIC EVOLUTION OF STROMATIC MIGMATITES FROM  
THE WESTERN ÖTZTAL-STUBAI CRYSTALLINE BASEMENT (TYROL, EASTERN ALPS)

by

W. Thöny<sup>1</sup>, P. Tropper<sup>1</sup> & F. Bernhard<sup>2</sup>

<sup>1</sup>Institute of Mineralogy and Petrography

University of Innsbruck, Innrain 52, A-6020 Innsbruck

<sup>2</sup>Institute of Engineering Geology and Applied Mineralogy

Technical University of Graz, Rechbauerstrasse 12, A-8010 Graz

The Austroalpine Ötztal-Stubai Crystalline Basement Complex (ÖSCB) in the Eastern Alps provides an excellent opportunity to study a metamorphic core complex which underwent several episodes of metamorphic overprints. Although extensive research has been performed on the two predominant orogenic episodes in the Eastern Alps namely the Variscan and Alpine orogenic events, very little attention has been paid to the pre-Variscan (Caledonian) metamorphic history so far. The pre-Variscan events are manifested in localized migmatite occurrences in the central and western ÖSCB. The migmatite from Verpel in the Kaunertal, western ÖSCB, is a stromatic migmatite containing narrow (1–2 cm width) bands of leucosome. The primary mineral assemblage is garnet + biotite + plagioclase + K-feldspar + quartz ± cordierite. Cordierite is rare and subsequently breaks down to form biotite + sillimanite aggregates. Late stage muscovite also occurs and replaces biotite.

Thermobarometry and estimation of the P-T- $\alpha$ (H<sub>2</sub>O) conditions of the pre-Variscan metamorphic event involves application of several different thermobarometric techniques such as cation exchange thermometry (Fe-Mg exchange between garnet and biotite) and multi-phase equilibrium calculations. The latter are performed using the thermodynamic data bases and phase diagram calculation programs THERMOCALC v. 2.7 (HOLLAND & POWELL, 1998), TWQ v. 2.02 (BERMAN, 1988) and WEBINVEQ (GORDON, 1992). Our results yield temperatures of 550–600°C and pressures of 6–7 kbar and low  $\alpha$ (H<sub>2</sub>O) of 0.2–0.4 for a mesosome sample. It is not clear yet, if these conditions are the final result of the pre-Variscan migmatization or the Variscan metamorphic overprint. The formation of cordierite due to the reaction biotite + sillimanite + quartz ⇌ cordierite + garnet + H<sub>2</sub>O/melt requires temperatures of at least 650–750°C between 3 and 6 kbar. These temperatures are high enough to induce melting as preliminary melting experiments at 700°C and 4 kbar with the natural biotite + plagioclase + quartz protolith rock show. Major element analyses of protolith rocks and adjacent mesosome samples show a decrease in SiO<sub>2</sub> and an increase in Al<sub>2</sub>O<sub>3</sub>, Fe<sub>2</sub>O<sub>3</sub> and MgO during migmatization.

The thermobarometric results above will be compared to petrogenetic grids for high-grade metapelites developed by SPEAR et al. (1999). The textural observations are in accordance with an isobaric heating path above 4 kbar from the study of SPEAR et al. (1999).

## **References**

- BERMAN, R. G. (1988): *J. Petrol.*, 29, 445-522.  
GORDON, T. (1992): *Geochim. Cosmochim. Acta* 56, 1793-1800.  
HOLLAND, T. J. B. & POWELL, R. (1998): *J. Metam. Geol.* 8, 89-124.  
SPEAR, F. S., KOHN, M. J. & CHENEY, J. T. (1999): *Contrib. Mineral. Petrol.* 134, 17-32.

CELADONITE: THE COLOUR-GIVING GREEN CLAY MINERAL OF THE CARBONATE  
MANGANESE ORE, ÚRKÚT, TRANSDANUBIAN CENTRAL RANGE, HUNGARY

by

E. Tóth<sup>1</sup>, T.G. Weiszburg<sup>1</sup> & D. Pop<sup>2</sup>

<sup>1</sup>Department of Mineralogy  
Eötvös Loránd University, Budapest

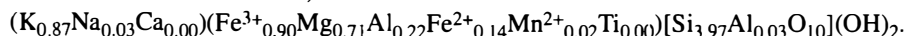
<sup>2</sup>Department of Mineralogy  
Babeş-Bolyai University, Cluj-Napoca

On the basis of full chemical analyses (ICP-MS) and TEM investigations done on carefully separated samples, new data on the 10 Å green clay mineral of the Úrkút Manganese Ore Formation (UMOF) are presented.

The UMOF is an Upper Liassic local facies in the Transdanubian Central Range zone and is related to the Toarcian anoxic event. The manganese mineralisation was formed in a pelagic environment. The thickness of the UMOF varies between 1 - 50 m. The carbonate manganese ore occurs in two horizons. The thickness of the Main Ore Bed (MOB) is 8 - 12 m, the MOB is overlain by an about 25 m thick dark thin-stratified radiolarian clay marl, then a 2 - 4 m thick manganese-carbonate layer follows (the so-called "Bed No. II"). The banded green ore itself is a mixed clay-sized material, consisting predominantly of carbonates (mainly rhodochrosite), goethite, quartz and different layer silicates, among them the colour-giving clay mineral. The studied samples were collected from the uppermost part of the MOB.

In the earliest studies the green clay mineral was described mainly as glauconite, and later on, as comprehensive XPD and IR data accumulated, "celadonite-glauconite", celadonite and aluminoceladonite. The most detailed summary of the former results is given in [1]. The uncertainty concerning the nature of this mineral was mainly due to separation problems.

Using a new three-step separation procedure developed for the given mineral assemblage [2], we were able to obtain reliable data on the chemical composition of this mineral. Based on a dioctahedral TOT mica structure, the chemical formula is:



The results were plotted in a charge diagram  $x_T-x_O-x_{IL}$ . The clay mineral can be classified as celadonite according to the three latest classification schemes [3, 4, 5].

TEM investigations of the pure sample revealed that the celadonite crystals are euhedral (the laths have a characteristic size range: 0.1 - 2.1  $\mu\text{m}$  in length and 0.07 - 1.14  $\mu\text{m}$  in width), which indicates primary precipitation. This contradicts the opinion of [6], where the formation of the green clay was explained by transformation from Fe-smectites during early diagenetic processes.

The presence of celadonite (as opposed to glauconite and green smectite) might be a new evidence in the row of indirect evidences [1] for some kind of submarine volcanic activity playing a role in the genesis of the Úrkút manganese deposit.

This work was supported by OTKA Grant #T25873.

## References

- [1] POLGARI, M. et al. (2000): Mangánércek Magyarországon / Manganese ores in Hungary. (in Hungarian with extended English summary). - Regional Committee of the Hungarian Academy of Sciences, Szeged, 652 p.
- [2] MIZAK, J. et al. (2000): Separation of the 10 Å green clay mineral from the carbonatic manganese ore, Úrkút, Hungary. - Acta Mineral. Petrogr. Szeged 41, Suppl.: 73.
- [3] BAILEY, S. W. (1980): Summary of recommendations of AIPEA nomenclature committee. - Clays Clay Miner. 28: 73-78.
- [4] BAILEY, S. W. (1986): Report of AIPEA nomenclature committee. - Suppl. AIPEA Newslett., 22: 1-3.
- [5] RIEDER, M. et al. (1998): Nomenclature of micas. - Can. Mineral. 36: 905-912.
- [6] VARENTSOV, I. M. et al. (1988): Ore formation in the early-Jurassic basin of Central Europe: Aspects of mineralogy, geochemistry and genesis of the Úrkút manganese deposit, Hungary. - Chem. Erde 48: 257-304.

PETROLOGY OF MANGANESE SILICATE-CARBONATE ROCKS FROM  
THE VEITSCH MN-DEPOSITS, GREYWACKE ZONE, EASTERN ALPS

by

P. Tropper<sup>1</sup>, F. Bernhard<sup>2</sup> & W. Postl<sup>3</sup>

<sup>1</sup>Institute of Mineralogy and Petrography

University of Innsbruck, Innrain 52, A-6020 Innsbruck

<sup>2</sup>Institute of Engineering Geology and Applied Mineralogy

Technical University of Graz, rechbauerstrasse 12, A-8010 Graz

<sup>3</sup>Referat für Mineralogie

Landesmuseum Joanneum, Raubergasse 10, A-8010 Graz

Within the Upper Austroalpine Greywacke Zone several carbonate-hosted Fe and Mn ore deposits occur. The Mn deposits of Veitsch at Kaskogel and south-east of Friedelkogel consists of lens-shaped Mn-carbonate bodies of up to 1.5 m thickness which are thought to have formed by syn-sedimentary processes. (HADITSCH, 1968). The primary manganese minerals described from these deposits are: rhodochrosite, tephroite, pyroxmangite, rhodonite, spessartine, Mn-chlorite, Mn-humite (manganhumite or sonolite) friedelite and jacobsite. (HADITSCH, 1968, POSTL et al., 1998). Sulfides such as sphalerite, galena, chalcopyrite and Co-Ni sulfides also occur. In addition, POSTL et al (1998) and NIEDERMAYR et al. (2000) described rare minerals such as helvine and sussexite from these deposits.

During this investigation, four samples of manganese silicate-carbonate rocks were studied. The sample from Kaskogel contains the mineral assemblage: tephroite + spessartine + rhodochrosite + Mn-chlorite + Mn-humite + friedelite. The three samples from Friedelkogel contain the mineral assemblages: Mn-humite + Mn-chlorite + rhodochrosite, Mn-humite + jacobsite + rhodochrosite and Mn-humite + jacobsite + rhodochrosite. All minerals grow in a matrix of rhodochrosite. In the sample from Kaskogel, tephroite grows along veins. Tephroite has a composition of  $\text{Te}\text{ph}_{92}\text{F}\text{o}_7\text{Fa}_1$  and shows replacement by friedelite, which contains up to 3 wt.% Cl. The garnets also grow along veins, where two stages of garnet growth can be observed. The second stage appears as a replacement of the first garnet generation. Chemically, the garnets show a homogeneous first generation in the cores with a composition of  $\text{Sp}_{97}\text{Gr}_{2}\text{And}_{1}$ . The second garnet generation at the rims has slightly higher CaO contents and a composition of  $\text{Sp}_{92}\text{Gr}_{7}\text{Prp}_{0.5}\text{And}_{0.5}$ .

Based on experimental investigations in the system Mn-Al-Si-O (ABS-WURMBACH & PETERS, 1999) and the system MnO-SiO<sub>2</sub>-CO<sub>2</sub>-H<sub>2</sub>O (PETERS et al., 1973) it is possible to place T-X(CO<sub>2</sub>)-f(O<sub>2</sub>) constraints on the assemblage tephroite + rhodochrosite + spessartine. The formation of tephroite probably took place around 400 - 450°C under low X(CO<sub>2</sub>) of < 0.02 and negligibly low f(O<sub>2</sub>). These data are in accordance with pre-Alpine greenschist facies P-T estimates from the Greywacke zone of 300 - 400°C and 3 - 5 kbar (NEUBAUER et al., 1999).

## References

- ABS-WURMBACH, I. & PETERS, T. (1999): Eur. J. Mineral. 11, 45-68.  
HADITSCH (1968): Arch. F. Lagerstättenforsch. 7, 112-169.  
NEUBAUER et al. (1999): Schweiz. Mineral. Petrogr. Mitt. 79, 41-62.  
NIEDERMAYR et al. (2000): Carinhia II 190/110, 181-224.  
PETERS, T., SCHWANDER, H. & TROMMSDORFF, V. (1973): Contrib. Mineral. Petrol. 42, 325-332.  
POSTL, W., BERNHARD, F. & HOFER, F. (1998): Mitt. Abt. Miner. Joanneum 62/63, 59-64.

**DIE SPATMAGNESIT-LAGERSTÄTTE BREITENAU (STEIERMARK),  
EINE PALÄOZOISCHE MAGNESIT-MINERALISATION  
AUS DEM GRAZER PALÄOZOIKUM**

von

**W. Tufar<sup>1</sup>, U. Siewers<sup>2</sup> & Ch. Weber<sup>3</sup>**

<sup>1</sup>Fachbereich Geowissenschaften

Philipps-Universität Marburg, Hans-Meerweinstrasse, D-35032 Marburg

<sup>2</sup>Bundesanstalt für Geowissenschaften und Rohstoffe

Stilleweg 2, D-30631 Hannover

<sup>3</sup>VRD-Europa, Veitsch-Radex GmbH

Werk Breitenau, A-8614 Breitenau am Hochlantsch

Die Magnesit-Lagerstätte Breitenau im NE Grazer Paläozoikum, die größte Spatmagnesit-Lagerstätte der Ostalpen mit einem Gesamtinhalt von etwa 50 Millionen Tonnen Spatmagnesit, liegt am Nordabfall des Hochlantsch in der schwach regio-nalmetamorph überprägten Laufnitzdorfer Gruppe (Obersilur - Oberdevon), deren Gesteine im Lagerstättengrenzbereich dem Obersilur zugeordnet werden können. Auffällig ist bereits, daß sich die Nebengesteinsserie der Magnesit-Lagerstätte durch einen ausgesprochenen Mangel an Karbonatgestein auszeichnet. Eine erhebliche Karbonatführung weisen dagegen die beiden benachbarten Serien auf, die "Kalk-schieferfolge" (Unterdevon - Oberdevon) und erstreckt die höchste tektonische Einheit, die Hochlantschgruppe (Unterdevon - Oberkarbon) mit dem bis zu 800 m mächtigen Hochlantschkalk, die sich beide jedoch durch eine völlige Abwesenheit von Magnesit auszeichnen.

Der Spatmagnesit von Breitenau gehört einem stratiformen Lagerstättenzug an, der über einen Bereich von mehreren Kilometern in der Laufnitzdorfer Gruppe durch Ausbisse bzw. Vorkommen von Magnesit markiert wird. Der Magnesitkörper der Breitenau streicht etwa E-W, fällt mit ca. 25° nach S und ist auf etwa 1.7 - 2 km von ca. 800 m über NN im Tagbau bis in eine Teufe von ca. 240 m über NN zu verfolgen. Die Mächtigkeit kann bis 200 m betragen. Im liegenden Bereich wird der Magnesit, mit scharfer Begrenzung, von einem feinkörnigen sedimentären Obersilur-Dolomit begleitet. Liegendes der Magnesit-Lagerstätte bildet ein kohlenstoffführender phyllitischer Schiefer, Hangendes Metatuffit und kohlenstoffreicher phyllitischer Schiefer, der Lydit führt. Tektonisch wurde die Lagerstätte teilweise stark beansprucht, gestört und weist dementsprechend u. a. zahlreiche Störungen und Verwürfe auf.

Magnesit (Spatmagnesit, Ø: 2.69 Gew.-% FeO, 0.295 Gew.-% MnO; < 2 - 1651 g/t Sr) tritt praktisch als monomineralischer Lagerstätten- bzw. Gesteinsbildner auf und ist öfters in relativ großen Kristallen und Kristallaggregaten anzutreffen, die mehrere cm Länge erreichen können.

Es liegen mehrere Typen von Spatmagnesit vor. Häufig zu beobachten ist weißer, aber auch hell- bis dunkelgrauer, stellenweise außerdem fast schwarzer Spatmagnesit. Ausgesprochen charakteristisch für die Lagerstätte sind Bändermagnesit und "Magnesit-Sonnen", während pionierhafter Magnesit nur untergeordnet vorliegt.

Die Bänderung des Bändermagnesites ist primär angelegt und geht auf ursprüngliche, rhythmische Wechselfolgen bzw. Abfolgen von weißen, reinen und dunkleren, zumeist grauen, unreinen, etwas bituminösen und teilweise auch Pyrit sowie toniges Material führende Karbonatlagen zurück. Bei der Spätdiagenese konnte Magnesit in den reinen Lagen häufig ungehindert wachsen bzw. rekristallisieren und liegt somit in diesen zumeist in größeren Körnern vor, in den unreinen Lagen dagegen wurde sein Wachstum bzw. seine Rekristallisation teilweise gehemmt und unterdrückt. Die dunklen Lagen bzw. Bänder (Straten) von Magnesit sind stellenweise zerbrochen, teilweise auch angelöst oder sogar weggelöst. Obwohl der Bändermagnesit später abschließend schwach regionalmetamorph überprägt wurde, sind primäre Texturen und Gefüge erhalten geblieben. Als eine Besonderheit weist Bändermagnesit sogar noch Belastungsmarken ("load casts") auf und lässt erkennen, daß ursprünglich unverfestigte, plastische, rhythmische Magnesit-Wechselfolgen vorlagen, in denen einzelne Lagen bzw. Bänder einbrachen und in unterlagernde Magnesitbänder eindrückten.

Äußerst kennzeichnend für die Lagerstätte sind "Magnesit-Sonnen", die eine Kristallisation von Magnesit (z. T. in beachtlicher Größe bzw. Länge) in freie, große Hohlräume belegen: Dunkelgraue bis fast schwarze, meist bereits lithifizierte, stellenweise aber auch noch plastische Bänke und Lagen von feinkörnigem Magnesit mit kohliger Substanz und öfters auch etwas Pyrit werden als Substrat häufig angelöst und zeigen als Folge einer spätdiagenetischen Zementation aufgewachsen mehrere cm lange, (hell-)graue "Magnesit-Tapeten" (1. Generation Zement), die noch ein wenig kohlige Substanz als färbendes Pigment enthalten können, gefolgt von weißen, ebenfalls mehrere cm langen "Magnesit-Tapeten" (2. Generation Zement), die ebenfalls weiter in den freien Hohlräum hineinwachsen und auf die stellenweise noch Dolomit in großen Kristallen ("Röß Zahndolomit", 3. Generation Zement) als Resthohlräumfüllung folgen kann.

Tektonische Beanspruchung hat den Magnesit teilweise deutlich betroffen, stellenweise liegen sogar mächtigere Magnesit-Breccien vor. Magnesit kann daher erhebliche postkristalline Deformation mit Kataklase und sogar Rekristallisation aufweisen.

Dolomit tritt als Neben- bis Übergemengteil auf, weitere Übergementeile und nur örtlich Nebengemengteile bilden Quarz und Chlorit. Gelegentlich ist Calcit als Übergemengteil anzutreffen. Talk, der in Paragenese mit Magnesit erwartet werden könnte, fehlt in dieser Lagerstätte. Kohlige Substanz und Pyrit liegen als Übergemengteile bis Nebengemengteile vor, erstere kann auch etwas reichlicher beibrechen und findet sich häufig als "Graphit-Spiegel" auf Störungsflächen und Harnischen. Als Übergemengteile sind gelegentlich u. a. Zinkblende, Kupferkies und Rutil zu beobachten. Von mineralogischem Interesse ist im Magnesit ein lokales Auftreten von Magnetit, der in seinen Pseudomorphosen erkennen läßt, daß auch ein älterer Hämatit vorlag, der vollständig verdrängt und pseudomorphosiert wurde (Muschketowit). Seinerseits wird aber Magnetit dann selbst von einem jüngeren Hämatit verdrängt (Martit). Als junge Bildungen in der Lagerstätte sind z. B. Baryt oder Zinkblende auf Klüften, Zinnober und Millerit anzuführen.

Auch das Beispiel der Magnesit-Lagerstätte Breitenau läßt ersehen, daß die Spurenelement-Analyse der Seltenen Erden ( $\Sigma$  SEE ohne Y: 1.515 g/t bis 125.889 g/t, Ø: 20.621 g/t; deutliche Abnahme in den "Magnesit-Sonnen" vom feinkörnigen Magnesit-Substrat zu den Magnesit-Tapeten) keine eindeutige Aussage über die Genese des Magnesites ermöglicht. Rückschlüsse über die Genese der Lagerstätte lassen sich jedoch aus den geologischen Befunden ableiten.

Kennzeichnend für die Magnesit-Lagerstätte Breitenau ist ihr Auftreten in einer obersilurischen Gesteinsserie mit ausgesprochenem Mangel an Karbonatgestein. Der Magnesit liegt eingebettet in eine Schwarzschieferfazies, wurde durch diagenetische und postdiagenetische Veränderungen überprägt und zeigt einen Zusammenhang mit Absenkung sowie damit in Verbindung stehenden vulkanischen Einflüssen mit Auswirkung auf eine Bildung salinarer Lösungen. Die Magnesit-Lagerstätte zeigt dieselbe tektonische Beanspruchung bzw. die verschiedenen tektonischen Verformungsakte und die schwache Regionalmetamorphose wie die umgebende Laufnitzdorfer Gruppe, in welcher der Magnesit liegt und hat deren gesamte tektonische und metamorphe erdgeschichtliche Entwicklung durchlaufen. Mit der Lagerstätte Breitenau im Obersilur des Grazer Paläozoikums liegt eine nur schwach regionalmetamorph überprägte Spatmagnesit-Lagerstätte vom Typ Radenthein vor.

**DIE SPATMAGNESIT-LAGERSTÄTTE RADENTHEIN (MILLSTÄTTER ALPE, KÄRNTEN),  
EINE VORALPIDISCHE MAGNESIT-MINERALISATION  
AUS DEM MITTELOSTALPINEN ALTKRISTALLIN DER OSTALPEN**

von

**W. Tufar<sup>1</sup>, U. Siewers<sup>2</sup> & Ch. Weber<sup>3</sup>**

<sup>1</sup>Fachbereich Geowissenschaften

Philipps-Universität Marburg, Hans-Meerweinstrasse, D-35032 Marburg

<sup>2</sup>Bundesanstalt für Geowissenschaften und Rohstoffe

Stilleweg 2, D-30631 Hannover

<sup>3</sup>VRD-Europa, Veitsch-Radex GmbH

Werk Breitenau, A-8614 Breitenau am Hochlantsch

Die Magnesit-Lagerstätte Radenthein im Altkristallin auf der Millstätter Alpe stellt eine der großen Spatmagnesit-Lagerstätten der Ostalpen dar, deren bergwirtschaftliche Bedeutung durch einen Gesamtinhalt von etwa 35 Millionen Tonnen Spatmagnesit unterstrichen wird. Sie ist im Gegensatz zu anderen Vorkommen in den Ostalpen, z. B. in karbonatreichen Sedimentserien in der Grauwackenzone, durch ihr Auftreten in einer Altkristallin-Serie mit einem ausgesprochenen Mangel an Karbonatgestein gekennzeichnet. Dieses polymetamorphe Altkristallin wird im Liegenden aus der nach N abtauchenden Millstätter Serie gebildet, die sich durch ein Zurücktreten an Granat, teilweise auch an Amphibolit, auszeichnet, aber mächtige Marmorzüge und reichlich pegmatitische Bildungen aufweist. Darüber folgt die Serie des Radentheiner Glimmerschiefers, der die Magnesit-Lagerstätte enthält und vorherrschend aus Muskovit-Glimmerschiefer mit oft reichlich Granat aufgebaut wird. Außerdem treten im Radentheiner Glimmerschiefer Hornblende-Gesteine, Graphit-führender Glimmerschiefer und Quarzit auf, während Marmor nur sehr untergeordnet anzutreffen ist und Pegmatit fehlt. Die hangende Priedöfgneis-Serie besteht aus mächtigeren, häufig quarzitischen Paragneisen.

Die Magnesit-Lagerstätte liegt etwa 6 km NW von Radenthein entfernt, in der Nordostflanke der Millstätter Alpe in ca. 1250 m bis 1870 m über NN und gehört einem stratiformen, etwa 5 km langen, N–S streichenden und steil nach E einfallenden Lagerstättenzug im Radentheiner Glimmerschiefer an. Im Bereich der Lagerstätte zeichnet sich der Radentheiner Glimmerschiefer vor allem durch Granat-Glimmerschiefer ("Grönnit": extrem reich an Granat, bis Granatfels) aus und enthält Einlagerungen von Amphibolit, Hornblende-Garbenschiefere sowie etwas Marmor (Calcit-, Dolomit-Marmor). Der im Bereich des Kontaktes stellenweise anzutreffende "Radentheinit" stellt eine Besonderheit dar und besteht aus Disthen, Granat und Biotit. Eine reiche Magnesit-Führung mit größerer Mächtigkeit (30 - 80 m) ist im nördlichen Bereich auf etwa 1.2 km bekannt. In der Abfolge wird Magnesit von etwas Dolomit begleitet und stellenweise von einer Magnesit-Dolomit-Übergangszone überlagert.

In der Lagerstätte tritt Magnesit (Spatmagnesit, Ø: 1.65 Gew.-% FeO, 0.066 Gew.-% MnO, 20.4 g/t Sr) praktisch als monomineralischer Lagerstätten- bzw. Gesteinsbildner auf, häufig in relativ großen Kristallaggregaten bzw. Porphyroblasten oder Idioblasten, die sogar mehrere cm Länge erreichen können. Es liegt Magnesit-Marmor vor, der mehrere Typen beobachten lässt. Vorherrschend ist weißer Spatmagnesit, daneben tritt stellenweise Pignolit-Magnesit und außerdem Bänder-Magnesit auf. Beim Pignolit-Magnesit handelt es sich um einen grobkristallinen, unreinen Magnesit-Marmor, dessen Magnesit-Porphyroblasten bzw. -Idioblasten ursprünglich in einer Tonschiefermatrix aufgesproßt sind. Der Bänder-Magnesit zeichnet sich durch eine charakteristische rhythmische Bänderung bzw. Abfolge im mm- bis cm-Bereich von Magnesit und meist dünnen, dunkleren, häufig reichlicher Talk führenden Lagen ("Tonschiefer") aus und kann Graphit als färbendes Pigment enthalten. Einschlüsse, vor allem von Dolomit und/oder Calcit, sind im Magnesit, auch in seinen pignolitischen und bänderigen Typen, stellenweise verbreitet, z. T. fein ausgebildet und teilweise zonar im Magnesit angeordnet oder liegen als "Durchstäubung" in seinen Porphyroblasten und Idioblasten vor. Als Einschluß, selbst in den "Durchstäubungen", tritt stellenweise sogar relikтив erhaltener, älterer Magnesit auf. Starke tektonische Beanspruchung sowie regional-metamorphe Überprägung hat den Magnesit deutlich betroffen. Er zeigt dementsprechend erhebliche postkristalline Deformation mit Kataklase und sogar Rekristallisation, reliktische Kataklasten von Magnesit, teilweise mit Längung im Zusammenhang mit einer gewissen (Fließ-) Schieferung, liegen häufig eingebettet in jüngeres Rekristallitat von Magnesit.

Dolomit und/oder Calcit, in geringen Gehalten, liegen meistens in Verwachsung mit Magnesit vor, können diesen verdrängen oder werden stellenweise selbst von jüngeren Magnesit-Generationen verdrängt. Weitere Neben- bis Übergemengteile bilden u. a. Talk, der gelegentlich auch etwas reichlicher auftritt, eisenarmer Biotit bzw. Phlogopit, Klinochlor, Quarz, Disthen (z.T. mehrere cm lang, häufig von Talk und Klinochlor verdrängt und pseudomorphosiert), Mg-reicher Amphibol, Sulfide (vor allem Pyrit, gelegentlich etwas Kupferkies, Magnetkies, z. T. sogar mit Pentlandit-Flammen, Zinkblende usw.), Rutil, Turmalin und Graphit. Turmalin kann im Kontaktbereich der Lagerstätte örtlich deutlich angereichert als Turmalingestein ("Turmalinit") vorliegen und macht auf eine erhebliche Bor-Konzentration aufmerksam, wie sie in Evaporit-Bildungen auftritt. Magnesit und die mit ihm vergesellschafteten Silikate sowie Graphit repräsentieren eine metamorphe Paragenese, die im Metamorphosegrad mit der umgebenden Altkristallin-Serie des Radentheiner Glimmerschiefers übereinstimmt.

Die Verteilung der Seltenen Erden ( $\text{Ø } \Sigma \text{ SEE ohne Y: } 8.43 \text{ g/t}$ ) im Magnesit weist meist eine positive Eu-Anomalie auf, zum Teil ist ein Verlust an Ytter-Erden zu beobachten. Bezüglich der Isotopen-Zusammensetzung zeigt der Magnesit beim Kohlenstoff streuende negative und positive Werte, beim Sauerstoff eine starke Streuung der negativen Werte.

Magnesit besitzt meist nur sehr kleine Flüssigkeits-Einschlüsse. Vorherrschend sind einphasige, zweiphasige (Lösung und Gasphase) treten nur untergeordnet auf, dreiphasige Flüssigkeits-Einschlüsse (Lösung, Gasphase und Tochterkristall) liegen nur gelegentlich vor. Die Gasphase besteht vorherrschend aus  $\text{CO}_2$ , daneben treten  $\text{CH}_4$  und  $\text{N}_2$  auf. Bei den Homogenisierungs-Temperaturen zweiphasiger Primäreinschlüsse zeichnen sich mehrere Maxima ab (um 30°C, zwischen 230°C und 240°C sowie um 305°C).

Von Interesse sind außerdem Flüssigkeits-Einschlüsse, die im Temperaturintervall von 29.8°C bis 30.9°C in die flüssige Phase homogenisieren, da in diesen flüssiges CO<sub>2</sub> ("kritisches CO<sub>2</sub>") vorliegt. Ermittlungen des Schmelzpunktes der H<sub>2</sub>O-reichen Phase ( $T_m$ <sub>Eis</sub>) zeichnen vor allem Werte zwischen -8.3 und -9.2°C sowie zwischen -11.2 und -11.6°C ab. Auslaugungsanalysen von Flüssigkeits-Einschlüssen des Magnesites ergaben als mineralbildende Lösungen Chlorid-Hydrogencarbonat-Lösungen von Alkali- und Erdalkalimetallen mit relativ hohen Gehalten an Natrium, Kalium und Magnesium sowie Chlorid- und Hydrogencarbonationen, während Calcium etwas und Strontium stark zurücktreten.

Radenthein repräsentiert weltweit die Typlokalität einer regionalmetamorphen Spatmagnesit-Lagerstätte, die durch ihr Auftreten im Kristallin gekennzeichnet ist, obendrein in einer poly-metamorphen Kristallinserie, die ausgeprägte Diaphthorese zeigt und einen ausgesprochenen Mangel an Karbonatgestein aufweist. Ursprünglich handelt es sich um eine vulkanogen-sedimentäre (Geosynklinal-) Serie, in welcher der Magnesit-Lagerstättenzug auf eine Bildung in einem abgeschnürten Becken mit salinaren Lösungen zurückgeführt werden kann, in dem auch eine Schwarzschieferfazies (Graphit!) vorlag. Die gesamte (Geosynklinal-) Serie mit ihrem Magnesit-Lagerstättenzug wurde präalpidisch progressiv stark regional-metamorph umgebildet (mesozonal, z. B. Staurolith) und in alpidischer Zeit diaphthoritisch überprägt. Die Magnesit-Lagerstätte weist dieselbe tektonische Beanspruchung, Durchbewegung, bzw. die verschiedenen tektonischen Verformungsakte, Schieferung und Regionalmetamorphosen wie die umgebende polymetamorphe Serie der Radentheiner Glimmerschiefer auf, in der sie liegt und hat deren gesamte tektonische und metamorphe erdgeschichtliche Entwicklung durchlaufen.

SYNCHRONOUS CONTRASTING LATE MIOCENE ALKALINE VOLCANIC SERIES  
RELATED TO THE CHEB-DOMAŽLICE GRABEN, WESTERN BOHEMIA:  
GEOCHEMISTRY AND MINERALOGY

by

J. Ulrych<sup>1</sup>, J. Svobodová<sup>1</sup>, J. K. Novák<sup>1</sup> & K. Balogh<sup>2</sup>

<sup>1</sup>Institute of Geology

Academy of Science of the Czech Republic, Rozvojová 135, CR-165 02 Praha

<sup>2</sup>Institute of Nuclear Research

Hungarian Academy of Sciences, Bemrér 18/c, H-4026 Debrecen

The Cenozoic alkaline volcanism of the Bohemian Massif is an integral part of the Central European Volcanic Province. It is associated with large, sheet-like region of upwelling in the upper mantle, extending from the eastern Atlantic Ocean to central Europe and the western Mediterranean [1]. Cenozoic volcanism in W Bohemia is associated with the uplifted northeastern flank of the young Cheb-Domažlice Graben formed mostly by the Teplá Crystalline Complex. The most common volcanic forms are small stocks and diatremes (basaltic rocks), flows (differentiated trachyandesitic products), bulbous domes (trachyte), laccoliths with preserved gneissic roof (rhyolite), and rare complex volcanoes (with products of basanite and olivine nephelinite composition – Vlčí hora and Podhorní vrch Hills). The volcanic activity was probably coeval with the incipient graben formation dated from the Upper Miocene ? (older than 11.7 Ma) onwards and continuing with the Upper Pliocene sedimentary fill. Two coexisting Tertiary volcanic series have been recognised there:

(i) weakly alkaline series - WAS [alkali basalt/basanite I trachybasalt I trachyandesite - trachyte - rhyolite; 12.9 - 11.3 Ma] and

(ii) strongly alkaline series SAS [(melilite-bearing) olivine nephelinite/basanite II tephrite/trachybasalt II; 12.4 - 8.3 Ma].

Both series represent cogenetic association of contrasting silica-saturated to oversaturated and undersaturated rocks belonging to the intraplate continental magma types. These contrasting series are comparable with the volcanic suites of Siebengebirge, Westerwald and Cantal within the Cenozoic European Volcanic Province.

Rocks of the WAS are characterised by wide ranges in Mg# (72 - 8), SREE (170 - 530 ppm), and the (La/Yb)<sub>N</sub> (16.3 - 39.6) and Th/U (2.4 - 13.4) ratios. An expressive negative Eu/Eu\* anomaly (0.33) and high contents of Th (72 ppm) are present in rhyolites and some Q-rich trachytes. Rocks of the SAS are typical in their more narrow ranges in Mg# (74 - 49), SREE (200 - 470 ppm), and the (La/Yb)<sub>N</sub> (21.9 - 43.0) and Th/U (1.9 - 7.4) ratios. No expressive negative Eu/Eu\* anomaly is present (0.7 - 0.9).

Based on patterns in PM-normalised multielement variation diagrams, two initial, mantle-derived parental magmas, represented by alkali basalt/basanite I and olivine nephelinite/basanite II were recognised. Individual rock types differ in the magnitude of Rb and K negative anomaly and Nb/Ta ratio. Negative K and Rb anomalies in both representatives of initial magmas point to the origin of the magmas from the source containing phlogopite (amphibole). However, one uniform source cannot explain geochemical features observed in the mentioned rocks, and multiple mantle components (mantle plume, metasomatised mantle lithosphere) were probably involved in the generation of initial magmas. Parental magma of olivine nephelinites was derived from metasomatised mantle lithosphere with slight influence of plume material only, whereas the plume component prevailed in the parental magma of basanites (alkali basalts). Two different sources of Tertiary basanites and nephelinites from the southwestern Poland were reported by [2].

Olivine nephelinites/basanites II are geochemically similar to some tephrites/trachybasalts II. Geochemical variations within this group of rocks can be explained by different degrees of partial melting of a single magma source and olivine and moderate clinopyroxene fractionation. Relatively stable incompatible trace elements ratios indicate very slight or no crustal contamination.

Parental magma of alkali basalts/basanites I evolved to trachybasalts-basaltic trachyandesites-trachyandesites-trachytes-rhyolites. Variable Ba/Rb, K/Rb, Nb/Zr, Y/Nb, Zr/Rb and Th/U ratios indicate upper crustal contamination. Magma probably evolved in an upper crustal magma chamber by the AFC process. Olivine, clinopyroxene, Fe-Ti oxide and, in later stages, also apatite and K-feldspar fractionated. Late-crystallised apatite, Fe-Ti oxide and K-feldspar fractionation led to the depletion in Ti, Ba, Sr, Eu and P in rhyolites and some trachytes.

The ultramafic (peridotite, harzburgite) xenoliths are present in the SAS (basanite, olivine nephelinite), chemical compositions of some olivine nephelinite samples is shifted by granite (macro) and microxenoliths. Olivine nephelinite from Podhorní vrch Hill near Mariánské Lázně contains coarse-grained pegmatoid segregations of ijolite to turjaite composition [3]. Well-known megacrysts of oxykaersutite > diopside >> olivine occur in the basanite of Vlčí hora Hill together with cumulates of kaersutite.

Felsic derivatives (rhyolite and trachyte) reveal anomalous concentrations of Mn, both in rare primary ferromagnesian manganese minerals (diopside-hedenbergite, sodian magnesio-arfvedsonite, winchite, biotite-phlogopite, titanian magnetite), and in secondary hydrothermal Mn-oxyhydroxides and carbonates (rhodochrosite-calcite). The presence of sulphur in cavities along fissures accompanied by alteration of host rock indicates postmagmatic activity (i.e., presence of sulphur gases) within the trachytic intrusion of Špicák Hill.

The most widespread rocks of the WAS, i.e., Q-normative trachytes, differ only partly from rhyolite displaying higher contents of normative feldspar and lower content of quartz. Feldspars are the most substantial minerals of all these rocks forming usually more than 80 vol. %. Nevertheless, the presence of ternary feldspars and anhydrous ferromagnesian minerals indicate high temperatures of their origin and special crystallisation pathways. The most common reaction in these rock types (Q-normative trachytes and rhyolites) would be the crystallisation of alkali feldspars through the reaction of plagioclase with melt.

This explains the presence of partially resorbed cores of high-temperature ternary plagioclases and/or ternary alkali feldspars (generally anorthoclase rimmed by sanidine) in K-feldspar phenocrysts in the Špičák Hill trachyte. This phenomenon has been described from many localities of trachytes and rhyolites. The extent of resorption of plagioclase probably depended on the pressure, the bulk H<sub>2</sub>O content and the bulk composition of the melt. Partial to complete resorption of plagioclase can also occur in Q-normative trachytes under H<sub>2</sub>O buffered conditions, particularly if silica saturation is not attained until the late stages of crystallisation. For detail see [4].

### Literature

- [1] HOERNLE, K., ZHANG, Y. & GRAHAM, D. (1995): Seismic and geochemical evidence for large-scale mantle upwelling beneath the Eastern Atlantic and Western and central Europe. - *Nature*, 374: 34-39.
- [2] ALIBERT, C., LETERRIER, J., PANASIUK, M. & ZIMMERMANN, J. L. (1985): Trace and isotope geochemistry of the alkaline Tertiary volcanism in southwestern Poland. - *Lithos*, 20: 311-321.
- [3] ULRYCH, J., PIVEC, E., LANG, M. & LLOYD, F. E. (2000): Ijolite segregations in melilite nephelinite of Podhorní vrch volcano, Western Bohemia. - *N. Jb. Mineral., Abh.*, 175: 317-348.
- [4] PIVEC, E., ULRYCH, J., LANG, M., ÁRVA-SOS, E. & NEKOVARÍK, Č. (in press): Weakly-alkaline trachy-basalt-rhyolite series from the Teplá Highland, Western Bohemia: geochemical constraints. - *Geol. bavarica*, 22 pp.

**CHEMISMUS UND GENESE ORGANISCHER MINERALE  
IN DEUTSCHEN UND ÖSTERREICHISCHEN BRAUNKOHLEN**

von

**N. Vávra**

Institut für Paläontologie  
Universität Wien, Geozentrum, Althanstrasse 14, A-1090 Wien

Aus einer Reihe von Kohlelagerstätten sind im Laufe der Zeit verschiedenste organische Minerale beschrieben worden, die allerdings nur zum Teil mit modernen chemischen Methoden untersucht bzw. revidiert worden sind. Meist handelt es sich um Substanzen, die zu Terpenen in Beziehung gesetzt werden können; es sind dies meist fossile Harze ("Bernstein" im weitesten Sinne), Kohlenwasserstoffe bzw. entsprechende Gemische oder in einigen Fällen sogar Kautschuk ("fossil laticifers"). Die einzelnen Minerale sind dabei nicht nur aufgrund ihres oft sehr eigenartigen Chemismus sondern vielmehr auch im Zusammenhang mit Details der Inkohlungsprozesse sowie als Lieferanten von "Chemofoossilien" (molecular fossils) von Interesse, die – trotz aller gebotenen Vorsicht – gewisse Rückschlüsse bezüglich der Erzeugerpflanzen gestatten.

Unter den in Kohlelagerstätten als eigenes, gut definiertes Mineral vorkommenden Kohlenwasserstoffen ist vor allem der Hartit zu erwähnen. Seine Typuslokalität ist der seit 1949 eingestellte, einst nicht unbedeutende Glanzkohlenbergbau [1] von Hart (W Gloggnitz, N.Ö.), am Ostende der Norischen Senke gelegen (Miozän, Karpat). Hartit – später als Phyllocladan identifiziert – wurde in der Folge von zahlreichen weiteren Fundpunkten des In- und Auslandes beschrieben, z.T. jedoch unter anderen Namen, die als jüngere Synonyma zu betrachten sind (Hofmannit, Branchit, Josen etc.); anhand von Material aus Bílina (Tschechien) wurde vor wenigen Jahren eine moderne Revision veröffentlicht [2]. Ein als Köflachit aus dem Köflach-Voitsberger Tertiärbecken (Steiermark) beschriebenes Mineral [3] erwies sich bei einer Neubearbeitung [4] als ein Gemisch verschiedener Kohlenwasserstoffe, wobei allerdings Phyllocladan die Hauptmenge ausmachte. Ähnliche Resultate liegen mittlerweile auch für den Ixolyt (Hart bei Gloggnitz) sowie für den Jaulingit (Jauling=Jaulingwiese, nahe St. Veit a.d. Tr., 5 km SE Berndorf; Miozän, Karpat) vor: hier ist das Phyllocladan mit Abstand der dominierende Bestandteil. Diesen beiden Resultaten kommt insoferne besondere Bedeutung zu, als hier Typusmaterial analysiert werden konnte, was beim Köflachit bisher leider nicht möglich war. Bezuglich Jaulingit und Ixolyt wären jetzt freilich noch Belegstücke der anderen in der Literatur behaupteten Vorkommen dieser beiden Minerale zu überprüfen. Hinsichtlich einer Identifizierung einer möglichen Erzeugerpflanze lässt sich angeben, daß es sich bei Phyllocladan um ein Diageneseprodukt von Phyllocladen, und/oder Isophyllocladen – vielleicht auch von Phyllocladol – handelt, von Substanzen, die Bestandteile von Coniferenblatt- und -rindenölen sind,

sich aber kaum zur Charakterisierung von Familien und Gattungen eignen. Mit einiger Vorsicht kann man allerdings bestimmte Vertreter der Taxodiaceae (Sciadopitys und/oder Cryptomeria) als mögliche Erzeugerpflanzen annehmen [5], [6].

Unter den aus Kohlelagerstätten bekanntgewordenen fossilen Harzen sind jene Fälle von besonderem Interesse, wo aufgrund von bestimmten Chemofossilien eine Herleitung von Angiospermen angenommen werden kann. Dies trifft beispielsweise auf den Glessit zu, ein Harz, das anhand des Vorkommens von Amyrin – einem pentazyklischen Triterpen – bereits vor längerer Zeit als Angiospermenharz verdächtigt worden war [7]. Mit moderner Methodik konnte dieser Befund anhand von Material aus Bitterfeld (Sachsen) dahingehend erweitert werden, daß sowohl  $\beta$ - als auch  $\alpha$ -Amyrin vorliegt und zwar in etwa jenem Verhältnis, wie diese beiden Isomeren in rezenten Elemi-Harzen vorkommen (1 : 2.01 bzw. 1 : 1.90). Dies wurde als weiterer Hinweis gewertet, Glessit als ein fossiles Burseraceen-Harz zu deuten [8]. Aus dem Eozän Kärntens (Sonnberg bei Guttaring) stammt der Rosthornit, ein fossiles Harz, das aufgrund des Nachweises der beiden Amyrine gleichfalls als Burseraceen-Harz interpretiert werden kann [8].

Ein weiteres Beispiel eines Angiospermenharzes, das schon sehr früh als ein solches erkannt worden war, ist der Siegburgit [9]; eine Neubearbeitung [10] dieses Materials ergab eindeutig, daß es sich um ein Polymeres von Polystyrol-ähnlicher Struktur handelt. Dazu kam noch der Nachweis eines Esters der Zimtsäure, sodaß die Beziehung zur Familie der Hammamelidaceae als Erzeugerpflanzen gegeben erscheint (rezent z.B. Liquidambar orientalis mit einem vergleichbaren Chemismus). In diesem Zusammenhang sei auch der Nachweis von Zimtsäure und Dihydrozimtsäure (als Diageneseprodukt) in fossilen Harzen aus dem Eozän der Umgebung von Kassel [11] sowie aus einigen Harzproben aus Helmstedt [12] erwähnt: hier scheint sich hiemit eine weitere Gruppe von Angiospermenharzen abgrenzen zu lassen.

Als wohl bekanntestes organisches Material aus deutschen Kohlevorkommen sei noch an das "Affenhaar" aus dem Geiseltal (bei Halle a.d. S.) erinnert: schon früh als fossiler Kautschuk erkannt, hat dieses Material erst in jüngerer Zeit eine eingehendere Bearbeitung erfahren [13]; weniger bekannt dürfte jedoch das Vorkommen von fossilem Kautschuk aus der Braunkohle des Lavanttales (Kärnten) sein. Es handelte sich um einen dünnen Kohlestreifen, bei dem die spröden Kohleteile mit einer elastischen Substanz verbunden waren. Anhand eines Infrarotspektrums wurden Vergleiche mit Naturkautschuk angestellt und aufgrund des eher geringen Schwefelgehaltes sogar die Vermutung, daß hier möglicherweise ein nur "schwach vulkanisierter Weichgummi" vorläge, ausgesprochen [14].

## Literatur

- [1] WEBER, L. & WEISS, A. (1983): Bergbaugeschichte und Geologie der österreichischen Braunkohlevorkommen. - Arch. Lagerst. forsch. Geol. Bundesanst., 4: 1-317.
- [2] BOUSKA, V. et al. (1998): Hartite from Břílina. - Amer. Mineralogist, 83: 1340-1346.
- [3] DOELTER, C. (1878): Ueber ein neues Harzvorkommen bei Köflach. - Mitt. naturwiss. Ver. Steiermark, 1877: 93-96.

- [4] VAVRA, N. (1993): Organische Mineralien aus der Steiermark, I. (Hartit, Köflachit, Retinit, Trinkerit).  
Matrixx Miner. Nachr. Österr., 2: 24-38.
- [5] HEGNAUER, R. (1962–1986): Chemosystematik der Pflanzen. Eine Übersicht über die Verbreitung und die systematische Bedeutung der Pflanzenstoffe, Band 1 sowie Band 7 mit Nachträgen, Birkhäuser, Basel.
- [6] VAVRA, N. (1998): Phyllocladan, Simonellit und andere Chemofossilien aus Kohleproben des Korneuburger Beckens (Karpat, Miozän, Niederösterreich). - Beitr. Paläont. 23: 57-65.
- [7] FRONDEL, J. W. (1967): X-ray Diffraction Study of fossil Elemis. - Nature, 215: 1360-1361.
- [8] VAVRA, N. (1999): Fossil Resins from Austria: Biomarkers detected in Rosthornite (Eocene, Carinthia), Köflachite (Miocene, Styria) and a resin from the Lower Cretaceous of Salzburg. - In: KOSMOWSKA-CERANOWICZ, B. & PANER, H.(eds.): Investigations into amber. - Archaeol. Mus. Gdansk, Museum of the Earth, PAN, Gdansk.
- [9] LASAULX, A.v. (1875): Siegburgit, ein neues fossiles Harz. - N. Jb. Min. Geol. Paläont., Jgg. 1875: 128-133.
- [10] PASTOROVA, I., WEEDING, T. & BOON, J. J. (1998): 3-Phenylpropylcinnamate, a copolymer unit in Siegburgite fossil resin: a proposed marker for the Hammamelidaceae. - Org. Geochem., 29, 5-7: 1381-1393.
- [11] VAVRA, N. (in Vorbrtg.): Analyse des "Bernsteins" aus den eozänen Braunkohlen von Stolzenbach bei Kassel. -Documenta naturae.
- [12] VAHLDIEK, B.-W. (1986): Bernstein aus den eozänen Braunkohlen von Helmstedt (Bundesrepublik Deutschland, Niedersachsen) Stratigraphie und Ausbildung. - Aufschluss, 37: 165-177.
- [13] MAHLBERG, P. G. et al. (1984): Fossil laticifers from Eocene Brown Coal deposits of the Geiseltal. - Amer. J. Bot., 71, 9: 1192-1200.
- [14] BECK-MANNAGETTA, P. (1964): Fossiler Kautschuk aus der Braunkohle des Lavanttales (Ostkarnten). - N. Jb. Geol. Paläont. Mh., 1964, 11: 655-659.

**INFRARED BAND ASSIGNMENT OF AL-SI MULLITE AND SiO<sub>2</sub>-FREE COMPOUNDS  
WITH MULLITE STRUCTURE**

by

**D. Voll<sup>1</sup>, A. Beran<sup>1</sup> & H. Schneider<sup>2</sup>**

<sup>1</sup>Institut für Mineralogie und Kristallographie  
Universität Wien, Geocenter, Althanstrasse 14, A-1090 Wien  
<sup>2</sup>Institut für Werkstoff-forschung  
Deutsches Zentrum für Luft- und Raumfahrt, D-51147 Köln

Mullite is an aluminium silicate with the general formula  $\text{Al}_2[\text{Al}_{2+2x}\text{Si}_{2-2x}]\text{O}_{10-x}$ , where x denotes the number of oxygen vacancies per unit cell. SiO<sub>2</sub>-free phases with mullite structure can be obtained by the substitution of silicon by germanium and aluminium by gallium, or by addition of alkali metal ions for charge compensation of a mullite-type Al<sub>2</sub>O<sub>3</sub>. FTIR spectroscopic investigations were performed on synthesized powders of Al-Si, Al-Ge, Ga-Ge and alkali (Na, K, Rb) aluminates mullites. The IR spectra of Al-Si mullite and the germanate mullites in the lattice vibration region (1400 - 400 cm<sup>-1</sup>) are characterized by the presence of three main band groups, which are located for Al-Si mullite in the (a) 1200 - 1100 cm<sup>-1</sup>, (b) 1000 - 700 cm<sup>-1</sup> and (c) 650 - 400 cm<sup>-1</sup> spectral range. For Al-Ge and Ga-Ge mullites these band groups show a strong shift towards lower wavenumbers, which can be explained with the increasing size of the polyhedra in the substituted mullites. In IR spectra of the alkali aluminates only two band groups, (b) and (c), are observed, which are also shifted to the low energy region compared to Al-Si mullite due to increased Al-O distances [1]. The IR spectrum of the Na aluminite mullite exhibits a fine structure, which continuously vanishes in a solid solution from Na- to K-Al mullite. It can be assumed, that ordering effects are responsible for the more complex band structure of the Na aluminite.

The infrared absorption bands of the mullite-type compounds were deconvoluted into a minimum number of nine single bands. On the basis of observed band shifts and the polarization behaviour of a mullite single crystal [2, 3] the following assignment for the infrared bands of mullite is proposed: Bands in the high energy region (a) are assigned to Si-O and Ge-O stretching vibrations, mainly occurring along the short (Si, Ge)-O bond within the (001) plane. The absence of group (a) bands in the mullite-type silica-free alkali aluminates strongly supports this interpretation. Group (b) bands are mainly determined by stretching vibrations of Al and Ga on tetrahedral sites and T-O-T bending vibrations. The bands of group (c) can be assigned to stretching vibrations of Al and Ga in octahedral coordination and to O-T-O bending vibrations.

## **References**

- [1] FISCHER, R. X. et al. (2001): Crystal structure of Na and K aluminate mullite.s - Am. Mineral., submitted for publication.
- [2] RÜSCHER, C. H. (1996): Phonon spectra of 2:1 mullite in infrared and Raman experiments. - Phys. Chem. Minerals 23: 50-55.
- [3] VOLL, D. et al. (2001): Infrared band assignment and Rietveld refinement of Al-Si, Al-Ge, and Ga-Ge mullites. - Eur. J. Mineral. 13, in press.

**EINSATZMÖGLICHKEITEN VON TONEN AUS DEM BEREICH DES  
BRAUNKOHLETAGBAUES OBERDORF, WESTSTEIRISCHES TERTIÄRBECKEN,  
ALS ROHSTOFF IN DER INDUSTRIE**

von

**D. Wagner & H. Kurzweil**

Institut für Petrologie  
Universität Wien, Geozentrum, Althanstrasse 14, A-1090 Wien

Die im Tagebau Oberdorf verbreiteten Braunkohle-führenden, neogenen Sedimentabfolgen (Ott-  
nang, 17.6 Ma) sind als Ablagerungen eines ehemals randfaziellen, fluviatilen Environments in  
der Köflach-Voitsberger Bucht im wesentlichen schluffig-tonige Überflutungssedimente, die im  
Hinblick auf ihre Verfügbarkeit und ihre einheitliche Ausbildung hinsichtlich Kornaufbau und  
Mineralogie ein für industrielle Zwecke potentiell nutzbares Rohstoffvorkommen darstellen.

Die gegenständlichen Untersuchungen wurden zur Charakterisierung und Verwendbarkeit dieser  
Tone, insbesonders für industrielle Einsatzbereiche, an drei großtechnisch gewonnenen Durch-  
schnittsproben durchgeführt.

Das Untersuchungsprogramm umfaßte

- o Korngrößenanalytik (Siebungen, SEDIGRAPH)
- o Mineralogische Untersuchungen (XRD, DTA/DTG, REM/EDAX)
- o Chemische Analytik (XRF - Haupt- und Spurenelemente)

sowie die Ermittlung der Kennwerte von:

- o Anmachwassergehalt
- o Wasseraufnahmefähigkeit (ENSLIN)
- o Fließ- und Ausrollgrenze
- o Bildsamkeit
- o Trocken- und Brennschwindung
- o Methylenblau-Wert
- o Kationenaustauschvermögen.

## **Ergebnisse**

Nach ihrer Korngrößenzusammensetzung entsprechen die Rohstoffproben schlecht sortierten schluffigen Tonen, die in dieser Zusammensetzung nach der Klassifizierung im WINKLER-Diagramm für Ziegeltone in den Dach- bzw. Decken-ziegelbereich fallen.

Die durchschnittliche mineralogische Zusammensetzung mit den Schichtsilikaten der Glimmer- (ca. 36 %), der Chlorit- (ca. 8 %), der Kaolinit- (ca. 7 %) und der Smektitgruppe (ca. 5 %), sowie den Gemengteilen Quarz (ca. 40 %) und Feldspat (ca. 4 %) entspricht einem Tongestein in der üblichen Ausbildung Weststeirischer Beckensedimente.

Dem entspricht auch die durchschnittliche chemische Zusammensetzung der Tone mit Werten von  $\text{SiO}_2$  61.9 %,  $\text{Al}_2\text{O}_3$  16.9 %,  $\text{Fe}_2\text{O}_3$  7.8 %,  $\text{MgO}$  1.1 %,  $\text{CaO}$  0.6 %,  $\text{Na}_2\text{O}$  0.3 % und  $\text{K}_2\text{O}$  2.8 %. Auffällig bei den Spurenelementgehalten ist Vanadium mit Werten um ca. 200 ppm.

An Ergebnissen herstellungsrelevanter Eigenschaften der Tone sind vorliegend:

- o Anmachwassergehalt: 23 bis 30 %,
- o Wasseraufnahmefähigkeit (ENSLIN): 199 bis 229 % nach 4 Tagen,
- o Fließ- und Ausrollgrenze: schwach bis mittelmäßige Plastizität,
- o Bildsamkeit: schwach bis mittelbindig,
- o Trocken- und Brennschwindung: 8 bis 11% (1100°C).

Sie charakterisieren zur Herstellung von Hohlloch- und Dachziegeln geeignete Ziegeltone.

Mit Methylenblau-Werten von 3.00 - 4.45 (0/2 mm), 4.00 - 4.75 (0/0.063 mm) und 11.00 - 13.00 (0/0.002 mm) wird schließlich der Anteil der Glimmergruppe (Illit) am Aufbau der Tone unterstrichen.

Die Untersuchungsergebnisse korrelieren insgesamt sehr gut. Sie beschreiben Ziegeltone ohne höherwertige Verwendungen des Rohstoffs in Aussicht zu stellen.

## **Literatur**

- HAAS, M. (1999): Die frühmiozänen Sedimente der Braunkohletagebaue Oberdorf und Zangtal. - Diss. Formal- und Naturwiss. Fak. Univ. Wien.
- LORENZ, W. & GWOSDZ, W. (1997): Bewertungskriterien für Industriemineral, Steine und Erden. - Jb. Geol., H.2, Teil I, 91-101.
- SCHMIDT, H. (1979): Rohstoff-Untersuchungsverfahren in der Grobkeramik, III.: Physikal. Grunduntersuchung. - Sprechsaal, 112. Jg., H.3, 163-169.

**ANDALUSIT, SILLIMANIT UND KYANIT  
VOM SCHNEESTELLKOPF, KREUZECKGRUPPE, KÄRNTEN**

von

**F. Walter & K. Ettinger**

Institut für Mineralogie und Petrologie  
Karl-Franzens-Universität Graz, Universitätsplatz 2, A-8010 Graz

Quarzgänge, die bis 35 cm lange und 10 cm im Querschnitt messende Andalusitkristalle führen, sind aus der Kreuzeckgruppe schon seit einigen Jahrzehnten bekannt [1]. Als Fundort wird das Gebiet zwischen Schneestellkopf und Eisenriegel im Talschluß der Teuchl genannt. Eine weite Verbreitung von Andalusit in der Kreuzeckgruppe wurde vom Wöllatal im Westen über Strieden-obere Raggalalm - Schneestellkopf bis ins Teuchtal im Osten über rund 9 km festgestellt (pers. Mitt. J. MÖRTL). Die Andalusit-Quarzgänge treten in Metapeliten diskordant und teilweise stark boudiniert auf, einige Gänge sind bis zu 2 m mächtig.

Die Metamorphose der Strieden Einheit wurde als amphibolitfaziell mit mehr als 550°C bestimmt, wobei weiter nach Osten das Stabilitätsfeld für Sillimanit erreicht wird [2].

Im Rahmen einer Exkursion des Naturwissenschaftlichen Vereins für Kärnten wurden im Blockfeld südlich Schneestellkopf in 2360 m SH Andalusit-Quarzmobilisate beprobt, die bereits makroskopisch erkennbar weiße Nadeln im fleischroten Andalusit führen.

Die zahlreichen nur wenige mm bis einige cm großen Andalusitkristalle sind meist idiomorph entwickelt oder zu Haufen bzw. cm dicken Lagen im Quarz mit mehr als 50 Vol.-% angereichert. Akzessorisch sind im Andalusit Fluorapatit, Monazit und Relikte von Chloritoid vorhanden.

Die bereits makroskopisch sichtbaren Nadeln sind Kyanit, treten nur in Andalusit auf und sind an der Korngrenze zu Quarz scharf abgeschnitten. Der Kyanit ist idiomorph ausgebildet (Abb. 1 u. 2) und erstreckt sich oft über mehrere Andalusiteinkristalle. Auffallend ist ein Saum aus Schichtsilikaten (Paragonit-Muskowit Mischkristalle mit 80 - 20 mol% Paragonit), die stets den Kyanit umhüllen (Abb. 2). Dieses Gefüge läßt den Schluß zu, daß Kyanit nach Andalusit in diesem kristallisierte, wobei das geringere Molvolumen (rund -14 %) des Kyanits Platz für die Glimmerminerale schuf.

Sillimanit tritt als Fibrolith im Andalusit meist in unmittelbarer Nähe zu Quarz auf und ist auch im Quarz in Rissen und cm-breiten Nestern anzutreffen. Die Bestimmung erfolgte röntgenographisch, nur in den Anreicherungen im Quarz konnte Sillimanit mineraloptisch eindeutig identifiziert werden. Sillimanit kommt im Andalusit ohne Glimmersäume vor, die Differenz der Molvolumina (rd. 3 %) beider Minerale ist für einen entsprechenden Umhüllungshohlraum um Sillimanit auch sehr gering.

Die Mineralabfolge der drei Alumosilikate könnte aus Abb. 1 folgend gedeutet werden: Andalusit – Sillimanit – Kyanit. Sillimanit ist in diesem Andalusitkorn reichlich enthalten, im Kyanit, der diesen Andalusit idiomorph durchrennt, ist jedoch kein Sillimanit eingeschlossen. Die Sillimanitbildung wäre somit zeitlich vor dem Kyanit abgeschlossen.

Entlang von Rissen im Andalusit treten myrmekitartige Verwachsungen aus Kyanit + Quarz auf. Quarz ist dabei in unmittelbarer Nähe im Überschuß vorhanden (Abb. 3). Einen weiteren Hinweis, daß Kyanit nach Andalusit gebildet wurde, geben dm-große idiomorphe Andalusitkristalle mit beginnender Paramorphosenbildung von Kyanit nach Andalusit [1].

Feldspäte sind in der Paragenese der Andalusit-Quarzgänge nicht vorhanden, sodaß Natrium und Kalium als Bestandteile der fluiden Phase zugeführt wurden. Paragonitreiche, teils grobkristalline Glimmer wurden während oder kurz nach der Kristallisation von Kyanit gebildet. Als letzte Mineralbildung treten feinstkristalliner Muskowit (ohne Paragonitgehalt) und Diaspor als Alterationsprodukte von Andalusit, Sillimanit und Kyanitauf (Abb. 3). Diese Umwandlung der Alumosilikate kommt bevorzugt an Rissen und Korngrenzen vor.

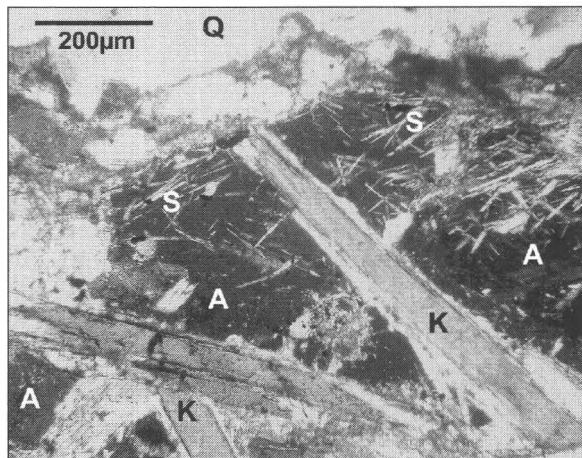


**Abb.1**  
Andalusit (A) – Sillimanit (S) – Kyanit (K)  
Abfolge im Andalusit-Quarzgang (Q) vom  
Schneestellkopf, Kreuzeckgruppe, Kärn-  
ten. Dünnschliff, gekreuzte Nicols.

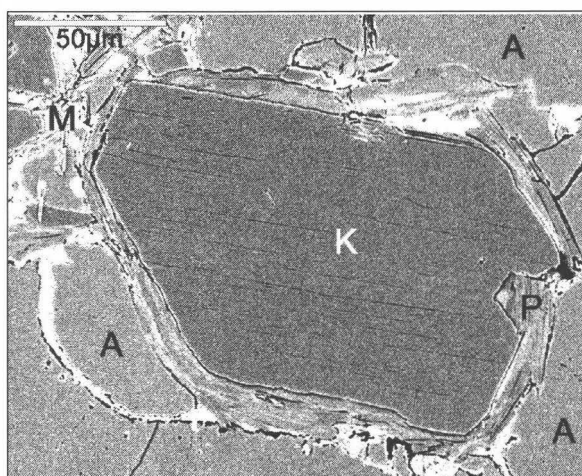


**Abb.2**  
Querschnitte eines idiomorphen Kyanitkri-  
stalles (K) mit Paragonit (P) und Musko-  
wit (M) Urmhüllung im Andalusit (A). BSE-  
Bild.

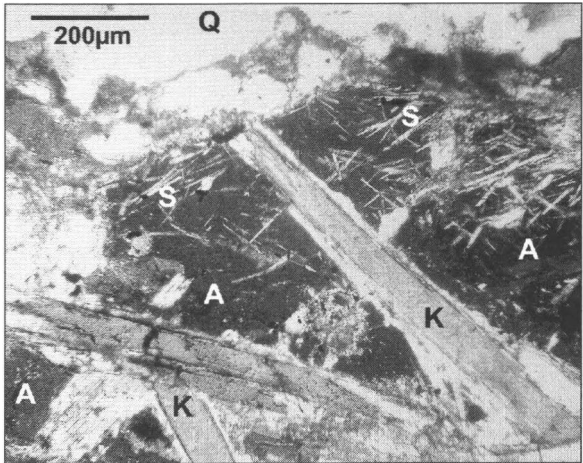


Abb.3

Myrmekitartige Verdrängung (Kyanit + Quarz) von Andalusit (A) mit angrenzendem Paragonit (P). Relikte von Sillimanit sind in Andalusit und Quarz (Q) erhalten. Muskowit (M) und Diaspor (D) sind die letzten Alterationsprodukte von Andalusit. BSE-Bild.

## Literatur

- [1] MEIXNER, H. (1971): Ein Vorkommen von Andalusit-Kristallen und von Paramorphosen von Disthen nach solchen sowie Cordierit und Apatit aus der Kreuzeckgruppe, Kärnten. - Carinthia II, Sh. 28: 239-243.
- [2] SCHUSTER, R. et al. (1999): Permo-triassic high temperature/low pressure (HT/LP) metamorphism in Austro-alpine basement units (Eastern Alps). - EUG 10 abstr.: 295.

DIE KRISTALLSTRUKTURVERFEINERUNG EINES FAST ALKALIFREIEN MINERALS  
DER OSUMILITHGRUPPE:  $K_{<0.1}(Fe,Mg)_2(Mg,Fe)_3[Si_{12}O_{30}]$

von

F. Walter & K. Ettinger

Institut für Mineralogie und Petrologie  
Karl-Franzens-Universität Graz, Universitätsplatz 2, A-8010 Graz

Die Kristallstruktur von Mineralen der Osumilithgruppe mit der allgemeinen Formel  $CB_2A_2T_2_3Tl_{12}O_{30}$  ist durch Doppelsechsringe von  $(Si,Al)O_4$ -Tetraedern (T1) geprägt. Diese Doppelringe sind entlang c gestapelt und werden durch T2-Tetraeder und A-Oktaeder miteinander verknüpft. In die durch die Doppelringe gebildeten Kanäle parallel c können große Alkali- bzw. Erdalkali-Kationen eintreten (C). Die Position B, meist mit Na besetzt, liegt zwischen zwei A-Oktaedern parallel zur c-Achse [1]. Die Alkaligehalte von Mineralen der Osumilithgruppe reichen von  $Na+K = 4$  (in der Formeleinheit) für Eifelit, über  $Na+K = 2$  für Roedderit, Merrihueit etc., bis  $Na+K = 1$  für Chayesit. Alkalifreie Minerale dieser Gruppe wurden bisher nicht beschrieben, von einer synthetischen alkalifreien Phase mit Osumilithstruktur liegt eine Strukturverfeinerung vor [2].

Aus Vulkaniten des steirisch-burgenländischen Vulkangebietes konnten bisher folgende Minerale der Osumilithgruppe nachgewiesen werden: Osumilith, Merrihueit, Roedderit und Chayesit. Diese meist hypidiomorphen, gelb bis dunkelblau gefärbten, kurzprismatischen hexagonalen Kristalle treten in kleinen Blasenhohlräumen als Reaktionsprodukte von basaltischem Magma und Si-reichen Xenolithen auf.

Aus einem Xenolith vom Stradner Kogel südlich Bad Gleichenberg, Steiermark wurde über ein nahezu alkalifreies Mineral der Osumilithgruppe berichtet [3]. Zur Klärung der Kationenbesetzung wurde an diesem Mineral eine Kristallstrukturuntersuchung durchgeführt. Ein  $0.16 \times 0.16 \times 0.07$  mm großer Kristall wurde am STOE-Vierkreisdiffraktometer (Institut für Chemie, Universität Graz) mit MoK $\alpha$ -Strahlung ( $\lambda = 0.71073$  Å) gemessen. Die Parameter der hexagonalen Zelle sind  $a = 10.050(1)$  Å und  $c = 14.338(2)$  Å. 3237 Reflexe mit  $2\theta < 51.8^\circ$  wurden mit  $\omega$ -scan ( $\Delta\omega = 0.8^\circ$ ) gemessen und für LP korrigiert. Über die systematischen Auslösungen konnten P6/mcc als Raumgruppe und 428 unabhängige Reflexe mit  $R(int) = 0.083$ ,  $R(\sigma) = 0.044$  ermittelt werden.

Als Startparameter der Koordinaten für die Positionen T1, T2 und A wurden jene des synthetischen MAS-Osumiliths [2] verwendet, entsprechend der chemischen Analyse [3] wurden T1 mit Silizium und T2 und A mit Magnesium und Eisen besetzt. Der geringe Mn- und Zn-Gehalt wurden als Fe berücksichtigt.

Die Verfeinerung mit dem Programm SHELX-97 [4] ergab eine Mg-Fe-Verteilung der Besetzung in T2 mit 38 % Fe und in A mit 65 % Fe. Über die anschließende Differenzfourieranalyse konnte nur für die Position C (0, 0, .25) ein schwacher Peak nachgewiesen werden. Die Verfeinerung der Besetzung mit Kalium in C ergab rd. 5 % K und 95 % Leerstelle. Die Position B für Natrium ist unbesetzt. Die chemische Analyse [3] für Na weist Konzentrationen nahe der Nachweisgrenze auf und bestätigt obiges Ergebnis. Die Verfeinerung mit anisotropen thermischen Parametern resultierte in  $R_1 = 0.028$  für 350  $F_o > 4\sigma(F_o)$  und  $wR_2 = 0.053$  für alle Reflexe.

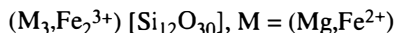
Die T1-O Abstände betragen 1.606 - 1.615 Å und weisen auf eine vollständige Besetzung mit Si hin [1]. Auch die Tetraederwinkel von 106.2 - 111.0° für O-T1-O belegen ein nur gering verzerrtes Tetraeder. Das die Doppelsechsringe vernetzende Tetraeder T2 ist dagegen extrem verzerrt: O-T2-O = 88.6 - 131.5°. Der Abstand T2-O3 (4x) mit 1.932(2) Å wird durch die Mg und Fe-Besetzung dieses Tetraeders geprägt und liegt im Wertebereich für T2-O Abstände der Roedderit-Chayesit-Mischkristalle [5]. Der A-O3 Abstand (6x) mit 2.032(2) Å ist für ein  $MgO_6$  Oktaeder zu kurz, sodaß hier der hohe Fe-Gehalt von 65 % in der Position A realistisch ist. Der wesentlichste Unterschied zu allen bisher bekannten Osumilith-Mineralen ist die hier nahezu leere Position C. Dies wird auch durch die Verlängerung der C-O Abstände belegt: C-O2 = 3.123(2) Å (12x) verglichen mit C-O2 Abständen in Roedderit-Chayesit von 3.062 - 3.066 Å [5]. Nur der synthetische MAS-Osumilith [2] zeigt mit der leeren Position C eine noch größere Distanz zu O2 mit 3.179(14) Å.

Ein weiterer Hinweis auf die Nichtbesetzung der Position C ist der Winkel O2-T1-O2: Ist C besetzt, beobachtet man Winkel von 102.4 - 105.0° [2], bei Roedderit-Chayesit 104.4 - 104.6° [5]. Im nahezu alkalifreien Mineral der Osumilithgruppe vom Stradner Kogel liegt O2-T1-O2 bei 108.8(2)° und im MAS-Osumilith bei 110.9°. Die kleinen Winkel kompensieren dabei den energetisch bevorzugten C-O Abstand, bei nichtbesetzter Position C wird dieser Winkel entspannt [2].

Aus der Kristallstrukturverfeinerung des Minerals der Osumilithgruppe vom Stradner Kogel kann folgende Formel angegeben werden:



Über den Wertigkeitsausgleich liegen 80 % des Eisens als  $Fe^{3+}$  vor. Berechnungen der Bindungsstärken für die Positionen T2 und A liefern Hinweise für das Vorliegen von Fe in unterschiedlichen Wertigkeitsstufen. Die Oxidation von  $Fe^{2+}$  zu  $Fe^{3+}$  wird auch in der Kristallchemie der Roedderit-Chayesit-Mischreihe über die Beziehung  $(K,Na)+Fe^{2+} = \square + Fe^{3+}$  angegeben [5]. Der Chemismus des hier untersuchten Minerals der Osumilithgruppe würde somit nahezu einem neuen Endglied mit der Summenformel



entsprechen (Abb. 1).

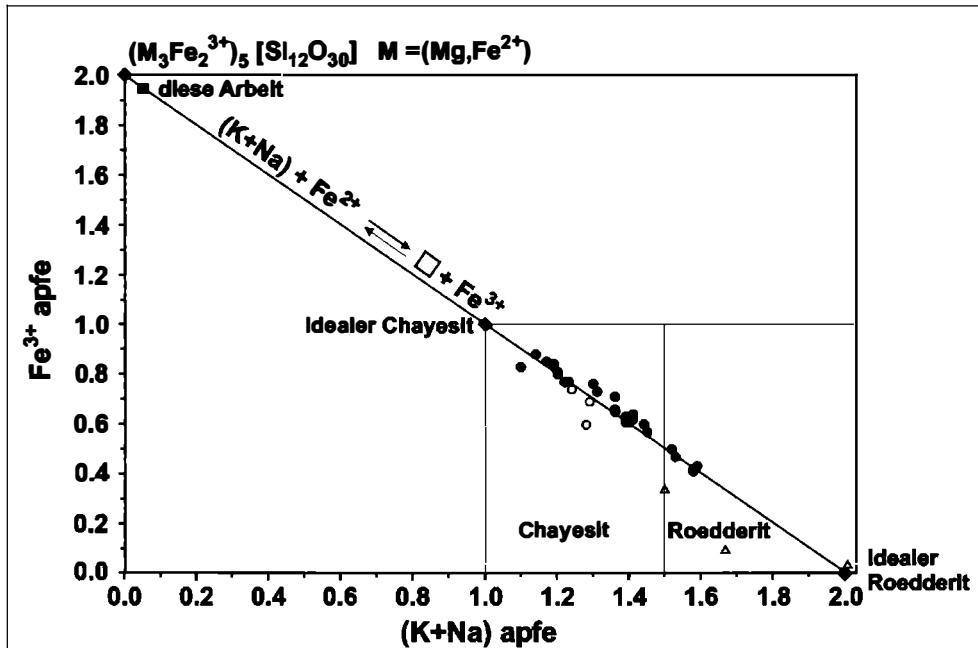


Abb. 1:  
Roedderit-Chayesit Mischreihe, modifiziert nach [5]

## Literatur

- [1] HAWTHORNE, F. C. et al. (1991): The crystal chemistry of the milarite-group minerals. - Am. Mineral. 76: 1836-1856.
- [2] WINTER, W. et al. (1995): Crystal structure refinement of synthetic osumilite-type phases: BaMg<sub>2</sub>Al<sub>6</sub>Si<sub>9</sub>O<sub>30</sub>, SrMg<sub>2</sub>Al<sub>6</sub>Si<sub>9</sub>O<sub>30</sub> and Mg<sub>2</sub>Al<sub>4</sub>Si<sub>11</sub>O<sub>30</sub>. - Eur. J. Mineral. 7, 277-286.
- [3] POSTL, W. et al. (2000): Über ein nahezu Alkali-freies Mineral der Osumilith-Gruppe aus dem Nephelinit-Steinbruch am Stradner Kogel bei Wilhelmsdorf, südlich Bad Gleichenberg, Steiermark, Österreich. - Joannea Min. 1: 53-64.
- [4] SHELDICK, G. M. (1997): SHELX-97, program for crystal structure determination. - University of Göttingen, Germany.
- [5] ALIETTI, E. et al. (1994): The roedderite-chayesite series from Spanish lamproites: crystal-chemical characterization. - Mineral. Mag. 58: 655-662.

**PLATIMETALLE IN MESOZOISCHEN OPHIOLITEN DER OSALPEN**

von

**H. H. Weinke<sup>1</sup>, F. Koller<sup>2</sup> & E. Pernicka<sup>3</sup>**

<sup>1</sup>Institut für Geochemie

Universität Wien, Geozentrum, Althanstrasse 14, A-1090 Wien

<sup>2</sup>Institut für Petrologie

Universität Wien, Geozentrum, Althanstrasse 14, A-1090 Wien

<sup>3</sup>Archäometallurgie

Technische Universität Bergakademie Freiberg

### **Einleitung**

Sehr geringe Gehalte an siderophilen Elementen in ultramafischen Gesteinen stellen ein analytisches Problem dar. Sie können möglicherweise auch inhomogen verteilt sein, deshalb ist es anzustreben, aus einer relativ großen Probenmenge (5 bis 10 g) aussagekräftige Analysenergebnisse zu erhalten. Die Platinmetalle können in diesen Konzentrationen nicht direkt mittels instrumenteller Neutronenaktivierungsanalyse gemessen werden, sondern erst nach einem Anreicherungsschritt über Nickelsulfid [1,2] wurden die Proben bestrahlt und danach radiochemisch aufgearbeitet.

### **Methodik**

In der vorliegenden Arbeit wurde durch Variation des Aufschlusses versucht, den Trennungsschritt der Platinmetalle mit Hilfe von Nickelsulfid zu optimieren sowie im Austauscherschritt nach der Aktivierung Cr, Co und Cu möglichst quantitativ in das Eluat zu entfernen, da in der anschließenden gammaspektroskopischen Messung eine nicht vollständige Abtrennung dieser Elemente zu einer deutlichen Erhöhung des Hintergrundes führt und damit die Nachweisgrenze signifikant verringert.

- ⇒ Aufschluss in einem Kohlenstofftiegel bei 1000°C (2h) einer Mischung von 5 g Probe mit Ni-Pulver, Schwefel, Li-Borat, Na-Karbonat und SiO<sub>2</sub>-Pulver.
- ⇒ Nach dem Erkalten wird aus dem Schmelzkuchen der NiS-König in 100 ml HCl<sub>(conc)</sub> herausgelöst.
- ⇒ Die reduzierende Lösung über Teflon-Filter abgenutscht und mit Methanol gespült, anschließend das Filter in Polypropylenfolie zur Bestrahlung eingeschweißt.
- ⇒ Für 2 Tage im Karussell bei einem thermischen Neutronenfluss von 7.0 10<sup>6</sup> pro cm<sup>2</sup> bestrahlt.
- ⇒ Gelöste Probe kühlen, mit 15 ml Dowex 1X8 sorgfältig schwenken und dann mit HCl<sub>(conc)</sub> ansäuern.

- ⇒ Ionen austauschersäule aus PVC-Schlauch mit etwa 2 ml unverbrauchtem Harz aufgießen und nach dem Absetzen darauf Probe mit aufgeschlämmten Harz gießen.
- ⇒ Waschen mit 10 ml 0.1N HCl, damit Fremdaktivität herausgelöst wird (z.B. Fe, Cu).
- ⇒ Anschließend mit  $\text{FeCl}_2$ -Lösung behandeln, da  $\text{Fe}^{2+}$  Cr zu  $\text{Cr}^{3+}$  reduziert, die PGE werden jedoch in der Säule gehalten; Überprüfung durch Kontrollmessungen auf dem Detektor.
- ⇒ Harz trockenlaufen lassen, in Plastikflasche überführen und mit etwas HCl nachspülen.
- ⇒ 1. Messung sofort nach Beendigung des Austauschvorganges für 2h.
- ⇒ anschließend mehrere Messdurchgänge von 2 bis 10 Stunden.
- ⇒ zwischendurch Messung der ebenfalls aufgeschlossenen Standards.

### **Ophiolitproben**

Als Beispiel wurden verschiedene, serpentiniisierte Ultramafititkomplexe der Mantelabfolge aus mesozoischen Ophioliten aus den Ostalpen ausgewählt. Verwendet wurden Harzburgite aus dem Idalm-Ophiolit des Unterengadiner Fensters (UM-ID), weiters Harzburgite aus der Rechnitzer Fenstergruppe (UM-RS) sowie Lherzolithe aus dem Reckner-Komplex im Unterostalpinen Rahmen des Tauernfensters (UM-UOA). Die Harzburgite der penninischen Fenster weisen sehr niedrige Al-Gehalte um 1.3 Gew.%  $\text{Al}_2\text{O}_3$  auf und entsprechen einem sehr stark verarmten Mantel eines MOR-Ophiolit. Die Lherzolithe des Reckner hingegen mit ~ 4 Gew.%  $\text{Al}_2\text{O}_3$  belegen deutlich deren geringeren Aufschmelzungsgrad.

### **Zusammenfassung**

Die Chondriten-normierten Pattern der untersuchten Ultramafititproben werden diskutiert. Sehr gut ist die starke Verarmung der PGE-Elemente zu beobachten. Die Lherzolithe des Unterostalpins (UM-UOA) weisen die geringsten Gehalte auf.

### **Danksagung**

Herrn Dietrich Kaether vom Max-Planck-Institut für Kernphysik, Heidelberg, sei für die engagierte Hilfe in der Radiochemie und Gammaspektroskopie herzlich gedankt.

### **Literatur**

- [1] ROBERT, R. V. D., VANWYK, E. & PALMER, R. (1971): Concentration of the Noble Metals by a Fire-Assay Technique using Nickel Sulphide as the Collector. - Nat. Inst Metall Rep. 1371, Johannesburg.
- [2] SCHMIDT, G. & PERNICKA, E. (1994): The determination of platinum group elements (PGE) in target rocks and fall-back material of Nördlinger Ries impact crater, Germany. - Geochim. Cosmochim. Acta 58: 5083-5090.
- [3] JOCHUM, K. P. (1996): Rhodium and other platinum-group elements in carbonaceous chondrites. - Geochim. Cosmochim. Acta 60: 3353-3357.

**SYNTHETIC COBALTOMENITE,  $\text{CoSeO}_3 \cdot 2\text{H}_2\text{O}$ , AND RELATED Co-COMPOUNDS  
AS MODEL PHASES FOR THE APPLICATION OF  
THE SUPERPOSITION MODEL (SM) OF CRYSTAL FIELDS IN GEOSCIENCES**

by

**M. Wildner & M. Andrus**

Institut für Mineralogie und Kristallographie  
Universität Wien, Geozentrum, Althanstrasse 14, A-1090 Wien

The Superposition Model (SM) of crystal fields was originally developed to separate the geometrical and physical information inherent in crystal field parameters [1, 2]. It is based on the assumption that the crystal field can be expressed as the sum of axially symmetric contributions of all  $i$  nearest neighbour ligands of the transition metal ion. The crystal field parameters  $B_{kq}$  can then be obtained from

$$B_{kq} = \sum \bar{B}_k(R_0) \left( \frac{R_0}{r} \right)^{t_k} K_{kq}(\Theta_i, \Phi_i)$$

where  $\bar{B}_k$  are the intrinsic parameters (related to a reference metal-ligand distance  $R_0$ ),  $t_k$  are the power law exponent parameters, both for each rank  $k$  of the crystal field,  $R_i$  are the individual metal-ligand distances, and  $K_{kq}(\Theta_i, \Phi_i)$  are the coordination factors calculated from the angular polar coordinates of the ligands.

Since its introduction by BRADBURY & NEWMAN [3], the SM has been applied with considerable success for the analysis of lanthanide crystal fields. Contrary, SM investigations on d-block transition elements are scarce up to date. Hence, the necessary intrinsic and power law exponent parameters for application to systems containing d-elements, e.g. in geosciences, are practically missing or were obtained from natural, dilute phases, where the local structure around the particular transition ion is not exactly known, e.g.  $\text{Cr}^{3+}$  in aluminosilicates [4, 5]. In order to provide reliable SM parameters of  $3\text{d}^n$  elements for future applications in geosciences, we started to investigate inorganic model compounds, i.e. pure synthetic endmember phases, where the (local) structure is precisely known from concurrent or recent structure investigations.

The first complete SM parameter set for  $\text{Co}^{2+}$  ( $\bar{B}_4 = 4740$ ,  $\bar{B}_2 = 7000 \text{ cm}^{-1}$ ;  $t_4 = 3.1$ ,  $t_2 = 5.5$ ) was extracted from polarised electronic absorption spectra of  $\text{Li}_2\text{Co}_3(\text{SeO}_3)_4$ , which is characterised by a strong bond length and angle distortion of its  $\text{CoO}_6$  polyhedra with low symmetries  $C_1$  and  $C_i$  [6]. Subsequently, we performed SM analyses of temperature dependent polarised spectra of brucite-type  $\text{Co}(\text{OH})_2$  [7], where the  $\text{Co}^{2+}$  ions occupy a high-symmetry site ( $D_{3d}$ ) within a compressed hexagonal close packing of oxygen atoms. In general, the magnitude of the intrinsic  $B_k$  parameters was confirmed ( $\bar{B}_4 = 5320$ ,  $\bar{B}_2 = 3900 \text{ cm}^{-1}$ ; the  $t_k$  were not refined due to symmetry restrictions). On closer inspection, however, it appeared that the specific position of closely related ligands within the spectrochemical series (i.e.  $\text{Q}_3\text{Se}^{2-}$  vs.  $\text{OH}^-$ ) affects the intrinsic  $\bar{B}_k$ .

Therefore, especially for mixed-ligand coordinations, it might be worthwhile to apply some empirical correction factor for the ligand type in the SM equation – resembling the *f*-factor formerly introduced by JØRGENSEN [8] – instead of refining different SM parameter sets for each ligand type.

Consequently, we modified our program suite [9] (performing the SM calculations with varying parameter sets, preparing the input files for a modified HCFLDN2 crystal field program package by YEUNG [10], and interpreting its output files) in such a way that

$$B_{kq} = \sum_i \bar{B}_k(R_0) \left( \frac{R_0}{R_i} \right)^{t_k} K_{kq}(\Theta_i, \Phi_i) \cdot f_i$$

where  $f_i$  represents a fixed or adjustable correction factor for different ligand types, according to their position in the spectrochemical series of ligands. By default,  $f_i$  is set to unity. As a  $\text{Co}^{2+}$  model phase with a distorted mixed-ligand coordination relevant for geosciences, synthetic cobaltomenite,  $\text{CoSeO}_3 \cdot 2\text{H}_2\text{O}$ , was chosen. There, the  $\text{Co}^{2+}$  cations are octahedrally coordinated to four oxygen atoms belonging to  $\text{SeO}_3$  groups ( $\text{Co}-\text{O} = 2.07 - 2.16 \text{ \AA}$ ) as well as two water molecules ( $\text{Co}-\text{O} = 2.04$  and  $2.19 \text{ \AA}$ ) in *cis*-position [11]. However, the calculations reveal only a marginal deviation of  $f_{\text{H}_2\text{O}}$  from unity. In this case, a reason for this unexpected result might be an additional perturbation and hence complication of the crystal field due to the linkage of the  $\text{CoO}_6$  octahedra to  $\text{Co}_2\text{O}_{10}$  dimers. Preliminary SM,  $f_{\text{H}_2\text{O}}$ , and interelectronic repulsion parameters for  $\text{CoSeO}_3 \cdot 2\text{H}_2\text{O}$  are:  $B_4 = 5080 \text{ cm}^{-1}$ ,  $t_4 = 5.4$ ,  $B_2 = 8000 \text{ cm}^{-1}$ ,  $t_2 = 0$ ,  $f_{\text{H}_2\text{O}} = 1.01$ , Racah B =  $800 \text{ cm}^{-1}$ , and Racah C =  $3300 \text{ cm}^{-1}$ . With the exception of the second rank exponent  $t_2$ , which might also be biased by the polyhedral linkage, the obtained SM and Racah parameters comply quite well with the expectations for  $\text{Co}^{2+}$  in oxygen crystal fields.

## References

- [1] NEWMAN, D. J. (1971): Theory of lanthanide crystal fields. - *Adv Phys*, 20, 197-256.
- [2] NEWMAN, D. J. & NG, B. (1989): The superposition model of crystal fields. - *Rep. Prog. Phys.*, 52, 699-763.
- [3] BRADBURY & NEWMAN (1967)
- [4] YEUNG, Y. Y., QIN, J., CHANG, Y. M. & RUDOWICZ, C. (1994): Correlation of spectroscopic properties and substitutional sites of  $\text{Cr}^{3+}$  in aluminosilicates: I. Kyanite. - *Phys. Chem. Min.*, 21, 526-531.
- [5] QIN, J., RUDOWICZ, C., CHANG, Y. M. & YEUNG, Y. Y. (1994): Correlation of spectroscopic properties and substitutional sites of  $\text{Cr}^{3+}$  in aluminosilicates: II. Andalusite and sillimanite. - *Phys. Chem. Min.*, 21, 532-538.
- [6] WILDNER, M. & ANDRUT, M. (1999): Crystal structure, electronic absorption spectra, and crystal field superposition model analysis of  $\text{Li}_2\text{Co}_3(\text{SeO}_3)_4$ . - *Z. Kristallogr.*, 214, 216-222.
- [7] ANDRUT, M. & WILDNER, M. (2001): Superposition Model analysis from polarised electronic absorption spectra of  $\text{Co}^{2+}$  in trigonally distorted octahedra in brucite-type  $\text{Co}(\text{OH})_2$ . - *J. Phys. Cond. Matter* (submitted).
- [8] JØRGENSEN, C. K. (1962): Absorption spectra and chemical bonding in complexes. - Oxford, Pergamon Press.
- [9] WILDNER, M. & ANDRUT, M. (1998-2001): SMM2, program suite for Superposition Model calculations. (unpublished).
- [10] CHANG, Y. M., RUDOWICZ, C. & YEUNG, Y. Y. (1994): Crystal field analysis of the  $3d^N$  ions at low symmetry sites including the "imaginary" terms. - *Computers in Physics*, 8, 583-588.
- [11] WILDNER, M. (1990): Crystal structure refinements of synthetic cobaltomenite ( $\text{CoSeO}_3 \cdot 2\text{H}_2\text{O}$ ) and ahlfeldite ( $\text{NiSeO}_3 \cdot 2\text{H}_2\text{O}$ ). - *N. Jb. Min. Mh.*, 1990, 353-362.

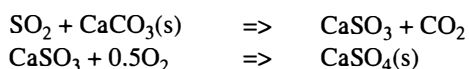
**URSACHEN FÜR RESTKARBONAT IM GIPS  
AUS EINER RAUCHGASENTSCHWEFELUNGSANLAGE**

von

**P. Wilflingseder<sup>1</sup>, R. Abart<sup>1</sup> & K. Bärnthaler<sup>2</sup>**

<sup>1</sup>Institut für Mineralogie und Petrologie  
Universität Graz, Universitätsplatz 2, A-8010 Graz  
<sup>2</sup>Babcock Borsig Power  
Austrian Energy, Waagner Biro Strasse 105, A-8021 Graz

Kalkstein basierte Flüssig-Gas Entschwefelung - "wet flue gas desulfurization" (WFGD) ist die kosteneffektivste Methode zur Entschwefelung von Rauchgasen im industriellen Maßstab. Das Verfahren basiert auf der Absorption von Schwefeldioxid aus dem Rauchgas an Tröpfchen einer wässrigen Suspension von Kalkpartikeln. Der Rauchgaswäscher ist ein vertikaler, innen gummierteter Stahlzylinder. Im unteren Drittel befindet sich der Wäschersumpf, im oberen Drittel die Reingaszone. Im mittleren Drittel, der sogenannten Kontaktzone, wird die Wäschersuspension über das heraufziehende Rauchgas mittels Sprühdüsen vaporisiert. Die für die Wäschersuspension verwendeten Kalksteine sind gewissen Kriterien der Betreiber unterworfen. Die Kriterien wären über 95 Gew.% CaCO<sub>3</sub>, unter 3 Gew.% MgCO<sub>3</sub> und 90 % der Körner sollten eine Größe zwischen 90 und 44 µm haben. In der Suspension erfolgt eine gipsbildende Reaktion, die vereinfacht formuliert werden kann als [ 1 ]:



Diese Reaktion läuft nicht immer vollständig ab. Zurückbleibende Restkarbonatsanteile sind störend bei der Weiterverarbeitung des Gipes in der Zement oder Gipsplattenindustrie. Untersucht wurde ein Rauchgaswäscher mit stark schwankenden Restkarbonatgehalten. Das Restkarbonat tritt vor allem in Form von Agglomeraten gemeinsam mit Glimmern, Tonmineralen und dolomitischen Körnern und untergeordnet als korrodierte Körner auf. Das gänzliche Fehlen von Gips/Kalzit Verwachsungen legt nahe, dass die Reaktion auf einer vollständigen Auflösung des Kalzits beruht und es zu keiner Fest-Fest Reaktion zwischen Gips und Kalzit kommt. Die Gipskörner nukleieren somit neu aus der Suspension. Es wurde untersucht ob die auftretenden Restkarbonate durch eine lokale Übersättigung an Kohlendioxid sekundär entstanden sind. Dazu wurde eine Separation des Restkarbonates von Gips mittels Rütteltisch und per Handauslese durchgeführt. Das Rohmaterial und das Restkarbonat wurden auf ihre Kohlenstoff- und Sauerstoffisotopie analysiert.

Das Ausgangsmaterial und das Restkarbonat stimmen in ihren  $^{13}\text{C}$ -Werten innerhalb der analytischen Genauigkeit überein. Die  $^{18}\text{O}$ -Werte des Restkarbonates sind gegenüber den  $^{18}\text{O}$ -Werten des Ausgangskalkes leicht erhöht. Die Übereinstimmung der Kohlenstoffisotopenwerte von Ausgangskalk und Restkarbonat lässt die Vermutung zu, dass im Restkarbonat vorwiegend aus dem Kalzit des Ausgangskalkes besteht und kein sekundäres Karbonat gebildet wurde. Die Differenz in den Sauerstoffisotopenwerten lässt sich aus der Verunreinigung der Restkarbonatproben mit Gips erklären.

Zusätzlich wurden ausgewählte Spurenelemente (V, Fe, Mn, Sr, Pb, Zn, Cd) mittels ICP-MS analysiert. Das Spurenelementmuster von Ausgangskalk, Gips und Restkarbonat zeigen einen sehr ähnlichen Verlauf. Gewisse Abweichungen dürften mit dem Materialeintrag über das Rauchgas oder mit Heterogenitäten im Ausgangskarbonat zusammenhängen. Besonders fällt bei den Spurenelementmustern auf, dass die untersuchten Elemente im Restkarbonat eine Anreicherung gegenüber dem Ausgangskarbonat zeigen.

Das Auftreten der Restkarbonate in den charakteristischen Agglomeraten wird durch die Koagulation von primären Karbonatpartikeln im Rauchgaswäscher erklärt. Das Auftreten von Glimmern in den Agglomeraten lässt vermuten, dass die oberflächenaktiven Schichtsilikate die "Kolloidbildung" fördern. In Form der Agglomerate scheint das Karbonat relativ schlecht löslich zu sein und bildet den Hauptanteil des unerwünschten Restkarbonates. Die Schwankungen im Restkarbonatanteil in der untersuchten Entschwefelungsanlage werden auf die schwankende Qualität des verwendeten Kalkes im Hinblick auf den Glimmer und Tonmineralgehalt zurückgeführt. Diese Ergebnisse lassen eine Erweiterung der Qualitätskriterien für den in der Suspension zu verwendenden Kalk im Hinblick auf den Glimmer- und Tonmineralgehalt als sinnvoll erscheinen.

## Literatur

- [1] BROGREN & KARLSSON (1997): A Model for Prediction of Limestone Dissolution in Wet Flue Gas Desulfurization. - Applications Ind. Eng. Chem. Res. 1997, 36, 3889-3897.

**PETROGRAPHICAL DATA ON THE LOWER CRETACEOUS  
FOSSIL RESIN DEPOSIT, GOLLING/SALZBURG**

by

**W. Winkler & E. Ch. Kirchner**

Institute of Mineralogy  
University of Salzburg, Hellbrunnerstrasse 34, A-5020 Salzburg

Already in 1885 the first geological hiking routes have been described between Grubach and the Lammer valley [1]. Detailed geological work of this area was carried out by PLÖCHINGER [2], later by FAUPL & TOLLMANN [3]. In 1962 the first resin samples were found in a clayey bed rich in coal (embedded in the sandstone of the Upper Roßfeld strata) after blastings for a freight road [2, 4-5].

The Upper Roßfeld strata (Hauterive to Apt) consist of coarsely clastic accretion and sandstones with higher carbonate content than the sandstones of the Lower Roßfeld strata, silification and layers of chert. In the sedimentological model, the Upper Roßfeld strata are the result of small sediment fans, which advance from the slope perpendicular to the deep sea trench and are supplied with material from canyons. The black stone layers, which include the resins, are typical for the Upper Roßfeld strata of the Apt [2-3, 6-7].

The majority of the resin samples is translucent and dark brown, or of a lighter brown color, other samples are completely opaque and of a milky brown color. The milky brown areas seem to be the contact zones with the surrounding sediment, where thermal influence during orogenesis could take effect. Smaller resin particles within thin coal strata are completely altered, the strata themselves are deformed by tectonic activity. Occurrence of calcite veins, pyrite, and limonite together with the resin rodlets was documented [4, 8]. SCHLEE [9-10] describes the red variety of the resin surrounded with remains of "rusty" sediments instead of coal as speciality. Usually these samples show a very intense red color. They were found in a small area of about one m<sup>3</sup> embedded in the other brown resins [8].

Microscopical investigations on several polished thin sections of completely new fossil resin material from Golling have proved an enormous richness in microfossils. The numerous microfossils, which have not been documented in any previous studies, may help form a more detailed picture of the flora of the former Araucaria-woods.

The microfossils found range from sizes less than 10 mm to sizes more than 50 mm and have not been identified, yet, except wood fragments and possible hyphas. Many microfossils follow an obvious flow trend (also detectable with UV-fluorescence) - possibly due to the flow of the original resin material as well as the kneading of the re-softened resin mass during orogenic activities. Some inclusions seem stretched or slightly deformed by this process.

The deposit from the Lower Cretaceous in Golling (Salzburg) was investigated concerning the resin samples as well as their surrounding coal by X-ray diffraction (Siemens D500). The coal samples include quartz, gypsum, pyrite, muscovite, albite and/or calcite, in one coal sample lepidocrocite could be detected. Gypsum in the coal samples is in some cases even visible as small crystals.

The fossil resin samples show similar mineral inclusions, such as quartz, gypsum, pyrite, muscovite, albite, calcite, and bassanite in one totally milled sample. The oxidation crust of the red variety additionally includes lepidocrocite and clinochlore. Thus, lepidocrocite in the red samples from the very restricted area (about one m<sup>3</sup>) within the former and now reforested mine from Golling could be identified as the coloring substance.

The bedrock with quartz, pyrite, muscovite, albite, calcite, clinochlore, and marcasite exhibits similar mineral content.

The white oxidation crust of brittle brown samples, according to the other components, includes rozenite and melanterite, the oxidation products of pyrite.

The fracture fillers are quartz and pyrite, whereby the quartz fillings deserve special attention. The fillings originate in the surrounding sediment and especially the agate- and chalcedony-structures within larger cavities point towards crystallization of a fluid phase, which is transported into the cavities over fractures from the surface. The agates are banded in white to grey and are translucent in thin sections [10-12].

Further investigations concerning relative age dating have been conducted by Raman spectroscopy. A number of differently aged samples have been included in a comparative study concerning age-dependent intensity changes of typical Raman bands in the resins [13].

### Acknowledgements

Many thanks go to the private collectors who supported the investigations on the fossil resin deposit in Golling/Austria with sample material and personal messages.

### References

- [1] FUGGER, E. & KASTNER, C. (1885): Naturwissenschaftliche Studien und Beobachtungen aus und über Salzburg. - Salzburg: Herm Kerber.
- [2] PLÖCHINGER, B. (1968): Die Hallstätter Deckscholle östlich von Kuchl/Salzburg und ihre in das Aptien reichende Roßfeldschichten-Unterlage. - Verh. Geol. B.-A.: 80-86.
- [3] FAUPL, P. & TOLLMANN, A. (1979): Die Roßfeldschichten: Ein Beispiel für Sedimentation im Bereich einer tektonisch aktiven Tiefseerinne aus der kalkalpinen Unterkreide. - Geologische Rundschau 68: 93-120.
- [4] STRASSER, A. (1968): Über den Neufund eines fossilen Harzes in der Weitenau bei Golling/Salzburg. - Der Aufschluß 19: 17.
- [5] STRASSER, A. (1989): Die Minerale Salzburgs. - Salzburg: Druckhaus Salzburg.
- [6] PLÖCHINGER, B. (1979): Argumente für die intramalmische Eingleitung von Hallstätter Schollen bei Golling (Salzburg). - Verh. Geol. B. A. 2: 181-194.

- [7] PLÖCHINGER, B. (1990): Erläuterungen zur geologischen Karte der Republik Österreich, Blatt 94 (1:50000), Vienna: Geologische Bundesanstalt.
- [8] FISCHER, G.: personal messages
- [9] SCHLEE, D. (1984b): Notizen über einige Bernsteine und Kopale aus aller Welt. - In: Bernstein-Neuigkeiten, ed. Staatliches Museum für Naturkunde in Stuttgart und Gesellschaft zur Förderung des Naturkundemuseums in Stuttgart, Stuttgarter Beiträge zur Naturkunde, Series C, 18: 29-37. Stuttgart: Calwer.
- [10] SCHLEE, D. (1985): Der österreichische Bernstein von Golling. - Goldschmiede Zeitung 8: 70-73.
- [11] SCHLEE, D. (1984): Bernstein-Neuigkeiten. Stuttgarter Beiträge zur Naturkunde, Ser. C, 18: 100 S.
- [12] SCHLEE, D. (1990): Das Bernstein-Kabinett. - Stuttgarter Beiträge zur Naturkunde, Series C, 28. Stuttgart: Staatliches Museum für Naturkunde in Stuttgart und Gesellschaft zur Förderung des Naturkundemuseums in Stuttgart.
- [13] WINKLER, W et al. (2001): A Raman spectroscopic approach to the maturation process of fossil resins. - J. Raman Spectrosc. 32: 59-63.

LARGE "GAHNITES" FROM NEAR OKAHUA, NAMIBIA:  
ONLY FE- AND ZN-BEARING SPINELS

by

**A. Wohlschläger, U. Kolitsch & E. Libowitzky**

Institut für Mineralogie und Kristallographie  
Universität Wien, Geozentrum, Althanstrasse 14, A-1090 Wien

Gahnite, ideally  $ZnAl_2O_4$ , is a Zn-dominant member of the spinel group, and a typical mineral in metamorphic and pegmatitic rocks. Recently, large (up to about 3 cm) blackish green "gahnite" crystals were reported from a private claim near Okahua about 30 km southeast of Otjiwarongo, central Namibia [1]. The host rocks are part of complex Precambrian metasediments consisting of marbles, calc-silicate rocks, quartz schists and chlorite-biotite schists, which are intruded by pegmatites and aplites [1].

Samples of "gahnite" and associated minerals, collected in September 2000 with the kind permission of the claim holder ("Namibia Minerals"), were investigated using single-crystal and powder X-ray diffraction, SEM-EDS, as well as IR and Raman spectroscopy. Large, blackish green octahedral "gahnite" crystals, associated with coarse-grained calcite, diopside, phlogopite and pale yellow forsterite, contain major Mg and Al, and minor amounts of Fe and Zn (1.0 - 1.3 wt.% ZnO). Their idealised empirical formula is  $(Mg_{0.81}Fe^{2+}_{0.17}Zn_{0.02})(Al_{1.9}Fe^{3+}_{0.1})O_4$ , and, consequently, they are Fe- and Zn-bearing spinels. IR spectroscopic investigations of a 0.5 mm thick polished platelet of a larger crystal showed nearly total absorption in the region between 10000 and 400  $\text{cm}^{-1}$  with only one small transparent region just before lattice vibrations cut off the transmitted light. This confirms the presence of both  $Fe^{3+}$  and  $Fe^{2+}$ .

In addition, small subhedral "gahnite" crystals, embedded in a dolomite marble and accompanied by orange subhedral clinohumite, have been collected from an outcrop about 30 m above the occurrence of the large spinels. Compared to the large octahedra, the small crystals have even less Zn being sometimes under the EDS detection limit (< 0.2 wt.% ZnO). Traces of manganese were detected in these tiny crystals that show a violet tint and are transparent under the binocular. Their Mg content is slightly higher and they contain less Fe than the large crystals.

Other minerals identified from the occurrence are meionite-dominant scapolite, wollastonite, titanite and epidote. The first two occur in narrow white veinlets. The chondrodite reported from the locality [1] has not been confirmed so far. Further studies are underway.

**References**

- [1] PALFI, A. G. & WARTHA, R. (2001): Das Gahnit-Vorkommen bei Okahua. In BAHMANN, U. & BAHMANN, A. (Eds.), Namibia – Zauberwelt edler Steine und Kristalle, Bode-Verlag, Haltern, Germany, pp. 140-142. (in German).

TEMPERATURE-RELATED DEHYDRATION AND STRUCTURAL DEVELOPMENT  
OF SOL-GEL PREPARED TYPE I MULLITE PRECURSORS

by

R. Zahiri<sup>1</sup>, D. Voll<sup>1</sup>, A. Beran<sup>1</sup> & H. Schneider<sup>2</sup>

<sup>1</sup>Institut für Mineralogie und Kristallographie  
Universität Wien, Geocenter, Althanstrasse 14, A-1090 Wien  
<sup>2</sup>Institut für Werkstoff-forschung  
Deutsches Zentrum für Luft- und Raumfahrt, D-51147 Köln

Mullite is an important compound in the field of advanced ceramics. For the preparation of ultrafine and pure precursor powders, the sol-gel route is a convenient method. Mullite precursors are characterized by different crystallization paths [1]. Type I precursors are non-crystalline up to 900°C and crystallize to mullite above this temperature. Precursor type II consists of weakly crystalline pseudo-boehmite and an amorphous silica-rich phase; mullite formation starts at temperatures  $\geq 1200^{\circ}\text{C}$ . Type III precursors are amorphous up to 900°C and crystallization of  $\gamma$ -alumina with  $\text{SiO}_2$ -rich amorphous phase is observed above this temperature; crystallization of mullite occurs above 1200°C.

Two sol-gel derived precursors for stoichiometric mullite ( $3\text{Al}_2\text{O}_3 \cdot 2\text{SiO}_2$ ), synthesized by slow hydrolysis methods, were investigated by FTIR spectroscopy, thermogravimetry and determination of the analytical water content. Precursor A was prepared by use of aluminium nitrate and tetraethoxysilane (TEOS) as starting materials, precursor B was synthesized from aluminium sec.-butoxide and TEOS. The 150°C-dried precursor powders (as-prepared) were heat-treated in 100°C steps in the range from 200 to 1000°C. Due to their crystallization behaviour, both samples correspond to type I precursors.

The IR absorption bands of the  $\text{H}_2\text{O}$  ( $5160\text{ cm}^{-1}$ ) and ( $\text{Si}, \text{Al}$ )-OH ( $4540\text{ cm}^{-1}$ ) combination mode, the ( $\text{H}_2\text{O}, \text{OH}$ ) stretching modes ( $3430\text{ cm}^{-1}$ ) and the  $\text{H}_2\text{O}$  bending modes ( $1635\text{ cm}^{-1}$ ) were used to monitor the temperature-dependent dehydration behaviour. Molecular water as well as OH groups are present in the as-prepared powders and in the heat-treated precursor phases. Precursor A shows a continuous loss of  $\text{H}_2\text{O}$  molecules and OH groups in the temperature range from as-prepared to 600°C, where most of  $\text{H}_2\text{O}$  and OH is released. Further dehydration occurs in the temperature step from 800 to 900°C. In precursor B the OH group content remains almost constant up to 500°C and is continuously reduced above this temperature.  $\text{H}_2\text{O}$  molecules are continuously removed over the whole temperature range. At 900°C both precursors show only minor amounts of  $\text{H}_2\text{O}$  and OH.

The IR spectra of the heat-treated samples in the range of lattice vibrations (1400 - 400 cm<sup>-1</sup>) show the structural changes of the precursor phases. The spectrum of the as-prepared sample of precursor A is characterized by two main band groups, located in the regions 1250 - 850 cm<sup>-1</sup> and 780 - 500 cm<sup>-1</sup>. With increasing temperature up to 600°C the low-energy band is splitted in two bands, which continuously change in their relative intensity, and the high-energy band shifts to higher wavenumbers. The absorption bands of the samples heat-treated between 600 and 900°C show only slight changes. Precursor A additionally exhibits a strong absorption band at around 1400 cm<sup>-1</sup> in the as-prepared sample, attributed to nitrate, which continuously vanishes up to 500°C. The temperature-related changes of the absorption bands of precursor B up to 800°C are less significant than for precursor A. Between 800 and 900°C remarkable changes of the spectrum are observed and the band pattern becomes very similar to that of precursor A. The IR spectra of the 1000°C-samples of both precursors closely match that of an alumina-rich mullite.

### References

- [1] SCHNEIDER, H. et al. (1993): Mullite precursor phases. - J. Europ. Ceram. Soc. 11: 87-94

PETROGENETIC SIGNIFICANCE OF  
SULFIDE INCLUSIONS IN ULTRAMAFIC CUMULATE XENOLITHS  
FROM NOGRAD-GÖMÖR VOLCANIC FIELD, PANNONIAN BASIN

by

Z. Zajacz, Cs. Szabó & I. Kovács

Department of Petrology and Geochemistry  
Lithosphere Research Group, Eötvös University, Múzeum krt.4/A, H-1088 Budapest

In this paper we provide new information about the evolution of the lithosphere beneath the Nógrád-Gömör Volcanic Field (northern Pannonian Basin) studying sulfide inclusions in cumulate-origin ultramafic xenoliths. These clinopyroxene rich xenoliths, representing the lower crust and upper mantle of the region studied, went through metasomatic alteration which resulted in formation of amphiboles.

We have carried out a detailed petrographic observation of sulfide inclusions using reflected light microscope and analyzed numerous back scattered electron images of the most typical sulfide inclusions. Based on these petrographic studies, only rounded or elongated or negative crystal shaped single inclusions occurring randomly in clinopyroxenes and amphiboles, and rarely in olivines and spinels have been selected for detailed electron microprobe analysis. Textural fabrics listed above are typical of primary inclusions. The sulfide blebs consist mostly of pyrrhotite and minor chalcopyrite, cubanite and pyrite, based on optical properties (Figure 1 and 2).

Chemical compositions of the sulfide phases show that pyrrhotite, which is the major phase in all inclusions, is sulfur rich (up to 40.2 - 41.4 m/m%) and nickel poor (max 6.1 m/m%). Chalcopyrite is also sulfur rich (up to 36.7 m/m%) and deficient in Cu content (down to 27.7 m/m%). Pyrite and cubanite show regular compositions and were identified only in one xenolith.

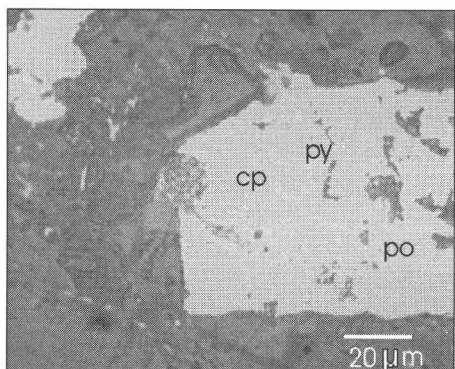


Figure 1  
Elongated sulfide inclusion containing spherical chalcopyrite surrounded by thin pyrite rind in clinopyroxene.  
The rest of the inclusion consists of pyrrhotite.

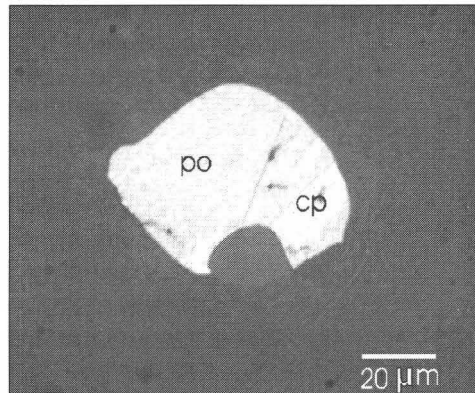


Figure 2

*Spool-shaped sulfide inclusion containing pyrrhotite and minor exsolved chalcopyrite lamellas in clinopyroxene.*

The bulk compositions of sulfide blebs calculated by mass balance calculation form a tight compositional range and are enriched in Fe compared to those in Type-I peridotite xenoliths from the same volcanic field (Figure 3) (SZABO & BODNAR, 1995). This indicates a distinct evolution history (FALUS et al., 2000).

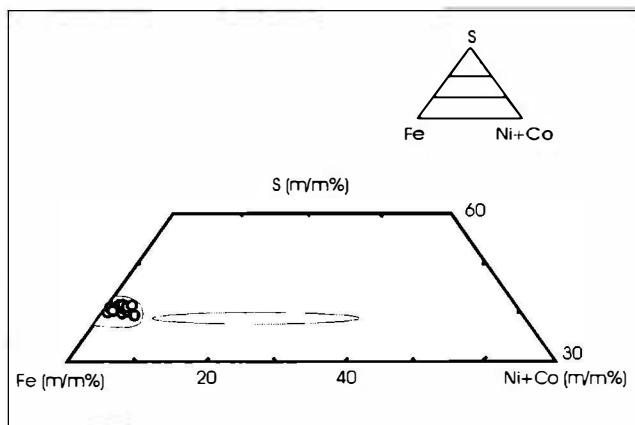


Figure 3

*Calculated bulk composition of sulfide blebs in cumulate xenoliths (black circles) in comparison to those of Type-I peridotitic xenoliths (grey field) (SZABO & BODNAR, 1995) from the Nógrád-Gömör Volcanic Field.*

Based on our study, it can be concluded that the sulfide blebs studied could have formed from sulfide melt which coexisted with silicate melt which was the source of host clinopyroxene rich cumulates. The sulfide blebs (mineralogically pyrrhotite) went through a high and low temperature evolution producing the other sulfide phases (chalcopyrite, cubanite, pyrite) present in the blebs. Chalcopyrite exsolved from pyrrhotite at relatively low temperature. Pyrite is a product of low temperature alteration process of pyrrhotite.

Study of the sulfide blebs also provides significant information to the origin of amphiboles in the host cumulate xenoliths. Textural features of the amphiboles (e.g., presence of amphibole lamellas in clinopyroxenes along their cleavages) refer to their metasomatic origin. However, sulfide blebs occurring either in clinopyroxenes or amphiboles show no differences in textural features and chemical compositions. The metasomatic process produced amphiboles did not affect the sulfide inclusions. If amphiboles have igneous origin, their sulfide inclusions should be different in compositions and fabrics from those in clinopyroxenes.

## **References**

- [1] SZABO, CS. & BODNAR, R. (1995): Chemistry and origin of mantle sulfides in spinel peridotite xenoliths from alkaline basaltic lavas, Nógrád – Gömör Volcanic Field, northern Hungary and southern Slovakia  
Geochim. et. Cosmochim. Acta, 59, 3917-3927.
- [2] FALUS, GY., SZABO, CS., AZBEJ, T., KOVACS, I. & ZAJACZ, Z. (2000): Mantle evolution beneath the Carpathian-Pannonian Region: Evidence from sulphide inclusions in upper mantle xenoliths. - Vjesti 37/3, PANCARDI 2000 Abstracts, 37.